UNIVERSITÀ DEGLI STUDI DI MILANO
DOCTORATE SCHOOL OF CHEMICAL SCIENCES AND TECHNOLOGIES
DEPARTMENT OF ORGANIC AND INDUSTRIAL CHEMISTRY
PHD COURSE IN CHEMICAL SCIENCES, XXIV CYCLE

PEPTIDOMIMETICS CONTAINING NEW BIFUNCTIONAL 2,5-DIKETOPIPERAZINE SCAFFOLDS: SYNTHESIS, CONFORMATIONAL ANALYSIS AND USE AS POTENT INTEGRIN LIGANDS

CHIM/06 Organic Chemistry

MATTIA MARCHINI
R08322

Tutor: Prof. Cesare GENNARI
Co-Tutor: Prof. Umberto PIARULLI (Università dell'Insubria)

Co-ordinator: Prof. Silvia ARDIZZONE

A.Y. 2010/2011

The present work was led by:	Prof. C. Gennari and Prof. U. Piarulli	
Doctoral Final Oral Examination:	January, 11th 2012	
Examination Committee:	Chairperson:	Prof. E. Beccalli
	Second Member:	Prof. Giuseppe Faita
	Third Member:	Prof. Massimo Sisti

The work herein described was performed at the University of Milan at the Department of Organic and Industrial Chemistry in the period from January 2009 to December 2011 under the supervision of Prof. Cesare Gennari, and at the Institute of Organic Chemistry at the University of Regensburg in the period from October 2010 to March 2011 under the supervision of Prof. Dr. O. Reiser.

I sincerely acknowledge my supervisors, Prof. C. Gennari and Prof. U. Piarulli, for providing me with interesting topics, for their ability in carrying out this work and for their steady support.

TABLE OF CONTENTS

ABBREVIATIONS

1D, 2D, 3D	One / two / three- dimensional
Ac	acetyl
ACC	aminocyclopropanecarboxylic acid
AcOH	acetic acid
ACPC	aminocyclopentanecarboxylic acid
All	allyl
aq.	aqueous solution
Ar	aryl
Bn	benzyl
Boc	tert-butyloxycarbonyl-
Bu	Butyl
c-	cyclo
Cbz	Benzyloxycarbonyl-
CD	Circular Dichroism
Conc.	Concentrated
COSY	Correlation Spectroscopy
DBU	1,8-diazabicyclo[5.4.0]undec-7-ene
DCC	dicyclohexylcarbodiimide
DCM	dichloromethane
DIAD	diisopropylazadicarboxylate
DIC	diisopropylcarbodiimide
DIPEA	diisopropylethylamine
DKP	diketopiperazine
DMAP	dimethylaminopyridine
DMF	dimethylformamide
DMSO	dimethylsulfoxyde
DPPA	diphenylphosphoric acid azide
ECM	Extracellular matix
EDC	Ethyl-N,N-dimethyl-3-aminopropyl carbodiimide
eq.	equivalents
ESI	electrospray ionisation
Et	Ethyl
Fmoc	9-Fluorenylmethoxycarbonyl
Fn	Fibronectin
h	hours
HATU	O-(7-azabenzotriazol-1-yl)-tetramethyl-uronium hexafluorophosphate
HBTU	O-benzotriazole-N,N,N’,N’-tetramethyl-uronium hexafluorophosphate
HMBC	heteronuclear multiple bond correlation
HOAt	1-Hydroxy-7-azabenzotriazole
HOBt	N-Hydroxybenzotriazole
HPLC	high performance liquid chromatography
HSQC	heteronuclear single quantum correlation
IC	inhibitory capacity
*i*PrOH	propan-2-ol
IR	Infrared Spectroscopy
J	Scalar coupling constants
KHMDS	potassium hexamethyldisilazane
MALDI	Matrix-assisted laser desorption ionization
MC	Monte Carlo
MD	molecular dynamics
Me	methyl
MeOH	methanol
MIDAS	Metal ion dependent site
min.	minutes
MS	Mass Spectroscopy
MW	Molecular weight
NMR	Nuclear Magnetic Resonance
NOE	Nuclear Overhauser Effect
PG	Protecting group
Ph	Phenyl
ppb	Part per billion
ppm	Part per million
Py	Pyridine
quant.	quantitative
quat.	quaternary
r.t.	room temperature
Rf	Retention faktor
RMSD	Root Mean Square Deviation

ROESY	Rotating Frame NOE spectroscopy	TFE	Trifluoroethanol
sat.	saturated	THF	tetrahydrofurane
SPPS	solid phase peptide synthesis	TIS	triisopropylsilane
*t*Bu	tert-butyl	TMS	trimethylsilyl
TEA	triethylamine	TOCSY	Total Correlation Spectroscopy
tert	tertiary	tol	toluene
Tf	triflate	UV	Utraviolet Spectroscopy
TFA	trifluoroacetic acid	δ	Chemical shift

Amino acid	**One-letter code**	**Three-letter code**
Alanine	A	Ala
Arginine	R	Arg
Asparagine	N	Asn
Aspartic	D	Asp
Cysteine	C	Cys
Glutamine	Q	Gln
Glutamic acid	E	Glu
Glycine	G	Gly
Histidine	H	His
Isoleucine	I	Ile
Leucine	L	Leu
Lysine	K	Lys
Methionine	M	Met
Phenylalanine	F	Phe
Proline	P	Pro
Serine	S	Ser
Threonine	T	Thr
Tryptophan	W	Trp
Tyrosine	Y	Tyr
Valine	V	Val
Unspecified amino acid	X	Xaa, Yaa

D-amino acids are described by D-Xaa in the three-letter code and with the small letter in the one-letter code.

GENERAL INTRODUCTION

In the past 50 years a wide variety of naturally occurring peptides have been discovered. These peptides and their higher relatives proteins play a fundamental role in almost all processes of the living cell. As neurotransmitters, immunomodulators, enzyme inhibitors, substrates and hormones peptides are responsible for the regulation of biochemical processes such as cell-cell communication and control of vital functions like metabolism, immune response, digestion, respiration, sensitivity to pain, reproduction, behavior and electrolyte levels.

Unfortunately, peptides show several limits in their clinical application: 1) being composed of natural amino acids, they are readily degraded by specific or non-specific proteases under physiological conditions; 2) they tend to be quite conformationally flexible, so that they can bind to more than one receptor or receptor subtype, leading to undesired side effects; 3) due to their high molecular mass and to the lack of a specific delivery system, they are characterized by poor bioavailability.[1]

Peptidomimetics are designed to circumvent some of these problems. The essential elements (pharmacophores) in a peptdomimetic mimic a natural peptide or protein in 3D space retaining the ability to interact with the biological target, producing or blocking the same biological effect.

The design process begins by developing structure-activity relationships (SAR) that can define a minimal active sequence or major pharmacophore elements, and identify the key residues that are responsible for the biological effect. Then structural constraints are applied to probe the 3-D arrangement(s) of these features. In this process, the peptide complexity is reduced and the basic pharmacophore model is defined by its critical structural features in 3D space. As one of the major efforts in organic chemistry, a variety of molecules have been designed to mimic the secondary structures of peptides, such as α-helices, β-turns, and β-sheets. Peptides composed of naturally occurring α-amino acids usually must have a length of at least 12 units in order to adopt a stable conformation in solution, while oligopeptides constructed from unnatural amino acids surprisingly assume stable secondary structures even in short oligomers of several units. This is a reason why in most successful approaches to small molecule mimetics, the chemical modifications involve the restriction of conformations performed either by the cyclization of peptides or by the incorporation of conformationally restricted building blocks, mostly unnatural amino acids and dipeptide surrogates.

The other tactic involves replacing a particular peptide bond with its isostere.

A variety of methodologies and strategies have been developed and continue to be developed to establish systematic tools for transformation of peptides into peptidomimetics or further into small drug-like molecules.[2]

As a result of such endeavors, the advantage of peptidomimetics over the native peptides has been demonstrated by: (1) increasing the potency and selectivity; (2) decreasing the side effects; (3) improving oral bioavailability, and the half-life of the activity through minimizing enzymatic degradation.

1 Peptide secondary structure elements

Secondary structure is the local conformation of a polypeptide chain or the spatial relationship of amino acid residues that are close together in the primary sequence. In globular proteins the three basic units of secondary structure are the: α-helix, β-sheet and turns.

It is the formation of regular secondary structures into complicated patterns of protein folding that ultimately leads to the characteristic functional properties of proteins and peptides.

1.1 α-helix

α-helix (Figure 1) is the most common repetitive feature of peptide secondary structure. It can be visualized as a poliamide "cylinder" in which the tightly coiled main chain forms the inner part of it, while the side chains extend outwards. The α-helix is defined as 3.6_{13}, 3.6 indicating the number of residues per turn and 13 the number of atoms in the ring formed by hydrogen bonds between backbone CO and NH in *i* and *i*+4 residues, respectively, which stabilize the structure. Because of the right-handed helicity of an α-helix, carbonyls are pointing downward in the direction of the C-terminus, while the NHs point upward in the direction of the N-terminus.[3]

A less common helical secondary structure is the 3_{10} helix. Having three residues per turn, carbonyl on residue *i* is hydrogen-bonded to the amide NH on residue *i*+3, forming 10-membered repetitive rings.3

Aminoacids are featured by a peculiar propensity to form helices. Helix propensities accumulate over a peptide segment, with Ala being the most helix-stabilizing and Gly the least.

A number of methods devoted to the stabilization of this kind of secondary structure can be helpful in the design of helices-mimics:

- introduction of Ala residues;
- design of covalent or non-covalent interactions between residues side chains one turn apart (S-S bridges, H-bonds, …);
- addition of nonpeptide templates to initiate helix formation;
- introduction of charged residues near the N or C termini to electrostatically stabilize the helix;
- replacement of one of the main chain intramolecular hydrogen bonds with a covalent linkage, by introduction of an hydrogen-bond surrogate.3

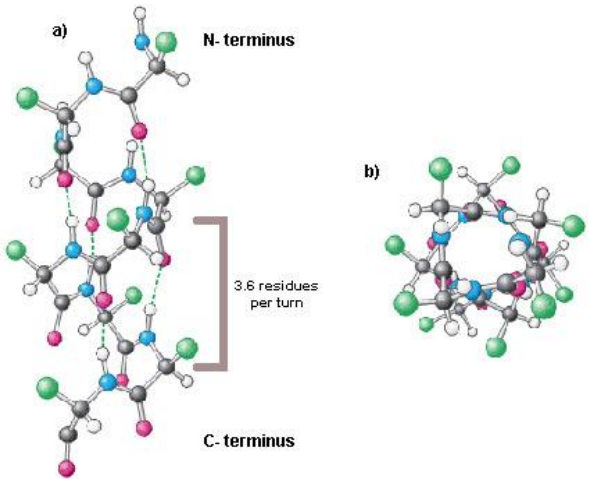

Figure 1 – representation of an α-helix a) from aside and b) from above.

1.2 β-strand and β sheet

The β-strand is the second type of periodic secondary structure and is an extended conformation when compared with the α-helix.

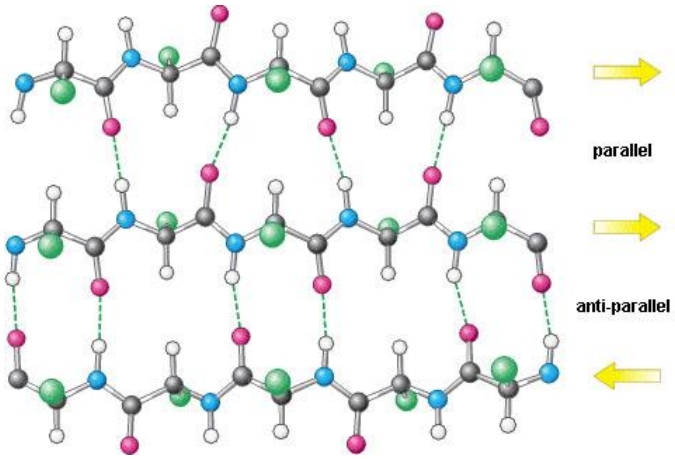

Figure 2 – β-strands forming a β-sheet

A single β-strand (Figure 2) is not stable largely because of the limited number of local stabilizing interactions. However, the backbone of N–H and C=O groups are oriented approximately perpendicular to the direction of the chain and therefore these groups are available for interstrand hydrogen bonding.

Consequently, hydrogen bonds can be formed between two or more β-strands leading to a stable sheet arrangement. These β-sheets result in significant increase in the overall stability and in the formation of backbone H-bonds between adjacent strands that may involve residues widely separated in the

primary sequence. Adjacent strands can align in antiparallel or parallel arrangements with the orientation established by determining the direction of the polypeptide from the N- to the C-terminal. Antiparallel association of β-strands leads to colinear N–H ••• O=C hydrogen bonds and, consequently, to a network of 10- and 14-membered H-bonded rings, while a parallel association of strands leads to deviation from colinearity and to a network of 12-membered H-bonded rings (Figure 2). On average β-sheets containing antiparallel strands are more common than sheets made up entirely of parallel strands. Antiparallel sheets are often formed from just two β-strands running in opposite directions whilst it is observed that at least four β-strands are required to form parallel sheets.

1.3 - Loops, turns, templates

Reverse turns constitute one of the most common structural features in globular proteins. Turns have the universal role of enabling the polypeptide to change direction and in some cases to reverse back on itself. Besides its structural role in the protein fold, turns play also a key role in many of the molecular recognition events in biological systems. These events include interactions between peptide hormones and their receptors, antibodies and antigens, and regulatory enzymes and their corresponding substrates.[4]

Reverse turns comprise the widely distributed β-turns, as well as the less prevalent γ-turns and α-turns, and may include well-defined loops, such as Ω-loops.[5] In current practice, the classification of a turn is based on the preferred torsion angles (ϕ and ψ) of the backbone chain, the position of the stabilizing hydrogen bond, and the length of the chain where the turn occurs.[6] Analysis of the amino acid composition of turns reveals that bulky or branched side chains occur at very low frequencies. Instead, residues with small side chains such as glycine, aspartate, asparagine, serine, cysteine and proline are found preferentially.5

A γ-turn (Figure 3) contains three residues and frequently links adjacent strands of antiparallel β-sheets. This kind of turn is characterized by the fact that the middle residue (i+1) does not participate in H-bonding whilst the first and third residues can form the final and initial H-bonds of the antiparallel β-stands, resulting in a 7-membered hydrogen-bonded ring. The change in direction of the polypeptide chain caused by a γ-turn is reflected in the values of ϕ and ψ for the central residue. As result of the size and conformational flexibility, glycine is a favoured residue in this position although other amino acids can be found.

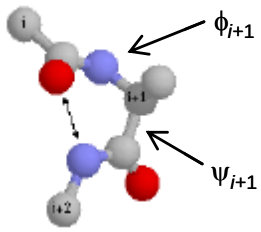

TURN TYPE	ϕ_{i+1}	ψ_{i+1}
CLASSIC γ-TURN	70º to 85º	-60º to -70º
INVERSE γ-TURN	-70º to -85º	60º to 70º

Figure 3 - Torsion angles of classic and inverse γ-turns.

Four residue turns, meaning β-turns, are more commonly found in proteins and both linear and cyclic peptides. According to the last revaluation of the β-turn classification, nine distinct structural types were suggested based on the ϕ and ψ torsion angles in residues *i*+1 and *i*+2 (Figure 4).[7] β-turns, may (classical β-turn) or may not (open β-turn) be stabilized by an intramolecular H-bond formed between the C=O of the first residue (*i*) and the N–H of the fourth residue (*i*+3) (abbreviated as 4 → 1 H-bond), giving rise to a 10-membered H-bonded ring. Two major classes of β-turns meet the stereochemical criteria, with all peptide bonds being *trans*: type I and type II (Figure 4).[8] These turns differ in the orientation of the peptide bond between the *i*+1 and *i*+2 residues, and consequently in the preferred side chain dispositions in these positions. In a type I turn, both the *i*+1 and *i*+2 positions accommodate L-residues, however proline preferentially fits in the *i*+2 position. Type I turns are the most prevalent in naturally occurring proteins. In a type II turn, the *i*+1 position can accommodate an L-residue (usually proline) and the *i*+2 position favours a glycine, small polar L-residues, or a D-residue because of steric clash with a side chain in the L-configuration. Proline in the *i*+1 position is a strong sequence determinant for either a type I or II turn because of the restriction on the ϕ angle from the cyclic side chain.8

Other turn geometries are also found. For example, the mirror images of types I and II are known respectively as types I' and II', and are energetically equivalent if residues of the opposite chirality occupy corresponding sequence positions. This means that, for example, a D-Pro residue would be favoured in position *i*+1 of a type I' turn or in position *i*+2 of a type II' turn. On the other hand, the intervening peptide bond (between residue *i*+1 and *i*+2) can adopt a cis conformation and still allow the turn to form an i to *i*+3 hydrogen bond and link to two β-strands. The resulting turn is called a type VI turn.

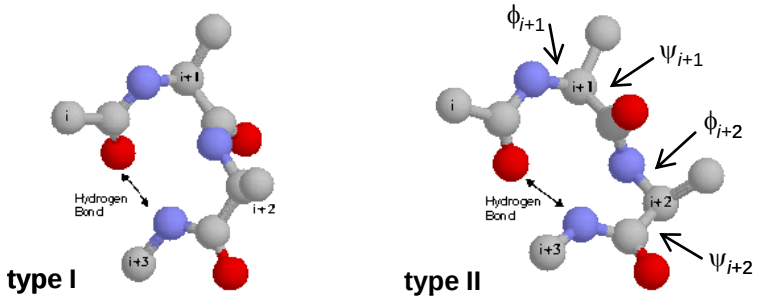

TURN TYPE	ϕ_{i+1}	ψ_{i+1}	ϕ_{i+2}	ψ_{i+2}
I	-60	-30	-90	0
I'	60	30	90	0
II	-60	120	80	0
II'	60	-120	-80	0
IV	-61	10	-53	17
VIa1	-60	120	-90	0
VIa2	-120	120	-60	0
VIb	-135	135	-75	160
VIII	-60	-30	-120	120

Figure 4 - Torsion angles of classic β-turns.

β-hairpins (Figure 5) are the simplest units that can be constructed from β-strands and β-turns. These occur widely in proteins and make up the fundamental building blocks of antiparallel β-sheet. They are also structures found in many naturally occurring bioactive cyclic peptides such as gramicidin S and the peptide hormones oxytocin and vasopressin.8

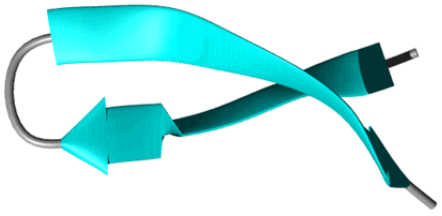

Figure 5 - β-hairpin.

β-hairpins are stabilized by virtue of turn propensities of amino acid residues as well cross-strand interactions between the sequences flanking the turn. Favourable energetic contributions to the stability of these structural features have been demonstrate to include cross-strand aromatic-aromatic, aromatic-polar, H-bonding and salt-bridge interactions in combination with loop conformational propensity and entropy terms dependent on loop length.[9]

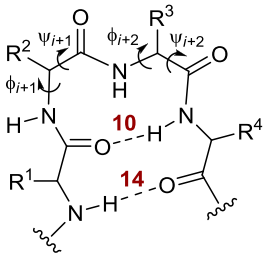

Figure 6 - Minimal β-hairpin.

A tetrapeptide can adopt a "minimal β-hairpin" conformation (Figure 6) with residues *i*+1 and *i*+2 involved in the β-turn. This structure is characterized by the presence of 10- and 14-membered H-bonded rings.

2 Structural determination

The knowledge of the three dimensional structure of a peptide is essential to understand its physical, chemical and biological properties. Hence, the assessment of the conformational stabilities of peptides and their three dimensional structure, which depends in general on the amino acids it comprises, can rely on a wide bouquet of techniques.

Xray diffraction allows structural investigations at atomic resolution. However, not all substances can be easily crystallized and, moreover, there might be a huge difference between the conformation in the solid state and the one seen in solution.

To gain information about the secondary structure of a peptide in solution, important tools such as circular dichroism spectroscopy, 1D and 2D NMR spectroscopy are employed.

NMR Spectroscopy has progressed to become the method for determination of protein structures in aqueous solution. Sophisticated NMR methods for protein analysis such as 2D-NMR spectroscopy with modern standard measurement options (COSY, TOCSY, HSQC $^{13}C/^{1}H$, HMBC $^{13}C/^{1}H$, NOESY, ROESY) and variable temperature ^{1}H-NMR contribute to the scope.

VT-NMR experiments detect amide protons chemical shift variations in function of temperature, thus temperature coefficients can be calculated ($\Delta\delta/\Delta T$). Evaluating $\Delta\delta/\Delta T$ values and chemical shifts (δ), much can be said about NH protons tendency to be involved in intramolecular H-bondings. Very low absolute values of $\Delta\delta/\Delta T$ are indicative of a proton involved in a very stable intramolecular H-bonding, not exposed to solvent. A proton involved in an intramolecular H-bonding is usually characterized by a relatively low δ. The formation of a single H-bonding has a rather deshielding effect. When more H-bonds are formed with the solvent, higher δ values are generally observed. Moreover, high $\Delta\delta/\Delta T$ coefficient absolute values are indicative of NH protons involved in an

equilibrium between intramolecular H-bonds and H-bonds with the solvent. More than one stable conformation can thus be expected.

COSY, TOCSY (revealing the proton crosspeaks in the same spin system) and NOESY (cross peaks due to dipolar coupling resulting from *through space* interactions) experiments allow the complete characterization of the synthesized compounds and assignment of all the proton chemical shifts, thus giving information on the primary structure. Medium- and long-range NOE contacts, detected from both NOESY and ROESY experiments, are significant in the determination of the preferential conformations adopted in solution.

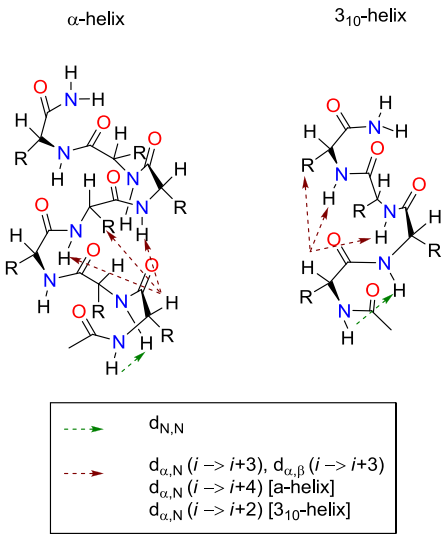

Figure 7 – short sequential and medium range ^{1}H-^{1}H distances

For example, some typical sequential and medium range NOEs may be observed in the case of regular repeating structures, such as helices (Figure 7).

Depending on the torsion angles that characterize the secondary structure of a peptide, sequential and medium-range ^{1}H-^{1}H-distances will have different values. For instance the *sequential* NH-NH and CH_α-NH contacts for a regular α-helix are about 2.8 Å and 3.5 Å respectively. The CH_β-NH contacts, since they depend also on the torsion angle on the side chain χ_i, vary between 2.5 and 4.1 Å for a α-helix.[10]

In the case of peptides, including proline or non proteinogenic amino acids there exists an increased possibility of *cis-trans* isomerization of the peptide bond. The influence of the *cis-trans* isomerization on the sequential ^{1}H-^{1}H-distances allows closer CH_α (*i*)-CH_α (*i*+1) and NH (*i*)-CH_α (*i*+1) contacts in the *cis* form whereas shorter CH_α (*i*)-CH_α (*i*+1) and NH (*i*)-CH_δ (*i*+1) contacts are observed for the *trans* form.[10]

Medium-range distances indicating helical-structures are $i \rightarrow i+2$, $i \rightarrow i+3$ and $i \rightarrow i+4$ contacts. In particular $i \rightarrow i+4$ contacts are especially useful since they are present in a regular α-helix and not in a

3_{10}-helix. Tight turns have close $i \rightarrow i+2$ values. In the case of β-structures short medium-range distances are not observed, since the polypeptide segments are almost fully extended.[10]

Circular dichroism (CD) is also widely used in the determination of the secondary structure of peptidomimetics. UV-CD is based on planar polarized light. Planar polarized light is the sum of the left and the right circularly polarized light. When planar polarized light hits an optically active substance, the left and the right circularly polarized components are absorbed in a different extent, so that polarized light results elliptical. Ellipticity can thus be measured.
The spectrum does not reflect the absorbance of each individual chromophore, but of a combination of the orientated chromophores in the three dimensional arrangement of the polymer. Hence, each type of peptide secondary structure gives rise to a unique and distinct CD spectrum.
CD spectra are recorded in the wavelength region below 300 nm, and a conformer present in the tiniest amount or a particular small segment of a macromolecule can make a very large contribution to the overall absorption of circularly polarized light. Clues on the presence of regular conformational patterns can be obtained observing the CD spectra of molecules of known secondary structure. For example, α-helix and β-sheet structures produce particular patterns in CD spectra.
Additionally there can be some contributions from aromatic residues (Phe, Tyr, Trp and His) and disulfide bonds. If there are a significant number of aromatic residues present in a molecule, the CD spectra can be affected in the region of far-UV. The contribution seen in near-UV is smaller. This region can be used to investigate changes of tertiary structures, for instance, those caused by ligand binding or folding/unfolding processes.[11]

The NMR data can be finally used as an indirect source of structural information, from which the overall 3D structure can be calculated. Hybrid **MC/MD simulations** are thus performed, starting from conformers that possess random torsion angle values and fitting them to the conformational restrains derived from the NMR measurements.
When investigating biologically active compounds, **docking studies** can also be performed. These computational techniques are used to explore the possible binding modes of a substrate to a given receptor, enzyme or other binding site, whose crystal structure or analogy model is known.

3 Aim of this work of thesis

In this thesis we describe our recent efforts on the design of two kinds of peptidomimetics containing a bifunctional diketopiperazine (DKP):

I. Cyclic peptidomimetics bearing a bifunctional DKP as a constrained scaffold and either the RGD or the *i*DGR sequence were synthesized and tested as selective ligands for the integrins $\alpha_v\beta_3$ and $\alpha_v\beta_5$;

II. A linear decapeptide was synthesized alternating a bifunctional DKP as a β,β-dipeptide mimic and two α-amino acids, in order to further evaluate DKP secondary-structure-inducing potentials.

References:

[1] M. Goodman, H. Shao, *Pure Appl. Chem.* **1996**, *68*, 1303-1308.

[2] J. Vagner, H. Qu, V. J. Hruby, *Curr Opin Chem Biol.* **2008**, *12*, 292-296.

[3] K. J. Jensen, De Novo Design of Proteins. In Peptide and Protein Design for Biopharmaceutical Peptide and Protein Design for Biopharmaceutical Applications, K. J. Jensen Ed., **2009**, John Wiley&Sons Ltd, Chapter 3, 207-215.

[4] G. D. Rose, L. M. Gierasch, J. A. Smith, *Adv. Protein Chem.* **1985**, *37*, 1-109.

[5] A. M. C. Marcelino, L. M. Gierasch, *Biopolymers* **2008**, *89*, 380-391.

[6] B. L. Sibanda, T. P. Blundell, J. M. Thornton, *J. Mol. Biol.* **1989**, *206*, 1425-1436.

[7] D. J. Hill, M. J. Mio, R. B. Prince, T. S. Hughes, J. S. Moore, *Chem. Rev.* **2001**, *101*, 3893-4012.

[8] E. G. Hutchinson, J. M. Thornton, *Protein Sci.* **1994**, *3*, 2207-2216.

[9] J. A. Patch, A. E. Barron, *Curr. Opin. Chem. Biol.* **2002**, *6*, 872-877.

[10] E. F. Plow, T. A. Haas, L. Zhang, J. Loftus, J. W. Smith, *J. Biol. Chem.* **2000**, *275*, 21785-21788.

[11] M. A. Horton, *Int. J. Biochem. Cell Biol.* **1997**, *29*, 721-725.

1 DIKETOPIPERAZINES

1 - Introduction

2,5-Diketopiperazines (DKPs), the smallest cyclic peptides (Figure 1.1), are an important class of biologically active compounds[1] and their research has been fundamental to many aspects of peptide chemistry. They were once believed to be only protein artifacts or degradation products, but they have regained interest from chemists and pharmacologists thanks to their numerous biological properties[2] that point to several therapeutic applications, ranging from antibiotics[3,4] to synthetic vaccines and anticancer agents.[5,6]

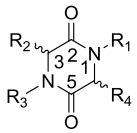

Figure 1.1 - General structure of 2,5-diketopiperazines.

2,5-Diketopiperazines have two *s-cis* secondary amide groups that can hydrogen bond horizontally within the ring plane. Due to the rigid cyclic structure bearing amide groups, DKPs are usually poorly soluble in organic solvents. In the solid state, most of the *N*-unsubstituted DKPs adopt a linear tape orientation (Figure 1.2a),[7] while the presence of one *N*-substituent leads to the formation of one-dimensional hydrogen bonded tapes through establishment of a non-reciprocal hydrogen-bond network (Figure 1.2b) or to hydrogen bonded dimers (Figure 1.2c).[8]

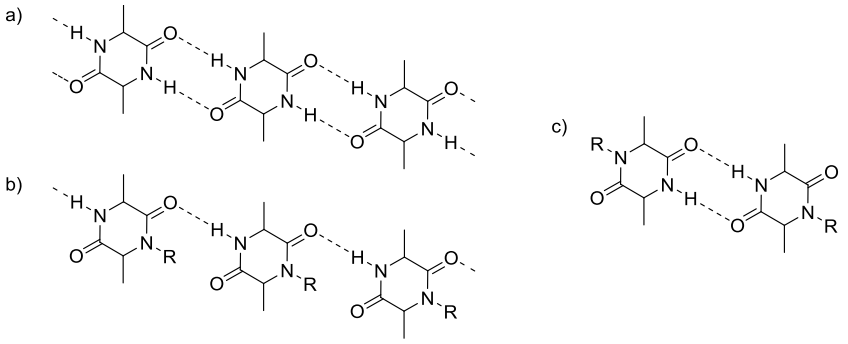

Figure 1.2 - Schematic view of hydrogen bond patterns in solid state structures of 2,5-diketopiperazines.

Due to the structural similarity of 2,5-diketopiperazines to peptides, medicinal chemists have been inspired to use DKPs to circumvent the limitations of peptides. Constraining the nitrogen atom of an α-amino amide into a DKP ring alters its physical properties, reduces the susceptibility to metabolic amide bond cleavage and induces conformational rigidity. These changes in structural and physical properties, as well as the presence of groups that can act as donors and acceptors of hydrogen bonds enhance favorable interactions with biological targets. Moreover, DKPs are simple heterocyclic scaffolds in which diversity can be introduced at up to four positions (N1, N4, C3, C6) and stereochemically controlled at two (C3, C6), while they can be prepared from readily available α-amino acids using conventional synthetic procedures,[9,10] solid-phase[11,12] and microwave-assisted organic synthesis.[13,14]

Considering all these properties, it is evident why these constrained bifunctional cyclopeptides have emerged as privileged structures for the discovery of new lead compounds and represent a useful toolset for those pursuing research in the areas of combinatorial biomedical chemistry,[15,16] de novo design of proteins[17] and functional molecular devices. Furthermore, DKP scaffolds are also interesting candidates as organocatalysts and have been used in the asymmetric hydrocyanation of aldehydes[18,19a] and imines,[19b] although in the latter case the results have been questioned.[19c]

Finally, in the last decade a relevant application of DKPs has gained importance: their use as templates capable of inducing a defined secondary structure in peptide sequences. In these cases, advantage can be taken from the synthesis of symmetrical and unsymmetrical DKPs bearing reactive functionalities (e.g., NH_2, COOH) in the lateral chains of the amino acids.

2 - Biological Activities

The peculiar DKP heterocycle, being found alone or as part of larger and more complex molecules in several natural products[20,21,22b] of various origin,[22,23] constitutes a rich source of new biologically

active compounds. The wide spectrum of their biological properties points to various therapeutic possibilities.[24]

The most important biological activities of diketopiperazines are probably the regulation of the P-glycoprotein (P-gp) activity, the inhibition of plasminogen activator inhibitor-1 (PAI-1)[25] and the alteration of cardiovascular and blood-clotting functions.[26] They also act as antitumour,[27,23c] antiviral,[28] antifungal,[29] antibacterial,[30] and antihyperglycaemic agents[31] and affinities for calcium channels and opioid,[32] GABAergic,[33] serotoninergic 5-HT_{1A}[34] and oxytocin receptors.[35,36]

Several examples of DKP-containing natural metabolites showing cytotoxicity (**1**-**4**, Figure 1.3),[22b,r,s,23c] inhibiting tumor growth (**5**, Figure 1.3),[22k,l,t] cell cycle (**6**-**9**, Figure 1.3)[22c,h,u] and cancer cell invasion (**10**, Figure 1.3),[23c] are reported in the literature.

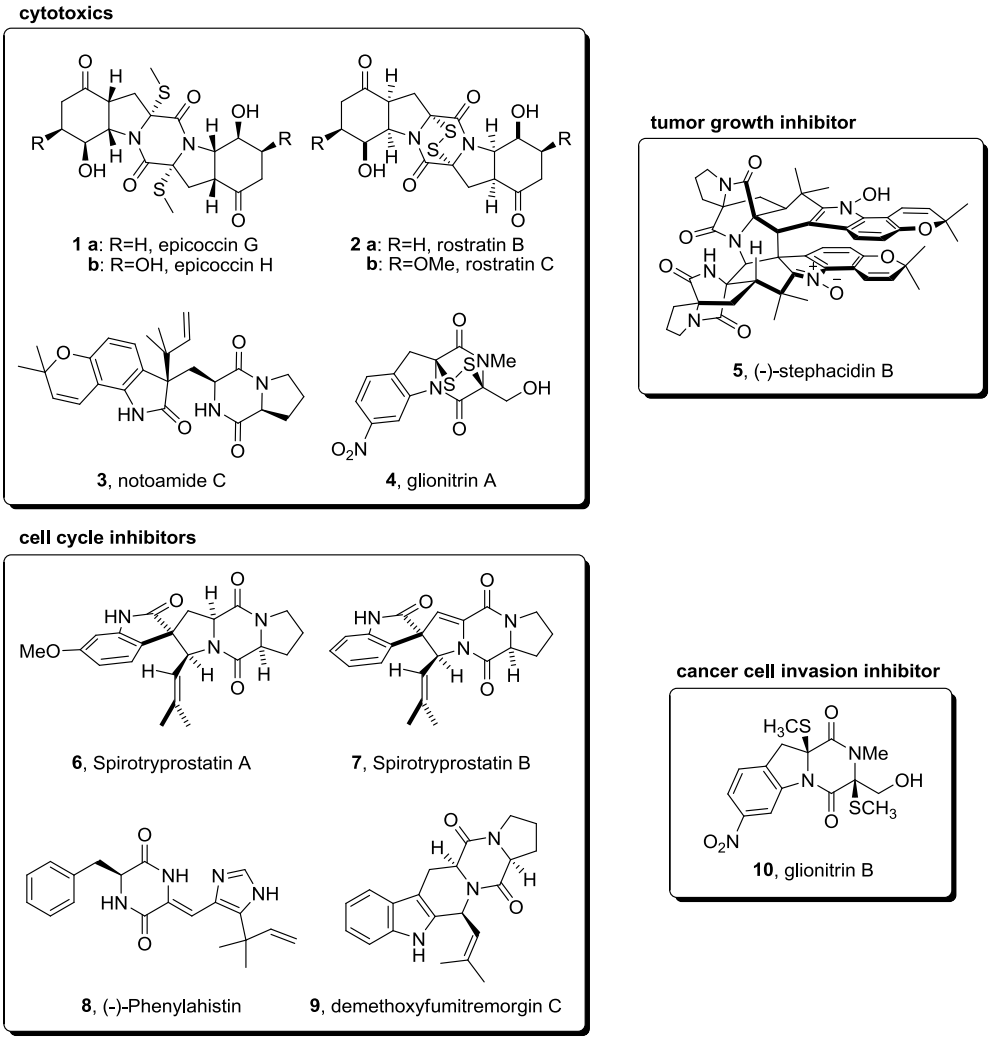

Figure 1.3 - examples of naturally occurring DKPs, showing cytotoxicity and other cancer related inhibitory activities.

Synthetic cytotoxic DKPs were also designed (Figure 1.4).[37,38]

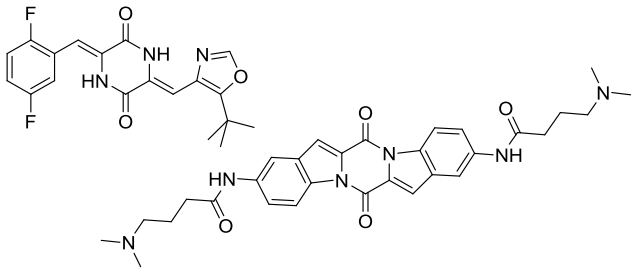

Figure 1.4 – Synthetic cytotoxic DKPs [37,38]

Some metabolites have shown an interesting activity as HIV-1 replication inhibitors (**1-2**, Figure 1.3; **11**, Figure 1.5),[22a,b] some other compounds have proven antibiotic and antibacterial properties(**12-17**, Figure 1.6),[21,22j,m,v,w,23f] in particular against *Mycobacterium tuberculosis* (**18**, Figure 1.6),[23d] resposible for tubercolosis.

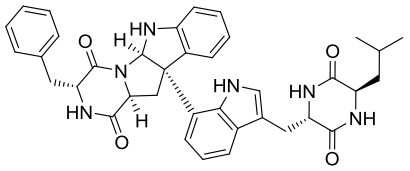

11, Pestalazine A

Figure 1.5 – DKP presenting HIV-1 replication inhibitory activity

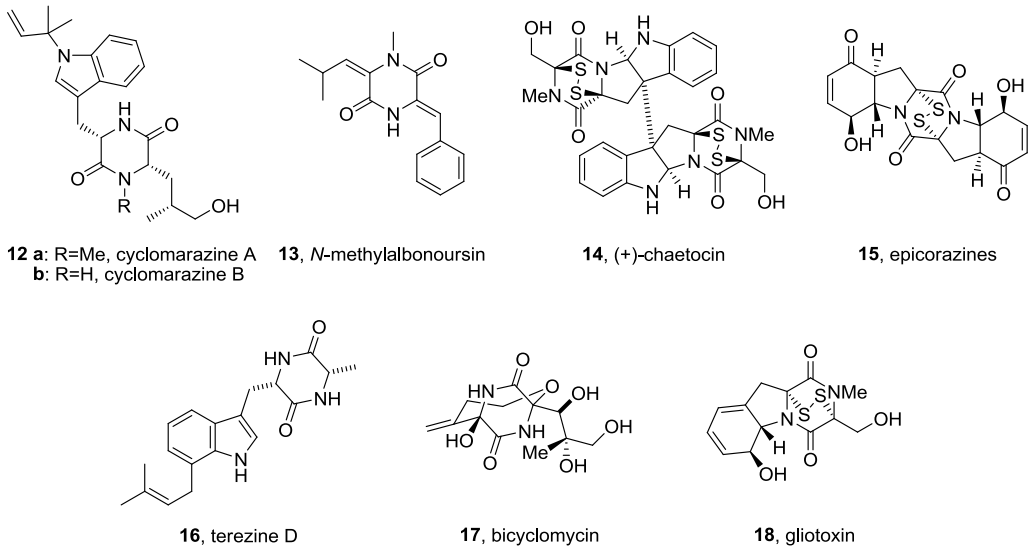

12 a: R=Me, cyclomarazine A
b: R=H, cyclomarazine B

13, *N*-methylalbonoursin

14, (+)-chaetocin

15, epicorazines

16, terezine D

17, bicyclomycin

18, gliotoxin

Figure 1.6 – examples of naturally occurring DKPs, showing antibiotic and antibacterial activities.

Gypsetin (**21**, Figure 1.7) was found to be a competitive ACAT (acyl coenzyme A:cholesterol acyltransferase) inhibitor with respect to oleoyl-CoA.[22d] ACAT enzyme has been identified as the rate-limiting enzyme in the absorption of cholesterol. Thus, the inhibition of ACAT has received much attention due to its potential in moderating the effect of elevated cholesterol level. One of the

applications might have been the prevention or the slowdown in the progession of atherosclerosis, even though this kind of inhibitors were recentely proven not to be effective for this purpose.[39]

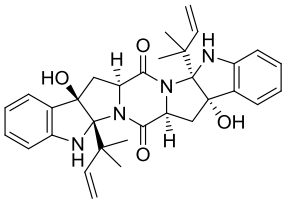

19, gypsetin

Figure 1.7 – ACAT inhibitor gypsetin

P-glycoproteins are part of a larger superfamily of efflux transporters found in the gut, gonads, kidneys, biliary system, brain and other organs named the ATP-binding cassette family (ABCs). P-gps appear to have developed as a mechanism to protect the body from harmful substances. Using ATP as an energy source, they transport certain hydrophobic substances in the following directions:

- into the gut;
- out of the brain;
- into urine;
- into bile;
- out of the gonads;
- out of other organs.

They contribute greatly to the distribution and elimination of many clinically important therapeutic substances. Prescription and OTC drugs, foods and substances made by the body may be inhibitors and/or inducers of these transporters.

P-gps (ABCB1) have been implicated as a primary cause of multidrug-resistance in tumors. The responsible gene has been found to be MDR1. Many oncological drugs are ABCB1(P-gp) substrates and are excluded from the brain at the blood-brain barrier (BBB). In cases of primary or secondary brain tumors, finding an ABCB1(P-gp) inhibitor could be found that would block the extrusion of the oncological drug from the BBB without causing toxicity, would possibly improve the efficacy of such drugs might be improved. Several generations of ABCB (P-gp) inhibitors have been evaluated with modest success. A recent study of paclitaxel with elacridar [a third generation ABCB1(P-gp) inhibitor] has proved promising. Moreover, the membrane efflux pump P-gp is overexpressed in many multidrug resistant cancer cell lines and is an important mechanism whereby cancer cell lines acquire resistance to clinically important anticancer agents. Inhibitors of P-gp represent a potential strategy to overcome this resistance.

A similar targeted strategy for improving drug efficacy could be useful for a wide range of brain disorders, from HIV and other infections to mood disorders.[40]

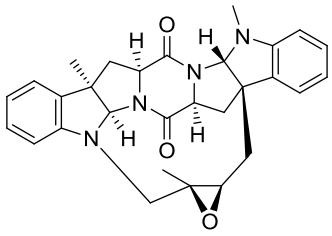

20, nocardioazine A

Figure 1.8 - noncytotoxic P-gp inhibitor nocardioazine A

Metabolite nocardioazine A (Figure 1.8), isolated form a culture of bacterium *Nocardiopsis sp.*, proved to be representative of a new class of noncytotoxic P-gp inhibitors, capable of reversing doxorubicin resistance in a P-gp overexpressing drug resistant colon cancer cell line.[23b]

Plasminogen activator inhibitor - type 1 (PAI-1), the main physiological inhibitor of the serine proteases and primary inhibitor of the tissue-type (tPA) and urokinase-type (uPA) plasminogen activators, has been implicated in a wide range of pathological processes, thus becoming an attractive target for pharmacologic inhibition. The plasminogen-converting enzymes generate active plasmin, which proteolytically degrades fibrin and components of the extracellular matrix. While tPA is an essential element in the fibrinolytic system, regulating the formation and degradation of clots, uPA is linked to extracellular proteolytic homeostasis and consequently related to detachment and cell migration events typical of metastasis, invasion and angiogenesis processes.[25]

When PAI-1 is quantitatively or qualitatively disrupted, a variety of modulated functions are implicated in several pathological situations such as thromboembolic disease due to highly active PAI-1,[25a] coronary heart disease, atherosclerosis, thrombosis[25b] and cancer progression[25c] associated with increased levels of circulating PAI-1. The correlation between PAI-1 and cancer has been demonstrated in mice: it has been shown that the administration of exogenous PAI-1 leads to an increasing number of metastases in animals previously injected with malignant cells, while the introduction of monoclonal antibodies to this macromolecular inhibitor reduced the metastatic potential.

The inhibitory capacity of PAI-1 depends on the conformation of the reactive centre loop (RCL) and on its availability to bind tPA or uPA, so its potential to be explored as a therapeutic macromolecular target for the treatment of cardiovascular diseases and cancer emphasises the importance of developing drugs as specific inhibitors.[25d] Diketopiperazines are the most potent PAI-1 inhibitors known,[25b] they

act through a mechanism involving conformational changes, which inactivate PAI-1 RCLcomplementarity, preventing its binding to the target protein.[25d]

Metabolite **21** isolated from *Streptomyces sp.*, as the first low-molecular-weight PAI-1 inhibitor, was the model for designing structural changes in order to obtain more active products (Figure 1.9). Using bioisosteric substitutions and combinatorial chemistry approaches, DKP **22** and **23** containing different side chains connected by exocyclic double bonds were synthesized and showed both *in vivo* and *in vitro* PAI-1 inhibitory activity (IC_{50} 3.5 μM and 0.2 μM, respectively).[25a] Other strategies, such as introduction of structural rigidity, were also applied to metabolite **21**, leading to compounds like **24** that also shows an interesting PAI-1 inhibitory activity (IC_{50} 0.3 μM).[25c]

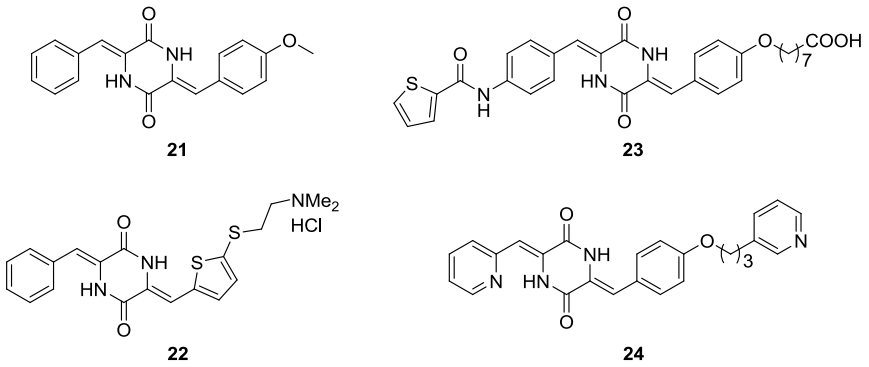

Figure 1.9 - Diketopiperazines as PAI-1 inhibitors.

Tumour cell pro-coagulant activity has been considered to favour metastatic processes by encasing malignant cells in a fibrin coat, which protects them from the host immunological system. Thus, components of the blood-clotting system are potential targets for a new class of therapeutic agents designed to selectively inhibit tumour growth and prevent metastasis. Haematological studies showed that cyclo(L-His-L-Tyr) DKP **25** significantly increases clotting time and prevents platelet adhesion and aggregation induced by adenosine diphosphate.[2] Cyclo(L-His-L-Phe) DKP **26** showed antitumour activity by significantly reducing the viability of HeLa, WHCO3 and MCF-7 cells, respectively from, cervical, oesophageal and mammary carcinoma.[2]

In relation to cardiac effects, compound **25** increased the heart rate in isolated rodent hearts, while compound **26** decreased cardiac output and the level of coronary blood flow (Figure 1.10). Much like several cyclic dipeptides that display potential activity for the treatment of cardiovascular dysfunctions, compounds **25** and **26** could be employed as antiarrhythmic agents, thus reducing mortality by ventricular fibrillation in myocardial infarction.[2]

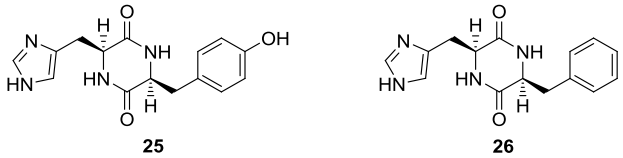

25 **26**

Figure 1.10 - DKPs which interfere in cardiovascular and blood-coagulation functions.

Figure 1.11 shows a representative set of DKP-based molecules exhibiting other biological activities.[28,31,32,33,34,35,36]

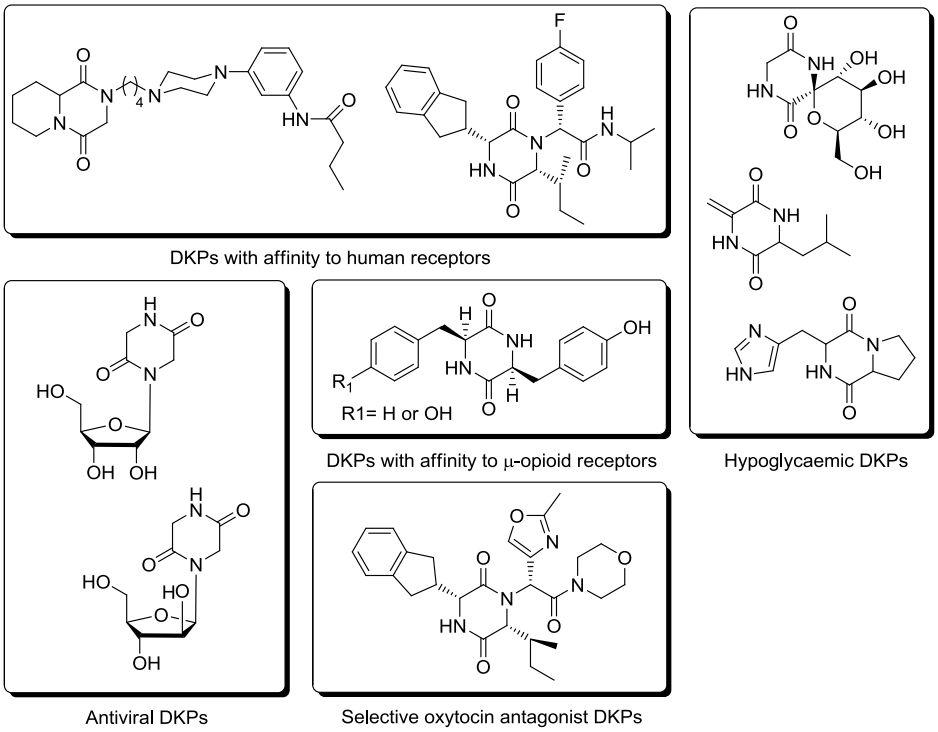

Figure 1.11

3 - Synthesis of diketopiperazines

3.1 - Mechanism of formation

The planar backbone amide bonds in polypeptides are known to occur predominantly in the *trans* conformation. Planarity is maintained through a rotational energy barrier because of the partial double bond character of the peptide bond. On average, the energy difference between *trans* and *cis* peptide bond isomers is of the order of 2.5 kcal/mol (Scheme 1.1).

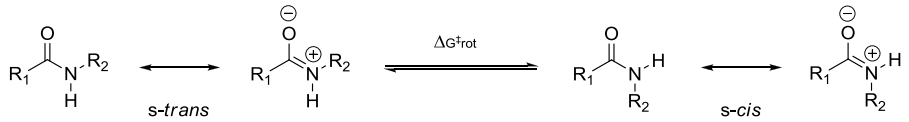

Scheme 1.1

Such isomerism is relevant to DKP formation because in a dipeptide derivative the intramolecular attack of the amino group on the terminal carboxylic group is possible only from a folded conformation containing a *cis* peptide bond (Scheme 1.2).

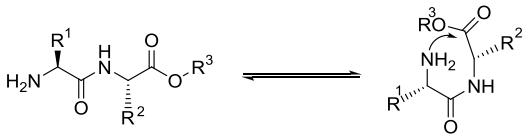

Scheme 1.2

Cis peptide bonds are not frequent in naturally occurring polypeptides, and this is thought to be due mostly to steric conflict between neighbouring C^{α}-substituents in the *cis* conformation. However, the actual frequencies of occurrence of *cis* peptide bonds in known protein structures do not correlate well with residue side-chain bulk. In a similar way, steric interactions between the side chains in the trans and cis isomers can not explain sufficiently the relative ease of DKP formation from a number of dipeptide derivatives. Particularly noteworthy in this respect are dipeptides involving α-alkyl amino acid residues. For such compounds one would predict large energy differences between *trans* and *cis* isomers on the basis of steric crowding in the *cis* isomer. Instead such peptides have been observed to cyclize quite readily. It is likely that the conformational constrains (on backbone torsional angles) introduced into a peptide by for example Aib residues result in amide bond isomerisation/cyclization mechanisms with low energy barriers that are favoured. Possibly such factors as overall proximity between terminal amino and carbonyl groups, as well as stabilizing intramolecular interactions may be involved.[12]

3.2 - Conventional synthetic procedures

The 2,5-DKPs, head-to-tail dipeptide dimers, are a common naturally occurring structural motif and consequently most biologically active DKPs are isolated from natural sources. They are also frequently generated as unwanted by-products or degradation products in the synthesis of oligopeptides. However, due to the relative structural simplicity of its basic nucleus, several synthetic methods are also available mainly based on reactions of dipeptides, easily prepared from α-amino acids by conventional methodology.

It is possible to prepare symmetrical DKPs simply by heating the free amino acid methyl esters in a sealed tube and this method can even be effective for DKPs derived from amino acids with reactive

side chains. However, it is generally better to use protected precursors since for example, Dab, Orn, and Lys derivatives can give rise do the corresponding pyrrolidone, piperidone and homopiperidone by-products. In the case of unsymmetrical DKPs, the oldest synthetic procedure consists in the dipeptide ester treatment with methanolic ammonia, but the strongly basic conditions in this procedure can lead to epimerization.

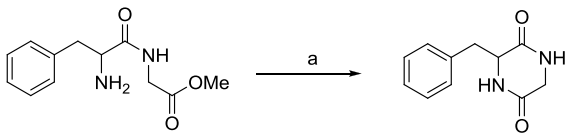

Scheme 1.3 - Solution-phase synthesis: a) MeOH, reflux, 14 h.

A method less prone to loss of chiral integrity consists of Boc-dipeptidyl methyl ester *N*-deprotection with formic acid, followed by reflux of the dipeptidyl ester formate salt in 2-butanol/toluene and removal of formic acid through azeotropic distillation.[41] However, for many DKPs, simple reflux of dipeptidyl methyl esters in low-boiling solvents, particularly methanol, is normally effective (Scheme 1.3).[42]

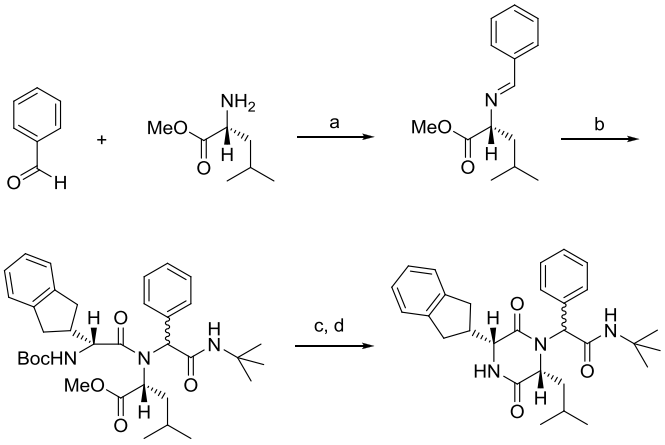

Scheme 1.4 - Ugi reaction: a) 1 equiv Et_3N, MeOH; b) *t*-Bu-isonitrile, *N*-Boc-*R*-indanylglycine; c) 4 N HCl/dioxane, 4 h; d) Et_3N.

Another method to obtain diketopiperazines is the Ugi reaction, a synthesis containing a small number of multicomponent steps, which allows substitutions on the secondary amino group.[15] The stereospecific synthesis illustrated in Scheme 1.4 was proposed as an alternative in the preparation of trisubstituted DKPs. However, it was not possible to control the stereochemistry of the chiral centre located in the α carbon of the tertiary amine.[43]

The problem of stereocontrol might be solved by using a symmetric keton as the starting carbonyl compound. As a relevant example in the discovery and synthesis of pharmacologically active

compounds involving this kind of Ugi-type reaction approach, aplaviroc is here mentioned (Scheme 1.5).[36] Aplaviroc is a CCR5 receptor antagonist and an investigational drug for HIV treatment.[44]

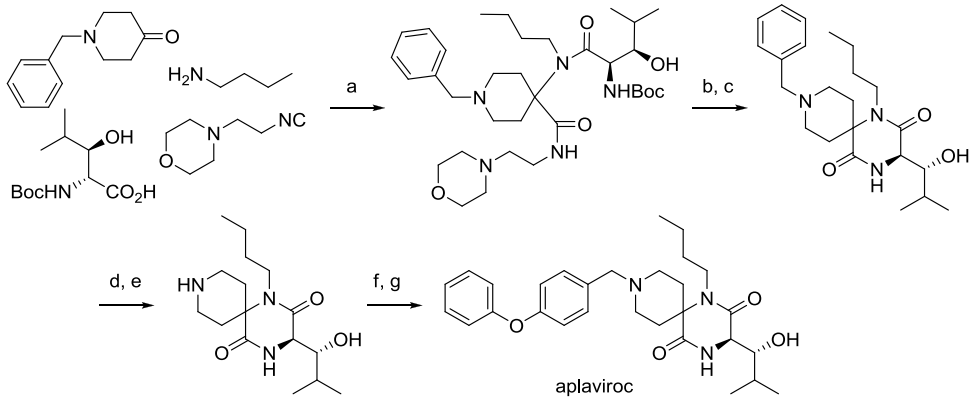

Scheme 1.5 – Synthesis of aplaviroc through a Ugi-type 5C-4CR, in solution: a) MeOH, 55°C; b) $HCl_{conc.}$ 55%; c) AcOH – toluene; d) H_2, $Pd(OH)_2/C$, 55°C; e) 4N HCl in EtOAc; f) RCHO, $NaBH(OAc)_3$, AcOH, DMF; g) 4N HCl in EtOAc.

As an alternative, the glycine cyclic dipeptide has been used as the starting material for the solution-phase synthesis of substituted diketopiperazines. The protocol outlined in Scheme 1.6 was used in the synthesis of several active compounds.[11] A similar strategy was employed to generate olefin derivatives of *N*-acetylated diketopiperazines with exocyclic double bonds,[42] or bis-epoxides, which would serve as precursors to more complex DKPs (Scheme 1.7).[45]

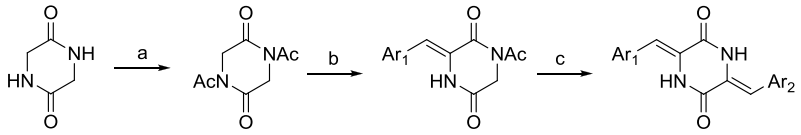

Scheme 1.6 - Synthesis of substituted diketopiperazines starting from cyclo(Gly-Gly): a) Ac_2O, reflux; b) *t*-BuOH, *t*-BuOK, Ar^1CHO, THF, rt; c) Ar^2CHO, Cs_2CO_3, DMF, 80-100ºC.

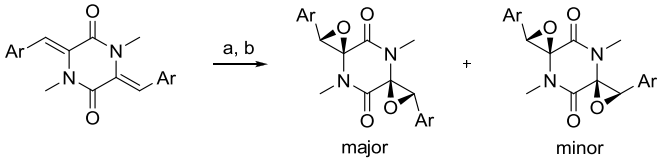

Scheme 1.7 - Synthesis of bis-epoxy diketopiperazines: a) NBS, H_2O; b) Et_3N.

An innovating strategy employing microwave heating was used to couple peptides intramolecularly, resulting in symmetrical dimeric DKP, without epimerisation in the α-position of the amino acids. N^{α}-benzoyl-Arg(NO_2)-Leu-NH_2, a PAR-2 receptor antagonist, was prepared by classical solution-phase synthesis. To the C-terminal end of this dipeptide pharmacophore, a glycine residue was introduced and activated for auto-condensation, resulting in the DKP cyclo(Gly-Gly) *N*-substituted by the

selected dipeptide. The cyclization reaction is exemplified in Scheme 1.8 and, compared to conventional heating, the microwave synthesis furnish the desired compounds in higher yields and shorter reaction times.[46]

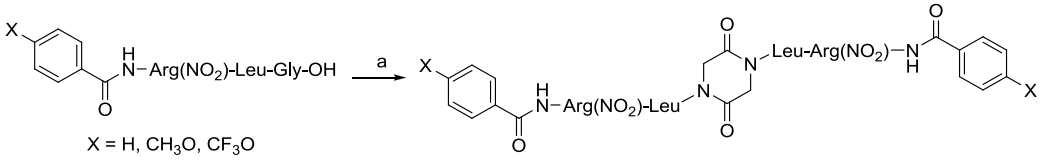

Scheme 1.8 - Dipeptide dimers obtained by microwave heating: a) HBTU/DMAP, DMF, 5 min, 40 ºC, 400 W.

Recently it was also reported a microwave-assisted stereoselective one-pot synthesis of symmetrical and unsymmetrical 2,5-DKPs from unprotected amino acids, through a phosphite-promoted one step coupling reaction (Scheme 1.9). This method is characterized by overall good yields, scalability, and tolerance to several base-stable protecting groups. Simple filtration through a pad of silica provides the pure compounds.[47]

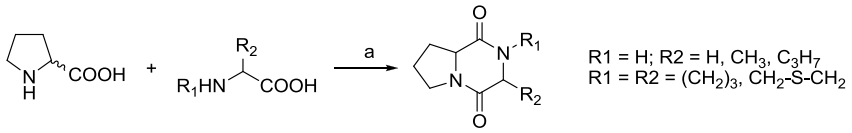

Scheme 1.9 - P^{III}-promoted coupling of amino acids: a) $MeOPCl_2$, NEt_3, toluene, MW: 84-97%.

Even more recently, an aqueous in situ one-pot *N*-Boc-deprotection-cyclization of *N*-Boc-dipeptidyl-*tert*-butyl and methyl esters was reported to provide optically pure *cis*-DKPs in excellent yields under microwave irradiation (Scheme 1.10).[48]

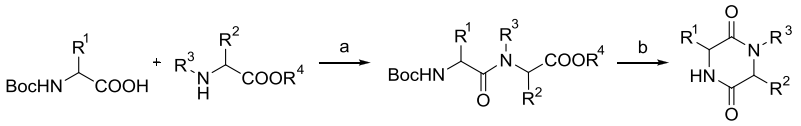

Scheme 1.10 - *N*-Boc-deprotection-cyclization of *N*-Boc-dipeptidylesters to DKPs: a) EDAC, HOBt, DMAP, TEA/CH_2Cl_2, 5°C, then overnight at rt; b) H_2O (1 mL), MW (250 °C, 250 W and 150 psi) for 10 min.

Phase-transfer catalysis seems to be another reliable method for the one-pot synthesis of symmetric 1,4-disubstituted-DKPs starting from a suitable amine and chloroacetyl chloride in presence of an aqueous base.[49]

O,N-acyl transfer is receiving greater attention in recent years, as a valuable method for the efficient synthesis of difficult peptide sequences and racemization-free segment condensation. This approach was also employed for the synthesis of hexa- and pentasubstituted diketopiperazines under mild conditions.[50] An activated ester of the first hindered aminoacid is reacting with the free carboxylic acid

of a second fragment forming a mixed anhydride, which is undergoing spontaneous rearrangement and procedes to the DKP product (Scheme 1.11). This strategy could also be used to achieve oligomers.

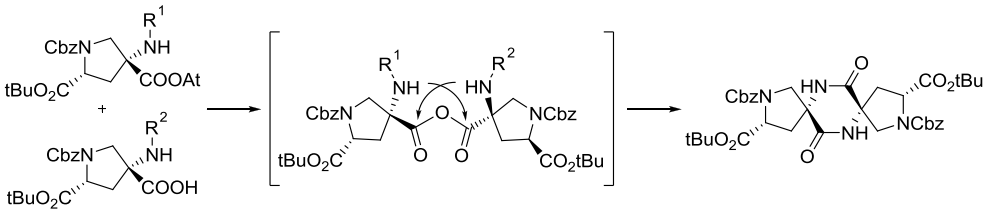

Scheme 1.11 – Synthesis of hexasubstituted DKPs *via O,N*-acyltransfer

DKP can form even when it is not desired. In fact, parallel DKP formation in reactions involving amino acids is a quite common side reaction. For example, attempts to perform nucleophilic substitutions in substituted pyrimidinic rings, by ethyl glycine chloride in the presence of a strong base, DABCO (1,4-diaza-bicyclo[2.2.2]octane), resulted in the glycine DKP produced by predominant auto-condensation of ethyl glycine.[51]

Although solution-phase synthesis presents the advantage of requiring a smaller number of reaction steps, solid-phase synthesis has been the most used method to synthesize DKPs, with variations in the type of resin, protecting groups and type of cleavage among others. In multistep protocols, a dipeptide having the first peptide bond generated *in situ* is attached to the solid support, and it remains bound through the carboxylic extremity up to the cycling step, that is then followed by separation from the matrix or release of the *N*-protective group of the amino acid (cyclative cleavage).[11,52,53]

A generic solid-phase protocol is shown in Scheme 1.12 for obtaining DKPs under mild conditions, using the phenacyl ester (*O*-Pac) bond to attach the carboxylic amino acid terminal to the resin. Deprotection of the Boc-amino group and coupling with the next amino acid afforded a dipeptide, subsequently deprotected and cyclized by intramolecular aminolysis.[52] Solid-phase synthesis of unsaturated 3-substituted DKP, employing a carbamate bond between the dipeptide N-terminal and the resin, was also described.[11]

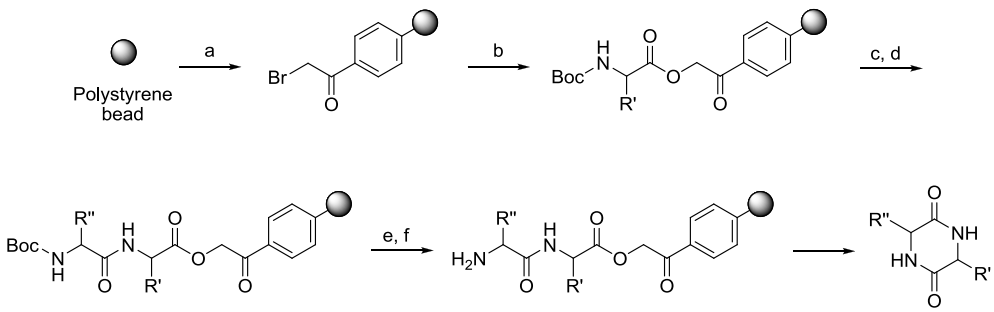

Scheme 1.12 - Solid-phase synthesis: a) $BrCH_2COBr$, $AlCl_3$, nitrobenzene/DCM (1:1); b) Boc-AA'-OH, Et_3N, DMF; c) 3.5 N HCl/AcOH; d) Boc-AA''-OH, HOBt, DCC, NMM, DMF; e) 10% DIPEA/EtOAc; f) 5% Et_3N/THF-H_2O (8:1).

Notwithstanding the successful use of activated ligands such *O*-Pac, the bond susceptible to nucleophilic attack requires amino acid side-chain group protection. This relative lability is generally considered responsible for small losses of the elongating peptides. Peptide attachment to the resin by the safety-catch technique circumvents this problem, because the stable bond is conveniently activated only after ending the peptide synthesis, allowing cleavage and cyclization. The strategy outlined in Scheme 1.13 permits the removal of protecting groups before cleavage, facilitating further workup.[15] The use of safety-catch ligands allowed the solid-phase generation of bicyclic and tricyclic DKP, which show even greater structural diversity.

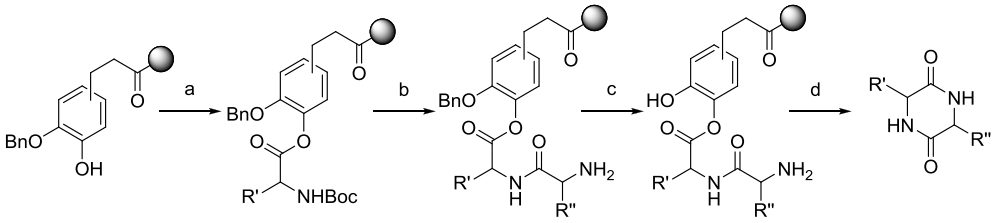

Scheme 1.13 - Solid-phase synthesis by safety-catch approach: a) Boc-AA'-OH, DIC, DIPEA; b) Boc-based solid-phase peptide synthesis; c) TFMSA, TFA; d) DIPEA.

References:

[1] D. T. Witiak, Y. Wei in *Progress in Drug Discovery* (Ed: E. Jucker), Birkhäuser Verlag, Basel, **1990**, vol. 35, pp. 249-363.

[2] K. McCleland, P. J. Milne, F. R. Lucieto, C. Frost, S. C. Brauns, M. Van De Venter, J. Du Plessis, K. Dyason, *J. Pharm. Pharmacol.* **2004**, *56*, 1143–1153.

[3] Y. Funabashi, T. Horiguchi, S. Iinuma, S. Tanida, S. Harada, *J. Antibiot.* **1994**, *47*, 1202–1218.

[4] F. Fdhila, V. Vazquez, J. L. Sanchez, R. Riguera, *J. Nat. Prod.* **2003**, *66*, 1299–1301.

[5] W. A. Loughlin, R. L. Marshall, A. Carreiro, K. E. Elson, *Bioorg. & Med. Chem. Lett.* **2000**, *10*, 91–94.

[6] B. Nicholson, G. K. Lloyd, B. R. Miller, M. A. Palladino, Y. Kiso, Y. Hayashi, S. T. C. Neuteboom, *Anti-Cancer Drugs* **2006**, *17*, 25–31.

[7] Y. Du, C. J. Creighton, B. A. Tounge, A. B. Reitz, *Org. Lett.* **2004**, *6*, 309-312.

[8] R. A. Weatherhead-Kloster, H. D. Selby, W. B. Miller III, E. A. Mash, *J. Org. Chem.* **2005**, *70*, 8693-8702.

[9] I. L. Rodionov, L. N. Rodionova, L. K. Baidakova, A. M. Romashko, T. A. Balashova, V. T. Ivanov, *Tetrahedron* **2002**, *58*, 8515–8523.

[10] For a review on synthetic approaches to all three DKP isomers (2,3-, 2,5- and 2,6-), see: C. J. Dinsmore, D. C. Beshore, *Tetrahedron* **2002**, *58*, 3297-3312, and references therein.

[11] W.-R. Li, J. H. Yang, *J. Comb. Chem.* **2002**, *4*, 106-108.

[12] For a recent review, see: P. M. Fischer, *J. Pept. Sci.* **2003**, *9*, 9-35, and references therein.

[13] A. Lopez-Cobenas, P. Cledera, J. D. Sanchez, P. Lopez-Alvarado, M. T. Ramos, C. Avendano, J. C. Menendez, *Synthesis* **2005**, *19*, 3412-3422.

[14] For a recent review, see: J. C. O'Neill, H. E. Blackwell, *Comb. Chem. High Throughput Screening* **2007**, *10*, 857-876, and references therein.

[15] D. A. Horton, G. T. Bourne, M. L. Smythe, *Mol. Divers.* **2000**, *5*, 289-304.

[16] A. F. Spatola, P. Romanovskis in *Combinatorial Peptide and Nonpeptide Libraries* (Ed: G. Jung), VCH, Weinheim, **1996**, pp. 327-347.

[17] G. Tuchscherer, M. Mutter, *J. Biotechnol.* **1995**, *41*, 197-210.

[18] J. I. Oku, S. Inoue, *J. Chem. Soc.-Chem. Commun.* **1981**, 229-230.

[19] a) E. F. Kogut, J. C. Thoen, M. A. Lipton, *J. Org. Chem.* **1998**, *63*, 4604-4610; b) M. S. Iyer, K. M. Gigstad, N. D. Namedev, M. Lipton, *J. Am. Chem. Soc.* **1996**, *118*, 4910-4911; c) C. Becker, C. Hoben, D. Schollmeyer, G. Scherr, H. Kunz, *Eur. J. Org. Chem.* **2005**, 1497–1499.

[20] M. B. Martins, I. Carvalho, *Tetrahedron* **2007**, *63*, 9923-9932.

[21] R. Huang, X. Zhou, T. Xu, X. Yang, Y. Liu, *Chem. Biodiv.* **2010**, *7*, 2809-2829.

[22] DKP natural compounds of *fungi* origin: a) G. Ding, L. Jiang, L. Guo, X. Chen, H. Zhang, Y. Che, *J. Nat. Prod.* **2008**, *71*, 1861-1865; b) H. Guo, B. Sun, H. Gao, X. Chen, S. Liu, X. Yao, X. Liu, Y. Che, *J. Nat. Prod.* **2009**, *72*, 2115-2119; c) C. Cui, H. Kakeya, H. Osada, *Tetrahedron* **1996**, *52*, 12651-12666; d) J. M. Schkeryantz, J. C. G. Woo, S. J. Danishefsky, *J. Am. Chem. Soc.* **1995**, *117*, 7025-7026; e) J. M. Roe, R. a B. Webster, A. Ganesan, *Organic letters* **2003**, *5*, 2825-2827; f) A. A. L. Gunatilaka, *J. Nat. Prod.* **2006**, *69*, 509-26; g) Y. Shiono, K. Akiyama, H. Hayashi, *Biosci. Biotechnol. Biochem.* **2000**, *64*, 1519-1521; h) K. Kanoh, S. Kohno, T. Asari, T. Harada, J. Katada, M. Muramatsu, H. Kawashima, H. Sekiya, I. Uno, *Bioorg. Med. Chem. Lett.* **1997**, *7*, 2847-2852; i) P. R. Hewitt, E. Cleator, S. V. Ley, *Org. Biomol. Chem.* **2004**, *2*, 2415-7; j) K. A. Gurney, P. G. Mantle, *J. Nat. Prod.* **1993**, *56*, 1194-1198; k) J. E. Wulff, S. B. Herzon, R. Siegrist, A. G. Myers, *J. Am. Chem. Soc.* **2007**, *129*, 4898-9; l) S. U. Lee, Y. Asami, D. Lee, J.-hyuk Jang, J. S. Ahn, H. Oh, *J. Nat. Prod.* **2011**, 1284-1287; m) E. Iwasa, Y. Hamashima, S. Fujishiro, E. Higuchi, A. Ito, M. Yoshida, M. Sodeoka, *J. Am. Chem. Soc.* **2010**, *132*, 4078-4079; n) D. O. Guimarães,

W. S. Borges, N. J. Vieira, L. F. de Oliveira, C. H. T. P. da Silva, N. P. Lopes, L. G. Dias, R. Durán-Patrón, I. G. Collado, M. T. Pupo, *Phytochemistry* **2010**, *71*, 1423-1429; o) P. S. Baran, C. a Guerrero, E. J. Corey, *J. Am. Chem. Soc.* **2003**, *125*, 5628-9; p) C. Pérez-Balado, A. R. de Lera, *Org. Biomol. Chem.* **2010**, *8*, 5179-5186; q) T. Iizuka, S. Takiguchi, Y.-suke Kumakura, N. Tsukioka, K. Higuchi, T. Kawasaki, *Tetrahedron Letters* **2010**, *51*, 6003-6005; r) R. X. Tan, P. R. Jensen, P. G. Williams, W. Fenical, *J. Nat. Prod.* **2004**, *67*, 1374-1382; s) H. Kato, T. Yoshida, T. Tokue, Y. Nojiri, H. Hirota, T. Ohta, R. M. Williams, S. Tsukamoto, *Angew. Chem. Int. Ed.* **2007**, *46*, 2254-2256; t) J. Qian-Cutrone, S. Huang, Y.-Z. Shu, D. Vyas, C. Fairchild, A. Menendez, K. Krampitz, R. Dalterio, S. E. Klohr, Q. Gao, *J. Am. Chem. Soc.* **2002**, *124*, 14556-14557; u) H. Wang, A. Ganesan, *Org. Lett.* **1999**, *1*, 1647-1649; v) M. A. A. Al-Fatimi, W.-D. Jülich, R. Jansen, U. Lindequist, *Evid. Based complement. Alternat. Med.* **2006**, *3*, 87-92; w) Y. Wang, J. B. Gloer, J. a Scott, D. Malloch, *J. Nat. Prod.* **1995**, *58*, 93-99; x) G. Strobel, B. Daisy, U. Castillo, J. Harper, *J. Nat. Prod.* **2004**, *67*, 257-268.

[23] DKP natural compounds of *bacteria* origin: a) R. M.-B. Ameur, L. Mellouli, F. Chabchoub, S. Fotso, S. Bejar, *Chem. Nat. Compd.* **2004**, *40*, 510-513; b) R. Raju, A. M. Piggott, X.-C. Huang, R. J. Capon, *Org. Lett.* **2011**, *13*, 2770-2773; c) H. B. Park, Y.-J. Kim, J.-S. Park, H. O. Yang, K. R. Lee, H. C. Kwon, *J. Nat. Prod.* **2011**, ASAP, DOI: 10.1021/np200563x; d) T. C. McMahon, S. Stanley, E. Kazyanskaya, D. Hung, J. L. Wood, *Tetrahedron Letters* **2011**, *52*, 2262-2264; e) D. L. Boger, J. Zhou, *J. Am. Chem. Soc.* **1993**, *115*, 11426–11433; f) A. Magyar, X. Zhang, F. Abdi, H. Kohn, W. R. Widger, *J. Biol. Chem.* **1999**, *274*, 7316-7324.

[24] D. D. Long, R. J. Tennant-Eyles, J. C. Estevez, M. R. Wormald, R. a Dwek, M. D. Smith, G. W. J. Fleet, *J. Chem. Soc., Perkin Trans. 1* **2001**, 807-813.

[25] a) Folkes, A.; Roe, M. B.; Sohal, S.; Golec, J.; Faint, R.; Brooks, T.; Charlton, P., *Bioorg. Med. Chem. Lett.* **2001**, *11*, 2589; b) Wang, S.; Golec, J.; Miller, W.; Milutinovic, S.; Folkes, A.; Williams, S.; Brooks, T.; Hardman, K.; Charlton, P.; Wren, S.; Spencer, *J. Bioorg. Med. Chem. Lett.* **2002**, *12*, 2367; c) Brooks, T. D.; Wang, S.W.; Brünner, N.; Charlton, P. A., *Anti-Cancer Drugs* **2004**, *15*, 37; d) Einholm, A. P.; Pedersen, K. E.; Wind, T.; Kulig, P.; Overgaard, M. T.; Jensen, J. K.; Bodker, J. S.; Christensen, A., *Biochem. J.* **2003**, *373*, 723.

[26] K. McCleland, P. J. Milne, F. R. Lucieto, C. Frost, S. C. Brauns, M. Van De Venter, J. Du Plessis, K. Dyason, *J. Pharm. Pharmacol.* **2004**, *56*, 1143-1153.

[27] a) Kanoh, K.; Kohno, S.; Katada, J.; Takahashi, J.; Uno, I., *J. Antibiot.* **1999**, *52*, 134; b) Nicholson, B.; Lloyd, G. K.; Miller, B. R.; Palladino, M. A.; Kiso, Y.; Hayashi, Y.; Neuteboom, S. T. C. *Anti-Cancer Drugs* **2006**, *17*, 25; c) Kanzaki, H.; Imura, D.; Nitoda, T.; Kawazu, K., *J. Biosci. Bioeng.* **2000**, *90*, 86.

[28] Sinha, S.; Srivastava, R.; De Clercq, E.; Singh, R. K., *Nucleosides Nucleotides Nucleic Acids* **2004**, *23*, 1815.

[29] a) Asano, N., *Glycobiology* **2003**, *13*, 93R; b) Houston, D. R.; Synstad, B.; Eijsink, V. G. H.; Stark, M. J. R.; Eggleston, I. M.;Van Aalten, D. M. F., *J. Med. Chem.* **2004**, *47*, 5713; c) Byun, H.-G.; Zhang, H.; Mochizuki, M.; Adachi, K.; Shizuri, Y.; Lee,W.-J.; Kim, S.-K. J. Antibiot. 2003, 56, 102.

[30] a) Fdhila, F.; Vàzquez, V.; Sanchez, J. L.; Riguera, R., *J. Nat. Prod.* **2003**, *66*, 1299; b) Kanokmedhakul, S.; Kanokmedhakul, K.; Phonkerd, N.; Soytong, K.; Kongsaeree, P.; Suksamrarn, A., *Planta Med.* **2002**, *68*, 834; c) Sugie, Y.; Hirai, H.; Inagaki, T.; Ishiguro, M.; Kim, Y. J.; Kojima, Y.; Sakakibara, T.; Sakemi, S.; Sugiura, A.; Suzuki, Y.; Brennan, L.; Duignan, J.; Huang, L. H.; Sutcliffe, J.; Kojima, N., *J. Antibiot.* **2001**, *54*, 911; d) Abraham, W.-R. Drug Des. Rev. 2005, 2, 13. 22. De Kievit, T. R.; Iglewski, B. H., *Infect. Immun.* **2000**, *68*, 4839; e) Kozlovsky, A. G.; Zhelifonova,V. P.; Adanin,V. M.; Antipova, T. V.; Ozerskaya, S. M.; Ivanushkina, N. E.; Grafe, U., *Appl. Biochem. Microbiol.* **2003**, *39*, 393.

[31] a) Kwon, O. S.; Park, S. H.; Yun, B. S.; Pyun, Y. R.; Kim, C. J., *J. Antibiot.* **2000**, *53*, 954; b) Song, M. K.; Hwang, I. K.; Rosenthal, M. J.; Harris, D. M.; Yamaguchi, D. T.; Yip, I.; Go, V. L. W., *Exp. Biol. Med.* **2003**, *228*, 1338; c) Hwang, I. K.; Harris, D. M.; Yip, I.; Kang, K.W.; Song, M. K. *Diabetes Obes. Metab.* **2003**, *5*, 317.

[32] Kilian, G.; Jamie, H.; Brauns, S. C. A.; Dyason, K.; Milne, P. J., *Pharmazie* **2005**, *60*, 305.

[33] Imamura, M.; Prasad, C., *Peptides* **2003**, *24*, 445.

[34] Lòpez-Rodrìguez, M. L.; Morcillo, M. J.; Fernàndez, E.; Porras, E.; Orensanz, L.; Beneytez, M. E.; Manzanares, J.; Fuentes, J. A., *J. Med. Chem.* **2001**, *44*, 186.

[35] a) Wyatt, P. G.; Allen, M. J.; Borthwick, A. D.; Davies, D. E.; Exall, A. M.; Hatley, R. J. D.; Irving, W. R.; Livermore, D. G.; Miller, N. D.; Nerozzi, F.; Sollis, S. L.; Szardenings, A. K., *Bioorg. Med. Chem. Lett.* **2005**, *15*, 2579; b) Liddle, J. PCT Int. Appl. CODEN: PIXXD2;WO2005000840; A1 20050106, 2005; *Chem. Abstr.* **2005**, *142*, 114102; c) Brooks, D. P. PCT Int. Appl. CODEN: PIXXD2; WO 2005000311; A1 20050106, 2005; *Chem. Abstr.* **2005**, *142*, 114098.

[36] A. Dömling, Y. Huang, *Synthesis* **2010**, 2859-2883.

[37] Y. Yamakazi, Y. Hayashi, Analogs of Dehydrophenylahistins, **2011**, PCT Int. Appl. WO 2011/084962.

[38] D. L. Boger, B. E. Fink, M. P. Hedrick, *Bioorg. Med. Chem. Lett.* **2000**, *10*, 1019-1020.

[39] M. C. Meuwese, E. de Groot, R. Duivenvoorden, M. D. Trip, L. Ose, F. J. Maritz, D. C. G. Basart, J. J. P. Kastelein, R. Habib, M. H. Davidson, et al., *J. Am. Med. Assoc.* **2009**, *301*, 1131-1139.

[40] J. Oesterheld, M.D. "*P-gp (ABCB1) Introduction"*, GeneMedRX, http://www.genemedrx.com/PGP_Introduction.php (21.10.2011).

[41] D. E. Nitecki, B. Halpern, J. W. Westley, *J. Org. Chem.* **1968**, *33*, 864-866.

[42] Y. Hayashi, S. Orikasa, K. Tanaka, K. Kanoh, Y. Kiso, *J. Org. Chem.* **2000**, *65*, 8402-5.

[43] S. L. Sollis, *J. Org. Chem.* **2005**, *70*, 4735-40.

[44] J. F. Demarest, S. S. Sparks, K. Schell, S. Shibayama, C. B. McDanal, L. Fang, K. K. Adkison, A. Shachoy-Clark, S. C. Piscitelli, *J. Clin. Pharmacol.* **2008**, *48*, 1179-1188.

[45] S. Ando, A. L. Grote, K. Koide, *J. Org. Chem.* **2011**, 1155-1158.

[46] V. Santagada, F. Fiorino, E. Perissutti, B. Severino, S. Terracciano, G. Cirino, G. Caliendo, *Tetrahedron Letters* **2003**, *44*, 1145-1148.

[47] M. Jainta, M. Nieger, S. Bräse, *Eur. J. Org. Chem.* **2008**, *2008*, 5418-5424.

[48] L. Pérez-Picaso, J. Escalante, H. F. Olivo, M. Y. Rios, *Molecules* **2009**, *14*, 2836-2849.

[49] E. O'Reilly, L. Pes, F. Paradisi, *Tetrahedron Letters* **2010**, *51*, 1696-1697.

[50] Z. Z. Brown, C. E. Schafmeister, *Org. Lett.* **2010**, *12*, 1436-1439.

[51] D. S. Ermolat'ev, E. V. Babaev, *Molecules* **2003**, *8*, 467-471.

[52] D.-X. Wang, M.-T. Liang, G.-J. Tian, H. Lin, H.-Q. Liu, *Tetrahedron Letters* **2002**, *43*, 865-867.

[53] T. Guo, A. E. P. Adang, G. Dong, D. Fitzpatrick, P. Geng, K.-K. Ho, C. H. Jibilian, S. G. Kultgen, R. Liu, E. McDonald, et al., *Bioorg. Med. Chem. Lett.* **2004**, *14*, 1717-20.

2 | *DIKETOPIPERAZINES AS TEMPLATES*

1 - Examples in the literature [1]

Having emerged as privileged structures, DKPs were recently used as templates capable of inducing a defined secondary structure in peptide sequences. This relevant application, which has gained importance in the last decade, inherently takes advantage from the synthesis of symmetrical and unsymmetrical DKPs bearing reactive functionalities (e.g., NH_2, COOH) in the lateral chains of the amino acids. This let them being incorporated into a peptidomimetic moiety.

These constrained heterocyclic scaffolds were reported to be used in receptors, for the selective recognition of small peptides and anions, and in peptidomimetics mimicking topologically relevant elements of secondary structure of proteins (e.g., β-turns, β-hairpins, and α-helices).

1.1 - DKPs as two-armed receptors

Two-armed receptors consisting of a central scaffold and two, generally symmetrical, lateral modules containing several binding sites, have been synthesized (often via a combinatorial approach) and reported to bind different kinds of guests (e.g., anions, cations, small molecules, amino acids and short peptides). The importance of the central scaffold resides in its ability to: i) create a cleft with an adequate size to accommodate the guest, and ii) protrude the two side-arms with the correct geometry to wrap the guest with a sufficient number of binding points. Diketopiperazines, with their rather flat core and lateral chains of variable size and shape have been proficiently used to this purpose. For instance, Wennemers and co-workers have prepared several symmetrical DKP-based two-armed receptors, derived from 4-amino-proline where the two amino groups (with a *cis* disposition) were functionalized with two tripeptide side chains (Figure 2.1).[2,3]

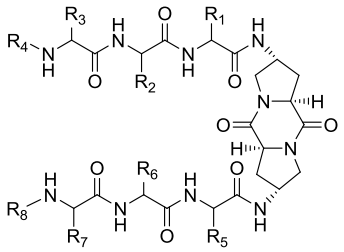

Figure 2.1 - General structure of di-(2*S*,4*R*)-4-aminoproline diketopiperazine two-armed receptors.

Five different receptors were prepared. The use of 4-amino-proline imparted the necessary distance between the two side arms in order to avoid intramolecular recognition between the two tripeptide arms and collapse of the receptor.

The resulting two-armed receptors were screened towards an encoded[4] resin-bound tripeptide library with the general structure Ac-AA3-AA2-AA1-NH$(CH_2)_6$-CONH-PS.

The screening revealed highly selective binding properties in organic solvents; in particular, each of the five structurally similar receptor prototypes selects for different tripeptides within the library. In particular, the di-(2*S*,4*R*)-4-aminoproline diketopiperazine shows a highly preorganized, turn-like conformation which imparts a defined orientation to the tripeptide side arms.

Water soluble diketopiperazine receptors were also synthesized, containing aspartic acid residues in the side arms, and were shown to bind to arginine-rich peptides in aqueous solution.[5] Interestingly, the addition of surfactants to this water-soluble receptor led to the formation of receptor-surfactant complexes with thermotropic liquid-crystalline properties.[6] Later on, the same group reported the synthesis of macrocyclic diketopiperazine receptors and demonstrated that the macrocyclization can alter the binding properties of the two-armed receptors since macrocyclic receptors bind their peptidic substrates with lower binding affinities compared to flexible two-armed receptors. The extent of altered binding selectivities depends on the length of the linker used to connect the receptor arms.[7]

Jolliffe and co-workers have reported another example of symmetrical diketopiperazine-based receptor with potential applications as sensor capable of discriminating anions that are ubiquitous in biological processes.[8] The authors designed and synthesized a diketopiperazine-based receptor bearing two dipicolylamino (DPA) arms (disposed in a *cis* configuration), by cyclization of the dipeptide Orn(DPA)-Orn(DPA)-OMe. Addition of $Zn(OAc)_2$ to the diketopiperazine-based receptor gave the bis[zinc(II)] complex for anion binding studies (Figure 2.2). The receptor showed significant selectivity for di- and triphosphate oxoanions over other anions tested (e.g., the sodium salts of nitrate, sulfate, bromide, iodide, acetate, (+)-tartrate, citrate, hydrogenphosphate, phosphotyrosine, phosphothreonine) in aqueous solution at physiological pH (pH = 7.4).

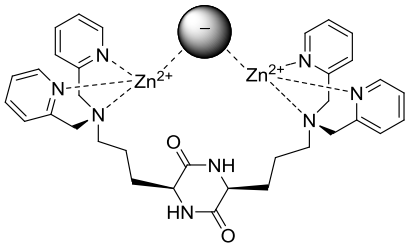

Figure 2.2 - Diketopiperazine-based anion receptor.

1.2 - DKPs as β-turn mimics

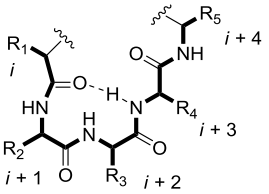

Figure 2.3 - β-turn

As already mentioned, a β-turn is defined as any tetrapeptide sequence, showing a typical 10-membered intramolecular H-bonded ring (Figure 2.3).

Although there has been much discussion in the literature on what constitutes a β-turn mimic and how different types of mimics are to be characterized,[9] these can be roughly classified into three broad classes, which are illustrated in Figure 2.4: a) internal β-turn mimics, b) β-hairpin mimics (where a rigid scaffold induces reversal of the peptide chain), and c) external β-turn inducers.

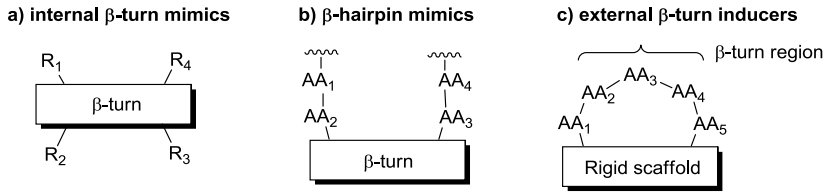

Figure 2.4 – classification of β-turn mimics.

1.2.1 - *Internal β-turn mimics*

The first class of β-turn mimics includes scaffolds displaying side chains with trajectories mimicking a peptide reverse turn. Several examples of this type of DKP-based scaffolds are reported in the literature. Golebiowski and co-workers have developed a solid-supported high-throughput synthesis of bicyclic diketopiperazines, starting from racemic piperazine-2-carboxylic acid.[10] A library of β-turn mimics was prepared (general structure, Figure 2.5), in which the first two (R^4 and R^5) substituents

were introduced via the Petasis reaction and subsequent amide bond formation, whereas R^1 and R^2 substituents were originated from an α-amino acid and were introduced in the amidation reaction.

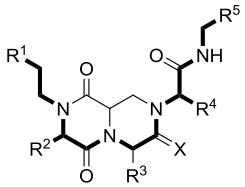

Figure 2.5 – examples of DKP-based internal β-turn mimics.

Later on, the same authors were able to introduce the missing R^3 substituent by developing a solid-phase protocol based on the Ugi reaction and using both L- and D-diaminopropionic acid as starting material, leading to two (complementary) epimeric series of β-turn mimics **27** (Figure 2.6).[11,12]

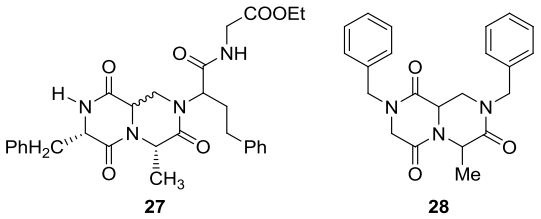

Figure 2.6 – examples of DKP-based internal β-turn mimics.

Simulated annealing calculations were performed on both epimers of structure **27** to determine their propensity to adopt a β-turn. The obtained data suggest that both *R*- and *S*- epimers of structure **27** fit more closely a type I β-turn.[12] Starting from simple α-amino acids, Kahn and co-workers have also reported the solution-phase synthesis of a conformationally restricted β-turn mimic **28** based on a similar bicyclic diketopiperazine scaffold (Figure 2.6).[13]

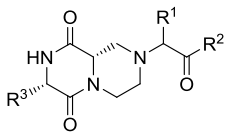

Figure 2.7 – examples of DKP-based internal β-turn mimics.

A cyclopropyl derivative of this heterocycle was also reported by Belov et al.[14] Finally, in 2010, Jurckak and co-workers reported the solid-supported synthesis of a library of β-turn mimics based on the general structure reported in Figure 2.7, using the original Golebiowski's strategy (three-component Petasis condensation and 2,5-DKP formation) but starting from optically pure (*S*)-

piperazine-2-carboxylic acid, with the purpose of decreasing the number of diastereomers of the final bicyclic scaffolds.[15]

Burgess and co-workers described the use of diketopiperazine scaffolds in antagonists of tropomysin receptor kinase C.[16] Selectivities for this particular receptor were achieved by using amino acid side chains corresponding to those present in the β-turn regions of the parent neurotrophin ligands. The diketopiperazine scaffolds used in this work (Figure 2.8) are functionalized at the N1 and C3, and the substituents at these two positions were calculated to overlay well with the side chains of the *i*+1 and *i*+2 residues of a type-I β-turn.

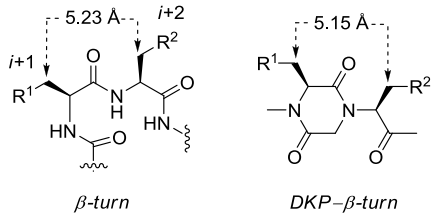

Figure 2.8 – DKP mimics of a type I β-turn.

1.2.2 - *DKPs as β-hairpin inducers*

The second class of β-turn mimics consists of a rigid scaffold, which, when incorporated into a peptide or pseudo-peptide chain, causes a reversal of the chain.[17] In strictest terms, these structures themselves should adopt a β-turn conformation, but quite often they lack substitution at the important *i*+1 and *i*+2 residues of the turn region or the means to introduce significant diversity at these positions. As β-hairpin inducers, the scaffolds can promote the formation of parallel or antiparallel β-sheets depending whether the side chains contain the same (e.g., two amine or carboxylic groups) or complementary functionalities (one amine and one carboxylic function). Gellerman and co-workers have reported the synthesis of orthogonally protected optically pure diketopiperazine scaffolds, starting from N_α-carboxymethyl ω-Alloc ornithine and orthogonally protected L-lysine.[18,19] The resulting non-symmetrical diketopiperazine scaffold **29** (Figure 2.9) bears two amine functionalities [AllocNH-$(CH_2)_3$, generated from Orn and FmocNH-$(CH_2)_4$, generated from Lys] in the arms of the DKP core and a complementary N_α-carboxymethyl group, which could be further manipulated via solid-phase organic chemistry (SPOC).

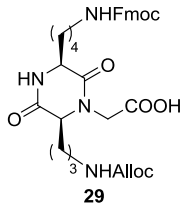

29

Figure 2.9 – example of DKP-based β-turn mimic

Alternatively, two different functionalities can be created in the lateral chains of the two amino acids forming the DKP core, such as an amine (e.g., derived from Lys, Orn or diaminobutyric acid) and a carboxylic acid (e.g., derived from Asp or Glu). Davies and co-workers performed some calculations on the minimum constraint requirement for a β-turn, which would fit tightly at the turn without causing steric hindrance, and preserve the polar backbone at the β-turn.[20] The result turned out to be a reverse *cis*-amide link in the form of a DKP ring containing an amino and a carboxylic groups in a *cis*-orientation, which would mimic a β-turn (correct angles and distances) and induce the formation of β-sheet structures.

1.2.3 - *DKPs in cyclic peptidomimetics, as external β-turn inducers*

In the case of external β-turn inducers, a rigid template is used to constrain the backbone of a cyclic peptide in order to stabilize the peptidic residue into a β-turn conformation. Notable examples of this type of β-turn mimic, based on a DKP scaffold, have been reported by Robinson and co-workers.[21]

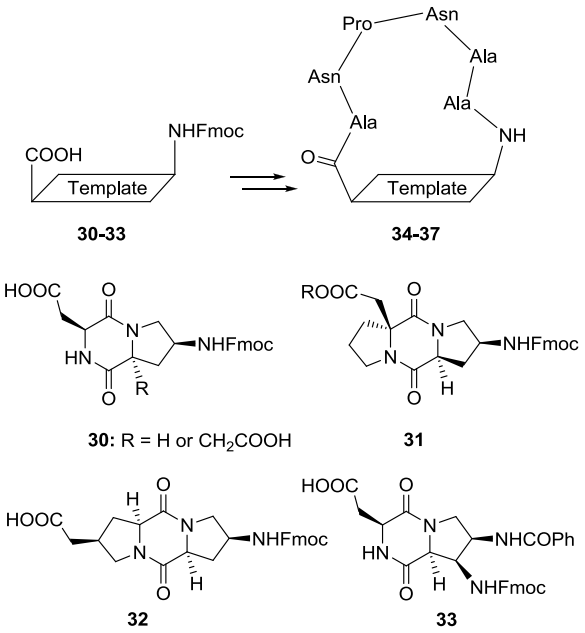

Figure 2.10 - Examples of diketopiperazine-based scaffolds as "external" β-turn mimics.

The authors have reported an extensive investigation of proline-based diketopiperazine templates (Figure 2.10), that were used to stabilize turn and hairpin conformations in cyclic peptides containing the Asn-Pro-Asn-Ala (NPNA) sequence. This tetrapeptide motif, which is found as a repeated unit in the circumsporozoite (CS) surface protein of the malaria parasite *Plasmodium falciparum*, has a tendency to adopt type-I β-turns in aqueous solution in linear peptides containing tandemly repeated NPNA sequence, and this secondary structure appears to be important for immune recognition of the folded CS protein. Several bifunctional bi- and tri-cyclic diketopiperazine scaffolds were prepared and

inserted into cyclic peptides containing the ANPNAA sequence. The first bicyclic scaffolds **30** derives from the cyclization of L-aspartic acid and (2*S*,4*S*)-4-aminoproline[21] or (2*R*,4*S*)-4-amino-2-carboxymethylproline[22] which are obtained starting from readily available (2*S*,4*R*)-4-hydroxyproline. These were incorporated into the cyclic loop mimics **34** containing the tetrapeptide motif Asn-Pro-Asn-Ala (NPNA), by solid-phase peptide synthesis, using Fmoc-chemistry. The conformational studies of loop mimics **34** were performed by ^{1}H-NMR spectroscopy and MD calculations.[23] Structure calculations using NOE-derived distance restraints indicate that the NPNA motif in **34** adopts a type-I β-turn conformation, while a bulged loop backbone conformation, rather than a stable β-hairpin is induced in the cyclopeptide by the pseudoequatorial position of 4-amido substituent of the pyrrolidine ring. Immunological studies revealed that these compounds can elicit anti-sporozoite antibodies in mice. Template **31** is closely related to **30**, but the additional pyrrolidine ring provides an extended framework for incorporating new functional groups. The synthesis of this scaffold started again from readily available (2*S*,4*R*)-4-hydroxyproline and L-proline. The template was then incorporated into cyclic peptide mimic **35** containing the sequence ANPNAA.[24] The solution conformation of **35** was studied by NMR in 10% D_2O/H_2O at pH 5.0. Average solution structures calculated with NOE restraints showed again the NPNA motif in a type-I β-turn conformation, and indeed the entire loop backbone conformation was very similar to that found with template **30** in mimic **34**. On the other hand, the tricyclic template **32** comprises a *cis*-fused bis-proline-derived diketopiperazine, where both proline rings are functionalized at the C4 position with an amino and carboxymethyl functionalities. Scaffold **32** was incorporated into cyclic peptide mimic **36** containing the usual ANPNAA sequence.[25]

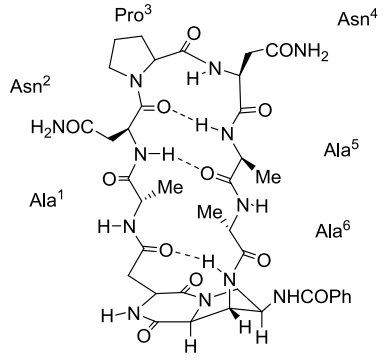

37

Figure 2.11 - β-Hairpin structure in the cyclic peptidomimetic **37**, containing the DKP template **33**.

Compared to templates **30** and **31**, the *N*- and *C*-termini of the peptide are anchored to template **32** in a quite different geometric relationship, which enforces a different backbone conformation on the peptide loop. This was confirmed by NMR spectroscopy in aqueous solution.[25] In particular, the tetrapeptide NPNA motif populates an extended conformation, rather than the β-turn seen in mimics **34** and **35**. Finally, template **33** was synthesized with the purpose of creating an additional *N*-substituent at the Cβ position of the pyrrolidine ring, that should remain axial and so be ideally

positioned as an anchoring group to restrain a peptide loop into a β-hairpin geometry. Template **33** was synthesized using (2*S*, 3*R*, 4*R*)-3,4-diaminoproline as a building block and was used to construct loop mimic **37** (Figure 2.11) whose conformation was studied by NMR and MD methods.[26]

A relatively stable β-hairpin conformation in the backbone of **37** was detected in the NOESY spectra (DMSO-d_6 solutions), by means of NOE contacts connecting H_α(Ala^1) as well as NH(Asn^2) with NH(Ala^5). In addition, a β-turn in the NPNA motif was also indicated by a relatively strong Asn^4 to Ala^5 $d_{N,N}$ NOE, as well as NOE contacts between Asn^2 H(β)s and Ala^5 NH, as observed in earlier studies of **34**. Average solution structures were determined by dynamic simulated annealing (SA) using distance restraints derived from NOESY spectra. The SA structures revealed a well defined β-hairpin backbone conformation, including a type I β-turn in the NPNA motif (Figure 2.11).

Scaffold **30** (R = H) was also introduced into the cyclic peptide **38** containing the Arg-Gly-Asp (RGD) sequence (Figure 2.12).[21]

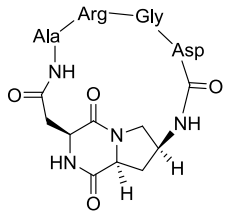

38

Figure 2.12 - Cyclic RGD peptidomimetics containing bicyclic DKP template **30**.

A conformational study to determine the three-dimensional presentation of the RGD motif in peptidomimetic **38** was performed by ^{1}H-NMR spectroscopy. However, no conclusive evidence of a defined conformation could be found, and it seems very likely that the peptide backbone of **38** is interconverting rapidly between two or more conformational states in aqueous solution.

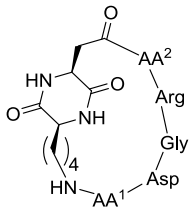

39 a: AA^1, AA^2 = not present
b: AA^1 = not present, AA^2 = Gly
c: AA^1, AA^2 = Gly

Figure 2.13 - cyclic RGD peptidomimetics containing cyclo[Lys-Asp].

In a similar approach, Royo, Albericio and co-workers have prepared cyclic peptidomimetics containing cyclo[Lys-Asp] as a template (**39**, Figure 2.13).[27] The side arms of the diketopiperazine were then used to link the amino and carboxy termini of three different peptides containing the RGD sequence (RGD, RGDG, and GRGDG), following a solid phase approach.

1.3 - DKPs in helical structures

Bis-peptides were recently introduced by Schafmeister and co-workers as "synthetic oligomers assembled from cyclic, stereochemically pure monomers coupled through pairs of amide bonds to form rigid spiroladder oligomers with predefined and programmable three-dimensional structures".[28]

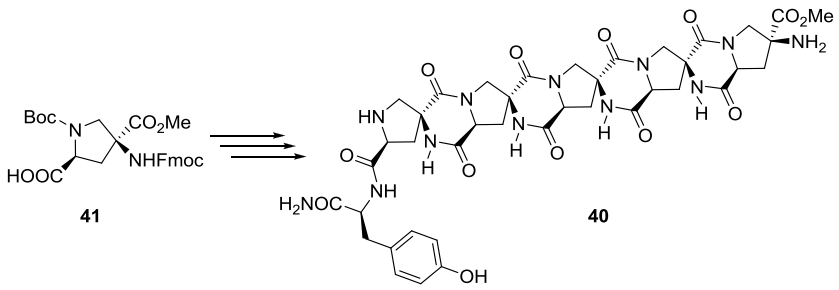

Figure 2.14

A "molecular rod" **40** (Figure 2.14) was synthesized starting from the "bis-amino acid" 4-amino-4-carboxy proline **41**.[29] This substituted proline was prepared in multi-gram quantities in nine synthetic steps from commercially available *trans*-4-hydroxy-L-proline. The synthesis of the "molecular rod" **40** occurred in two stages: a first "assembly" stage where the linear oligomer was grown, coupling the proline COOH to the primary amine in 4-position, by solid-phase peptide synthesis. A "rigidification" stage followed after cleavage from the resin. In this step, the diketopiperazines were cyclized by an intramolecular aminolysis reaction, in which the secondary amine of each monomer attacked the methyl ester of the previous monomer.

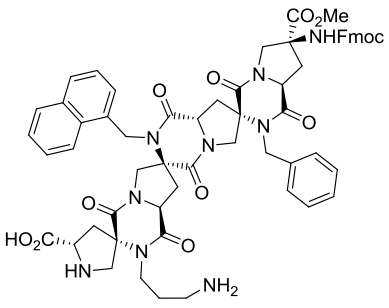

Figure 2.15 - Bis-peptide **42** with a left-handed helical arrangement.

Interestingly, when the bis-amino acid **41** was functionalized by reductive alkylation with different aldehydes at the primary amine group, the bis-peptide **42** resulting from the coupling of the corresponding homochiral monomers, adopted a left-handed helical arrangement, and the nitrogen substituents superimposed well on the side chains of a model α-helical peptide (Figure 2.15).[30]

2 - Previous work of our research group in the field

Recently, our group reported the synthesis of a new class of bifunctional DKP scaffolds (**DKP1**, **DKP2**, Figure 2.16), formally derived from aspartic acid and 2,3-diaminopropionic acid, bearing a carboxylic acid and an amino functionalities.[31] As a consequence of the absolute configuration of the two α-amino acids forming the cyclic dipeptide unit, the two reactive functionalities (amino and carboxylic acid) are locked in a *cis*- (**DKP1**) or *trans*-configuration (**DKP2**). In addition, while being derived from α-amino acids, these DKP scaffolds can be seen as a conformationally constrained dipeptide formed by two β-amino acids (see Figure 2.16), and in particular a β^2- and a β^3-amino acids (following Seebach's nomenclature).[32]

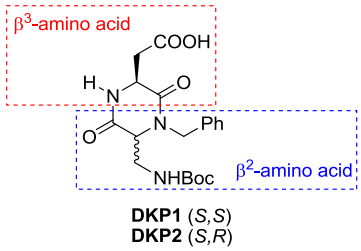

Figure 2.16 - Structure of bifunctional DKP scaffolds highlighting the conformationally constrained β2–β3 dipeptide sequence.

In particular, the bifunctional scaffold **DKP1**, derived from L-aspartic acid and (*S*)-2,3-diaminopropionic acid, bears the amino and carboxylic acid functionalities in a *cis* relationship and, as such, can be seen as a β-turn mimic and promoter of antiparallel β-sheet. In view of these potential properties, the synthesis of several peptidomimetics was performed by solution phase peptide synthesis (Boc strategy). Conformational analysis of these derivatives[31] was carried out by a combination of ^{1}H-NMR spectroscopy (chemical shift and NOE studies), IR spectroscopy, CD spectroscopy and molecular modeling, and revealed the formation of β-hairpin mimics involving 10- and 18-membered H-bonded rings and a reverse turn of the growing peptide chain (**43**, **44**, Figure 2.17). The β-hairpin conformation of the longer derivatives (**44 a** and **b**) was detected also in competitive, dipolar and even protic solvents such as dimethylsulfoxide and methanol, thus showing the high stability of these structures and the very good turn-inducing ability of the scaffold.

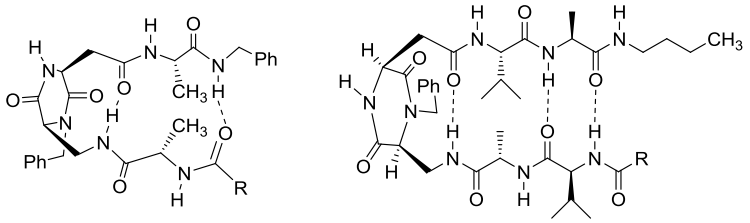

43 a: R = O-*t*Bu
b: R = CH_3

44 a: R = O-*t*Bu
b: R = CH_3

Figure 2.17 - Peptidomimetics containing scaffold **DKP1**.

This attitude was further confirmed in the conformational analysis of two oligomers of **DKP1**, namely the trimer Boc-(**DKP1**)$_3$-NH*n*Bu (**45**, Figure 2.18), and the tetramer Boc-(**DKP1**)$_4$-NH*n*Bu (**46**, Figure 2.18).[33] The conformational preferences in solution of these foldamers were investigated by ^{1}H-NMR and CD spectroscopy and molecular modeling. In the case of the trimeric structure, the conformational studies suggest the possible formation of two turns for the first and third residues, while the tetramer Boc-(**DKP1**)$_4$-NH*n*Bu (**46**, Figure 2.18) is best described as a β-bend ribbon conformation which is characterized by a succession of β-turns forming a linear peptide with a ribbon-like shape.

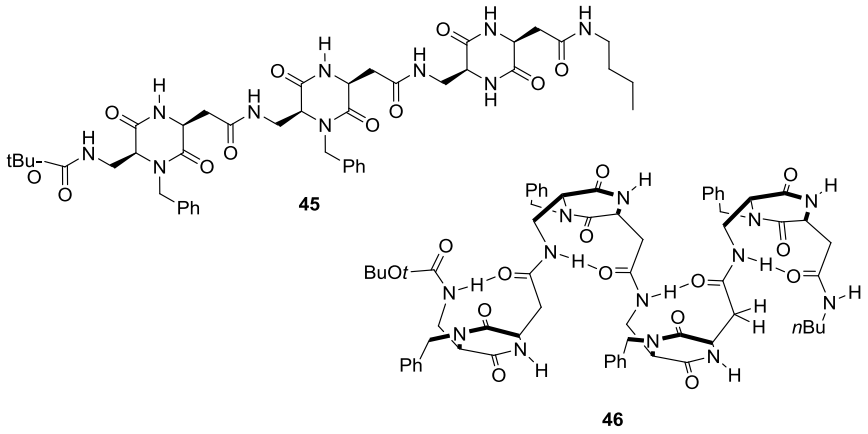

45

46

Figure 2.18 - Structure of trimer **45** and tetramer **46**.

The most peculiar feature of the β-turn structure present both in the hairpin and β-bend ribbon are the CD spectra which display a rather strong minimum around 200 nm and a weaker one at 225 nm with a negative maximum at 215 nm (Figure 2.17). This was shown, by NMR studies, to adopt a turn-like conformation with a 10-membered H-bonded ring induced by the β^2–β^3 unit.

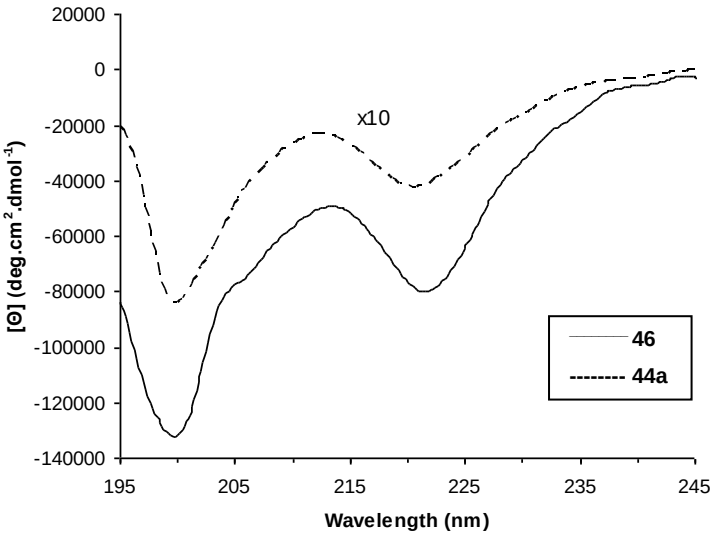

Figure 2.19 - CD spectrum of the tetramer **46** and the hairpin peptidomimimetic **44a**. The data of the latter compound have been multiplied by a factor 10 to magnify the appearance of the curve.

Our group has reported the synthesis, conformational analysis and investigation of the biological activity of cyclic RGD-peptidomimetics **47** and **48** (Figure 2.20), containing the bifunctional diketopiperazine scaffolds **DKP1** (*cis*) and **DKP2** (*trans*) (Figure 2.16).[34]

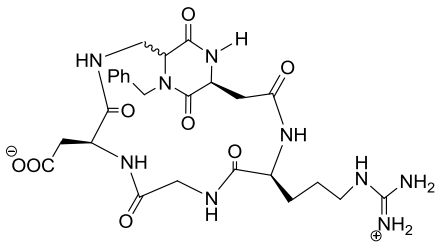

Figure 2.20 - Cyclic RGD peptidomimetics containing scaffolds **DKP1** and **DKP2**.

The conformational studies of cyclic RGD peptidomimetics were performed by NMR spectroscopy (^{1}H-NMR and NOESY spectra of dilute H_2O/D_2O 9:1 solutions) and by computational methods [Monte Carlo/Stochastic Dynamics (MC/SD) simulations].

RGD-peptidomimetic **47** exists in two different preferred conformations: one characterized by a γ-turn centered at the Gly residue and a βII'-turn at Gly-Asp and the second featuring a γ-turn at Arg and a βII'-turn at Arg-Gly (respectively, **47 A** and **B** in Figure 2.21). In both cases, the RGD sequence displays a kinked, non-extended arrangement with a rather short (6.5-7.4 Å) C_β(Arg)–C_β(Asp) distance. On the contrary, compound **48** adopts a single extended arrangement of the RGD sequence [C_β(Arg)–C_β(Asp) average distance = 9.3 Å] characterized by a pseudo β-turn at DKP-Arg and the formation of an inverse γ-turn at Asp (Figure 2.21).

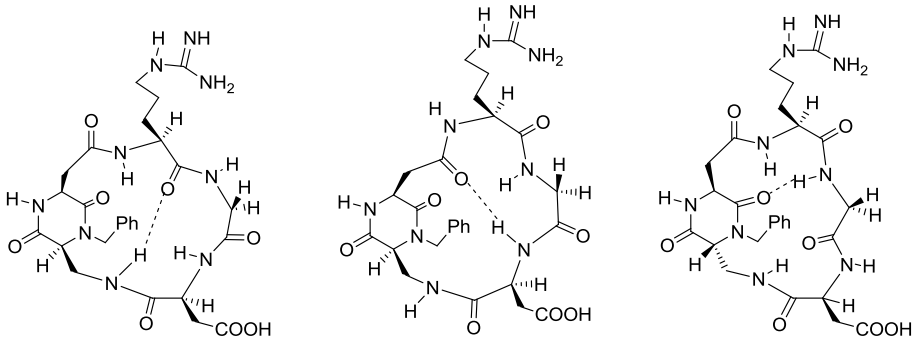

Figure 2.21 - Preferred intramolecular hydrogen-bonded patterns proposed for compound **47** and **48** on the basis of spectroscopic data. The arrows indicate significant NOE contacts.

3 - Library of DKP scaffolds

On the basis of the goals previously achieved by our research group, a library of bifunctional diketopiperazines structurally similar to **DKP1** and **DKP2** (see Figure 2.16) was prepared, varying their stereochemistry and substitution pattern (**DKP3-DKP8**, Figure 2.22). A second generation of scaffolds **DKP1-DKP3** was also prepared (**DKP1***, **DKP2***, **DKP3***, Figure 2.22), in which the amino group is masked as azide.

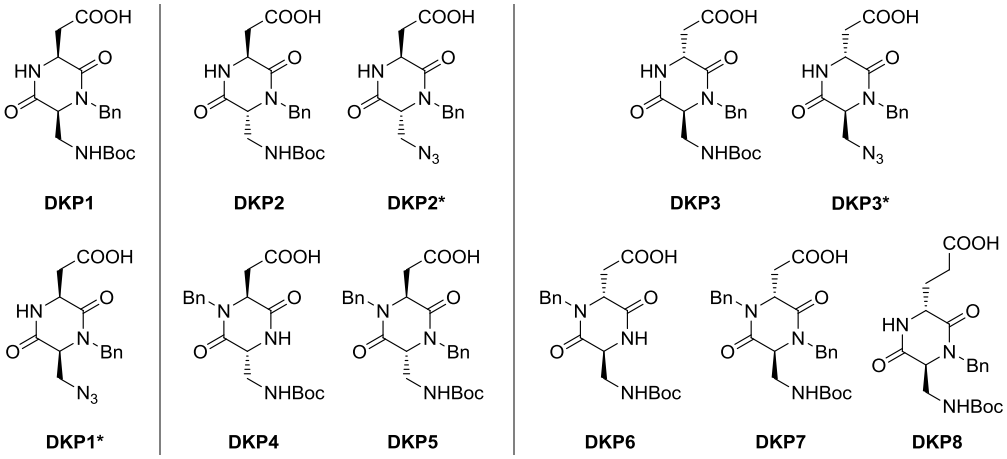

Figure 2.22 – Library of bifunctional diketopiperazine scaffolds **DKP1-DKP8** and second generation scaffolds **DKP1*-DKP3***

3.1 - Conception of the library

DKP1 and **DKP2** already revealed interesting and valuable constrained rigid scaffolds which, bearing a carboxylic acid and an amino functionalities, could be successfully employed as secondary structure inducers for several applications.

Tiny variations in their stereochemistry, ring substitutions or degrees of freedom, may dramatically change the behavior of these scaffolds when inserted into a peptidomimetic moiety. Having a wide range of scaffolds available may be of great impact expecially when aiming at the modulation of a biological target. For these reasons a library of eight diketopiperazines (Figure 2.22), structurally similar to **DKP1** and **DKP2**, was conceived.

In particular the scaffolds in the library differ for their relative stereochemistry, namely *cis* (**DKP1**) or *trans* (**DKP2**–**8**). The *trans* scaffolds differ for their absolute stereochemistry [either 3*R*,6*S* (**DKP2**, **DKP4, DKP5**) or 3*S*,6*R* (**DKP3**, **DKP6**, **DKP7**, **DKP8**)], for the substitution at the endocyclic nitrogens, which can be either hydrogen or benzyl (**DKP2**, **DKP3**, **DKP4**, **DKP6, DKP8**) or dibenzyl (**DKP5**, **DKP7**), and for the length of side-arm bearing the carboxylic group, which can be either carboxymethyl (**DKP1**–**7**) or carboxyethyl (**DKP8**).

A second generation of scaffolds, containing an amino functionality masked as azide (**DKP1***-**DKP3***), was created when we attempted to use this kind of scaffolds as building blocks for Fmoc solid phase synthesis. The azido function, which is stable in certain solid-phase peptide coupling conditions, stands here in place of a protecting group, alternative to Fmoc.

3.2 - Synthesis

A solution phase Boc-strategy was chosen for the synthesis of all the scaffolds. Different synthetic approaches were devised depending on the diketopiperazine nitrogen substitution.

3.2.1 - *Synthesis of DKP1 - DKP3 and DKP1* - DKP3**

The synthesis of **DKP-1**, **DKP-2** and **DKP-3** (bearing a benzyl group at nitrogen N-4, Figure 2.22) was performed according to procedures already developed in the group.[31]

Hydroxymethyl diketopiperazine **49** was identified as a suitable precursor.

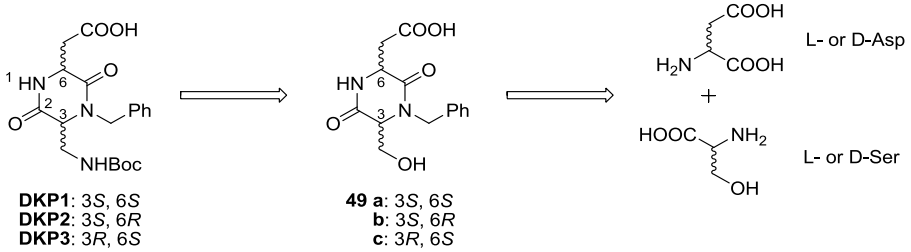

Scheme 2.1 – retrosynthetic approach to **DKP1-DKP3**.

The diketopiperazine ring was supposed to be provided by the cyclization of the dipeptide methylester derived from suitably protected and functionalized L- or D-aspartic acid and L- or D-serine (Scheme 2.1).

Therefore, aspartic acid was protected orthogonally to Boc and methylester on the β carboxylic acid functionality as an allylester. Either L- or D-aspartic acid were accordingly esterified by treatment with acetyl chloride in allyl alcohol to give aspartic acid β-allylester hydrochloride **50** (Scheme 2.2). The reaction of acetyl chloride with an alcohol (allyl alcohol here) is used to generate HCl *in situ* leading to the formation of allyl acetate, which can be removed if necessary by evaporation under reduced pressure. This procedure is reported to be selective for the β-carboxylic group esterification, but some bis-allylation can still take place.[35] In order to minimize the α-carboxylic acid esterification the reaction was performed at low temperature (0–10 ºC). The amino group was then protected as its *N*-*tert*-butoxycarbonyl derivative, under standard conditions, to give *N*-(*tert*-butoxycarbonyl)-aspartic acid β-allyl ester (**51**, Scheme 2.2). On the other hand, the OH group of the serine side-chain was thought not to interfere with the subsequent coupling reaction. Hence, only α-carboxylic acid group was protected as its methyl ester. Serine methyl ester hydrochloride **52** was obtained by esterification of the corresponding free amino acid in refluxing methanol, in the presence of acetyl chloride. The serine α-amino group was then alkylated through a reductive alkylation, thus obtaining *N*-benzylserine methyl ester **53**. As we mentioned previously (see Chapter 1.3.1), the presence of a tertiary amine decreases the energy difference between *cis* and *trans* peptide bond isomers, thus facilitating the cyclization step and DKP formation.

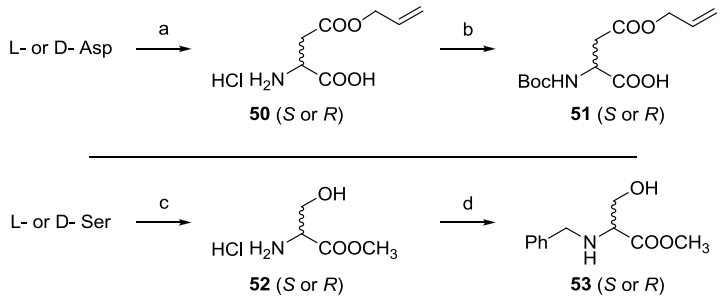

Scheme 2.2 – Synthesis of precursors: a) CH_3COCl, CH_2=$CHCH_2OH$: 80%; b) Et_3N, Boc_2O, 1:1 H_2O/THF: 96%; c) CH_3COCl, CH_3OH: 100%; d) Et_3N, PhCHO, CH_3OH, then $NaBH_4$: 93%.

The hydrochloric salt **52** was treated with benzaldehyde in methanol, in the presence of *i*Pr_2EtN to obtain the corresponding imine, that was subsequently reduced with sodium borohydride (Scheme 2.2). In order to minimize racemization during this latest step, special attention should be given to both temperature (-10°C during addition of reagents) and reaction time.[36] A procedure using sodium triacetoxyborohydride was recently attempeted, obtaining more reproducible results in terms of optical purity, but slightly lower yields.

It was then envisaged to couple protected aspartic acid **51** with *N*-benzylserine **53**. This reaction was reported using Carpino's reagent HATU, and the formation of dipeptides **54** was declared to occur in good yield (72%).[31] After Boc-deprotection with TFA in dichloromethane, and subsequent basic

activation in a biphasic medium ($NaHCO_{3\ aq.}$ 1M, AcOEt), diketopiperazines **49** were to be formed through an intramolecular 6-*exo* ring closing (Scheme 2.3).

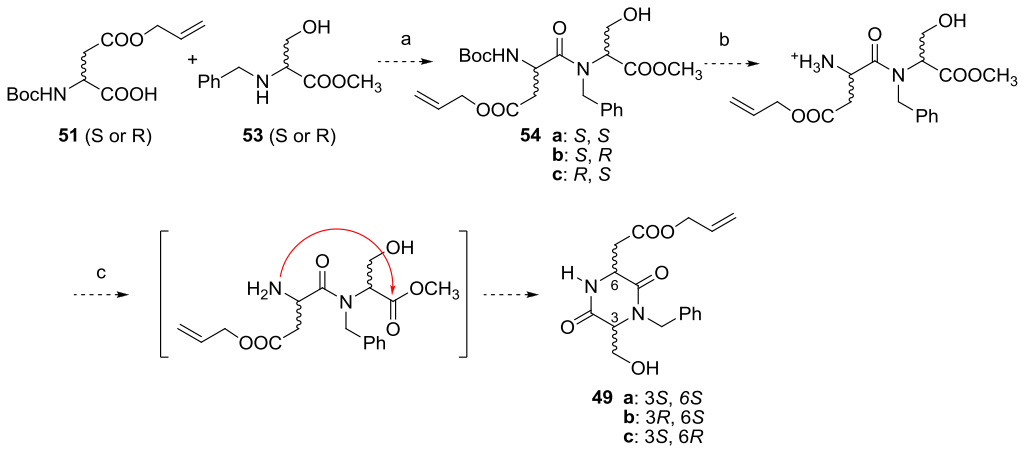

Scheme 2.3 – synthetic route to diketopiperazine **53**, as reported in the literature: a) HATU, HOAt, *i*Pr_2EtN, DMF, 72%; b) CF_3COOH/CH_2Cl_2 1:1; c) $NaHCO_{3\ aq.}$ 1M, AcOEt, 77% over two steps.

Indeed diketopiperazines **49** were actually obtained in good yields through these synthetic steps. The structure of the *cis* compound **DKP1** (Figure 2.22), which was obtained following the same strategy, was in fact confirmed by X-ray.[31]

Being sure of having obtained compounds of structure **49**, we decided to investigate the coupling between aspartic acid derivatives **51** and the hydroxyl-unprotected serin derivatives **53** more carefully. The spectroscopic properties of the intermediates obtained from the coupling reaction were closer inspected, revealing that the formation of the isopeptides **55** had instead occurred, *via* the selective acylation of the unprotected β-hydroxy group of either (*S*)- or (*R*)-*N*-benzylserine (Scheme 2.4).[37]

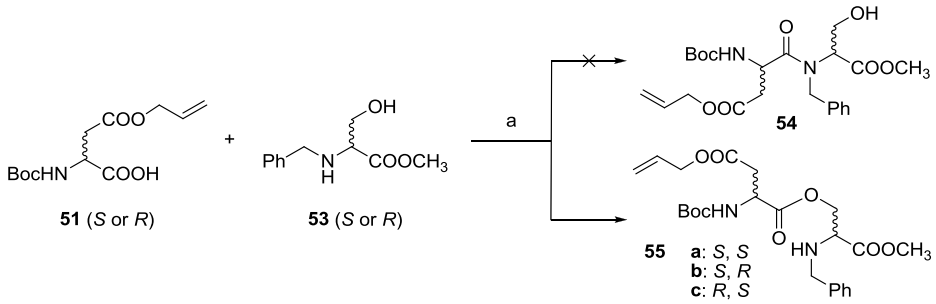

Scheme 2.4 – formation of an isodipeptide by direct coupling of compounds **51** and **53**: a) HATU, HOAt, *i*Pr_2EtN, DMF, 72%.

Diagnostic of this outcome were the NMR spectra, studied in particolar for compounds **55a** and **55b**: (i) in the ^{1}H NMR spectrum, the O-CH_2 protons of serine were rather deshielded [**55a**: δ 4.32-4.48, m, 2H ($CDCl_3$); **55b**: δ 4.30, dd, 1H and δ 4.39, dd, 1H (CD_2Cl_2)]; (ii) in the HMBC (Heteronuclear Multiple Bond Coherence) spectrum of both compounds, a long range coupling (through three bonds)

was clearly evident between the O-CH_2 protons of serine and the α-carbonyl carbon of aspartic (Figure 2.23).

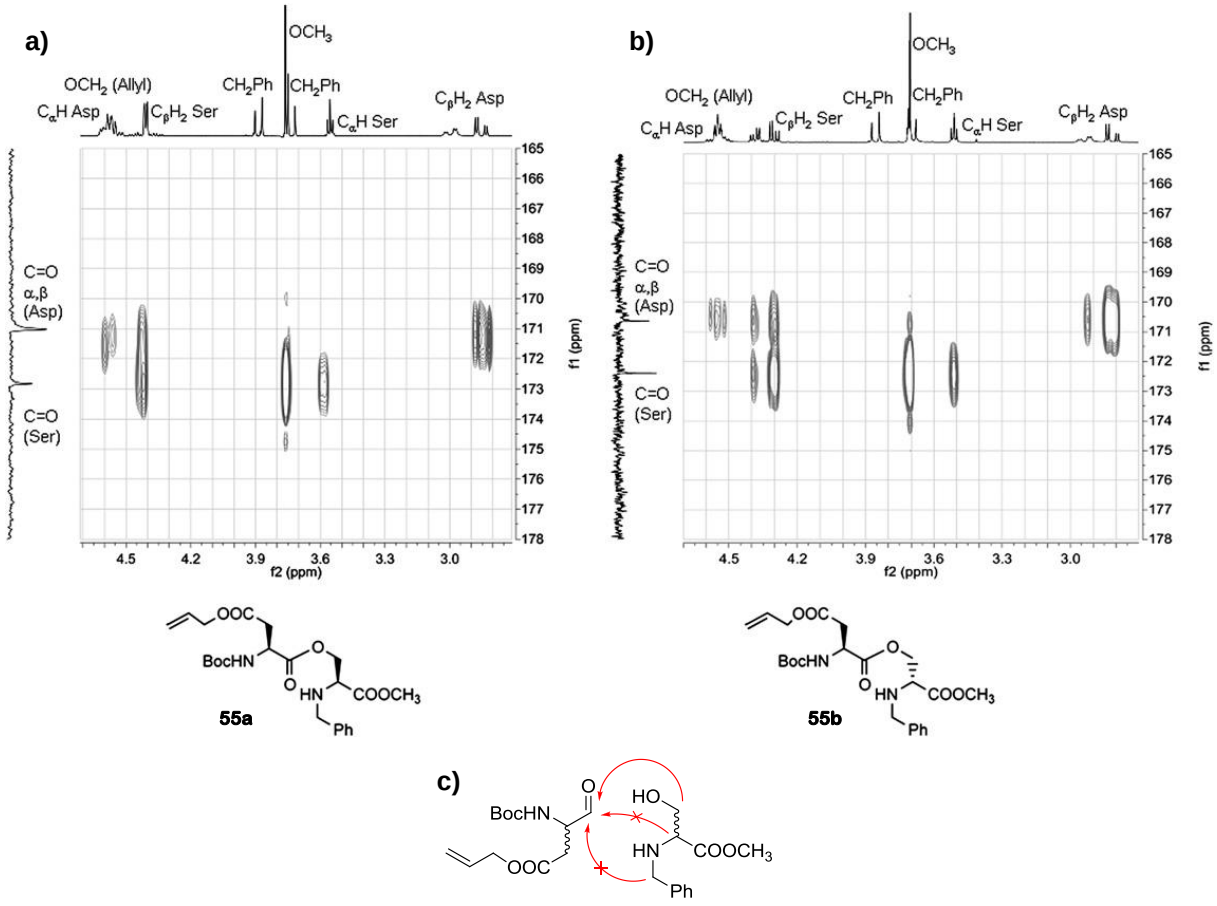

Figure 2.23 – HMBC spectra of isopeptides a) **55a** ($CDCl_3$) and b) **55b** (CD_2Cl_2), highlighting the long range coupling (through three bonds) between the O-CH_2 protons of Ser and the α-carbonyl carbon of Asp; c) scheme representing the long range couplings highlighted from the HMBC spectra.

Had we been in presence of dipeptide **54**, we might have probably expected other long range couplings, in particular between the the α-carbonyl carbon of Asp and both the CH_2-Ph and the C_α-H of Ser. In order to further prove our hypothesis, an extra experiment was conducted on compound **55b**. Capping compound **55b** with acetic anhydride provided isopeptide **56** (Scheme 2.5). In this case, a long range coupling (through three bonds) between the benzylic CH_2 protons of benzylserine and the acetyl carbonyl carbon was detected, confirming that acetylation had occurred on the secondary amine group of serine, which was therefore not involved in an amide bond with the aspartic fragment (Figure 2.24).

Thus, as compound **49** was obtained after Boc deprotection of compounds **55** with TFA and subsequent treatment with four equivalents of Et_3N or *i*Pr_2EtN in methanol, it was clear that the deprotected isopeptide intermediate had to procede through an *O*,*N*-acyl transfer while forming the diketopiperazine ring.

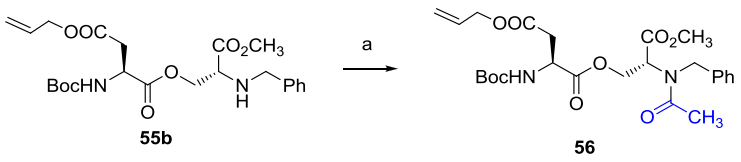

Scheme 2.5 – acetylation of isopeptide **55b**: a) Ac_2O, pyridine.

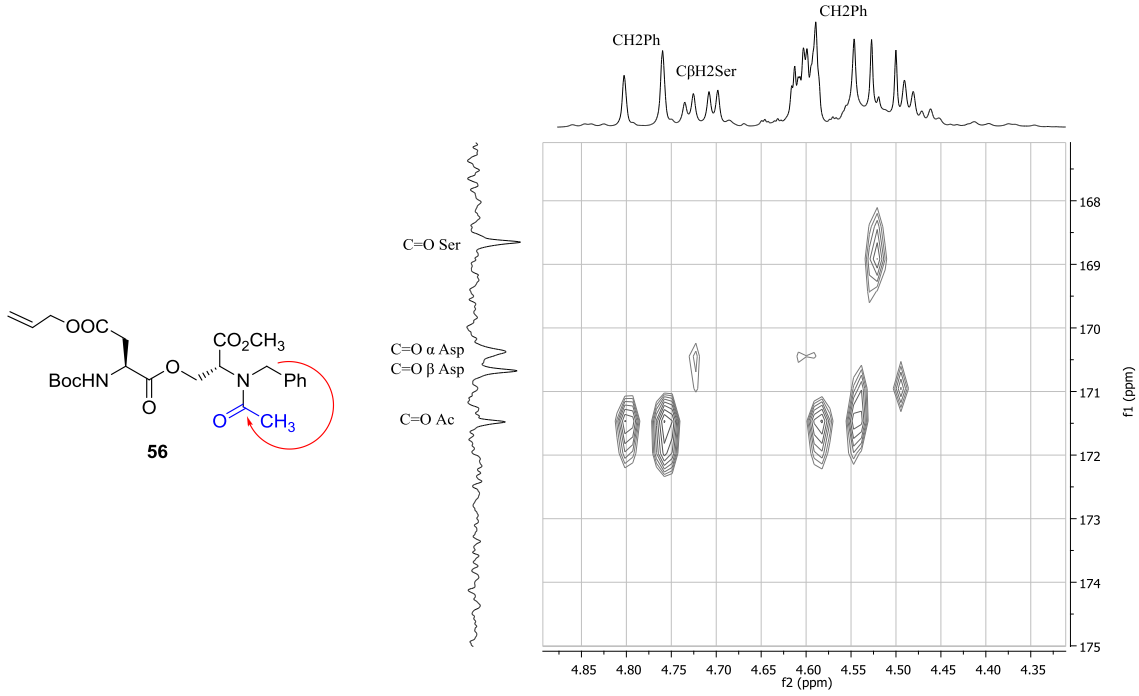

Figure 2.24 - HMBC spectrum of **56** in CD_2Cl_2.

Puzzled by this behavior, we decided to investigate the conditions promoting *O,N*-acyl transfer/cyclization reactions, and the relevant mechanism that leads to diketopiperazine **49b** from isopeptide **55b**. Despite the presence of a nucleophilic nitrogen, isopeptide **55b** was stable both in solid state and in solution (dichloromethane). Instead, a complete degradation of the product was observed in methanol after 72 h, which could be attributed (as revealed from ^{1}H-NMR spectra) to the transesterification of the aspartate β-allyl ester and to the cleavage of the isopeptidic bond, giving rise to *N*-(tert-butoxycarbonyl)-aspartic acid dimethylester and *N*-benzylserine methyl ester. In any case, isomerisation to dipeptide **54b** was never observed.

Since the *O,N*-acyl transfer indeed occurred during the formation of diketopiperazine **49b** upon nitrogen deprotection, the Boc group of isopeptide **55b** was cleaved by reaction with TFA to give the bis-TFA salt **57**, which was fully characterized (Scheme 2.6).

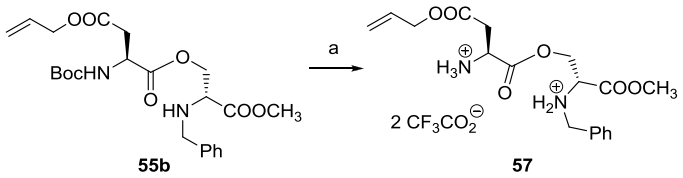

Scheme 2.6 – cleavage of the Boc group on **59b**: a) CF_3CO_2H/CH_2Cl_2, 1:1, 2h, quantitative.

In this case too, the HMBC spectrum of **57** confirmed that no *O*,*N*-acyl shift had occurred (Figure 2.25), as, again, no long range couplings were detected between the α-carbonyl carbon of Asp and either the CH_2-Ph or the C_α-H of Ser. Only a long range coupling between the O-CH_2 of Ser and the α-carbonyl carbon of Asp was highlighted in the spectrum.

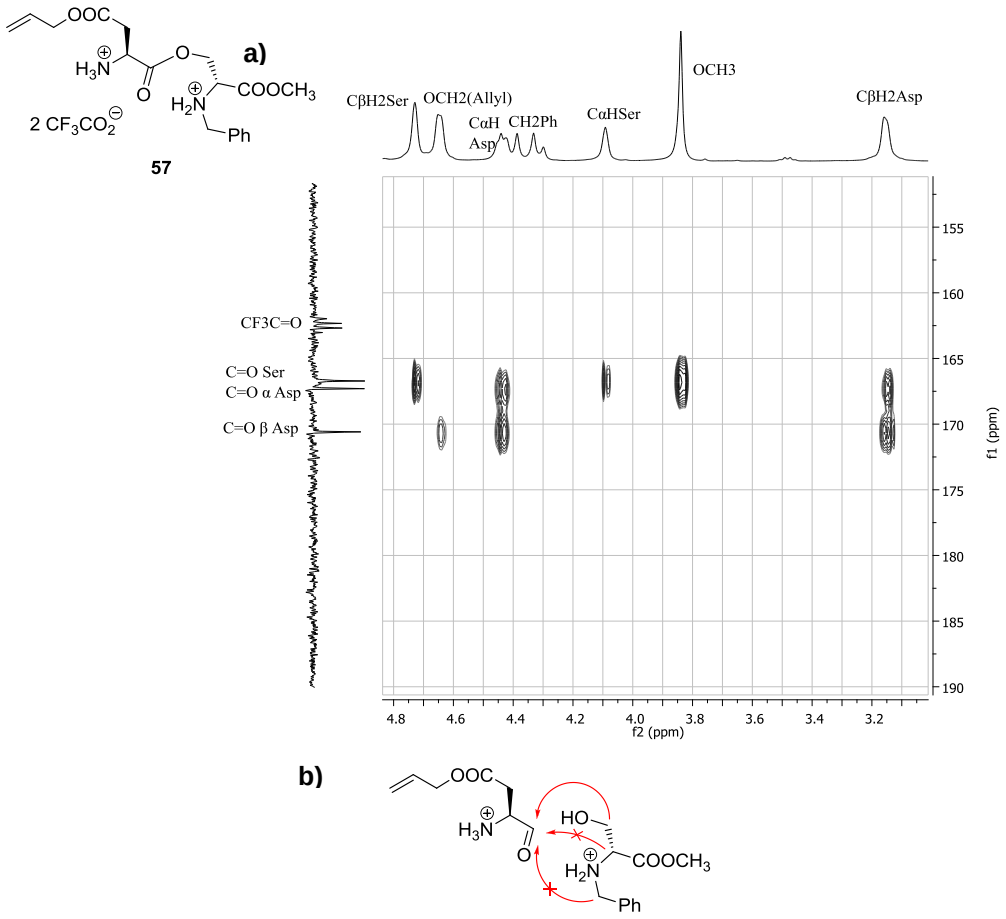

Figure 2.25 – a) HMBC spectrum of isopeptide bis trifluoroacetate salt **57** ($CDCl_3$), highlighting the long range coupling (through three bonds) between the O-CH_2 protons of Ser and the α-carbonyl carbon of Asp; b) scheme representing the long range couplings highlighted from the HMBC spectrum.

Reactivity of bis-TFA salt **57** was then investigated. No *O*,*N*-acyl migration was observed after 48 h, monitoring a dichloromethane solution of compound **57** by ^{1}H-NMR; conversely, when dissolved in methanol, complete methanolysis of isopeptide bis-TFA salt was detected in 6 h, giving rise to (2*S*)-

aspartic acid β-allyl ester α-methylester and *N*-benzylserine methyl ester. Isomerization to the dipeptide was not observed, even in this case.

Upon addition of 4 equivalents of a base (Et_3N or iPr_2EtN) to a solution of bis-TFA salt **57** in methanol, ring closure occurred rapidly and was virtually complete after 2 h. However, monitoring the reaction by ^{1}H-NMR spectroscopy (CD_3OD / 4 eq. Et_3N), the dipeptide **54b** resulting from the *O,N*-acyl shift was never detected, and only signals concerning the starting bis-TFA salt **57** and the resulting diketopiperazine **49b** were identified.

As can be clearly seen in Figure 2.26, the two dd at δ 4.32 and δ 4.45, belonging to the O-CH_2 protons of benzylserine in the isopeptide bis-TFA salt **57**, decreased in intensity with time, while the dd at δ 3.93 and δ 4.02, corresponding to the same O-CH_2 protons in **49b**, proportionally increased. The same holds for the two d of the benzylic CH_2 protons, which in the isopeptide salt **57** resonate at δ 3.73 and δ 3.87, while in **49b** shift to δ 4.12 and δ 5.38, and for the serine C_α-H which moves from δ 3.6 to δ 3.77.

The same transformation (bis-TFA salt **57** to **49b**) was followed by ^{1}H-NMR in an aprotic solvent (CD_2Cl_2 containing 4 eq. of Et_3N). In this case too, despite the much reduced reaction rate (only 32% conversion was observed after 15 h), no *O,N*-acyl shift product was ever detected (Figure 2.27).

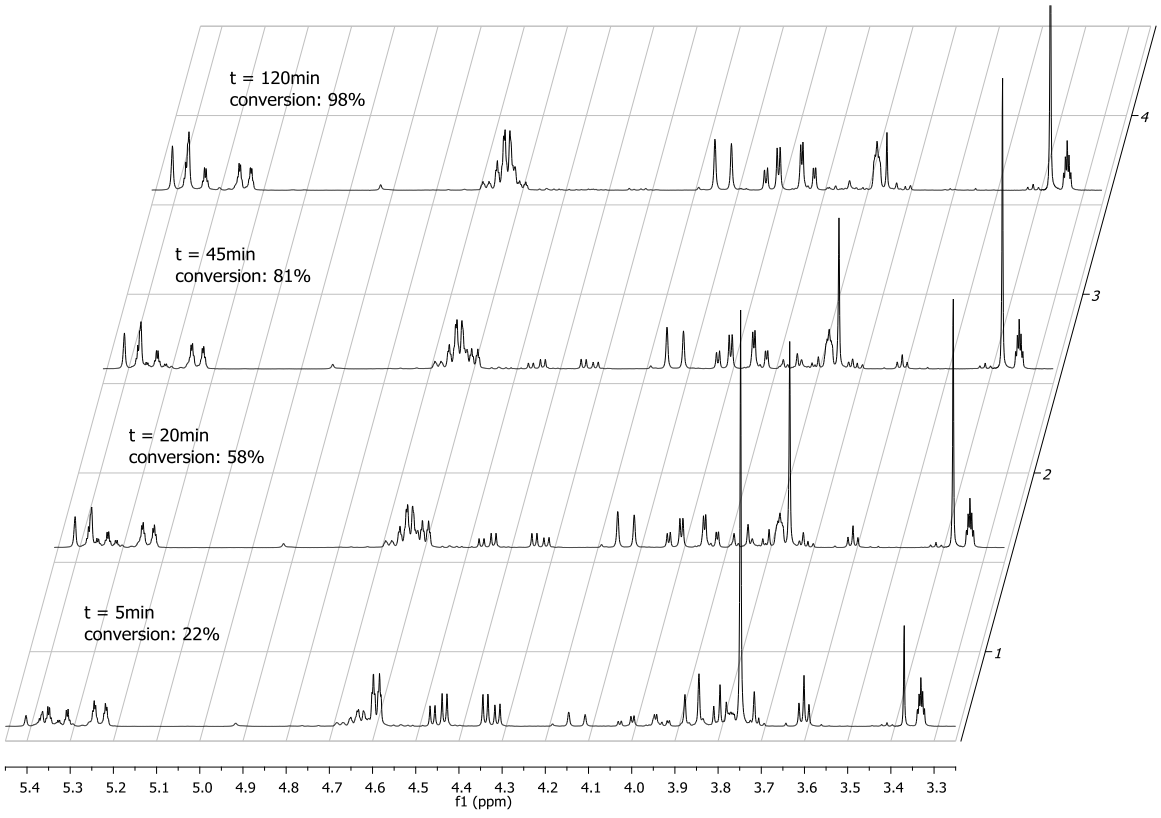

Figure 2.26 - ^{1}H-NMR monitoring of the transformation of isopeptide bis-TFA salt **57** into the diketopiperazine **49b** (CD_3OD / 4 eq. Et_3N).

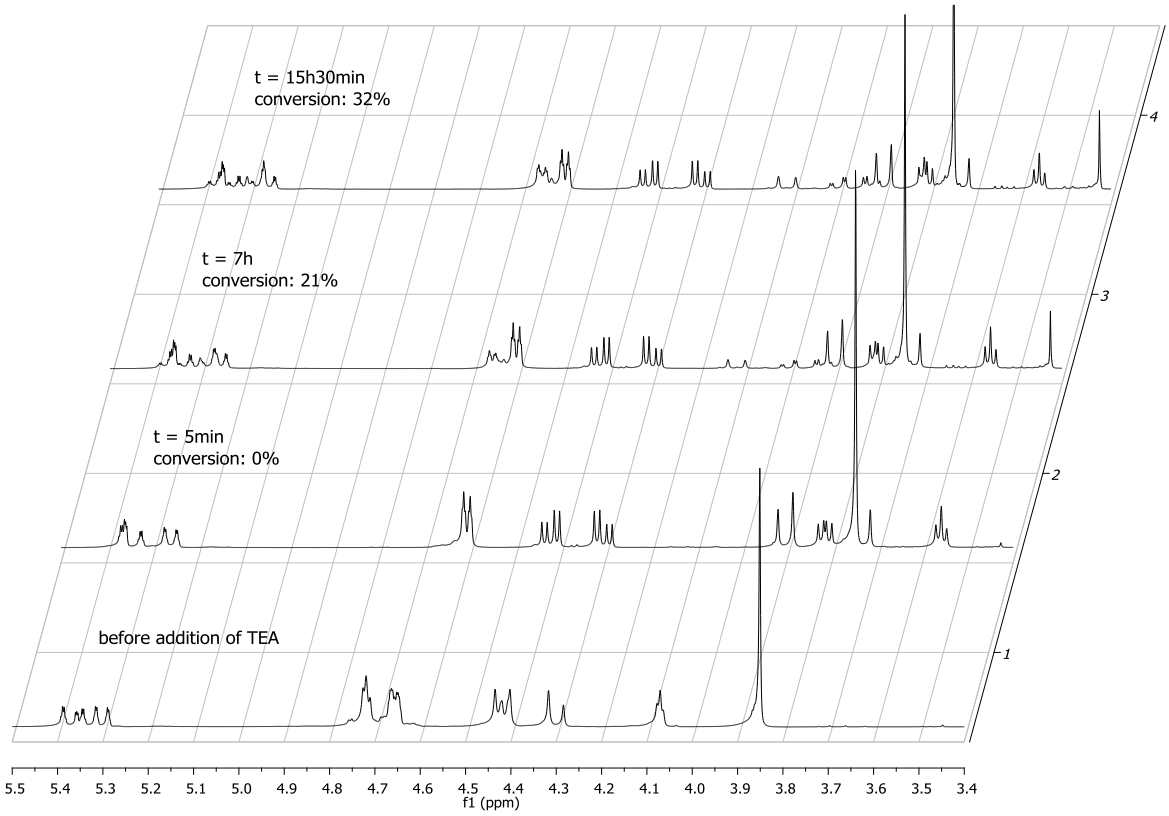

Figure 2.27 - ^{1}H-NMR monitoring of the transformation of isopeptide bis-TFA salt **57** into the diketopiperazine **49b** (CD_2Cl_2 / 4 eq. Et_3N).

Based on these experimental observations, a reasonable mechanistic explanation involves a rate limiting *O,N*-acyl transfer with simultaneous ring closure to DKP, so that no dipeptide intermediate can be detected (Scheme 2.7).

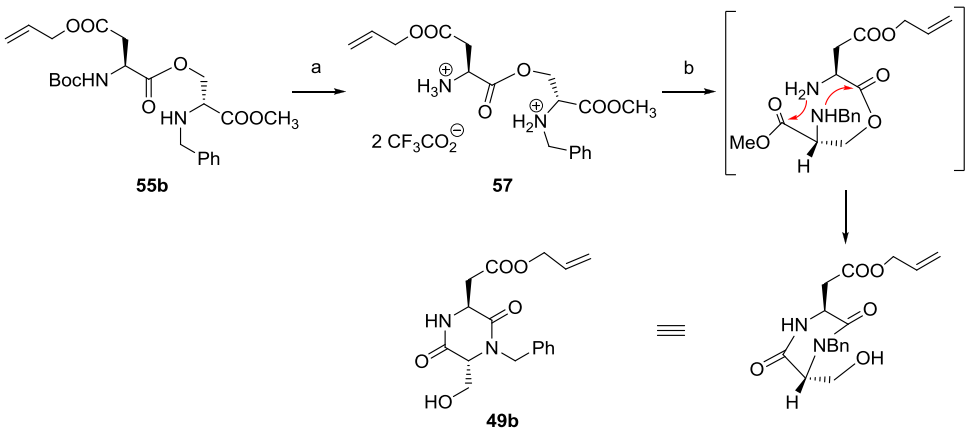

Scheme 2.7 – proposed diketopiperazine mechanism of formation: a) CF_3CO_2H/CH_2Cl_2, 1:1; b) 4 equiv. base (Et_3N or iPr_2EtN), MeOH.

On a preparative scale, the synthesis of diketopiperazine **49b** from bis-TFA salt **57** was more efficiently performed (94% isolated yield) with *i*Pr_2EtN (4 eq.) in *i*PrOH instead of MeOH, that in the long run leads to transesterification of aspartic allyl ester.[37]

Analogous results were also observed while synthesizing of both diketopiperazines **49a** (*cis*) and **49c** (*trans*).

In vision of a scaling up of the synthesis of isopeptide **55**, these studies gave us enough information on how to improve the coupling reaction between the two aminoacid derivatives **51** and **53**. Since an ester bond is formed instead of an amide bond, the more appropriate and better value coupling reagent EDC (1-ethyl-3-(3-dimethylaminopropyl) carbodiimide) in presence of a catalytic amount of DMAP (4-Dimethylaminopyridine) provided the best results (Scheme 2.8).

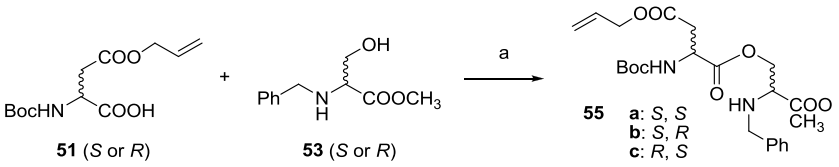

Scheme 2.8 - a) EDC, $DMAP_{cat.}$, CH_2Cl_2, 94%

Carpino's reagents (HATU, HOAt) are very useful to avoid epimerization on the α proton during aminoacid coupling, but also this methodology, monitoring temperature and reaction time, gives no epimerization on the α proton, as confirmed by ^{13}C-NMR. Furthermore, the yields we obtained were higher.

Once the coupling reaction and the subsequent diketopiperazine ring closure were improved, we focused on the transformation of the hydroxy moiety of **49** into the Boc-protected amino moiety present in **DKP1-DKP3**.

Functional group interconversion was accomplished by a Mitsunobu type reaction,[38] followed by reduction and *in situ* Boc-protection by Staudinger reaction of the obtained azides **58** into derivatives **59**. Deprotection of the allyl ester on compounds **59** was succesfully accomplished via a Pd^0 catalyzed Tsuji-Trost reaction, which proceeds quantitatively affording the final scaffolds **DKP1-DKP3** (Scheme 2.9):

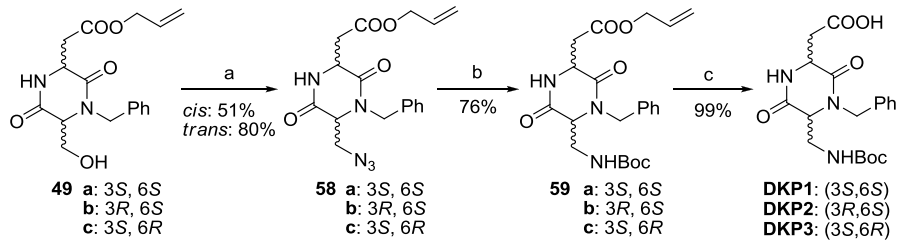

Scheme 2.9 – a) PPh_3, DIAD, H_3N.tol, DCM/toluene, -20°C; b) Me_3P, Boc-ON, THF, -20°C -> r.t; c) $[Pd(PPh_3)_4]$, PPh_3, pyrrolidine, DCM, 0°C.

Mitsunobu transformation on substrates **49** is a quite sensitive reaction, since the activated hydroxy group could β eliminate before reacting with the pronucleophile (HN_3). The C(6) proton can be in fact easily extracted due to its acidity, providing a diketopiperazine with an exocyclic double bond (**60**, Scheme 2.10).

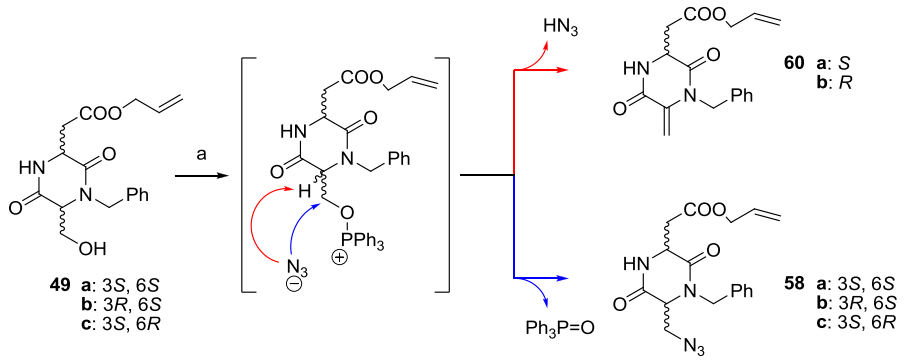

Scheme 2.10 – β elimination competing with the Mitsunobu nucleophilic attack: a) PPh_3, DIAD, H_3N.tol, DCM/toluene, -20°C.

Monitoring temperature (which should not exceed -20°C), reaction time and order of reagents addition, we were able to drastically reduce the amount of **60**, reducing the ratio **58a**:**60a** to 3:1, **58b**:**60a** and **58c**:**60b** to 8:1. Reaction was carried out in a toluene/dichloromethane 2:1 solution, since toluene is itself was not sufficient to solubilize diketopiperazines **49** at -20°C.

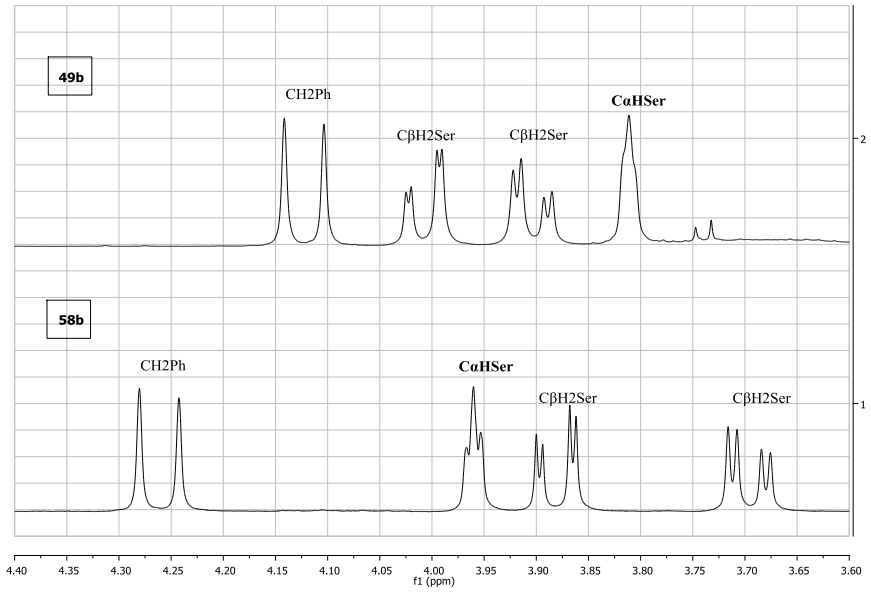

Figure 2.28

β elimination side reaction proved to be particularly competitive in the case of the *cis* substrate **49a**. Purification from the by-product revealed even more complicated, as product **58a** showed almost the

same elution time of the corresponding byproduct **60a**, with various eluents. These are the main reasons why yields are far lower for the *cis* product.
NMR evidence of the formation of azide **58b**, namely the shift of C_α-H and C_β-H_2 derived from serine, is reported in Figure 2.28.

The next step involved a one-pot Staudinger – Boc protection. The Staudinger reaction, a very mild azide reduction, involves the reaction of the azide with a phosphine to generate a phosphazide, which loses N_2 to form an iminophosphorane. Hydrolysis of this intermediate leads to the amine and the very stable phosphine oxide. The mechanism is reported in Scheme 2.11.

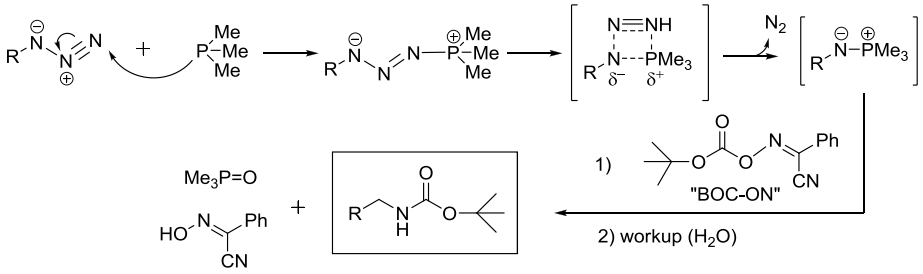

Scheme 2.11 – Staudinger reaction, mechanism.

In our case the intermediate iminophosphorane reacted directly with 2-(*t*-butoxycarbonyloxyimino)-2-phenylacetonitrile (Boc-ON),[39] present in the reaction medium, affording the desired Boc-protected amine in very good yield. Finally the DKP scaffold allyl esters **59** (Scheme 2.9), were de-allylated in the presence of a catalytic amount of *tetrakis*(triphenylphosphine) [$Pd(PPh_3)_4$] and pyrrolidine, *i.e.* a nucleophile acting as an allyl scavenger to give the amino acid derivatives **DKP1-DKP3** in quantitative yield. Such methodology is of special interest for peptide synthesis because the deprotection conditions are usually mild enough to be compatible with the presence of acid labile *t*-Bu and Boc protections.[40]

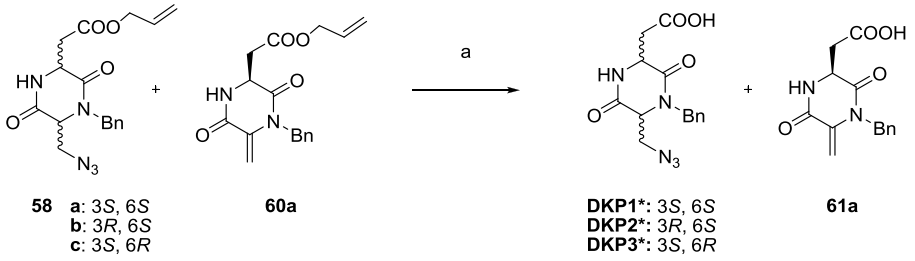

Scheme 2.12 – synthesis of second generation **DKP1*-DKP3*** from intermediate **58**: a) [Pd(PPh3)4], N-methyl aniline, DCM, 1h, r.t., 90%.

When scaffolds **DKP1-DKP3** needed to be used as building blocks in Fmoc-solid phase synthesis, a second generation of these scaffolds (**DKP1***, **DKP2***, **DKP3***, Figure 2.22) was conceived. We first

thought about reducing azides **58** to the corresponding free amines, which could then be Fmoc protected and de-allylated with the usual Tsuji-Trost procedure. However, aiming at reducing the number of steps, we decided instead to directly de-allylate azides **58**, using a similar, milder protocol, thus obtaining azido acids **DKP1*-DKP3*** (Scheme 2.12). Azides are in fact stable under solid phase coupling conditions (DCC, HOBt or DIC, HOAt), and can be seen as protecting groups of the amino functionality. The *in-situ* azide reduction is making the amino group available for the subsequent coupling step.

Moreover, de-allylation worked well even when performed on the *non*-separable mixture of azide **58a** and dehydroalanine-like elimination by-product **60a**, which were obtained from the Mitsunobu reaction. The two de-allylated products **DKP1*** and **61a** couldn't be separated by silica gel chromatography, as degradation occurred. However the remarkably different solubility properties of the two compounds allowed us obtain azido acid **DKP1*** with good purity, by successive precipitations of highly insoluble **61a** from concentrated dichloromethane solutions.

A scheme of the whole synthetic route to **DKP1-DKP3** and **DKP1*-DKP3*** is reported below (Scheme 2.13):

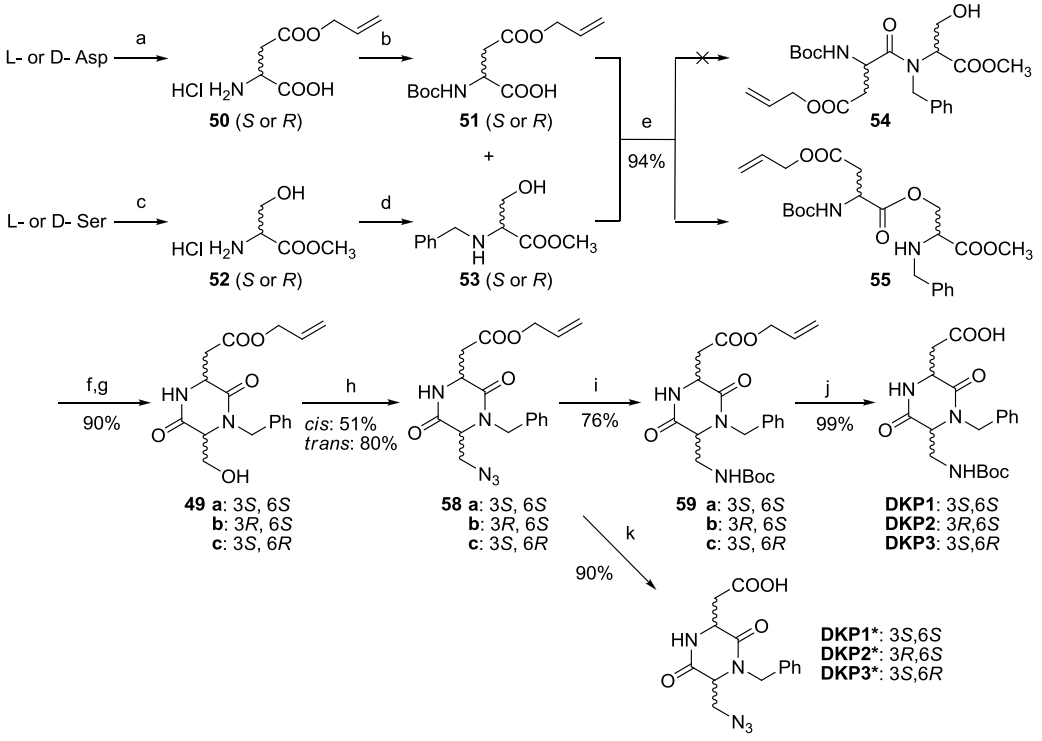

Scheme 2.13 – a) CH_3COCl, $CH_2{=}CHCH_2OH$; b) Et_3N, Boc_2O, 1:1 H_2O/THF; c) CH_3COCl, CH_3OH; d) Et_3N, PhCHO, CH_3OH, then $NaBH_4$; e) EDC, $DMAP_{cat.}$, DCM; f) TFA/DCM, 1:1; g) iPr_2EtN, *i*PrOH; h) PPh_3, DIAD, H_3N.tol, DCM/toluene, -20°C; i) Me_3P, Boc-ON, THF, -20°C -> r.t; j) $[Pd(PPh_3)_4]$, PPh_3, pyrrolidine, DCM, 0°C; k) [Pd(PPh3)4], N-methyl aniline, DCM, 1h, r.t..

3.2.2 - *Synthesis of **DKP4** and **DKP6***

A retrosynthetic analysis of scaffolds **DKP4** and **DKP6** (bearing a benzyl group at nitrogen N-1) suggested that, even in this case, the diketopiperazine ring **62** could be obtained from suitably protected aspartic acid and serine in the correct relative configuration (Scheme 2.14):

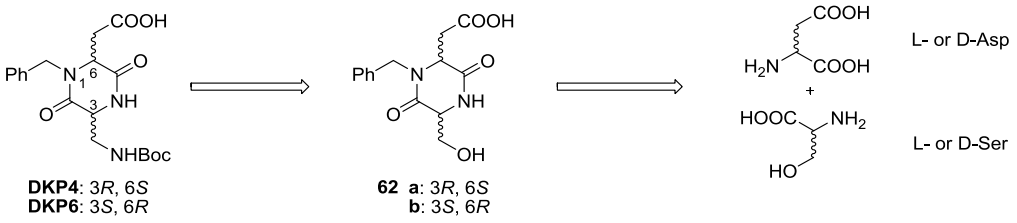

Scheme 2.14

We started investigating the synthesis of scaffold **DKP4**. As regards the aspartic acid derived fragment, both carboxylic acid moieties were protected as methyl esters and nitrogen was subsequently reductively alkylated to give derivative **63**. Protection of the Ser hydroxyl group was necessary to avoid self-condensation: we decided to non-orthogonally protect the hydroxyl (protected as -*t*Bu ether) and the amino functionalities (protected as –Boc), which, in this way, can be easily freed in an acidic medium (*e.g.* TFA solution) before diketopiperazine ring closure; such a protected Serine, derivative **64**, was commercially available (Fluorochem™) (Scheme 2.15).

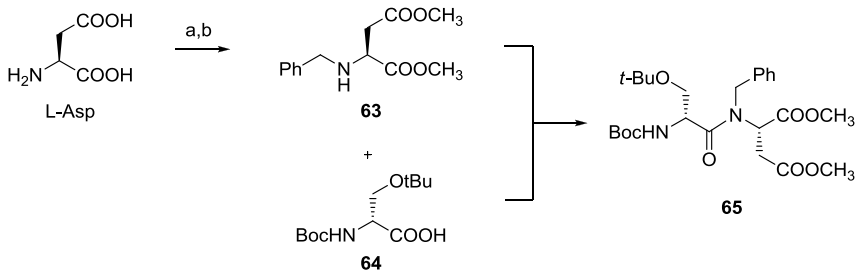

Scheme 2.15 - a) CH_3COCl, CH_3OH: 99%; b) $NaBH_3CN$, PhCHO, CH_3OH: 67%.

Coupling the two aminoacidic fragments **63** and **64** proved to be very challenging: the secondary nitrogen of Asp that should act as the nucleophile is very hindered and, moreover, serine carboxylic group is hindered as well, due to the two surrounding *t*Bu groups. The use of classical aminoacid coupling agents, such as HATU, DPPA, PyBrOP (reported to be very useful in the coupling of *N*-methyl aminoacids),[41] was attempted first, nevertheless not providing desired dipeptide **65** (curiously, reaction with PyBrOP provided a pyrrolidine serine derivative in good yield) (Scheme 2.16).

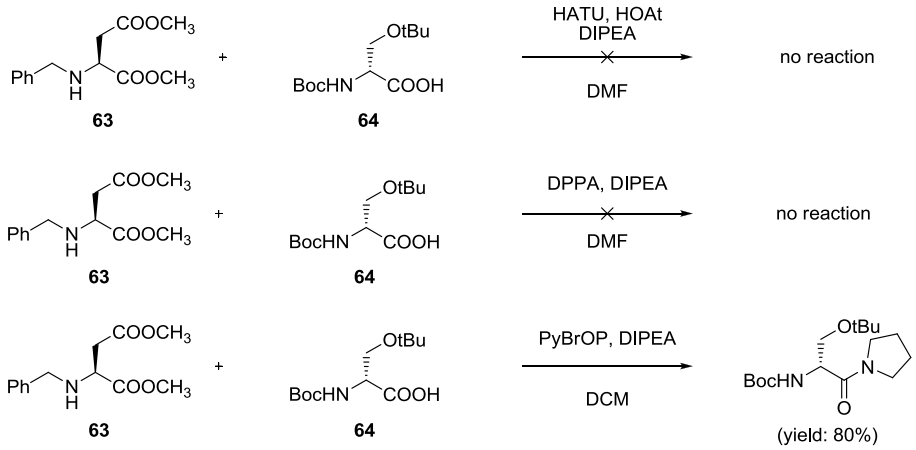

Scheme 2.16

Other methods envisaging carboxyl activation *via N*-carboxyl anhydride (NCAs) derivatives were employed.[42] Original procedures prompted the treatment of the aminoacid with unprotected carboxy functionality with phosgene. Milder reactants, such as diphosgene ($ClCO_2CCl_3$) or chlorosilanes (such as Cl_2SiMe_2, were later developed to generate an NCA derivative (these compounds generate silylated NCA derivatives). We attempted to use both of these mild methodologies to generate NCA activated derivatives of H-D-Ser(tBu)-OH (Fluorochem™). Unfortunately, only reaction with dimethylchlorosilane led to the NCA-like compound. Also this kind of activation did not prove anyway strong enough to induce dipeptide formation when reacted with nucleophile **63** (Scheme 2.17).

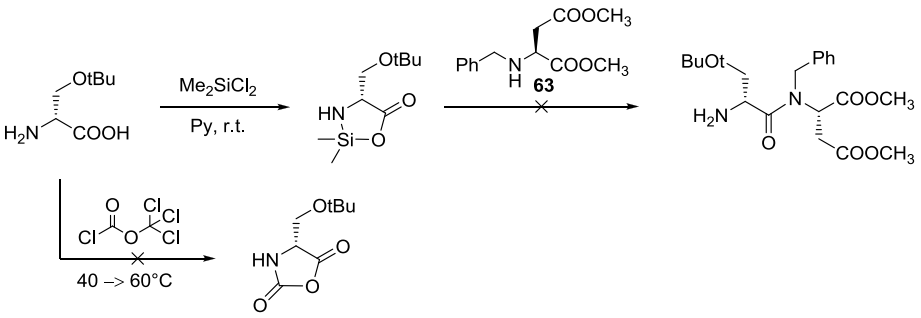

Scheme 2.17

During the '90s, Carpino et al. introduced the use of aminoacid fluorides as active species for coupling.[43] The *pKa* value of hydrogen fluoride, which is generated as a byproduct during the coupling reaction, is far higher than those of hydrogen chloride or bromide, thus allowing this procedure to be compatible with acid labile protective groups (e.g.: -Boc). The acyl fluoride derivative of **64** was prepared in crystalline form using cyanuric fluoride and was subjected to reaction with compound **63**, without previous purification: isolated yield after workup and chromatography purification was extremely low (only 10%) (Scheme 2.18).

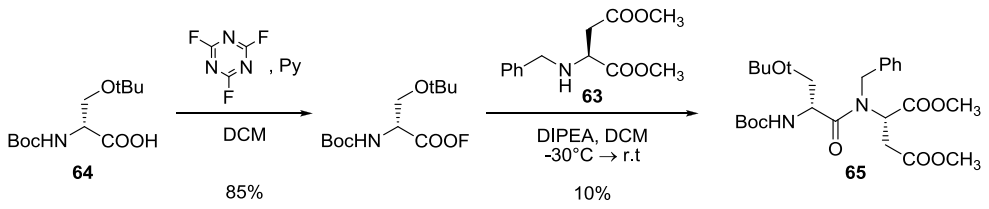

Scheme 2.18

We made two last coupling attempts, activating Ser as its mixed and symmetric anhydrides.[44] The mixed anhydride of compound **64**, obtained after reaction with isobutylchloroformate (IBCF), was made to react in a one-pot procedure with aspartic derivative **63**. The nucleophile preferentially attacked on the wrong carbonyl carbon of the mixed anhydride (probably due to steric factors), leading to a carbamate that regenerated aspartic derivative **63** after workup (Scheme 2.19).

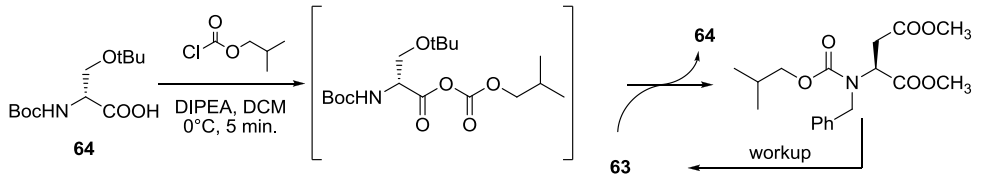

Scheme 2.19

Finally, the symmetric anhydride of the serine derivative, generated from DCC, gave the desired results. Of course, the coupling procedure needed an extensive synthetic set up to avoid starting material waste and to improve yields. The symmetric anhydride was promptly separated from its byproduct, DCU, in order to prevent the formation of a useless acylated derivative of **64** derived from the condensation between them (Scheme 35). Being DCU mostly insoluble in dichloromethane, the symmetric anhydride could be isolated by filtration. Reaction between the symmetric anhydride and aspartic derivative **63** led at last to the desired dipeptide **65**. Furthermore, almost the whole unreacted serine **64**, resulting from the breakdown of the symmetric anhydride, was recovered during workup (Scheme 2.20).

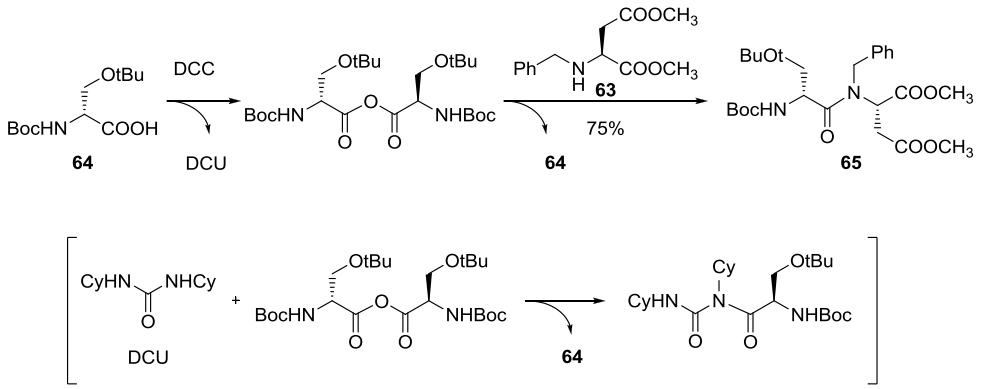

Scheme 2.20

Treatment of dipeptide **65** with trifluoroacetic acid (to deprotect both the amino and the hydroxy group of serine) and subsequent ring closing reaction in methanol, led to diketopiperazine **62a** (Scheme 2.21).

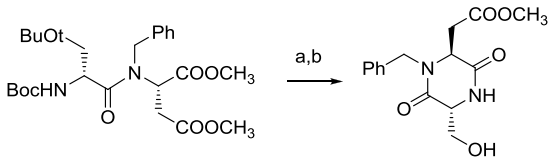

65 **62a**

Scheme 2.21 - a) TFA/DCM; b) MeOH, DIPEA, 85%.

Planning to transform hydroxy group of **62a** in protected amino group, we ran Mitsunobu reaction under the same conditions used for the synthesis of scaffolds **DKP1**-**DKP3** (toluene/DCM, -20 °C), but we only recovered starting material. Hence we tried to run the reaction again increasing temperature gradually, from -20 °C to 0 °C, without any results. Finally, Mitsunobu reaction performed at r.t. led to azide **66**, although major product resulted to be the β-elimination derivative **67** (ratio **66**/**67** 2:3) (Scheme 2.22).

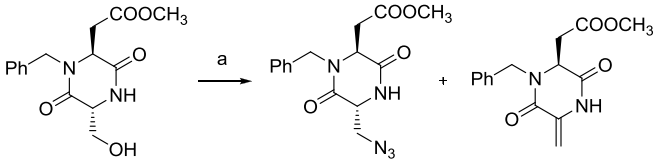

62a **66** **67**

Scheme 2.22 – a) PPh_3, DIAD, HN_3·Tol, toluene/DCM, r.t.

At this point, aiming at scaling up the syntheses of both **DKP4** and **DKP6**, we realized that we might try to circumvent the problem of β-elimination, by performing the Mitsunobu reaction on Boc-Ser-OMe (either L or D) (**68**), thus directly transforming the Ser OH group into the azide. This could also contribute to simplify the synthetic sequence avoiding the use of an additional protecting group (*t*Bu).

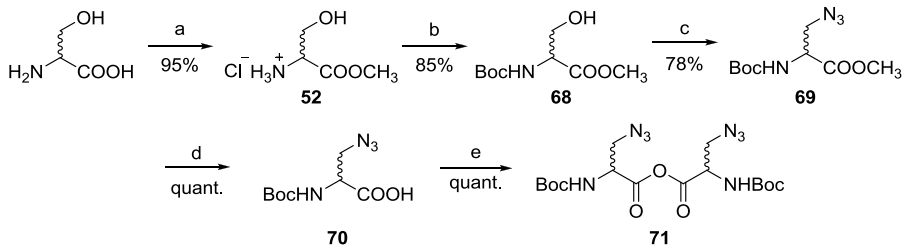

Scheme 2.23 - Synthesis of symmetric anhydrides **71**: a) CH_3COCl, CH_3OH; b) Boc_2O, THF/H_2O 1:1; c) HN_3, DIAD, PPh_3, THF; d) LiOH, THF/H_2O 1:1; e) DCC, DCM.

The Mitsunobu reaction with HN_3 proceeded uneventfully in good yield (78%) to give compound **69**, which was then saponified with LiOH. Treatment of freshly prepared acid **70** with DCC afforded the

symmetric anhydride **71** in a quantitative yield, which was isolated by filtering off DCU and evaporating the solvent, and immediately used in the next synthetic step without further purification (Scheme 2.23).

Coupling of 3-azido-2-*N*-*tert*-butoxycarbonylaminopropionic anhydride (**71**) to either (*S*)- or (*R*)- *N*-benzyl-aspartic acid dimethylester occurred in 80% yield, while the subsequent Boc cleavage and cyclization to diketopiperazines **66** were nearly quantitative (Scheme 2.24).

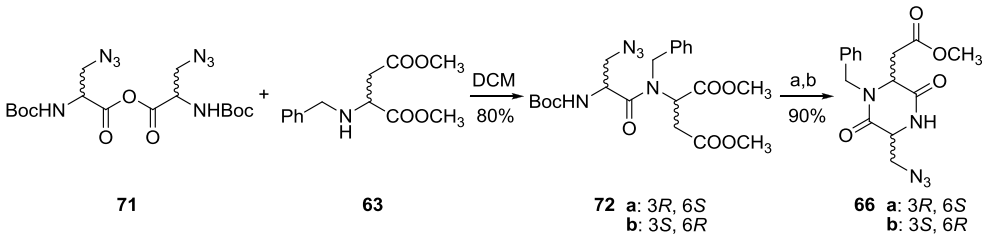

Scheme 2.24 - Synthesis of diketopiperazines **66**: a) TFA/DCM 1:2; b) DIPEA, *i*PrOH.

The same Staudinger-type reaction used for the synthesis of **DKP1-DKP3** (see § 4.2.1, in this chapter) could be employed to reduce azides **66**. Moreover, the absence, in this case, of an allyl ester, allowed us to use the more reliable catalytic hydrogenation, which provides amine **74**, followed by a Boc protection, obtaining compound **75**. A final hydrolysis of the methyl ester provided diketopiperazines **DKP4** and **DKP6** in 90% overall yield (Scheme 2.25).

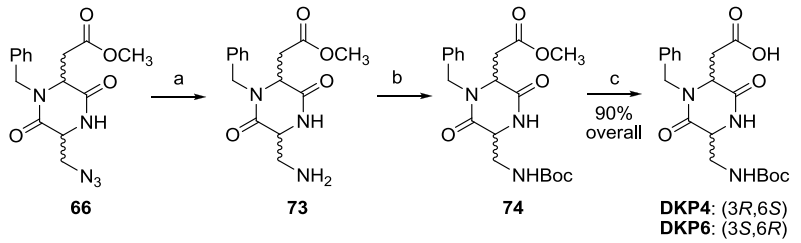

Scheme 2.25 - Synthesis of **DKP4** and **DKP6**: a) H_2, Pd-C, THF; b) Boc_2O, THF; c) LiOH, THF/H_2O 1:1.

3.2.3 - *Synthesis of **DKP5** and **DKP7***

The synthesis of scaffolds **DKP5** and **DKP7** can in principle be achieved through the benzylation of the second diketopiperazine nitrogen of an advanced intermediate in the synthesis of either **DKP2** and **DKP4**, or **DKP3** and **DKP6**, respectively (Figure 2.29). Aiming at minimizing the use of protecting groups, the only suitable intermediate for a nitrogen alkylation was identified in the azide derivative. The diketopiperazine intermediates bearing a free hydroxyl group or a Boc protected amino functionality could in fact give over-alkylated by-products. The azido group might serve as a protecting group here, being stable in the reaction conditions.

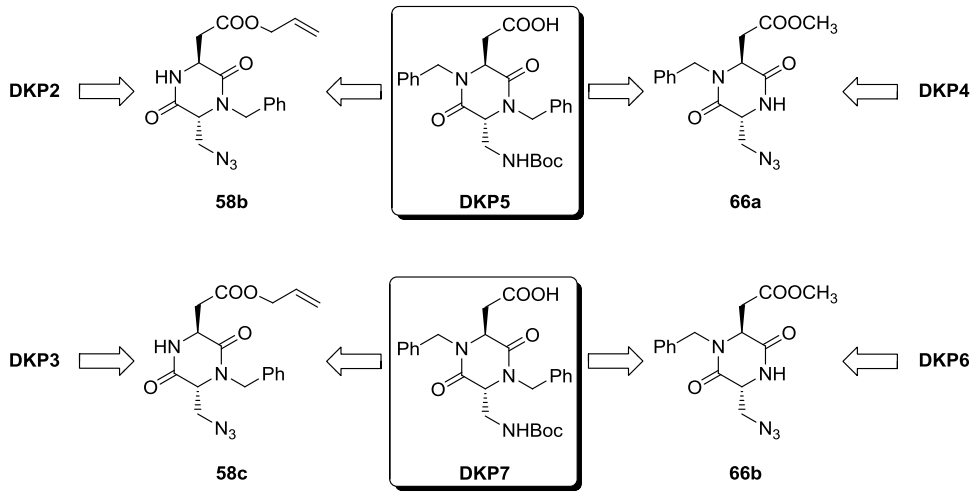

Figure 2.29

As we had intermediates **58b-c** available, we started to investigate *N*-benzylation on these substrates. Nitrogen N-4 alkylation was first attempted using sodium hydride and benzyl bromide in dimethylformamide. This typical experimental procedure generally provides good yields for amide benzylation but, unfortunately, our major product proved to be an elimination derivative (compounds **60a-b**, Scheme 2.10). $-N_3$ acted as leaving group in presence of a strong non-hindered base, such as NaH. Better results were obtained using KHMDS (potassium bis(trimethylsilyl)amide), being a more hindered base, in presence of benzyl bromide, lowering temperature of reaction between -70°C and -40°C. Azides **75** were converted into **DKP5** and **DKP7** following the same protocols used in the synthesis of **DKP2** and **DKP3**; namely, a Staudinger reduction provided *N*-Boc protected amine **76**, which underwent a Tsuji-Trost-like ester deallylation (Scheme 2.26).

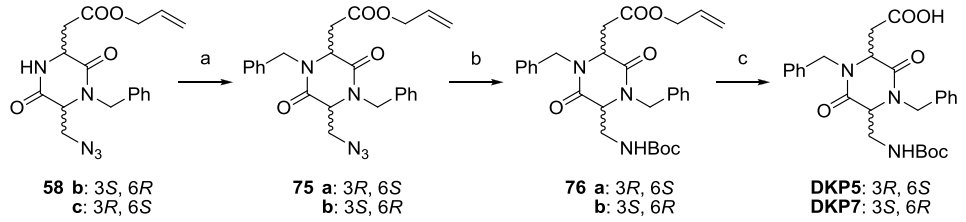

Scheme 2.26 – Synthesis of **DKP5** and **DKP7**, starting from intermediates **58b** and **58c**, respectively: a) KHMDS, BnBr, THF/DMF 7:3, 76%; b) Me_3P, BocON, toluene, 65%; c) pyrrolidine, PPh_3, $[Pd(PPh_3)_4]$, DCM.

Intermediates **66a-b** resulted even less prone to β-elimination under *N*-alkylation conditions. Azides **77** are catalytically hydrogenated to the corresponding amines, which could be easily Boc protected (**78**). Methyl ester hydrolysis finally afforded the desired products (Scheme 2.27).

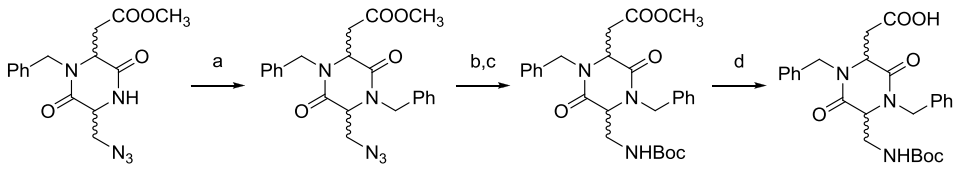

66 a: 3*R*, 6*S* **b**: 3*S*, 6*R* **77 a**: 3*R*, 6*S* **b**: 3*S*, 6*R* **78 a**: 3*R*, 6*S* **b**: 3*S*, 6*R* **DKP5**: 3*R*, 6*S* **DKP7**: 3*S*, 6*R*

Scheme 2.27 - Synthesis of **DKP5** and **DKP7**, starting from intermediates **66a** and **66b**, respectively: a) KHMDS, BnBr, THF/DMF 7:3; b)) Me_3P, BocON, toluene, 87%; c) LiOH, THF/H_2O 1:1; 75% overall.

This last approach seems to be slightly better than the previous one, even if the two methods are reliable enough to be considered equivalent.

3.2.4 - *Synthesis of **DKP8***

Scaffold **DKP-8**, bearing a carboxyethyl side chain, was obtained through a synthetic strategy similar to the one adopted in the case of compounds **DKP1-DKP3** (see § 4.2.1, in this Chapter), starting from (*S*)-*N*-benzylserine methyl ester **53** (Scheme 2.2) and (*R*)-*N*-(*tert*-butoxycarbonyl)glutamic acid γ-methyl ester **79**.[45] In this case too, direct coupling of these fragments afforded isopeptide **80**, which was deprotected and cyclized to diketopiperazine **81**. Azidation of the -CH_2OH group *via* a Mitsunobu reaction, reduction by catalytic hydrogenation, protection with Boc_2O and final hydrolysis of the methylester afforded **DKP-8** (Scheme 2.28).

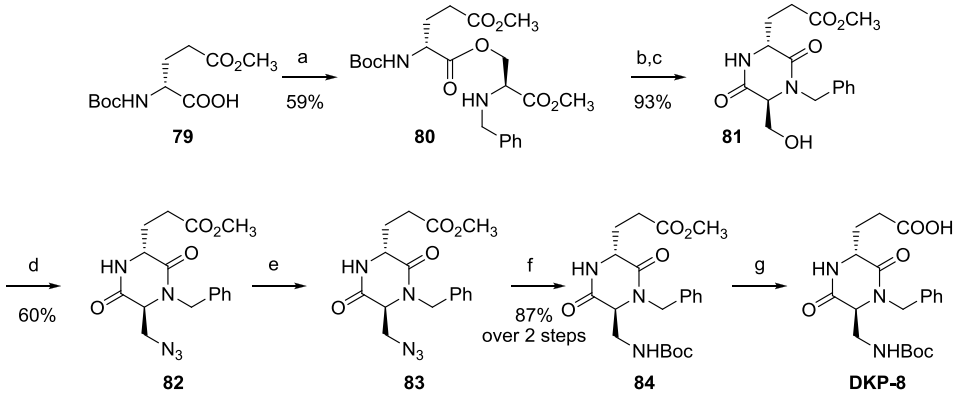

79 **80** **81** **82** **83** **84** **DKP-8**

Scheme 2.28 – a) **53**, HATU, HOAt, DIPEA, DMF; b) TFA/CH_2Cl_2 1:2; c) DIPEA, *i*PrOH; d) HN_3, DIAD, PPh_3, CH_2Cl_2/toluene/DMF; e) H_2, Pd-C, THF; f) Boc_2O, THF; g) LiOH, THF/30% H_2O_2 1:1.

This latest step was at first performed in the conditions already described for the synthesis of **DKP4-DKP7**, treating **84** with LiOH in a 1:1 mixture of THF and water. The reaction did not procede as fast and completely as observed in the other cases and, moreover, extensive racemization problems were detected when **DKP8** thus obtained was used in the synthesis of a macrocyclic peptidomimetic. Hence a milder yet more selective procedure involving the *in situ* formation of LiOOH was adopted. Enantiomerically pure **DKP8** was this time obtained quantitatively.

References:

[1] A. S. M. Ressurreição, R. Delatouche, C. Gennari, U. Piarulli, *Eur. J. Org. Chem.* **2011**, 217-228.

[2] H. Wennemers, M. Conza, M. Nold, P. Krattiger, *Chem. Eur. J.* **2001**, *7*, 3342-3347.

[3] M. Conza, H. Wennemers, *J. Org. Chem.* **2002**, *67*, 2696-2698.

[4] a) M. H. J. Ohlmeyer, R. N. Swanson, L. W. Dillard, J. C. Reader, G. Asouline, R. Kobayashi, M. H. Wigler, W. C. Still, Proc. *Natl. Acad. Sci. USA* **1993**, **90**, 10922-10926; b) H. P. Nestler, P. Bartlett, W. C. Still, *J. Org. Chem.* **1994**, *59*, 4723-4724.

[5] P. Krattiger, H. Wennemers, *Synlett* **2005**, 706-708.

[6] C. F. J. Paul, P. Krattigger, B. M. Smarsky, H. Wennemers, *J. Mater. Chem.* **2008**, *18*, 2962-2967.

[7] J. Bernard, H. Wennemers, *Org. Lett.* **2007**, *9*, 4283-4286.

[8] J. V. Carolan, S. J. Butler, K. A. Jolliffe, *J. Org. Chem.* **2009**, *74*, 2992-2296.

[9] K. Burgess, *Acc. Chem. Res.* **2001**, *34*, 826-835.

[10] A. Golebiowski, S. R. Klopfenstein, J. J. Chen, X. Shao, *Tetrahedron Lett.* **2000**, *41*, 4841-4844.

[11] A. Golebiowski, S. R. Klopfenstein, X. Shao, J. J. Chen, A. O. Colson, A. L. Grieb, A. F. Russell, *Org. Lett.* **2000**, 2, 2615-2617.

[12] A. Golebiowski, J. Jozwik, S. R. Klopfenstein, A. O. Colson, A. L. Grieb, A. F. Russell, V. L. Rastogi, C. F. Diven, D. E. Portlock, J. J. Chen, *J. Comb. Chem.* **2002**, *4*, 584-590.

[13] H.-O. Kim, H. Nakanishi, M. S. Lee, M. Kahn, *Org. Lett.* **2000**, *2*, 301-302.

[14] V. N. Belov, C. Funke, T. Labahn, M. Es-Sayed, A. de Meijere, *Eur. J. Org. Chem.* **1999**, 1345-1356.

[15] A. Mieczkowski, W. Kozminski, J. Jurczak, *Synthesis* **2010**, 221-232.

[16] J. Liu, F. Brahimi, H. U. Saragovi, K. Burgess, *J. Med. Chem.* **2010**, *53*, 5044-5048.

[17] J. A. Robinson, *Acc. Chem. Res.* **2008**, *41*, 1278-1288.

[18] G. Gellerman, E. Hazan, T. Brider, T. Traube, A. Albeck, S. Shatzmiler, *Int. J. Pept. Res. Ther.* **2008**, *14*, 183-192.

[19] G. Gellerman, E. Hazana, M. Kovaliov, A. Albeck, S. Shatuniler, *Tetrahedron* **2009**, *65*, 1389-1396.

[20] J. S. Davies, M. Stelmach-Diddams, R. Fromentin, A. Howells, R. Cotton, *J. Chem. Soc., Perkin Trans. 1* **2000**, 239-243.

[21] C. Bisang, C. Weber, J. A. Robinson, *Helv. Chim. Acta* **1996**, *79*, 1825–1842.

[22] F. Emery, C. Bisang, M. Favre, L. Jiang, J. A. Robinson, *Chem. Commun.* **1996**, 2155–2156.

[23] C. Bisang, L. Jiang, E. Freund, F. Emery, C. Bauch, H. Matile, G. Pluschke, J. A. Robinson, *J. Am. Chem. Soc.* **1998**, *120*, 7439–7449.

[24] M. E. Pfeifer, A. Linden, J. A. Robinson, *Helv. Chim. Acta* **1997**, *80*, 1513–1527.

[25] R. Beeli, M. Steger, A. Linden, J. A. Robinson, *Helv. Chim. Acta* **1996**, *79*, 2235–2248.

[26] a) M. E. Pfeifer, J. A. Robinson, *Chem. Commun.* **1998**, 1977–1978; b) M. E. Pfeifer, K. Moehle, A. Linden, J. A. Robinson, *Helv. Chim. Acta* **2000**, *83*, 444–464.

[27] M. Royo, W. Van den Nest, M. del Fresno, A. Frieden, D. Yahalom, M. Rosenblatt, M. Chorev, F. Albericio, *Tetrahedron Lett.* **2001**, *42*, 7387–7391.

[28] C. E. Schafmeister, Z. Z. Brown, S. Gupta, *Acc. Chem. Res.* **2008**, *41*, 1387-1398.

[29] C. G. Levins, C. E. Schafmeister, *J. Am. Chem. Soc.* **2003**, *125*, 4702-4703.

[30] Z. Z. Brown, C. E. Schafmeister, *Org. Lett.* **2010**, *12*, 1436-1439.

[31] A. S. M. Ressurreicao, A. Bordessa, M. Civera, L. Belvisi, C. Gennari, U. Piarulli, *J. Org. Chem.* **2008**, *73*, 652-660.

[32] The superscripted number after β specifies the position of the side chain on the corresponding β-amino acid, see: T. Hintermann, D. Seebach, *Synlett* **1997**, 437-438.

[33] R. Delatouche, M. Durini, M. Civera, L. Belvisi, U. Piarulli, Tetrahedron Lett. **2010**, *51*, 4278-4280.

[34] A. S. M. Ressurreicao, A. Vidu, M. Civera, L. Belvisi, D. Potenza, L. Manzoni, S. Ongeri, C. Gennari, U. Piarulli, *Chem.-Eur. J.* **2009**, *15*, 12184–12188.

[35] K. L. Webster, A. B. Maude, M. E. O'Donnell, A. P. Mehrotra, D. Gani, *J. Chem. Soc., Perkin Trans. 1* **2001**, 1673-1695.

[36] C. M. Thompson, J. A. Frick, D. L. C. Green, *J. Org. Chem.* **1990**, *55*, 111-116.

[37] M. Marchini, M. Mingozzi, R. Colombo, C. Gennari, M. Durini, U. Piarulli, *Tetrahedron* **2010**, *51*, 4278–4280.

[38] O. Mitsunobu, Y. Yamada, *Bull. Chem. Soc. Japan* **1967**, *40*, 2380-2382.

[39] X. Ariza, F. Urpí, C. Viladomat, J. Vilarrasa, *Tetrahedron Lett.* **1998**, *39*, 9101-9102.

[40] C. David, L. Bischoff, H. Meudal, A. Mothé, N. De Mota, S. DaNascimento, C. Llorens-Cortes, M.-C. Fournié-Zaluski, B. P. Roques, *J. Med. Chem.* **1999**, *42*, 5197-5211.

[41] J. Coste, E. Frerot, P. Jouin, *J. Org. Chem.* **1994**, *59*, 2437-2446.

[42] J. A. Fehrentz, C. G. Dellac, M. Amblard, F. Winternitz, A. Loffet, J. Martinez, *J. Pept. Sci.* **1995**, *1*, 124–131.

[43] L. A. Carpino, E.-S. M. E. Mansour, D. Sadat-Aalaee, *J. Org. Chem.* **1991**, *56*, 2611-2614.

[44] a) R. G. Denkewalter, *J.Am.Chem.Soc.* **1966**, *88*, 3163-3164; b) K. Jensen, J. Alsina, M. F. Songster, J. Vagner, F. Albericio, G. Barany, *J.Am.Chem.Soc.* **1998**, *120*, 5441 5452.

[45] V. Bavetsias, A. L. Jackman, R. Kimbell, W. Gibson, F. T. Boyle, G. M. F. Bisset, *J. Med. Chem.* **1996**, *39*, 73-85.

3 SYNTHESIS AND CONFORMATIONAL ANALYSIS OF PEPTIDOMIMETICS CONTAINING A BIFUNCTIONAL DIKETOPIPERAZINE SCAFFOLD, AS INTEGRIN LIGANDS

1 - Targeting Integrins

Integrins are the major family of adhesion receptors known in the kingdom Animalia, being involved in cell adhesion to extracellular matrix proteins and also playing important roles, in vertebrates, in certain cell-cell adhesions. In addition to mediating cell adhesion, integrins make transmembrane connections to the cytoskeleton and activate many intracellular signaling pathways. Since the recognition of the integrin receptor family around 20 years ago,[1] they have become the best-understood cell adhesion receptors. Integrins and their ligands play key roles in the pathogenesis of inflammatory disease, leukocyte traffic, aggregation, tumor progression as well as osteoporosis and macular degeneration. The role of integrins in pathological conditions makes them attractive pharmacological targets.[2]

Research in the last two decades has been directed to the discovery and the development of integrin antagonists for clinical applications.[3] The early discovery of the structural basis of the recognition between integrins and their natural ligands by means of short amino acid sequences,[4] together with outstanding crystallographic, electron microscopy, and computational analyses[5,6] on selected integrin subfamilies provided a breakthrough for the rational design of a wide variety of class-selective or promiscuous integrin inhibitors.

1.1 - Integrins: family, function, structure

Integrins are heterodimeric membrane glycoproteins comprised non-covalently associated α- and β-subunits, mediating dynamic linkages between extracellular adhesion molecules and the intracellular actin cytoskeleton. They are expressed by all multicellular animals, but their diversity varies widely among species; for example, 19 α and 8 β subunit genes are present in mammals, encoding for 25 different heterodimers, whereas the Drosophila and Caenorhabditis genomes encode only five and two integrin α and β subunits respectively.

Each integrin subunit consists of an extracellular domain, a single transmembrane region, and a short (~30–40 amino acids) cytoplasmic region. Figure 3.1 depicts the mammalian subunits and their αβ associations; 8 β subunits can assort with 18 α subunits to form 24 distinct integrins.[7]

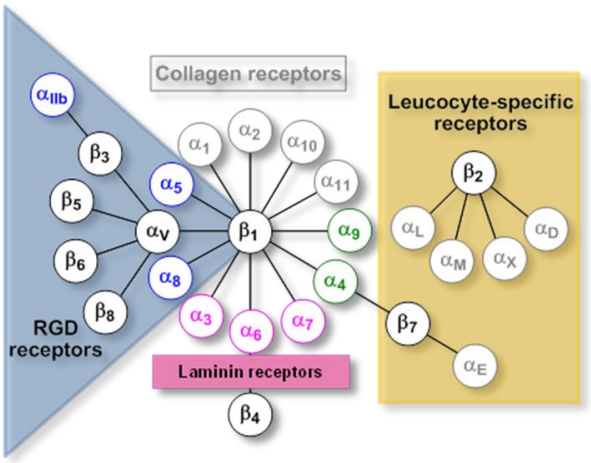

Figure 3.1

Each integrin subunit consists of an extracellular domain, a single transmembrane region, and a short (~30–40 amino acids) cytoplasmic region.

The N-terminus of the α-chain consists of a β-propeller domain that is formed by seven repeats of 60 amino acids each.[8] The β-propeller domain is linked to the transmembrane domain by three regions that have been named the Thigh, Calf-1, and Calf-2 domains (Figure 3.2 a). In addition, a highly flexible region is present between the Thigh and Calf-1 domains.5 Half of all α-chains have an additional 200 amino acid inserted domain between repeats two and three of the β- propeller (the I-domain) (Figure 3.2 a).[9] The I-domain functions as the major ligand-binding site in those integrins with this domain, whereas the β-propeller serves as the ligand binding in integrins without I-domains.[10] Cytoplasmic tail domains of individual α-subunits are well-conserved across species boundaries.[11]

The N-terminal region of the β-subunit consists of a cysteine-rich region termed the plexin-semaphorin-integrin (PSI) domain. C-terminal to this domain is an evolutionarily conserved I-like domain flanked on either side by immunoglobulin folds called hybrid domains. The membrane proximal region of the α-subunit contains four EGF-like repeats. The α-subunit also has a flexible "knee" region, which is formed by the hybrid domain and the first two EGF-like repeats (Figure 3.2 b).[10] The intracellular regions of the β-subunits are more conserved between subunits than are the α-subunit cytoplasmic tails.[12] These beta chain cytoplasmic tails play significant roles in regulating integrin activity.[5b]

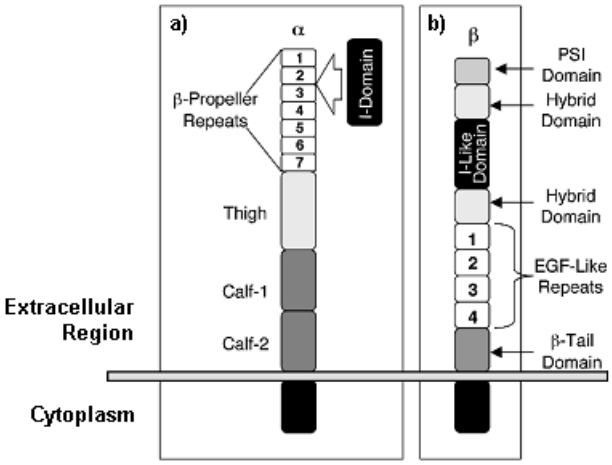

Figure 3.2 - Integrin structure: (**a**) Primary structure of integrin α-subunits. Half of the α-subunits also have an I-domain inserted between β-propeller repeats 2 and 3; (**b**) Primary structure of integrin β-subunits.

Each α-chain combines with a β-chain to form a unique heterodimer with selectivity for ECM proteins, cell surface molecules, plasma proteins, or microorganisms.[13] Integrins bind to their ligands in a divalent cation-dependent fashion.[14] Although some integrins recognize primarily a single ECM protein ligand (e.g., $\alpha_5\beta_1$ recognizes primarily fibronectin), others can bind several ligands (e.g., integrin $\alpha_v\beta_3$ binds vitronectin, fibronectin, fibrinogen, denatured or proteolyzed collagen, and other matrix proteins). Many integrins recognize the tripeptide Arg–Gly–Asp (RGD) (e.g. $\alpha_v\beta_3$, $\alpha_5\beta_1$, $\alpha_{IIb}\beta_3$, $\alpha_v\beta_6$, and $\alpha_3\beta_1$), but sequences flanking the RGD peptide are also important for selectivity.[13a,b] Other integrins recognize alternative short peptide sequences (e.g., integrin $\alpha_4\beta_1$ recognizes Glu lle Leu Asp Val (EILDV) and Arg Glu Asp Val (REDV) in alternatively spliced CS-1 fibronectin and $\alpha_{IIb}\beta_3$ binds KQAGDV in the fibrinogen γ chain).[15] In addition, some integrins can also bind cell surface receptors to induce cell–cell adhesion.[13b,c]

The ligands bound by common integrins and their recognition sites are shown in Table 3.1.[16]

Table 3.1 - Integrin ligands and recognition sequences

Integrin	***Ligands (recognition sequences)***
$\alpha_1\beta_1$	Collagen (GFOGER, fibrillar collagen domain) and laminin
$\alpha_2\beta_1$	Collagen (GFOGER, fibrillar collagen domain), laminin, and $\alpha_3\beta_1$
$\alpha_3\beta_1$	Fibronectin (RGD), collagen, laminin, epiligrin, entactin, and $\alpha_2\beta_1$
$\alpha_4\beta_1$	CS-1 fibronectin (EILDV) and VCAM-1 (QIDS)
$\alpha_5\beta_1$	Fibronectin (RGD), fibrinogen (RGD), and L1-CAM
$\alpha_6\beta_1$	Laminin (several sites), merosin, and Kalinin
$\alpha_7\beta_1$	Laminin
$\alpha_8\beta_1$	Fibronectin (RGD) and tenascin
$\alpha_9\beta_1$	Tenascin (AEIDGIEL), collagen, and laminin
$\alpha_{10}\beta_1$	Collagen
$\alpha_{11}\beta_1$	Collagen
$\alpha_L\beta_2$	ICAM-1, ICAM-2, and ICAM-3 (ICAM peptides)
$\alpha_M\beta_2$	iC3b, fibrinogen (P1 and P2 peptide in γ-chain), factor X, and ICAM-1 (ICAM peptides)
$\alpha_X\beta_2$	iC3b and fibrinogen (GPR in α-chain)
$\alpha_D\beta_2$	ICAM-3 and VCAM-1
$\alpha_v\beta_1$	Fibronectin (RGD) and vitronectin (RGD) Fibronectin (RGD), vitronectin (RGD), von Willebrand Factor (RGD dependent),
$\alpha_v\beta_3$	thrombospondin (Cryptic RGD site), tenascin (RGD), Del-1 (RGD), osteopontin (RGD), MMP2 (PEX domain), and bFGF (DGR)

$\alpha_v\beta_5$	Vitronectin (RGD and KKQRFRHRNRKG), osteopontin, and Del-1 (RGD)
$\alpha_v\beta_6$	Fibronectin (RGD) and tenascin (DLXXL)
$\alpha_v\beta_8$	Collagen, laminin, and fibronectin
$\alpha_{IIb}\beta_3$	Fibronectin (RGD), Fibrinogen (KQAGDV), vitronectin (RGD), and von Willebrand factor (RGD)
$\alpha_6\beta_4$	Laminin (several sites)
$\alpha_4\beta_7$	CS-1 fibronectin, VCAM-1, and MAdCAM-1 (LDT)
$\alpha_E\beta_7$	E-Cadherin

Integrins are not constitutively active, but rather exist in multiple activation states (Figure 3.3).[17] Integrin activation status is regulated by the delicate balance in a bidirectional signaling mechanism which drives reversible changes in integrin conformation and affinity for their ligands. Both extra- and intracellular stimuli are allowed to regulate activation.[7,18]

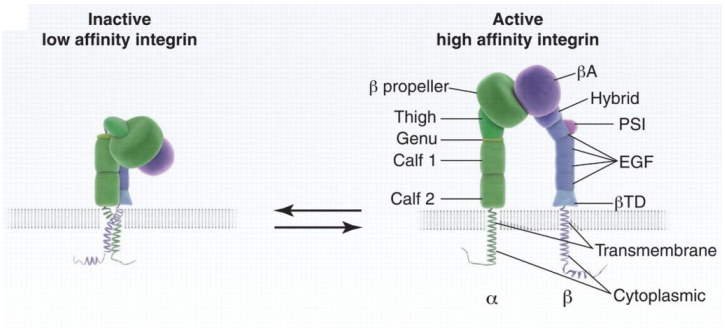

Figure 3.3 – representation of integrin activation states.

High affinity binding of integrins to ligands is promted in response to intracellular signaling events converging on the cytoplasmic domain that alter the tertiary and quaternary structure of the extracellular region, making the integrin ligand-competent (inside-out signaling).

Extracellular factors that influence integrin activation are ligand binding, divalent cation concentration, chemokine signaling and mechanical stress. Integrins transmit signals to the cell interior, which regulate organization of the cytoskeleton, activate kinase signaling cascades, and modulate the cell cycle and gene expression (outside-in signaling). Through this mechanism, integrins behave as mechanochemical transducers, orchestrating a synergic cross-talk with other extracellular matrix constituents and providing anchorage for endothelial cells.

The integrin tails serve as a site for the docking of various kinases and related adaptor proteins that comprise focal adhesions. Signals emanating from focal adhesions have been shown to promote survival, differentiation and proliferation.[19] In the absence of integrin ligation, these processes are abrogated therefore pharmacological inhibition of integrin ligation is of great interest for the therapy of numerous diseases resulting from abberant integrin mediated signaling.

Integrins are transducing information both into and out of the cell to promote cell adhesion, spreading and motility. Disruption of focal adhesions prevents integrin mediated cell adhesion and impaired cell motility and migration. Prolonged integrin inhibition in adhesion dependent cells results in anoikis, apoptotic cell death due to ECM deprivation.[20]

1.2 - Role in Angiogenesis

Angiogenesis is the process whereby new vessels form from pre-existing vessels. The growth of new blood vessels promotes embryonic development, wound healing, the female reproductive cycle, and also plays a key role in the pathological development of solid tumor cancers, hemangiomas, diabetic retinopathy, age-related macular degeneration, psoriasis, gingivitis, rheumatoid arthritis, and possibly osteoarthritis and inflammatory bowel disease.[21]

Several cell types within tumors, including tumor cells, monocytes, and fibroblasts, secrete growth factors, such as VEGF, that induce blood vessel growth into tumors (Figure 3.4).[22]

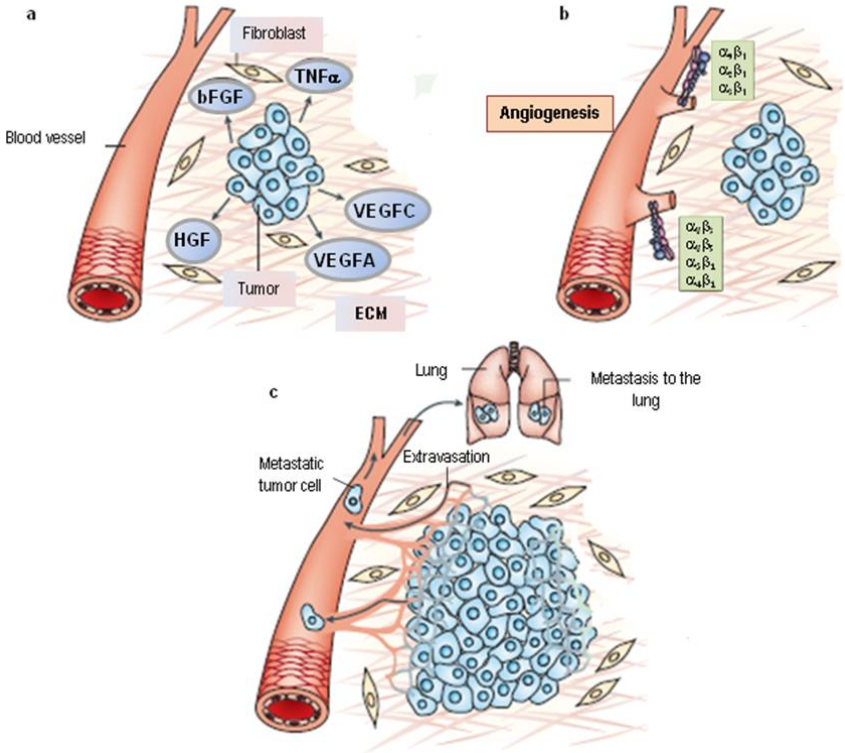

Figure 3.4 – a) Secretion of growth factors and Chemokines from tumor cells in vicinity of already existing blood vessels; b) activation or expression upregulation of integrins such as $\alpha_1\beta_1$, $\alpha_2\beta_1$, $\alpha_4\beta_1$, $\alpha_5\beta_1$ and $\alpha_V\beta_3$ on blood vessels; c) integrins promoting endothelial cell migration and survival during invasion of tumour tissue. New vessel sprouts are produced promoting tumour growth and providing a way to metastasis to local and distant sites, such as lung.

Studies have shown that angiogenesis plays a major role in tumor growth and that inhibiting angiogenesis can inhibit tumor progression and metastasis. Although growth factors and their receptors play key roles in angiogenic sprouting, adhesion to the ECM also regulates angiogenesis.

Formation of new vasculature requires endothelial cell attachment and migration on ECM proteins. One ECM protein, fibronectin is associated with vascular proliferation.[23] As integrins are critical for the cell to bind ECM, many integrins play crucial roles in regulating vascular growth, both during

embryonic development and in various pathologies. Proliferating endothelial cells express several integrins that are not expressed on quiescent blood vessels.

Recent studies suggest that inhibition of both $\alpha_v\beta_3$ and $\alpha_5\beta_1$ may be required for optimal effects on angiogenesis.[24]

1.2.1 - *Integrins $\alpha_v\beta_3$ and $\alpha_v\beta_5$*

Integrin $\alpha_v\beta_3$ is expressed on angiogenic blood vessels[25] but not on resting vessels. Inhibitors of $\alpha_v\beta_3$ antibody block angiogenesis in a variety of animal models. A key role of $\alpha_v\beta_3$ in vasculogenesis and angiogenesis has been outlined. Peptide and antibody antagonists of $\alpha_v\beta_3$ also block tumor angiogenesis and growth. Further analysis showed tumor regression related to apoptosis in the vasculature, induced by these antagonists.[26]

Different members of the integrin α_v subfamily transduce angiogenic signals by different growth factors. *in vivo* angiogenesis assays showed that bFGF or TNF-α depend on $\alpha_v\beta_3$ to initiate angiogenesis, whereas $\alpha_v\beta_5$ is required for TGF-α- and VEGF-mediated angiogenesis.[27] These data taken together have established a role for $\alpha_v\beta_3$ and $\alpha_v\beta_3$ integrins in angiogenesis and as important therapeutic targets.

One study showed that animals lacking β_3 or β_3 and β_5 subunits displayed increased tumor angiogenesis.[28] This led to the controversial conclusion that $\alpha_v\beta_3/\alpha_v\beta_5$ integrins might actually be involved in suppressing angiogenesis. However, it is likely that the apoptotic mechanism, which is generally induced by unligated integrins and controls tumor vascular growth, is responsible for the increased vascularization in β_3 - and β_5 -deficient tumors.[16,29]

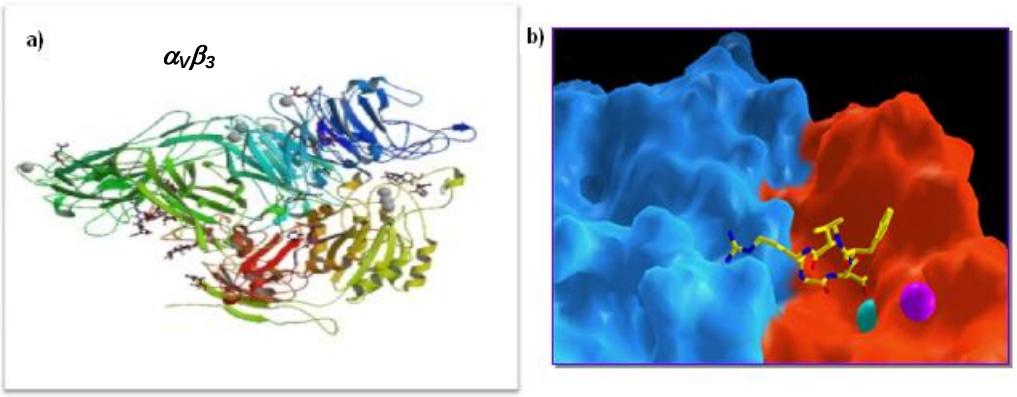

Figure 3.5 – a) Crystal structure of the extracellular segment of integrin $\alpha_V\beta_3$; b) Crystal structure of the extracellular segment of $\alpha_V\beta_3$ integrin in complex with the cyclic pentapeptide ligand Cilengitide, in its binding conformation.

The complete crystal structure of $\alpha_v\beta_3$ integrin ectodomain including an αβ transmembrane fragment has been very recently determined.[30] The earlier determination of the crystal structure of the

ectodomain of $\alpha_v\beta_3$ (ΔTM- $\alpha_v\beta_3$) (Figure 3.5 a) in the absence and presence of a prototypical RGD ligand (Cilengitide) (Figure 3.5 b), already revealed the modular nature of integrins and pivotal information on its divalent cation–mediated binding interactions with extracellular ligands.

A homology model for the closely related $\alpha_V\beta_5$ receptor was developed. The two integrins were found to mostly differ in the region comprising residues 159-188 in the β_3 subunit. A 'roof" was described for $\alpha_V\beta_5$ integrin featuring Tyr and Lys residues, which would hamper the binding of compounds containing bulky substituents nearby their Asp-mimicking group. Because of this difference, a few inhibitors of $\alpha_V\beta_3$ integrin displaying selectivity over $\alpha_V\beta_5$ have actually been found,[31] but specific inhibitors of $\alpha_V\beta_5$ integrins have not been described yet.

1.2.2 - *Integrins $\alpha_5\beta_1$*

Integrin $\alpha_5\beta_1$ is significantly upregulated in tumor angiogenesis in both mice and humans but is not expressed on quiescent endothelium. Antagonists of $\alpha_5\beta_1$ also inhibited tumor angiogenesis in chicks and mice, thus leading to tumor regression. [23]

Integrin $\alpha_5\beta_1$ -mediated adhesion promotes endothelial cell survival *in vivo* and *in vitro*[29] by suppressing the activity of protein kinase A (PKA). Integrin $\alpha_5\beta_1$ antagonists activate both PKA and caspase-8, thereby inducing apoptosis and inhibiting angiogenesis.[32] Although inhibition of integrin ligation can prevent cell attachment to the ECM, recent studies show that integrin $\alpha_5\beta_1$ antagonists also actively suppress signal transduction that leads to cell survival. Antagonists of $\alpha_5\beta_1$ suppress cell migration and survival on vitronectin, but not cell attachment to vitronectin, indicating that these antagonists affect the migration and survival machinery rather than integrin receptors for vitronectin.[16,33]

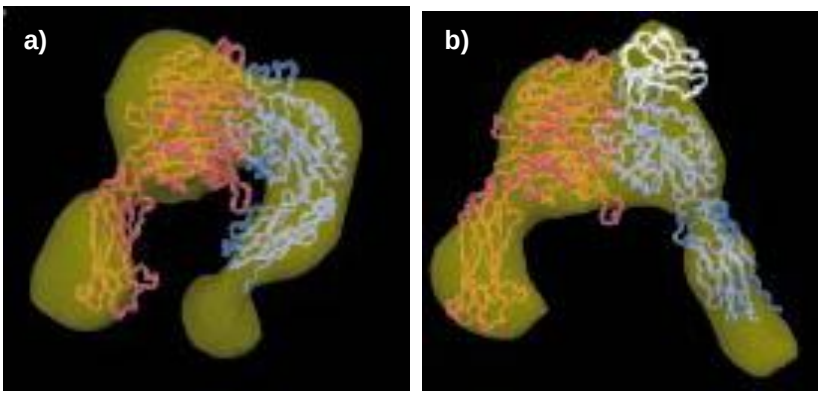

Figure 3.6 - Surface-rendered density maps of the $\alpha_5\beta_1$ headpiece in a) the unliganded closed and b) the ligand-bound open conformation.

The threedimensional structure of the ligand-binding headpiece of integrin $\alpha_5\beta_1$ complexed with fragments of its physiological ligand fibronectin was determined by mean of a molecular electron

microscopy. The density map for the unliganded $\alpha_5\beta_1$ headpiece shows a 'closed' conformation similar to that seen in the $\alpha_V\beta_3$ crystal structure. By contrast, binding to fibronectin induces an 'open' conformation (Figure 3.6).[34]

The lack of reliable structural data in the past, however, excluded $\alpha_5\beta_1$ as target for structure based drug design. However, the high homology between the different integrin subtypes makes them promising targets for homology modeling, which was achieved for $\alpha_V\beta_5$ integrin by Kessler and co-workers.[35,31b] Homology modeling of proteins is considered to be possible for a homology of 40% or greater.[36] This precondition is met by the integrins $\alpha_v\beta_3$ and $\alpha_5\beta_1$ with 53% homology for α_v/α_5 and 55% for β_3/β_1.

1.3 - Role in hemostasis and thrombosis

Thrombosis is a desease-related process consisting in the formation of a blood clot inside a blood vessel. It occurs when platelets adhere to damaged blood vessels and become activated,[37] thus recruiting other platelets. As a result a haemostatic plug is formed. This is an essential mechanism for preventing blood loss, but inappropriate thrombus formation can lead to a stroke or to a heart attack. It is probably the first clearly integrin associated process.

In the 1970s, it was noted that some patients suffering from Glanzmann's thrombasthenia, a known severe bleeding disorder, lacked two functional glycoproteins (GPIIb and GPIIIa) on their blood platelets, which are now known as the integrin $\alpha_{IIb}\beta_3$.[38] It was subsequently found that the platelet–platelet interaction that mediates thrombus formation is facilitated by fibrinogen binding to the platelet-specific integrin $\alpha_{IIb}\beta_3$ following platelet activation caused by thrombotic stimuli.[39,40]

1.3.1 - *Integrins $\alpha_{IIb}\beta_3$*

$\alpha_{IIb}\beta_3$ integrin (GPIIa/IIIb) is highly expressed on the surface of platelets,[41] comprising approximately 80% of the total surface proteins found on platelets. The final common pathway in blood coagulation involves the engagement of this integrin induced by platelet activation. Under normal conditions integrin $\alpha_{IIb}\beta_3$ is maintained in the inactivated state. Soluble factors in the blood such as thrombin, bind their respective platelet receptors to activate inside-out signaling pathways that cause conformational changes in $\alpha_{IIb}\beta_3$ integrin.[41] Changes in conformation lead to increases in receptor affinity and avidity, which promote platelet aggregation and clot formation through increased cell-to-cell contacts and cell-matrix contacts. Aberrant platelet aggregation or thrombosis is central to the pathophysiology of multiple Acute Coronary Syndromes (ACS), unstable angina, ischemic stroke and sickle cell anemia. Inhibition of $\alpha_{IIb}\beta_3$ prevents platelet aggregation and therefore has shown efficacy in the prevention of thrombosis for the treatment of ACS. Some $\alpha_{IIb}\beta_3$ integrin targeted drugs have already been approved so far.

The complete ectodomain structure of integrin $\alpha_{IIb}\beta_3$ was determined,[42] thus living information about its binding site, better understanding its biniding mode and conformation (Figure 3.7). The binding mode of RGD-based $\alpha_{IIb}\beta_3$ antagonists was established through mutagenesis experiments[43] and crystallographic analysis of the platelet fibrinogen receptor.[44]

Figure 3.7 - Crystal structure of the extracellular segment of integrin $\alpha_{IIb}\beta_3$.

1.4 - RGD and isoDGR recognition motifs

The arginine-glycine-aspartic acid (RGD) cell adhesion sequence was discovered in fibronectin 27 years ago.[45] Other adhesion proteins such as vitronectin, fibrinogen, von Willebrand factor, thrombospondin, laminin, entactin, tenascin, osteopontin, bone sialoprotein, and, under some conditions, collagens were then discovered to include RGD sites. It was soon confirmed with regard to fibronectin and then extended to other proteins that the RGD sequence is the endogenous recognition motif for cell attachment to proteins.

Cells expressing several α_V integrins (e.g. β_1, β_3, β_5, β_6 and β_8), as well as integrins $\alpha_{IIb}\beta_3$, $\alpha_5\beta_1$ and $\alpha_8\beta_1$, recognize the ubiquitous RGD sequence in their ligands. Naturally occurring integrin inhibitor proteins bearing the RGD motif are showing an extremely varied selectivity and potency in targeting RGD-recognizing integrins. Elucidations on their structure suggest that proper restriction of the RGD flexibility can lead to integrin inhibition.[46]

Hence, monomeric linear or confomationally constrained RGD-containing cyclic peptides, pseudo-peptides, and mimetics thereof displaying high potency and selectivity were conceived. The most significant advances in this field have led to the development of agents targeting $\alpha_{IIb}\beta_3$ integrin on platelets for inhibiting thrombosis[47] and inhibitors of $\alpha_V\beta_3$ and $\alpha_V\beta_5$ integrins against angiogenesis, cancer and bone resorption.[48] Among these, it is important to recall the nanomolar $\alpha_V\beta_3/\alpha_V\beta_5$ binder cyclic pentapeptide c-RGD-(D-Phe)-N-methyl-V developed by Kessler (known as Cilengitide or

EMD121974, which has recently entered phase III clinical investigation for patients with glioblastoma multiforme).[48j]

As already mentioned, a crucial enhancement in this field was achieved with the crystal structure resolution of the ectodomain of $\alpha_V\beta_3$ integrin, both unligated and complexed with Cilengitide,[5b] as well as the better crystal structure resolution of $\alpha_{IIb}\beta_3$ integrin complexed with the synthetic anti-trombotic drug *Eptifibatide.*[6d,49]

Besides the well defined RGD and other binding motifs, it has been proposed that the NGR and DGR sequences might also have a role in integrin recognition. Controversial results have however been reported.

The importance of the *iso*DGR sequence as an integrin binding motif was discovered by serendipity by Corti research group (S.Raffaele/MolMed).[50]

The NGR sequence, present in several endogenous molecules as well as in fibronectin FN-I_5 and FN-I_7, can easyly deamidate (also *in vivo*) on asparagine, giving *iso*DGR and DGR (Scheme 3.1). Although protein modifications typically causes loss of activity/function, it was recently suggested that *iso*DGR formation at NGR or DGR sites might result in a gain of function. The *iso*DGR sequence can in fact mimic RGD and interact with the RGD-binding site of integrins.[51]

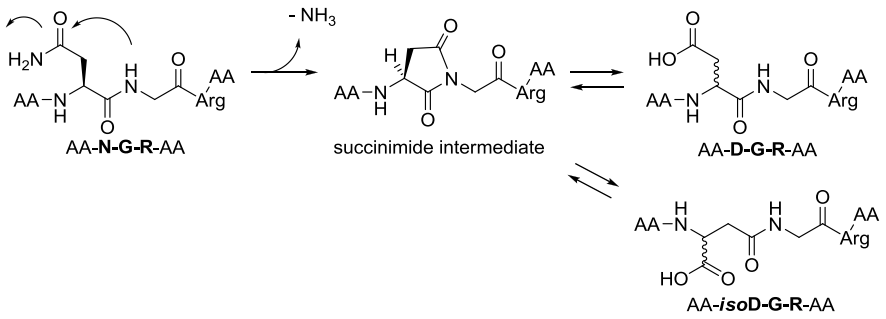

Scheme 3.1 – formation of DGR and isoDGR sequences by asparagine deamidation

*iso*DGR containing peptides can recognize members of the RGD-dependent integrin family, such as **$\alpha_v\beta_3$, $\alpha_v\beta_5$,** $\alpha_v\beta_6$, $\alpha_v\beta_8$ and **$\alpha_5\beta_1$,** but not other.[52] Both affinity and specificity of the interaction between *iso*DGR and integrin binding site is reported to be highly dependent on the flanking residues.

Notably, *iso*DGR docks onto the integrin binding site in an inverted orientation respect to RGD. This orientation allows *iso*DGR to bind to the $\alpha_v\beta_3$ binding pocket maintaining all the typical electrostatic-clamp interactions of the RGD motif. The acidic and basic residues are at the correct distance and orientation to engage stabilizing interactions with the polar regions of integrin: the *iso*Aspartic carboxylic side chain is interacting with MIDAS, Asn^{215}, Tyr^{122} and Arg^{214}, while Arginine guanidinium interacts with Asp^{218}, Asp^{150} and Gln^{180}. Moreover, additional stabilizing interactions are present: glycine recognizes the receptor via polar interactions and an H-bond between its amide and

carbonyl of Arg[216].[51] Therefore, *iso*DGR can be considered as a natural fit for the RGD binding pocket of $\alpha_v\beta_3$ integrin, suggesting that the naturally occurring transformation of NGR and DGR into *iso*DGR functions as a molecular switch able to activate integrin recognition.

Although *iso*DGR- and RGD-containing ligands can share the same integrin binding site, their effects on integrin finction might not be necessarily the same.[53]

1.4.1 - *RGD integrin ligands: state of the art*

The potential of $\alpha_v\beta_3$ inhibitor EMD121974 (**85**, Cilengitide, Figure 3.8) by Kessler was soon recognized by various clinical programs, opening the era of the integrin inhibitor class as investigational agents for antiangiogenic and anticancer therapies. The crystal structure analysis of the ectodomain of $\alpha_v\beta_3$ complexed with Cilengitide offered the first clear picture

of the RGD binding mode, which revealed a Cilengitide conformation featuring an inverse γ-turn centred on Asp, and a distorted βII'-turn with Gly and Asp at the i+1and i+2 positions, respectively. A distance of 8.9 Å between the C_β of Asp and Arg, accounting for an almost extended conformation of the RGD motif were observed. The most important interactions between the ligand and the receptor involved the Arg guanidinium group, which was forming salt bridges with Asp150 and Asp218 in the α subunit, and the Asp carboxylic group of the ligand, which interacts with the Mn^{2+} ion at MIDAS (Metal-Ion-Dependent Adhesion Site) in the β subunit. Moreover, several hydrophobic interactions were engaging the Gly residue, positioned at the interface between the α and β subunits.

An earlier example of RGD-based cyclic peptide had already been identified by Kessler, c(RGDfV)[54] **86** (Figure 3.8), which can be considered as an ancestor of Cilengitide. This compound was selectively active against $\alpha_V\beta_3$ integrin, and its overall conformation allowed the lateral chains of Asp and Arg to adopt a unstretched arrangement (distance C_β(Asp)- C_β(Arg) 6.9 Å).

Representative examples of semipeptidic $\alpha_V\beta_3$ inhibitors, bearing a non-peptidic and rigid turn-inducing motif to appropriately constrain the RGD motif, are reported in the literature.

Classic bicyclic, but also monocyclic scaffolds and simple linear tethers have been used to properly fold the RGD sequence within a macrocyclic template, to better fit within $\alpha_V\beta_3$ integrin binding site.[55]

Bicyclic heterocycles stand among the most popular constrained mimetics of natural amino acids in the structure-based design of peptidomimetics. Various successful examples of peptide are validating their use as preferred conformation inducing scaffolds.[56]

Kessler exploited azabicycloalkane and spyrocyclic systems, traditionally known as β-turn inducers, to prepare cyclic RGD-containing peptidomimetics.[57] The most active and less constrained compound of the series (**87**, Figure 3.8) was a fully promiscuous antagonist.

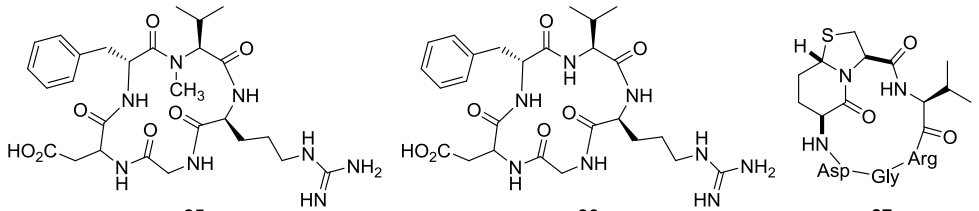

Figure 3.8

A stereoisomeric library of RGD pentapeptide mimetics incorporating 5,6- and 5,7-fused azabicycloalkane amino acids was generated by the group of Scolastico.[58] Among the high affinity ligands found within the collection, the most active compounds (**88** and ST1646 (**89**), Figure 3.9) demonstrated low nanomolar binders of $\alpha_V\beta_3$ and $\alpha_V\beta_5$ integrins. **89** was completely selective towards $\alpha_V\beta_3$ integrin respect to $\alpha_{IIb}\beta_3$ and $\alpha_5\beta_1$ integrins. Moreover, significant antiangiogenic activity of this compound emerged from *in vitro* experiments showing inhibition of the proliferation of endothelial cells.[59]

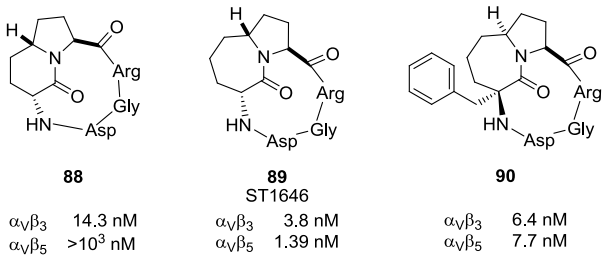

Figure 3.9

A strong dependence of the overall conformation of the cyclic peptides on the lactam ring size and stereochemistry was revealed. Almost the same interactions observed in the crystal structure of $\alpha_V\beta_3$ complexed with Cilengitide **85** were maintained. They observed an average distance between Arg and Asp C_β of 8.8 Å in the case of **88**, and 8.5 Å in **89**, indicative of an almost extended conformation of the RGD sequence.

Cyclopeptide **90** (Figure 3.9) emerged as a nanomolar antagonist of both $\alpha_V\beta_3$ and $\alpha_V\beta_5$ integrins comparable to ST1646 **89**. Docking studies revealed that the conformationscontaining an inverse γ-turn on Asp conserved the main contacts observed in the X-ray crystal structure with Cilengitide **85**.[60]

Also monocyclic turn-inducing scaffolds were used in the search for non peptidic RGD-containing systems, based on βII'/γ arrangement with the γ-turn centred on Gly.

Kessler inserted amino pyrrolidinone based motifs to hold the RGD moiety, providing macrocycles **91a** and **91b** (Figure 3.10).[61] A βII' turn conformation with Gly at the i+1 position was unexpectedly

observed for these compounds. **91a** was a moderate and selective antagonist of $\alpha_V\beta_3$ integrin, while **91b** proved to be a more active $\alpha_V\beta_3$ inhibitor, even though aspecific. The main difference between the two analogues was the orientation of the lactam bond in the turn-motif, which was found to be rotated by 180° in the two isomers, and involved in a H-bond with the receptor in the case of **91b**.

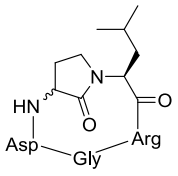

91a: (*S*) $\alpha_V\beta_3$ 40 nM
$\alpha_{IIb}\beta_3$ 2.8 μM

91b: (*R*) $\alpha_V\beta_3$ 0.8 nM
$\alpha_{IIb}\beta_3$ 8.5 nM

Figure 3.10

D- and L-morpholines were exploited by Guarna and co-workers to replace the *N*-Me-Val motif of Cilengitide **85**, grafting compounds **92** (Figure 3.11).[62] The different conformation of the peptide bond between D-Phe and the morpholine scaffold provided distinct structural arrangements for the two compounds. **92b** showed in particular a *cis* conformation in the docking analysis, with an RGD sequence arrangement comparable to that observed in the $\alpha_V\beta_3$-Cilengitide complex.

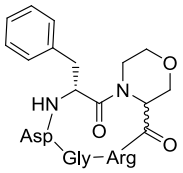

92a: (*S*) $\alpha_V\beta_3$ 157 nM
$\alpha_V\beta_5$ 15.1 nM

92b: (*R*) $\alpha_V\beta_3$ 32.6 nM
$\alpha_V\beta_5$ 21 nM

Figure 3.11

Kessler and Overhand designed several pyranoid and furanoid sugar δ- and ε-amino acid based compounds. Due to their high flexibility, they proved to be aspecific antagonists of $\alpha_V\beta_3$ and $\alpha_{IIb}\beta_3$ integrins. This aspecificity was also supported by the conformational analysis of this compounds, which showed an arrangement standing in between the typical kinked conformation of $\alpha_V\beta_3$-selective antagonists and the extended one required for targeting $\alpha_{IIb}\beta_3$ integrin. The two most representative members of this class of compounds are sketched in Figure 3.12 (**93**, **94**).[63,48k]

Casiraghi and colleagues, following an analogous inspiration, exploited furanoid carbasugar γ-amino acid equivalents to generate four stereoisomeric macrocycles (most active members **95**, Figure 3.12). Although an improvement in the affinity towards $\alpha_V\beta_3$ and $\alpha_V\beta_5$ was observed, their activity surprisingly proved to be almost irrespective of the configuration at the carbons bearing the amino acid functions. An inverted γ-turn, centered on Asp was revealed by NMR, displaying a C_β(Asp)-C_β(Arg) distance in the range of 8.0-8.4 Å.[64]

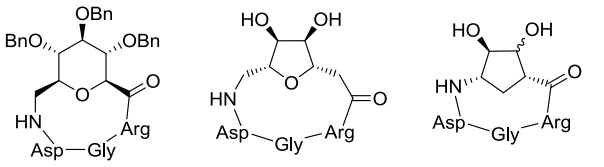

93

$\alpha_V\beta_3$ 25 nM
$\alpha_V\beta_5$ $>10^4$ nM
$\alpha_{IIb}\beta_3$ 13.4 nM

94

$\alpha_V\beta_3$ 1.49 μM
$\alpha_V\beta_5$ 0.38 μM

95

a (*S*): $\alpha_V\beta_3$ 51.4 nM
$\alpha_V\beta_5$ 165.5 nM
b (*R*): $\alpha_V\beta_3$ 44.7 nM
$\alpha_V\beta_5$ 125.4 nM

Figure 3.12

The same group incorporated 4-amino proline (Amp) scaffolds into a library of RGD peptides, to further extend these findings.[65] The compounds reported in Figure 3.13 (**96 a-d**) displayed exceptionally high affinity towards $\alpha_V\beta_3$ and $\alpha_V\beta_5$ integrins. A picomolar activity was observed for $\alpha_V\beta_3$ integrin in the high affinity status. A preferential conformation featuring an inverse γ-turn motif around Asp for the macrocycles containing a *cis*-disposed γ-amino acid motif was detected by NMR conformational analysis. On the contrary the macrocycles proved to be more flexible when a *trans* γ-amino acid was present. All the macrocycles showed a C_β(Asp)- C_β(Arg) distance in the 7.8-8.2 Å range. The most active analogues maintain the relevant key interactions observed for Cilengitide **85**. Compound **96a** was stabilized by a strong H-bonding contact between the NH in the aminoproline motif and Tyr178. Quite interestingly, the alkyl and acyl chains of **96 b** and **c** provided additional contacts for binding, pointing towards a large hydrophobic hollow rich with aromatic residues.

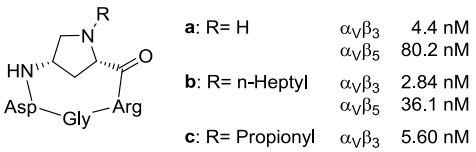

96

a: R= H
$\alpha_V\beta_3$ 4.4 nM
$\alpha_V\beta_5$ 80.2 nM

b: R= n-Heptyl
$\alpha_V\beta_3$ 2.84 nM
$\alpha_V\beta_5$ 36.1 nM

c: R= Propionyl
$\alpha_V\beta_3$ 5.60 nM
$\alpha_V\beta_5$ 94.0 nM

d: R= Bz
$\alpha_V\beta_3$ 5.15 nM
$\alpha_V\beta_5$ 86.6 nM

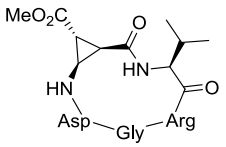

97

$\alpha_V\beta_3$ 20 nM
$\alpha_5\beta_1$ 1.5 μM

Figure 3.13

Pseudopentapeptides containing both enantiomers of *cis*-β-aminocyclopropanecarboxylic acid (β-Acc) were conceived, the most interesting of the two being sketched in Figure 3.13 (**97**).[48e]

Compound **97** resulted more active towards both $\alpha_V\beta_3$ and $\alpha_5\beta_1$ integrins, respect to the reference compound c(RGDfV) **86**. The C_β(Asp)- C_β(Arg) distance found for compound **97** resulted considerably shorter than expected (7.06 Å). Moreover, a γ-turn centered on Gly and a pseudo β-turn wherein (+)-β-Acc occupied the i+1 position were observed.

Despite the impressive work dedicated to the identification of semipeptide analogues, Cilengitide (**85**) is the only investigational agent of this class that has been developed for clinical testing on cancer patients. The growth inhibitory activity of Cilengitide observed in the clinic is likely due to a

combination of multifaceted mechanisms. These might depend on whether the drug is administered alone or in combination, and include inhibition of angiogenesis, direct cytotoxic activity on tumor cells, increase of endothelial cell permeability, and inhibition of cell adhesion, migration and invasion.[55,66]

Very recently, a paradoxical proangiogenic activity of low doses of Cilengitide was observed in certain preclinical studies.[67]

1.4.2 - *isoDGR integrin ligands*

As regards *iso*DGR-containing cyclic peptides or pseudo-peptides, not many examples appeared in the literature so far.

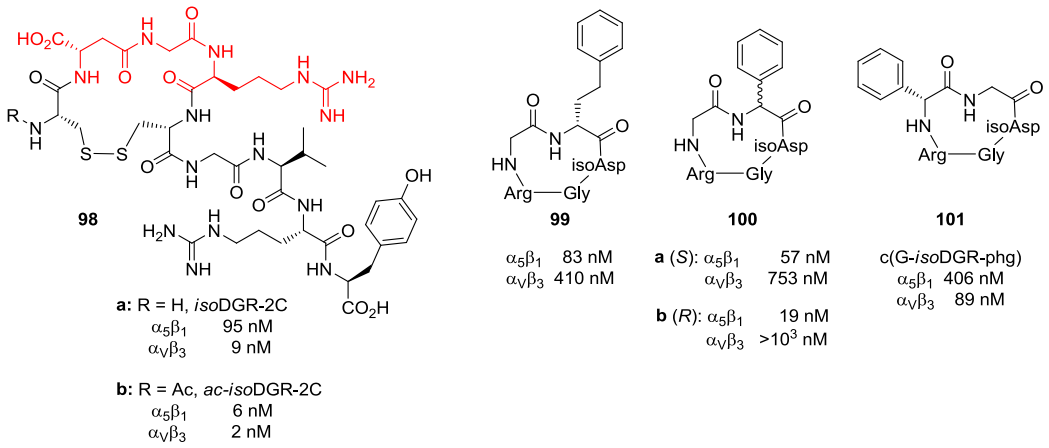

Figure 3.14

Being a relatively young research field (the earliest evidences dating back to 2006),[68] a lot more as been published on the structural basis for the interaction of *iso*DGR with the RGD-binding site of integrins, on the molecular switch ability of the NGR sequence to *iso*DGR and its possible applications in the discovery of innovative drugs. Still, extensive efforts in the understanding of the *iso*DGR motif potential need to be profused.

The most interesting examples appeared in the literature are reported in Figure 3.14.

Compound **98a** was the first to be discovered, by Corti and co-workers.[50,51] The efficacy of the cyclic motif C*iso*DGRC was demonstrated exchainging cysteine residues with glycine, and analogues such as **98b** were also prepared, obtaining enhanced affinity towards most of the integrins tested.[52]

These compounds have been tested for their competitive binding with ACDCRGDCFC-TNF to $\alpha_V\beta_3$ integrin. Being ACDCRGDCFC-TNF a quite weak ligand of $\alpha_V\beta_3$ integrin, the strikingly low nanomolar activity of these compounds might not be compared to other already shown activities.

Kessler and colleagues started an investigation in the field, synthesizing a small library of compounds based on the retrosequence of the highly active integrin-binding cyclic peptide c(RGDfV) **86**, for

example c(Vf*iso*DGR), obtaining moderate to poor results. Far better results were obtained flanking the *iso*DGR moiety with an aromatic aminoacid and a glycine (**99**-**101**, Figure 3.14). Hints on the importance of the flanking residues and, in particular, on the effects of a flanking aromatic moiety were given, and interesting selectivity towards $\alpha_5\beta_1$ integrin respect to $\alpha_V\beta_3$ integrin were obtained.[69]

2 - Cyclic [DKP-RGD] compounds

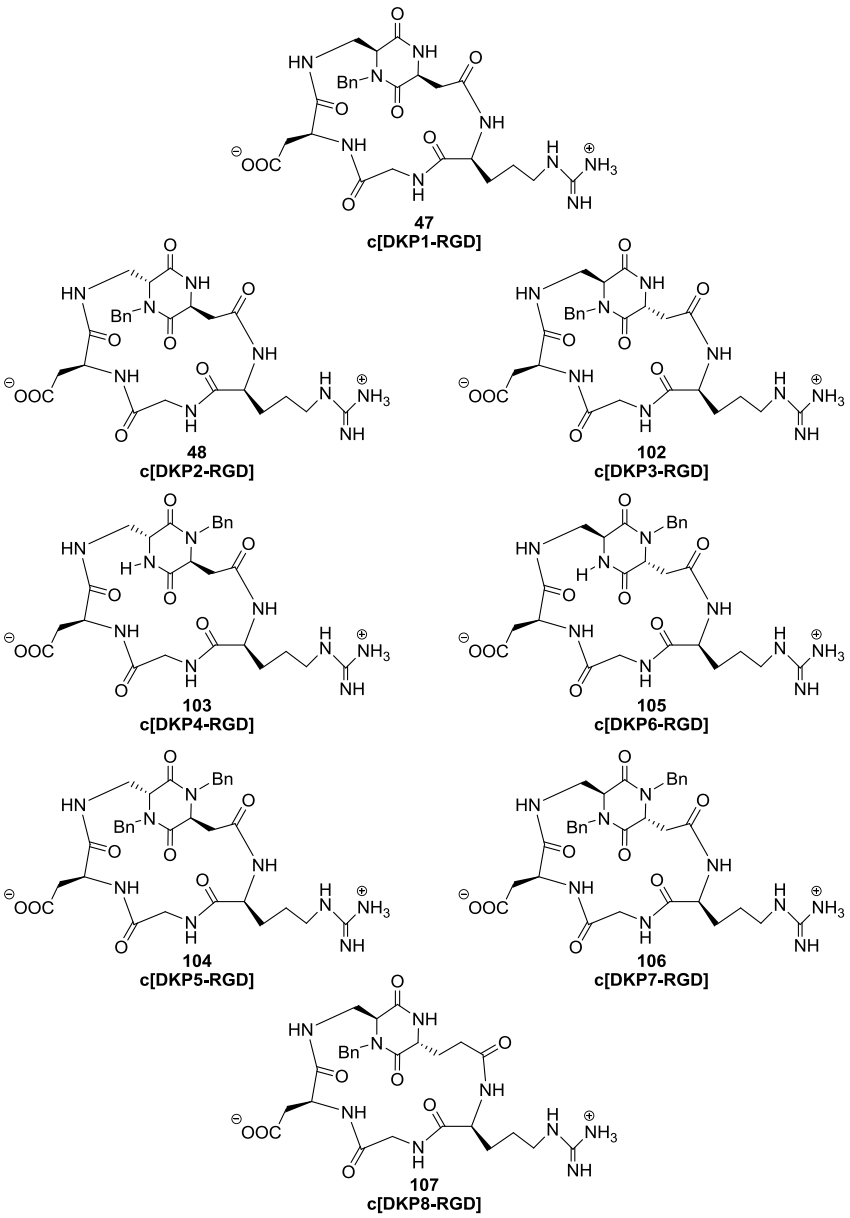

Figure 3.15 - Cyclic RGD-peptidomimetics (**47**, **48**, **102**-**107**) containing bifunctional diketopiperazine scaffolds **DKP1**-**DKP8**.

Our research group recently reported the synthesis of two cyclic peptidomimetic compounds containg the RGD sequence and bearing either **DKP1** or **DKP2** as a rigid scaffold (**47**-**48**, Figure 3.15).[70]

These compounds were examined *in vitro* for their ability to inhibit biotinylated vitronectin binding to the purified $\alpha_v\beta_3$ and $\alpha_v\beta_5$ receptors, giving strikingly different yet encouraging results. High micromolar IC_{50} values were obtained by compound **47** (IC_{50} ($\alpha_v\beta_3$): 3898 ± 418 nm; IC_{50} ($\alpha_v\beta_5$): > 10^4), while compound **48** gave low nanomolar values and demonstrated 50 fold more selective for the $\alpha_v\beta_3$ integrin with respect to the $\alpha_v\beta_5$ (IC_{50} ($\alpha_v\beta_3$): 3.2 ± 2.7; IC_{50} ($\alpha_v\beta_5$): 114 ± 99), in this kind of assay.

NMR characterization and conformational studies helped in giving an explanation of the different behavior of these two compounds. As already mentioned, a distance of ca. 9 Å between the C_β atoms of Asp and Arg, imparted by an extended conformation of the Arg-Gly-Asp sequence, is necessary for the best fitting into the active site of the $\alpha_V\beta_3$ integrin.The *cis* scaffold **DKP1** is inducing a less extended conformation in the RGD sequence (distance C_β(Asp)-C_β(Arg) = 5.9-7.9 Å) respect to what a *trans* scaffold like **DKP2** is doing (distance C_β(Asp)-C_β(Arg) = 9.4 Å).

Though, we decided to incorporate also diketopiperazine scaffolds **DKP3-8** into cyclic compounds of this kind (Figure 3.15).

2.1 - Synthesis

A solution phase synthetic strategy was adopted for the synthesis of the cyclic compounds reported in Figure 3.

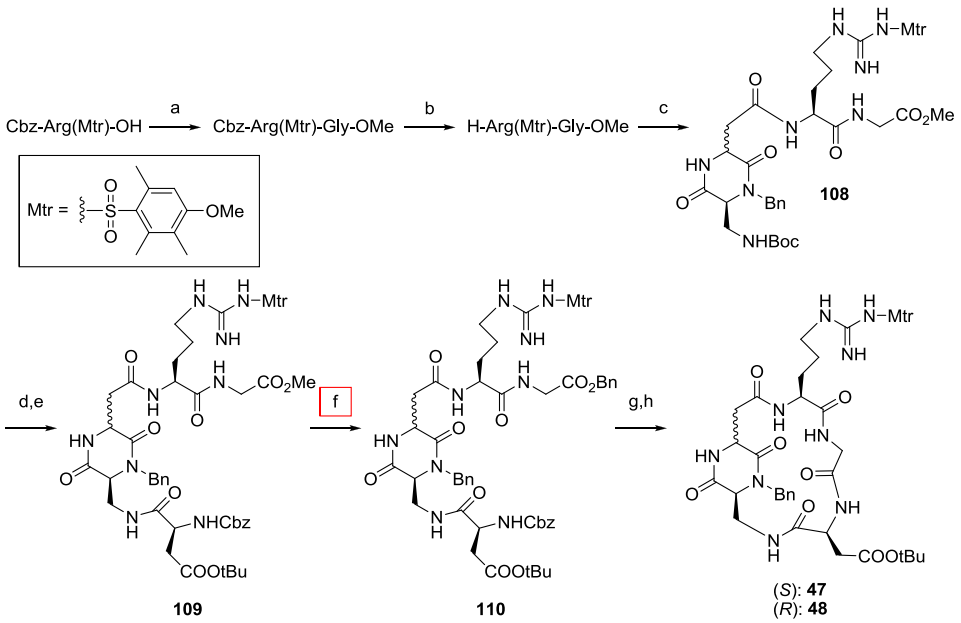

Scheme 3.2 – Synthesis of **47** and **48** as reported in the literature: a) HBTU, HOBt, DIPEA, HCl.Gly-OMe, DMF: 78%; b) H_2/Pd(OH)$_2$, MeOH: 98%; c) **DKP1** or **DKP2**, HBTU, HOBt, DIPEA, DMF; d) TFA/DCM 1:2; e) Cbz-Asp(OtBu)-OH, HATU, HOAt, DIPEA, DMF; f) BnOH (100 eq), Ti(*i*PrOH)$_4$ (1.05 eq), THF, 4Å MS, 90°C; g) H_2, Pd(OH)$_2$, MeOH; h) HATU, HOAT, collidine, DMF.

The reported synthesis of **47** and **48**[70] (Scheme 3.2) started from Cbz-Arg(Mtr)-OH, HCl.Gly-OMe and Cbz-Asp(*t*Bu)-OH, and envisaged the coupling of Arg(Mtr)-Gly-OMe to the acid of the appropriate diketopiperazine scaffold. After subsequent Boc deprotection of **108** the aspartic derivative Cbz-Asp(*t*Bu)-OH, was coupled. After transesterification of the glycine methyl ester **109** to the corresponding benzyl ester, the linear pentapeptides Cbz-D-DKP-RG-OBn **110** could be subjected to hydrogenolysis and subsequent macrolactamization.

The late stage transesterification on the linear pentapeptides resulted very capricious, giving non-reproducible yields. It was anyway an elegant idea to get to a non-orthogonally protected linear precursor. I decided then to by-pass transesterification using as starting materials Boc-Arg(Mtr)-OH and HCl.Gly-OBn, thus directly obtaining Cbz-D-DKP-RG-OBn in better yields (Scheme 3.2).

Linear pentapeptide precursors were deprotected in hydrogenolytic conditions at both the carboxyl group of glycine and the aspartic amino group, in presence of a catalytic amount of palladium on charcoal in methanol under an H_2 atmosphere. This was a quite slow reaction: the Cbz group was the last and harder to be cleaved, as revealed by HPLC-MS profiles. We recently realized that, performing the reaction in methanol, a methylated by-product is forming. In most cases, we were able to separate it from the main product by preparative HPLC after the cyclization step, but we thought we might better avoid its formation performing the reaction in a 1:1 THF/water mixture. These conditions are providing pure product in quantitative yields.

Table 3.2 – Optimization of macrolactamization conditions, on compound NH_2-D-**DKP3**-RG-OH (**115**).

Reagents and conditions	Purification	Yield
DPPA, DIPEA, 1.4 mM in DMF, 48 h	Flash silica gel column cromatography	75%
PyBrOP, DIPEA, 1.4 mM in DMF, 48 h	Flash silica gel column cromatography	28%
FDPP, DIPEA, 1.4 mM in DMF, 48 h	Flash silica gel column cromatography	73%
HATU, HOAt, collidine, 2 mM in DMF, 48 h	Flash silica gel column cromatography	30-40%

The macrocyclization step was optimized on **DKP3** containing compound **115**, screening several synthetic procedures and reactants. All the results are reported in Table 3.2.

It is clear that the best results were obtained when using DPPA or FDPP (75 and 73% respectively). DPPA was chosen, as FDPP left some impurities, visible from HPLC-MS profiles, that could not be removed with a mere flash chromatographic column.

Anyway, in order to avoid purification problems, all the other linear intermediates **115** (containing **DKP4-8**) were efficiently macrolactamized using the more conventional HATU, in presence of HOAt and *i*Pr_2EtN.

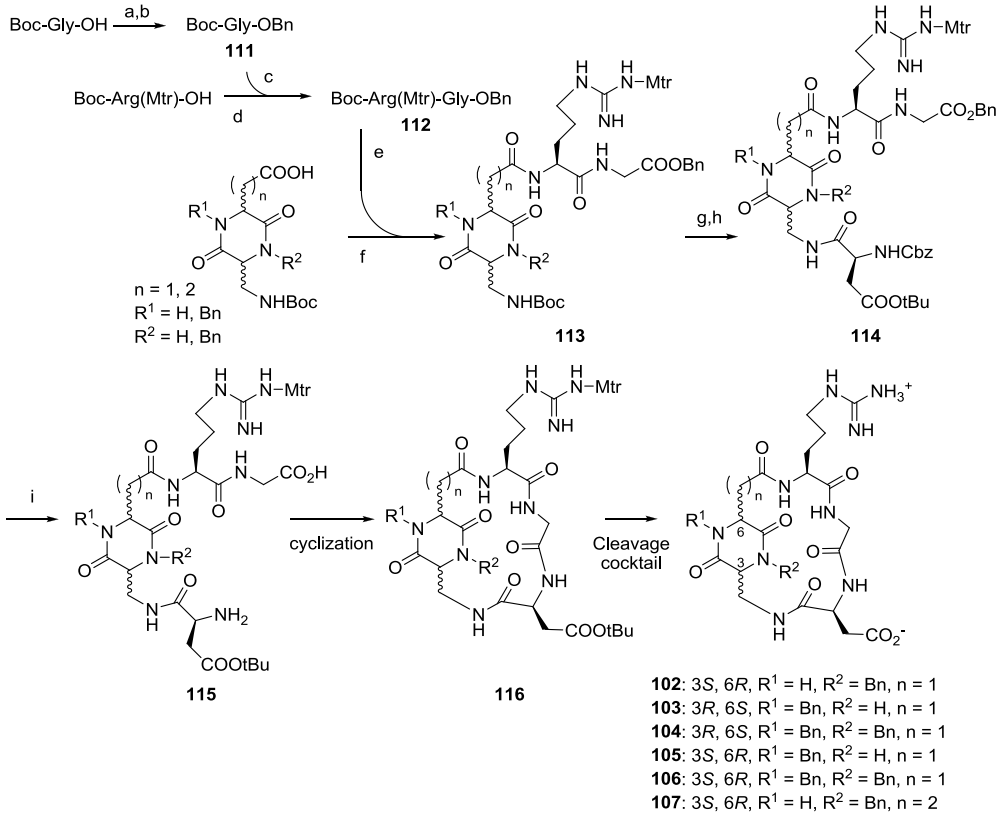

Scheme 3.3 – Synthesis of cyclic RGD peptidomimetics **102-107** containing scaffolds **DKP3-DKP8**: a) Cs_2CO_3, MeOH; b) BnBr, DMF: 95%; c) TFA/DCM 1:2; d) HBTU, HOBt, DIPEA, DMF: 90%; e) TFA/DCM 1:2; f) HATU, HOAt, *i*Pr_2EtN, DMF: 67%; g) TFA/DCM 1:2; h) Cbz-Asp(O*t*Bu)-OH, HATU, HOAt, *i*Pr_2EtN, DMF; i) H_2, Pd/C, THF/H_2O 1:1.

Final cleavage of the side chain protecting groups (Mtr on Arg and *t*Bu on Asp) was accomplished treating cyclized products **116** with a strongly acidic "cleavage cocktail". A first receipe envisaged a mixture TFA/triethylsilane/1,2-ethandithiol/phenol/thioanisole/H_2O 80:2.5:5:5:5:2.5. Far better results and cleaner crudes were however obtained with a mixture TFA/thioanisole/ethanedithiol/anisole 90:5:3:2.

In the case of the *N*-dibenzyl derivatives containing **DKP5** and **DKP7** (**104**, **106**), the molecules are displaying planar chirality. They can in fact exist as two different separable conformers (diastereomers) due to hindered rotation of one ring around the other (i.e., the DKP *N*-benzyl group cannot pass inside the macrolactam ring). We were able to isolate only one of the two diastereomers of **104**, either because it was formed exclusively or because it was formed predominantly and the minor one was not detected/isolated. Two diastereomers of compound **106** were instead isolated in a 2 (A) : 1 (B) ratio, Scheme 3.4).

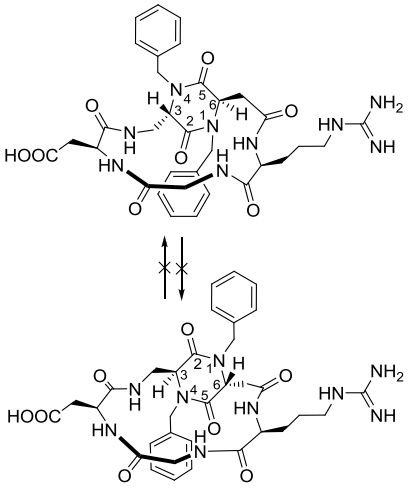

Scheme 3.4 - non-interconverting stereoisomers **106 A** and **B**.

2.2 - Biological evaluation [71]

The cyclic RGD peptidomimetics were examined *in vitro* for their ability to inhibit biotinylated vitronectin binding to the purified $\alpha_v\beta_3$ and $\alpha_v\beta_5$ receptors (Table 3.3).

Table 3.3 - Inhibition of biotinylated vitronectin binding to $\alpha_v\beta_3$ and $\alpha_v\beta_5$ receptors

Compound	Structure	$\alpha_V\beta_3$ IC_{50} [**nM**][a]	$\alpha_V\beta_5$ IC_{50} [**nM**][a]
47	*Cyclo* [**DKP1**-RGD] (*cis*)	3898 ± 418	$> 10^4$
48	*Cyclo* [**DKP2**-RGD] (*trans*)	3.2 ± 2.7	114 ± 99
102	*Cyclo* [**DKP3**-RGD] (*trans*)	4.5 ± 1.1	149 ± 25
103	*Cyclo* [**DKP4**-RGD] (*trans*)	7.6 ± 4.3	216 ± 5
104	*Cyclo* [**DKP5**-RGD] (*trans*)	12.2 ± 5.0	131 ± 29
105	*Cyclo* [**DKP6**-RGD] (*trans*)	2.1 ± 0.6	79 ± 3
106 A	*Cyclo* [**DKP7**-RGD] (A-major)	220.2 ± 82.3	$> 10^4$
106 B	*Cyclo* [**DKP7**-RGD] (B-minor)	0.2 ± 0.09	109 ± 15
107	*Cyclo* [**DKP8**-RGD] (*trans*)	7.5 ± 0.6	$> 10^3$
ref 1	c(RGDfV)	3.2 ± 1.3	7.5 ± 4.8
ref 2	ST1646	1.0 ± 0.5	1.4 ± 0.8

[a] IC_{50} values were calculated as the concentration of compound required for 50% inhibition of biotinylated vitronectin binding as estimated by GraphPad Prism software; all values are the arithmetic mean ± SD of triplicate determinations.

Screening assays were performed incubating the immobilized integrin receptors with various concentrations (10^{-10}–10^{-5} M) of the RGD ligands **47, 48, 102-107** in the presence of biotinylated vitronectin (1 μg/mL), and measuring the concentration of bound vitronectin in the presence of the competitive ligands. The ability of the new compounds to inhibit the binding of vitronectin to the isolated $\alpha_v\beta_3$ and $\alpha_v\beta_5$ receptors was compared with that of the reference compounds c(RGDfV)[72] (**86**, Figure 3.8) and ST1646[58] (**89**, Figure 3.9).

Low nanomolar values were obtained with all the ligands except *cyclo*[**DKP1**-RGD] (**47**) which incorporates a *cis* DKP and ligand **106 A**. The behavior of this last ligand is peculiar, considering that the diastereomeric compound **106 B** (see above for the definition of the two diastereomers) is the most potent ligand of this series, effectively inhibiting the binding of vitronectin to the isolated $\alpha_v\beta_3$ receptor at a 200 picomolar concentration. Interestingly, unlike reference compounds *c*(RGDfV) and ST1646, the RGD-peptidomimetics **47, 48, 102-107** were ca. 10-1000 fold more selective for the $\alpha_v\beta_3$ integrin with respect to the $\alpha_v\beta_5$, in this kind of assay, being **107** the most selective of the series.

2.3 - NMR characterization and conformational studies [73]

The structure and connectivity of ligands **47, 48, 102-107** and of their fully protected precursors were unambiguously assigned by means of mono- and bidimensional ^{1}H- and ^{13}C-NMR spectra.

The preferred conformations of the cyclic RGD peptidomimetics **47, 48, 102-107** in aqueous solution were then investigated, with the aim of rationalizing the affinity of these compounds for the $\alpha_v\beta_3$ receptor at a molecular level. In fact, as already mentioned, the high activity and selectivity of Cilengitide (**85**) has been attributed to an extended conformation of the RGD motif displaying a distance of ca. 9 Å between the C_β atoms of Asp and Arg, imparted by an extended conformation of the Arg-Gly-Asp sequence.[5] In such extended conformations, the carboxylate and guanidinium groups are properly positioned to effectively exert their function of electrostatic clamp.

Monodimensional ^{1}H-NMR experiments were conducted to detect intramolecular hydrogen bonds, by measuring the chemical shift of the N–H protons and their temperature coefficients ($\Delta\delta/\Delta T$). NOESY spectra were recorded to investigate both sequential and long-range NOE's that provide evidences of preferred conformations. The relevant NMR data are summarized in Table 3.4, while graphic in Figure 3.16 displays the temperature coefficients.

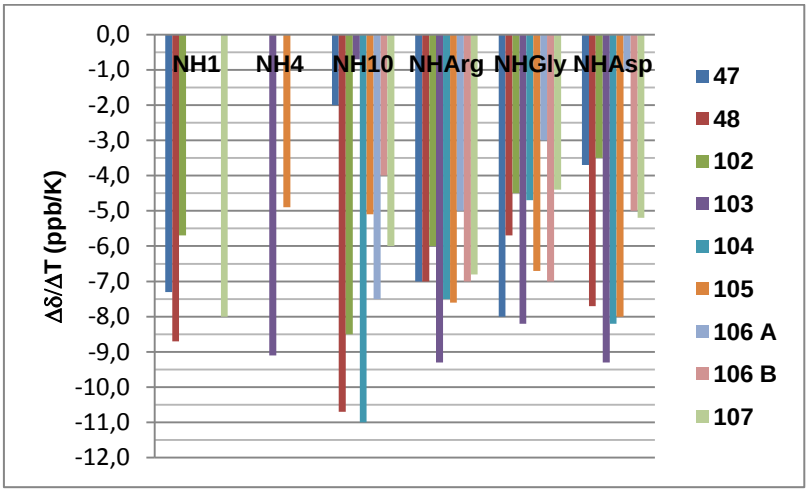

Figure 3.16 - Graphical illustration of temperature coefficients (Δδ/δT) for compounds **47, 48, 102-106** in H_2O/D_2O 9:1 between 290 K and 320 K.

As already reported in the literature,[70] ligand **47** exists as an equilibrium of two different preferred conformations. The NOESY spectrum shows two mutually exclusive long-range NOE contacts. The cross peak between DKP-NH_{10} and NH_{Asp} (strong) is indicative of a β-turn conformation at Gly-Asp stabilized by a hydrogen bond between DKP-NH_{10} and Arg-C=O (Type I H-bonding pattern, Figure 3.17 A). The chemical shift value (7.46 ppm) and the Δδ/ΔT value (-2 ppb/K) of the amide proton DKP-NH_{10} indicate that this proton is strongly locked in an intramolecularly H-bonded state. The cross peak between NH_{Gly} and NH_{Asp} (medium) is indicative of an alternative β-turn conformation at Arg-Gly, stabilized by a hydrogen bond between Asp-NH and C(8)=O (Type II H-bonding pattern, Figure 3.17 B).

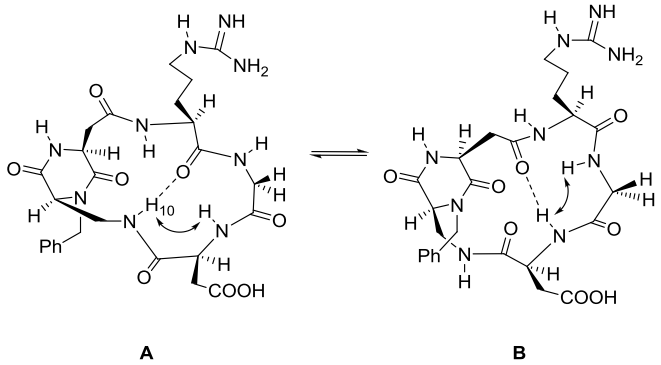

Figure 3.17 - Preferred intramolecular hydrogen-bonding pattern proposed for compound **47** on the basis of spectroscopic data. The arrows indicate significant NOE contacts. A) Type I H-bonding pattern, Gly-Asp β-turn motif. B) Type II H- H-bonding pattern, Arg-Gly β-turn motif .

Ligands **48** and **102** are characterized by a high conformational equilibrium, as ascertained by the values of chemical shifts and Δδ/ΔT reported in Table 3.4. The only exception is proton NH-Asp (7.85 ppm and the Δδ/ΔT value -3,5 ppb/K) of **27**, which might be involved in a Type II H-bonding pattern.

On the other hand, the presence in both cases of a NOE contact between NH_{Gly} and NH_{Arg} suggests the formation of a β-turn motif at DKP-Arg, stabilized by a hydrogen bond between NH_{Gly} and C(5)=O (appointed as Type III H-bonding pattern, Figure 3.18). The presence of this H-bond is also supported by the rather upfield chemical shift value of NH_{Gly} in these two ligands (8.18 and 8.00 ppm for **48** and **102**, respectively) and the relatively low temperature dependence (-5.7 and -4.5 ppb/K, respectively).

The similarity of the NMR data and hence of the conformation of these two ligands is quite surprising, considering the opposite configuration of the diketopiperazine scaffold (**DKP2**, 3*R*,6*S* in **48**; **DKP3**, 3*S*,6*R* in **102**) which should impart a different stereochemical orientation to the two side arms of the diketopiperazine.

Table 3.4 - ^{1}H-NMR and NOE data of cyclic RGD-peptidomimetics **47, 48, 102-107** in water.

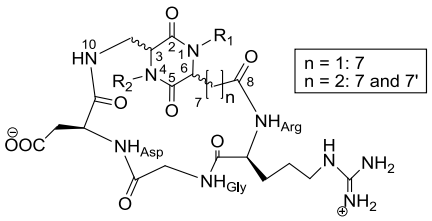

		NH_1	NH_4	NH_{10}	NH_{Arg}	NH_{Gly}	NH_{Asp}	Significant NOE contacts
47 cyclo[**DKP1**-RGD]	**δ** (ppm)	8,35	-	7,46	8,40	8,75	8,10	NH_{Asp}-NH_{10}; NH_{Asp}-NH_{Gly}
	Δδ/ΔT (ppb/K)	-7.3	-	-2.0	-7.0	-8.0	-3.7	
48 cyclo[**DKP2**-RGD]	**δ** (ppm)	8.35	-	8.78	8.57	8.18	8.29	NH_{Arg}-NH_{Gly}
	Δδ/ΔT (ppb/K)	-8.7	-	-10.7	-7.0	-5.7	-7.7	
102 cyclo[DKP-**3**-RGD]	**δ** (ppm)	8.10	-	8.28	8.80	8.00	7.85	NH_{Arg}-NH_{Gly}
	Δδ/ΔT (ppb/K)	-5.7	-	-8.5	-6.0	-4.5	-3.5	
103 cyclo[**DKP4**-RGD]	**δ** (ppm)	-	8.17	7.59	8.29	8.27	8.88	--
	Δδ/ΔT (ppb/K)	-	-9.1	-0.7	-9.3	-8.2	-9.3	
104 cyclo[**DKP5**-RGD]	**δ** (ppm)	-	-	8.58	8.48	8.23	8.42	NH_{Arg}-NH_{Gly}
	Δδ/ΔT (ppb/K)	-	-	-11.0	-7.5	-4.7	-8.2	
105 cyclo[**DKP6**-RGD]	**δ** (ppm)	-	8.07	7.90	8.32	8.35	8.80	NH_{Asp}-NH_{10}; NH_4-NH_{10};
	Δδ/ΔT (ppb/K)	-	-4.9	-5.1	-7.6	-6.7	-8.0	
106 A cyclo[**DKP7**-RGD]-A	**δ** (ppm)	-	-	8.04	8.66	7.93	7.76	NH_{Arg}-NH_{Gly}; NH_{Asp}-NH_{Gly}
	Δδ/ΔT (ppb/K)	-	-	-7.5	-5.0	-3.0	-1.0	
106 B cyclo[**DKP7**-RGD]-B	**δ** (ppm)	-	-	7.72	8.34	8.45	8.55	NH_{Asp}-NH_{10}
	Δδ/ΔT (ppb/K)	-	-	-4.0	-7.0	-7.0	-5.0	
107 cyclo[**DKP8**-RGD]	**δ** (ppm)	7.82	-	7.43	8.64	8.04	7.90	-
	Δδ/ΔT (ppb/K)	-8.0	-	-6.0	-6.8	-4.4	-5.2	

This conformational similarity can be interpreted in terms of a quasi-enantiomeric structure of the two ligands (excluding the configuration of the remote RD amino acid side chains, Figure 3.18).

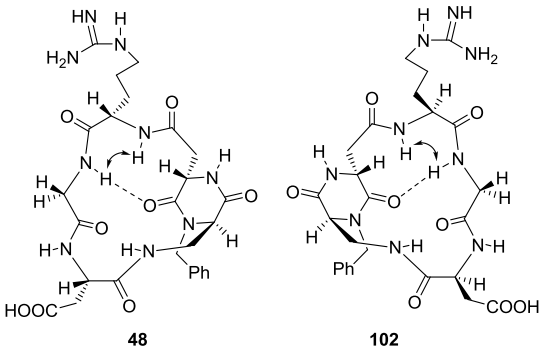

48 **102**

Figure 3.18 - Preferred intramolecular hydrogen-bonding pattern proposed for compound **48** and **102** on the basis of spectroscopic data. The arrows indicate significant NOE contacts. The DKP-Arg β-turn motif is referred as Type III H-bonding pattern.

Ligands **103** and **105**, featuring the diketopiperazine scaffolds **DKP4** (3*R*,6*S*) and **DKP6** (3*S*,6*R*) respectively (with the benzyl substitution at the endocyclic nitrogen N1, instead of N4), show a different NMR pattern. In particular, ligand **105** is characterized by a rather strong NOE contact between NH_{Asp} and NH_{10} and a moderate/weak one involving NH_4 and NH_{10}. These two contacts are mutually exclusive and hence indicative of an equilibrium between two different conformations, respectively Type I and Type IV H-bonding patterns (Figure 3.19 A and B).

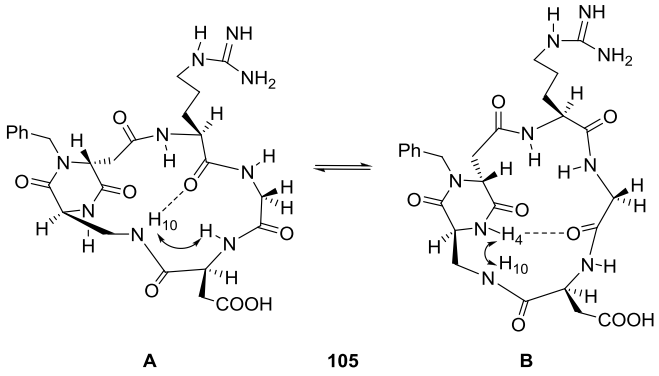

A **105** **B**

Figure 3.19 - Preferred intramolecular hydrogen-bonded pattern proposed for compound **105** on the basis of spectroscopic data. A) Type I H-bonding pattern is characterized by a β-turn motif at Gly-Asp stabilized by a hydrogen bond between NH_{10} and Arg-C=O. B) Type IV H-bonding pattern which is characterized by a pseudo β-turn at Asp-DKP stabilized by a hydrogen bond between NH_4 and Gly-C=O. The arrows indicate significant NOE contacts.

The hydrogen bonded status of the two amide protons NH_4 and NH_{10}, as indicated by their rather low temperature dependence (-4.9 and -5.1 ppb/K, respectively) and quite upfield chemical shift values (8.07 and 7.90 ppm, respectively), corroborate this assumption. The Type IV H-bonding pattern could feature a pseudo β-turn at Asp-DKP stabilized by a hydrogen bond between NH_4 and Gly-C=O (NOE contact between NH_4 and NH_{10}).

Ligand **103**, on the other hand, is characterized by the absence of relevant NOE contacts, a very low temperature dependence (-0.7 ppb/K) and a quite upfield chemical shift value (7.59 ppm) for proton NH_{10}. These two features suggest a Type I H-bonding pattern, notwithstanding the apparent lack of NOE contact between NH_{Asp} and NH_{10}.

The dibenzylated diketopiperazine containing peptidomimetics **104** and **106** were eventually studied. Ligand **104** shows NMR features similar to ligand **48** (Type III H-bonding pattern): a NOE contact between NH_{Gly} and NH_{Arg} and a rather shielded NH_{Gly} (8.23 ppm) with a relatively low temperature coefficient (-4.7 ppb/K). As discussed above, ligand *cyclo*[**DKP7**-RGD] was obtained as a mixture of two diastereomers **106 A** and **106 B**, whose conformations in solution were studied separately. In particular, **106 A** displays two mutually exclusive NOE contacts between NH_{Arg} and NH_{Gly} and between NH_{Asp} and NH_{Gly}. These three protons, on the other hand, show also a rather strong hydrogen bonded status, as indicated by their low temperature dependence and, at least for NH_{Asp} and NH_{Gly}, their upfield chemical shift (Table 3.4). These data indicate an equilibrium between two different conformations: one displaying a Type III H-bonding pattern and a second one showing a Type II H-bonding pattern (β-turn at Arg-Gly), like the low-affinity ligand **47**, *i.e. cyclo*[**DKP1**-RGD]. Finally, ligand **106 B** shows a single NOE contact between NH_{Asp} and NH_{10} and a hydrogen bonded status for NH_{10} (δ 7.72 ppm and $\Delta\delta/\Delta T$ -4 ppb/K, see Table 3.4). These values are indicative of a Type I H-bonding pattern.

No NOE contacts were identified for compound **107**, containing the superior omologous of **DKP3** (*i.e.* **DKP8**). Moreover, also temperature coefficients of the amide protons are not relevant for the identification of H-bonds.

Conformational analysis. Conformational studies of the cyclic RGD-peptidomimetics were performed by mixed-mode Metropolis Monte Carlo/Stochastic Dynamics (MC/SD) simulations, using the implicit water GB/SA solvation model[2] and the OPLS_2001 force field.

As already reported in a preliminary communication,[70] three-dimensional structures satisfying long-range NOE contacts were generated for RGD peptidomimetic **47** performing two 10 ns restrained MC/SD simulations and applying the DKP-NH_{10}/NH_{Asp} or the NH_{Asp}/NH_{Gly} distance restraint derived from NOESY spectra.

More than 90% of the conformations sampled during the first simulation adopted a non-extended arrangement of the RGD sequence characterized by a β-turn at Gly-Asp and the presence of the corresponding hydrogen bond between DKP-NH_{10} and Arg-C=O. In addition, the formation of a γ-turn at Gly stabilized by the hydrogen bond between NH_{Asp} and Arg-C=O was observed for 40% of the simulation. A Cβ(Arg)–Cβ(Asp) average distance of 7.4 Å was obtained during this MC/SD calculation. A representative energy minimized conformation selected by cluster analysis and featuring both H-bonds is shown in Figure 3.20 A (Type I-*cis* H-bonding pattern). Approximately 60% of the conformations sampled during the simulation of **47** featuring the NH_{Asp}/NH_{Gly} distance restraint, adopted a non-extended arrangement of the RGD sequence characterized by a β-turn at Arg-Gly and the corresponding hydrogen bond between NH_{Asp} and C(8)=O. In addition, the formation of a γ-turn at Arg stabilized by the hydrogen bond between NH_{Gly} and C(8)=O was observed for 40% of the

simulation. The Cβ(Arg)–Cβ(Asp) average distance in this MC/SD calculation was 6.8 Å. A representative energy minimized conformation selected by cluster analysis and featuring both H-bonds is shown in Figure 3.20 B (Type II H-bonding pattern).

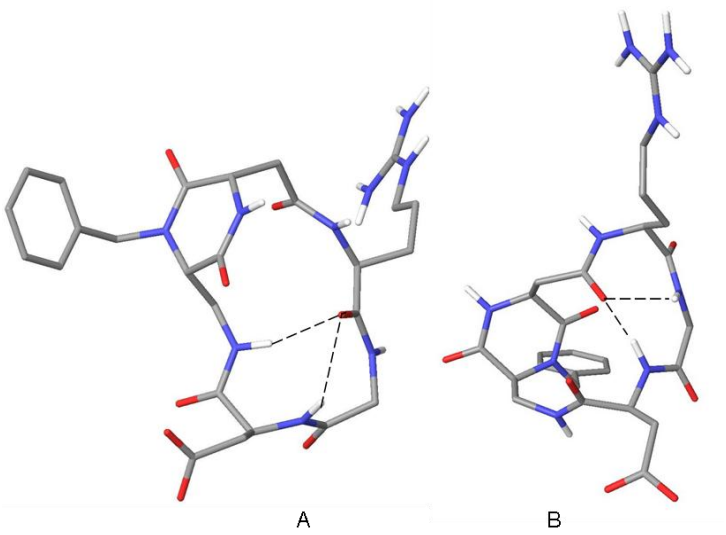

Figure 3.20 - Structures of **47** as obtained by restrained MC/SD simulations based on experimental distance information, after energy minimization. A) Type I-*cis* H-bonding pattern, γ-turn at Gly and βII'-turn at Gly-Asp [CβArg)–Cβ(Asp)=7.9 Å]. B) Type II H-bonding pattern, γ-turn at Arg and βII'-turn at Arg-Gly [Cβ(Arg)–Cβ(Asp)=6.6 Å].

The NOESY spectra of compounds **48** (containing *N*-4-benzylated **DKP2**, 3*R*,6*S*), **102** (containing *N*-4-benzylated **DKP3**, 3*S*,6*R*) and **104** (containing *N*-dibenzylated **DKP5** 3*R*,6*S*) show only one relevant long-range interaction between NHGly and NHArg: this NOE is indicative of a β-turn motif at DKP-Arg stabilized by a hydrogen bond between NHGly and C(5)=O (Figure 3.18, Type III H-bonding pattern). The distance restraint corresponding to the NOE contact between NHGly and NHArg was applied in the 10 ns MC/SD simulations of compounds **48**, **102** and **104**. More than 90% of the conformations sampled during each of these simulations adopted an extended arrangement of the RGD sequence characterized by a pseudo β-turn at DKP-Arg and the formation of the corresponding hydrogen bond between the NHGly and C(5)=O. Interestingly, only for compound **102**, the additional formation of a β-turn at Arg-Gly stabilized by the hydrogen bond between NHAsp and C(8)=O was observed for 15% of the simulation. These results and the NMR data (showing δ 7.85 ppm and Δδ/ΔT -3.5 ppb/K for NHAsp of **102**) suggest the contribution of a Type II/Type III H-bonding pattern to the conformational equilibrium of **102** (mainly populated by a Type III H-bonding pattern).

Cβ(Arg)-Cβ(Asp) average distances of 9.3, 8.8, and 9.1 Å were obtained during the MC/SD calculations of **48**, **102** and **104**, respectively. A representative energy minimized conformation selected by cluster analysis and featuring the H-bond between the Gly-NH and C(5)=O (Type III H-bonding pattern) is shown in Figure 3.21 for RGD peptidomimetic **48**.

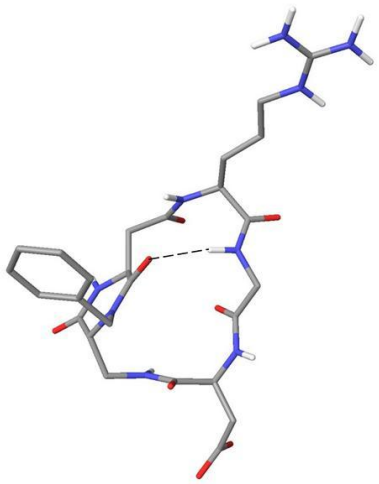

Figure 3.21 - Structure of **48** as obtained by restrained MC/SD simulations based on experimental distance information, after energy minimization (Type III H-bonding pattern, distorted inverse γ-turn at Asp and pseudo β-turn at DKP-Arg, Cβ(Arg)–Cβ(Asp)=9.4 Å).

Due to the absence of relevant long-range NOE contacts, several 10 ns runs of unconstrained MC/SD simulations were performed for RGD peptidomimetic **103** (containing N-1-benzylated **DKP4**, 3*R*,6*S*) starting from different 3D structures. Most of the conformations sampled during these simulations adopted an extended arrangement of the RGD sequence (Cβ(Arg)-Cβ(Asp) average distance of 8.8 Å) and approximately 40% of them are characterized by a β-turn at Gly-Asp and the presence of the corresponding hydrogen bond between DKP-NH_{10} and Arg-C=O. These results provide a structural model in agreement with NMR data showing a low temperature dependence (-0.7 ppb/K) and an upfield chemical shift value (7.59 ppm) for proton NH_{10}.

A representative energy minimized conformation selected by cluster analysis and featuring the H-bond between DKP-NH_{10} and Arg-C=O (Type I-*trans* H-bonding pattern) is shown in Figure 3.22 for RGD peptidomimetic **103**. It is worth noting how the combination of the *trans* **DKP4** scaffold with the Gly-Asp β-turn occurs by generating an extended RGD arrangement, while the combination of the *cis* **DKP1** scaffold with the same secondary motif resulted in a non-extended RGD disposition (see above, Figure 3.20 A). Accordingly, two Type I H-bonding patterns have been defined, depending on the *cis* or *trans* relative stereochemistry of the diketopiperazine scaffold.

Three-dimensional structures satisfying long-range NOE contacts were generated for RGD peptidomimetic **105** (containing N-1-benzylated **DKP6**, 3*S*,6*R*) performing two 10 ns restrained MC/SD simulations and applying the DKP-NH_{10}/NH_{Asp} or the NH_4/NH_{10} distance restraint derived from NOESY spectra (Table 3.4, Figure 3.19).

Most of the conformations sampled during the first simulation adopted an extended arrangement of the RGD sequence (Cβ(Arg)-Cβ(Asp) average distance of 9.0 Å) and approximately 40% of them are characterized by a β-turn at Gly-Asp and the corresponding hydrogen bond between DKP-NH_{10} and Arg-C=O. A representative energy minimized conformation selected by cluster analysis and featuring

this H-bond is shown in Figure 3.23 A (Type I-*trans* H-bonding pattern). Approximately 70% of the conformations sampled during the simulation of **105** featuring the NH_4/NH_{10} distance restraint, adopted an extended arrangement of the RGD sequence (Cβ(Arg)-Cβ(Asp) average distance of 8.8 Å) characterized by a pseudo β-turn at Asp-DKP and the corresponding hydrogen bond between NH_4 and Gly-C=O. In addition, the formation of a γ-turn at Asp stabilized by the hydrogen bond between NH_{10} and Gly-C=O was observed for 50% of the simulation A representative energy minimized conformation selected by cluster analysis and featuring these H-bonds is shown in Figure 3.23 B (Type IV H-bonding pattern).

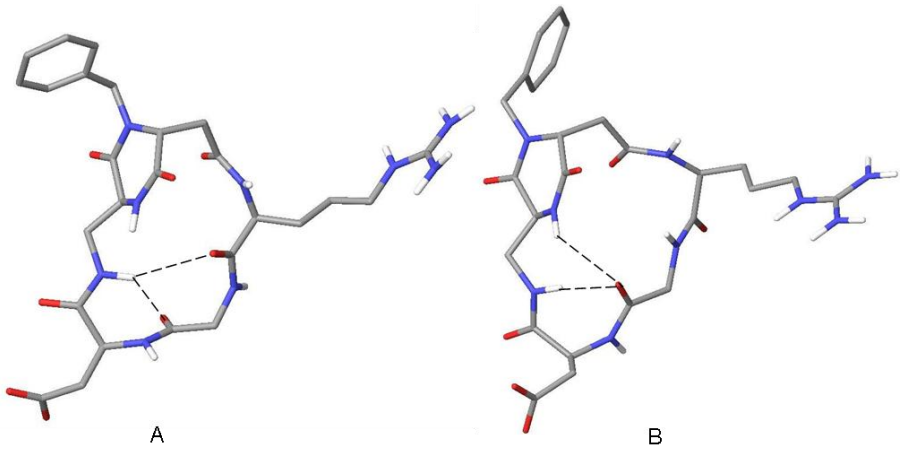

Figure 3.23 - Structures of **105** as obtained by restrained MC/SD simulations based on experimental distance information, after energy minimization. A) Type I-*trans* H-bonding pattern, inverse γ-turn at Asp and distorted βII'-turn at Gly-Asp [CβArg)–Cβ(Asp)=9.0 Å]. B) Type IV H-bonding pattern, inverse γ-turn at Asp and pseudo β-turn at Asp-DKP [Cβ(Arg)–Cβ(Asp)=8.8 Å].

Three-dimensional structures satisfying long-range NOE contacts were generated for RGD peptidomimetic **106** (containing *N*-dibenzylated **DKP7** 3*S*,6*R*) performing three 10 ns restrained MC/SD simulations and applying the distance restraints derived from NOESY spectra of diastereoisomers **106A** and **106B** (Table 3.4): in the first simulation NH_{Arg}/NH_{Gly} relevant in **106A**, in the second simulation NH_{Asp}/NH_{Gly} also relevant in **106A**, and in the third simulation DKP-NH_{10}/NH_{Asp} relevant in **106B**.

All the conformations sampled during the first two simulations adopted a non-extended arrangement of the RGD sequence [Cβ(Arg)-Cβ(Asp) average distance of 6.6 Å] characterized by the simultaneous presence of different turn motifs (pseudo β-turn at DKP-Arg, γ-turn at Gly and pseudo β-turn centered at the DKP unit). The structural models provided by these restrained MC/SD simulations differ from the conformations hypothesized on the basis of NMR data of **106A** [equilibrium between Type III (pseudo β-turn at DKP-Arg) and Type II (β-turn at Arg-Gly) H-bonding patterns, see the NMR section]. However, also the calculated structures are able to provide an explanation for the NOE contacts and the NMR temperature coefficients observed for **106A**.

The distance restraint corresponding to the NOE contact between DKP-NH_{10} and NH_{Asp} (observed in the NOESY spectrum of **106B**) was applied in the third 10 ns MC/SD simulation of compound **106**. Most of the conformations sampled during this simulation adopted an extended arrangement of the RGD sequence (Cβ(Arg)-Cβ(Asp) average distance of 9.0 Å) and approximately 50% of them are characterized by a β-turn at Gly-Asp and the corresponding hydrogen bond between DKP-NH_{10} and Arg-C=O. A representative energy minimized conformation selected by cluster analysis and featuring this H-bond is shown in Figure 3.24 (Type I-*trans* H-bonding pattern).

Contrary to what observed for the other cyclic RGD peptidomimetics containing DKP scaffolds, rotation of the DKP ring can not be observed during the simulations performed on compound **106**, confirming **106A** and **106B** as two different separable conformers (diastereomers) due to hindered rotation of one ring around the other.

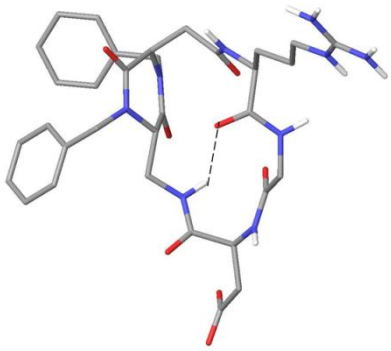

Figure 3.24 - Structure of **106B** as obtained by restrained MC/SD simulations based on experimental distance information, after energy minimization (Type I-*trans* H-bonding pattern, distorted inverse γ-turn at Asp and βII'-turn at Gly-Asp, Cβ(Arg)–Cβ(Asp)=9.2 Å).

Due to the absence of relevant long-range NOE contacts, two 10 ns runs of unconstrained MC/SD simulations were performed for RGD peptidomimetic **107** (containing *N*-4-benzylated **DKP8**, 3*S*,6*R*).

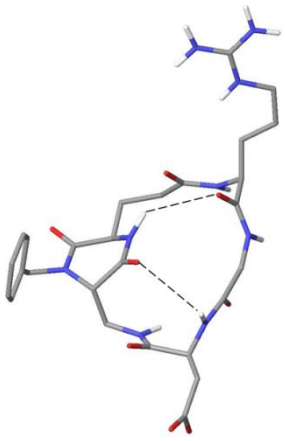

Figure 3.25 - Structure of **107** as obtained by MC/SD simulations, after energy minimization (Cβ(Arg)–Cβ(Asp)=9.5 Å).

All the conformations sampled during these simulations adopted an extended arrangement of the RGD sequence (Cβ(Arg)-Cβ(Asp) average distance of 9.8 Å) characterized by the formation of hydrogen bonds between NH_{Asp} and C(2)=O and between NH_1 and Arg-C=O.
A representative energy minimized conformation selected by cluster analysis and featuring these H-bonds is shown in Figure 3.25 for RGD peptidomimetic **107**.

Molecular docking. In order to rationalize, on a molecular basis, the affinity of cyclic RGD peptidomimetics for the $\alpha_v\beta_3$ receptor, docking studies were performed starting from the representative conformations obtained from the MC/SD simulations. The crystal structure of the extracellular segment of integrin $\alpha_v\beta_3$ complexed with the cyclic pentapeptide Cilengitide (1L5G, pdb code) was taken as a reference model for the interpretation of the docking results in terms of ligand-protein interactions. In the X-ray complex, Cilengitide binds to the interface of the α and β units forming specific electrostatic interactions.The acid and basic pharmacophoric groups and their orientation are essential for binding to the $\alpha_v\beta_3$ because they act like an electrostatic clamp, interacting with charged regions of the receptor binding site.
Docking calculations starting from geometries featuring the Type I-*cis* and Type II H-bonding patterns produced top-ranked poses conserving optimal interactions only with the α subunit of the $\alpha_v\beta_3$ receptor. Probably, the short Cβ(Arg)-Cβ(Asp) distances (values less than 8 Å) of these geometries prevent the guanidine and carboxylic groups from achieving the required separation for binding to the $\alpha_v\beta_3$ integrin. On the other hand, docking calculations starting from the RGD extended conformations featuring the Type I-*trans*, Type III and Type IV H-bonding patterns, produced top-ranked poses conserving all the important interactions of the X-ray complex (Figure 3.26).

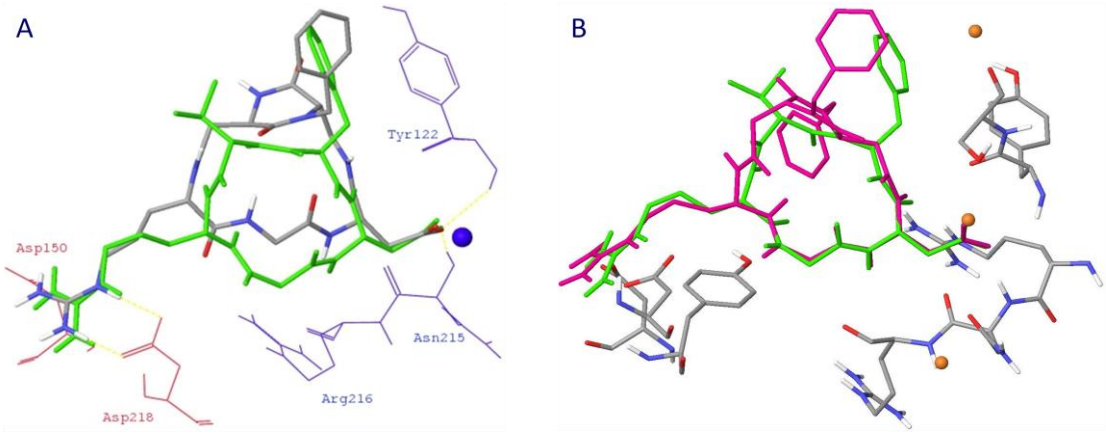

Figure 3.26 - Top-ranking binding mode of compounds A) ***cyclo*[DKP3-RGD] (102)** and B) ***cyclo*[DKP7-RGD] (106 B)** into the crystal structure of the extracellular domain of $\alpha_V\beta_3$ integrin overlaid on the bound conformation of Cilengitide (green).

The positively charged Arg guanidinium group of the ligand interacts with the negatively charged side chains of Asp218 and Asp150 in the α unit, one carboxylate oxygen of the ligand Asp side chain is coordinated to the metal cation in the metal-ion-dependent adhesion site (MIDAS) region of the β unit, while the second carboxylate oxygen forms hydrogen bonds with the backbone amides of Asn215 and Tyr122 in the β unit. Further stabilizing interaction involves the formation of a hydrogen bond between the ligand backbone NH of the Asp residue and the backbone carbonyl group of Arg216 in the β unit.

In light of all these considerations, the micromolar affinity of RGD peptidomimetics **47** and **106A** (3.9 and 0.2 μM, respectively) for $\alpha_v\beta_3$ (Table 1) can be explained in terms of their low pre-organization for binding. In fact, as determined by the computational and NMR studies, these compounds in solution mainly feature non-extended RGD conformations which, according to the docking results, are not able to properly fit into the $\alpha_v\beta_3$ receptor. On the contrary, the nanomolar affinity of RGD peptidomimetics **48**, **102-105**, **106B** and **107** for $\alpha_v\beta_3$ can be attributed to their high structural pre-organization. In fact, as determined by the computational and NMR studies, these compounds in solution mainly feature extended RGD conformations (principally determined by Type I-*trans*, Type III and Type IV H-bonding patterns) similar to the RGD bound conformation of Cilengitide.

2.4 - Depsipeptide side-project

Most of the problems in the synthesis of the compounds shown so far are probably related to the introduction of an amino moiety on the diketopiperazine scaffolds. This was accomplished, most of the times, thorugh a Mitsunobu-type reaction on compounds **49** in presence of HN_3 in toluene to give azides **58** (Scheme 2.9, Chapter 2, §3.2.1). A major drawback of this reaction was apart for the very low atom economy, the formation of varying amounts, depending on the substrate, of a dehydroalanine-like elimination by-product (**60**, Scheme 2.10, Chapter 2, §3.2.1).

At some point we wondered whether it was really necessary to introduce an amino functionality on our scaffolds, or if we could in principle incorporate into RGD-containing macrocyclic compounds a scaffold bearing an hydroxyl functionality, thus obtaining a depsipeptide (**117**, Figure 3.27).

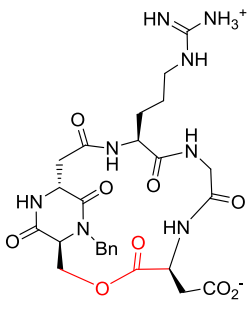

117

Figure 3.27 – Depsipeptide containing the RGD-sequence and **DKP3**-like scaffold. Depsi bond is highlighted in red.

This might have reduced the number of steps in the synthesis of RGD-cyclic compounds, enhacing most probably the overall yields. A depsi bond in the macrocycle might also have an effect, which we could not *a priori* define as positive or negative, on the conformation assumed and, hence, on their biological activity. The lower stability of the ester bond respect to the amide bond, expecially *in vivo*, might represent a major drawback.

We investigated the synthesis of compound **117** starting from diketopiperazine **49c**, a precursor in the synthesis of scaffold **DKP3** (Scheme 3.5). **49c** was coupled with Cbz-Asp(O*t*Bu)-OH in presence of EDC, DMAP and a catalytic amount of scandium triflate,[74] forming the ester bond. This mild procedure gave the best results among the other more common ones tried. The mechanism seems to procede through a carboxylic acid activated species (with carbodiimide, *N*-hydroxysuccinimide, or other reagents) which react with *N*-dimethylaminopyridine forming an acyl pyridinium intermediate. The role of $Sc(OTf)_3$ may be to coordinate with the carbonyl oxygen of this acyl pyridinium intermediate, providing a highly reactive species.

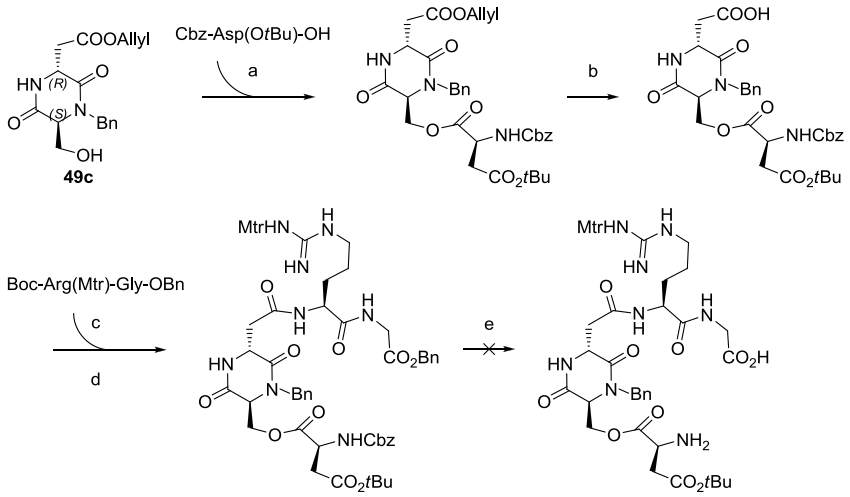

Scheme 3.5 – **Reagents and conditions:** a) $Sc(OTf)_3$, EDC, DMAP, DCM, -8°C → r.t, 2h: 90%; b) $[Pd(PPh_3)_4]$, PPh_3, pyrrolidine, DCM, 0°C: 100%; c) TFA/DCM 1:2, 3h; d) HATU, HOAt, DIPEA, DMF, 0°C → r.t., 2.5 days: 73 %; e) Pd/C 10%, H_2, MeOH, 2 days

Allyl ester was then cleaved quantitatively in the already described conditions, and the free carboxylic acid thus obtained was coupled with the Arg(Mtr)-Gly-OBn fragment in presence of HATU, HOAt and *i*Pr_2EtN (Scheme 3.5).

Several protocols were employed while trying to hydrogenolytically cleave both benzylester and Cbz (Pd/C 10%, MeOH; $Pd(OH)_2$/C 20%, MeOH; Pd/C 10% THF; $Pd(OH)_2$/C 20%, THF; Pd/C 10%, DCM; $Pd(OH)_2$/C 20%, DCM). Milder procedures provided a partially deprotected intermediate, in which Cbz had not been cleaved, while prolonging reaction times resulted in the break of the depsi bond. Feeling not confident enough on the efficacy of a depsipeptide *in vivo* (ester bond stability), and

considering that affording this new synthetic target revealed more troublesome and time consuming than expected, we decided to discontinue the project.

3 - Cyclic [DKP-*iso*DGR] compounds

The growing interest towards the *iso*DGR recognition motif and the encouraging results obtained by our cyclic RGD-containing compounds (see §2) led us to conceive a new class of cyclic peptidomimetics bearing the *iso*DGR sequence and incorporating a bifunctional diketopiperazine scaffold, which could serve as integrin antagonists.

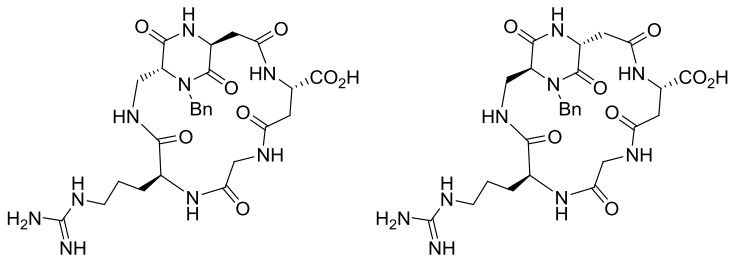

118 **119**

Figure 3.28 – *iso*DGR containing compounds **c[DKP2-*iso*DGR]** and **c[DKP3-*iso*DGR]**.

However, it must be kept in mind that simply replacing the RGD sequence with *iso*DGR within the context of an already existing compound might not provide the expected results, because an inverted orientation of the ligand is required to interact with the RGD-binding pocket. Moreover, flanking residues contribution in enhancing binding affinity and specificity might be affected. Lacking a reliable model for aprioristic prediction of binding affinities/ docking to the most interesting $\alpha_5\beta_1$ integrin, we decided to start an investigation synthesizing two compounds bearing our two progenitor *trans* diketopiperazines, namely **DKP2** and **DKP3**, as a scaffold (**118**, **119**, Figure 3.28).

3.1 - Synthesis

A synthesis *in solution*, very similar to the one adopted in the case of our RGD-containing pentapeptidomimetics, was planned at first. Considering the commercially available starting material, a Fmoc strategy was needed (Scheme 3.6). Thus, we envisaged the synthesis of dipeptide Fmoc-*iso*Asp(*t*Bu)-Gly-OBn, which was easily achieved in good yields using Carpino's coupling reagents (HATU, HOAt), and of a modified *N*-Fmoc protected diketopiperazine scaffold. Nevertheless, we soon discouraged from pursuing this approach, due to the annoing dirty cleavage of the Fmoc protecting group in solution.

The recent success in the synthesis of a DKP-containing decapeptide on solid phase (see Chapter 4), suggested to take advantage of a similar strategy, envisaging a solid phase synthesis of a linear advanced intermediate which could therefore be cyclized in solution.

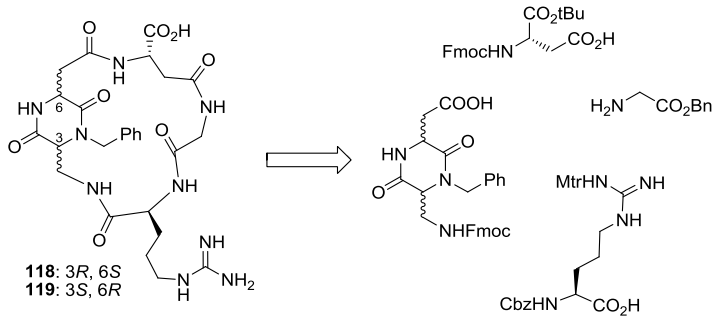

Scheme 3.6 – in solution approach to the synthesis of *iso*DGR-containing compounds, using Fmoc strategy.

I already had experience with the synthesis of modified diketopiperazine **DKP1*** (see Chapter 2), bearing the usual carboxy acid group and an amino group masked as azide. Similarly, modified versions of **DKP2** and **DKP3**, which could serve as building blocks in a Fmoc solid phase synthetic approach, were easily obtained (**DKP2*** and **DKP3***, Chapter 2).

We planned to build a linear pentapeptide on resin starting from commercially available Fmoc-Gly-OH, Fmoc-Asp(OH)-O*t*Bu and Cbz-Arg(Mtr)-OH, and easy accessible **DKP2*** or **DKP3*** (Scheme 3.7).

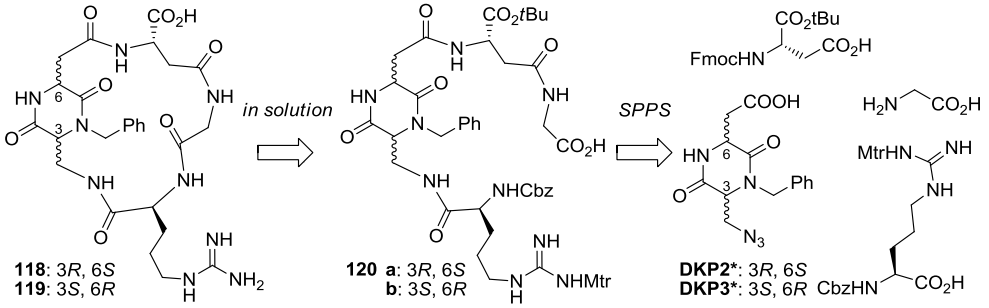

Scheme 3.7 – solid phase approach to the synthesis of *iso*DGR-containing compounds, using Fmoc strategy.

Cleavage from the resin needed to be orthogonal respect to side chain deprotection (acid labile *t*Bu-ester and Mtr-sulfonamide), thus SASRIN™ (Super Acid Sensitive resIN) was chosen as the solid support (Figure 3.29).

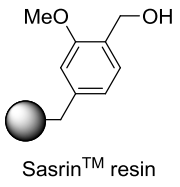

Figure 3.29

The first aminoacid, namely Gly, was treated with di*iso*propylcarbodiimide (DIC) and a catalytic amount of dimethylaminopyridine (DMAP) in dimethylformamide in order to form an ester bond with the resin linker (Scheme 3.8).

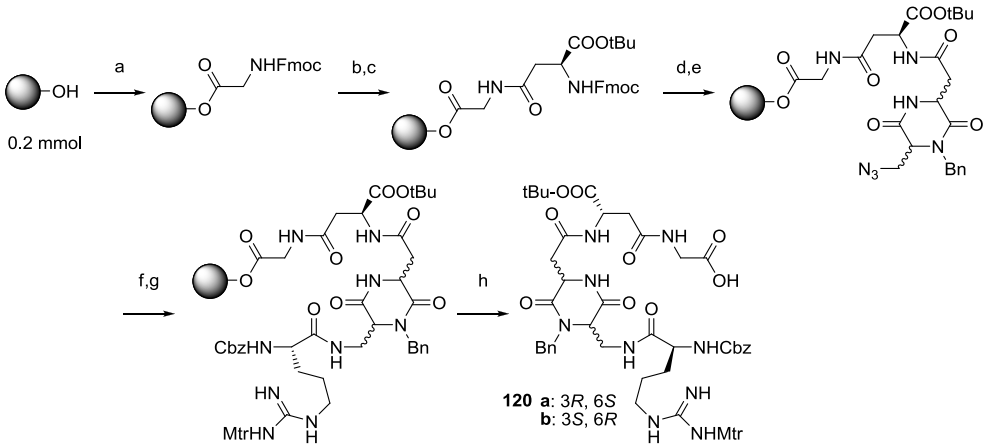

Scheme 3.8 – SPPS of linear pentapeptide intermediates: a) Fmoc-Gly-OH, DIC, $DMAP_{cat}$, DMF, 2h; b) piperidine 20%, in DMF; c) Fmoc-Asp(OH)-O*t*Bu, DIC, HOAt, DMF, 3h; d) piperidine 2%, DBU 2%, in DMF; e) **DKP2*** *or* **DKP3***, DIC, HOAt, DMF, 18h; f) Me_3P, dioxane/water 4:1; g) Cbz-Arg(Mtr)-OH, DIC, HOAt, DMF, 18h; h) 1% TFA, DCM: 88% overall yield.

Fmoc deprotections were performed either with 20% solutions of piperidine in DMF or, in milder conditions, with DMF solutions of piperidine (2%) and diazabicycloundecene (DBU) (2%), while all coupling reactions were performed using activated –OAt esters which were generated treating the corresponding amino acids with DIC and HOAt in DMF. The activated ester mixture was added to the resin, which was shaken at r.t.. Reaction times varied from 2h to 18h in the case of more challenging couplings (Scheme 3.8).

After coupling the diketopiperazine scaffold, an interesting *in situ* azide reduction was performed to free the amino group in presence of Me_3P (1M in toluene) in a 4:1 mixture of dioxane and water, which served to hydrolyze the iminophosphorane intermediate. After washing the resin, the free amine obtained was ready for the subsequent coupling reaction.

Only linear intermediate **120** was isolated, after cleavage form the resin in weakly acidic conditions (1% TFA in DCM) (Scheme 3.8).

After being cleaved from resin, linear peptide intermediate **120** needed extensive purification. Cbz hydrogenolytical cleavage in presence of Pd/C 10% in THF and subsequent macrolactamization using HATU, HOAt and DIPEA, in DMF, were then carried out in solution (Scheme 3.9). Both cyclization and final side-chain deprotection were performed in the same conditions already described for our RGD-containing peptides (see §2.1).

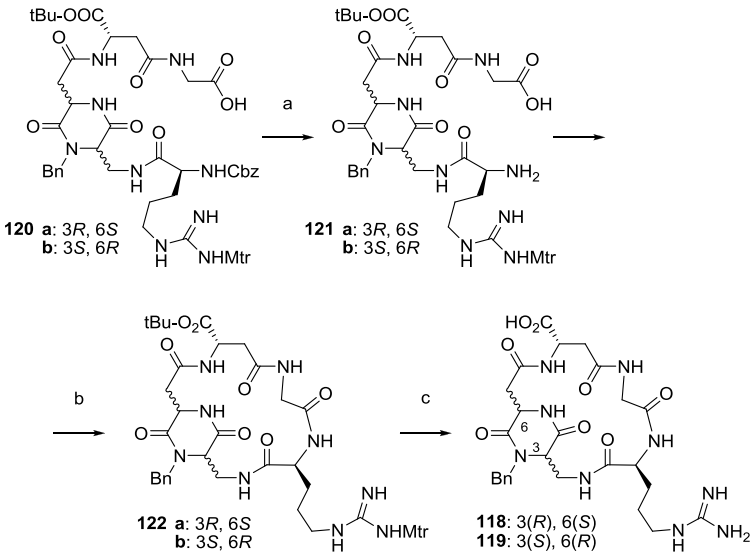

Scheme 3.9 – a) H_2, Pd/C 10%, THF/water 1:1; b) HATU, HOAt, DIPEA, 1.4 mM, DMF; c) TFA/thioanisole/EDT/anisole 90:5:3:2.

The latest step, in particular, provided products **118** and **119** in unexpected low yields, an will be hence object of optimization.

3.2 - Biological evaluation [71]

The cyclic *iso*DGR peptidomimetics were examined *in vitro* for their ability to inhibit biotinylated vitronectin binding to the purified $\alpha_v\beta_3$ and $\alpha_v\beta_5$ receptors (Table 3.5).

Screening assays were performed incubating the immobilized integrin receptors with various concentrations (10^{-10}–10^{-5} M) of the *iso*DGR ligands **118-119** in the presence of biotinylated vitronectin (1 μg/mL), and measuring the concentration of bound vitronectin in the presence of the competitive ligands. The ability of the new compounds to inhibit the binding of vitronectin to the isolated $\alpha_v\beta_3$ and $\alpha_v\beta_5$ receptors may be compared with that of *iso*DGR-containing compounds reported in the literature by Kessler et al. such as c(G-*iso*DGR-phg) (**101**, Figure 3.14), which where tested in the same kind of assay (Table 3.5).[69]

Compound **119**, incorporating diketopiperazine scaffold **DKP3**, displays low nanomolar affinity towards $\alpha_V\beta_3$ integrin (IC_{50}: 9.2 ± 1.1 nM), with a slight selectivity respect to $\alpha_V\beta_5$ integrin (IC_{50}: 312 ± 21 nM). Moreover, **119** appears ten fold more active in the inhibition of biotinylated vitronectin binding to $\alpha_V\beta_3$ integrin respect to c(G-*iso*DGR-phg) (**101**), which was chosen as a reference. These low nanomolar IC_{50} values are also comparable to those obtained by RGD containing compounds, such as c(RGDfV) (**86**) or ST1646 (**89**).

Unfortunately, the results related to compound **118** are still not available. This preliminary results should anyway be considered very promising.

Table 3.5 - Inhibition of biotinylated vitronectin binding to $\alpha_v\beta_3$ and $\alpha_v\beta_5$ receptors

Compound	Structure	$\alpha_V\beta_3$ IC_{50} [**nM**][a]	$\alpha_V\beta_5$ IC_{50} [**nM**][a]
118	*Cyclo* [**DKP2**-*iso*DGR]	n. a.	n. a.
119	*Cyclo* [**DKP3**-*iso*DGR]	9.2 ± 1.1	312 ± 21
ref	c(G-*iso*DGR-phg)	89 ± 19	-

[a] IC_{50} values were calculated as the concentration of compound required for 50% inhibition of biotinylated vitronectin binding as estimated by GraphPad Prism software; all values are the arithmetic mean ± SD of triplicate determinations.

NMR studies and conformational analysis are *in progress*.

References:

[1] R.O. Hynes, *Cell* **1987**, *48*, 549-554.

[2] M. Millard, S. Odde, N. Neamati, Theranostics 2011, 1, 154-188.

[3] a) M. Shimaoka, T.A. Springer, *Nature Rev. Drug Discov.* **2003**, *2*, 703-716; b) K.-E.Gottschalk; H. Kessler, *Angew. Chem. Int. Ed.* **2002**, *41*, 3767-3774; W.H. Miller, et al. *Drug Discovery Today* **2000**, *5*, 397-408; d) I. Ojima, *Bioorg. Med. Chem.* **1995**, *3*, 337-360.

[4] E. Ruoslahti, *Matrix Biol.* **2003**, *22*, 459-465; b) E. Ruoslahti, *Annu. Rev. Cell Dev. Biol.* **1996**, *12*, 967-715.

[5] a) J. P. Xiong, T. Stehle, B. Diefenbach, R. Zhang, R. Dunker, D. L. Scott, A. Joachimiak, S. L. Goodman, M. A. Arnaout, *Science* **2001**, *294*, 339-345; b) J. P. Xiong, T. Stehle, R. Zhang, A. Joachimiak, M. Frech, S. L. Goodman, M. A. Arnaout, *Science* **2002**, *296*, 151-155.

[6] a) W. Chen, C. Chang, M. K. Gilson, *J. Am. Chem. Soc*. **2006**, *128*, 4675-4684; b) L. Marinelli, A. Meyer, D. Heckmann, A. Lavecchia, E. Novellino, H. Kessler, *J. Med. Chem.* **2005**, *48*, 4204-4207; c) L. Marinelli, K.-E. Gottschalk, A. Meyer, E. Novellino, H. Kessler, *J. Med. Chem.* **2004**, *47*, 4166-4177; d) T. Xiao, J. Takagi, B. S. Coller, J.-H. Wang, T. A. Springer, *Nature* **2004**, *432*, 59-67; e) T. A. Springer, J. Zhu, T. Xiao, *J. Cell Biol.* **2008**, *182*, 791-800; f) T. J. You, D. S. Maxwell, T. P. Kogan, Q. Chen, J. Li, J. Kassir, G. W. Holland, R. A. F. Dixon, *Biophys. J.* **2002**, *82*, 447-457.

[7] R. O. Hynes, *Cell* **2002**, *110*, 673-687.

[8] T. A. Springer, *Proc. Natl. Acad. Sci. USA* **1997**, *94*, 65–72.

[9] M. J. Humphries, *Biochem. Soc. Trans.* **2000**, *28*, 311–339.

[10] M. Shimaoka, J. Takagi, T. A. Springer, *Annu. Rev. Biophys. Biomol. Struct.* **2002**, *31*, 485–516.

[11] S. C. Fagerholm, T. J. Hilden, C. G. Gahmberg, *Trends Biochem. Sci.* **2004**, *29*, 504–512.

[12] J. Ylanne, *Front. Biosci.* **1998**, *3*, 877–886.

[13] a) J. C. Loftus, J. W. Smith, M. H. Ginsberg, *J. Biol. Chem.* **1994**, *269*, 25235–25238; b) E. F. Plow, T. A. Haas, L. Zhang, J. C. Loftus, J. W. Smith, *J. Biol. Chem*. **2000**, *275*, 21785–21788; b) A. van der Flier, A. Sonnenberg, *Cell Tissue Res.* **2001**, *305*, 285–298.

[14] a) J. W. Smith, R. S. Piotrowicz, D. Mathis, *J. Biol. Chem.* **1994**, *269*, 960–967; b) A. P. Mould, S. K. Akiyama, M. J. Humphries, *J. Biol. Chem.* **1995**, *270*, 26270–26277.

[15] H. Jin, J. Varner, *Br J Cancer* **2004**, *90*, 561–565.

[16] B. A. Teicher, L. M. Ellis, Eds., *Antiangiogenic Agents in Cancer Therapy*, Humana Press, **2008**, *Chapter 3*, 49-71.

[17] M. Moser, K. R. Legate, R. Zent, R. Fässler, *Science* **2009**, *324*, 895-899.

[18] M. A. Arnaout, B. Mahalingam, and J.-P. Xiong, *Annu. Rev. Cell Dev. Biol.* **2005**, *21*, 381-410.

[19] K. Legate, S. Wickström, R. Fässler, *Genes Dev.* **2009**, *23*, 397-418.

[20] J. Desgrosellier, D. Cheresh, *Nat Rev Cancer*. **2010**, *10*, 9-22.

[21] P. Carmeliet, *Nat. Med.* **2003**, *9*, 653–660.

[22] N. Ferrara, R. S. Kerbel, *Nature* **2005**, *438*, 967–974.

[23] S. Kim, K. Bell, S. A.Mousa, J. A.Varner, *Am. J. Pathol.* **2000**, *156*, 1345–1362.

[24] N. Laurens, M. a Engelse, C. Jungerius, C. W. Löwik, V. W. M. van Hinsbergh, P. Koolwijk, *Angiogenesis* **2009**, *12*, 275-285.

[25] P. C. Brooks, R. A. Clark, D. A. Cheresh, *Science* **1994**, *264*, 569–571.

[26] P. C. Brooks, A. M. Montgomery, M. Rosenfeld, R. A. Reisfeld, T. Hu, G. Klier, D. A. Cheresh, *Cell* **1994**, *79*, 1157–1164.

[27] M. Friedlander, P. C. Brooks, R. W. Shaffer, C. M. Kincaid, J. A. Varner, D. A.Cheresh, *Science* **1995**, *270*, 1500–1502.

[28] L. E. Reynolds, L. Wyder, J. C. Lively, D. Taverna, S. D. Robinson, X. Huang, D. Sheppard, R. O. Hynes, K. M. Hodivala-Dilke, *Nat. Med.* **2002**, *8*, 27–34.

[29] D. G. Stupack, X. S. Puente, S. Boutsaboualoy, C. M. Storgard, D. A. Cheresh, *J. Cell Biol.* **2001**, *155*, 459–470.

[30] J.-P. Xiong, B. Mahalingham, J. L. Alonso, L. A. Borrelli, X. Rui, S. Anand, B. T. Hyman, T. Rysiok, D. Müller-Pompalla, S. L. Goodman, et al., *J. Cell Biol.* **2009**, *186*, 589-600.

[31] a) A. Meyer, J. Auernheimer, A. Modlinger, H. Kessler, *Curr. Pharm. Des.* **2006**, *12*, 2723-2747; b) L. Marinelli, K.-E. Gottschalk, A. Meyer, E. Novellino, H. Kessler, J. Med. Chem. 2004, 47, 4166-4177.

[32] S. Kim, M. Bakre, H. Yin, J. A. Varner, *J. Clin. Invest.* **2002**, *110*, 933–941.

[33] S. Kim, M. Harris, J. A. Varner, *J. Biol. Chem.* **2000**, *275*, 33920–33928.

[34] J. Takagi, K. Strokovich, T. A. Springer, T. Walz, *EMBO J.* **2003**, *22*, 4607-4615.

[35] L. Marinelli, A. Meyer, D. Heckmann, A. Laveccia, E. Novellino, H. Kessler, J. Med. Chem. 2005, 48, 4204-4207.

[36] A. Hillisch, L. F. Pineda, R. Hilgenfeld, *Drug Discov. Today* **2004**, *9*, 659-569.

[37] B. Furie, *Hematology* **2009**, 255–258.

[38] D. R. Phillips, P. P. Agin, *J. Clin. Invest.* **1977**, *60*, 535–545.

[39] B. S. Coller, S. J. Shattil, *Blood* **2008**, *112*, 3011–3025.

[40] D. Cox, M. Brennan, N. Moran, *Nat. Rev. Drug Discov.* **2010**, *9*, 804-820.

[41] D. Phillips, I. Charo, R. Scarborough, *Cell* **1991**, *65*, 359-362.

[42] a) J. Zhu, B. H. Luo, T. Xiao, C. Zhang, N. Nishida, T. A. Springer, *Mol. Cell* **2008**, *32*, 849-861; b) T. A. Springer, J. Zhu, T. Xiao, *J. Cell Biol.* **2008**, *182*, 791-800.

[43] T. Kamata, K. K. Tieu, T. A. Springer, Y. Takada, *J. Biol. Chem.* **2001**, *276*, 44275-44283.

[44] a) M. Hoefling, H. Kessler, K.-E. Gottschalk, *Angew. Chem. Int. Ed.* **2009**, *48*, 6590-6593; b) T. Xiao, J. Takagi, B. S. Coller, J.-H. Wang, T. A. Springer, *Nature*, **2004**, *432*, 59-67.

[27] Marinelli, L.; Meyer, A.; Heckmann, D.;

[45] M. D. Pierschbacher, E. Ruoslahti, *Nature* **1984**, *309*, 30-33.

[46] a) S. Swenson, S. Ramu, F.S. Markland, *Curr. Pharm. Des.* **2007**, *13*, 2860-2871; b) J. J. Calvete, C. Marcinkiewicz, D. Monleón, V. Esteve, B. Celda, P. Juárez, L. Sanz, *Toxicon* **2005**, *45*, 1063-1074; c) Y. Fujii, D. Okuda, Z. Fujimoto, Z., *J. Mol. Biol.* **2003**, *332*, 1115-1122; d) R. J. Gould, M. A. Polokoff, P. A. Friedman, T. F. Huang, J. C. Holt, J. J. Cook, S. Niewiarowski, *Proc. Soc. Exp. Biol. Med.* **1990**, *195*, 168-171.

[47] a) D. Simon, H. Xu, S. Ortlepp, C. Rogers, N. Rao, *Arterioscler. Thromb. Vasc. Biol.* **1997**, *17*, 528-535; b) M. Dennis, W. Henzel, R. Pitti, M. Lipari, M. Napier, T. Deisher, et al.. *Proc. Natl. Acad. Sci. U. S. A.* **1990**, *87*, 2471-2475; c) I. Ojima, S. Chakravarty, Q. Dong, *Bioorg. Med. Chem.* **1995**, *3*, 337-360.

[48] a) T. Doi, S. Kamioka, S. Shimazu, T. Takahashi, *Org. Lett.* **2008**, *10*, 817-819; b) M. Ishikawa, M. Tsushima, D. Kubota, Y. Yanagisawa, Y. Hiraiwa, Y. Kojima, K. Ajito, N. Anzai. *Org. Proc. Res. Dev.* **2008,** *12*, 596-602; c) D. Heckmann, A. Meyer, L. Marinelli, G. Zahn, R. Stragies, H. Kessler, *Angew. Chem. Int. Ed.* **2007**, *46*, 3571-3574; d) D. Heckmann, A. Meyer, B. Laufer, G. Zahn, R. Stragies, H. Kessler, *ChemBioChem* **2008**, *9*, 1397-1407; e) S. Urman, K. Gaus, Y. Yang, U. Strijowski, N. Sewald, S. De Pol, O. Reiser, *Angew. Chem. Int. Ed.* **2007**, *46*, 3976-3978; f) Stupp, R., Rüegg, C, *J. Clin. Oncol.* **2007**, *25*, 1637-1638; g) A. Del Gatto, L. Zaccaro, P. Grieco, E. Novellino, A. Zannetti, S. Del Vecchio, F. Iommelli, M. Salvatore, C. Pedone, M. Saviano, *J. Med. Chem.* **2006**, *49*, 3416-3420; h) Neri, D.; Bicknell, R., *Nature Rev.* **2005**, *5*, 436-446; i) P. Vianello, P. Cozzi, A. Galvani, M. Meroni, M. Varasi, D. Volpi, T. Bandiera, *Bioorg. Med. Chem. Lett.* **2004**, *14*, 657-661; j) Schaffner, P.; Dard, M.M., *Cell. Mol. Life Sci.* **2003**, *60*, 119-132; k) E. Lohof, E. Planker, C. Mang, F. Burkhart, M. A. Dechantsreiter, R. Haubner, H.-J. Wester, M. Schwaiger, G. Hölzemann, S. L. Goodman, H. Kessler, *Angew. Chem. Int. Ed.* **2000**, *39*, 2761-2764; l) M. A. Dechantsreiter, E. Planker, B. Mathä, E. Lohof, G. Hölzemann, A. Jonczyk, S. L. Goodman, H. Kessler, *J. Med. Chem.*

1999, *42*, 3033-3040; m) J. Wermuth, S. L. Goodman, A. Jonczyk, H. Kessler, *J. Am. Chem. Soc.* **1997**, *119*, 1328-1335; Paolillo, M.; n) M. A. Russo, M. Serra, L. Colombo, S. Schinelli, *Mini-Rev. Med. Chem.* **2009**, *9*, 1439-1446; o) Z. Liu, F. Wang, X. Chen, *Drug Dev. Res.* **2008**, *69*, 329-339.

[49] T. A. Springer, J. Zhu, T. Xiao, *J. Cell. Biol.* **2008**, *182*, 791-800.

[50] F. Curnis, A. Sacchi, A. Gasparri, R. Longhi, A. Bachi, C. Doglioni, C. Bordignon, C. Traversari, G.-P. Rizzardi, A. Corti, *Cancer Res.* **2008**, *68*, 7073-7082.

[51] A. Spitaleri, S. Mari, F. Curnis, C. Traversari, R. Longhi, C. Bordignon, A. Corti, G.-P. Rizzardi, G. Musco, *J. Biol. Chem.* **2008**, *283*, 19757-19768.

[52] F. Curnis, A. Cattaneo, R. Longhi, A. Sacchi, A. M. Gasparri, F. Pastorino, P. Di Matteo, C. Traversari, A. Bachi, M. Ponzoni, et al., *J. Biol. Chem.* **2010**, *285*, 9114-9123.

[53] A. Corti, F. Curnis, *J. Cell Sci.* **2011**, *124*, 515-522.

[54] M. Aumailley, M. Gurrath, G. Müller, J. Calvete, R. Timpl, H. Kessler *FEBS Lett.* **1991**, *291*, 50-54.

[55] L. Auzzas, F. Zanardi, L. Battistini, P. Burreddu, P. Carta, G. Rassu, C. Curti, G. Casiraghi, *Curr. Med. Chem.* **2010**, *17*, 1255-1299.

[56] a) S. Hanessian, L. Auzzas, *Acc. Chem. Res*. **2008**, *41*, 1241-1251; b) A. Trabocchi, D. Scarpi, A. Guarna, *Amino Acids* **2008**, *34*, 1-24; c) S. M. Cowell, Y. S. Lee, J. P. Cain, V. J. Hruby, *Curr. Med. Chem.* **2004**, *11*, 2785-98.

[57] Haubner, R.; Schmitt, W.; Hölzemann, G.; Goodman, S.L.; Jonczyk, A.; Kessler, H. *J. Am. Chem. Soc*. **1996**, *118*, 7881-91.

[58] a) L. Belvisi, A. Bernardi, M. Colombo, L. Manzoni, D. Potenza, C. Scolastico, G. Giannini, M. Marcellini, T. Riccioni, M. Castorina, P. LoGiudice C. Pisano, *Bioorg. Med. Chem.* **2006**, *14*, 169-180; b) L. Manzoni, L. Belvisi, D. Arosio, M. Civera, M. Pilkington-Miksa, D. Potenza, A. Caprini, E. M. V. Araldi, E. Monferrini, M. Mancino, F. Podestà, C. Scolastico, *ChemMedChem* **2009**, *4*, 615 –632.

[59] L. Belvisi, T. Riccioni, M. Marcellini, L. Vesci, I. Chiarucci, D. Efrati, D. Potenza, C. Scolastico, L. Manzoni, K. Lombardo, M. A. Stasi, A. Orlandi, A. Ciucci, B. Nico, D. Ribatti, G. Giannini, M. Presta, P. Carminati, C. Pisano, *Mol. Cancer Ther*. **2005**, *4*, 1670-1680.

[60] D. Arosio, L. Belvisi, L. Colombo, M. Colombo, D. Invernizzi, L. Manzoni, D. Potenza, M. Serra, M. Castorina, C. Pisano, C. Scolastico, *ChemMedChem* **2008**, *3*, 1589-1603.

[61] R. Haubner, W. Schmitt, G. Hölzemann, S. L. Goodman, A. Jonczyk, H. Kessler, *J. Am. Chem. Soc.* **1996**, *118*, 7881-7891.

[62] F. Sladojevich, A. Trabocchi, A. Guarna, *J. Org. Chem.* **2007**, *72*, 4254-4257.

[63] a) R. M. Van Well, L. Marinelli, C. Altona, K. Erkelens, G. Siegal, M. van Raaij, A. L. Llamas-Saiz, H. Kessler, E. Novellino, A. Lavecchia, J. H. van Boom, M. Overhand, *J. Am. Chem. Soc.* **2003**, *125*, 10822-10829; b) R. M. Van Well, H. S. Overkleeft, G. A. van der Marel, D. Bruss, G. Thibault, P. G. de Groot, J. H. van Boom, M. Overhand, *Bioorg.Med. Chem. Lett.* **2003**, *13*, 331-334.

[64] G. Casiraghi, G. Rassu, L. Auzzas, P. Burreddu, E. Gaetani, L. Battistini, F. Zanardi, C. Curti, G. Nicastro, L. Belvisi, I. Motto, M. Castorina, G. Giannini, C. Pisano, *J. Med. Chem.* **2005**, *48*, 7675-7687.

[65] F. Zanardi, P. Burreddu, G. Rassu, L. Auzzas, L. Battistini, C. Curti, A. Sartori, G. Nicastro, G. Menchi, N. Cini, A. Bottoncetti, S. Raspanti, G. Casiraghi, *J. Med. Chem.* **2008**, *51*, 1771-82.

[66] a) M. Weller, D. Reardon, B. Nabors, R. Stupp, *Nat. Med*. **2009**, *15*, 726; b) A. R. Reynolds, K. M. Hodivala-Dilke, *Nat. Med*. **2009**, *15*, 727.

[67] a) S. M. Weis, D. G. Stupack, D. A. Cheresh, *Cancer Cell* **2009**, *15*, 359-361; b) A. R. Reynolds, I. R. Hart, A. R. Watson, J. C. Welti, R. G. Silva, S. D. Robinson, Da Violante, M. Gourlaouen, M. Salih, M. C. Jones, D. T. Jones, G. Saunders, V. Kostourou, F. Perron-Sierra, J. C. Norman, G. C. Tucker, K. M. Hodivala-Dilke, *Nat. Med*. **2009**, *15*, 392-400. For recent examples of other antiangiogenic agents causing tumor progression in preclinical models, see: e) M.

Pàez-Ribes, E. Allen, J. Hudock, T. Takeda, H. Okuyama, F. Viñals, M. Inoue, G. Bergers, D. Hanahan, O. Casanovas, *Cancer Cell* **2009**, *15*, 230-231; f) J. M. L. Ebos, C. R. Lee, W. Cruz-Munoz, G. A. Bjarnason, J. G. Christensen, R. S. Kerbel, *Cancer Cell* **2009**, *15*, 232-239.

[68] F. Curnis, R. Longhi, L. Crippa, A. Cattaneo, E. Dondossola, A. Bachi, A. Corti, *J. Biol. Chem.* **2006**, *281*, 36466–36476

[69] A. O. Frank, E. Otto, C. Mas-Moruno, H. B. Schiller, L. Marinelli, S. Cosconati, A. Bochen, D. Vossmeyer, G. Zahn, R. Stragies, et al., *Angew. Chem. Int. Ed.* **2010**, *49*, 9278-9281.

[70] A. S. M. da Ressurreição, A. Vidu, M. Civera, L. Belvisi, D. Potenza, L. Manzoni, S. Ongeri, C. Gennari, U. Piarulli, *Chem. Eur. J.* **2009**, *15*, 12184-8.

[71] The biological studies reported in this section were carried out by Dr. Daniela Arosio from CNR-ISTM, Milan, whom I sincerely acknowledge for the kind collaboration.

[72] a) G. Müller, M. Gurrath, H. Kessler, *J. Comput.-Aided Mol. Des.* **1994**, *8*, 709-730; b) R. Haubner, R. Gratias, B. Diefenbach, S. L. Goodman, A. Jonczyk, H. Kessler, *J. Am. Chem. Soc.* **1996**, *118*, 7461-7472; c) M. Aumailley, M. Gurrath, G. Müller, J. Calvete, R. Timpl, H. Kessler, *FEBS Lett.* **1991**, *291*, 50-54.

[73] The NMR characterization and computational studies reported in this section were carried out by Dr. Donatella Potenza, Dr. Laura Belvisi and M.Sc. Ileana Guzzetti from the University of Milan, whom I sincerely acknowledge for the kind collaboration.

[74] H. Zhao, A. Pendri, R. B. Greenwald, *J. Org. Chem.* **1998**, *63*, 7559-7562.

4 DESIGN, SYNTHESIS AND CONFORMATIONAL ANALYSIS OF AN α/β-PEPTIDE FOLDAMER

As part of my project, I spent six months (October 2010 – March 2011) in the group of Prof. Oliver Reiser at the University of Regensburg, working on the design of α/β–peptide foldamers, containing diketopiperazine repeating units as secondary structure inducers.

1 - Foldamers

Foldamers were first defined by Gellmann in the mid-'90s as oligomers of modest length with a strong tendency to adopt a specific compact conformation in solution.[1]

Protein–protein interactions (PPIs) are involved in a large number of biological processes. As many diseases originate from their malfunction, inhibiting PPIs may represent a promising strategy for drug discovery. Small molecule inhibitors often failed in targeting protein surface motifs.[2] Over the past two decades many researchers have been looking for biopolymer-like folding behavior in unnatural oligomers,[3] with the aim of using compact and specific conformations to mimic biopolymer-like functions. Protein surface recognition by mimicking distinct folding patterns along with proteolytic stability is the main advantage of foldamers compared to α-peptides or small drug molecules.

Early efforts in the field focused on β-peptides,[4] and they remain subjects of intensive investigation today.[5] Other prominent representatives of this field are the γ-peptides,[6] azapeptides[7] and oligoureas[8] (Figure 4.1).

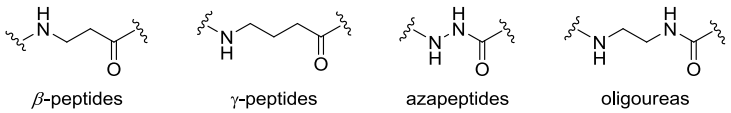

Figure 4.1 – Selected aliphatic foldamer backbones

However, foldamers with heterogeneous backbones having various periodic motifs,[9,10] such as α/β-peptides, gained interest in recent years. Heterogeneous backbones are intriguing at a fundamental level, since they diverge from the homogeneous backbones of the biological precedents, proteins and nucleic acids.

1.1 - *α*/*β*-Peptide foldamers

Foldamer design based on heterogeneous backbones offers benefits relative to an exclusive reliance on homogeneous backbones. For a given set of monomer classes, the number of candidate foldamer backbones is vastly larger if we include heterogeneous backbones than if we are limited to homogeneous backbones. Considering, for example, only *α*- and *β*-amino acids as building blocks, then the homogeneous approach limits us to *α*-peptides or *β*-peptides. The heterogeneous approach, in contrast, allows many different combinations (e.g., *α*-*β*-*α*-*β*-*α*-*β*-, *α*-*α*-*β*-*α*-*α*-*β*-, *α*-*β*-*β*-*α*-*β*-*β*-, *α*-*α*-*β*-*β*-, to name just a few).[11] The study of heterogeneous backbone foldamers has several advantages over that of their homogeneous backbone counterparts, including access to many new molecular shapes based on variations in the stoichiometries and patterns of the subunit combinations and improved prospects for side chain diversification.

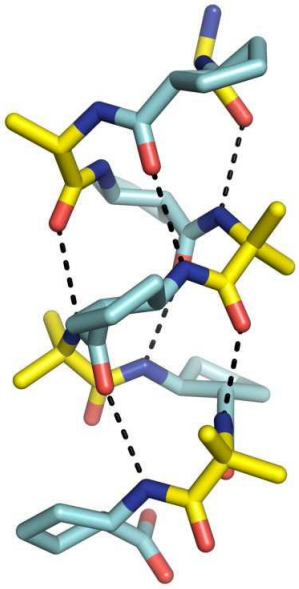

Figure 4.2 - Crystal structure of an *α*/β-peptide, with 1:1 *α*:β alternation in the backbone, in the 14/15-helical conformation. *α*-amino acid residues are yellow, and *β*-amino acid residues are blue.[12]

Recent efforts to develop α/*β*-peptide foldamers (Figure 4.2) can be divided into two conceptually distinct classes.[13] The first includes entities prepared using a "block" strategy, in which α-peptide segments and *β*-peptide segments are combined to form a hybrid oligomer. The second class encompasses designs in which α- and *β*-amino acid monomers are interspersed in a regular pattern throughout an oligomer sequence.

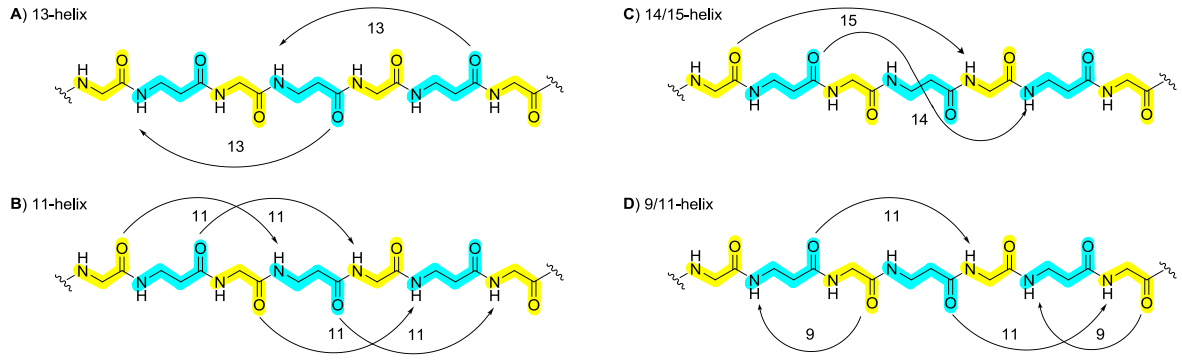

Figure 4.3 – Hydrogen bonding patterns observed in different helices formed by α/*β*-peptides with 1:1 backbone alternation.[10]

The "block" approach was mainly adopted to study sheet secondary structures, introducing reverse turn motifs within a strand-forming segment, thus promoting a hairpin.[14]

The first systematic structural studies of linear oligomers with backbone alternation of α- and *β*-residues were conducted independently by the groups of Reiser[15] and Gellman.[16]

Reiser and coworkers document the formation of a 13-helix (Figure 4.3, A) by α/*β*-peptides containing L-alanine residues alternating with 3-substituted *cis*-2-aminocyclopropanecarboxylic acid residues. Indicative of the adopted helical conformation is the $i \rightarrow i - 2$ C=O· ·H-N H-bonding pattern showed by heptamer **121** (Figure 4.4) in methanol.

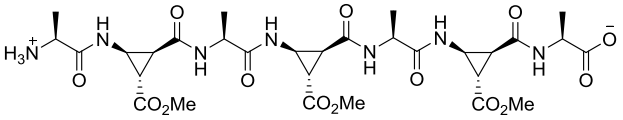

121

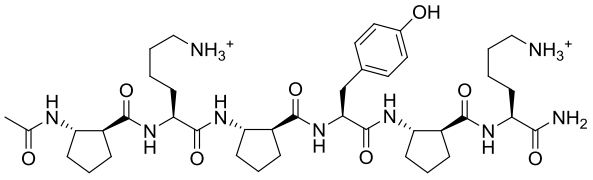

122

Figure 4.4

Earlier pharmacological studies showing that incorporation of a single *cis*-2-aminocyclopropanecarboxylic acid residue into a peptide corresponding to the C-terminus of neuropeptide Y gave rise to substantial affinity and unique selectivity toward the natural receptor proteins, inspired this structural work.[17]

On the other hand, Gellman and co-workers prepared hexamers and octamers containing either (*S*,*S*)-2-aminocyclohexanecarboxylic acid (ACHC) or (*S*,*S*)-2-aminocyclopentanecarboxylic acid (ACPC) alternating with either L- or D-*α*-amino acid residues, in order to find new foldamers. In fact, *β*-peptide sequences containing *trans*-ACHC or *trans*-ACPC already proved the ability of these conformationally preorganized structures to promote stable secondary structures (*i.e.* *β*-peptide helices) within short oligomers.[3b] Only the combination of (*S*,*S*)-ACPC with L-*α*-amino acid (**122**, Figure 4.4) gave rise to nonsequential NOEs, which resulted indicative of two different rapidly interconverting helical conformations: one involving $i \rightarrow i + 3$ and the other $i \rightarrow i + 4$ C=O· ·H-N H-bonds (11-helix and 14/15 helix, Figure 4.3 B,C). These H-bonding patterns are typically observed in *α*-peptide backbones, and correspond to 3_{10}- and α-helices respectively.[18]

A "mixed" H-bonding pattern such as 9/11-helix, featuring two distinct types of backbone C=O· ·H-N H-bonds with opposite orientations relative to the backbone direction (Figure 4.3 D), was also identified by Sharma, Kunwar, and co-workers (**123**, Figure 4.5).[19] Compounds of this type,

containing β^3-residues, are probably adopting a 14/15-helix-like conformation lacking intramolecular H-bonds, as postulated by Seebach and co-workers.[20]

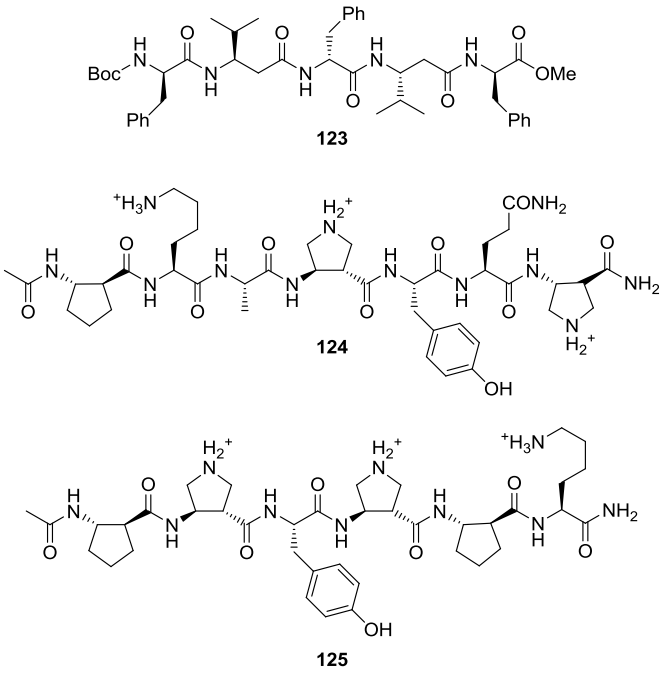

Figure 4.5

Foldameric behavior is not limited to α/β-peptides with a 1:1 α/β residue alternation. For example, both 2:1 and 1:2 α/β backbone patterns (such as **124** and **125**, respectively, Figure 4.5) were recently found to promote helix formation in short oligomers.[21]

Overall, the structural data obtained with short oligomers suggest that the propensity to form $i \rightarrow i + 3$ and/or $i \rightarrow i + 4$ C=O· ·H-N H-bonded helices, typical of 3_{10}- and α-helices, may be a common feature of foldamers that contain homochiral α- and β-amino acid residues, for most α:β proportions and sequence patterns.[10]

1.2 - Observed structures

The propensity of such diverse backbones to fold may be governed by many internal or external parameters. The overall shape and rigidity of the molecule and its ability to establish attractive or repulsive intramolecular non-covalent interactions depend on monomer size and shape, linkage orientation, rotational restrictions, local intramolecular interactions, and interactions between monomers remote from each other in a sequence. A common feature to all foldamers is a certain degree of backbone rigidity that limits the entropic cost of adopting an organized conformation. A further contribution to folding tendency is given by solvent effects such as hydrophobic effects.[22]

However, the secondary structures found in foldamers are much less diverse than the variety of their backbones. The typical motifs of biopolymers (helices, linear strands, turns and sheets) are present in

most classes of foldamers, being the helix the most frequently observed structure. Sheets are probably not less common, but less tractable and still awaiting to be discovered.

On the other hand, many unknown or uncommon folding motifs such as pillar-like architectures (stacks of aromatic rings),[23] knots,[24] spiral-like objects ('tail-biters'),[25] or non-canonical helices,[26] are displayed by foldamers.[22]

1.3 - *De novo* foldamer design

Mándity et al. developed an innovative concept of the so called stereochemical patterning approach, as a very promising tool for the *de novo* foldamer design based on the analysis of backbone torsion angles in β-peptides as well as in α/β-peptides.[27] The signs of the peptide bond-flanking dihedrals ($\psi_{(n-1)}][\phi_n$, where][indicates the CONH group) revealed to be crucial for the type of secondary structure that is induced. In particular, helical structures were observed when dihedrals of adjacent residues had the same sign. By correlating the signs of torsion angles and the absolute stereochemistry of building blocks, peptide sequences that would undergo a distinct helical folding could be readily predicted.

In order to test the predictive ability of the method, *cis*- or/and *trans*-ACPC residues along with acyclic α- and β-amino acids were employed for the synthesis of β- and α/β-peptide sequences either based on this $\psi][\phi$ sign, stereochemical pattern, or generated under quasi-randomized control. Theoretical predictions and experimental findings were in excellent agreement.

Residue type	Backbone configuration	Structuring effect
α	(*S*)-C_α	[–
α	(*R*)-C_α	[+
β	(*S*)-C_α	[–
β	(*R*)-C_α	[+
β	(*S*)-C_β	[–
β	(*R*)-C_β	[+

Table 4.1 - Signs of dihedral angles ([ψ and ϕ]) induced by the configurations of the backbone atoms.

Signs of $\psi][\phi$	Secondary structure
+][+	helix
–][–	helix
+][–	strand
–][+	strand

Table 4.2: The secondary structure preference of the $\psi][\phi$ building blocks.

This strategy may be of great impact in the fast rational design of molecules with tailored properties.[9]

1.4 - Biological applications

An emerging and challenging foldamer application is to mimic folded peptide segments found in proteins, in particular the α-helix. Indeed, the use of short α-peptide fragments to target biomacromolecules (e.g. proteins) is limited because they generally do not maintain their secondary structure once extracted from the protein context.[6a]

Recently, optimized careful combinations of α- and β-amino acids mimicking helical sequences, namely a mixed $\alpha\alpha\beta\alpha\alpha\alpha\beta$ heptamer, have been shown to effectively imitate the binding surface of a known α-peptide HIV inhibitor targeting the gp41 central trimeric coiled coil.[28] It is noteworthy that these foldamers were equipotent to the parent α-peptide in cell–cell fusion inhibition assays and in inhibition of HIV-1 infectivity.[22]

A major advance toward the development of biologically active foldamers was the identification of a chimeric peptide foldamer consisting of N-terminal α/β segment and a C-terminal α-peptide segment, which binds to the BH3-recognition cleft of the anti-apoptotic protein Bcl-x_L.[29] The crystal structure of the complex with Bcl-x_L reveals that the helical foldamer has the same orientation as the natural BH3 domains. The α/β-segment adopts a 14/15-helical structure with some cyclic β-amino acid residues making contacts with the protein surface, thus inhibiting the interaction between Bcl-x_L and its proapoptotic partner, that can trigger cancer.[30]

2 - Design, synthesis and conformational analysis of an α/β-peptide foldamer, containing DKP repeating units as secondary structure inducers

2.1 - Conception

As previously mentioned (Chapter 2, §3), the ability of **DKP1** to form well-defined folded structures, when introduced in peptide sequences had already been studied in our research group.[31] In particular, while inserted in hexapeptides, **DKP1** acts as a β-hairpin inducer, while oligomers of **DKP1 form** a β-bend ribbon conformation starting from four units of **DKP1**.

As inferred from these evidences, **DKP1** results well pre-organized to induce a reverse turn of the growing peptide chain, favouring the formation of regular H-bonding patterns throughout the backbone. Thus, the synthesis of longer hybrid peptides containing more than one **DKP1** repeating units alternated with alpha units might represent an improvement in the study of the behavior of our scaffold as a folding inducer.

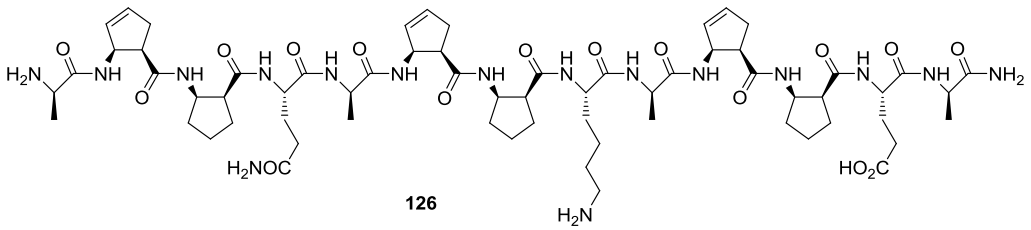

Figure 4.6

Very nice examples of highly pre-organized structures, such as helices, were obtained by the group of Reiser alternating two α- and two β- amino acids.

They have in fact just designed unprecedented 9/12/9/10 helical structures featuring the α,α,β,β sequential motif, by applying the stereochemical patterning approach.[27] The most representative of the 9-mers and 13-mers synthesized, which contain *cis*-ACPC and *α*-amino acid units, is sketched in Figure 4.6 (**126**). Properties and structures characterizing their foldamers were studied by means of CD and NMR spectroscopy, subsequent computational structure refinement. In contrast to the corresponding foldamers characterized by an *α,β,α,β* sequential motif, the helices formed tend to be very stable also in aqueous solutions.

Highly contributing to this outcome are also the favorable electrostatic interactions between the side-chains of α-amino acids such as Glu and Lys, as well as the hydrophobic interactions of the ACPC-rings. It is worth noticing is the behavior of *N*-terminal α-amino acids, which maintain significant flexibility.[32]

Taking advantage of the constrained *β*-dipeptide nature of **DKP1** we envisaged the design of a foldamer featuring the promising α,α,β,β sequential motif.

Taking into account the outcome of previous studies, we decided to investigate the synthesis of a pseudodecapeptide containing three **DKP1** units, two of them at the C- and N- termini, alternated with L-Ala-L-Ala units (**127**, Figure 4.7).

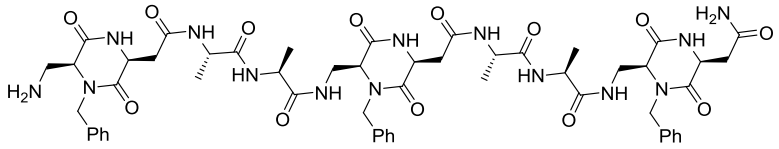

127

Figure 4.7

Although the design of **127** is in accordance with the stereochemical patterning approach, this peptide lacks the potential stabilizing electrostatic interactions between α-amino acid side chains. As we considered MM studies not predictive enough, we decided, on the basis of the already reported results, to gather preliminary evidences on **DKP1** behavior by preparing and analyzing a simple system. This study did not mean to be exhaustive, but, depending on the experimental results, it might represent a good starting point for the design of analogous DKP containing systems.

2.2 - Synthesis

As the coupling of *β*-amino acids can be challenging,[33] a solid-phase synthetic approach, using Fmoc chemistry, was adopted. Peptide **127** was built on Rink amide resin from C to N-terminus on a 0.1 mmol scale, and purified by preparative HPLC after cleavage.

DKP1* (Figure 4.8), which was chosen as the *β,β* building block, was synthesized in solution as already described in chapter 2 (§ 4.2.1). This scaffold is bearing a free carboxylic acid function and an

amino function masked as azide. Our diketopiperazine azido acids, and in particular **DKP1*** (*cis*), were shown to be very sensitive to basic conditions, as the azido moiety is prone to β-eliminate, giving a dehydroalanine-like derivative. For this reason, neutral carboxylic acid activation conditions were used for the synthesis of the linear peptide. Standard DCC/HOBt peptide coupling techniques revealed effective for the coupling of **DKP1***. Its –OBt activated ester was formed, adding a solution of HOBt and DCC in DCM to the carboxylic acid solution in DMF. The white precipitate (DCU) needed to be filtered off before adding the activated ester solution to the resin, which was shaken at room temperature. Reaction times varied from 3 h to 18 h, depending on the ease of the coupling.

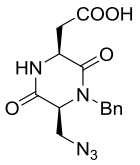

DKP1*

Figure 4.8 – **DKP1*** scaffold, used as the β,β building block.

Succinimidyl active esters of α-amino acids were employed in the synthesis. These kinds of active esters are sufficiently stable to be isolated and stored, and still react rapidly in peptide coupling. They are prepared treating the free carboxylic acid with DCC in presence of *N*-hydroxysuccinimide, in THF, and once isolated and purified by crystallization, they are merely dissolved and added to the resin.

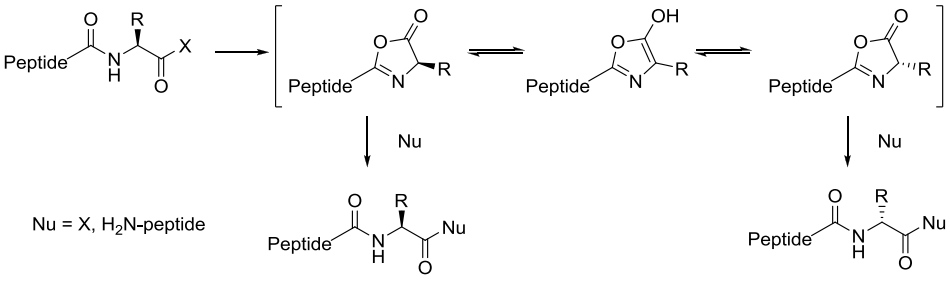

Scheme 4.1 – Epimerization *via* oxazolone formation.

Notably, the base-free conditions employed during coupling reactions allowed us to think about a more convergent synthesis, coupling, in one case, a Fmoc-L-Ala-L-Ala-OSu building block. Even though epimerization is a main concern in convergent peptide synthesis, due to the easy formation of oxazolones upon activation of the carboxylic acid participating in the amide bond formation (Scheme 4.1), we were able to avoid this problem.

The α,α- dipeptide building block was synthesized in solution according to procedures reported in the literature, starting from commercially available Fmoc-L-Ala-OH, whose activated succinimidyl ester was isolated, and unprotected L-Ala.[34] A succinimidyl ester of the dipeptide thus obtained was prepared (Scheme 4.2).

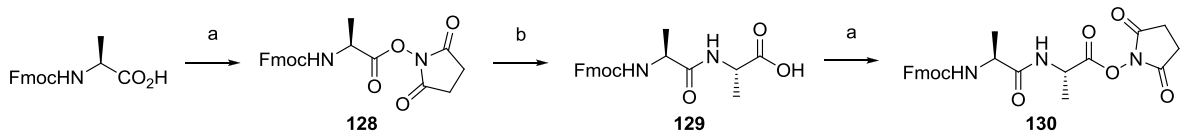

Scheme 4.2 – Reagents and conditions: a) NHS, DCC, THF, 0°C, 20h: 94%; b) H-L-Ala-OH, $NaHCO_3$, acetone/EtOH/water 1:4:1, 20h: 76%.

A general synthetic scheme is here reported in Scheme 4.3.

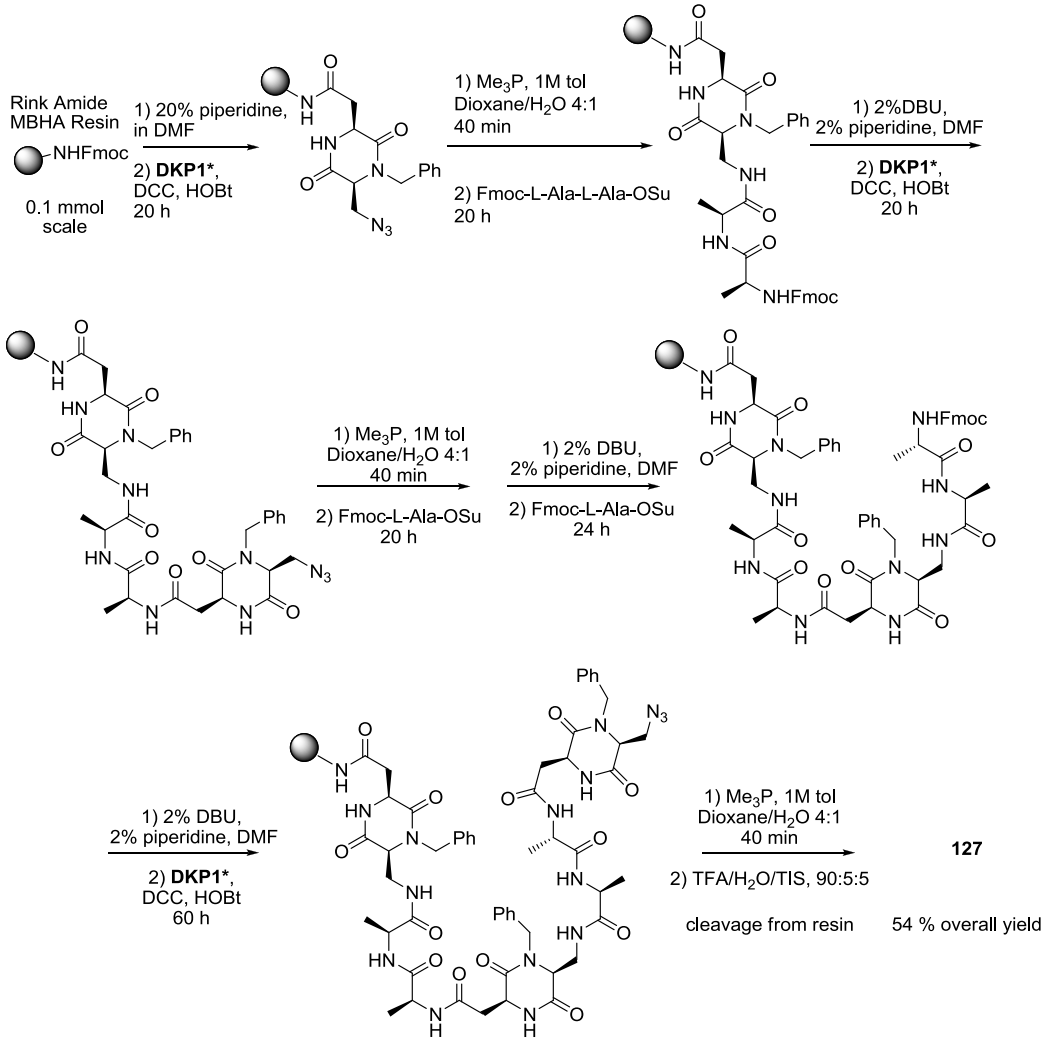

Scheme 4.3 – SPPS of peptide **127**.

Fmoc deprotections were performed treating the resin with either a 20% piperidine solution in DMF, or with a milder 2% piperidine, 2% DBU solution in DMF, and washing the resin carefully afterwards. Azides were reduced *in situ* in the presence of Me_3P (1 M solution in toluene) in a 4:1 dioxane/water solution, in order to obtain a free amine.

As the peptide grows (expecially after the sixth amino acid residue), coupling reactions are of course becoming more and more challenging. For this reason a step-wise approach was preferred after coupling the second diketopiperazine. Fmoc-L-Ala succinimidyl ester was used in two successive steps.

In order to monitor the coupling efficiency after each coupling step a slightly modified Kaiser test was performed and non-quantitative steps were repeated. When Kaiser test gave a positive result after the third coupling cycle, capping in presence of acetic anhydride and pyridine was performed, thus acetylating the amines still free.

A small cleavage from the resin was performed after the coupling of the α,α-dipeptide, treating a few beads with a 90:5:5 mixture of TFA, triisopropylsilane (TIS) and water, to check whether epimerization had occurred. LC/MS analysis and ^{13}C-NMR confirmed that only one species was present.

After the last coupling/azide reduction step cleavage of the linear peptide from the resin was carried out by treating the latter with a solution of TFA, TIS and water (90:5:5) for 2.5 h. The cleaved peptide was obtained with a C-terminal amide group that facilitated NMR assignment.

Subsequently, the peptide was precipitated from cold diethyl ether and dissolved in 10 % acetic acid in water. After lyophilization the peptide was purified by reversed phase preparative HPLC (RP-HPLC) in order to yield a pure compound, crucial for detailed structure analysis.

2.3 - Conformational Analysis

2.3.1 - *Variable temperature measurements*

VT-NMR measurements were carried out in order to get an insight into the backbone H-bonding pattern of peptide **127**.

As already mentioned in previous chapters, amide protons chemical shifts, as well as their dependence on temperature, may give first hints on the secondary structure. It has been shown that for α-peptides in water the analysis of temperature coefficients alone is not sufficient for the prediction of secondary structure formation. However, supported by lots of data for peptidic foldamers in various solvents together with other structural data we believe that the temperature gradients may help analyzing the structures of peptidic foldamers.[35] Temperature coefficients $\Delta\delta/\Delta T$ (ppb/K) relating to amide protons were calculated to detect the presence of hydrogen bonds within the peptide backbone.

Indeed, protons involved in H-bonding are usually characterized by rather upfield chemical shifts and a low dependence on temperature (low negative temperature coefficient values), while downfield chemical shifts and high absolute values of the temperature coefficient are indicative of solvent exposed amide protons, not involved in hydrogen bonding. Figure 4.9 shows the amide region of the ^{1}H-NMR spectra of peptide **127** in dimethylsulfoxide (DMSO-d_6) in a temperature range from 290 to 320 K.

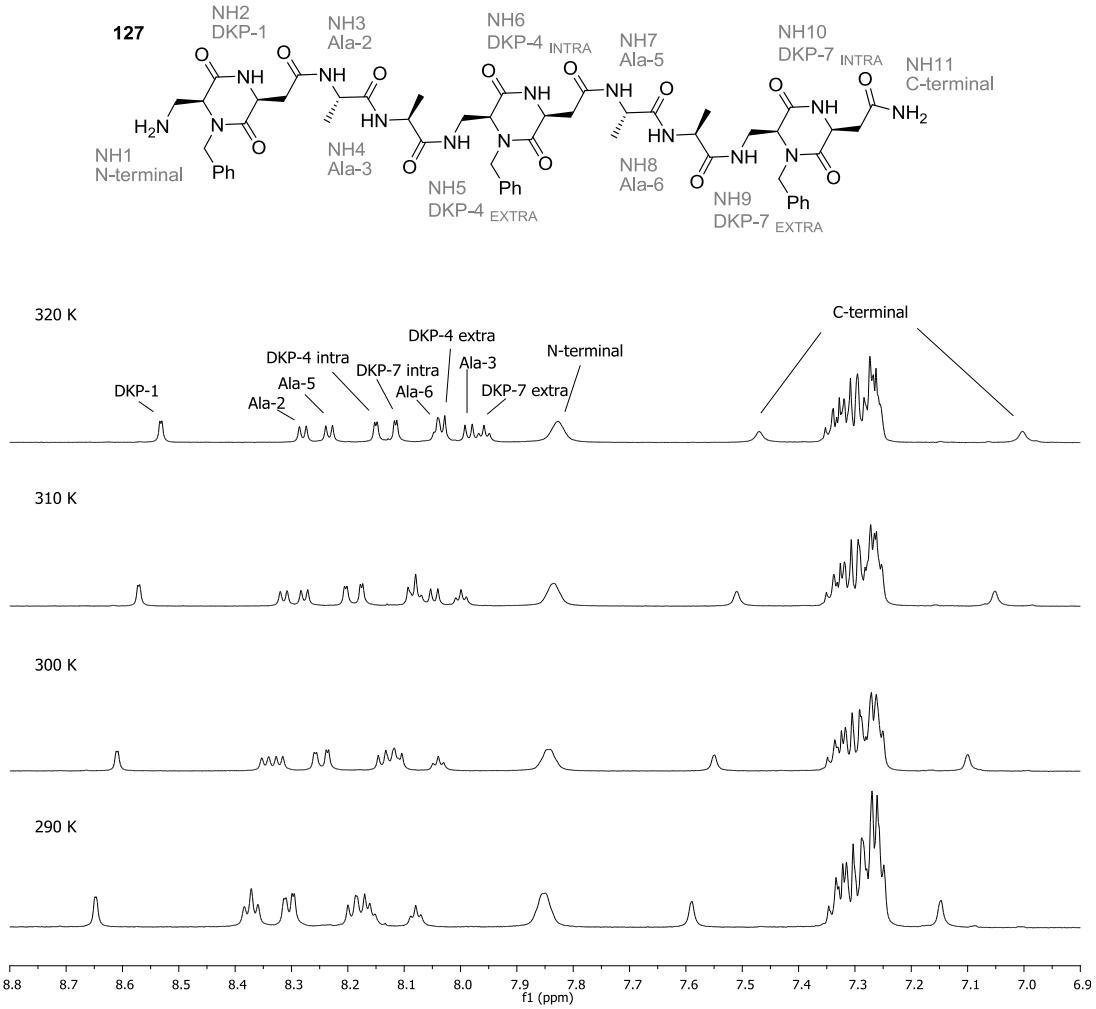

Figure 4.9 - Amide region in the ^{1}H-NMR spectra of peptide **127** in DMSO-*d*6 in a temperature range from 290 to 320 K (temperature increases from bottom to top; increment = 10 K).

Herein the changes of chemical shifts with increasing temperature can be observed. The temperature coefficients calculated for peptide **127** in DMSO-d_6 are reported in Table 4.3.

T [K]	290	300	310	320		**Δδ/ΔT** [ppb K^{-1}]
Spin system	δ [ppm]					
DKP-1	8.6474	8.6094	8.5708	8.5317		-3.86
Ala-2	8.3712	8.3465	8.3137	8.2796		-3.05
Ala-5	8.3712	8.3211	8.2771	8.2328		-4.61
DKP-4 INTRA	8.3115	8.2576	8.2037	8.1502		-5.38
DKP-7 INTRA	8.2970	8.2362	8.1756	8.1152		-6.06
Ala-6	-	-	-	-		-
DKP-4 EXTRA	-	-	-	-		-
Ala-3	-	-	8.0464	7.9856		-6.08
DKP-7 EXTRA	8.0792	8.0393	7.9990	7.9583		-4.03

Table 4.3 – Variation of backbone NH-protons chemical shifts (δ) with temperature, and corresponding temperature coefficients (Δδ/ΔT) in DMSO-*d*6 between 290 K to 320 K.

Unfortunately, protons NH5 (DKP-4_{extra}), NH8 (Ala-6), and in some extent NH4 (Ala-3) are overlapped. Therefore, no temperature coefficients could be calculated for NH5 and NH8, and a non-relevant value of Δδ/ΔT was reported for NH4. Thus little can be said on their tendency to be involved in H-bonding. N-terminal (Δδ/ΔT = -0.81) and C-terminal (Δδ/ΔT = -4.00; -4.83) NH protons are usually not taken into account in the prediction of a peptide secondary structure. Figure 4.10 gives a visual representation of the temperature coefficients values obtained.

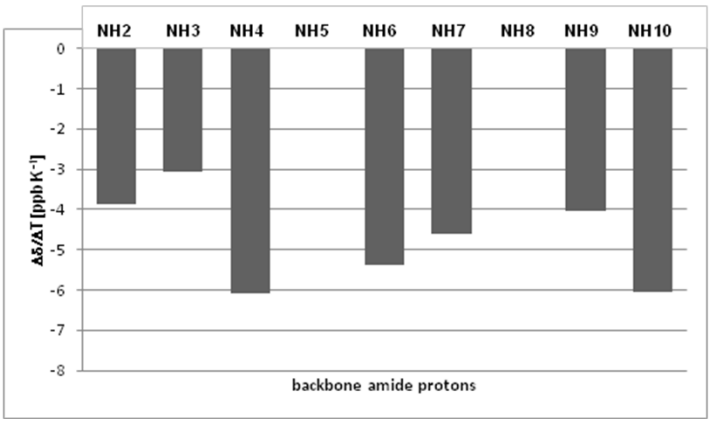

Figure 4.10 - Graphical illustration of temperature coefficients (Δδ/ΔT) for compound **127** in DMSO-*d*6 between 290 K and 320 K.

NH3 (Ala-2) displays the lowest Δδ/ΔT absolute value. This proton, as well as protons NH2 (DKP-1) and NH9 (DKP-7_{EXTRA}), having temperature coefficients in the range between -3 and -4 (ppb/K), may be involved in backbone H-bonding. Anyway, no strong H-bonding tendency was detected for **127**..

2.3.2 - *2D NMR measurements*

A detailed NMR solution analysis was performed on peptide **127** in DMSO-*d*6 to determine its structure in solution. For the assignment of the peptide standard homonuclear 2D NMR methods such as total correlation spectroscopy (TOCSY) and nuclear Overhauser effect spectroscopy (NOESY) as well as rotating frame nuclear Overhauser effect spectroscopy (ROESY) were applied.[36] 2D spectra were recorded at 310 K, in order to get the best signal resolution for the resonance assignment of the protons. Of course, the conspicuous presence of repeating alanine and **DKP1** residues did not make it an easy issue to unambiguously assign the whole structure.

Unfortunately only few ROE contacts were clearly detected from the ROESY spectrum, due to the bad signal resolution in some regions. The most relevant ROESY crosspeaks are depicted in Figure 4.11.

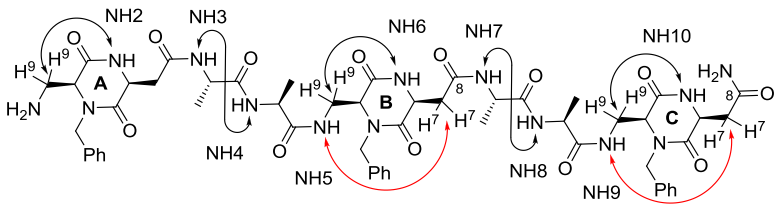

Figure 4.11 – Relevant medium-range ROE contacts.

The ROESY crosspeaks, which were found between NH3 and NH4 and between NH7 and NH8 amide protons as well as between NH2 and H9A and between NH6 and H9B, are not much contributing to the determination of the three-dimentional structure, as they are almost sequential.

On the other hand, the ROESY crosspeaks between NH5 and H7B and between NH9 and H7C, which were highlighted in Figure 4.11 in red and shown in the spectrum in Figure 4.12, may account for a β-turn induced by **DKP1**, forming a 10-membered H-bonding pattern which involves diketopiperazine extracyclic amide proton (NH5, NH9) and extracyclic C(8)=O carbonyl (B, C). The same kind of ROE contact was already observed for the **DKP1**- trimer and tetramer reported in the literature.[31b]

Not much can instead be inferred on the behavior of the rest of the backbone, as other relevant ROESY crosspeaks could not be unambiguously assigned so far. Further studies will be performed.

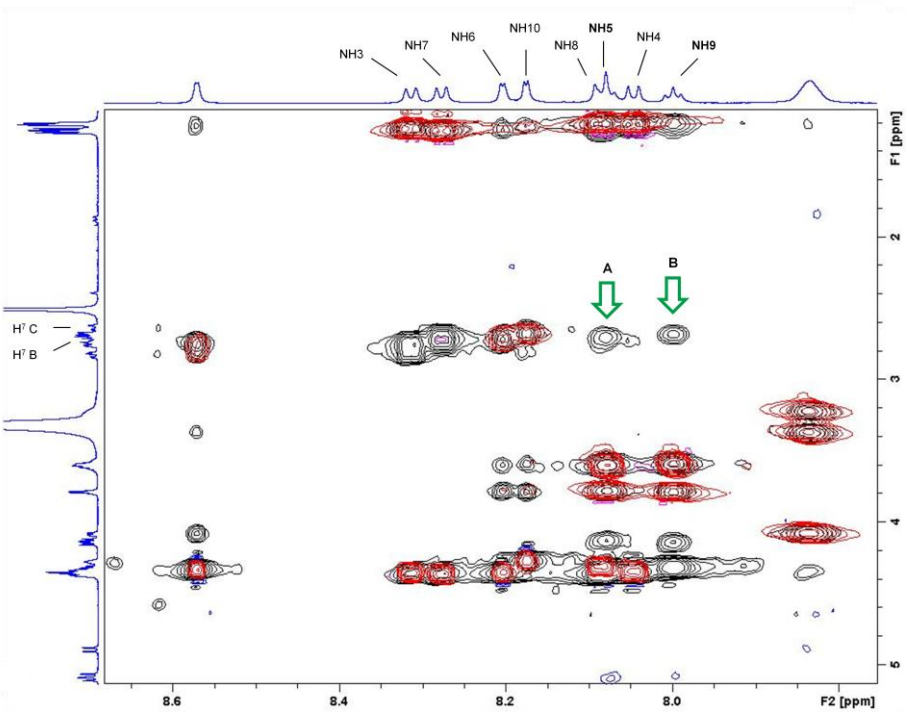

Figure 4.12 – Extract from the ROESY spectrum (grayscale) superimposed to the TOCSY spectrum (red) of peptide **127** in DMSO-*d*6 at 310 K, showing: A) NH5/H7B ROE contact; B) NH9/H7C ROE contact (relevant crosspeaks marked with green arrows).

2.3.3 - *CD spectroscopy*

CD spectra of the designed $\alpha,\alpha,\beta,\beta$-peptide were recorded between 190 and 280 nm in three different solvents, in order to identify regular structures in solution.

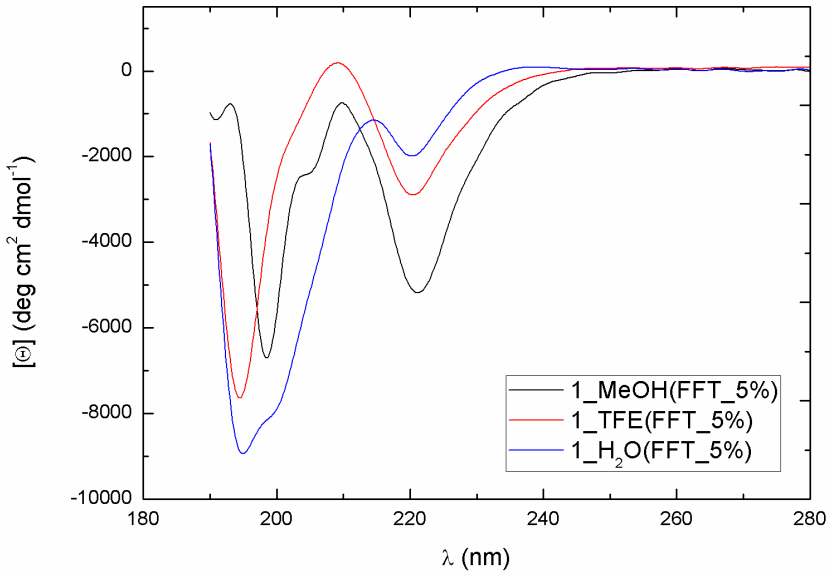

Figure 4.13 – Superimposed CD spectra of compound **127** recorded in MeOH, TFE and water.

In general, stabilization of secondary structures is higher in organic solvents. For these reason methanol was used at first. Trifluoroethanol (TFE) was then used. TFE is in fact known to further stabilize peptide secondary structures, removing alternative hydrogen-bonding partners and providing a low dielectric environment that favours the formation of intrapeptide hydrogen bonds.[37] Additionally, water was tested in order to check the behaviour of **127** under pseudo-physiological conditions.

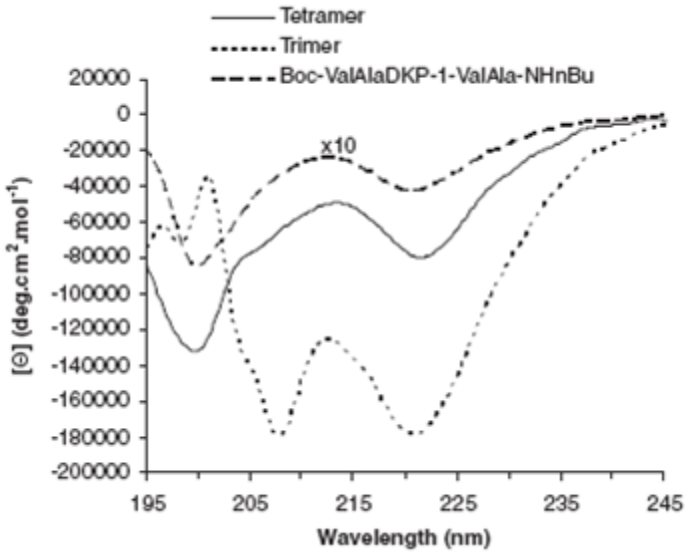

Figure 4.14 – Superimposed CD spectra of DKP1-tetramer, trimer,[31b] and the hairpin peptidomimetic Boc-ValAla-**DKP1**-ValAla-NH*n*Bu.[31a] The data of the latter compound have been multiplied by a factor 10 to magnify the appearance of the curve.

All CD spectra were normalized to peptide concentration, the number of amide bonds (13), and the curves were smoothed (FFT filter 5% cutoff with the Origin 8.0 program).

In all three cases, two minima around 195-200 nm and around 220 nm as well as a maximum around 210-215 nm were observed. These results resemble the ones reported in the literature for linear peptides containing **DKP1** as a template (Figure 4.14).[31]

Hence, also CD spectroscopy is giving evidence of **DKP1** tendency to induce a β-turn, and its prevailing contribution to the peptide secondary structure.

2.3.4 - *Computational studies*

Having evidences of a regular secondary structure in hands, a preliminary computational study, was performed for compound **127** applying the NH5/H7B and NH9/H7C distance restraints derived from ROE contacts. Our hypothesis of successive β-turns induced by the diketopiperazine scaffolds was confirmed by the results of constrained MC/SD simulations (Figure 4.15). Some of the representative conformations obtained show a characteristic C=O· ·H-N 10-membered hydrogen bonding pattern induced by both the C-terminal and the central DKP.

Of course, more ROE contacts might have been detected to achieve a more comprehensive result, which could take into account also the behavior of the α,α-portions.

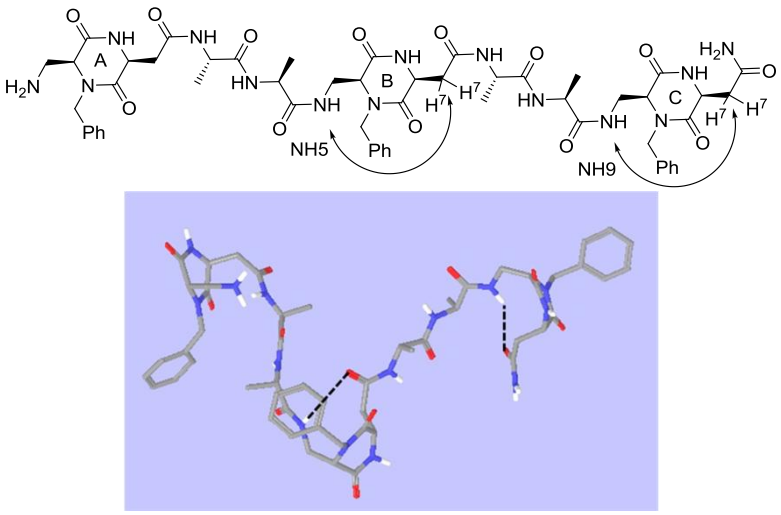

Figure 4.15 – Representative conformation obtained by 10ns MC/SD (AMBER* force field) restrained simulations.

References:

[1] a) D. H. Appella, L. A. Christianson, I. L. Karle, D. R. Powell, S. H. Gellman, *J. Am. Chem. Soc.* **1996**, *118*, 13071–13072; b) S. H. Gellman, *Acc. Chem. Res.* **1998**, *31*, 173–180.

[2] M. R. Arkin, J. A. Wells, *Nat. Rev. Drug Discov.* **2004**, *3*, 301–317.

[3] a) D. J. Hill, M. J. Mio, R. B. Prince, T. S. Hughes, J. S. Moore, *Chem. Rev.* **2001**, *101*, 3893–4011; b) R. P. Cheng, S. H. Gellman, W. F. DeGrado, *Chem. Rev.* 2001, *101*, 3219–323; c) I. Huc, *Eur. J. Org. Chem.* **2004**, 17–29; d) *Foldamers: Structure, Properties, and Applications*, S. Hecht, I. Huc, Eds.; Wiley-VCH: Weinheim, Germany, **2007**.

[4] R. P. Cheng, S. H. Gellman, W. F. DeGrado, *Chem. Rev.* **2001**, *101*, 3219-3232.

[5] D. Seebach, J. Gardiner, *Acc. Chem. Res.* **2008**, *41*, 1366-75.

[6] a) D. Seebach, A. K. Beck, D. J. Bierbaum, *Chem. Biodev.* **2004**, *1*, 1111; b) G. V. M. Sharma, K. R. Reddy, P. R. Krishna, A. R. Sankar, K. Narsimulu, S. K. Kumar, P. Jayaprakash, B. Jagannadh, A. C. Kunwar, *J. Am. Chem. Soc.* **2003**, *125*, 13670.

[7] P. Le Grel, A. Salaun, M. Potel, B. Le Grel, F. Lassagne, *J. Org. Chem.* **2006**, *71*, 5638.

[8] V. Semetey, D. Rognan, C. Hemmerlin, R. Graff, J. P. Briand, M. Marraud, G. Guichard, *Angew. Chem. Int. Ed.* **2002**, *41*, 1893.

[9] L. K. A. Pilsl, O. Reiser, *Amino acids* **2011**, *41*, 709-718.

[10] W. S. Horne, S. H. Gellman, *Acc. Chem. Res.* **2008**, 1399-1408.

[11] P. G. Vasudev, S. Chatterjee, N. Shamala, P. Balaram, *Chem. Rev.* **2011**, *111*, 657-87.

[12] "*FOLDAMERS: FROM DESIGN TO PROTEIN RECOGNITION*", http://foldamer.org/files/book_of_abstract_foldamers2010.pdf (20.12.2011)

[13] B. R. Huck, J. D. Fisk, S. H Gellman, *Org. Lett.* **2000**, *2*, 2607–2610.

[14] a) S. Krauthäuser, L. A. Christianson, D. R. Powell, S. H. Gellman, *J. Am. Chem. Soc.* **1997**, *119*, 11719–11720; b) H. N. Gopi, R. S. Roy, S. R. Raghothama, I. L. Karle, P. Balaram, *Helv. Chim. Acta* **2002**, *85*, 3313–3330.

[15] S. De Pol, C. Zorn, C. D. Klein, O. Zerbe, O. Reiser, *Angew. Chem. Int. Ed.* **2004**, *43*, 511–514.

[16] A. Hayen, M. A. Schmitt, F. N. Ngassa, K. A. Thomasson, S. H. Gellman, *Angew. Chem. Int. Ed.* **2004**, *43*, 505–510.

[17] N. Koglin, C. Zorn, R. Beumer, C. Cabrele, C. Bubert, N. Sewald, O. Reiser, A. G. Beck-Sickinger, *Angew. Chem. Int. Ed.* **2003**, *42*, 202–205.

[18] K. A. Bolin, G. L. Millhauser, *Acc. Chem. Res.* **1999**, *32*, 1027–1033.

[19] a) G. V. M. Sharma, P. Nagendar, P. Jayaprakash, P. R.Krishna, K. V. S. Ramakrishna, A. C. Kunwar, *Angew. Chem., Int. Ed.* **2005**, *44*, 5878–5882; b) G. Srinivasulu, S. K. Kumar, G. V. M. Sharma, A. C. Kunwar, *J. Org. Chem.* **2006**, *71*, 8395–8400.

[20] D. Seebach, B. Jaun, R. Sebesta, R. I. Mathad, O. Flögel, M. Limbach, H. Sellner, S. Cottens, *Helv. Chim. Acta* **2006**, *89*, 1801–1825.

[21] M. A. Schmitt, S. H. Choi, I. A. Guzei, S. H. Gellman, *J. Am. Chem. Soc.* **2006**, *128*, 4538–4539.

[22] G. Guichard, I. Huc, *Chem. Commun.* **2011**, *47*, 5933-5941.

[23] R. S. Lokey, B. L. Iverson, *Nature* **1995**, *375*, 303.

[24] J. Brüggemann, S. Bitter, S. Müller, W. M. Müller, U. Müller, N. M. Maier, W. Lindner, F. Vögtle, *Angew. Chem. Int. Ed.* **2007**, *46*, 254.

[25] C. A. Hunter, A. Spitaleri, S. Tomas, *Chem. Commun.*, **2005**, 3691.

[26] a) N. Delsuc, F. Godde, B. Kauffmann, J.-M. Léger, I. Huc, *J. Am. Chem. Soc.* **2007**, *129*, 11348; b) D. Seebach, S. Abele, K. Gademann, G. Guichard, T. Hintermann, B. Jaun, J. Mathews, J. V. Schreiber, *Helv. Chim. Acta* **1998**, *81*, 932.

[27] a) A. Hetényi, Z. Szakonyi, I. M. Mándity, E. Szolnoki, G. K. Tóth, T. a Martinek, F. Fülöp, *Chem. Commun.* **2009**, 177-179; b) I. M. Mándity, E. Wéber, T. A. Martinek, G. Olajos, G. K. Tóth, E. Vass, F. Fülöp, *Angew. Chem. Int. Ed.* **2009**, *48*, 2171-2175.

[28] W. S. Horne, L. M. Johnson, T. J. Ketas, P. J. Klasse, M. Lu, J. P. Moore, S. H. Gellman, *Proc. Natl. Acad. Sci. U. S. A.* **2009**, *106*, 14751.

[29] a) J. D. Sadowsky, M. A. Schmitt, H.-S. Lee, N. Umezawa, S. Wang, Y. Tomita, S. H. Gellman, *J. Am. Chem. Soc.* **2005**, *127*, 11966–11968; b) J. D. Sadowsky, W. D. Fairlie, E. B. Hadley, H.-S. Lee, N. Umezawa, Z. Nikolovska-Coleska, S. Wang, D. C. S. Huang, Y. Tomita, S. H. Gellman *J. Am. Chem. Soc.* **2007**, *129*, 139–154; c) J. D. Sadowsky, J. K. Murray, Y. Tomita, S. H. Gellman, *ChemBioChem* **2007**, *8*, 903–916.

[30] a) E. F. Lee, J. D. Sadowsky, B. J. Smith, P. E. Czabotar, K. J. Peterson-Kaufman, P. M. Colman, S. H. Gellman, W. D. Fairlie, *Angew. Chem. Int. Ed.* **2009**, *48*, 4318–4322; b) B. Baptiste, G. Godde, I. Huc, *ChemBioChem* **2009**, *10*, 1765–1767.

[31] a) A. S. M. Ressurreição, A. Bordessa, M. Civera, L. Belvisi, C. Gennari, U. Piarulli, *J. Org. Chem.* **2008**, *73*, 652-660; b) R. Delatouche, M. Durini, M. Civera, L. Belvisi, U. Piarulli, *Tetrahedron Lett.* **2010**, *51*, 4278-4280.

[32] L. Berlicki, L. Pilsl, E. Wéber, I. M. Mándity, C. Cabrele, T. A. Martinek, F. Fülöp, O. Reiser, *Angew. Chem. Int. Ed.*, *in press.*

[33] C. Zorn, F. Gnad, S. Salmen, T. Herpin, O. Reiser, *Tetrahedron Lett.* **2001**, *42*, 7049-7053.

[34] a) G. Sosnovsky, M. Baysal, E. Erciyas, J. Pharm. Sci. **1994**, *83*, 999–1005; b) Y. Zhang, H. Gu, Z. Yang, B. Xu, *J. Am. Chem. Soc.* **2003**, *125*, 13680-13681.

[35] It has been shown that for α-peptides in water the analysis of temperature coefficients alone is not sufficient for the prediction of secondary structure formation. However, supported by lots of data for peptidic foldamers in various solvents together with other structural data we believe that the temperature gradients may help analyzing the structures of peptidic foldamers: N. H. Andersen, J. W. Neidigh, S. M. Harris, G. M. Lee, Z. Liu, H. Tong *J. Am. Chem. Soc.* **1997**, *119*, 8547–8561.

[36] For compounds with a molecular weight of about 1000 Da, NOE crosspeak intensities in NOESY spectra can be very low, therefore ROESY spectra are the better alternative in this case.

[37] a) A. Kentsis, T. R. Sosnick, *Biochem.* **1998**, *37*, 14613-14622; b) D. Roccatano, G. Colombo, M. Fioroni, A. E. Mark, *Proc. Nat. Ac. Sci. U.S.A.* **2002**, *99*, 12179–12184.

5 CONCLUSIONS

Diketopiperazines (DKPs) are the smallest, simplest cyclic peptides known, being derived from the cyclization of a dipeptide. They are very easily synthesized, and in several cases the cyclization occurs from the dipeptide as an undesired side reaction.[1] Diketopiperazines are simple heterocyclic scaffolds in which diversity can be introduced at up to four positions (N1, N4, C3, C6) and stereochemically controlled at two (C3, C6). Constraining the nitrogen atom of an α-amino amide into a DKP ring alters its physical properties, reduces the susceptibility to metabolic amide bond cleavage and induces conformational rigidity. These changes in structural and physical properties, as well as the presence of groups that can act as donors and acceptors of hydrogen bonds enhance favorable interactions with biological targets. For all these reasons, diketopiperazines have recently been considered privileged structures for drug discovery, useful scaffolds for peptidomimetics and also interesting candidates as organocatalysts.[2]

A library of 11 bifunctional 2,5-diketopiperazine scaffolds (**DKP1-DKP8**, **DKP1*-DKP3***), derived from L- or D-Ser and either L- or D-Asp (**DKP1-DKP7**, **DKP1*-DKP3***) or D-Glu (**DKP8**), was designed and prepared. All the scaffolds feature a carboxylic acid functionality and an amino moiety, either protected as Boc (**DKP1-DKP8**) or masked as azide (**DKP1*-DKP3***), which can be locked in a *cis*- (**DKP1**, **DKP1***) or *trans*-relationship (**DKP2-DKP8**, **DKP2*-DKP3***) as a consequence of the absolute configurations of the two α-amino acids. Moreover, the DKP scaffolds differ each from the other for the substitution at the intracyclic nitrogens (*N*-1, *N*-4), as they are either mono (**DKP1-DKP4**, **DKP6**, **DKP8**, **DKP1*-DKP3***) or bis-benzylated (**DKP5**, **DKP7**). While being derived from α-amino acids, they can be seen as a constrained dipeptide formed by two β- or a β- and a γ-amino acids.

Two different synthetic strategies were devised to obtain the mono-benzylated scaffolds, depending on the nitrogen substitution. In particular, the synthesis of **DKP1-DKP3**, **DKP1*-DKP3*** and **DKP8** (bearing a benzyl group at nitrogen N-4, derived from serine) was realized making use of the serine ligation strategy.[3] Selective *O*-acylation of the unprotected β-hydroxy group of *N*-benzylserine methyl

ester is preferred to the formation of the tertiary amide during the coupling reaction with the appropriate *N*-Boc protected amino acid. The resulting isopeptide is stable in solution to *O,N*-acyl transfer.

O,N-acyl migration was triggered by cleavage of the Boc protecting group and treatment of the corresponding trifluoroacetate salt in a polar protic solvent with a base, which also promotes immediate cyclization to diketopiperazine. The nitrogen functionality was introduced, in these cases, with a Mitsunobu-type reaction in presence of hydrazoic acid, thus affording an azide.

On the other hand, the synthesis of **DKP4** and **DKP6** (bearing a benzyl group at nitrogen N-1, aspartic acid derived) occurred *via* dipeptide, without formation of a isopeptide intermediate. The β-hydroxy group of serine was converted into azide with a Mitsunobu-type reaction prior to the formation of the symmetric anhydride, which was used in the coupling with a *N*-benzyl dimethyl aspartate derivative.

Bis *N*-benzyl substituted scaffolds (**DKP5**, **DKP7**) could be easily accessed benzylating mono-substituted advanced intermediates.

The 11 scaffolds of the prepared library were used as templates in the synthesis of cyclic integrin ligands containing either the RGD- or the *iso*DGR recognition sequences, and in the preparation of a linear α,α,β,β-decapeptide, whose folding properties were studied.

Integrins are transmembrane heterodimeric cell adhesion receptors, consisting of an α- and a β-subunit, involved in many fundamental processes, such as cell growth, cell division, cell survival, cellular differentiation, apoptosis. As a consequence, integrin malfunction is connected to a large variety of diseases (*e.g.* thrombosis, cancer, osteoporosis, inflammation), and integrins themselves represent attractive targets for pharmacological research.

Of the 24 different heterodimers known, the RGD-binding integrins $\alpha_V\beta_3$, $\alpha_V\beta_5$, $\alpha_5\beta_1$ are key-factors of angiogenesis, *i.e.* the formation and maturation of new blood vessels. A small localized tumor releases angiogenic growth factors, promoting the generation of abnormal blood vessels which can feed the tumor. Hence, angiogenesis plays a pivotal role in tumor growth and metastatic spreading.

Particular integrins are able to selectively bind different spatial presentations of a single binding motif (RGD) in multiple ECM proteins. Therefore, synthetic RGD-ligands can bind and inhibit endogenous-ligand-binding to integrins with an RGD-recognition specificity ($\alpha_V\beta_3$, $\alpha_V\beta_5$, $\alpha_5\beta_1$), thus significantly inhibiting angiogenesis, tumor growth and metastasis.

An efficient synthesis in solution of constrained peptides (**47**, **48**,[4] **102**-**107**) containing the **Arg-Gly-Asp** (RGD) motif and diketopiperazine scaffolds **DKP1-DKP8** was developed and optimized. Notably, two different separable conformers (diastereomers) formed during the cyclization of compound **106**, containing bis-benzylated scaffold **DKP7**, due to hindered rotation of one ring around the other.

Ligands **47**, **48**, **102-107** were tested for their ability to inhibit biotinylated vitronectin binding to $\alpha_v\beta_3$ and $\alpha_v\beta_5$ receptors. All the ligands, except for the one containing a *cis*-scaffold, displayed low nanomolar affinity for both $\alpha_V\beta_3$ and $\alpha_V\beta_5$ integrins, with a slight selectivity towards the former receptor. Interestingly, the two diastereomeric compounds showing atropoisomerism (**106 A**, **106 B**) are the most and the least selective and potent of the series.

Our ligands were fully characterized by NMR spectroscopy, detecting both H-bondings and long-range NOE contacts. Moreover, three-dimensional structures satisfying long-range NOE contacts were generated by restrained simulations. Five different H-bonding patterns were observed for our ligands on the basis of the conformational analysis, each one featuring at least a β-turn motif. A Cβ (Asp)-Cβ (Arg) distance of around 9 Å was detected from the structures obtained by restrained MC/SD simulations for the ligands displaying good affinity towards $\alpha_V\beta_3$ and $\alpha_V\beta_5$ integrins, while shorter distances were observed for the *cis* compound (**47**). Hence, a distance of ca. 9 Å, which accounts for an extended arrangement of the RGD motif, may be relevant for a positive binding to integrin. The extended arrangement of the RGD sequence in Cilengitide (**85**, Cβ(Arg)-Cβ(Asp) = 8.9 Å), one of the most potent compounds of this class, whose crystal structure in the bound conformation is known, corroborates this assumption. In order to rationalize, on a molecular basis, the affinity of cyclic RGD peptidomimetics for the $\alpha_v\beta_3$ receptor, docking studies were performed starting from the representative conformations obtained from the MC/SD simulations. The crystal structure of the extracellular segment of integrin $\alpha_v\beta_3$ complexed with the cyclic pentapeptide Cilengitide (1L5G, pdb code) was taken as a reference model for the interpretation of the docking results in terms of ligand-protein interactions. In most of the cases the electrostatic clamp interactions of the pharmacophoric groups were maintained; moreover, further stabilizing interactions were observed in the case of higher affinity compounds.

Besides the well defined RGD motif, it was proposed that also the *iso*DGR sequence might be involved in integrin recognition. In fact, *iso*DGR sequence can mimic RGD and interact with RGD binding site of integrins (such as $\alpha_v\beta_3$, $\alpha_v\beta_5$ and $\alpha_5\beta_1$) in an inverted orientation, maintaining all the typical electrostatic-clamp interactions of the RGD motif and presenting additional stabilizing interactions. Hence, two constrained peptides (**118-119**) containing the ***iso*Asp-Gly-Arg** (*iso*DGR) motif and diketopiperazine scaffolds **DKP2*-DKP3*** were prepared, combining a solid phase and an homogeneous synthetic approach. Very promising results (low nanomolar) were obtained for their ability to inhibit biotinylated vitronectin binding to $\alpha_v\beta_3$ and $\alpha_v\beta_5$ receptors.

As part of my project, I spent six months (October 2010 – March 2011) in the group of Prof. Oliver Reiser at the University of Regensburg, working on the design of α/β-peptide foldamers, containing diketopiperazine repeating units as secondary structure inducers.

Foldamers were defined by Gellman as "any polymer with strong tendency to adopt a specific compact conformation". Major advances have been made in the last decades, showing the ability of foldamers to adopt specific conformations able to mimic biopolymer-like functions. Thus, they have been used with success in the inhibition of protein protein interactions. In particular, protein surface recognition by mimicking distinct folding patterns along with proteolytic stability is the main advantage of foldamers compared to α-peptides or small drug molecules.

On the wake of the good results recently obtained by the group of Reiser in the design of *helices*,[5] alternating 2 α- and 2 β-amino acids, a linear decapeptide (**127**) was prepared alternating **DKP1***, which serves as a β,β-constrained dipeptide, and Ala-Ala, as the α,α-subunit.

A conformational analysis was performed with NMR spectroscopy, CD spectroscopy and computational methods. The results obtained, though not exhaustive, are indicative of a turn inducing ability of **DKP1**, that had already been reported in the literature.[6]

References:

[1] G. Barany, F. Albericio, J. Am. Chem. Soc. 1985, 107, 4936-4942.

[2] For a recent review on diketopiperazines, see: A. S. M. Ressurreição, R. Delatouche, C. Gennari, U. Piarulli, Eur. J. Org. Chem. 2011, 217-228.

[3] M. Marchini, M. Mingozzi, R. Colombo, C. Gennari, M. Durini, U. Piarulli, *Tetrahedron* **2010**, *66*, 9528-9531.

[4] A. S. M. da Ressurreição, A. Vidu, M. Civera, L. Belvisi, D. Potenza, L. Manzoni, S. Ongeri, C. Gennari, U. Piarulli, Chem. Eur. J. 2009, 15, 12184-12188.

[5] L. Berlicki, L. Pilsl, E. Wéber, I. M. Mándity, C. Cabrele, T. A. Martinek, F. Fülöp, O. Reiser, *Angew. Chem. Int. Ed.*, *in press.*

[6] a) A. S. M. Ressurreicao, A. Bordessa, M. Civera, L. Belvisi, C. Gennari, U. Piarulli, *J. Org. Chem.* **2008**, *73*, 652-660; b) R. Delatouche, M. Durini, M. Civera, L. Belvisi, U. Piarulli, *Tetrahedron Lett.* **2010**, *51*, 4278-4280.

6 EXPERIMENTAL SECTION

1 - General remarks and procedures

MATERIALS AND METHODS: All manipulations requiring anhydrous conditions were carried out in flame-dried glassware, with magnetic stirring and under a nitrogen atmosphere. All commercially available reagents were used as received. Anhydrous solvents were purchased from commercial sources and withdrawn from the container by syringe, under a slight positive pressure of nitrogen. (*S*)-and-(*R*)-serine methyl ester hydrochloride,[1] (*S*)-*N*-benzylserine methyl ester,[2] (2*R*)-aspartic acid β-allyl ester hydrochloride,[3] *N*-(tert-butoxycarbonyl)-(2*R*)-aspartic acid β-allyl ester,[3] (*S*)-and-(*R*)-*N*-Boc-serine methyl ester,[4] (*S*)-and-(*R*)-methyl 3-azido-2-(tert-butoxycarbonylamino)propanoate,[5] (*S*)-and-(*R*)-3-azido-2-(tert-butoxycarbonylamino) propanoic acid,[5] (*S*)-and-(*R*)-dimethyl aspartate hydrochloride,[6] (*S*)-and-(*R*)-*N*-benzyl-dimethyl aspartate,[7] γ-methyl glutamate hydrochloride[8] and *N*-Boc-glycine benzyl ester[9] were prepared according to literature procedures and their analytical data were in agreement with those already published. The reactions were monitored by analytical thin-layer chromatography (TLC) using silica gel 60 F_{254} pre-coated glass plates (0.25 mm thickness). Visualization was accomplished by

irradiation with a UV lamp and/or staining with a potassium permanganate alkaline solution or ninhydrin. Flash column chromatography was performed according to the method of Still and co-workers[10] using Chromagel 60 ACC (40-63 μm) silica gel. Melting points were obtained in an open capillary apparatus and are uncorrected. Proton NMR spectra were recorded on a spectrometer operating at 400.16 MHz. Proton chemical shifts are reported in ppm (δ) with the solvent reference relative to tetramethylsilane (TMS) employed as the internal standard. The following abbreviations are used to describe spin multiplicity: s = singlet, d = doublet, t = triplet, q = quartet, m = multiplet, br = broad signal, dd = doublet of doublet. Carbon NMR spectra were recorded on a spectrometer operating at 100.63 MHz, with complete proton decoupling. Carbon chemical shifts are reported in ppm (δ) relative to TMS with the respective solvent resonance as the internal standard. Infrared spectra were

recorded on a standard FT-IR. Optical rotation values were measured on an automatic polarimeter with a 1 dm cell at the sodium D line and are given in units of 10^{-1} deg cm^2 g^{-1}. High resolution mass spectra (HRMS) were performed on a Fourier Transform Ion Cyclotron Resonance (FT-ICR) Mass Spectrometer APEX II & Xmass software (Bruker Daltonics) – 4.7 T Magnet (Magnex) equipped with ESI source, available at CIGA (Centro Interdipartimentale Grandi Apparecchiature) c/o Università degli Studi di Milano. Low resolution mass spectra (MS) were recorded on Waters Acquity UPLC-MS (ESI ion source).

Circular dichroism (CD) spectra were measured on a JASCO J-710/720 spectrometer at the Institute of Analytical Chemistry at the University of Regensburg at room temperature between 180 and 350 nm in the specified solvents. The length of the cylindrical cuvettes was 0.2 mm and of the rectangular cuvettes was 1.0 mm. The resolution was 0.2 nm, the band width 1.0 nm, the sensitivity 100 mdeg, the response 0.25 s and the speed 20 nm/min. The background was subtracted for each spectrum. The absorption values were measured as molar ellipticies (deg cm^2 $dmol^{-1}$) and normalized to unit chromophore (number of residues).

GENERAL PROCEDURES:

In solution:

GENERAL PROCEDURE FOR Boc-DEPROTECTION REACTIONS:

GP1: To a solution of the *N*-Boc-protected amino acid or peptide in CH_2Cl_2 (0.13 M) was added half volume of TFA. The reaction mixture was stirred at for 2 h r.t. and then concentrated at reduced pressure. The excess TFA was azeotropically removed from the residue with toluene. Diethyl ether was added to the residue and the resulting suspension was evaporated under reduced pressure to afford the corresponding TFA salt.

GENERAL PROCEDURE FOR COUPLING REACTIONS:

GP2: To a solution of the *N*-protected amino acid in DMF, under nitrogen atmosphere and at 0 ºC, HATU (1.2 eq.), HOAt (1.2 eq.) and DIPEA (4 eq.) were added successively. After 30 min, a solution of the *N*-deprotected TFA salt of the peptide in DMF was added and the reaction mixture was stirred at 0 ºC for 1 h and at r.t. overnight. The mixture was afterwards diluted with EtOAc and consecutively washed with 1 M $KHSO_4$ (2×), aqueous $NaHCO_3$ (2×) and brine (2×), and dried over Na_2SO_4. Volatiles were evaporated under reduced pressure to afford the crude product.

GENERAL PROCEDURE FOR Cbz AND OBn HYDROGENOLYTIC CLEAVAGE:

GP3: protected compound (1 eq.) was dissolved in a mixture of THF/H_2O (1:1) and Pd/C 10% (0.1 eq.) was added. The reaction mixtures were subjected to three vacuum/hydrogen cycles and then left stirring overnight at room temperature under 1 bar of hydrogen. The mixture was filtered through Celite, and the cake thus obtained was washed thoroughly with THF/H_2O (1:1). The filtrate was concentrated and dried to give the crude product as white solid (100%).

GENERAL PROCEDURE FOR MACROLACTAMIZATION:

GP4: to a 1.4 mM solution of deprotected linear compound (1 eq.) in DMF, under nitrogen atmosphere and at 0 ºC, HATU (4 eq.), HOAt (4 eq.) and DIPEA (6 eq.) were added successively. After stirring the reaction mixture at 0 ºC for 1 h, it was allowed to reach r.t., and stirred overnight. DMF was then removed under reduced pressure and the residue was purified by flash chromatography on silica gel to afford the product as white foam (31-74%).

GENERAL PROCEDURE FOR Mtr AND O*t*Bu ESTER REMOVAL:

GP5: protected macrolactams was treated with TFA (0.01 M solution), in the presence of ion scavengers: thioanisole (5%), ethanedithiol (3%), anisole (2%). After TFA removal, under reduced pressure, the residue was dissolved in a 1:1 mixture of diisopropyl ether/water. Phases were separated and the aqueous layer was washed several times with diisopropyl ether. The aqueous phase was concentrated under reduced pressure to give the crude product, which was purified by HPLC to give the desired compound as white solid (60-80%).

Solid phase peptide synthesis:

Fmoc DEPROTECTION:

GP 6: The washed and swollen resin was treated twice with a solution of piperidine (20%) in DMF (v/v), 5 min and 15 min, respectively and washed with DMF (5x), DCM (5x), and again DMF (4x).

GP 7: The washed and swollen resin was treated twice with a solution of piperidine (2%) and DBU (2%) in DMF (v/v), 5 min and 15 min, respectively and washed with DMF (5x), DCM (5x), and again DMF (4x).

AZIDE REDUCTION:

GP 8: Azidopeptidyl resin (0.1 mmol, 1 eq.) was suspended in a 4:1 mixture of dioxane/water. Trimethylphosphine (1M solution in toluene, 0.6 ml, 0.6 mmol, 6 eq.) was added and the reaction vessel was shaken for 40 min. The resin was washed with dioxane (3x).

CAPPING

GP9: Acetic anhydride (50 eq.) and pyridine (50 eq.) were dissolved in DMF (1M) and added to the washed peptidyl resin, which was shaken for 30 min. at r.t.. The solution was sucked away, and the resin was washed in the order with DMF (4x) and *i*PrOH (3x). Kaiser test was performed before proceeding to the next step.

GP10: A 2M solution of acetic anhydride in DMF (1M) was added to the washed peptidyl resin, which was shaken for 20 min. at r.t.. The solution was sucked away, and the resin was washed in the order with DMF (4x) and *i*PrOH (3x). Kaiser test was performed before proceeding to the next step.

KAISER TEST:

Phenol (80% solution in ethanol), ninhydrin (6% solution in ethanol) and pyridine (two drops each) were added to a small sample of the resin and then heated in a boiling water bath for 60 s. If the color

of the solution maintained yellow, quantitative coupling was achieved. In the case of a slight blue color the coupling step was not fully completed and had to be repeated.

2 - Synthesis of diketopiperazine scaffolds DKP1-DKP8 and DKP1*-DKP3*

Preparation of hydrazoic acid

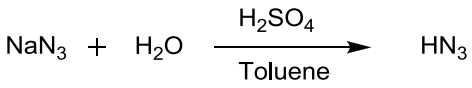

In a three-necked flask were dissolved 3 g of NaN_3 in 3 ml H_2O. Once totally diluted, 20 ml of toluene were added and the reaction flask was put in an ice bath under vigorous stirring. When the solution was at 0°C, 1.2 ml of concentrated H_2SO_4 were added extremely slowly in order not to exceed 10°C for the solution temperature. The reaction was let one hour at 0°C and was then filtered on cotton wool. The salt residue was washed twice with more toluene. The toluene solution was titrated by diluting 1 ml of the toluene solution in distilled water in a total volume of 50 ml. Titration was accomplished by addition of 0.1 M NaOH controlled with a pH meter allowing to calculate the HN_3 concentration in the mother solution when the equivalence volume was reached.

2.1 - <u>DKP1-DKP3</u> and <u>DKP1*-DKP3*</u>

(*R*)- and (*S*)-β-allyl aspartic acid hydrochloride (50)

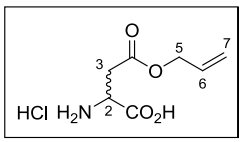

$C_7H_{12}ClNO_4$
MW: 209,63

In a round bottom flask cooled at 0°C were diluted 5 g (37.57 mmol) of L- or D- aspartic acid in 45 mL of allylic alcohol. Acetyl chloride (10.4 mL, 146.5 mmol, 3.9 eq.) were then slowly added dropwise with a dropping funnel into the reaction mixture. Once the addition was finished, the reaction flask was removed from the ice bath and let react at room temperature for 18 h. The reaction mixture was diluted in Et_2O making the product precipitate entirely. The salt was filtered through a glass filter and washed twice with more Et_2O. The salt was recovered and dried under vacuum affording 5.94 g (80%) of the monoallylated aspartic acid hydrochloride white solide.

[α]D20=+22.7 (*S*-; MeOH, *c*=1.00); mp: 181 - 183 °C. litt. = 184 - 185 °C; ^{1}H NMR (400 MHz, D_2O) δ 5.96-5.86 (m, 1H, H_6), 5.33-5.23 (m, 2H, H_7), 4.64 (d, *J*=5.74 Hz, 2H, H_5), 4.37-4.34 (m, 1H, H_2), 3.14-3.08 (dd, *J1*=4.8 Hz, *J2*=18.4 Hz, 2H, H_3); ^{13}C NMR (101 MHz, D_2O) δ 171.5 (C=O), 171.2 (C=O), 131.8 (C_6), 119.3 (C_7), 67.1 (C_5), 49.7 (C_2), 34.4 (C_3); IR (cm^{-1}): 3437, 2913, 1742, 1726, 1505, 1227, 1206.

N-Boc-(*R*)- and (S)-β-allyl aspartic acid (51)

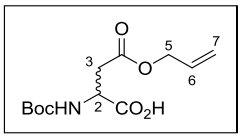

$C_{12}H_{19}NO_6$
MW: 273,28

In a round bottom flask were solved 5.9 g (28.14 mmol) of either (*R*)- or (S)- allyl aspartic acid hydrochloride **50** in 120 mL of THF/water 1:1 solution. The reaction flask was lowered into an ice bath and 11.77 mL (84.42 mmol, 3 eq.) of triethylamine were added. Then, 7.37 g (33.77 mmol, 1.2 eq.) of Boc_2O were added and the reaction was stirred at room temperature for 24 h. The reaction mixture was then diluted with 200 mL of EtOAc and washed with aqueous $KHSO_4$ 1M until pH = 3 and brine. The organic phase was dried over Na_2SO_4, filtered and concentrated under reduced pressure. The product was then dried under high vacuum for a few hours affording 7.38 g (96%) of the pure expected product as viscous transparent oil.

R_f=0.1 (EtOAc 100%); [α]D20=+33.3 (*S*-, $CHCl_3$, *c*=1.00); ^{1}H NMR (400 MHz, $CDCl_3$) δ 9,90 (bs, 1H, OH), 5.94-5.86 (m, 1H, H_6), 5.57 (d, *J*=8.4, 1H, NH), 5.19-5.32 (m, 2H, H_7), 4.52- 4.60 (m, 3H, H_2, H_5), 3.07 (dd, *J*1=4.2 Hz, *J2*=17.2 Hz, 1H, H_{3a}), 2.89 (dd, *J*1=4.8Hz, *J*2=17.1 Hz, 1H, H_{3b}), 1.46 (s, 9H, *t*Bu); ^{13}C NMR (101 MHz, $CDCl_3$) δ 176.0 (C=O), 171.2 (C=O), 156.0 (C=O), 132.0 (C_6), 119.1 (C_7), 80.9 ($\underline{C}(CH_3)_3$), 66.2 (C_5), 50.2 (C_2), 36.9 (C_3), 28.7 ($C(\underline{C}H_3)_3$); IR (cm^{-1}): 3331, 2980, 1732, 1504, 1385, 1163.

(S)- and (R)-serine methyl ester hydrochloride (52)

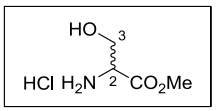

$C_4H_{10}ClNO_3$
MW: 155,58

In a round bottom flask at 0°C were dissolved 6 g (57.09 mmol) of L- or D-serine in 45mL MeOH. Acetyl chloride (16.2 mL, 228 mmol, 4 eq.) was added dropwise in the reaction mixture. Once the addition was finished, the reaction flask was equipped with a condenser and the mixture was heated to reflux. After 2.5 h reflux was then stopped and the flask was cooled to room temperature. 200 mL of Et_2O were added provoking the precipitation of the resulting salt which was filtered on a glass funnel and dried under high vacuum affording 8.79 g (99%) of serine methyl ester hydrochloride as a white solid.

mp: 162-164 °C; [α]D20=+3.98 (*S*-,MeOH, *c*=1.00); ^{1}H NMR (400 MHz, D_2O) δ 4.25 (t, *J*=3.8 Hz, 1H, H_2), 4.08 (dd, *J1*=4.3 Hz, *J2*=12.6 Hz, 1H, H_{3a}), 3.98 (dd, *J1*=3.4 Hz, *J2*=12.6 Hz, 1H, H_{3b}), 3.83 (s, 3H, OCH_3); ^{13}C NMR (101 MHz, D_2O) δ 169.3 (C=O), 59.6 (C_3), 55.1 (C_2), 54.1 (OCH_3); *S*: IR (cm^{-1}): 3358, 2928, 1750, 1595, 1510, 1260, 1095, 1040; *R*: IR (cm^{-1}): 3366, 2924, 1748, 1595, 1508, 1256, 1094, 1036.

(*S*)- and (*R*)-*N*-benzyl-serine methyl ester (53)

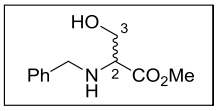

$C_{11}H_{15}NO_3$
MW: 209,24

6 g (38.6 mmol) of *S*- or *R*- serine methylester hydrochloride **52** were dissolved in 90 mL MeOH, and the mixture was cooled to -10°C. 9.4 mL of *i*Pr_2EtN (54.0 mmol, 1.4 eq.) and 0,79 mL (7.71 mmol, 1eq.) of freshly distilled benzaldehyde were successively added dropwise. The reaction was stirred for 4 hours at r.t.. The temperature was then lowered again to -10°C and 2.9 g (76.6 mmol, 2eq.) of $NaBH_4$ were added portionwise over 30 min. The reaction mixture was again let react for half an hour, then, reaction was quenched by adding at low temperature HCl 4 M until no more gas formation was observed. The mixture was washed 3 times with Et_2O. The organic phases were combined and extracted with HCl 4 M twice. The aqueous phases were then combined and neutralized by careful addition of saturated $NaHCO_3$ solution until a pH=8 was reached. The aqueous phase was then extracted 4 times with Et_2O. The organic phase was separated and dried over Na_2SO_4, filtered, concentrated under reduced pressure and dried under vacuum affording 7.35 g (91%) of benzyl serine methyl ester as transparent oil.

R_f=0.2 (EtOAc/ hexane 1:1); [α]20=+39.4 (*R*-; $CHCl_3$, *c*=1.00); ^{1}H NMR (400 MHz, $CDCl_3$) δ 7.38 – 7.26 (m, 5H, C_6H_5), 3.91 (d, *J* = 13.0, 1H, CH_2Ph), 3.82 (dd, *J* = 4.4, 10.9, 1H, H_3), 3.77 (m, 4H, CH_2Ph, OCH_3), 3.66 (dd, *J* = 6.2, 10.8, 1H, H_3), 3.46 (dd, *J* = 4.5, 6.1, 1H, H_2), 2.78 (s, 1H, OH); ^{13}C NMR (101 MHz, $CDCl_3$) δ 173.6 (C=O), 139.3 (C_6H_5 quat), 129.0 (C_6H_5), 128.8 (C_6H_5), 127.8(C_6H_5), 62.8 (C_3), 62.2 (C_2), 52.6 (OCH_3), 52.4 (CH_2Ph); *S*: IR (cm -1): 3320, 2951, 1736, 1454, 1202, 1142, 1057; *R*: IR (cm -1): 3320, 2951, 1738, 1202, 1142, 1057.

4-allyl 1-[2-(benzylamino)-3-methoxy-3-oxopropyl] *N*-(*tert*-butoxycarbonyl)-aspartate (55 a-c)

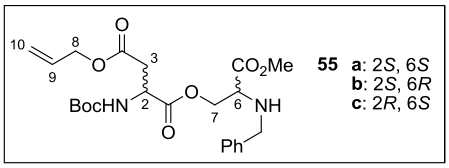

55 **a**: 2*S*, 6*S*
b: 2*S*, 6*R*
c: 2*R*, 6*S*

$C_{23}H_{32}N_2O_8$
MW: 464,51

To a solution of either (*R*)- or (*S*)-*N*-benzylserine methyl ester **53** (734 mg, 3.51 mmol, 1 eq.) and EDC·HCl (3.4 g, 17.6 mmol, 5 eq.) in dry CH_2Cl_2 (20 ml) at 0°C under a N_2 atmosphere, *β*-allyl (2*R*)- or (*2S*)-*N*-(tert-butoxycarbonyl) aspartate ester **51** (1.92 g, 7.01 mmol, 2 eq.) was added as a solution in CH_2Cl_2. After 30 min, DMAP (214 mg, 1.76 mmol, 0.5 eq.) was added in one portion. The mixture was stirred at 0°C for 2 h and for additional 4 h at r.t.. The resulting mixture was diluted with EtOAc (70 ml) and washed with $KHSO_4$ 1M aqueous solution (2x40 ml), aqueous $NaHCO_3$ (2x40 ml) and brine (2x40 ml), dried over Na_2SO_4, and volatiles were removed under reduced pressure. The residue was purified by flash chromatography on silica gel (Hexane/EtOAc, 7:3) to afford the desired product as a transparent oil (1.54 g, 94%).

R_f=0.30 (Hexane/EtOAc 6:4);

a) [α]D20=-2.65 (c=1.00, $CHCl_3$); ^{1}H NMR (400 MHz, $CDCl_3$) δ 7.24-7.34 (m, 5H, C_6H_5), 5.83-5.93 (m, 1H, H_9), 5.48 (d, J = 8.5 Hz, 1H, NHBoc), 5.30 (d, J = 17.2 Hz, 1H, H_{10a}), 5.23 (d, J = 10.4 Hz, 1H, H_{10b}), 4.51-4.61 (m, 3H, H_2, H_8), 4.32-4.48 (m, 2H, H_7), 3.88 (d, J = 13.1 Hz, 1H, C$\underline{H_2}$Ph), 3.75 (s, 3H, OCH_3), 3.73 (d, J = 13.1 Hz, 1H, C$\underline{H_2}$Ph), 3.55 (t, J = 4.7 Hz, 1H, H_6), 2.99 (dd, J_1 = 17.0 Hz, J_2=4.3 Hz, 1H, H_{3a}), 2.85 (dd, J_1=17.0 Hz, J_2=4.7 Hz, 1H, H_{3b}), 2.21 (bs, 1H, OH), 1.45 (s, 9H, $C(CH_3)_3$); ^{13}C NMR (101 MHz, $CDCl_3$) δ 172.8 (C=O), 171.0 (2C=O), 155.7 (COBoc), 139.6 (C_6H_5 - quat), 132.1 (C_9), 128.9 (C_6H_5), 128.7 (C_6H_5), 127.6 (C_6H_5), 119.1 (C_{10}), 80.6 ($\underline{C}(CH_3)_3$), 66.2 (C_8), 66.1 (C_7), 59.5 (C_6), 52.7 (C_2), 52.2 (CH_2Ph), 50.3 (OCH_3), 37.1 (C_3), 28.7 ($C(\underline{C}H_3)_3$); IR (cm^{-1}): 3358, 2928, 1738, 1500, 1454, 1385, 1163, 1053.

b) [α]D20=+11 (c=1.00 in $CHCl_3$); ^{1}H NMR (400 MHz, $CDCl_3$) δ 7.26-7.34 (m, 5H, C_6H_5), 5.83-5.93 (m, 1H, H_9), 5.47 (d, J = 8.4, 1H, NHBoc), 5.32 (d, J = 17.2, 1H, H_{10a}), 5.25 (d, J = 10.5, 1H, H_{10b}), 4.66 – 4.52 (m, 3H, H_2, H_8), 4.46 (dd, J = 4.6, 11.0, 1H, H_{7a}), 4.35 (dd, J = 4.8, 11.0, 1H, H_{7b}), 3.89 (d, J = 13.1, 1H, C$\underline{H_2}$Ph), 3.80 – 3.68 (m, 4H, OCH_3, C$\underline{H_2}$Ph), 3.55 (t, J = 4.7, 1H, H_6), 3.01 (dd, J = 4.3, 17.0, 1H, H_{3a}), 2.86 (dd, J = 4.7, 17.1, 1H, H_{3b}), 1.96 (s, 1H, OH), 1.45 (s, 9H, $C(CH_3)_3$); IR (cm^{-1}): 3362, 2978, 1740, 1500, 1455, 1368, 1167, 1053.

c) ^{1}H NMR (400 MHz, CD_2Cl_2) δ 7.37-7.20 (m, 5H), 5.95-5.82 (m, 1H), 5.41 (br d, 1H, J = 7.9 Hz), 5.34-5.18 (m, 2H), 4.61-4.48 (m, 3H), 4.39 (dd, 1H, J = 10.9, 4.6 Hz), 4.30 (dd, 1H, J = 10.9, 4.9 Hz), 3.86 (d, 1H, J = 13.1 Hz), 3.71 (s, 3H), 3.70 (d, 1H, J = 13.1 Hz), 3.51 (t, 1H, J = 4.7 Hz), 2.94 (dd, 1H, J = 17.2, 4.7 Hz), 2.82 (dd, 1H, J = 17.0, 4.8 Hz), 1.42 (s, 9H); ^{13}C NMR (101 MHz, CD_2Cl_2) δ 172.4, 170.6, 139.7, 131.9, 128.3, 128.2, 127.1, 118.1, 65.9, 65.6, 59.1, 52.0, 51.8, 50.0, 36.7, 28.0; HRMS (ESI) *m/z* calcd for $[C_{23}H_{33}N_2O_8]^+$: 465.22314 $[M+H]^+$; found: 465.22267.

OH-DKP1-CO_2Allyl (49 a); OH-DKP2-CO_2Allyl (49 b); OH-DKP3-CO_2Allyl (49 c)

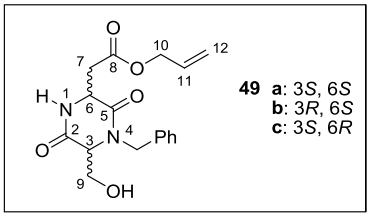

49 **a**: 3*S*, 6*S*
b: 3*R*, 6*S*
c: 3*S*, 6*R*

$C_{17}H_{20}N_2O_5$
MW: 332,35

Compound **55** (1.08 g, 1.82 mmol, 1 eq.) was deprotected according to general procedure **GP1**. The corresponding trifluoroacetate salt **57** was dissolved in *i*PrOH (20 ml) and *i*Pr_2EtN (0.9 ml, 5.6 mmol, 4 eq.) was added at r.t.. The reaction was stirred for 18 h at r.t., monitoring the formation of DKP by TLC (EtOAc/Hexane: 8/2). The solution was then concentrated under reduced pressure and the residue was purified by flash chromatography on silica gel (Hexane/EtOAc, 75:25) to afford the desired product as a white foam (543.8 mg, 90%).

57: R_f=0.37 (DCM/MeOH 95:5); [α]D32=–8.7 (c=1.50 in $CHCl_3$); ^{1}H NMR (400 MHz, CD_2Cl_2) δ 7.59-7.37 (m, 5H), 6.01-5.86 (m, 1H), 5.41-5.25 (m, 2H), 4.78-4.59 (m, 4H), 4.48-4.37 (m, 2H),

4.29 (d, *J*=12.98 Hz, 1H), 4.08-4.01 (br, 1H), 3.89-3.81 (s, 3H), 3.17 (dd, *J*=18.33 , 3.91 Hz, 1H), 3.10 (dd, J_1=18.53 Hz, J_2=6.10 Hz, 1H); ^{13}C NMR (100 MHz, CD_2Cl_2) δ 170.1, 166.3, 165.9, 131.2, 130.5, 130.0, 129.3, 118.9, 66.5, 62.7, 56.1, 53.9, 53.7, 53.4, 53.2, 52.9, 50.6, 49.4, 33.4; IR (film): ν_{max} 2921, 2850, 1759, 1681, 1539, 1456, 1392, 1202, 1137; HRMS (ESI) m/z calcd for $[C_{18}H_{25}N_2O_6]^+$: 365.17071 $[M+H]^+$; found: 365.17033.

49 a) R_f=0.25 (EtOAc/Hexane: 8/2); [α]D20=-72.1 (*c*= 1.00 in $CHCl_3$); ^{1}H NMR (300 MHz, $CDCl_3$) δ 7.41 – 7.19 (m, 5H, C_6H_5), 7.02 (d, *J* = 2.1 Hz, 1H, NH), 5.96 – 5.78 (m, *J* = 17.1, 10.4, 5.8 Hz, 1H, H_{11}), 5.38 – 5.19 (m, 3H, H_{12}, $C\underline{H_2}Ph$), 4.67 – 4.53 (m, 2H, H_{10}), 4.53 – 4.43 (m, 1H, H_6), 4.06 (d, *J* = 15.0 Hz, 1H, $C\underline{H_2}Ph$), 4.00 – 3.91 (m, *J* = 6.7 Hz, 1H, C_{9a}), 3.91 – 3.80 (m, *J* = 3.1 Hz, 2H, C_{9b}, C_3), 3.20 (dd, *J* = 17.6, 3.5 Hz, 1H, C_{7a}), 3.11 (dd, *J* = 17.6, 10.1 Hz, 1H, C_{7b}); ^{13}C NMR (101 MHz, $CDCl_3$) δ 171.8 (C=O), 166.8 (C=O), 166.2 (C=O), 135.6 (C_6H_5 – quat.), 131.9 (C_{11}), 129.5 (C_6H_5), 128.6 (C_6H_5), 128.6 (C_6H_5), 119.5 (C_{12}), 66.4 (C_{10}), 61.2 (C_3), 60.6 (C_9), 52.8 (C_6), 47.8 (CH_2Ph), 40.7 (C_7); IR (cm^{-1}): 3427, 2928, 1740, 1653, 1452, 1383, 1339, 1275, 1184, 1128.

49 b) R_f=0.10 (EtOAc/Hexane 8:2); [*a*]D20=-35.3 (*c*=1.00 in $CHCl_3$); ^{1}H NMR (400 MHz, CD_2Cl_2) δ 7.43 - 7.25 (m, 5H), 7.20 (br s, 1H), 6.02 - 5.83 (m, 1H), 5.39 - 5.20 (m, 3H), 4.70 - 4.55 (m, 3H), 4.12 (d, 1H, *J* = 15.2 Hz), 4.01 (dd, 1H, *J* = 11.8, 1.9 Hz), 3.90 (dd, 1H, *J* = 11.8, 3.1 Hz), 3.81 (bs, 1H,), 3.21 (dd, 1H, *J* = 17.4, 4.0 Hz), 2.86 (dd, 1H, *J* = 17.4, 8.0 Hz); ^{13}C NMR (101 MHz, CD_2Cl_2) δ 170.8, 168.2, 166.6, 135.9, 131.8, 128.8, 127.9, 127.9, 127.8, 118.3, 117.9, 65.7, 61.9, 61.6, 51.1, 47.3, 37.1; IR (neat): ν_{max} 3364, 3032, 2942, 1738, 1651, 1452, 1383, 1329, 1273, 1183, 1129; HRMS (ESI) *m/z* calcd for $[C_{17}H_{20}N_2NaO_5]^+$: 355.12644 $[M+Na]^+$; found: 355.12590.

N_3-DKP1-CO_2Allyl (58 a); N_3-DKP2-CO_2Allyl (58 b); N_3-DKP3-CO_2Allyl (58 c)

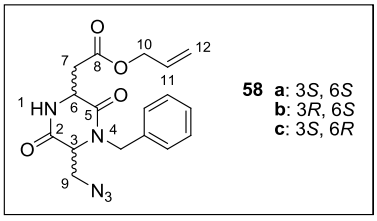

58 **a**: 3*S*, 6*S*
b: 3*R*, 6*S*
c: 3*S*, 6*R*

$C_{17}H_{19}N_5O_4$
MW: 357,36

To a solution of diketopiperazine **49** (559 mg, 1.7 mmol, 1 eq.) in CH_2Cl_2/toluene (6.6 ml/12.2 ml), under a nitrogen atmosphere and at -20 ºC, PPh_3 (535 mg, 2.0 mmol, 1.2 eq.) was added and the mixture was stirred until a solution was obtained. Addition of hydrazoic acid (0.45 M in toluene, 7.5 ml, 3.4 mmol, 2 eq.) was followed by dropwise addition of DIAD (0.42 ml, 2.0 mmol, 1.2 eq.) and the reaction was stirred at -20ºC during 3.5 h. The reaction mixture was loaded onto a silica gel column (Hexane/EtOAc, 6:4) thus removing the hydrazo-derivative. The resulting crude residue was further purified by flash chromatography (CH_2Cl_2/MeOH, 99:1) to afford the desired product as a white foam (**a:** 309 mg, 51%; **b-c:** 486 mg, 80%).

In the case of the *cis* isomer, an almost unseparable mixture of compounds **58a** and **60a** was obtained in a 2-3:1 ratio.

a) R_f=0.25 (EtOAc/Hexane: 8/2); [α]D20=-72.1 (*c*= 1.00 in $CHCl_3$) ^{1}H NMR (400 MHz, $CDCl_3$) δ 7.39 – 7.21 (m, 5H, C_6H_5), 6.77 (s, 1H, NH), 5.84-5.91 (m, 1H, H_{11}), 5.41 – 5.27 (m, 2H, H_{12}), 5.25 (d, *J* = 15.0, 1H, C$\underline{H_2}$Ph), 4.70 – 4.57 (m, 2H, H_{10}), 4.52 (dt, *J* = 2.7, 10.7, 1H, H_6), 4.17 (d, *J*=15.0 Hz, 1H, C$\underline{H_2}$Ph), 4.03 (q, *J* = 3.5, 1H, H_3), 3.92 – 3.85 (m, 2H, H2, H_9), 3.24 (dd, *J* = 2.7, 17.7, 1H, H_{7a}), 3.16 (br s, 1H, OH); 3.11 (dd, *J* = 10.9, 17.7, 1H, H_{7b}); ^{13}C NMR (101 MHz, $CDCl_3$) δ 171.8 (C=O), 166.8 (C=O), 166.2 (C=O), 135.6 (C_6H_5 – quat.), 131.9 (C6), 129.5 (C_6H_5), 128.6 (C_6H_5), 128.6 (C_6H_5), 119.5 (C_7), 66.4 (C_5), 61.2 (C_2), 60.6 (C_4), 52.8 (C_1), 47.8 (CH_2Ph), 40.7 (C_3); IR (cm^{-1}): 3427, 2928, 1740, 1653, 1452, 1383, 1339, 1275, 1184, 1128.

c) R_f=0.13 (Hexane/EtOAc 6:4); [*a*]D20=+55.9 (*c*=1.00 in $CHCl_3$); ^{1}H NMR (400 MHz, CD_2Cl_2) δ 7.39 – 7.26 (m, 5H), 7.09 (d, 1H, *J* = 11.3 Hz), 6.00 – 5.83 (m, 1H), 5.35 (dq, 1H, *J* = 1.5, 17.2 Hz), 5.28 (dq, 1H, *J* = 1.3, 10.4 Hz), 5.16 (d, 1H, *J* = 15.1 Hz), 4.69 – 4.60 (m, 3H), 4.26 (d, 1H, *J* = 15.1 Hz), 3.95 (t, 1H, *J* = 2.9 Hz), 3.89 (dd, 1H, *J* = 2.3, 12.7 Hz), 3.65 (dt, 1H, *J* = 6.6, 13.2 Hz), 3.29 (dd, 1H, *J* = 3.6, 17.5 Hz), 2.84 (dd, 1H, *J* = 8.9, 17.5 Hz); ^{13}C NMR (101 MHz, CD_2Cl_2) δ 171.0, 166.8, 166.4, 135.61, 131.9, 129.5, 128.7, 128.5, 119.4, 66.3, 59.5, 52.1, 51.5, 51.4, 48.3, 37.6; IR (cm^{-1}): v_{max} 3250, 2937, 2118, 1732, 1694, 1447, 1329, 1277, 1184; MS (ESI) *m/z* calcd for $[C_{17}H_{20}N_5O_4]^+$: 380.13 $[M+H]^+$; found: 380.2.

N-Boc-DKP1- CO_2Allyl (59 a); *N*-Boc-DKP2- CO_2Allyl (59 b); *N*-Boc-DKP3- CO_2Allyl (59 c)

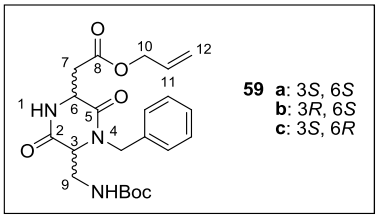

59 **a**: 3*S*, 6*S*
b: 3*R*, 6*S*
c: 3*S*, 6*R*

$C_{22}H_{29}N_3O_6$
MW: 431,48

To a solution of azide **58** (268 mg, 0.75 mmol, 1 eq.) in THF (2.5 ml), under a nitrogen atmosphere and at -20 ºC, Me_3P (0.83 ml of 1 M solution in THF, 0.83 mmol, 1.1 eq.) and 2-(*t*-butoxycarbonyloxyimino)-2-phenylacetonitrile (Boc-ON, 206 mg, 0.83 mmol, 1.1 eq.) were added successively. After stirring for 5 h at r.t., the solution was diluted with CH_2Cl_2 (60 ml) and washed with H_2O (3x30 ml) and brine. The organic phase was dried over Na_2SO_4 and volatiles were removed under reduced pressure. The residue was purified by flash chromatography on silica gel (CH_2Cl_2/MeOH, 99:1) to afford the desired product as a white foam (**a**: 308 mg, 95%; **b**: 246 mg, 76%).

a) R_f=0.2 (CH_2Cl_2/MeOH 97:3); [*a*]D20=-123.7 (*c*=1.00 in $CHCl_3$); ^{1}H NMR (400 MHz, $CDCl_3$) δ 7.33 (m, 5H, C_6H_5), 6.99 (s, 1H, NH), 5.92 (m, 1H, H_{11}), 5.56 (d, *J* = 15.1, 1H, C$\underline{H_2}$Ph), 5.35 (dd, *J* = 1.3, 17.2, 1H, H_{12b}), 5.28 (dd, *J* = 0.9, 10.4, 1H, H_{12b}), 5.20 (t, *J* = 6.4, 1H, NHBoc), 4.65 (d, *J* = 5.7, 2H, H_{10}), 4.50 (dt, *J* = 2.6, 11.2, 1H, H_6), 4.09 (d, *J* = 15.1, 1H, C$\underline{H_2}$Ph), 3.90 – 3.76 (m, 2H,

H_2, H_{9a}), 3.49 (m, 1H, H_{9b}), 3.28 (dd, *J* = 2.4, 17.6, 1H, H_{7a}), 2.84 (dd, *J* = 11.2, 17.6, 1H, H_{7b}), 1.46 (s, 9H, $C(CH_3)_3$); ^{13}C NMR (101 MHz, $CDCl_3$) δ 171.5 (C=O), 166.7 (C=O), 164.9 (C=O), 156.2 (C=O), 135.6 (C_6H_5 – quat.), 131.8 (C_{11}), 129.4 (C_6H_5), 128.9 (C_6H_5), 128.5 (C_6H_5), 119.3 (C_{12}), 80.8 ($\underline{C}(CH_3)_3$), 66.4 (C_{10}), 59.2 (C_3), 52.4 (C_6), 47.2 ($\underline{C}H_2Ph$), 40.8 (C_9), 40.6 (C_7), 28.7 ($C(\underline{C}H_3)_3$); IR (cm^{-1}): 3389, 2928, 1663, 1524, 1453, 1339, 1271, 1169.

b) R_f=0.14 (DCM/MeOH 97:3); [*a*]D20=+16.9 (*c*=1.00 in $CHCl_3$); ^1H NMR (400 MHz, $CDCl_3$) δ 7.41 – 7.21 (m, 5H), 6.94 (s, 1H), 5.91 (m, 1H), 5.51 (d, 1H, *J* = 15.1 Hz), 5.39 – 5.23 (m, 2H), 5.05 (br s, 1H), 4.64 (d, 2H, *J* = 5.6 Hz), 4.49 (dd, 1H, *J* = 2.8, 9.3 Hz), 4.09 (d, 1H, *J* = 15.1 Hz), 3.83 – 3.76 (m, 2H), 3.61 – 3.47 (m, 1H), 3.35 (dd, 1H, *J* = 3.3, 17.6 Hz), 2.79 (dd, 1H, *J* = 9.4, 17.6 Hz), 1.45 (s, 9H); ^{13}C NMR (101 MHz, $CDCl_3$) δ 171.3, 167.6, 165.3, 156.3, 135.8, 131.8, 129.4, 128.8, 128.5, 119.4, 80.8, 66.4, 59.7, 51.3, 47.6, 41.1, 38.3, 28.7; IR (cm^{-1}): ν_{max} 3328, 2980, 1692, 1524, 1453, 1329, 1273, 1171; MS (ESI) *m/z* calcd for $[C_{22}H_{30}N_3O_6]^+$: 432.21 $[M+H]^+$; found: 432.3.

N-Boc-DKP-COOH (DKP1-DKP3)

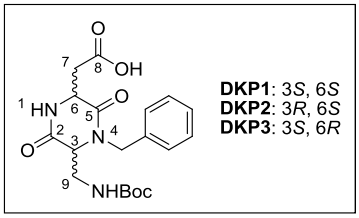

$C_{19}H_{25}N_3O_6$
MW: 391,42

Allyl ester **59** (363 mg, 0.84 mmol, 1 eq.) was dissolved in CH_2Cl_2 (6.0 ml) under a nitrogen atmosphere. After cooling the solution at 0 ºC, pyrrolidine (83 µl, 1.01 mmol, 1.2 eq), PPh_3 (40 mg, 0.15 mmol, 0.18 eq) and $[Pd(PPh_3)_4]$ (39 mg, 0.034 mmol, 0.04 eq) were added successively. After stirring for 1 h at 0°C, the mixture was diluted with EtOAc (25 ml) and extracted with aqueous $NaHCO_3$ (4x10 ml). The combined aqueous phases were acidified to pH 2 with a 1 M $KHSO_4$ solution and then extracted with CH_2Cl_2. The resulting organic phase was dried over Na_2SO_4 and the solvent was evaporated to afford the desired product as a fluffy white solid (327 mg, 99%) that was used without further purification.

N_3-DKP-CO_2H (DKP1*-DKP3*) [11]

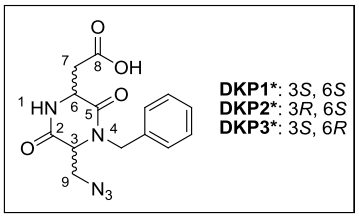

$C_{14}H_{15}N_5O_4$
MW: 317,30

Allyl ester **58** (300 mg, 0.84 mmol, 1 eq.) was dissolved in CH_2Cl_2 (8.0 ml) under a nitrogen atmosphere, and the mixture was cooled to 0°C. $[Pd(PPh_3)_4]$ (290 mg, 0.25 mmol, 0.3 eq) and freshly distilled *N*-methyl aniline (109µl, 1.0 mmol, 1.2 eq.) were added successively. The mixture was then

allowed to reach r.t.. After 1 h of stirring, the mixture was diluted with EtOAc (40 ml) and extracted with aqueous $NaHCO_3$ (4 x 20 ml). The combined aqueous phases were acidified to pH 2 by adding a $KHSO_4$ 1M solution and then extracted with CH_2Cl_2 (4 x 20 ml). The resulting organic phase was dried over Na_2SO_4 and the solvent was evaporated to afford the desired product as a slightly yellow solid (241 mg, 90%) which was used without further purification.

In the case of the *cis* isomer, a mixture of compounds **58a** and **60a** could be used as the starting material, without affecting reactivity. A mixture of free carboxylic acids **DKP1*** and **61a** was thus obtained. Successive precipitations of by-product with small amounts of CH_2Cl_2 afforded **DKP1*** in good purity.

DKP1*: ^{1}H NMR (300 MHz, $CDCl_3$) δ 8.83 (s, 1H, COOH), 7.42 – 7.19 (m, 5H, C_6H_5), 5.16 (d, J = 15.1 Hz, 1H, C$\underline{H_2}$Ph), 4.56 (dt, J = 11.6, 2.6 Hz, 1H, H_6), 4.21 (d, J = 15.1 Hz, 1H, C$\underline{H_2}$Ph), 3.97 (t, J = 2.1 Hz, 1H, H_3), 3.86 (dd, J = 12.8, 1.9 Hz, 1H, H_{9a}), 3.66 (dd, J = 12.8, 3.5 Hz, 1H H_{9b}), 3.31 (dd, J = 18.0, 2.6 Hz, 1H, H_{7a}), 3.05 (dd, J = 18.0, 11.7 Hz, 1H, H_{7b}).

DKP3*: ^{1}H NMR (400 MHz, $CDCl_3$) δ 8.12 (s, 1H, COOH), 7.42 – 7.31 (m, 3H, C_6H_5), 7.31 – 7.23 (m, J = 7.9 Hz, 2H, C_6H_5), 5.18 (d, J = 15.1 Hz, 1H, C$\underline{H_2}$Ph), 4.66 (dd, J = 9.8, 2.9 Hz, 1H, H_6), 4.27 (d, J = 15.1 Hz, 1H, C$\underline{H_2}$Ph), 3.96 (t, J = 2.4 Hz, 1H, H_3), 3.89 (dd, J = 12.8, 2.2 Hz, 1H, H_{9a}), 3.69 (dd, J = 12.8, 3.4 Hz, 1H H_{9b}), 3.38 (dd, J = 17.9, 3.2 Hz, 1H, H_{7a}), 2.80 (dd, J = 17.9, 9.9 Hz, 1H, H_{7b}).

2.2 - DKP4-DKP6

N-benzyl-dimethyl aspartate (63) [6,7]

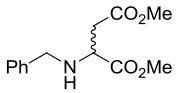

$C_{13}H_{17}NO_4$
MW: 251,28

At 0 °C to 50 ml of anhydrous methanol, 3.75 ml (47.5 mmol) of thinly chloride was added dropwise. The solution was stirred at 0 °C for 30 min and then 6.332 g (47.5 mmol) of Asp was added. The reaction mixture was stirred at r.t. for 24 h and TLC (CH_3Cl/CH_3OH, 9:1) indicated complete disappearance of Asp. The reaction mixture was evaporated under reduced pressure and the residue was triturated with petroleum ether repeatedly to provide 7.495 mg (98%) of HCl•Asp-$(OCH_3)_2$ as a colorless which was directly used for the next reaction.

To a vigorously stirred solution of 500 mg (2.54 mmol) of dimethyl aspartate hydrochloride and 160 mg (2.54 mmol) of sodium cyanoborohydride in 12 mL of methanol at rt was added 265 mg (2.54 mmol) of benzaldehyde in one portion. After being stirred for 4 h, the mixture was cooled in an ice bath, and the pH was lowered to ca. 1 with concd HCl. The mixture was then allowed to warm to r.t. for 2 h, and the methanol was removed under reduced pressure at r.t.. The white residue was dissolved into a minimum volume of water, and the pH was raised to ca. 10 with saturated aqueous Na_2CO_3. After three ethyl acetate extractions, combined organic portions were washed with brine, dried over Na_2CO_3, and evaporated to give a pale yellow oil.

methyl 3-azido-2-(tert-butoxycarbonylamino)propanoate (69)

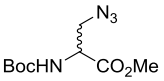

$C_9H_{16}N_4O_4$
MW: 244,25

In a round bottom flask were solved (10.0 g, 64.3 mmol, 1 eq.) of serine methyl ester hydrochloride in 232 mL of THF/water 1:1 solution. The reaction flask was lowered into an ice bath and 27 ml (193 mmol, 3 eq.) of triethylamine were added. Then, 16.8 g (77.1 mmol, 1.2 eq.) of Boc_2O were added and the reaction was stirred at room temperature for 24 h. The reaction mixture was then diluted with 200 mL of EtOAc and washed with aqueous $KHSO_4$ 1M until pH = 3 and brine. The organic phase was dried over Na_2SO_4, filtered and concentrated under reduced pressure. The product was then dried under high vacuum for a few hours affording 12.3 g (90 %) of pure Boc-Ser-OMe **68** as viscous transparent oil which was used in the next step without purification.

To triphenyl phosphine (1.45 g, 5.54 mmol, 1.2 eq.) in THF (11 mL) at -78 °C was added DIAD (1 ml, 5.54 mmol, 1.2 eq.) in THF (10 mL) followed by the HN_3 solution (1.8 M in toluene, 3.1 ml, 5.54mmol, 1.2 eq.) and Boc-serine methyl ester **68** (1.00 g, 4.62 mmol) in THF (10 mL). After the mixture stirred at -78 °C for 30 min and then allowed to slowly reach 0°C (within 3 h). The solvent was evaporated and the residue was chromatographed with hexane/EtOAc 9:1 to provide 839 mg (74%) of the azide as a mobile oil which crystallizes upon standing in the refrigerator.

3-azido-2-(tert-butoxycarbonylamino)propanoic acid (70)

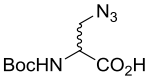

$C_8H_{14}N_4O_4$
MW: 230,22

Compound **69** (350.0 mg, 1.433 mmol) in THF (6 mL) at 0 °C was treated with LiOH monohydrate (84.0 mg, 2.00 mmol) in water (4 mL). After 1 h the mixture was concentrated, diluted with water, washed with ether, acidified with 1 M $KHSO_4$, and extracted into DCM which was dried and evaporated to provide 329.2 mg (quant.) of a colorless oil.

(*R*)-dimethyl-2-((*S*)-3-azido-*N*-benzyl-2-(*tert*-butoxycarbonylamino)propanamido)succinate (72 a);

(*S*)-dimethyl-2-((*R*)-3-azido-*N*-benzyl-2-(*tert*-butoxycarbonylamino)propanamido)succinate (72 b)

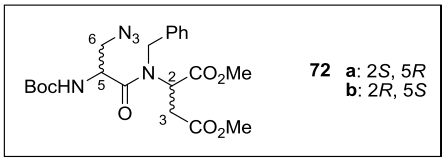

72 **a**: 2*S*, 5*R*
b: 2*R*, 5*S*

$C_{21}H_{29}N_5O_7$
MW: 463,48

DCC (1.77 g, 8.56 mmol, 1 eq.) was added to a solution of *N*-Boc-Ser(N_3)-OH (**69**) (3.94g, 17.11 mmol, 2 eq.) 60 ml of CH_2Cl_2, in one portion. A white precipitate (DCU) formed and stirring continued for 1h at r.t.. The mixture was then filtered on a cotton wool to remove DCU. The white

DCU residue was washed twice with cold CH_2Cl_2. The filtrate was concentrated under reduced pressure at r.t., and dried under high vacuum to afford symmetric anhydride **70a** or **70b** as a pale yellow foam, which was used without further purification. *N*-benzyl-aspartic acid dimethylester **63** (1.51 g, 6.01 mmol, 0.7 eq.) was dissolved in CH_2Cl_2 (50 ml) and the mixture was cooled to 0°C. A solution of symmetric anhydride in 50 ml of CH_2Cl_2 was then added dropwise, very slowly. The reaction mixture was let to reach r.t. and stirred overnight. The solvent was afterwards removed under reduced pressure and the residue was purified by flash chromatography on silica gel (Hexane/EtOAc, 8:2) to afford the desired product as a viscous transparent oil (2.22 g, 80%).

R_f=0.37 (Hexane/EtOAc, 7:3); [*a*]D20=-38.6 (**72 a**, *c*=1.0 in $CHCl_3$); ^{1}H NMR (400 MHz, CD_2Cl_2) (rotamers ratio in CD_2Cl_2 A/B = 4:1) δ 7.51 – 7.11 (m, 5H), 5.61 – 5.50 (m, 1H$_B$), 5.40 – 5.28 (m, 1H$_B$, overlapping with solvent signal), 5.17 (t, 1H$_B$, *J* = 7.1 Hz), 5.07 – 4.99 (m, 1H$_B$), 4.86 – 4.69 (m, 3H$_A$, 1H$_B$), 4.54 – 4.38 (m, 1H$_A$, 1H$_B$), 3.74 (dd, 1H$_B$, *J* = 12.3, 5.4 Hz), 3.69 – 3.65 (m, 3H$_A$, 1H$_B$), 3.63 (s, 3H$_A$), 3.52 (dd, 1H$_A$, *J* = 12.4, 6.3 Hz), 3.41 (dd, 1H$_A$, *J* = 12.3, 6.0 Hz), 3.28 (dd, 1H$_A$, *J* = 16.9, 7.4 Hz), 3.05 (dd, 1H$_B$, *J* = 17.1, 7.0 Hz), 2.71 (dd, 1H$_B$, *J* = 17.2, 7.3 Hz), 2.55 (dd, 1H$_A$, *J* = 16.1, 6.1 Hz), 1.45 (s, 9H); ^{13}C NMR (101 MHz, CD_2Cl_2) δ 171.9, 171.3, 170.4, 155.5, 136.3, 129.5, 129.3, 129.2, 129.1, 129.0, 128.8, 128.2, 128.0, 127.9, 80.9, 58.0, 56.9, 56.6, 53.4, 53.1, 53.0, 52.6, 52.4, 51.4, 48.1, 35.3, 34.9, 28.6; IR (neat): ν_{max} 3343, 2979, 2953, 2106, 1739, 1712, 1651, 1497, 1438, 1367, 1289, 1250, 1166; MS (ESI) *m/z* calcd for $[C_{21}H_{29}N_5NaO_7]^+$: 486.20 $[M+Na]^+$; found: 486.3.

N_3-DKP4-CO_2Me (66 a); N_3-DKP6-CO_2Me (66 b)

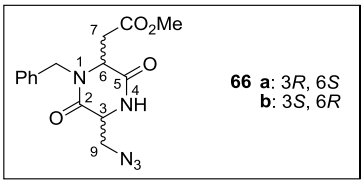

66 a: 3*R*, 6*S*
b: 3*S*, 6*R*

$C_{15}H_{17}N_5O_4$
MW: 331,33

Dipeptide **72** (1.44 g, 3.11 mmol, 1 eq.) was deprotected according to general procedure **GP1**, with the addition of Et_3SiH (1.24 ml, 7.78 mmol, 2.5 eq.) as an ion scavenger. The corresponding trifluoroacetate salt was dissolved in *i*PrOH (40 ml) and *i*Pr_2EtN (2.13 ml, 12.44 mmol, 4 eq.) was added at r.t.. The reaction was stirred for 5 h at r.t., then the solution was concentrated under reduced pressure and the residue was purified by flash chromatography on silica gel (EtOAc/Hexane, 8:2) to afford the desired product as a white foam (927.4 mg, 90%).

R_f=0.33 (Hexane/EtOAc 2:8); [*a*]D20=+32.2 (**66 a**, *c*=1 in $CHCl_3$); ^{1}H NMR (400 MHz, CD_2Cl_2) δ 7.45 – 7.24 (m, 5H), 6.83 (s , 1H), 5.13 (d, 1H, *J* = 15.3 Hz), 4.53 – 4.47 (m, 1H), 4.24 (d, 1H, *J* = 15.3 Hz), 4.12 (t, 1H, *J* = 4.7 Hz), 3.91 (dd, 1H, *J* = 12.5, 5.8 Hz), 3.85 (dd, 1H, *J* = 12.5, 3.6 Hz), 3.65 (s, 3H), 3.07 (dd, 1H, *J* = 17.5, 3.3 Hz), 2.88 (dd, 1H, *J* = 17.5, 5.0 Hz); ^{13}C NMR (101 MHz, CD_2Cl_2) δ 170.4, 167.6, 164.5, 135.6, 128.9, 127.9, 127.8, 56.0, 54.3, 52.0, 47.4, 34.6; IR (neat): ν_{max} 3249, 3066, 3030, 3007, 2953, 2924, 2852, 2362, 2342, 2117, 1736, 1558, 1496, 1449, 1372, 1332, 1281, 1204, 1180, 1138; MS (ESI) *m/z* calcd for $[C_{15}H_{18}N_5O_4]^+$: 332.14 $[M+H]^+$; found: 332.3.

NH_2-DKP4-CO_2Me (73 a); NH_2-DKP6-CO_2Me (73 b)

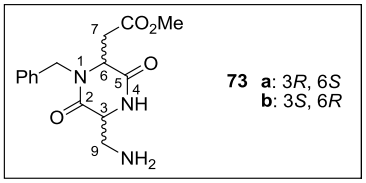

73 **a**: 3*R*, 6*S*
b: 3*S*, 6*R*

$C_{15}H_{19}N_3O_4$
MW:305,33

Compound **66** (737 mg, 2.22 mmol, 1 eq.) was dissolved in THF (45 ml) and Pd/C (237 mg, 0.22 mmol, 0.1 eq.) was added. The flask was thoroughly purged with H_2, and the system was closed. The reaction mixture was stirred at r.t. for 4 h, and then filtered through a Celite pad. The cake thus obtained was washed thoroughly with THF. The filtrate was concentrated and dried to give the crude product as a transparent paste (643.9 mg, 95%) which was used without further purification.

R_f=0.13 (CH_2Cl_2/MeOH 95:5); [*a*]D20=+83.2 (**73 a**, *c*=1 in $CHCl_3$); ^{1}H NMR (400 MHz, CD_2Cl_2) δ 7.30 – 7.09 (m, 5H), 6.75 (br s, 1H), 4.99 (d, 1H, *J* = 15.3 Hz), 4.15 – 4.04 (m, 2H), 4.00 (br s, 1H), 3.53 (s, 3H), 3.18 (dd, 1H, *J* = 13.1, 3.6 Hz), 2.99 – 2.84 (m, 2H), 2.73 (dd, 1H, *J* = 17.0, 5.1 Hz), 1.33 (s, 2H); ^{13}C NMR (101 MHz, CD_2Cl_2) δ 170.3, 167.4, 166.2, 136.1, 128.8, 127.7, 56.3, 55.9, 51.9, 47.2, 44.2, 35.0; IR (neat): ν_{max} 1736, 1685, 1659, 1496, 1449, 1371, 1318, 1254, 1203, 1179, 1109; MS (ESI) *m/z* calcd for $[C_{15}H_{20}N_3O_4]^+$: 306.14 $[M+H]^+$; found: 306.3.

NHBoc-DKP4-CO_2Me (74 a); NHBoc-DKP6-CO_2Me (74 b)

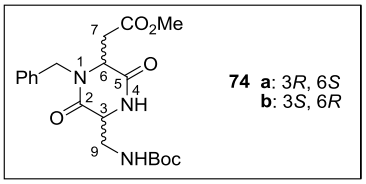

74 **a**: 3*R*, 6*S*
b: 3*S*, 6*R*

$C_{20}H_{27}N_3O_6$
MW: 405,44

To a solution of **73** (586 mg, 1.92 mmol, 1 eq.) in THF (35 ml) Boc_2O (461 mg, 2.11 mmol, 1.1 eq.) was added in one portion. After stirring the mixture at r. t. overnight, EtOAc (60 ml) was added. The solution was washed with 1 M $KHSO_4$ (4x) and brine (1x). The organic phase was dried over Na_2SO_4 and volatiles were removed under reduced pressure, to afford the desired product as a white foam (739.5 mg, 95%), which was used without further purification.

R_f=0.23 (EtOAc/Hex 7:3); [*a*]D20=+82.2 (**74 a**, *c*=1 in $CHCl_3$); ^{1}H NMR (400 MHz, CD_2Cl_2) δ 7.33 – 7.06 (m, 5H), 6.69 (br s, 1H), 5.12 (br s, 1H), 4.96 (d, 1H, *J* = 15.2 Hz), 4.26 (s, 1H), 4.14 (d, 1H, *J* = 15.3 Hz), 4.00 (s, 1H), 3.68 – 3.57 (m, 3H), 3.56 – 3.45 (m, 4H), 2.86 (d, 1H, *J* = 16.9 Hz), 2.72 (dd, 1H, *J* = 17.1, 4.9 Hz), 1.35 (s, 9H); ^{13}C NMR (101 MHz, CD_2Cl_2) δ 170.3, 167.3, 166.0, 146.7, 135.9, 128.8, 127.8, 127.6, 79.9, 56.6, 55.9, 51.9, 47.7, 42.2, 35.1, 28.0; IR (neat): ν_{max} 3328, 3004, 2979, 2953, 2934, 1809, 1737, 1690, 1586, 1508, 1497, 1450, 1393, 1368, 1333, 1250, 1208, 1168, 1119; MS (ESI) *m/z* calcd for $[C_{20}H_{28}N_3O_6]^+$: 406.20 $[M+H]^+$; found: 406.3.

NHBoc-DKP4-COOH (DKP4); NHBoc-DKP6-COOH (DKP6)

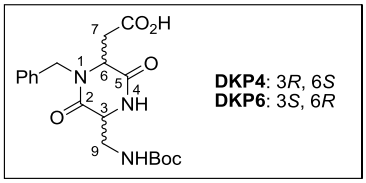

$C_{19}H_{25}N_3O_6$
MW: 391,42

Compound **74** (710 mg, 1.75 mmol, 1 eq.) was dissolved in THF (60 ml) and the mixture was cooled to 0 °C. A solution of $LiOH \cdot H_2O$ (183.7 mg, 4.38 mmol, 2.5 eq.) in H_2O (30 ml) was added dropwise. The resulting solution was let reacting for 1 h at 0 °C. Then, maintaining the temperature at 0 °C, the mixture was acidified with HCl 1M to pH = 1-2, and extracted with CH_2Cl_2 (4x). The collected organic phases were dried over Na_2SO_4 and volatiles removed under reduced pressure. Either **DKP4** or **DKP6** were afforded as a white foam (685 mg, 100%), which was used in subsequent steps without further purification.

2.3 - DKP5-DKP7

N_3-DKP5-CO_2Me (77 a); N_3-DKP7-CO_2Me (77 b)

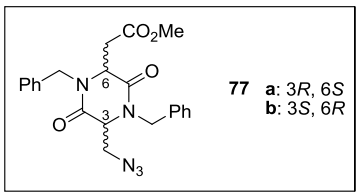

$C_{22}H_{23}N_5O_4$
MW: 421,45

A flame-dried flask under N_2 was charged with a solution of **66** (640 mg, 1.93 mmol, 1 eq.) in dry THF (32 ml). The temperature was lowered to -78°C and KHMDS (4.25 ml of a 0.5 M solution in toluene, 2.12 mmol, 1.1 eq.) was added dropwise. After 30 min benzyl bromide (1.18 ml, 9.65 mmol, 5 eq.) was added, and a final solvent ratio THF/DMF 7:3 was reached by adding DMF (13.6 ml). The mixture was allowed to reach -40°C and stirred for 3 h. Then aqueous NH_4Cl was slowly added and the mixture was extracted with EtOAc (3x). Organic phases were washed with brine and dried over Na_2SO_4. Volatiles were removed under reduced pressure and the residue was purified by flash chromatography on silica gel (Hex/EtOAc, 7:3) to afford the desired product as a viscous transparent oil (761 mg, 86%).

R_f=0.20 (Hexane/EtOAc 6:4); [*a*]D20=+14.8 (**77 b**, *c*=1 in $CHCl_3$); ^{1}H NMR (400 MHz, CD_2Cl_2) δ 7.46 – 7.27 (m, 10H), 5.42 – 5.34 (m, 1H, overlapping with solvent signal), 5.29 (d, 1H, J = 15.5 Hz), 4.31 – 4.25 (m, 1H), 4.23 – 4.14 (m, 3H), 4.11 (dd, 1H, J = 12.9, 2.0 Hz), 3.82 (dd, 1H, J = 12.8, 3.2 Hz), 3.61 (s, 3H), 3.26 (dd, 1H, J = 17.5, 2.9 Hz), 2.93 (dd, 1H, J = 17.5, 5.1 Hz); ^{13}C NMR (101 MHz, CD_2Cl_2) δ 170.9, 166.7, 165.6, 136.0, 129.5, 128.8, 128.4, 127.3, 104.3, 59.0, 55.7, 52.5, 52.1, 47.8, 47.6, 35.4; IR (neat): ν_{max} 2117, 1735, 1660, 1449, 1439, 1362, 1329, 1267, 1216, 1174; MS (ESI) *m/z* calcd for $[C_{22}H_{24}N_5O_4]^+$: 422.18 $[M+H]^+$; found: 422.3.

NHBoc-DKP5-CO_2Me (78 a); NHBoc-DKP7-CO_2Me (78 b)

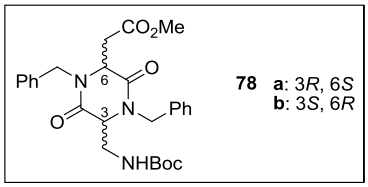

78 **a**: 3*R*, 6*S*
b: 3*S*, 6*R*

$C_{27}H_{33}N_3O_6$
MW: 495,57

To a solution of azide **77** (751 mg, 1.78 mmol, 1 eq.) in THF (48 ml), under a nitrogen atmosphere and at -20 ºC, 2-(*t*-butoxycarbonyloxyimino)-2-phenylacetonitrile (Boc-ON, 964 mg, 3.92 mmol, 2.2 eq.) and Me_3P (3.57 ml of 1 M solution in toluene, 3.56 mmol, 2 equiv) were added successively. After stirring for 6 h at r.t., the solution was diluted with CH_2Cl_2 and washed with H_2O (3x) and brine. The organic phase was dried over Na_2SO_4 and volatiles were removed under reduced pressure. The residue was purified by flash chromatography on silica gel (CH_2Cl_2/EtOAc, 8:2) to afford the desired product as a white foam (716 mg, 87%).

R_f=0.39 (CH_2Cl_2/EtOAc, 9:1); [*a*]D20=-103.6 (**78 b**, *c*=1.5 in $CHCl_3$); ^{1}H NMR (400 MHz, CD_2Cl_2) δ 7.48 – 7.24 (m, 10H), 5.56 (d, 1H, *J* = 15.3 Hz), 5.12 (d, 1H, *J* = 15.1 Hz), 4.98 (br s, 1H), 4.36 – 4.18 (m, 3H), 4.05 (s, 1H), 3.87 – 3.63 (m, 2H), 3.57 (s, 3H), 3.23 (dd, 1H, *J* = 17.3, 2.7 Hz), 2.92 (dd, 1H, *J* = 17.3, 4.9 Hz), 1.47 (s, 9H); ^{13}C NMR (101 MHz, CD_2Cl_2) δ 170.8, 166.7, 166.4, 156.5, 136.5, 136.3, 129.6, 129.4, 129.2, 128.5, 128.4, 80.3, 59.4, 56.0, 52.5, 48.0, 47.1, 41.5, 35.7, 28.8; IR (neat): ν_{max} 3323, 2978, 1738, 1714, 1658, 1497, 1450, 1366, 1330, 1252, 1202, 1168; MS (ESI) *m/z* calcd for $[C_{27}H_{34}N_3O_6]^+$: 496.24 $[M+H]^+$; found: 496.3.

NHBoc-DKP5-CO_2H (DKP5); NHBoc-DKP7-CO_2H (DKP7)

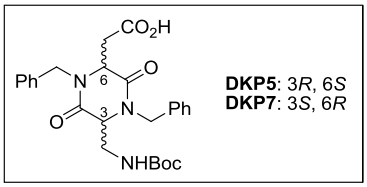

DKP5: 3*R*, 6*S*
DKP7: 3*S*, 6*R*

$C_{26}H_{31}N_3O_6$
MW: 481,54

Compound **78** (370 mg, 0.75 mmol, 1 eq.) was dissolved in THF (30 ml) and the mixture was cooled to 0 °C. A solution of LiOH·H_2O (78.3 mg, 1.86 mmol, 2.5 eq.) in H_2O (15 ml) was added dropwise. The resulting solution was let reacting for 1 h at 0 °C. Then, maintaining the temperature at 0 °C, the mixture was acidified with HCl 1M to pH = 1-2, and extracted with CH_2Cl_2 (4x). The collected organic phases were dried over Na_2SO_4 and volatiles removed under reduced pressure. Either **DKP5** or **DKP7** were afforded as a white foam (361 mg, 100%), which was used in subsequent steps without further purification.

2.4 - DKP8

(*R*)-*N*-(tert-butoxycarbonyl)glutamic acid γ-methyl ester (79)

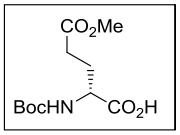

$C_{11}H_{19}NO_6$
MW: 261,27

To a flask containing MeOH (4,6 ml) and cooled to -14 °C was slowly added Acetyl chloride (1.3ml, 18.4 mmol, 2.7 eq) followed by D-glutamic acid (1g, 6.8 mmol, 1eq). Cooling bath was removed, and the solution was stirred for 30 min at r.t. and then poured into Et2O (330 mL). The precipitate was filtered off and washed well with Et_2O (50 mL) to give (*R*)- glutamic acid γ-methyl ester hydrochloride (1.25 g, 93%) as a white solid, which was used without further purification.

In a round bottom flask was solved 1 g (5.06 mmol, 1 eq) of (*R*)- glutamic acid γ-methyl ester hydrochloride in 20 mL of THF/water 1:1 solution. The reaction flask was lowered into an ice bath, and triethylamine (2.12 ml, 15.2 mmol, 3 eq.) and Boc_2O (1.21 g, 5.56 mmol, 1.1 eq) were added. After stirring at r.t. for 24 h. The reaction mixture was diluted with 60 mL of EtOAc and washed with aqueous $KHSO_4$ 1M until pH = 3 and brine. The organic phase was dried over Na_2SO_4, filtered and concentrated under reduced pressure. The product was then dried under high vacuum for a few hours affording 1.3 g (98%) of the pure expected product as viscous transparent oil.

(*R*)-1-((*S*)-2-(benzylamino)-3-methoxy-3-oxopropyl)5-methyl2-(tert-butoxycarbonylamino)pentanedioate (80)

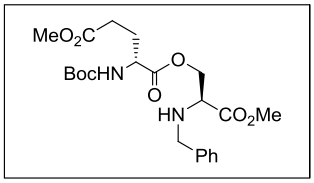

$C_{22}H_{32}N_2O_8$
MW: 452,50

(*R*)-*N*-(tert-butoxycarbonyl)glutamic acid γ-methyl ester **79** (1.0 g, 3.8 mmol, 1.3 eq.) was coupled with (*S*)-*N*-benzylserine methyl ester **53** (607 mg, 2.9 mmol, 1 eq.) according to general procedure **GP2**. The crude product was purified by flash chromatography on silica gel (Hexane/EtOAc, 7:3) to afford the desired product as a transparent oil (774 mg, 59%).

R_f=0.35 (Hexane/EtOAc 7:3); [*a*]D27=-4 (*c*=1.00 in $CHCl_3$); ^{1}H NMR (400 MHz, $CDCl_3$) δ 7.31 (m,5H), 5.12 (m, 1H), 4.47 (dd, *J* = 11.0, 4.9 Hz, 1H), 4.30 (dd, *J* = 11.0, 4.9 Hz, 1H), 3.90 (d, *J* = 13.1 Hz, 1H), 3.79 – 3.74 (m, 4H), 3.71 (d, *J* = 10.3 Hz, 1H), 3.68 (s, 3H), 3.56 (t, *J* = 4.9 Hz, 1H), 2.49 – 2.34 (m, 2H), 2.17 (dt, *J* = 13.3, 7.4 Hz, 1H), 1.95 (dt, *J* = 14.8, 7.9 Hz, 1H), 1.45 (s, 9H); ^{13}C NMR (101 MHz, CD_2Cl_2) δ 173.7, 173.1, 172.5, 155.8, 140.3, 129.0, 128.8, 127.7, 80.3, 66.2, 59.8, 53.5, 52.7, 52.4, 52.2, 30.5, 28.6, 28.2; IR (neat): ν_{max} 3368, 2976, 2953, 1739, 1716, 1509, 1454, 1367, 1249, 1201, 1166, 1051; MS (ESI) *m/z* calcd for $[C_{22}H_{33}N_2O_8]^+$: 453,22 $[M+H]^+$; found: 453.6.

HO-DKP8-CO_2Me (81)

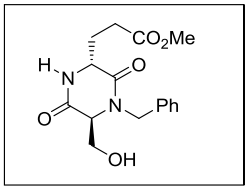

$C_{16}H_{20}N_2O_5$
MW: 320,34

Isopeptide **80** (440 mg, 0.97 mmol, 1 eq.) was deprotected according to general procedure **GP1**. The corresponding trifluoroacetate salt was dissolved in *i*PrOH (12 ml) and *i*Pr_2EtN (0.7 ml, 3.9 mmol, 4 eq.) was added at r.t. The reaction was stirred for 18 h at r.t., monitoring the formation of DKP by TLC (EtOAc). The solution was then concentrated under reduced pressure and the residue was purified by flash chromatography on silica gel (EtOAc) to afford the desired product as a white foam (289 mg, 93%).

R_f=0.12 (EtOAc); [*a*]D28=+29.5 (*c*=1.00 in $CHCl_3$); ^{1}H NMR (400 MHz, $CDCl_3$) δ 7.41 – 7.25 (m, 5H), 5.32 (d, *J* = 15.1 Hz, 1H), 4.43 (t, *J* = 4.4 Hz, 1H), 4.13 (d, *J* = 15.1 Hz, 1H), 3.95 (dd, *J* = 11.7, 2.4 Hz, 2H), 3.80 (t, *J* = 2.1 Hz, 1H), 3.67 (s, 3H), 2.53 – 2.26 (m, 3H), 2.23 – 2.10 (m, 1H); ^{13}C NMR (101 MHz, CD_3OD) δ 174.35, 169.95, 168.69, 136.75, 129.19, 128.77, 128.25, 128.17, 62.82, 61.46, 53.77, 51.51, 47.41, 29.05, 27.25; IR (neat): ν_{max} 3420, 2952, 1732, 1682, 1653, 1496, 1449, 1328, 1259, 1175, 1122, 1070; MS (ESI) *m/z* calcd for $[C_{16}H_{21}N_2O_5]^+$: 321,14 $[M+H]^+$; found: 321.4.

N_3-DKP8-CO_2Me (82)

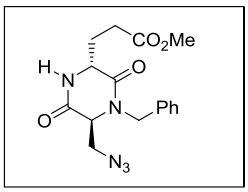

$C_{16}H_{19}N_5O_4$
MW: 345,35

To a solution of diketopiperazine **81** (104 mg, 0.32 mmol, 1 eq.) in CH_2Cl_2/toluene/DMF (3 ml / 2.5 ml / 1 ml), under nitrogen atmosphere and at -20 ºC, PPh_3 (128 mg, 0.49 mmol, 1.5 eq.) was added and the mixture was stirred until a solution was obtained. Hydrazoic acid (1.9 M in toluene, 0.51 ml, 0.97 mmol, 3 eq.) was added followed by dropwise addition of DIAD (0.096 ml, 0.49 mmol, 1.5 eq.) and the reaction was stirred at -20ºC overnight. The reaction mixture was loaded onto a silica gel column (EtOAc/Hexane 8:2) to afford the desired product as a white foam (72 mg, 65%).

R_f=0.52 (EtOAc); [*a*]D28=+57.9 (*c*=1.00 in $CHCl_3$); ^{1}H NMR (400 MHz, $CDCl_3$) δ 7.44 – 7.30 (m, 3H), 7.30 – 7.23 (m, 2H), 5.15 (d, *J* = 15.0 Hz, 1H), 4.43 (t, *J* = 4.7 Hz, 1H), 4.25 (d, *J* = 15.0 Hz, 1H), 3.94 (d, *J* = 2.7 Hz, 1H), 3.88 (dd, *J* = 12.8, 2.4 Hz, 1H), 3.71 (s, 3H), 3.64 (dd, *J* = 12.7, 3.4 Hz, 1H), 2.61 – 2.46 (m, 2H), 2.34 (dd, *J* = 9.1, 3.7 Hz, 2H); ^{13}C NMR (101 MHz, $CDCl_3$) δ 174.58, 167.72, 167.37, 136.06, 129.82, 128.97, 128.71, 78.02, 77.70, 59.99, 54.39, 52.71, 52.42, 48.51, 30.24, 27.73; IR (neat): ν_{max} 2116, 1733, 1686, 1654, 1437, 1327, 1289, 1258, 1174; MS (ESI) *m/z* calcd for $[C_{16}H_{20}N_5O_4]^+$: 346,15 $[M+H]^+$; found: 346.3.

NHBoc-DKP8-CO_2Me (84)

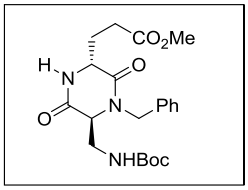

$C_{21}H_{29}N_3O_6$
MW: 419,47

Azide **82** (192 mg, 0.55 mmol, 1 eq.) was dissolved in 12 ml of THF. After addition of 59 mg of Pd/C 10% (0.05 mmol, 0.1 eq.), the mixture was hydrogenated under vigorous stirring over 3 h. Pd/C was then filtered off on a celite pad, which was thoroughly washed with THF. The filtrate was concentrated to dryness, obtaining amine **83** as a white solid, which was dissolved in THF. The mixture was cooled to 0°C before adding Boc anhydride (132 mg, 0.6 mmol, 1.1 eq.) and *i*Pr_2EtN (0.19 ml, 1.1 mmol, 2 eq.). The mixture was afterwards let to reach r.t. and stirred for 18 h. Volatiles were then removed under reduced pressure, and the residue was purified by flash chromatography on silica gel (EtOAc/Hexane, 1:1) to afford the desired product as a white foam (201 mg, 87%).

R_f=0.34 (EtOAc); [*a*]D20=-4.4 (*c*=1.00 in $CHCl_3$); ^{1}H NMR (400 MHz, $CDCl_3$) δ 7.44 (d, *J* = 9.9 Hz, 1H), 7.39 – 7.14 (m, 5H), 5.48 (d, *J* = 15.1 Hz, 1H), 5.29 (s, 1H), 4.25 (t, *J* = 4.4 Hz, 1H), 4.06 (d, *J* = 15.0 Hz, 1H), 3.80 (s, 1H), 3.77 – 3.57 (m, 4H), 3.57 – 3.43 (m, 1H), 2.60 – 2.42 (m, 2H), 2.38 – 2.19 (m, *J* = 6.1 Hz, 2H), 1.43 (s, 9H); ^{13}C NMR (101 MHz, $CDCl_3$) δ 174.56, 168.93, 166.59, 156.62, 136.35, 129.64, 128.92, 128.66, 80.80, 60.21, 53.98, 52.59, 47.78, 41.22, 29.96, 28.96, 28.28; IR (neat): ν_{max} 3298, 2978, 2952, 1689, 1523, 1448, 1393, 1366, 1329, 1253, 1169, 1059; MS (ESI) *m/z* calcd for $[C_{21}H_{30}N_3O_6]^+$: 420.21 $[M+H]^+$; found: 420.3.

NHBoc-DKP8-CO_2H (DKP8)

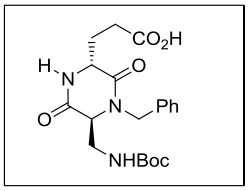

$C_{20}H_{27}N_3O_6$
MW: 405,44

Compound **84** (117 mg, 0.28 mmol, 1 eq.) was dissolved in THF (7 ml). The mixture was cooled to 0°C and a 2.7M solution of LiOOH in H_2O_2 (453 mg of LiOH in 7 ml of H_2O_2 35%) was added dropwise. The mixture was stirred for additional 30 min at 0°C, then warmed up to r.t. and stirred for 7h. After the addition of Na_2SO_3 (30.6 mg, 0.24 mmol, 6 eq.) the reaction mixture was diluted with 8 ml of THF/H_2O 1:1. $KHSO_4$ 1M was added to reach pH = 1-2, and the mixture was extracted with DCM (4x). The collected organic phases were dried over Na_2SO_4 and volatiles removed under reduced pressure, to afford crude **DKP8** as a yellowish solid. Crude product was dissolved in EtOAc and extracted with $NaHCO_3$ sat.; collected aqueous layers were acidified with $KHSO_4$ 1M to reach pH 1-2, and extracted with DCM (4x). Collected organic phases were dried over Na_2SO_4 and volatiles removed under reduced pressure, to afford DKP-8 as a white foam (100 mg, 90%) which was used without further purification.

3 - Synthesis of *cyclic*[DKP-RGD] compounds 102-107

Boc-Arg(Mtr)-Gly-OBn (112)

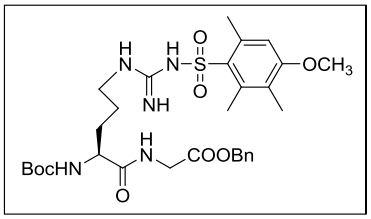

$C_{30}H_{43}N_5O_8S$
MW: 633,76

N-Boc glycine benzylester **111** (1.6 mg, 6 mmol, 1.2 eq.) was deprotected according to general procedure **GP1**. The corresponding trifluoroacetate salt was then coupled with Boc-Arg(Mtr)-OH (2.5g, 5.14 mmol, 1 eq.) according to general procedure **GP2**. The residue was purified by flash chromatography on silica gel (CH_2Cl_2/MeOH; 97:3) to afford the desired product as white foam (2.9 g, 90%).

R_f=0.21 (CH_2Cl_2/MeOH 97:3); [*a*]D20=-6.0 (*c*=0.5 in $CHCl_3$); ^{1}H NMR (400 MHz, CD_2Cl_2) δ 7.40 - 7.31 (m, 5H), 7.27 (br, 1H), 6.58 (s, 1H), 6.19 (s, 2H), 6.00 (br, 1H), 5.50 (d, 1H, *J* = 6.6), 5.15 (s, 2H), 4.24 (m, 1H), 4.09 (dd, 1H, *J* = 17.5, 6.4), 3.99 (dd, 1H, *J* = 17.9, 5.7), 3.84 (s, 3H), 3.25 (m, 2H), 2.67 (s, 3H), 2.60 (s, 3H), 2.14 (s, 3H), 1.84 (m, 2H), 1.61 (m, 2H), 1.43 (s, 9H); ^{13}C NMR (101 MHz, CD_2Cl_2) δ 172.9, 170.0, 158.5, 156.5, 156.0, 138.4, 136.5, 135.4, 133.4, 128.5, 128.4, 128.2, 124.8, 111.7, 80.1, 67.1, 55.4, 50.5, 41.2, 40.4, 30.0, 28.0, 25.1, 23.8, 18.1, 11.6; IR (neat): ν_{max} 3343, 2937, 1669, 1621, 1555, 1455, 1366, 1307, 1251, 1171, 1120; MS (ESI) *m/z* calcd for $[C_{30}H_{44}N_5O_8S]^+$: 634.29 $[M+H]^+$; found: 634.3.

N-Boc-DKP-Arg(Mtr)-Gly-OBn (113)

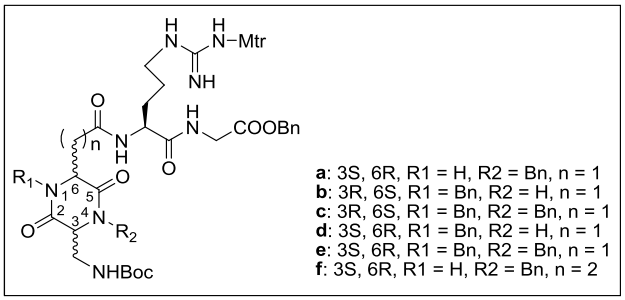

a) *N*-Boc-DKP3-Arg(Mtr)-Gly-OBn

Compound **112** (973.5 mg, 1.54 mmol, 1.2 eq.) was deprotected according to general procedure **GP1**. The corresponding trifluoroacetate salt was then coupled with **DKP3** (500 mg, 1.28 mmol, 1 eq.) according to general procedure **GP2**. The residue was purified by flash chromatography on silica gel (CH_2Cl_2/MeOH, 93:7) to afford the desired product as white foam (811 mg, 70%).

R_f=0.34 (CH_2Cl_2/MeOH 9:1); [*a*]D20=-1.8 (*c*=0.2 in $CHCl_3$); ^{1}H NMR (400 MHz, CD_2Cl_2) δ 7.85 (br, 1H), 7.69 (br, 1H), 7.53 – 7.28 (m, 11H), 6.56 (s, 1H), 6.35 – 6.03 (br, 3H), 5.64 (br, 1H), 5.35 (m, 1H), 5.12 (d, 2H, *J* = 8.3), 4.60 (m, 1H), 4.50 (m, 1H), 4.09 – 4.97 (m, 3H), 3.84 – 3.80 (m,

4H), 3.66 – 3.45 (m, 2H), 3.30 – 2.79 (m, 4H), 2.65 (s, 3H), 2.59 (s, 3H), 2.12 (s, 3H), 1.95 – 1.50 (m, 4H), 1.39 (s, 9H); ^{13}C NMR (101 MHz, CD_2Cl_2) δ 172.5, 170.6, 170.4, 169.9, 167.7, 166.4, 158.5, 156.6, 156.1, 138.4, 136.5, 135.8, 135.4, 133.3, 128.8, 128.5, 128.4, 128.2, 127.9, 124.8, 111.7, 79.8, 67.2, 67.1, 60.0, 55.4, 52.7, 51.5, 47.4, 41.2, 40.8, 39.7, 38.1, 31.6, 29.7, 28.0, 25.1, 23.8, 22.6, 18.1, 13.8, 11.7; IR (neat): ν_{max} 3335, 2937, 1651, 1557, 1455, 1307, 1251; MS (ESI) *m/z* calcd for $[C_{44}H_{59}N_8O_{11}S]^+$: 907.40 $[M+H]^+$; found: 907.6.

b) *N*-Boc-DKP4-Arg(Mtr)-Gly-OBn

Compound **112** (973.5 mg, 1.54 mmol, 1.2 eq.) was deprotected according to general procedure **GP1**. The corresponding trifluoroacetate salt was then coupled with **DKP4** (500 mg, 1.28 mmol, 1 eq.) according to general procedure **GP2**. The residue was purified by flash chromatography on silica gel (CH_2Cl_2/MeOH, 93:7) to afford the desired product as white foam (811 mg, 70%).

R_f=0.36 (CH_2Cl_2/MeOH 9:1); [*a*]D20=+21.7 (*c*=1 in $CHCl_3$); ^{1}H NMR (400 MHz, Acetone-d_6) δ 7.85 (t, 1H, *J* = 5.8 Hz), 7.61 (d, 1H, *J* = 7.7 Hz), 7.44 – 7.23 (m, 10H), 6.69 (s, 1H), 6.54 (br s, 2H), 6.19 (br s, 1H), 5.24 (d, 1H, *J* = 15.2 Hz), 5.17 (s, 2H), 4.56 – 4.47 (m, 1H, *J* = 8.1 Hz), 4.35 (t, 1H, *J* = 4.8 Hz), 4.17 (d, 1H, *J* = 15.2 Hz), 4.10 (t, 1H, *J* = 5.4 Hz,), 4.00 (d, 2H, *J* = 5.9 Hz), 3.85 (s, 3H), 3.77 – 3.68 (m, 1H), 3.62 – 3.50 (m, 1H), 3.34 – 3.11 (m, 2H), 2.92 (d, 2H, *J* = 5.4 Hz), 2.69 (s, 3H), 2.64 (s, 3H), 2.12 (s, 3H), 1.97 – 1.79 (m, 1H), 1.69 – 1.49 (m, 3H), 1.43 (s, 9H); ^{13}C NMR (101 MHz, Acetone-d_6) δ 138.9, 137.4, 136.9, 135.6, 129.3, 129.1, 128.7, 128.5, 128.2, 124.6, 112.3, 79.3, 66.8, 57.6, 55.9, 55.6, 53.1, 47.4, 42.9, 41.5, 40.8, 37.3, 28.4, 26.1, 24.0, 18.5, 11.9; IR (neat): ν_{max} 3331, 2936, 1681, 1555, 1454, 1392, 1366, 1333, 1306, 1249, 1172, 1120; MS (ESI) *m/z* calcd for $[C_{44}H_{59}N_8O_{11}S]^+$: 907.40 $[M+H]^+$; found: 907.5.

c) *N*-Boc-DKP5-Arg(Mtr)-Gly-OBn

Compound **112** (410 mg, 0.65 mmol, 1.2 eq.) was deprotected according to general procedure **GP1**. The corresponding trifluoroacetate salt was then coupled with **DKP5** (260 mg, 0.54 mmol, 1 eq.) according to general procedure **GP2**. The residue was purified by flash chromatography on silica gel (CH_2Cl_2/MeOH, 97:3) to afford the desired product as white foam (323 mg, 60% yield).

R_f=0.44 (CH_2Cl_2/MeOH, 9:1); [*a*]D20=-51.2 (*c*=0.6 in $CHCl_3$); ^{1}H NMR (400 MHz, CD_2Cl_2) δ 7.69 (br s, 1H), 7.41 (br s, 1H), 7.38 – 7.22 (m, 15H), 6.57 (s, 1H), 6.26 (br s, 2H), 5.33 (d, 1H, *J* = 15.6 Hz), 5.24 (d, 1H, *J* = 15.3 Hz), 5.12 (s, 2H), 4.77 (br s, 1H), 4.51 – 4.41 (m, 1H), 4.36 (br s, 1H), 4.28 (d, 1H, *J* = 15.5 Hz), 4.17 (d, 1H, *J* = 15.4 Hz), 4.08 – 3.95 (m, 3H), 3.84 (s, 3H), 3.76 – 3.65 (m, 1H), 3.64 – 3.53 (m, 1H), 3.34 – 3.13 (m, 2H), 3.07 (d, 1H, *J* = 13.3 Hz), 2.93 (dd, 1H, *J* = 15.8, 6.6 Hz), 2.66 (s, 3H), 2.58 (s, 3H), 2.11 (s, 3H), 2.01 – 1.88 (m, 1H), 1.75 – 1.48 (m, 3H), 1.42 (s, 9H); ^{13}C NMR (101 MHz, CD_2Cl_2) δ 172.9, 170.6, 170.3, 167.8, 166.7, 159.1, 157.1, 139.1, 137.1, 136.5, 136.1, 134.0, 129.6, 129.5, 129.2, 128.9, 128.9, 128.6, 128.5, 128.4, 125.4, 112.4, 67.7, 59.8, 56.3, 56.1, 47.6, 41.9, 41.6, 41.1, 37.2, 30.3, 29.5, 28.7, 26.2, 24.5, 18.8, 12.3; IR (neat): ν_{max} 3329, 2938, 2357, 2341, 1750, 1719, 1660, 1652, 1557, 1455, 1369, 1301, 1257, 1176, 1121; MS (ESI) *m/z* calcd for $[C_{51}H_{65}N_8O_{11}S]^+$: 997.45 $[M+H]^+$; found: 997.5.

d) *N*-Boc-DKP-6-Arg(Mtr)-Gly-OBn

Compound **112** (973 mg, 1.54 mmol, 1.2 eq.) was deprotected according to general procedure **GP1**. The corresponding trifluoroacetate salt was then coupled with **DKP6** (500 mg, 1.28 mmol, 1 eq.) according to general procedure **GP2**. The residue was purified by flash chromatography on silica gel (CH_2Cl_2/MeOH, 93:7) to afford the desired product as white foam (811 mg, 70%).

R_f=0.38 (CH_2Cl_2/MeOH 9:1); [*a*]D20=+23.4 (*c*=1 in $CHCl_3$); ^{1}H NMR (400 MHz, Acetone-d_6) δ 7.93 (t, 1H, *J* = 5.8 Hz), 7.73 (d, 1H, *J* = 8.1 Hz,), 7.45 – 7.24 (m, 10H), 6.69 (s, 1H), 6.59 (br s, 2H), 6.24 (br s, 1H), 5.34 (d, 1H, *J* = 15.2 Hz,), 5.16 (s, 2H), 4.68 – 4.58 (m, 1H), 4.34 (t, 1H, *J* = 4.6 Hz), 4.17 (d, 1H, *J* = 15.1 Hz), 4.11 – 3.93 (m, 3H), 3.85 (s, 3H), 3.75 – 3.65 (m, 1H), 3.65 – 3.54 (m, 1H), 3.32 – 3.11 (m, 2H), 3.07 (dd, 1H, *J* = 15.2, 5.8 Hz), 2.97 – 2.85 (m, 1H, overlapping with water signal), 2.70 (s, 3H), 2.65 (s, 3H), 2.11 (s, 3H), 1.92 – 1.80 (m, 1H), 1.67 – 1.47 (m, 3H), 1.42 (s, 9H); ^{13}C NMR (101 MHz, Acetone-d_6) δ 172.5, 170.2, 169.7, 168.7, 167.2, 158.7, 157.4, 157.3, 138.9, 137.1, 136.9, 136.8, 135.6, 129.4, 129.1, 128.8, 128.6, 128.2, 124.6, 112.3, 79.3, 66.9, 57.3, 56.1, 55.7, 52.7, 47.0, 43.1, 41.5, 40.8, 37.1, 30.5, 28.4, 25.7, 24.1, 18.5, 11.9; ; IR (neat): ν_{max} 3329, 2932, 1687, 1560, 1451, 1387, 1361, 1338, 1310, 1243, 1177, 1121; MS (ESI) *m/z* calcd for $[C_{44}H_{59}N_8O_{11}S]^+$: 907.40 $[M+H]^+$; found: 907.5.

e) *N*-Boc-DKP7-Arg(Mtr)-Gly-OBn

Compound **112** (327 mg, 0.52 mmol, 1.1 eq.) was deprotected according to general procedure **GP1**. The corresponding trifluoroacetate salt was then coupled with DKP-7 (227 mg, 0.47 mmol, 1 eq.) according to general procedure **GP2**. The residue was purified by flash chromatography on silica gel (CH_2Cl_2/MeOH, 95:5) to afford the desired product as white foam (286 mg, 61%).

R_f=0.45 (CH_2Cl_2/MeOH 9:1); [*a*]D20=-55.6 (*c*=0.7 in $CHCl_3$); ^{1}H NMR (400 MHz, Acetone-d_6) δ 7.85 (t, 1H, *J* = 5.7 Hz), 7.55 (d, 1H, *J* = 8.2 Hz), 7.51 – 7.22 (m, 15H), 6.68 (s, 1H), 6.54 (br s, 2H), 6.26 (br s, 1H), 5.92 (br s, 1H), 5.50 (d, 1H, *J* = 15.6 Hz), 5.29 (d, 1H, *J* = 15.3 Hz), 5.16 (s, 2H), 4.68 – 4.56 (m, 1H), 4.32 (d, 2H, *J* = 15.2 Hz), 4.26 – 4.20 (m, 1H), 4.06 (t, 1H, *J* = 3.3 Hz), 4.03 – 3.92 (m, 2H), 3.84 (s, 3H), 3.79 – 3.65 (m, 2H), 3.40 – 3.22 (m, 1H), 3.22 – 2.99 (m, 3H), 2.69 (s, 3H), 2.64 (s, 3H), 2.10 (s, 3H), 1.96 – 1.79 (m, 1H), 1.68 – 1.48 (m, 3H), 1.43 (s, 9H); ^{13}C NMR (101 MHz, Acetone-d_6) δ 171.7, 169.4, 169.1, 166.8, 166.4, 158.0, 156.7, 155.9, 138.3, 136.3, 128.7, 128.5, 128.3, 128.1, 127.6, 127.3, 123.9, 111.6, 78.5, 66.1, 58.9, 55.5, 54.9, 51.8, 46.5, 46.2, 40.8, 40.5, 39.9, 36.1, 27.7, 25.1, 23.4, 17.8, 11.2; IR (neat): ν_{max} 3326, 2936, 2361, 2343, 1748, 1714, 1659, 1650, 1555, 1453, 1366, 1306, 1253, 1172, 1120; MS (ESI) *m/z* calcd for $[C_{51}H_{65}N_8O_{11}S]^+$: 997.45 $[M+H]^+$; found: 997.6.

f) *N*-Boc-DKP8-Arg(Mtr)-Gly-OBn

Compound **112** (200 mg, 0.31 mmol, 1.1 eq.) was deprotected according to general procedure **GP1**. The corresponding trifluoroacetate salt was then coupled with **DKP-8** (116 mg, 0.29 mmol, 1 eq.) according to general procedure **GP2**. The residue was purified by flash chromatography on silica gel (CH_2Cl_2/MeOH, 95:5) to afford the desired product as white foam (163 mg, 61%).

R_f=0.4 (CH_2Cl_2/MeOH 9:1); [*a*]D29=-2.0 (*c*=0.2 in $CHCl_3$); ^{1}H NMR (400 MHz, CD_3OD) δ 7.42 – 7.26 (m, 10H), 6.67 (s, 1H), 5.39 (d, 1H, *J* = 15.3 Hz), 5.16 (s, 2H), 4.43 – 4.36 (m, 1H), 4.30 (t, 1H, *J* = 3.7 Hz), 4.09 – 4.00 (m, 2H), 3.93 (d, 1H, *J* = 17.6 Hz), 3.84 (s, 3H), 3.82 – 3.73 (m, 2H), 3.45 (d, 1H, *J* = 13.2 Hz), 3.25 – 3.09 (m, 2H), 2.69 (s, 3H), 2.63 (s, 3H), 2.46 – 2.22 (m, 3H), 2.22 – 2.16 (m, 1H), 2.14 (s, 3H), 1.87 – 1.76 (m, 1H), 1.68 – 1.52 (m, 3H), 1.44 (s, 9H); ^{13}C NMR (101 MHz, CD_2Cl_2) δ 173.7, 173.1, 170.3, 168.8, 167.0, 158.8, 157.0, 156.5, 138.8, 136.8, 136.5, 135.8, 133.9, 129.2, 128.9, 128.7, 128.5, 128.3, 125.1, 112.1, 80.0, 67.4, 60.6, 55.8, 53.9, 53.0, 48.0, 41.6, 41.1, 40.8, 31.6, 30.3, 28.4, 28.0, 25.6, 24.2, 18.5, 12.1; IR (neat): ν_{max} 3328, 3066, 3007, 2974, 2937, 1747, 1660, 1550, 1455, 1392, 1366, 1306, 1254, 1173, 1120; MS (ESI) *m/z* calcd for $[C_{45}H_{61}N_8O_{11}S]^+$: 921.42 $[M+H]^+$; found: 921.7.

Cbz-Asp(O*t*Bu)-DKP-Arg(Mtr)-Gly-OBn (114)

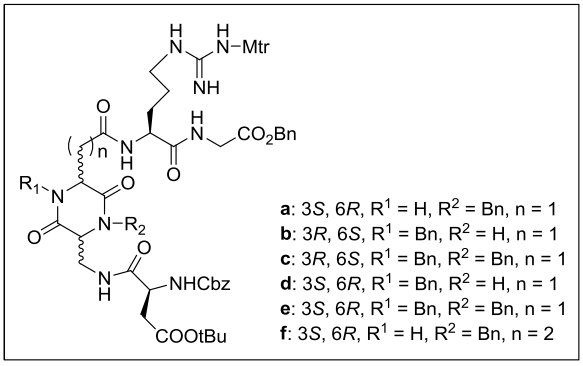

a) Cbz-Asp(O*t*Bu)-DKP3-Arg(Mtr)-Gly-OBn

Compound **113 a** (290 mg, 0.32 mmol, 1 eq.) was deprotected according to general procedure **GP1**. The corresponding trifluoroacetate salt was then coupled with Cbz-L-Asp(O*t*Bu)-OH (155 mg, 0.48 mmol, 1.5 eq.) according to general procedure **GP2**. The residue was purified by flash chromatography on silica gel (CH_2Cl_2/MeOH, 9:1) to afford the desired product as white foam (320 mg, 90%).

R_f=0.25 (CH_2Cl_2/MeOH 9:1); [*a*]D20=-7.0 (*c*=1 in $CHCl_3$); ^{1}H NMR (400 MHz, CD_2Cl_2) δ 7.85 – 7.55 (m, 3H), 7.41 – 7.16 (m, 16H), 6.55 (s, 1H), 6.36 – 6.00 (br, 3H), 5.24 (d, 1H, *J* = 13.9 Hz), 5.17 – 5.03 (m, 3H), 4.92 (d, 1H, *J* = 12.3 Hz), 4.70 – 4.39 (m, 3H), 4.17 (d, 1H, *J* = 14.7 Hz), 4.01 – 3.71 (m, 7H), 3.68 – 3.53 (m, 1H), 3.31 – 2.48 (m, 12H), 2.11 (s, 3H), 2.02 – 1.48 (m, 4H), 1.42 (s, 9H); ^{13}C NMR (101 MHz, CD_2Cl_2) δ 172.5, 172.0, 171.4, 170.6, 170.4, 170.0, 167.5, 166.6, 165.9, 165.7, 158.5, 156.6, 138.4, 136.5, 136.2, 135.8, 135.4, 133.5, 128.8, 128.5, 128.3, 127.9, 127.8, 124.8, 111.7, 81.6, 67.1, 59.5, 55.4, 52.4, 51.7, 51.2, 47.5, 41.2, 40.5, 39.6, 38.6, 37.3, 31.6, 29.7, 27.7, 25.1, 23.8, 22.6, 18.1, 13.8, 11.7; IR (neat): ν_{max} 3327, 2938, 1730, 1651, 1549, 1455, 1367, 1306, 1254, 1158, 1120; MS (ESI) *m/z* calcd for $[C_{55}H_{70}N_9O_{14}S]^+$: 1112.48 $[M+H]^+$; found: 1112.6.

b) Cbz-Asp(O*t*Bu)-DKP4-Arg(Mtr)-Gly-OBn

Compound **113 b** (290 mg, 0.32 mmol, 1 eq.) was deprotected according to general procedure **GP1**. The corresponding trifluoroacetate salt was then coupled with Cbz-L-Asp(O*t*Bu)-OH (124 mg, 0.38 mmol, 1.2 eq.) according to general procedure **GP2**. The residue was purified by flash chromatography on silica gel (CH_2Cl_2/MeOH, 9:1) to afford the desired product as white foam (327 mg, 92%).

R_f=0.45 (CH_2Cl_2/MeOH 9:1); [*a*]D20=+22.1 (*c*=1 in $CHCl_3$); ^{1}H NMR (400 MHz, Acetone-d_6) δ 7.84 (t, 1H, *J* = 5.8 Hz), 7.77 (t, 1H, *J* = 5.9 Hz), 7.60 (d, 1H, *J* = 8.0 Hz), 7.46 – 7.21 (m, 16H), 6.77 (d, 1H, *J* = 8.2 Hz), 6.69 (s, 1H), 6.54 (br s, 2H), 6.43 – 6.17 (br, 1H), 5.23 (d, 1H, *J* = 15.2 Hz), 5.19 – 5.10 (m, 3H), 5.06 (d, 1H, *J* = 12.5 Hz), 4.58 (td, 1H, *J* = 7.8, 5.6 Hz), 4.53 – 4.46 (m, 1H), 4.43 (t, 1H, *J* = 5.3 Hz), 4.18 (d, 1H, *J* = 15.2 Hz), 4.12 (t, 1H, *J* = 5.3 Hz), 4.06 – 3.93 (m, 2H), 3.93 – 3.81 (m, 4H), 3.70 – 3.59 (m, 1H), 3.31 – 3.11 (m, 2H), 2.97 – 2.89 (m, 2H), 2.87 – 2.77 (m, 1H, overlapping with water signal), 2.76 – 2.58 (m, 7H), 2.12 (s, 3H), 1.97 – 1.77 (m, 1H), 1.70 – 1.48 (m, 3H), 1.42 (s, 9H).; ^{13}C NMR (101 MHz, Acetone-d_6) δ 172.3, 172.0, 170.2, 169.8, 169.4, 168.5, 166.4, 158.4, 157.1, 156.5, 138.7, 137.4, 137.1, 136.6, 135.4, 129.1, 128.8, 128.7, 128.4, 128.2, 127.9, 124.3, 112.0, 80.9, 66.7, 66.6, 57.4, 55.4, 54.7, 47.1, 41.7, 41.3, 40.6, 37.9, 36.9, 29.9, 29.7, 29.6, 29.4, 29.2, 29.0, 28.8, 27.7, 25.8, 23.8, 18.2, 11.6; IR (neat): ν_{max} 3317, 2937, 1726, 1667, 1548, 1454, 1367, 1306, 1254, 1190, 1156, 1120; MS (ESI) *m/z* calcd for $[C_{55}H_{70}N_9O_{14}S]^+$: 1112.48 $[M+H]^+$; found: 1112.5.

c) Cbz-Asp(O*t*Bu)-DKP5-Arg(Mtr)-Gly-OBn

Compound **113 c** (147 mg, 0.15 mmol, 1 eq.) was deprotected according to general procedure **GP1**. The corresponding trifluoroacetate salt was then coupled with Cbz-L-Asp(O*t*Bu)-OH (58 mg, 0.18 mmol, 1.2 eq.) according to general procedure **GP2**. The residue was purified by flash chromatography on silica gel (CH_2Cl_2/MeOH, 95:5) to afford the desired product as white foam (172 mg, 96%).

R_f=0.43 (CH_2Cl_2/MeOH 95:5); [*a*]D20=-23.6 (*c*=0.7 in $CHCl_3$); ^{1}H NMR (400 MHz, Acetone-d_6) δ 7.89 (t, 1H, *J* = 5.9 Hz), 7.51 – 7.19 (m, 20H), 6.75 – 6.65 (m, 2H), 6.55 (br s, 2H), 6.33 (br s, 1H), 5.39 (d, 1H, *J* = 15.4 Hz), 5.16 (s, 2H), 5.10 (d, 1H, *J* = 13.8 Hz), 5.04 (d, 1H, *J* = 15.5 Hz), 4.59 – 4.49 (m, 3H), 4.46 (d, 1H, *J* = 15.6 Hz), 4.28 (d, 1H, *J* = 15.5 Hz), 4.20 – 4.15 (m, 1H), 4.08 – 3.91 (m, 3H), 3.84 (s, 3H), 3.81 – 3.73 (m, 1H), 3.39 – 3.24 (m, 1H), 3.22 – 3.11 (m, 1H), 3.08 (dd, 1H, *J* = 15.9, 3.5 Hz), 2.92 (dd, 1H, *J* = 15.9, 6.4 Hz), 2.87 – 2.77 (m, 4H), 2.73 – 2.60 (m, 4H), 2.08 (s, 3H, overlapping with solvent signal), 1.95 – 1.81 (m, 1H), 1.69 – 1.50 (m, 3H), 1.42 (s, 9H); ^{13}C NMR (101 MHz, Acetone-d_6) δ 171.7, 171.2, 169.8, 169.4, 166.1, 162.8, 158.0, 156.7, 147.4, 136.9, 136.5, 128.7, 128.6, 128.3, 128.1, 128.0, 127.8, 127.6, 127.3, 111.6, 80.4, 66.3, 66.1, 58.5, 55.9, 54.9, 52.2, 52.0, 46.8, 46.6, 40.9, 40.1, 39.3, 37.2, 35.9, 27.3, 25.6, 23.4, 17.8, 11.2; IR (neat): ν_{max} 3324, 2938, 1731, 1660, 1654, 1546, 1451, 1368, 1310, 1253, 1160, 1122; MS (ESI) *m/z* calcd for $[C_{62}H_{76}N_9O_{14}S]^+$: 1202.52 $[M+H]^+$; found: 1202.5.

d) Cbz-Asp(O*t*Bu)-DKP6-Arg(Mtr)-Gly-OBn

Compound **113 d** (400 mg, 0.44 mmol, 1 eq.) was deprotected according to general procedure **GP1**. The corresponding trifluoroacetate salt was then coupled with Cbz-L-Asp(O*t*Bu)-OH (171 mg, 0.52 mmol, 1.2 eq.) according to general procedure **GP2**. The residue was purified by flash chromatography on silica gel (CH_2Cl_2/MeOH, 9:1) to afford the desired product as white foam (451 mg, 92%).

R_f=0.46 (CH_2Cl_2/MeOH 9:1); [*a*]D20=+25.1 (*c*=1 in $CHCl_3$); ^{1}H NMR (400 MHz, Acetone-d_6) δ 7.92 (br s, 1H), 7.82 (br s, 1H), 7.70 (br s, 1H), 7.43 – 7.22 (m, 15H), 6.81 (d, 1H, *J* = 8.1 Hz), 6.68 (s, 1H), 6.58 (br s, 2H), 5.31 (d, 1H, *J* = 15.1 Hz), 5.19 – 5.10 (m, 3H), 5.05 (d, 1H, *J* = 12.6 Hz), 4.60 (m, 2H), 4.41 (t, 1H, *J* = 5.1 Hz), 4.17 (d, 1H, *J* = 15.1 Hz), 4.10 – 3.91 (m, 3H), 3.89 – 3.80 (m, 4H), 3.80 – 3.68 (m, 1H), 3.31 – 3.11 (m, 2H), 3.04 (dd, 1H, *J* = 15.3, 5.7 Hz), 2.98 – 2.86 (m, 1H, overlapping with water signal), 2.82 (dd, 1H, *J* = 16.2, 5.4 Hz), 2.70 (s, 3H), 2.65 (s, 3H), 2.11 (s, 3H), 1.92 – 1.79 (m, 1H), 1.70 – 1.46 (m, 3H), 1.41 (s, 9H); ^{13}C NMR (101 MHz, Acetone-d_6) δ 172.7, 172.5, 170.4, 170.2, 169.7, 168.7, 167.0, 158.7, 157.4, 156.9, 138.9, 137.7, 137.1, 136.9, 136.8, 135.6, 129.4, 129.3, 129.1, 129.0, 128.8, 128.7, 128.5, 128.2, 124.6, 112.3, 81.1, 66.9, 57.3, 55.7, 55.3, 52.8, 52.7, 47.1, 44.0, 43.7, 41.9, 41.5, 40.8, 38.6, 38.3, 37.0, 30.5, 28.0, 25.8, 24.1, 18.5, 11.9; IR (neat): ν_{max} 3312, 2943, 1729, 1672, 1553, 1453, 1369, 1309, 1259, 1186, 1161, 1124; MS (ESI) *m/z* calcd for $[C_{55}H_{70}N_9O_{14}S]^+$: 1112.48 $[M+H]^+$; found: 1112.5.

e) Cbz-Asp(O*t*Bu)-DKP7-Arg(Mtr)-Gly-OBn

Compound **113 e** (210 mg, 0.21 mmol, 1 eq.) was deprotected according to general procedure **GP1**. The corresponding trifluoroacetate salt was then coupled with Cbz-L-Asp(O*t*Bu)-OH (82 mg, 0.25 mmol, 1.2 eq.) according to general procedure **GP2**. The residue was purified by flash chromatography on silica gel (CH_2Cl_2/MeOH, 97:3) to afford the desired product as white foam (226 mg, 90%).

R_f=0.45 (CH_2Cl_2/MeOH 95:5); [*a*]D20=-28.9 (*c*=0.8 in $CHCl_3$); ^{1}H NMR (400 MHz, Acetone-d_6) δ 7.85 (t, 1H, *J* = 5.8 Hz), 7.53 (d, 1H, *J* = 8.1 Hz), 7.50 – 7.21 (m, 21H), 6.71 (d, 1H, *J* = 8.3 Hz), 6.67 (s, 1H), 6.53 (br s, 2H), 6.24 (br s, 1H), 5.44 (d, 1H, *J* = 15.5 Hz), 5.24 (d, 1H, *J* = 15.2 Hz), 5.18 – 5.10 (m, 3H), 5.07 (d, 1H, *J* = 12.6 Hz), 4.64 – 4.50 (m, 2H), 4.39 – 4.30 (m, 2H), 4.27 (s, 1H), 4.14 (t, 1H, *J* = 3.5 Hz), 4.06 – 3.94 (m, 2H), 3.94 – 3.77 (m, 5H), 3.38 – 3.22 (m, 1H), 3.20 – 3.01 (m, 3H), 2.84 – 2.78 (m, 1H, overlapping with water signal), 2.69 (s, 3H), 2.66 – 2.56 (m, 4H), 2.09 (s, 3H), 1.94 – 1.78 (m, 1H), 1.66 – 1.45 (m, 3H), 1.41 (s, 9H); ^{13}C NMR (101 MHz, Acetone-d_6) δ 172.1, 171.5, 170.0, 169.8, 169.5, 167.5, 166.7, 158.4, 157.1, 138.6, 136.7, 136.6, 129.2, 128.9, 128.8, 128.7, 128.6, 128.5, 128.4, 128.2, 127.9, 127.6, 124.3, 111.9, 80.7, 66.6, 66.5, 58.7, 55.9, 55.4, 52.3, 52.2, 47.0, 46.6, 41.2, 40.3, 39.5, 37.7, 36.4, 30.2, 27.7, 25.6, 23.8, 18.2, 11.6; IR (neat): ν_{max} 3322, 2936, 1729, 1659, 1651, 1549, 1454, 1367, 1306, 1256, 1161, 1120; MS (ESI) *m/z* calcd for $[C_{62}H_{76}N_9O_{14}S]^+$: 1202.52 $[M+H]^+$; found: 1202.5.

f) Cbz-Asp(O*t*Bu)-DKP8-Arg(Mtr)-Gly-OBn

Compound **113 f** (143 mg, 0.16 mmol, 1 eq.) was deprotected according to general procedure **GP1**. The corresponding trifluoroacetate salt was then coupled with Cbz-L-Asp(O*t*Bu)-OH (62 mg, 0.19 mmol, 1.2 eq.) according to general procedure **GP2**. The residue was purified by flash chromatography on silica gel (CH_2Cl_2/EtOH, 95:5) to afford the desired product as white foam (155 mg, 86%).

R_f=0.5 (CH_2Cl_2/MeOH 9:1); [*a*]D20=-3.0 (*c*=0.35 in $CHCl_3$); ^{1}H NMR (400 MHz, Acetone-d_6) δ 8.02 (s, 1H), 7.97 – 7.89 (m, 2H), 7.58 (d, 1H, *J* = 7.9 Hz), 7.39 – 7.21 (m, 15H), 6.87 (d, 1H, *J* = 8.6 Hz), 6.66 (s, 1H), 6.54 (br s, 2H), 5.31 (d, 1H, *J* = 15.2 Hz), 5.16 – 5.09 (m, 3H), 5.01 (d, 1H, *J* = 12.5 Hz), 4.61 – 4.52 (m, 2H), 4.41 (br s, 1H), 4.14 (d, 1H, *J* = 15.2 Hz), 4.04 (dd, 1H, *J* = 17.6, 6.0 Hz), 3.95 (dd, 1H, *J* = 17.6, 5.8 Hz), 3.90 – 3.86 (m, 1H), 3.85 – 3.76 (m, 4H), 3.76 – 3.66 (m, 1H), 3.28 – 3.10 (m, 2H), 2.81 (dd, 1H, *J* = 16.3, 5.3 Hz), 2.70 – 2.59 (m, 7H), 2.56 – 2.40 (m, 2H), 2.36 – 2.24 (m, 1H), 2.23 – 2.11 (m, 1H), 2.08 (s, 3H), 1.89 – 1.78 (m, 1H), 1.70 – 1.49 (m, 3H), 1.38 (s, 9H); ^{13}C NMR (101 MHz, Acetone-d_6) δ 174.0, 173.2, 172.7, 170.7, 170.5, 168.5, 167.6, 158.9, 157.6, 157.2, 139.1, 137.8, 137.1, 137.0, 135.8, 129.6, 129.3, 129.2, 129.0, 128.8, 128.7, 128.4, 124.9, 112.5, 81.3, 67.3, 67.2, 60.6, 55.9, 54.2, 53.3, 53.0, 48.0, 41.8, 41.1, 40.4, 38.3, 31.9, 30.5, 28.2, 28.0, 26.3, 24.3, 18.7, 12.1; IR (neat): ν_{max} 3309, 2932, 2359, 1731, 1652, 1541, 1455, 1258, 1120; MS (ESI) *m/z* calcd for $[C_{56}H_{72}N_9O_{14}S]^+$: 1126.49 $[M+H]^+$; found: 1126.7.

H-Asp(O*t*Bu)-DKP-Arg(Mtr)-Gly-OH (115)

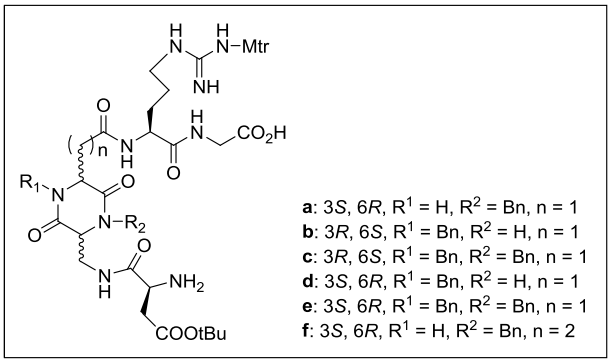

a) H-Asp(O*t*Bu)-DKP3-Arg(Mtr)-Gly-OH

Compound **114 a** (307 mg, 0.28 mmol, 1 eq.) was treated with Pd/C 10% (29.3 mg, 0.03 mmol, 0.1 eq.) in the conditions described in general procedure **GP3**. The crude product was obtained as white solid (248 mg, 100%) that was used without further purification.

b) H-Asp(O*t*Bu)-DKP4-Arg(Mtr)-Gly-OH

Compound **114 b** (307 mg, 0.28 mmol, 1 eq.) was treated with Pd/C 10% (29.3 mg, 0.03 mmol, 0.1 eq.) in the conditions described in general procedure **GP3**. The crude product was obtained as white solid (248 mg, 100%) that was used without further purification.

c) H-Asp(O*t*Bu)-DKP5-Arg(Mtr)-Gly-OH

Compound **114 c** (170 mg, 0.14 mmol, 1 eq.) was treated with Pd/C 10% (14.9 mg, 0.014 mmol, 0.1 eq.) in the conditions described in general procedure **GP3**. The crude product was obtained as white solid (137 mg, 100%) that was used without further purification.

d) H-Asp(O*t*Bu)-DKP6-Arg(Mtr)-Gly-OH

Compound **114 d** (400 mg, 0.36 mmol, 1 eq.) was treated with Pd/C 10% (38.1 mg, 0.04 mmol, 0.1 eq.) in the conditions described in general procedure **GP3**. The crude product was obtained as white solid (322 mg, 100%) that was used without further purification.

e) H-Asp(O*t*Bu)-DKP7-Arg(Mtr)-Gly-OH

Compound **114 e** (218 mg, 0.18 mmol, 1 eq.) was treated with Pd/C 10% (19.3 mg, 0.018 mmol, 0.1 eq.) in the conditions described in general procedure **GP3**. The crude product was obtained as white solid (176 mg, 100%) that was used without further purification.

f) H-Asp(O*t*Bu)-DKP8-Arg(Mtr)-Gly-OH

Compound **114 f** (148 mg, 0.13 mmol, 1 eq.) was treated with Pd/C 10% (13.8 mg, 0.013 mmol, 0.1 eq.) in the conditions described in general procedure **GP3**. The crude product was obtained as white solid (124 mg, 100%) that was used without further purification.

***Cyclo*[Arg(Mtr)-Gly-Asp(O*t*Bu)-DKP] (116)**

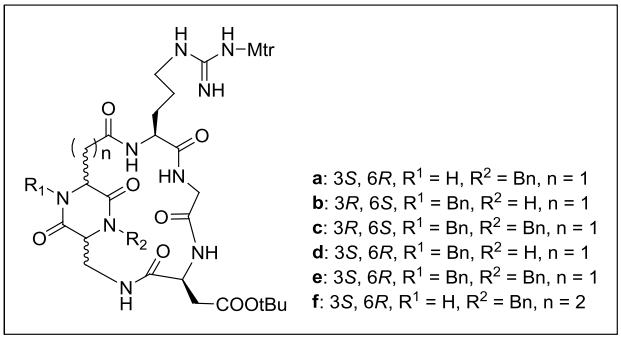

a: 3*S*, 6*R*, R^1 = H, R^2 = Bn, n = 1
b: 3*R*, 6*S*, R^1 = Bn, R^2 = H, n = 1
c: 3*R*, 6*S*, R^1 = Bn, R^2 = Bn, n = 1
d: 3*S*, 6*R*, R^1 = Bn, R^2 = H, n = 1
e: 3*S*, 6*R*, R^1 = Bn, R^2 = Bn, n = 1
f: 3*S*, 6*R*, R^1 = H, R^2 = Bn, n = 2

a) *Cyclo*[Arg(Mtr)-Gly-Asp(O*t*Bu)-DKP3]

To a solution of **115 a** (80 mg, 0.09 mmol, 1 eq.) in DMF (64 ml), under nitrogen atmosphere and at 0 ºC, DIPEA (92 µl, 0.54 mmol, 6 eq.) and DPPA (58 µl, 0.27 mmol, 3 eq.) were added successively. After stirring the reaction mixture at 0 ºC for 5 h, it was allowed to reach r.t., and stirred for 2 days. DMF was then removed under reduced pressure and the residue was purified by flash chromatography on silica gel (CH_2Cl_2/MeOH, 95:5) to afford the desired product as white foam (58.7 mg, 75%).

R_f=0.34 (CH_2Cl_2/MeOH, 9:1); ^{1}H NMR (400 MHz, CD_3OD) δ 7.33 – 7.14 (m, 5H), 6.57 (s, 1H), 5.06 (d, 1H, *J* = 15.1 Hz), 4.87 – 4.79 (m, 1H), 4.49 – 4.40 (m, 1H), 4.33 (d, 1H, *J* = 17.2 Hz), 3.92 – 3.80 (m, 3H), 3.74 (s, 3H), 3.69 (dd, 1H, *J* = 10.2, 4.6 Hz), 3.45 – 3.34 (m, 2H), 3.10 (t, 2H, *J* = 6.6 Hz), 2.78 (dd, 1H, *J* = 16.4, 8.5 Hz), 2.64 (dd, 1H, *J* = 13.4, 10.1 Hz), 2.58 (s, 3H), 2.51 (s, 3H), 2.46 – 2.33 (m, 2H), 2.03 (s, 3H), 2.01 – 1.76 (m, 2H), 1.58 – 1.37 (m, 2H), 1.32 (s, 9H); ^{13}C NMR

(101 MHz, CD_3OD) δ 173.8, 173.3, 172.3, 171.7, 171.2, 159.8, 158.2, 139.5, 137.9, 136.9, 134.9, 130.1, 129.1, 125.7, 114.2, 112.9, 82.4, 60.3, 56.0, 53.2, 50.4, 48.4, 43.6, 39.6, 38.5, 37.1, 28.3, 27.5, 27.0, 24.2, 18.8, 12.1**;** MS (ESI) *m/z* calcd for $[C_{40}H_{56}N_9O_{11}S]^+$: 870.38 $[M+H]^+$; found: 870.8.

b) *Cyclo*[Arg(Mtr)-Gly-Asp(O*t*Bu)-DKP4]

Compound **115 b** (224 mg, 0.25 mmol, 1 eq.) was cyclized in the conditions described in general procedure **GP4**, in presence of HATU (380.2 mg, 1 mmol, 4 eq.), HOAt (136.1 mg, 1 mmol, 4 eq.) and DIPEA (0.26 ml, 1.5 mmol, 6 eq). The crude product was purified by flash chromatography on silica gel (CH_2Cl_2/MeOH, 95:5) to afford yellowish solid that was further purified by Biotage (gradient: 95% H_2O / 5% acetonitrile to 5% H_2O / 95% acetonitrile), to obtain the product as white foam (133 mg, 61%).

R_f=0.45 (CH_2Cl_2/MeOH 9:1); ^{1}H NMR (400 MHz, CD_3OD) δ 7.41 – 7.21 (m, 5H), 6.68 (s, 1H), 5.36 (br s, 1H), 4.53 – 4.41 (m, 1H), 4.39 – 4.28 (m, 1H), 4.24 – 3.89 (m, 3H), 3.85 (s, 1H), 3.78 (d, 1H, *J* = 10.6 Hz,), 3.68 – 3.48 (m, 1H), 3.31 – 3.26 (m, 1H) 3.20 (t, 2H, *J* = 5.7 Hz), 2.98 – 2.86 (m, 1H), 2.83 – 2.72 (m, 2H), 2.72 – 2.56 (m, 7H), 2.14 (s, 3H), 1.89 – 1.75 (m, 1H), 1.74 – 1.52 (m, 3H), 1.49 (s, 9H); ^{13}C NMR (101 MHz, CD_3OD) δ 172.3, 172.1, 169.9, 169.4, 168.4, 166.9, 158.5, 138.1, 136.5, 128.6, 127.5, 124.3, 111.4, 81.3, 56.8, 54.6, 53.2, 41.9, 40.7, 40.1, 35.8, 30.7, 27.8, 26.9, 22.8, 17.3, 10.7; MS (ESI) *m/z* calcd for $[C_{40}H_{56}N_9O_{11}S]^+$: 870.38 $[M+H]^+$; found: 870.4.

c) *Cyclo*[Arg(Mtr)-Gly-Asp(O*t*Bu)-DKP5]

Compound **115 c** (224 mg, 0.25 mmol, 1 eq.) was cyclized in the conditions described in general procedure **GP4**, in presence of HATU (103.4 mg, 0.27 mmol, 4 eq.), HOAt (37.3 mg, 0.27 mmol, 4 eq.) and DIPEA (54 µl, 0.41 mmol, 6 eq). The crude product was purified by flash chromatography on silica gel (CH_2Cl_2/MeOH, 95:5) to afford yellowish solid that was further purified by Biotage (gradient: 95% H_2O / 5% acetonitrile to 5% H_2O / 95% acetonitrile), to obtain the product as white foam (20 mg, 31%).

R_f=0.33 (CH_2Cl_2/MeOH 9:1); ^{1}H NMR (400 MHz, Acetone-d_6) δ 8.00 (d, 1H, *J* = 6.9 Hz), 7.84 (d, 1H, *J* = 6.7 Hz), 7.79 – 7.70 (m, 1H), 7.58 (d, 1H, *J* = 7.7 Hz), 7.48 – 7.17 (m, 10H), 6.69 – 6.62 (m, 2H), 6.52 (br s, 2H), 6.38 (br s, 2H), 5.30 (d, 1H, *J* = 15.4 Hz), 5.24 (d, 1H, *J* = 16.0 Hz), 5.02 (d, 1H, *J* = 8.2 Hz), 4.65 – 4.38 (m, 2H), 4.38 – 3.89 (m, 5H), 3.82 (s, 3H), 3.52 (dd, 1H, *J* = 15.6, 2.3 Hz), 3.42 (dd, 1H, *J* = 13.9, 4.4 Hz), 3.28 – 3.13 (m, 2H), 2.87 (dd, 1H, *J* = 16.2, 8.2 Hz), 2.72 – 2.54 (m, 9H), 2.08 (s, 3H), 1.91 – 1.78 (m, 1H), 1.73 – 1.48 (m, 3H), 1.40 (s, 9H); ^{13}C NMR (101 MHz, Acetone-d_6) δ 172.1, 171.7, 171.6, 169.4, 169.1, 166.9, 158.0, 156.6, 138.5, 138.2, 136.3, 136.1, 128.9, 128.5, 127.9, 127.7, 127.0, 123.9, 111.6, 80.4, 58.9, 58.7, 54.9, 50.8, 49.3, 46.7, 41.9, 40.3, 39.4, 39.2, 36.8, 27.7, 27.3, 26.2, 23.3, 17.7, 11.2; MS (ESI) *m/z* calcd for $[C_{47}H_{62}N_9O_{11}S]^+$: 960.43 $[M+H]^+$; found: 960.7.

d) *Cyclo*[Arg(Mtr)-Gly-Asp(O*t*Bu)-DKP6]

Compound **115 d** (322 mg, 0.36 mmol, 1 eq.) was cyclized in the conditions described in general procedure **GP4**, in presence of HATU (547.2 mg, 1.44 mmol, 4 eq.), HOAt (195.8 mg, 1.44 mmol, 4 eq.) and DIPEA (0.37 ml, 2.2 mmol, 6 eq). The crude product was purified by flash chromatography on silica gel (CH_2Cl_2/MeOH, 95:5) to afford yellowish solid that was further purified by Biotage (gradient: 95% H_2O / 5% acetonitrile to 5% H_2O / 95% acetonitrile), to obtain the product as white foam (180 mg, 58%).

R_f=0.47 (CH_2Cl_2/MeOH 9:1); ^{1}H NMR (400 MHz, DMSO-d_6) δ 9.08 – 8.95 (m, 1H), 8.37 (d, 1H, J = 8.2 Hz), 7.95 (br s, 1H), 7.71 – 7.61 (m, 1H), 7.46 (br s, 1H, J = 7.6 Hz), 7.39 – 7.22 (m, 5H), 6.88 – 6.64 (m, 2H), 6.55 – 6.25 (m, 1H), 5.14 (d, 1H, J = 14.9 Hz), 4.21 (br s, 2H), 4.05 (d, 1H, J = 16.0 Hz), 3.99 – 3.92 (m, 1H), 3.90 – 3.75 (m, 5H), 3.63 – 3.43 (m, 3H), 3.01 (m, 2H), 2.88 (dd, 1H, J = 16.2, 7.4 Hz), 2.78 – 2.48 (m, 8H, overlapping with solvent signal), 2.44 (dd, 1H, J = 16.3, 7.0 Hz), 2.06 (s, 3H), 1.74 – 1.58 (m, 1H), 1.56 – 1.26 (m, 12H); ^{13}C NMR (101 MHz, DMSO-d_6) δ 172.3, 171.6, 170.9, 169.8, 167.4, 166.7, 158.6, 157.2, 138.8, 137.8, 136.7, 135.7, 129.8, 128.8, 128.5, 124.7, 112.9, 81.2, 58.5, 56.6, 55.6, 53.4, 51.5, 47.2, 43.6, 42.1, 36.6, 35.5, 32.4, 29.9, 28.8, 26.8, 24.7, 19.1, 12.9; MS (ESI) *m/z* calcd for $[C_{40}H_{56}N_9O_{11}S]^+$: 870.38 $[M+H]^+$; found: 870.4.

e) *Cyclo*[Arg(Mtr)-Gly-Asp(O*t*Bu)-DKP7]

Compound **115 e** (167 mg, 0.17 mmol, 1 eq.) was cyclized in the conditions described in general procedure **GP4**, in presence of HATU (259.7 mg, 0.68 mmol, 4 eq.), HOAt (93 mg, 0.68 mmol, 4 eq.) and DIPEA (0.17 ml, 1.02 mmol, 6 eq). The crude product was purified by flash chromatography on silica gel (CH_2Cl_2/MeOH, 95:5) to afford yellowish solid that was further purified by Biotage (gradient: 95% H_2O / 5% acetonitrile to 5% H_2O / 95% acetonitrile), to obtain the product (75 mg, 46%) as a 2:1 mixture of two inseparable diastereomers.

R_f=0.32 (CH_2Cl_2/MeOH 9:1); ^{1}H NMR (400 MHz, CD_3OD) δ (two diastereomers A and B; A/B = 2:1) 7.47 – 7.19 (m, 10H_A+ 10H_B), 6.70 – 6.65 (m, 1H_A + 1H_B), 5.40 (d, 1H_B, J = 15.2 Hz), 5.35 (d, 1H_B, J = 16.6 Hz), 5.19 (d, 1H_A, J = 14.9 Hz), 5.05 – 4.94 (m, 2H_A), 4.78 (dd, 1H_A, J = 11.5, 2.1 Hz), 4.57 (t, 1H_B, J = 6.7 Hz), 4.52 (d, 1H_B, J = 16.7 Hz), 4.46 (d, 1H_A, J = 17.4 Hz), 4.43 – 4.39 (m, 1H_B), 4.34 (d, 1H_B, J = 16.5 Hz), 4.29 – 4.19 (m, 1H_A + 2H_B), 4.13 (d, 1H_A, J = 15.1 Hz), 4.08 – 3.96 (m, 2H_A), 3.91 (d, 1H_B, J = 15.3 Hz), 3.88 – 3.78 (m, 3H_A + 4H_B), 3.70 (dd, 1H_A, J = 10.4, 4.1 Hz), 3.66 – 3.56 (m, 1H_A + 1H_B), 3.53 – 3.42 (m, 1H_A + 1H_B), 3.28 – 3.09 (m, 2H_A + 2H_B), 3.03 – 2.80 (m, 2H_A + 1H_B), 2.78 – 2.65 (m, 4H_A + 4H_B), 2.63 (s, 3H_B), 2.60 (s, 3H_A), 2.58 – 2.43 (m, 1H_A + 2H_B), 2.15 (s, 3H_B), 2.13 (s, 3H_A), 2.11 – 2.00 (m, 1H_A), 1.94 – 1.81 (m, 1H_A + 1H_B), 1.80 – 1.70 (m, 1H_B), 1.66 – 1.52 (m, 2H_A + 2H_B), 1.49 – 1.44 (m, 9H_A + 9H_B); ^{13}C NMR (101 MHz, CD_3OD) δ (two rotamers) 173.2, 172.2, 171.7, 171.1, 170.7, 170.4, 169.8, 168.5, 167.5, 158.5, 156.7, 138.1, 136.9, 136.5, 135.8, 135.5, 133.5, 128.7, 128.6, 128.5, 128.3, 127.9, 127.8, 127.0, 126.9, 126.1, 124.3, 111.4, 80.9, 59.7, 58.4, 56.9, 56.8, 54.6, 53.8, 50.2, 48.7, 43.2, 42.2,

39.7, 38.2, 35.9, 35.6, 35.1, 28.3, 26.9, 26.0, 25.5, 22.9, 17.4, 13.0, 10.7; MS (ESI) *m/z* calcd for $[C_{47}H_{62}N_9O_{11}S]^+$: 960.43 $[M+H]^+$; found: 960.5.

f) *Cyclo*[DKP-8-Arg(Mtr)-Gly-Asp(O*t*Bu)]

Compound **115 f** (124 mg, 0.13 mmol, 1 eq.) was cyclized in the conditions described in general procedure **GP4**, in presence of HATU (197 mg, 0.52 mmol, 4 eq.), HOAt (70 mg, 0.52 mmol, 4 eq.), and DIPEA (137 µl, 0.8 mmol, 6 eq.). The crude product was purified by flash chromatography on silica gel (CH_2Cl_2/MeOH, 93:7) to afford the desired product as white foam (85 mg, 74%).

R_f=0.4 (CH_2Cl_2/MeOH, 9:1); ^{1}H NMR (400 MHz, CD_3OD) δ 7.41 – 7.22 (m, 5H), 6.66 (s, 1H), 5.31 (d, 1H, *J* = 15.3 Hz), 4.47 (dd, 1H, *J* = 8.4, 4.9 Hz), 4.27 (dd, 1H, *J* = 8.7, 5.8 Hz), 4.18 – 4.08 (m, 2H), 4.05 (d, 1H, *J* = 15.3 Hz), 3.97 (d, 1H, *J* = 16.8 Hz), 3.88 – 3.79 (m, 4H), 3.67 (d, 1H, *J* = 16.8 Hz), 3.55 (d, 1H, *J* = 13.7 Hz), 3.26 – 3.14 (m, 2H), 2.91 (dd, 1H, *J* = 16.6, 4.9 Hz), 2.76 (dd, 1H, *J* = 16.6, 8.4 Hz), 2.71 – 2.56 (m, 7H), 2.56 – 2.42 (m, 2H), 2.12 (s, 3H), 1.86 – 1.52 (m, 5H), 1.44 (s, 9H); ^{13}C NMR (101 MHz, CD_3OD) δ 176.4, 175.9, 175.0, 173.9, 171.6, 171.6, 169.6, 169.5, 159.9, 158.2, 139.5, 138.0, 137.4, 134.8, 130.0, 129.0, 125.7, 112.8, 82.4, 60.4, 56.0, 54.9, 53.0, 52.4, 48.2, 44.0, 41.1, 40.2, 37.5, 31.8, 30.7, 29.0, 28.3, 27.4, 24.4, 18.9, 12.1**;** MS (ESI) *m/z* calcd for $[C_{41}H_{58}N_9O_{11}S]^+$: 884.40 $[M+H]^+$; found: 884.46.

***Cyclo*[Arg-Gly-Asp-DKP]**

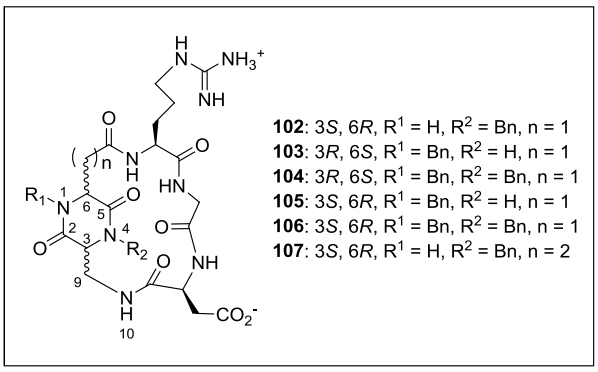

102: 3*S*, 6*R*, R^1 = H, R^2 = Bn, n = 1
103: 3*R*, 6*S*, R^1 = Bn, R^2 = H, n = 1
104: 3*R*, 6*S*, R^1 = Bn, R^2 = Bn, n = 1
105: 3*S*, 6*R*, R^1 = Bn, R^2 = H, n = 1
106: 3*S*, 6*R*, R^1 = Bn, R^2 = Bn, n = 1
107: 3*S*, 6*R*, R^1 = H, R^2 = Bn, n = 2

(102) *Cyclo*[Arg-Gly-Asp-DKP3]

Compound **116 a** (50 mg, 0.06 mmol) was fully deprotected in the conditions described in general procedure **GP5**. The crude product was purified by HPLC (Water's Atlantis 21 mm x 10 cm column, gradient: 90% H_2O / 10% acetonitrile to 70% H_2O / 30% acetonitrile) to give the desired compound (as trifluoroacetate salt) as white solid (34 mg, 80%).

^{1}H NMR (600 MHz, H_2O/D_2O 9:1, T= 298K) δ 8.76 (d, 1H, *J* = 8.2 Hz, Arg-NH), 8.28 (t, 1H, *J* = 6.7 Hz, DKP-NH10), 8.06 (s, 1H, DKP-NH1), 8.02 – 7.95 (m, 1H, Gly-NH), 7.85 (d, 1H, *J* = 8.6 Hz, Asp-NH), 7.37 – 7.18 (m, 5H, H-Ar), 7.10 (t, 1H, *J* = 5.9 Hz, NH-guan), 5.01 (m, 1H, $\underline{CH_2}$-Ph), 4.76 (m, 1H, αH-Asp), 4.48 (m, 1H, DKP-H6), 4.21 (dd, 1H, *J* = 17.7, 8.2 Hz, αH-Gly), 4.16 – 4.00 (m, 3H, DKP-H3 + $\underline{CH_2}$-Ph + αH-Arg), 3.90 (dd, 1H, *J* = 15.8, 7.1 Hz, DKP-H9), 3.63 –

3.47 (m, 2H, DKP-H9 + αH-Gly), 3.13 (dd, 2H, *J* = 13.2, 6.8 Hz, δH-Arg), 2.86 – 2.76 (m, 2H, DKP-H7, βH-Asp), 2.68 (dd, 1H, *J* = 17.1, 7.0 Hz, DKP-H7), 2.56 (dd, 1H, *J* = 14.4, 5.3 Hz, βH-Asp), 1.95 – 1.84 (m, 1H, βH-Arg), 1.77 – 1.66 (m, 1H, βH-Arg), 1.63 – 1.46 (m, 2H, γH-Arg); ^{13}C NMR (151 MHz, H_2O/D_2O 9:1, T= 298K) (obtained by HSQC experiment) *δ* 128.7, 127.6, 127.5, 59.3, 53.8, 51.9, 49.3, 47.7, 42.4, 40.5, 39.1, 37.8, 34.7, 25.5, 24.4; MS (ESI) *m/z* calcd for $[C_{26}H_{36}N_9O_8]^+$: 602.27 $[M+H]^+$; found: 602.3.

(103) *Cyclo*[Arg-Gly-Asp-DKP4]

Compound **116 b** (93.7 mg, 0.11 mmol) was fully deprotected in the conditions described in general procedure **GP5**. The crude product was purified by HPLC (Water's Atlantis 21 mm x 10 cm column, gradient: 90% H_2O / 10% acetonitrile to 70% H_2O / 30% acetonitrile) to give the desired compound as white solid (62 mg, 80%).

^{1}H NMR (400 MHz, H_2O/D_2O 9:1, T= 298K) *δ* 8.88 (br s, 1H, Asp-NH), 8.37 – 8.23 (m, 2H, Arg-NH + Gly-NH), 8.20 (m, 1H, DKP-NH4), 7.59 (m, 1H, DKP-NH10), 7.35 – 7.19 (m, 5H, H-Ar), 7.11 (t, 1H, *J* = 6.1 Hz, NH-guan), 5.08 (m, 1H, $\underline{CH_2}$-Ph), 4.35 (m, 1H, αH-Asp), 4.29 – 4.14 (m, 2H, αH-Arg + DKP-H6), 4.01 – 3.82 (m, 2H, αH-Gly + DKP-H3), 3.77 – 3.58 (m, 2H, αH-Gly + DKP-H9), 3.34 (m, 1H, DKP-H9), 3.12 (m, 2H, δH-Arg), 3.01 – 2.67 (m, 4H, DKP-H7 + βH-Asp), 1.85 – 1.43 (m, 4H, βH-Arg + γH-Arg); ^{13}C NMR (151 MHz, H_2O/D_2O 9:1, T= 298K) (obtained by HSQC experiment) *δ* 128.7, 127.6, 57.5, 53.5, 53.3, 52.0, 47.3, 42.3, 40.7, 40.6, 35.7, 34.3, 28.0, 24.4; HRMS (ESI) *m/z* calcd for $[C_{26}H_{35}N_9O_8Na]^+$: 624.25008 $[M+Na]^+$; found: 624.24942.

(104) *Cyclo*[Arg-Gly-Asp-DKP5]

Compound **116 c** (20 mg, 0.02 mmol) was fully deprotected in the conditions described in general procedure **GP5**. The crude product was purified by HPLC (Water's Atlantis 21 mm x 10 cm column, gradient: 90% H_2O / 10% acetonitrile to 30% H_2O / 70% acetonitrile) to give the desired compound (as trifluoroacetate salt) as white solid (9.5 mg, 60%).

^{1}H NMR (400 MHz, H_2O/D_2O 9:1, T= 298K) *δ* 8.61 – 8.53 (m, 1H, DKP-NH10), 8.48 (d, 1H, *J* = 6.6 Hz, Arg-NH), 8.42 (d, 1H, *J* = 8.3 Hz, Asp-NH), 8.23 (d, 1H, *J* = 9.6 Hz, Gly-NH), 7.44 – 7.19 (m, 10H, H-Ar), 7.11 – 7.03 (m, 1H, NH-guan), 5.10 (m, 1H, $\underline{CH_2}$-Ph), 5.00 (m, 1H, $\underline{CH_2}$-Ph), 4.62 (m, 1H, αH-Asp), 4.41 (m, 1H, DKP-H6), 4.37 (m, 1H, $\underline{CH_2}$-Ph), 4.33 (m, 1H, DKP-H3), 4.32 (m, 1H, DKP-H9), 4.23 (m, 1H, αH-Gly), 4.15 (d, 1H, *J* = 15.4 Hz, $\underline{CH_2}$-Ph), 4.11 (m, 1H, αH-Arg), 3.42 (d, 1H, *J* = 17.3 Hz, αH-Gly), 3.34 (m, 1H, DKP-H9), 3.10 (dd, 2H, *J* = 12.6, 6.6 Hz, δH-Arg), 2.86 (dd, 1H, *J* = 16.8, 7.8 Hz, βH-Asp), 2.70 (dd, 1H, *J* = 17.0, 7.2 Hz, βH-Asp), 2.55 (m, 2H, DKP-H7), 1.82 – 1.50 (m, 4H, βH-Arg + γH-Arg);^{13}C NMR (151 MHz, H_2O/D_2O 9:1, T= 298K) (obtained by HSQC experiment) *δ* 128.7, 128.5, 126.2, 59.5, 55.1, 51.5, 50.1, 48.3, 48.1, 41.9, 40.3, 39.7, 39.4, 38.6, 26.8, 24.3; HRMS (ESI) *m/z* calcd for $[C_{33}H_{41}N_9O_8Na]^+$: 714.29703 $[M+Na]^+$; found: 714.29588.

(105) *Cyclo*[Arg-Gly-Asp-DKP6]

Compound **116 d** (80.2 mg, 0.09 mmol) was fully deprotected in the conditions described in general procedure **GP5**. The crude product was purified by (Water's Atlantis 21 mm x 10 cm column, gradient: 90% H_2O / 10% acetonitrile to 70% H_2O / 30% acetonitrile) to give the desired compound (as trifluoroacetate salt) as white solid (54 mg, 82%).

^{1}H NMR (400 MHz, H_2O/D_2O 9:1, T= 298K) δ 8.80 (d, 1H, *J* = 6.4 Hz, Asp-NH), 8.40 – 8.26 (m, 2H, Gly-NH + Arg-NH), 8.07 (s, 1H, DKP-NH4), 7.89 (t, 1H, *J* = 6.1 Hz, DKP-NH10), 7.40 – 7.22 (m, 5H, H-Ar), 7.10 (t, 1H, *J* = 5.7 Hz, NH-guan), 5.06 (d, 1H, *J* = 17.9 Hz, $\underline{CH_2}$-Ph), 4.35 (m, 1H, αH-Asp), 4.29 (m, 1H, αH-Arg), 4.26 – 4.19 (m, 2H, DKP-H6 + $\underline{CH_2}$-Ph), 3.96 – 3.89 (m, 1H, DKP-H3), 3.90 – 3.75 (m, 2H, αH-Gly + DKP-H9), 3.67 (dd, 1H, *J* = 15.6, 6.1 Hz, αH-Gly), 3.58 – 3.43 (m, 1H, DKP-H9), 3.13 (dd, 2H, *J* = 12.9, 6.9 Hz, δH-Arg), 2.81 – 2.67 (m, 3H, DKP-H7 + βH-Asp), 2.56 (dd, 1H, *J* = 16.1, 8.3 Hz, βH-Asp), 1.84 – 1.48 (m, 4H, βH-Arg + γH-Arg);^{13}C NMR (151 MHz, H_2O/D_2O 9:1, T= 298K) (obtained by HSQC experiment) δ 128.6, 127.6, 57.6, 54.9, 53.1, 51.3, 47.7, 47.1, 42.8, 40.4, 35.4, 35.0, 27.8, 24.2; HRMS (ESI) *m/z* calcd for $[C_{26}H_{35}N_9O_8Na]^+$: 624.25008 $[M+Na]^+$; found: 624.24929.

(106) *Cyclo*[Arg-Gly-Asp-DKP7]

Compound **116 e** (65 mg, 0.068 mmol) was fully deprotected in the conditions described in general procedure **GP5**. The crude product was purified by HPLC (Water's Atlantis 21 mm x 10 cm column, gradient: 90% H_2O / 10% acetonitrile to 40% H_2O / 60% acetonitrile) to give **31A** (as trifluoroacetate salt) (21.3 mg) and **31B** (as trifluoroacetate salt) (10.6 mg) as white solids (60% overall).

106 A: ^{1}H NMR (400 MHz, H_2O/D_2O 9:1, T= 298K) δ 8.66 (d, 1H, *J* = 7.7 Hz, Arg-NH), 8.04 (t, 1H, *J* = 6.6 Hz, DKP-NH10), 7.95 – 7.89 (m, 1H, Gly-NH), 7.77 – 7.70 (m, 1H, Asp-NH), 7.44 – 7.16 (m, 10H, H-Ar), 7.10 – 7.04 (m, 1H, NH-guan), 5.06 – 4.99 (m, 1H, $\underline{CH_2}$-Ph), 4.89 (m, 1H, αH-Asp), 4.80 (m, 1H, $\underline{CH_2}$-Ph), 4.69 (m, 1H, DKP-H6), 4.57 (m, 1H, $\underline{CH_2}$-Ph), 4.39 – 4.33 (m, 2H, αH-Gly, DKP-H3), 4.14 – 4.07 (m, 1H, αH-Arg), 4.04 (d, 1H, *J* = 14.8 Hz, $\underline{CH_2}$-Ph), 3.91 (dd, 1H, *J* = 15.4, 7.1 Hz, DKP-H9), 3.71 – 3.61 (m, 1H, DKP-H9), 3.60 – 3.52 (m, 1H, αH-Gly), 3.10 (dd, 2H, *J* = 12.9, 6.9 Hz, δH-Arg), 2.90 – 2.76 (m, 2H, DKP-H7, βH-Asp), 2.62 (dd, 1H, *J* = 17.1, 6.3 Hz, βH-Asp), 2.58 – 2.49 (m, 1H, DKP-H7), 2.01 – 1.87 (m, 1H, βH-Arg), 1.73 – 1.58 (m, 1H, βH-Arg), 1.55 – 1.42 (m, 2H, γH-Arg); ^{13}C NMR (151 MHz, H_2O/D_2O 9:1, T= 298K) (obtained by HSQC experiment) δ 128.1, 48.0, 43.2, 40.9, 39.7, 37.7, 36.9, 25.4, 24.4; MS (ESI) *m/z* calcd for $[C_{33}H_{42}N_9O_8]^+$: 692,31 $[M+H]^+$; found: 692.4.

106 B: ^{1}H NMR (400 MHz, H_2O/D_2O 9:1, T= 298K) δ 8.55 (d, 1H, *J* = 8.1 Hz, Asp-NH), 8.45 (t, 1H, *J* = 5.8 Hz, Gly-NH), 8.34 (d, 1H, *J* = 5.9 Hz, Arg-NH), 7.73 (d, 1H, *J* = 8.4 Hz, DKP-NH10), 7.46 – 7.16 (m, 10H, H-Ar), 7.16 – 7.10 (m, 1H, NH-guan), 5.27 – 5.15 (m, 2H, $\underline{CH_2}$-Ph), 4.52 (m, 1H, αH-Asp), 4.44 (m, 1H, DKP-H6), 4.36 – 4.29 (m, 1H, $\underline{CH_2}$-Ph), 4.20 (d, 1H, *J* = 14.8 Hz, $\underline{CH_2}$-Ph), 4.16 – 4.07 (m, 2H, αH-Arg, DKP-H3), 3.80 (dd, 1H, *J* = 15.2, 4.1 Hz, αH-

Gly), 3.76 – 3.63 (m, 2H, αH-Gly, DKP-H9), 3.38 – 3.28 (m, 1H, DKP-H9), 3.16 (dd, 2H, *J* = 13.6, 7.1 Hz, δH-Arg), 2.94 (dd, 1H, *J* = 14.9, 6.1 Hz, DKP-H7), 2.87 – 2.72 (m, 2H, DKP-H7, βH-Asp), 2.60 (dd, 1H, *J* = 16.6, 7.2 Hz, βH-Asp), 1.77 (dd, 2H, *J* = 15.6, 8.3 Hz, βH-Arg), 1.69 – 1.52 (m, 2H, γH-Arg);^{13}C NMR (151 MHz, H_2O/D_2O 9:1, T= 298K) (obtained by HSQC experiment) δ 128.4, 60.7, 56.8, 53.6, 51.4, 49.6, 47.5, 43.5, 40.6, 39.3, 36.7, 35.6, 27.8; MS (ESI) *m/z* calcd for $[C_{33}H_{42}N_9O_8]^+$: 692,31 $[M+H]^+$; found: 692.3.

(107) Cyclo[Arg-Gly-Asp-DKP8]

Compound **116 f** (50 mg, 0.06 mmol) was fully deprotected in the conditions described in general procedure **GP5**. The crude product was purified by HPLC HPLC (Water's Atlantis 21 mm x 10 cm column, gradient: 95% H_2O / 5% acetonitrile to 80% H_2O / 20% acetonitrile) to give the desired compound (as trifluoroacetate salt) as white solid (34 mg, 80%).

^{1}H NMR (400 MHz, D_2O, 291 K) δ 8.21 – 8.14 (m, 1H), 7.35 – 7.12 (m, 5H), 5.07 (d, *J* = 15.7 Hz, 1H), 4.45 (t, *J* = 6.3 Hz, 1H), 4.24 – 4.16 (m, 1H), 4.10 – 3.94 (m, 3H), 3.90 – 3.72 (m, 4H), 3.61 (d, *J* = 14.8 Hz, 1H), 3.08 (t, *J* = 6.6 Hz, 2H), 2.76 (t, *J* = 5.4 Hz, 2H), 2.47 (m, 4H), 1.78 – 1.42 (m, 6H). MS (ESI) *m/z* calcd for $[C_{27}H_{38}N_9O_8]^+$: 616,28 $[M+H]^+$; found: 616.3.

4 - Synthesis of *cyclic*[DKP-*iso*DGR] compounds

4.1 - Solid phase peptide synthesis

GENERAL REMARKS: The syntheses of compounds **120** were carried out by manual coupling using Fmoc/*t*Bu strategy on SASRIN™ resin (200-400 mesh, 1.02 mmol/g) on a 0.1 mmol scale. Swelling of the resin was achieved suspending it in either DCM or DMF for 15 min.

SASRIN™ RESIN LOADING: The first Fmoc protected amino acid (Fmoc-GlyOH, 119 mg, 0.4 mmol, 4 eq.) residue was dissolved in the minimum amount of DMF, and the solution was cooled to 0° C. DIC (62 μl, 0.4 mmol, 4 eq.) was added dropwise. The mixture was stirred for 20 min at the same temperature before adding it to the resin (98 mg, 0.1 mmol, 1 eq.). DMAP (1.2 mg, 0.01 mmol, 0.1 eq.) was then added in one portion. The reaction vessel was gently shaken for 1 h at r.t.. Resin was thoroughly washed in the order with DMF (4x), DCM (4x), *i*PrOH (3x). Capping was performed (see general procedure **GP10**).

COUPLING REACTIONS: A sample vial equipped with a magnetic stirrer was charged with the appropriate *N*-protected-amino acid (2.5 - 4 eq.), which was dissolved in a 1:1 mixture of DCM/DMF. After cooling the mixture to 0 °C DIC (2.5 – 4 eq.) and HOAt (2.5 – 4 eq.) were added successively. The mixture was stirred for 20 min at the same temperature. The solution was then added to the *N*-deblocked swelled peptidylresin (0.1 mmol, 1 eq.). The resin was gently agitated for 2-18 h and, after sucking off the solution, it was washed in the order with DMF (4x), DCM (4x), *i*PrOH (3x) and/or Et_2O (2x). If a Fmoc-amino acid was coupled, Kaiser test was performed. If resin gives a positive

colour test, coupling procedure was repeated with fresh reagents. After a maximum of 3 coupling cycles, capping was performed (see general procedure **GP10**).

Exact amounts of the used amino acids and coupling reagents for SPPS are reported in Table 5.1.

Table 5.1 - Exact amounts of the used amino acids and coupling reagents for SPPS

REAGENTS	eq.	n (mmol)	AMOUNTS
Fmoc-L-Asp(OH)-O*t*Bu	3	0.3	123 mg
DIC	3	0.3	47 μl
HOAt	3	0.3	41 mg
DKP2* or **DKP3***	2.5	0.25	79 mg
DIC	2.5	0.25	38 μl
HOAt	2.5	0.25	34 mg
Cbz-L-Arg(Mtr)-OH · CHA	4	0.4	248 mg
DIC	4	0.4	62 μl
HOAt	4	0.4	27 mg

Fmoc DEPROTECTION: After successful coupling, washing and Fmoc deprotecting steps were carried out as described in general procedure **GP7**. This deprotection/coupling strategy was applied for each synthetic step involving N-Fmoc protected α-amino acids.

AZIDE REDUCTION: After successful coupling of **DKP*** building blocks, washing and azide reduction steps were carried out as described in general procedure **GP8**.

Cbz-Arg(Mtr)-DKP-*iso*Asp(O*t*Bu)-Gly-OH (120)

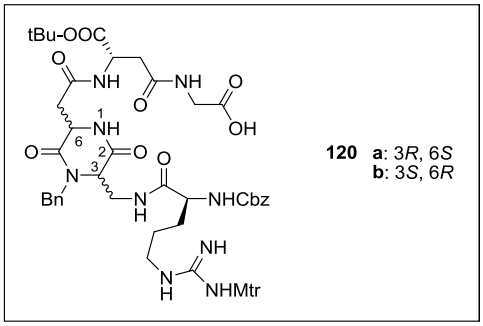

120 **a**: 3*R*, 6*S*
b: 3*S*, 6*R*

$C_{48}H_{63}N_9O_{14}S$
MW: 1022,13

CLEAVAGE FROM SASRIN™ RESIN: The resin was thoroughly washed with DCM (5 to 10 times) and then treated with 1% TFA in DCM (2ml) for 2-5 min. The mixture was filtered off with a N_2 pressure into a vial containing at least 2 eq. of pyridine in MeOH (0.2 ml 2M). The filtrate was checked for the peptide by TLC (DCM:MeOH=9:1). Treatment with 1% TFA in DCM was repeated as long as peptide was cleaving from the resin (5-8 times). Peptide containing fractions were combined and half of the DCM volume was removed at reduced pressure. The mixture was then diluted with aboundant EtOAc and washed with 1M $KHSO_{4\ aq.}$ (4x) to remove pyridinium trifluoroacetate and free the carboxylic acid. The organic layer was dried over Na_2SO_4, filtered and evapourated to afford a

white solid which was purified by flash chromatography (DCM:MeOH=9:1) (**a**: 89 mg, 88%; **b**: 90 mg, 88%).

a) ^{1}H NMR (400 MHz, MeOD) δ 8.35 (d, J = 6.2 Hz, 1H), 8.30 – 8.14 (m, 1H), 7.47 – 7.24 (m, 9H), 7.19 (d, J = 7.6 Hz, 1H), 6.65 (s, 1H), 5.38 (d, J = 15.4 Hz, 1H), 5.09 (q, J = 12.4 Hz, 2H), 4.75 – 4.56 (m, 2H), 4.13 (dd, J = 17.2, 9.3 Hz, 2H), 3.90 (dd, J = 12.5, 5.7 Hz, 4H), 3.82 (s, 1H), 3.60 (dd, J = 15.6, 4.8 Hz, 3H), 3.16 (s, 2H), 3.05 (dd, J = 16.3, 4.0 Hz, 1H), 2.83 (dd, J = 16.4, 6.8 Hz, 1H), 2.77 (d, J = 6.2 Hz, 2H), 2.68 (s, 3H), 2.62 (s, 3H), 2.12 (s, 3H), 1.73 (d, J = 5.6 Hz, 1H), 1.65 – 1.49 (m, 3H), 1.47 (s, 9H); ^{13}C NMR (101 MHz, MeOD) δ 175.0, 172.5, 171.8, 170.9, 170.8, 168.2, 167.6, 159.1, 157.7, 138.8, 137.4, 137.1, 136.5, 134.1, 129.2, 128.8, 128.4, 128.3, 128.1, 125.0, 112.1, 82.6, 67.2, 59.8, 55.5, 55.3, 51.4, 50.7, 41.2, 39.5, 37.5, 29.5, 27.5, 23.7, 18.1, 11.4; MS (ESI) *m/z* calcd for $[C_{48}H_{64}N_9O_{14}S]^+$: 1022.43 $[M+H]^+$; found: 1022.8.

b) ^{1}H NMR (400 MHz, MeOD) δ 7.43 – 7.22 (m, 9H), 6.67 (s, 1H), 5.38 (d, J = 15.3 Hz, 1H), 5.19 – 5.01 (m, 2H), 4.71 (t, J = 5.9 Hz, 1H), 4.62 (s, 1H), 4.18 – 4.06 (m, 2H), 4.02 – 3.92 (m, 1H), 3.90 (dd, J = 6.7, 3.7 Hz, 1H), 3.87 – 3.79 (m, 2H), 3.67 – 3.55 (m, 4H), 3.16 (dd, J = 13.2, 6.5 Hz, 1H), 3.05 – 2.91 (m, 1H), 2.88 – 2.74 (m, 3H), 2.69 (s, 3H), 2.62 (s, 3H), 2.13 (s, 3H), 1.75 (bs, 1H), 1.67 – 1.51 (m, 4H), 1.47 (s, 9H); ^{13}C NMR (101 MHz, MeOD) δ 172.5, 171.7, 170.9, 170.9, 168.2, 167.7, 159.2, 157.7, 157.4, 138.8, 137.4, 137.2, 136.3, 129.6, 129.2, 129.0, 128.8, 128.4, 128.3, 128.2, 125.0, 112.08, 82.71, 67.09, 59.76, 55.32, 55.26, 51.69, 50.63, 41.09, 39.41, 38.02, 37.52, 34.20, 32.33, 32.0, 30.0, 29.9, 29.7, 29.7, 29.5, 27.4, 25.3, 23.6, 23.0, 18.1, 13.7, 11.4; MS (ESI) *m/z* calcd for $[C_{48}H_{64}N_9O_{14}S]^+$: 1022.43 $[M+H]^+$; found: 1022.9.

4.2 - *In solution*

H-Arg-DKP-*iso*Asp(O*t*Bu)-Gly-OH (121)

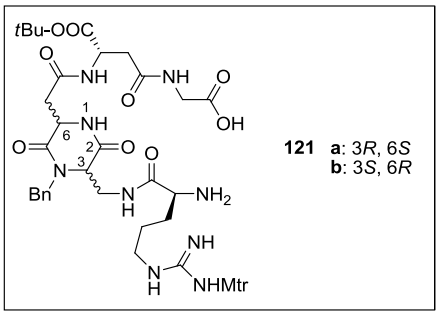

121 **a**: 3*R*, 6*S*
b: 3*S*, 6*R*

$C_{40}H_{57}N_9O_{12}S$
MW: 888,00

a) H-Arg-DKP2-*iso*Asp(O*t*Bu)-Gly-OH

Compound **120 a** (89 mg, 0.09 mmol, 1 eq.) was treated with Pd/C 10% (9.2 mg, 0.009 mmol, 0.1 eq.) in the conditions described in general procedure **GP3**. The crude product was obtained as white solid (77 mg, 100%) that was used without further purification.

b) H-Arg-DKP3-*iso*Asp(O*t*Bu)-Gly-OH

Compound **120 a** (90 mg, 0.09 mmol, 1 eq.) was treated with Pd/C 10% (9.3 mg, 0.009 mmol, 0.1 eq.) in the conditions described in general procedure **GP3**. The crude product was obtained as white solid (78 mg, 100%) that was used without further purification.

***Cyclo* [*iso*Asp(O*t*Bu)-Gly-Arg(Mtr)-DKP] (122)**

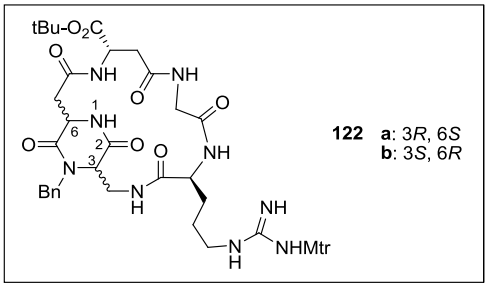

122 **a**: 3*R*, 6*S*
b: 3*S*, 6*R*

$C_{40}H_{55}N_9O_{11}S$
MW: 869,98

a) *Cyclo* [*iso*Asp(O*t*Bu)-Gly-Arg(Mtr)-DKP2]

Compound **121 a** (77 mg, 0.09 mmol, 1 eq.) was cyclized in the conditions described in general procedure **GP4**, in presence of HATU (136 mg, 0.36 mmol, 4 eq.), HOAt (49 mg, 0.36 mmol, 4 eq.) and DIPEA (93 µl, 0.54 mmol, 6 eq). The crude product was purified by flash chromatography on silica gel (CH_2Cl_2/MeOH, 95:5) to afford the desired product as white foam (41 mg, 55%).

^{1}H NMR (400 MHz, MeOD) δ 7.49 – 7.16 (m, 5H), 6.68 (s, 1H), 5.37 (d, J = 15.3 Hz, 1H), 5.03 (t, J = 6.9 Hz, 1H), 4.80 – 4.67 (m, 1H), 4.31 – 4.01 (m, 4H), 3.85 (s, 5H), 3.39 (d, J = 1.6 Hz, 1H), 3.26 – 3.13 (m, 2H), 2.79 (dd, J = 14.0, 4.5 Hz, 1H), 2.75 – 2.71 (m, 1H), 2.69 (s, 3H), 2.62 (s, 3H), 2.15 (s, 3H), 1.82 – 1.56 (m, 4H), 1.51 (s, 9H); ^{13}C NMR (101 MHz, MeOD) δ 174.2, 171.5, 170.7, 170.1, 169.7, 167.1, 166.7, 158.5, 156.8, 138.1, 136.5, 135.6, 133.5, 128.6, 127.8, 127.6, 124.3, 111.4, 82.0, 59.1, 54.6, 53.9, 50.7, 48.5, 48.2, 48.0, 47.8, 47.6, 47.4, 47.2, 47.0, 46.4, 41.4, 41.4, 40.0, 38.3, 37.3, 29.3, 27. 6, 26.8, 25.6, 22.8, 17.4, 10.7; MS (ESI) *m/z* calcd for $[C_{40}H_{56}N_9O_{11}S]^+$: 870.38 $[M+H]^+$; found: 870.8.

b) *Cyclo* [*iso*Asp(O*t*Bu)-Gly-Arg(Mtr)-DKP3]

Compound **121 b** (78 mg, 0.09 mmol, 1 eq.) was cyclized in the conditions described in general procedure **GP4**, in presence of HATU (137 mg, 0.36 mmol, 4 eq.), HOAt (49 mg, 0.36 mmol, 4 eq.) and DIPEA (93 µl, 0.54 mmol, 6 eq). The crude product was purified by flash chromatography on silica gel (CH_2Cl_2/MeOH, 95:5) to afford the desired product as white foam (31 mg, 35%).

^{1}H NMR (400 MHz, MeOD) δ 7.62 – 7.01 (m, 4H), 6.68 (s, 1H), 5.44 (d, J = 15.3 Hz, 1H), 5.06 (dd, J = 11.8, 3.2 Hz, 1H), 4.65 – 4.55 (m, 1H), 4.32 – 4.19 (m, 2H), 4.07 (d, J = 15.3 Hz, 1H), 3.84 (s, 4H), 3.72 (dd, J = 33.2, 14.8 Hz, 3H), 3.30 – 3.12 (m, 3H), 2.91 (dd, J = 14.7, 3.3 Hz, 2H), 2.69 (s, 3H), 2.63 (s, 3H), 2.40 – 2.22 (m, 1H), 2.14 (s, 3H), 1.91 – 1.74 (m, 2H), 1.73 – 1.56 (m, 5H), 1.50 (s, 9H); ^{13}C NMR (101 MHz, MeOD) δ 175.8, 172.5, 171.8, 170.9, 170.5, 168.4, 167.1, 162.7, 162.4, 159.2, 157.5, 138.7, 137.1, 136.4, 134.0, 129.3, 129.2, 128. 8, 128.7, 128.34, 128.3, 125.0, 112.1, 112.09, 82.9, 59.7, 55.3, 54.3, 51.3, 50.1, 47.2, 41.9, 39.2, 38.5, 37.8, 30.0, 29.0,

27.4, 26.5, 23.6, 18.1, 11.4; MS (ESI) *m/z* calcd for $[C_{40}H_{56}N_9O_{11}S]^+$: 870.38 $[M+H]^+$; found: 870.8.

***Cyclo* [*iso*Asp-Gly-Arg-DKP] (118) (119)**

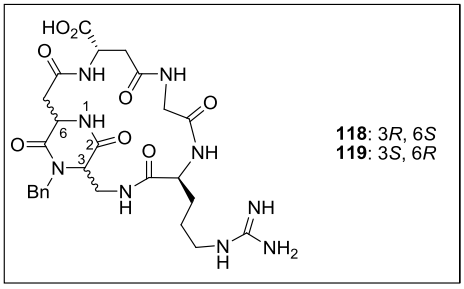

118: 3*R*, 6*S*
119: 3*S*, 6*R*

$C_{26}H_{35}N_9O_8$
MW: 601,61

(118) *Cyclo* [*iso*Asp-Gly-Arg-DKP2]

Compound **122 a** (41 mg, 0.05 mmol) was fully deprotected in the conditions described in general procedure **GP5**. The crude product was purified by HPLC (Water's Atlantis 21 mm x 10 cm column, gradient: 90% H_2O / 10% acetonitrile to 40% H_2O / 60% acetonitrile) to give the desired compound (as trifluoroacetate salt) as white solid (7 mg, 24%)

MS (ESI) *m/z* calcd for $[C_{26}H_{36}N_9O_8]^+$: 602,27 $[M+H]^+$; found: 602,3.

(119) *Cyclo* [*iso*Asp-Gly-Arg-DKP3]

Compound **122 b** (31 mg, 0.035 mmol) was fully deprotected in the conditions described in general procedure **GP5**. The crude product was purified by HPLC (Water's Atlantis 21 mm x 10 cm column, gradient: 90% H_2O / 10% acetonitrile to 60% H_2O / 40% acetonitrile) to give the desired compound (as trifluoroacetate salt) as white solid (6 mg, 29%).

MS (ESI) *m/z* calcd for $[C_{26}H_{36}N_9O_8]^+$: 602,27 $[M+H]^+$; found: 602,2.

5 - Synthesis of α/β-peptide foldamer [DKP1-Ala-Ala]$_2$-DKP1-NH$_2$ (127)

(S)-N-(((2S,5S)-5-(2-amino-2-oxoethyl)-1-benzyl-3,6-dioxopiperazin-2-yl)methyl)-2-((S)-2-(2-((2S,5S)-5-(((S)-2-((S)-2-(2-((2S,5S)-5-(aminomethyl)-4-benzyl-3,6-dioxopiperazin-2-yl) acetamido)propanamido)propanamido)methyl)-4-benzyl-3,6-dioxopiperazin-2-yl) acetamido)propanamido)propanamide (127)

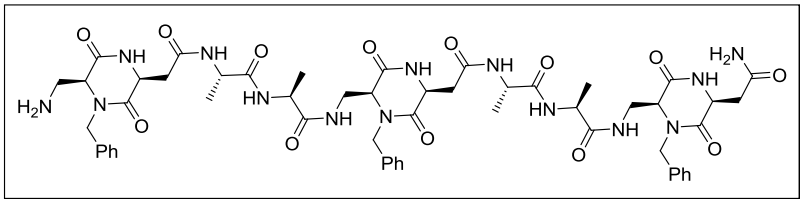

$C_{54}H_{68}N_{14}O_{13}$
MW: 1121,20

GENERAL REMARKS: The synthesis was carried out by manual coupling using Fmoc/*t*Bu strategy on the acid labile Rink amide MBHA resin (loading 0.6 mmol/g) pre-modified with an Fmoc

protecting group on a 0.1 mmol scale. Swelling of the resin was achieved suspending it in either DCM or DMF for 15 min.
Resin Fmoc deprotection was aceived following general procedure **GP6**.

COUPLING REACTIONS:
Fmoc-α-amino acid residues: A 1M solution (in either a 1:1 mixture of DCM/DMF or dioxane) of the appropriate *N*-Fmoc-protected succinimidyl ester (0.4 mmol, 4 eq.) was added to the resin, which was gently shaken for 2-18 h. The resin was washed in the order with DMF (4x), DCM (4x), *i*PrOH (3x) and/or Et_2O (2x). Kaiser test was performed. If resin gives a positive colour test, coupling procedure was repeated with fresh reagents (half of the amounts). After a maximum of 3 coupling cycles, capping was performed (see general procedure **GP9**). Preparation of amino acid succinimidyl esters: DCC (1.1 eq) was added to a stirring solution of the appropriate Fmoc-amino acid and *N*-hydroxy succinimide in dry THF, at 0 °C. The reaction mixture was stirred at 0° C for 4 h, and then allowed to stand in a refrigerator at 0° C for 16 h. The separated solid was removed by filtration and washed with THF (2x). The filtrate and washings were combined, and volatiles were removed at reduced pressure. The residue was dissolved in a small amount of DCM, and solution was filtered to remove insoluble material. Removal of volatiles at reduced pressure gave a foamy solid, which might be crystallized from a 1:1 mixture of DCM:PE. The isolated solid could be stored at -20 °C.
DKP1*: A sample vial equipped with a magnetic stirrer was charged **DKP1*** (80 mg, 0.25 mmol, 2.5 eq.) and HOBt (42 mg, 0.275 mmol, 2.75 eq.). A minimum amount of DMF to dissolve was added. After cooling the mixture to 0 °C DCC (57 mg, 0.275 mmol, 2.75 eq.) was added as a solution in DCM (1M), dropwise. The mixture was stirred for 20 min at the same temperature. DCU, which formed as a white solid, was let to settle and then filtered off. The solution was then added to the *N*-deblocked swelled peptidylresin (0.1 mmol, 1 eq.). The resin was gently agitated for 18 h and, after sucking off the solution, it was washed in the order with DMF (4x), DCM (4x), *i*PrOH (3x) and/or Et_2O (2x).

Exact amounts of the used amino acids for SPPS are reported in Table 5.2.

Table 5.2 - Exact amounts of the used amino acids for SPPS

REAGENTS	eq.	n (mmol)	AMOUNTS
Fmoc-L-Ala-L-Ala-OSu (**130**)	4	0.4	191 mg
Fmoc-L-Ala-OSu (**128**)	4	0.4	163 mg

Synthesis of Fmoc-L-Ala-L-Ala-OH (**129**): A solution of Fmoc-L-Ala-OSu (686 mg, 1.68 mmol, 1 eq.) in a mixture of EtOH/Acetone 4:1 was added under stirring to 2 ml of a water solution containing 150 mg of L-Ala-OH (1.68 mmol, 1 eq.) and 283 mg of $NaHCO_3$ (3.37 mmol, 2 eq.). After stirring the

mixture for 20 h, the organic solvent was evapourated and additional 15 ml of water were added. Insoluble impurities were removed by filtration. The filtrate was then acidified adding $HCl_{conc.}$, and the precipitate was collected and washed several times with water to obtain pure product in 76% yield (490 mg).

^{1}H NMR (300 MHz, $CDCl_3$) δ 7.75 (d, J = 7.5 Hz, 2H), 7.57 (d, J = 7.4 Hz, 2H), 7.39 (t, J = 7.3 Hz, 2H), 7.35 – 7.22 (m, 3H), 6.87 (d, J = 6.6 Hz, 1H), 5.57 (dd, J = 6.4, 2.9 Hz, 1H), 4.93 (p, J = 7.3 Hz, 1H), 4.45 – 4.25 (m, J = 7.0 Hz, 3H), 4.24 – 4.06 (m, J = 6.9 Hz, 1H), 3.73 (s, 1H), 2.81 (d, J = 9.5 Hz, 2H), 1.56 (d, J = 7.2 Hz, 1H), 1.42 – 1.36 (m, 2H).

Fmoc DEPROTECTION: After successful coupling, washing and Fmoc deprotecting steps were carried out as described in general procedure **GP7**. This deprotection/coupling strategy was applied for each synthetic step involving N-Fmoc protected α-amino acids.

AZIDE REDUCTION: After successful coupling of **DKP1*** building blocks, washing and azide reduction steps were carried out as described in general procedure **GP8**.

CLEAVAGE FROM RINK AMIDE RESIN:

Small cleavage: 0.5 ml of a solution of TFA, TIS and water (90:5:5) was added to a few beads of the resin in a sample vial. The mixture was gently agitated for 2 h. Cold Et_2O was added and volatiles were removed with a N_2 flux. Addition of more cold ether resulted in the precipitation of the product. Et_2O was removed with a pipette. The process was repeated twice, in order to purify the peptide. MeOH was then added, dissolving the peptide. The resin beads were separated and washed with more MeOH. Volatiles were then removed under a N_2 flux, affording the peptide.

Final cleavage: 1.5 ml of a solution of TFA, TIS and water (90:5:5) was added to the resin. The mixture was gently agitated for 2.5 h. After removal of the TFA under reduced pressure the peptides were precipitated from ice-cold diethyl ether. After filtering off the solution the peptides were acidified with conc. acetic acid and dissolved in a solution of 10 % acetic acid in water. The solvent was removed via lyophilization overnight and the crude peptides purified by preparative RP-HPLC.

60 mg of **127** were obtained (0.053 mmol, 53%).

Preparative reversed-phase HPLC of compound **127** was performed on Phenomenex Luna C18 100 Å 3 μm column (150mm x 2 mm). 97% (5.9‰ TFA in water) / 3% acetonitrile to 2% (5.9‰ TFA in water) / 98 % acetonitrile; linear gradient has been used during 30 min, at a flow rate of 0.3 mL/min, with detection at 206 nm.

^{1}H NMR (600 MHz, DMSO, 310 k) δ 8.57, 8.57, 8.32, 8.31, 8.28, 8.27, 8.21, 8.20, 8.18, 8.17, 8.09, 8.09, 8.08, 8.05, 8.04, 8.00, 7.84, 7.51, 7.35, 7.35, 7.34, 7.33, 7.33, 7.32, 7.32, 7.31, 7.29, 7.29, 7.28, 7.27, 7.27, 7.26, 7.25, 7.05, 7.05, 5.10, 5.08, 5.08, 5.06, 4.90, 4.87, 4.37, 4.37, 4.37, 4.36, 4.35, 4.35, 4.34, 4.33, 4.33, 4.32, 4.31, 4.30, 4.28, 4.28, 4.27, 4.27, 4.26, 4.26, 4.15, 4.13, 4.13, 4.11, 4.09, 4.08, 4.07, 4.07, 3.79, 3.79, 3.78, 3.77, 3.62, 3.60, 3.60, 3.59, 3.59, 3.59, 3.59, 3.59, 3.58, 3.58, 3.57, 2.84, 2.83, 2.81, 2.80, 2.76, 2.76, 2.75, 2.74, 2.74, 2.74, 2.73, 2.72, 2.72, 2.70, 2.70, 2.69, 2.68, 2.68, 2.67,

2.66, 2.64, 2.64, 2.62, 2.62, 2.61, 2.61, 1.26, 1.25, 1.24, 1.23, 1.21, 1.20, 1.20, 1.19; MS (ESI) *m/z* calcd for $[C_{54}H_{69}N_{14}O_{13}]^+$: 1121.52 $[M+H]^+$; found: 1121.7.

References:

[1] Y. Huang, D. R. Dalton, P. J. Carroll, *J. Org. Chem.* **1997**, *62*, 372-376.

[2] C. M. Thompson, J. A. Frick, D. L. Green, *J. Org. Chem.* **1990**, *55*, 111-116.

[3] K. L.Webster, A. B.Maude, M. E. O'Donnell, A. P. Mehrotra, D. J. Gani, *Chem. Soc. Perkin Trans. 1* **2001**, 1673-1695.

[4] M.C. Pirrung, S.W. Shuey, *J. Org. Chem.* **1994**, *59*, 3890-3897.

[5] S H. Rosenberg, K. P. Spina, K. W. Woods, J. Polakowski, D. L. Martin, Z. Yao, H. H. Stein, J. Cohen, J. L. Barlow, D. A. Egan, K. A. Tricarico, W. R. Baker, H. D. Kleinert, *J. Med. Chem.* **1993**, *36*, 449-459.

[6] K. Gu, L. Bi, M. Zhao, C. Wang, J. Juc, S. Peng, *Bioorg. Med. Chem.* **2007**, *15*, 6273-6290.

[7] J. M. Humphrey, R. J. Bridges, J. A. Hart, A. R. Chamberlin, *J. Org. Chem.* **1994**, *59*, 2467-2472.

[8] V. Bavetsias, A. L. Jackman, R. Kimbell, W. Gibson, F. T. Boyle, G. M. F. Bisset, *J. Med. Chem.* **1996**, *39*, 73-85.

[9] Y. Narukawa, K. N. Juneau, D. Snustad, D. B. Miller, L. S. Hegedus, *J. Org. Chem.* **1992**, *57*, 5453-5462.

[10] W. C. Still, M. Kahn, A. Mitra, *J. Org. Chem.* **1978**, *43*, 2923-2925.

[11] W. Xie, D. Ding, W. Zi, G. Li, D. Ma, *Angew. Chem. Int. Ed.* **2008**, *47*, 2844-2848.

APPENDIX OF NMR DATA

50: β-allyl aspartic acid hydrochloride

^{1}H NMR (400 MHz, D_2O):

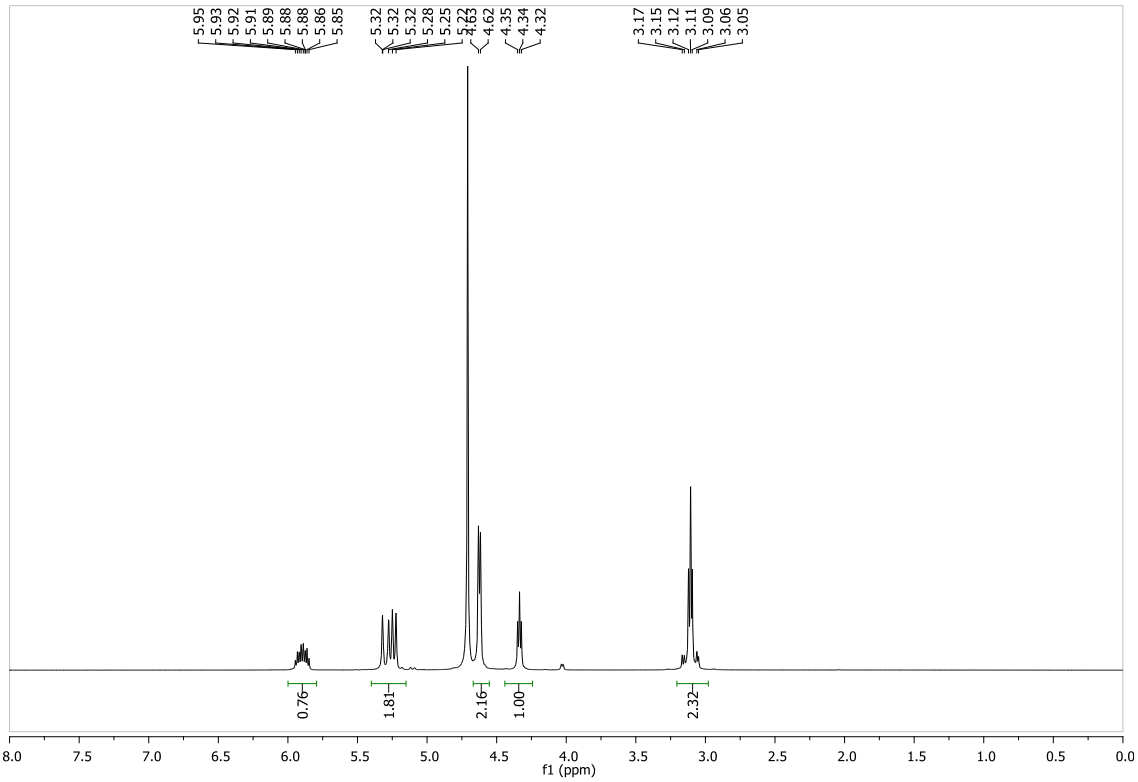

51: *N*-Boc-β-allyl aspartic acid

^{1}H NMR (300 MHz, $CDCl_3$):

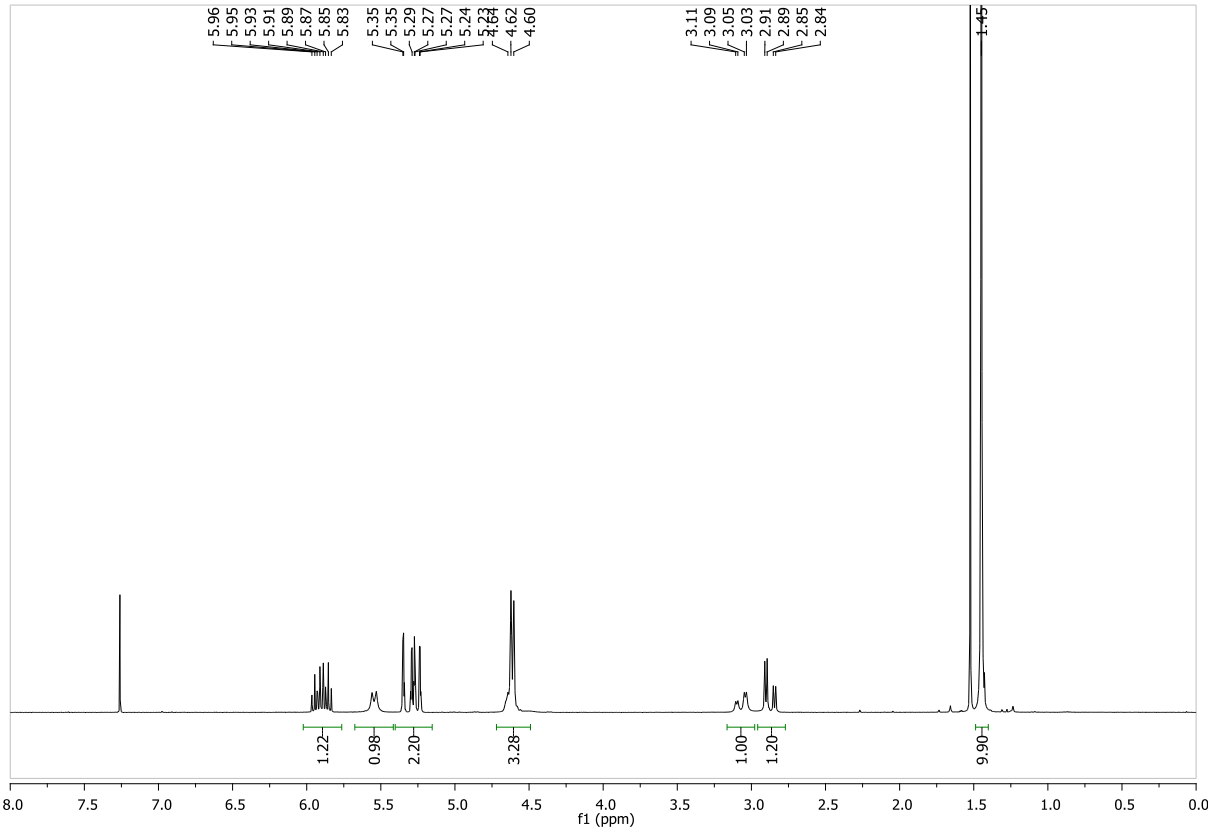

52: serine methylester hydrochloride

^{1}H NMR (300 MHz, D_2O):

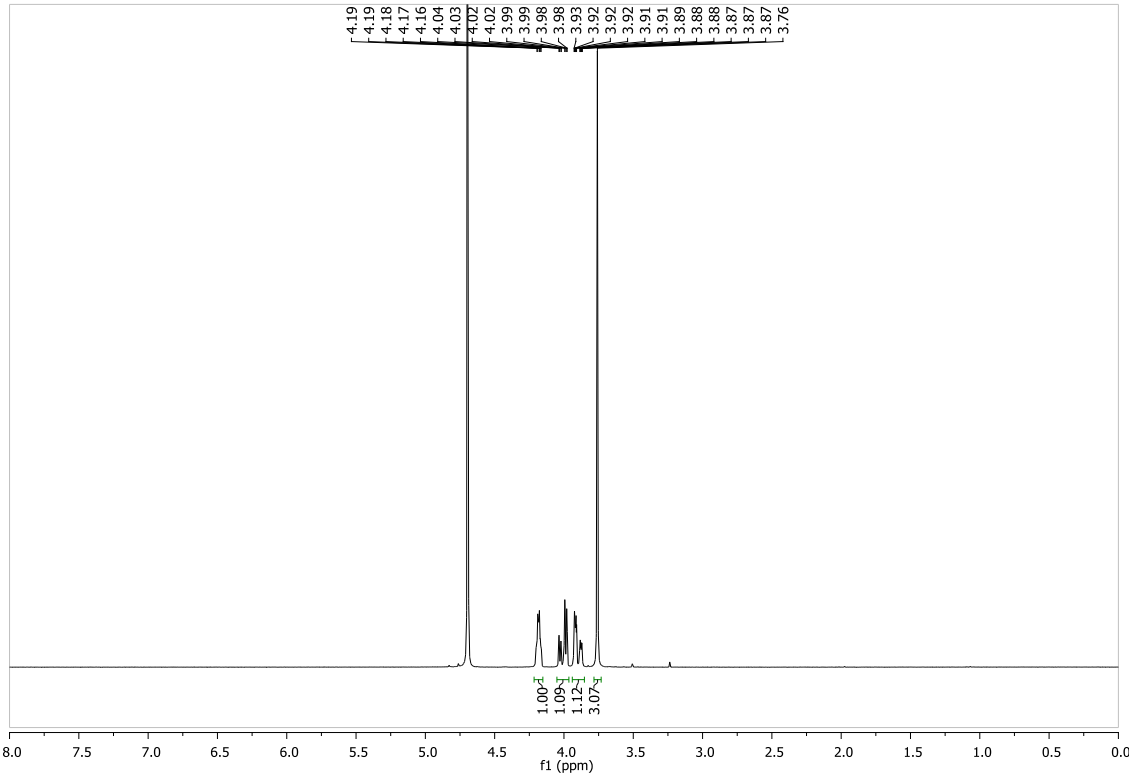

53: *N*-Bn-Ser-OMe

^{1}H NMR (300 MHz, $CDCl_3$):

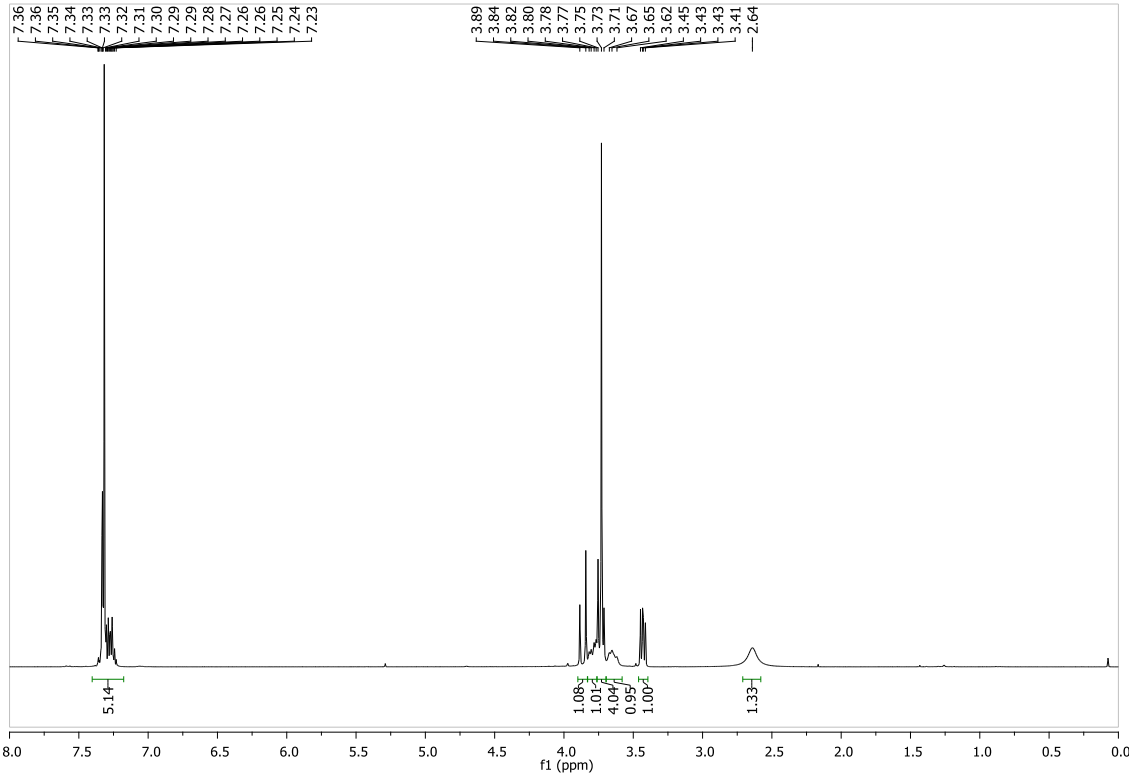

55 a + b: *N*-Bn-Ser(O-(*S*)-*N*-Boc-Asp(OAll))-OMe

^{1}H NMR (300 MHz, $CDCl_3$):

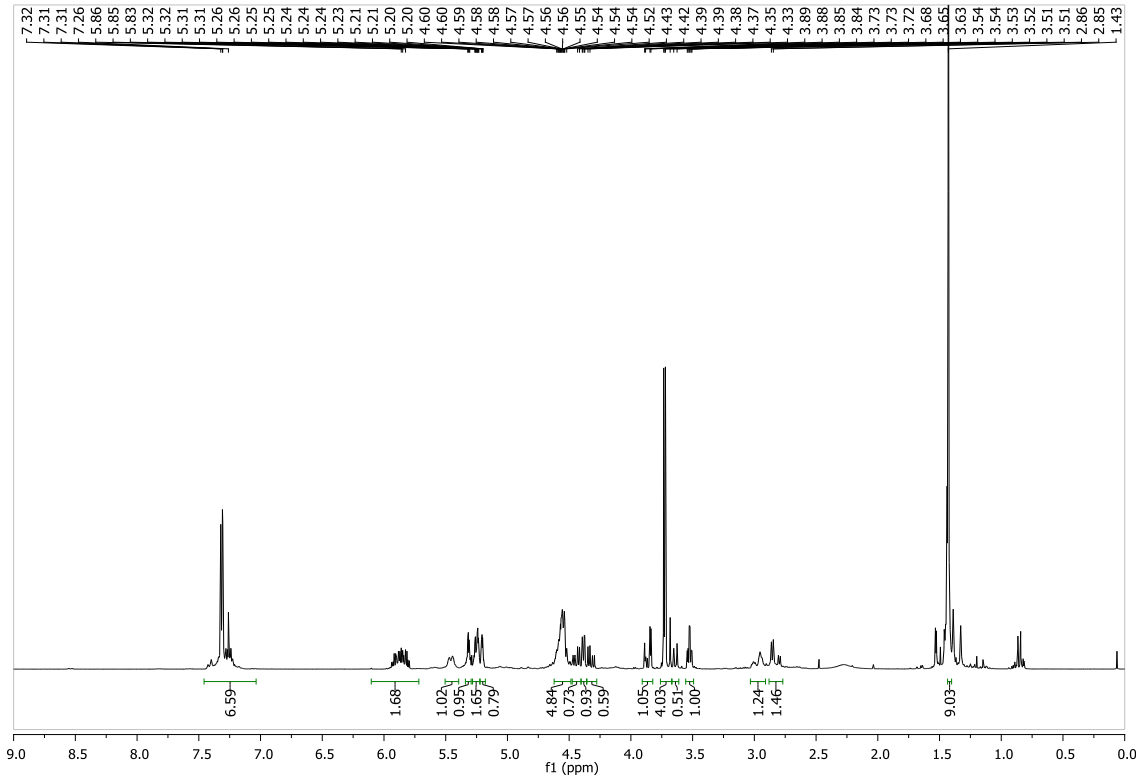

55 c: (*S*)-*N*-Bn-Ser(O-(*R*)-*N*-Boc-Asp(OAll))-OMe

^{1}H NMR (400 MHz, CD_2Cl_2):

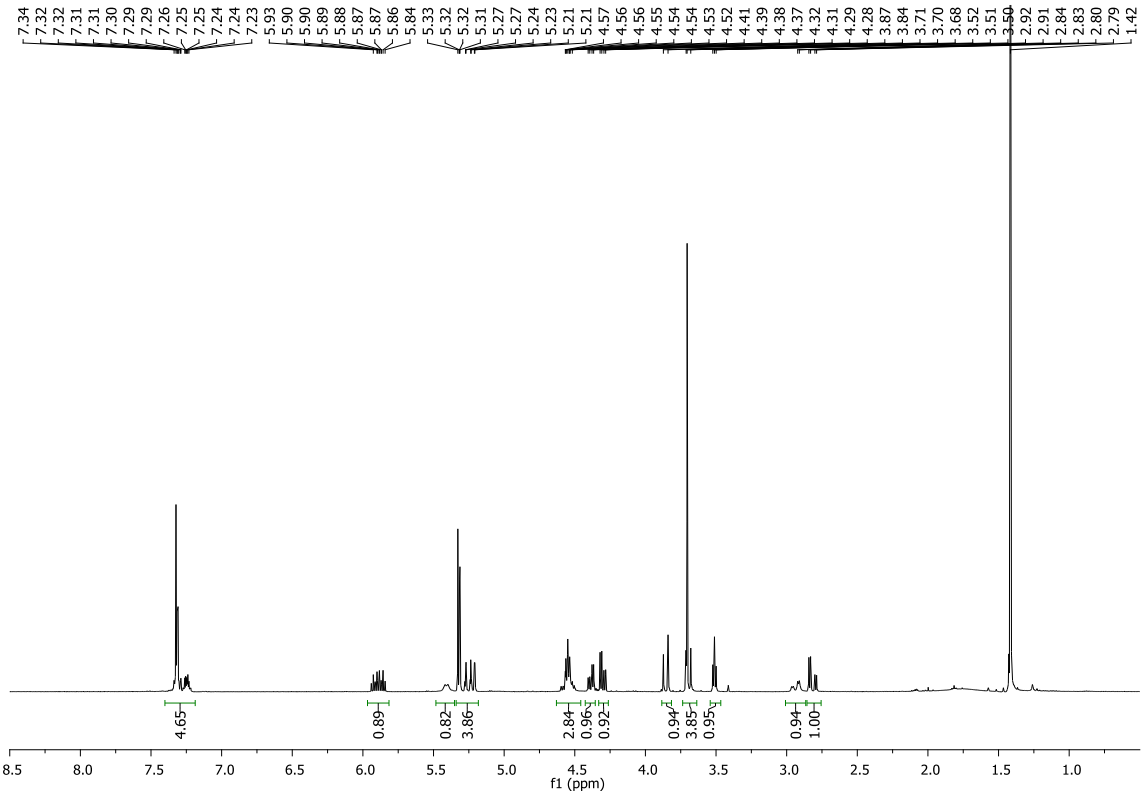

^{13}C NMR (101 MHz, CD_2Cl_2):

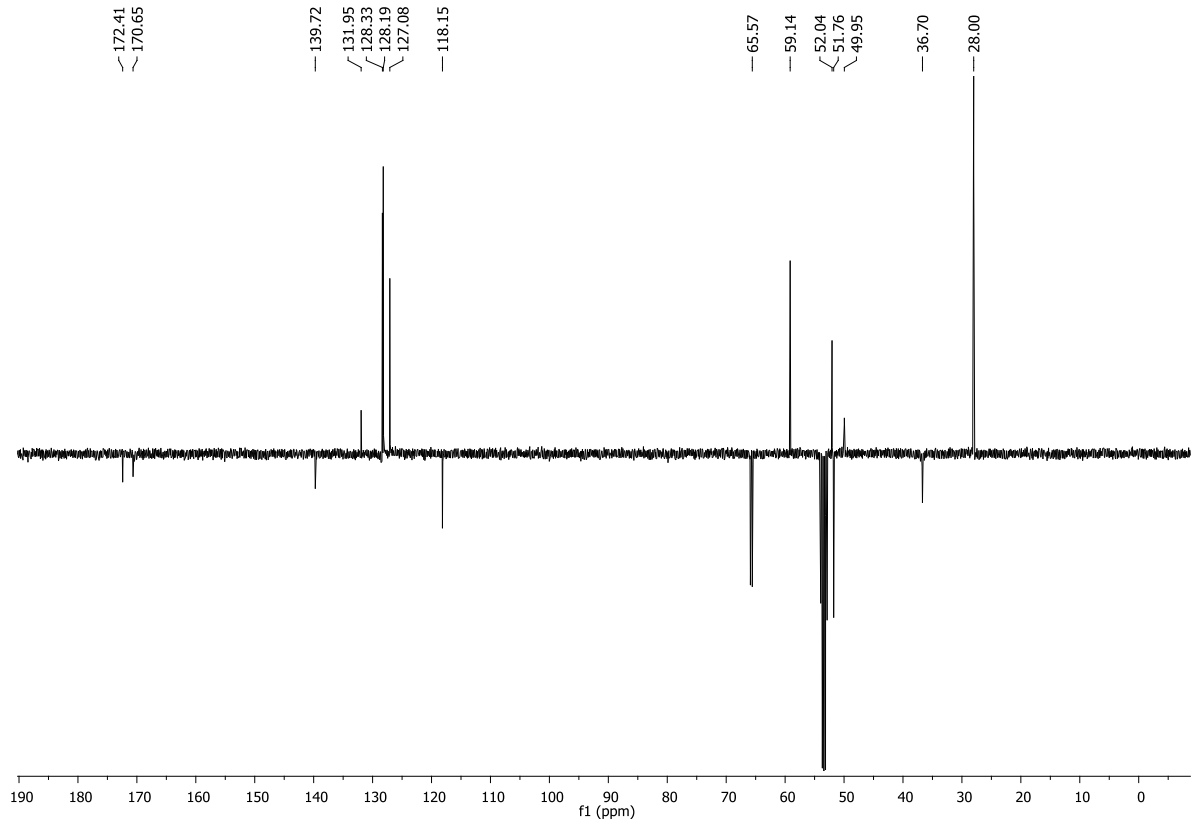

57 c: (*S*)-*N*-Bn-Ser(O-(*R*)-Asp(OAll))-OMe bis-trifluoroacetate

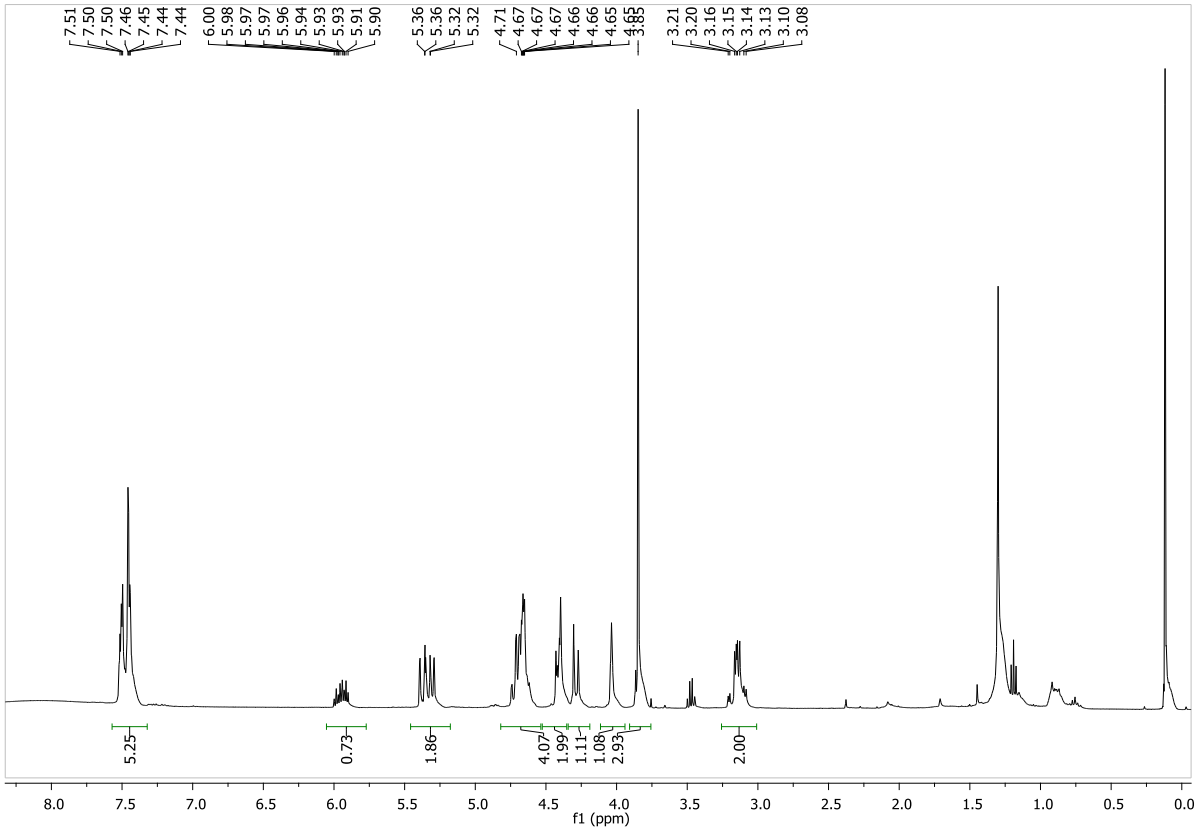

49 a: OH-DKP1-OAll

^{1}H NMR (300 MHz, $CDCl_3$):

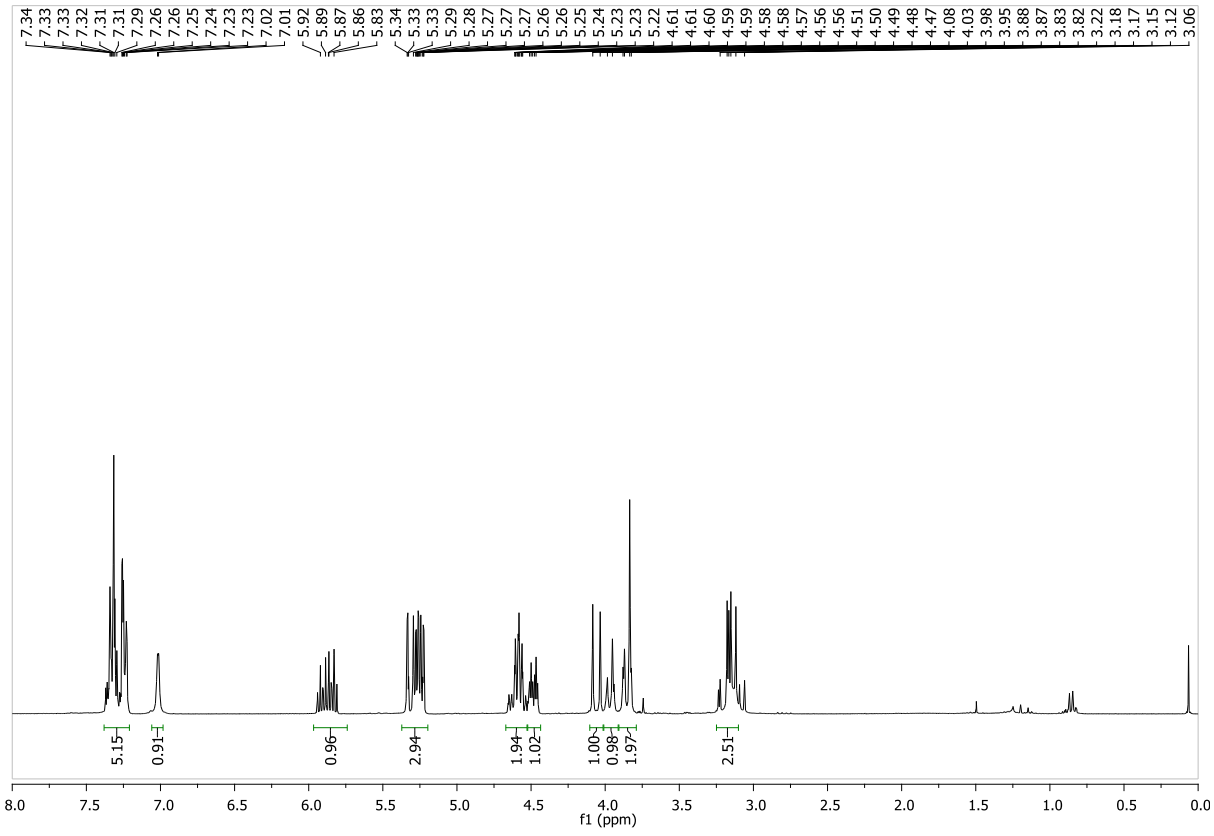

49 c: OH-DKP3-OAll

^{1}H NMR (400 MHz, CD_2Cl_2):

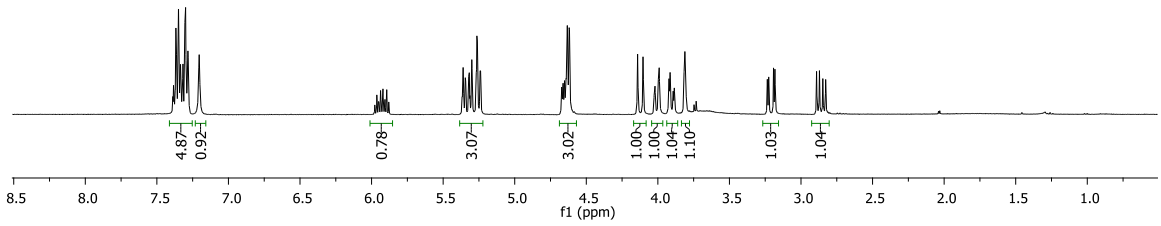

^{13}C NMR (101 MHz, CD_2Cl_2)

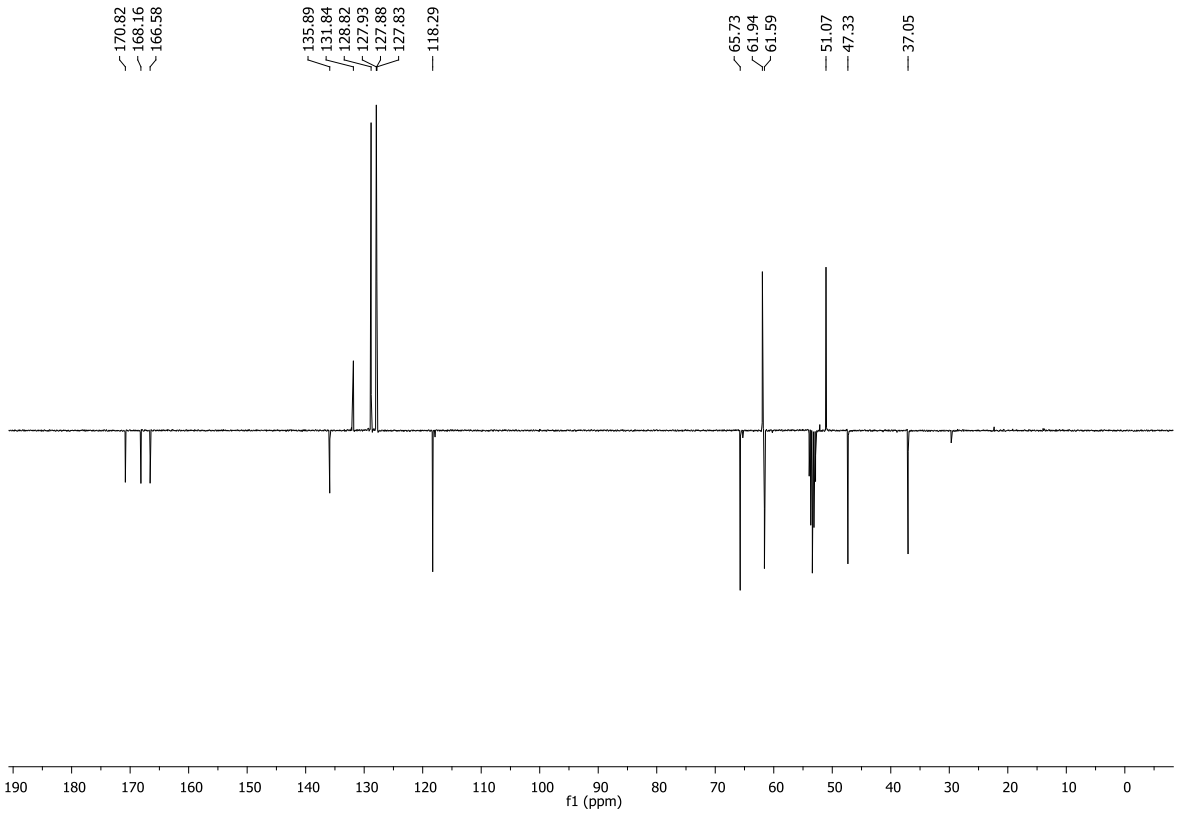

58 a: N_3-DKP1-CO_2Allyl + 60 a: H_2C=DKP-CO_2Allyl

^{1}H NMR (300 MHz, $CDCl_3$):

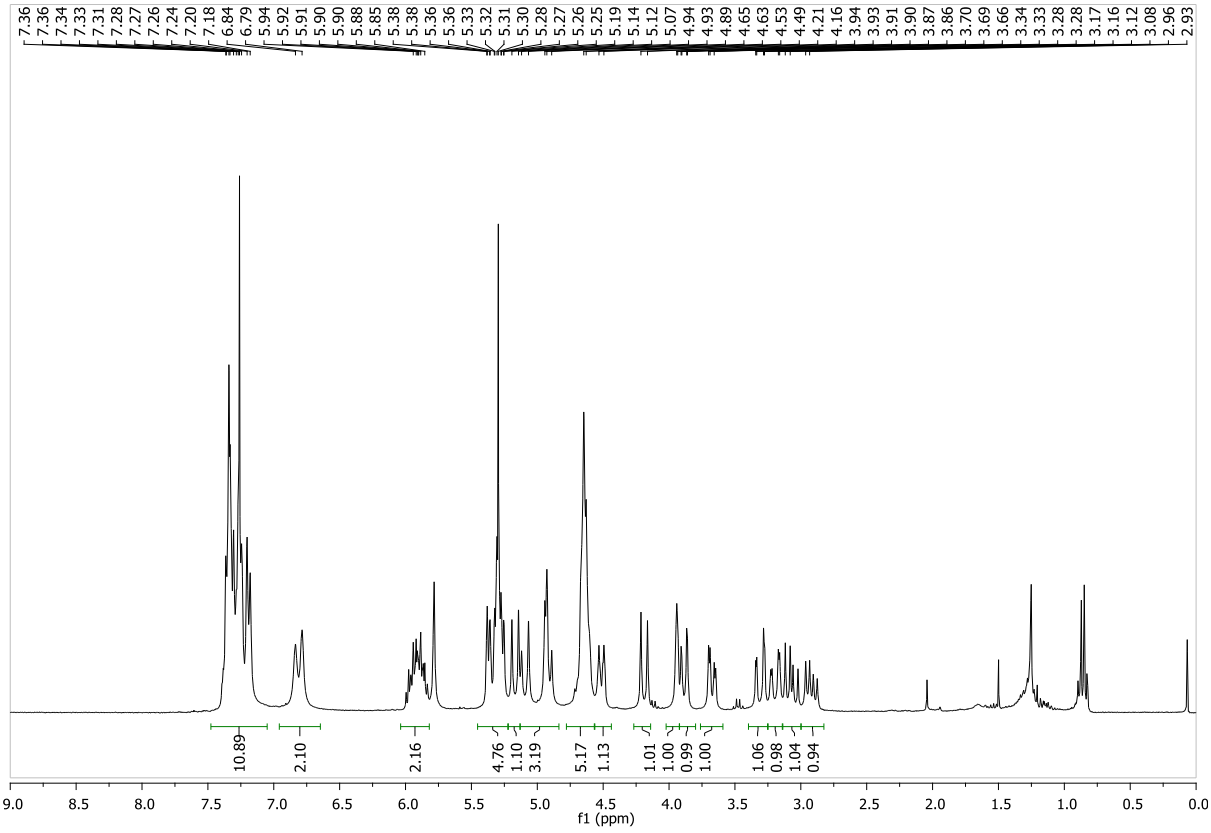

58 c: N_3-DKP3-CO_2Allyl

^{1}H NMR (400 MHz, CD_2Cl_2):

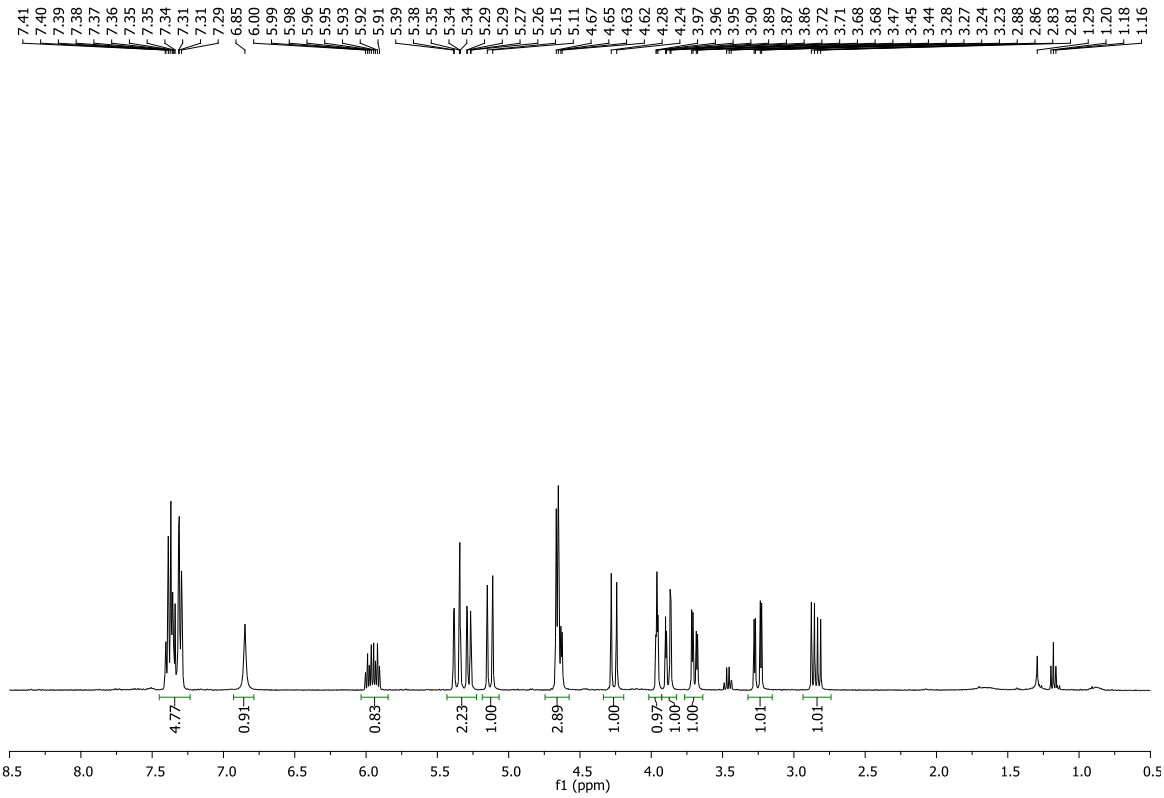

^{13}C NMR (101 MHz, CD_2Cl_2):

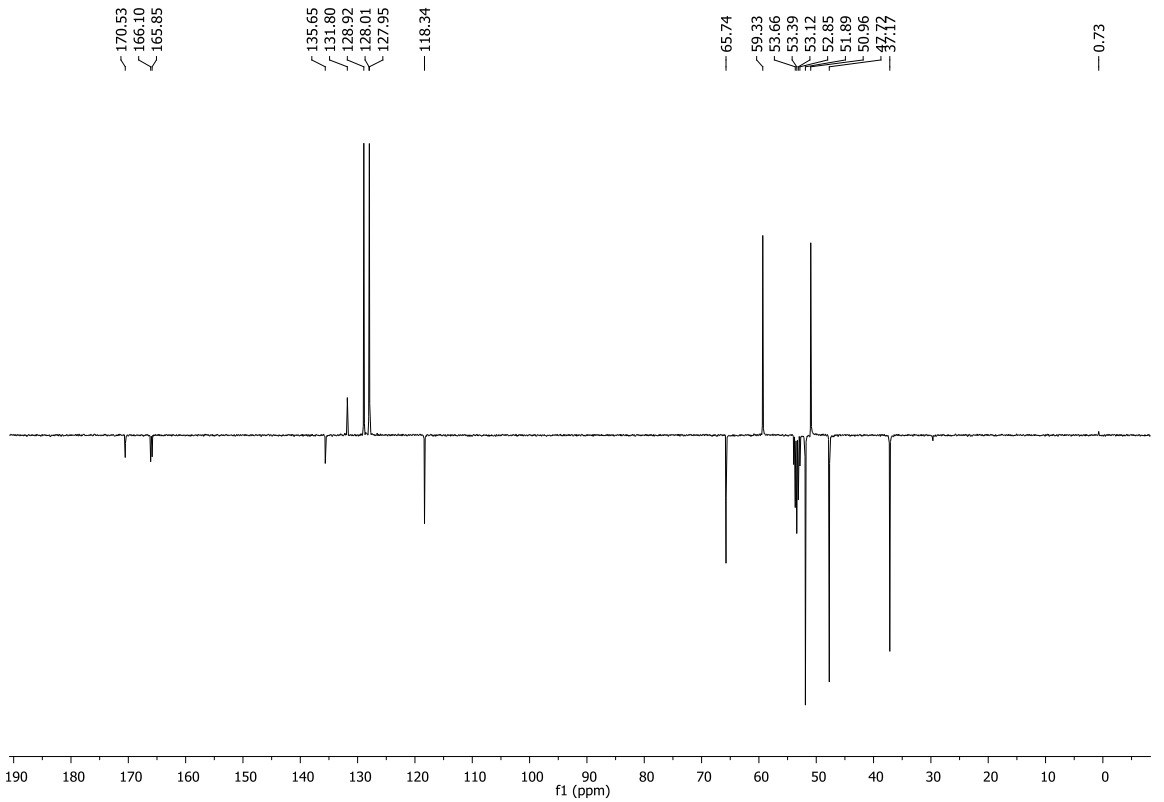

59 c: *N*-Boc-DKP3- CO_2Allyl

^{1}H NMR (400 MHz, CD_2Cl_2):

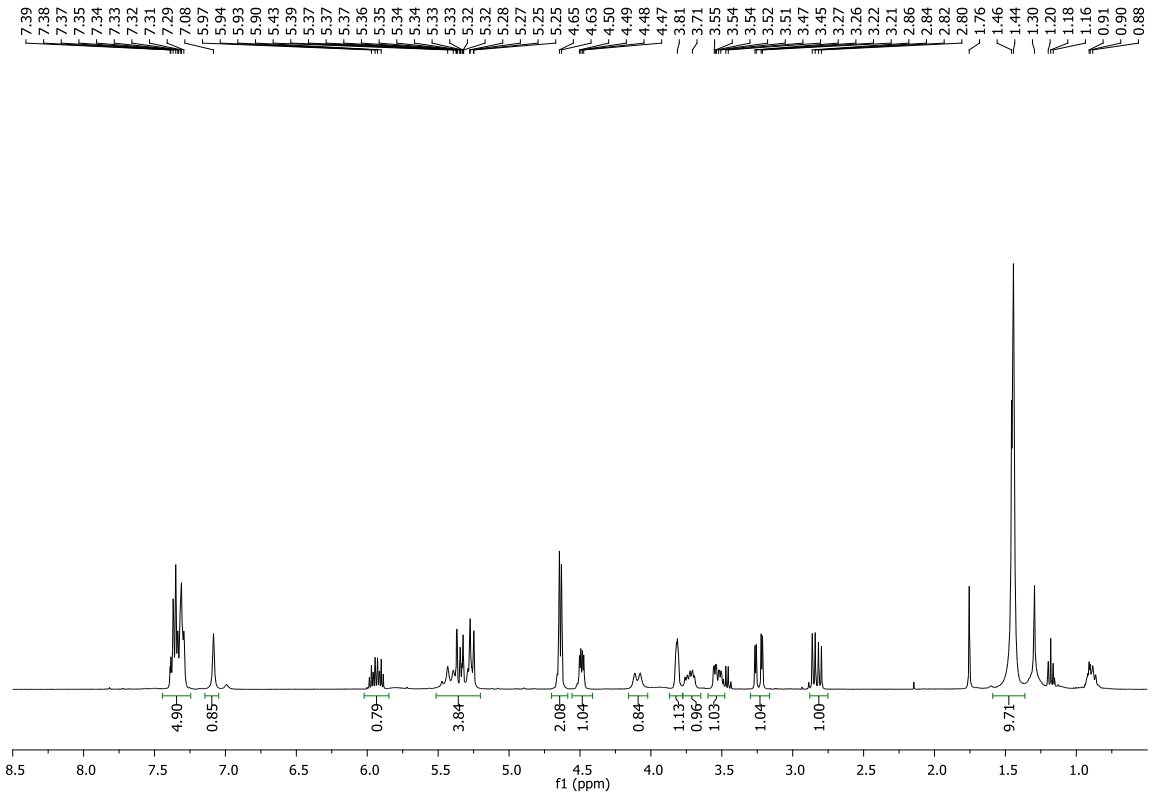

^{13}C NMR (101 MHz, CD_2Cl_2):

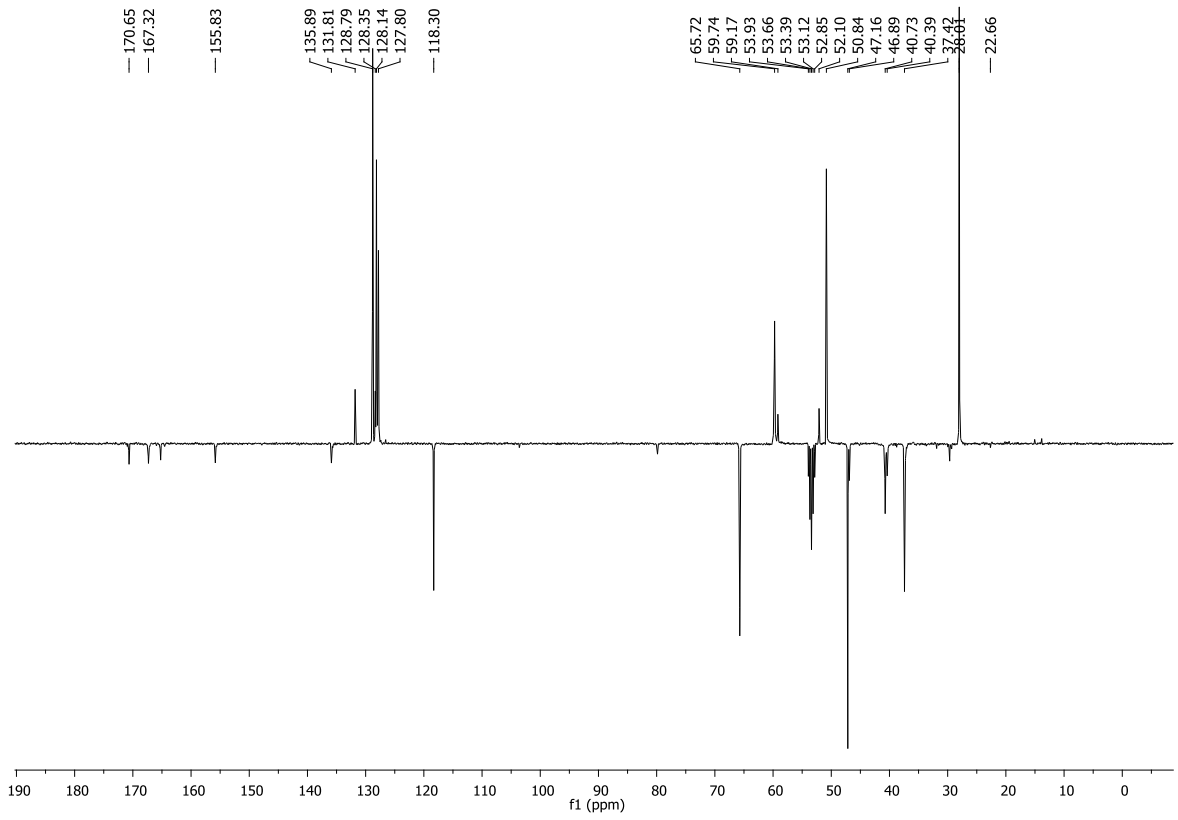

DKP1* - ^{1}H NMR (300 MHz, $CDCl_3$):

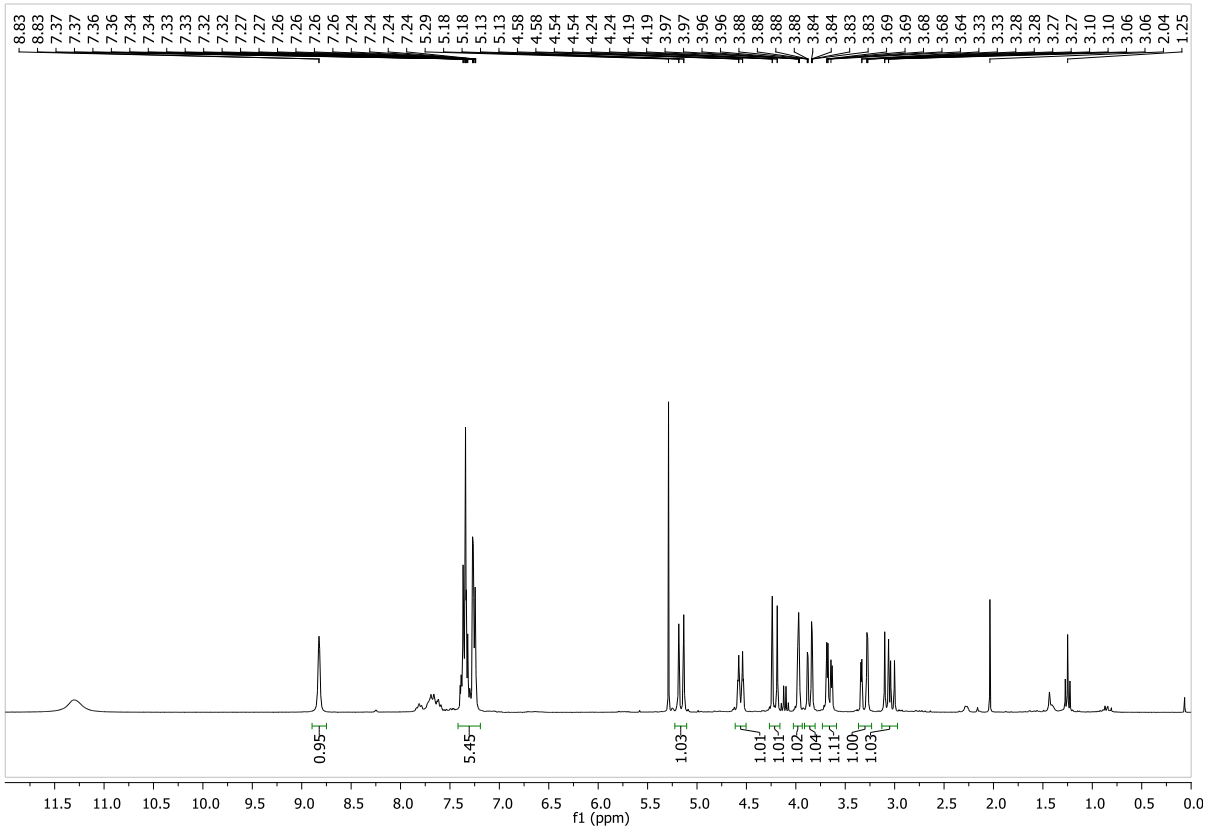

DKP3* - ^{1}H NMR (400 MHz, $CDCl_3$):

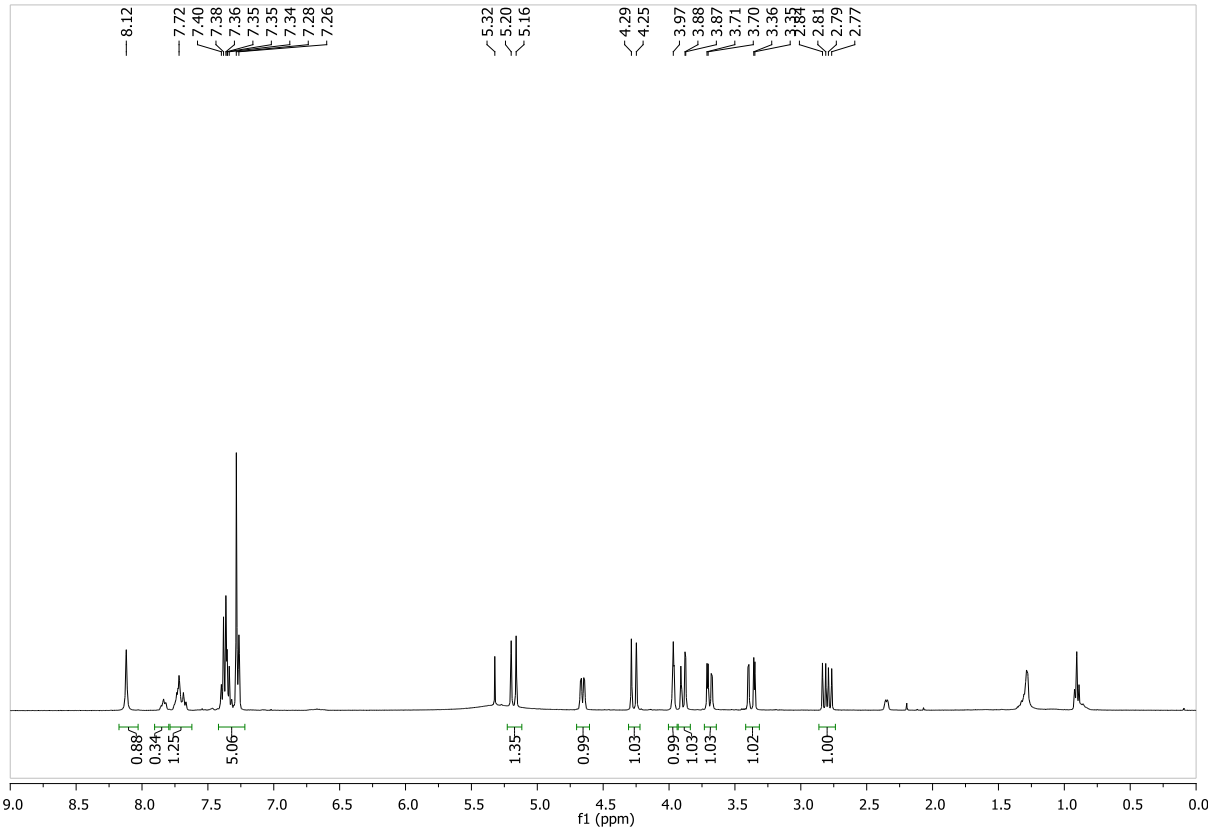

72 a: *N*-Boc-(*R*)-Ser(N_3)-*N*-Bn-(*S*)-Asp(OMe)-OMe

^{1}H NMR (400 MHz, CD_2Cl_2):

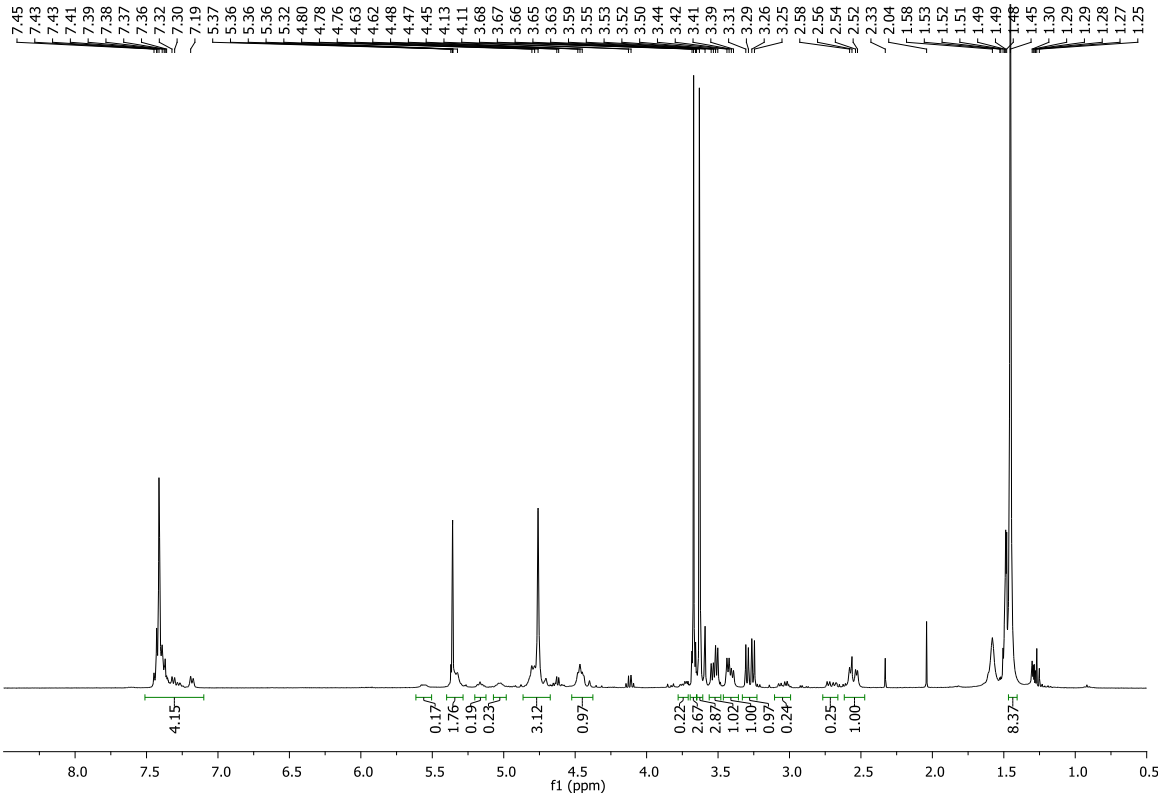

^{13}C NMR (101 MHz, CD_2Cl_2):

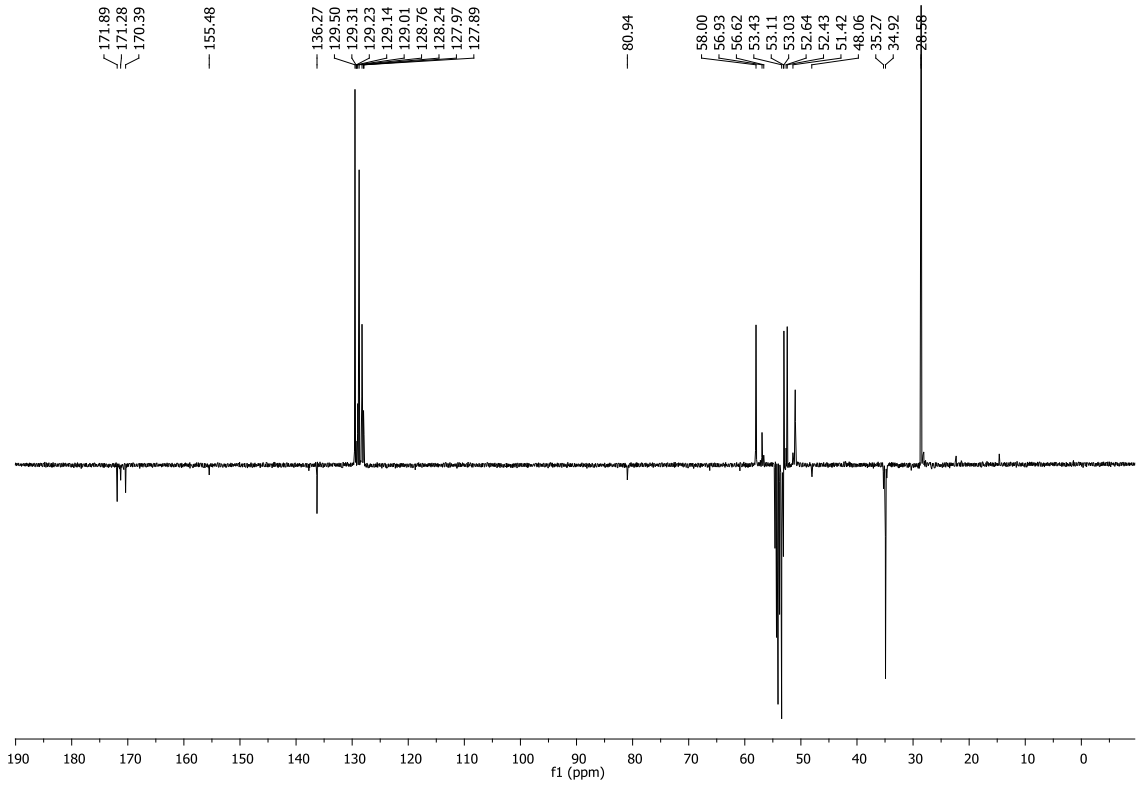

66 a: N_3-DKP4-CO_2Me

^{1}H NMR (400 MHz, CD_2Cl_2):

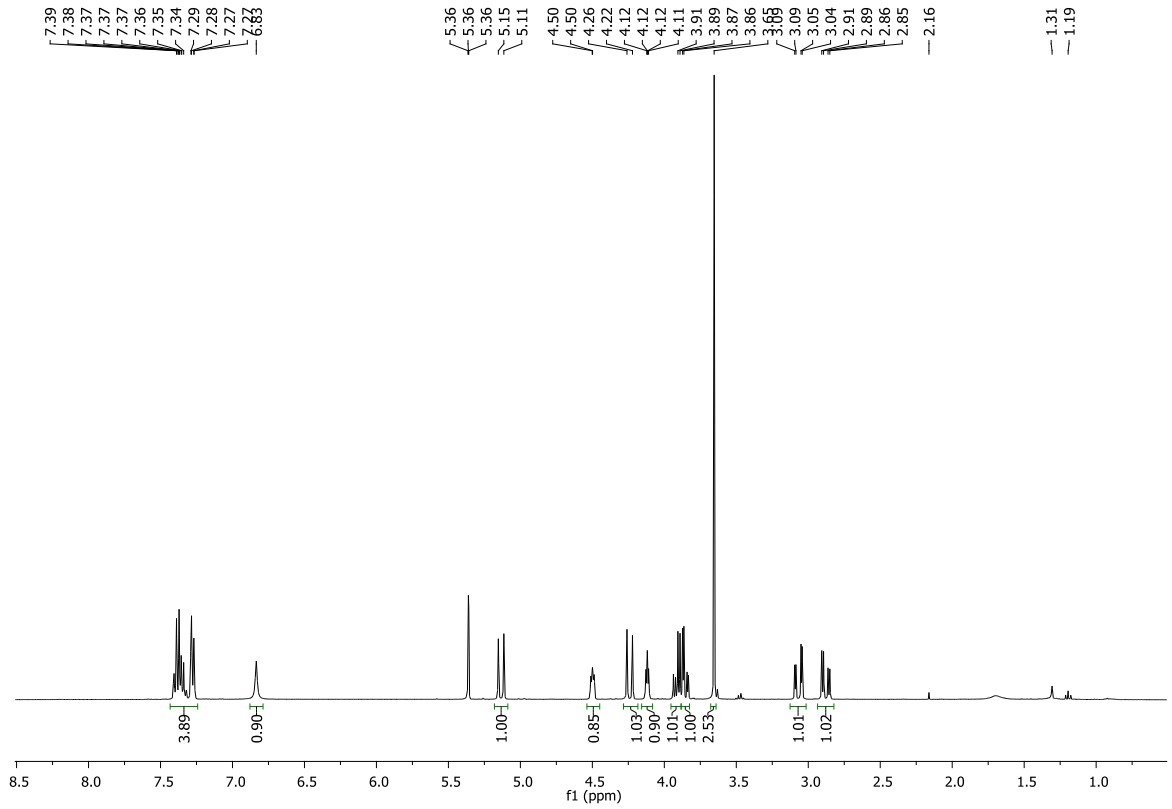

^{13}C NMR (101 MHz, CD_2Cl_2):

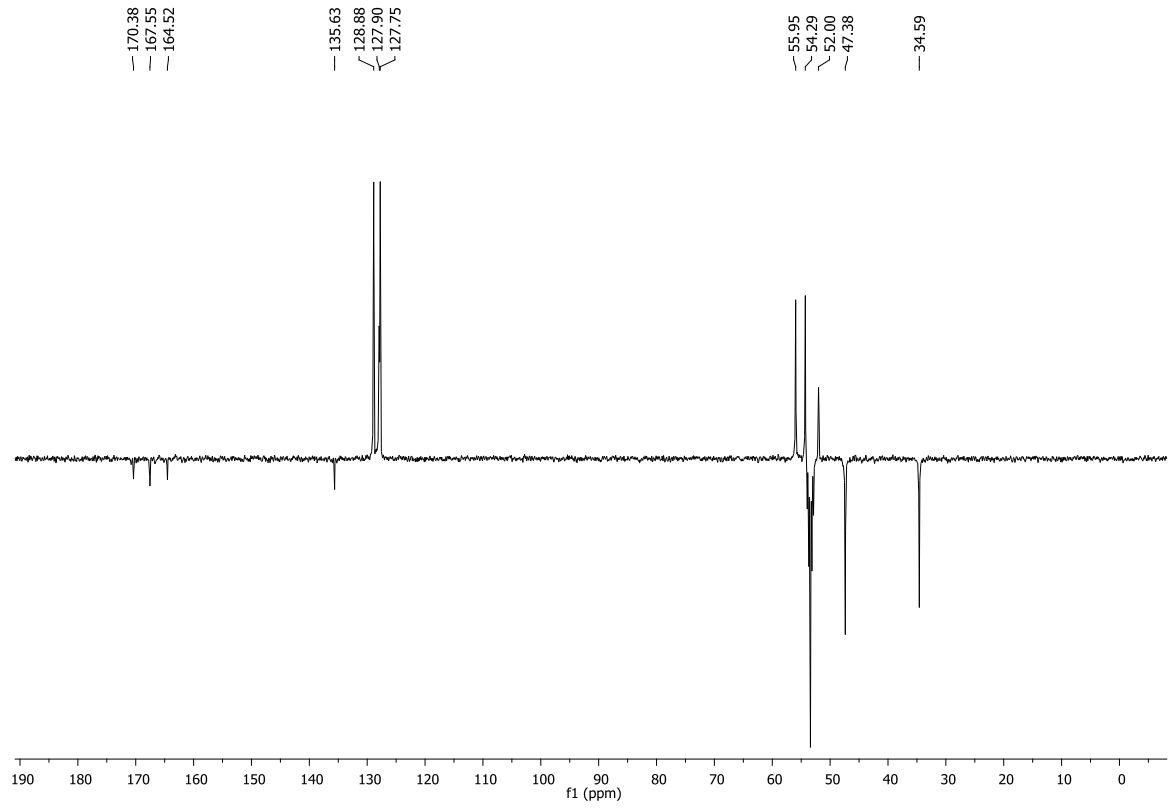

73 a: NH_2-DKP4-CO_2Me

^{1}H NMR (400 MHz, CD_2Cl_2):

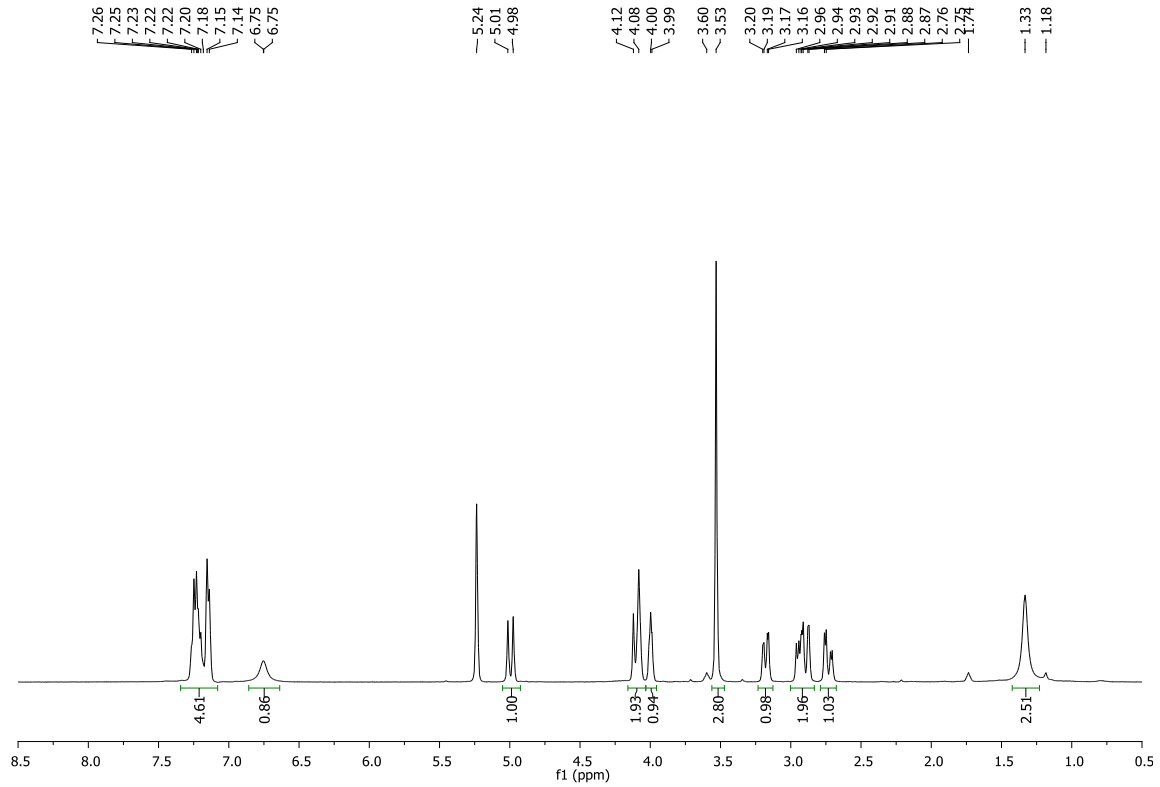

^{13}C NMR (101 MHz, CD_2Cl_2):

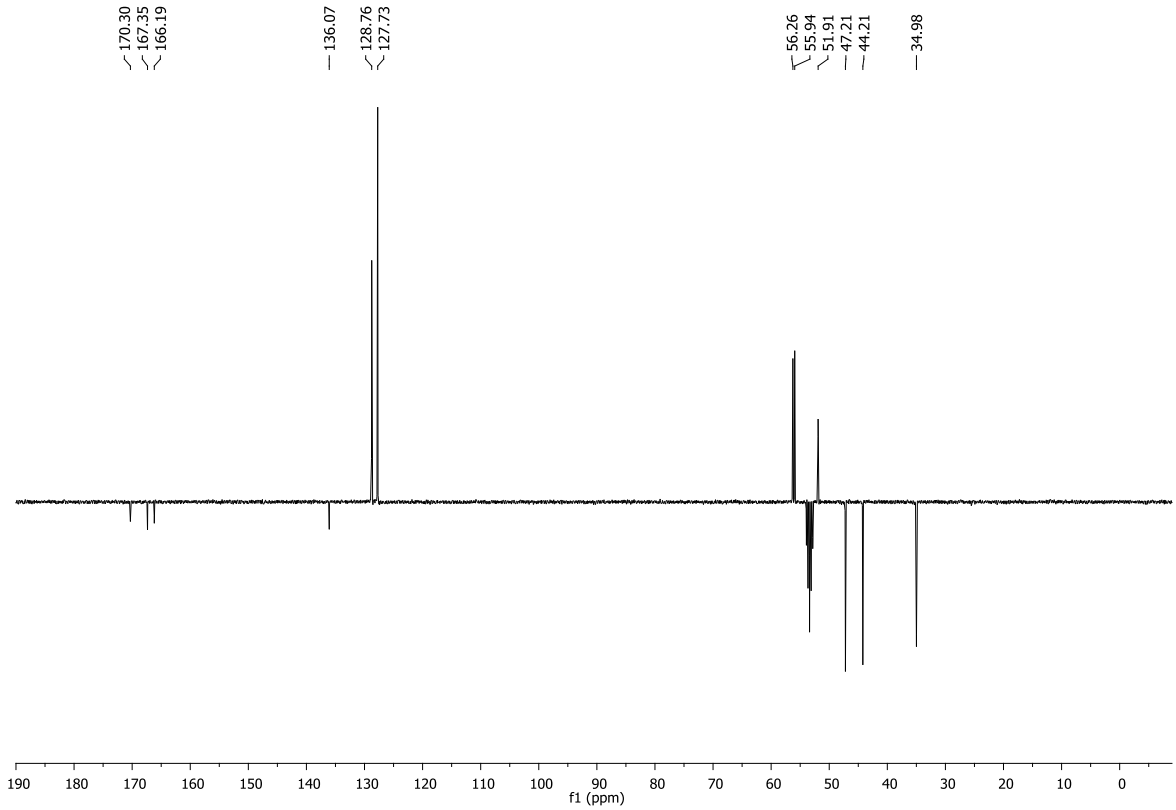

74 a: NHBoc-DKP4-CO_2Me

^{1}H NMR (400 MHz, CD_2Cl_2):

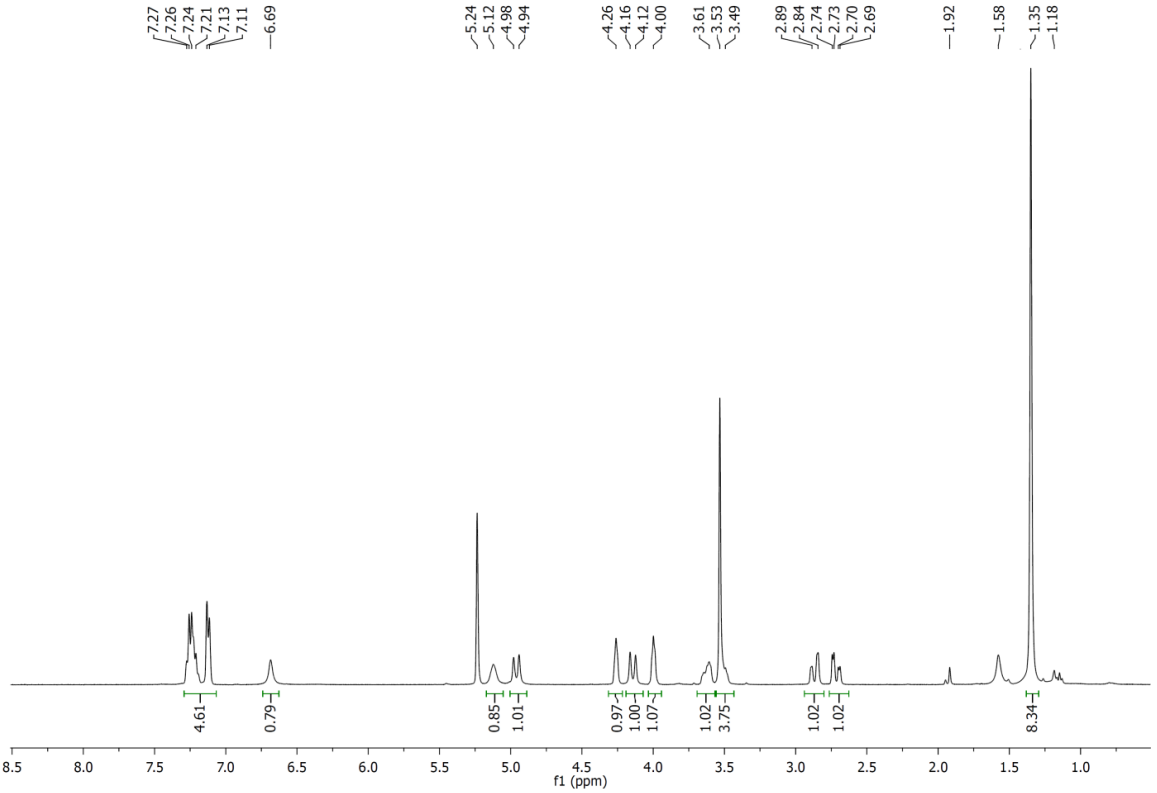

^{13}C NMR (101 MHz, CD_2Cl_2):

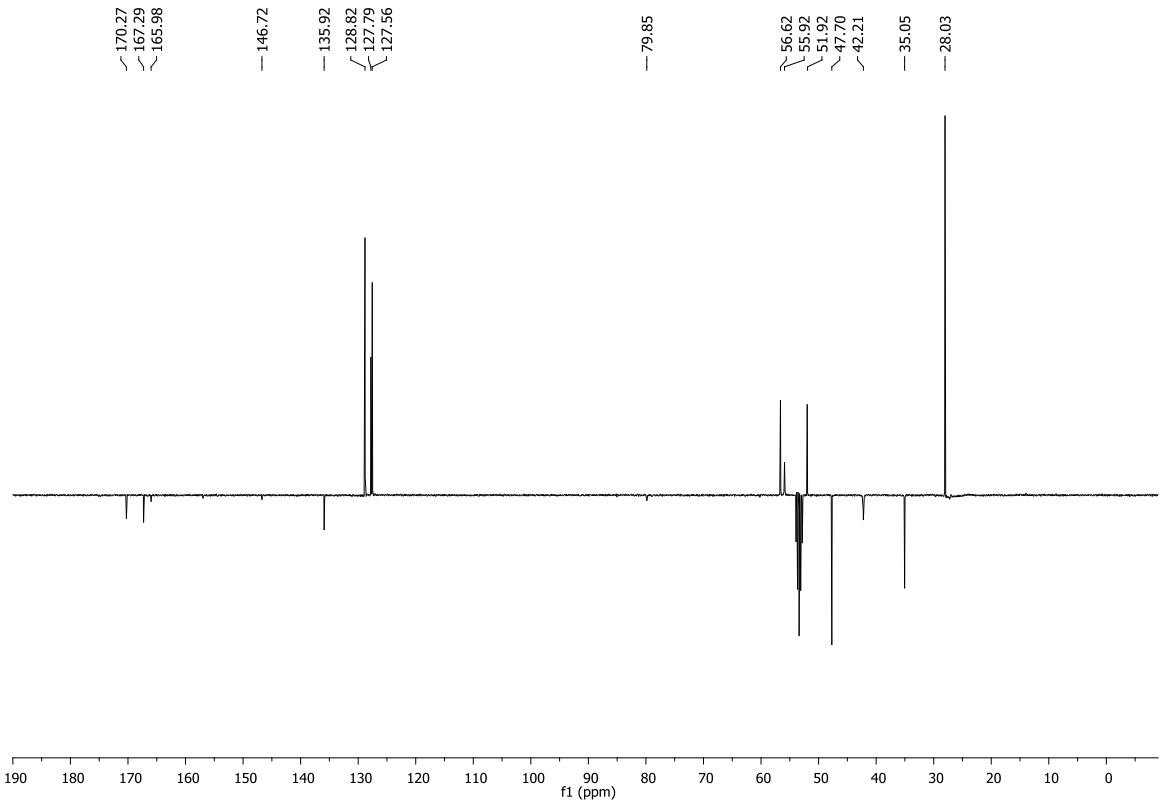

77 b: N_3-DKP7-CO_2Me

^{1}H NMR (400 MHz, CD_2Cl_2):

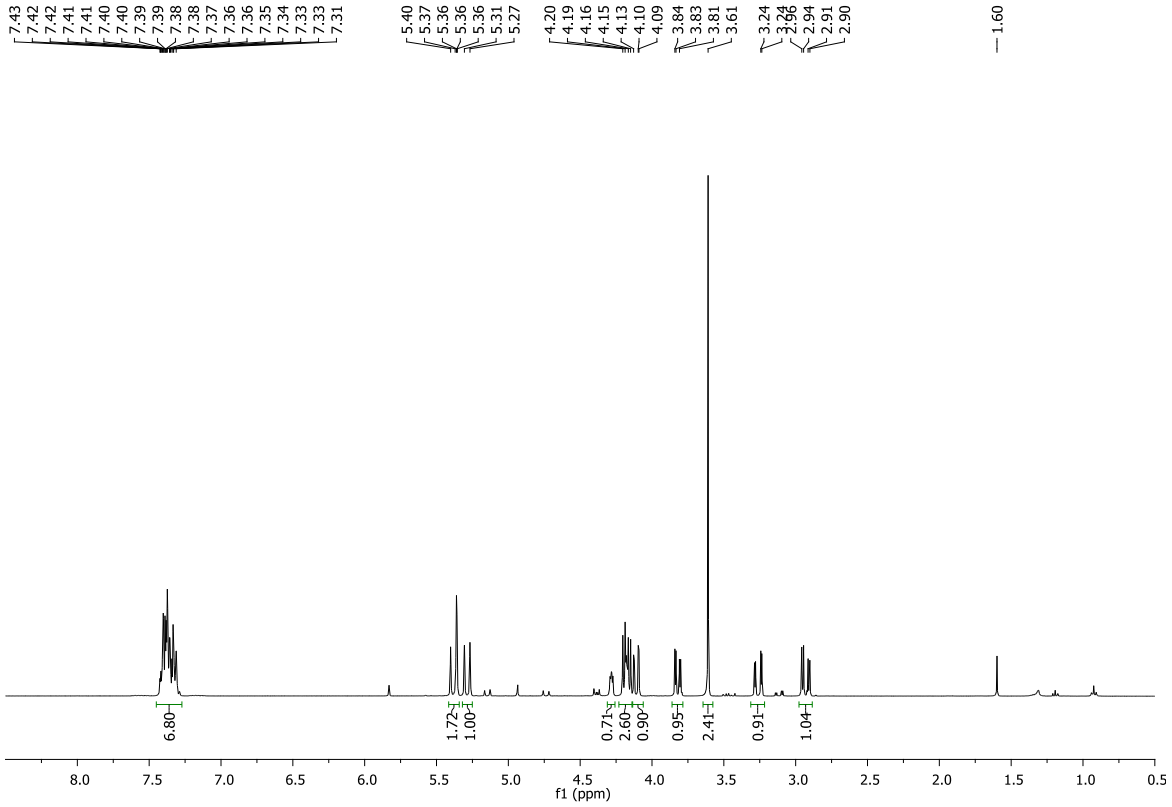

^{13}C NMR (101 MHz, CD_2Cl_2):

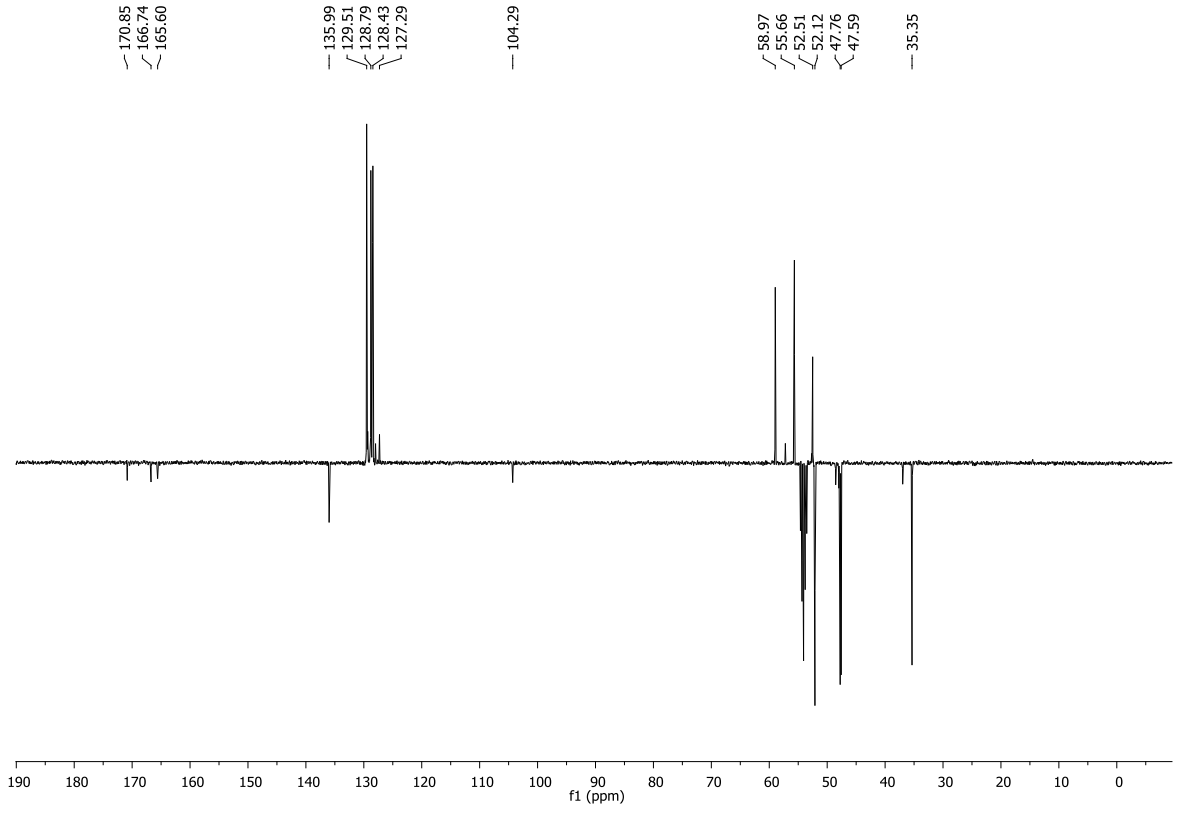

78 b: NHBoc-DKP7-CO_2Me

^{1}H NMR (400 MHz, CD_2Cl_2):

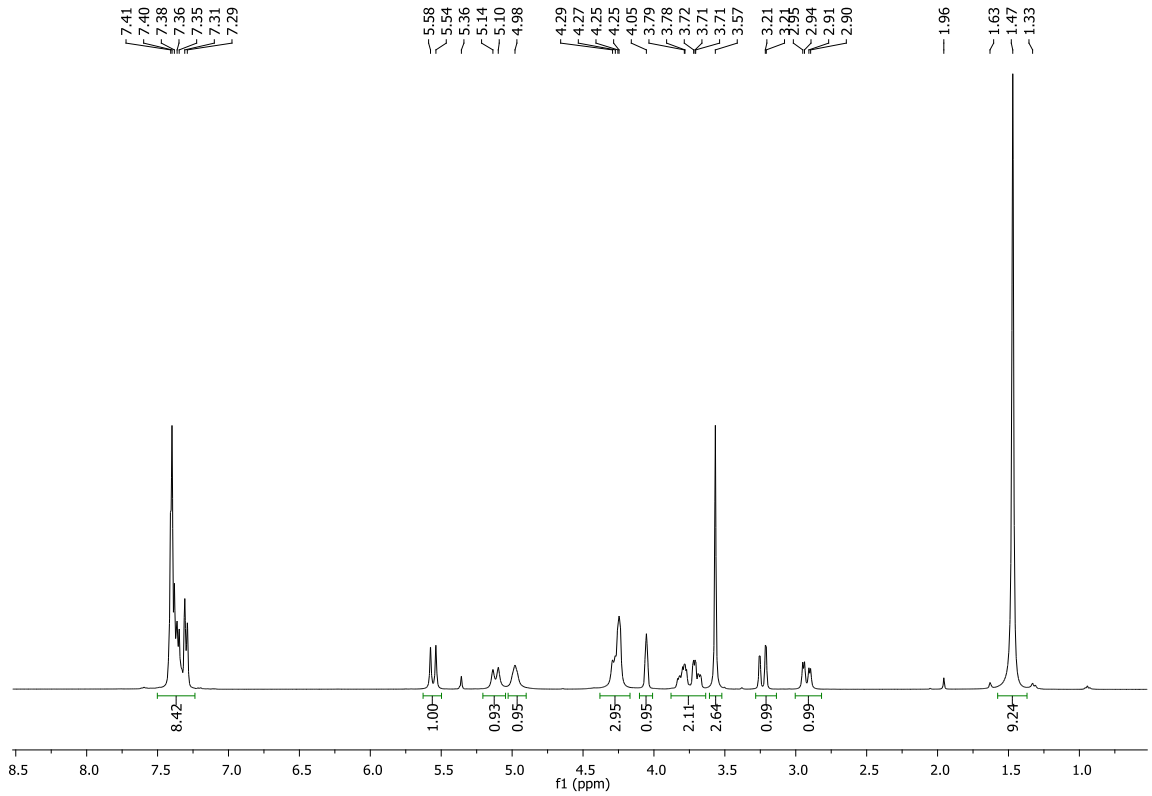

^{13}C NMR (101 MHz, CD_2Cl_2):

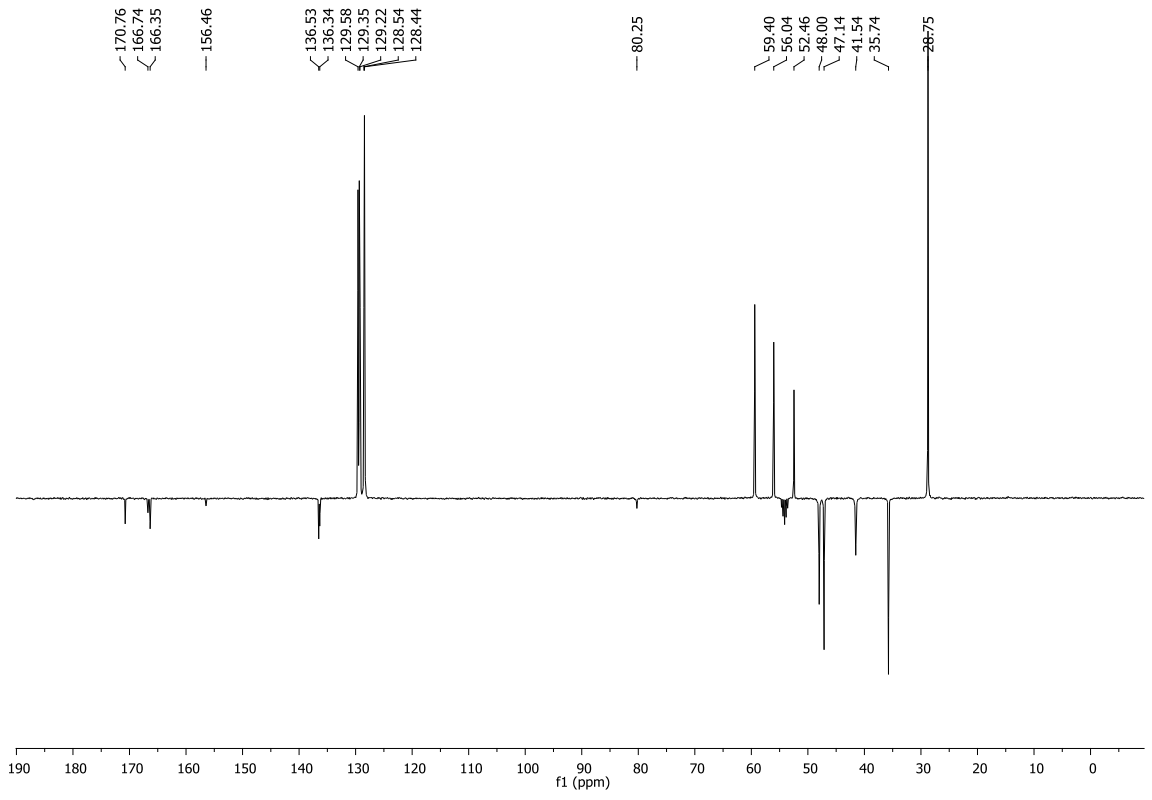

80: (*S*)-*N*-Bn-Ser(O-(*R*)-*N*-Boc-Glu(OMe))-OMe

^{1}H-NMR (400 MHz, $CDCl_3$):

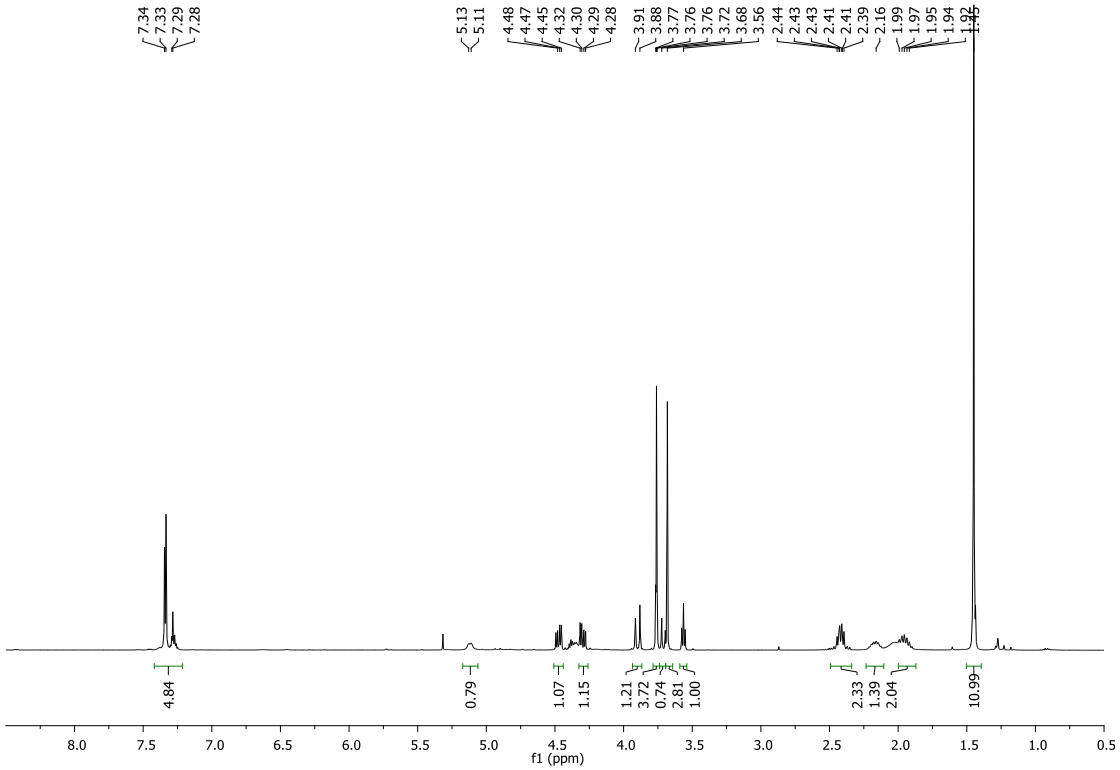

^{13}C-NMR (101 MHz, CD_2Cl_2):

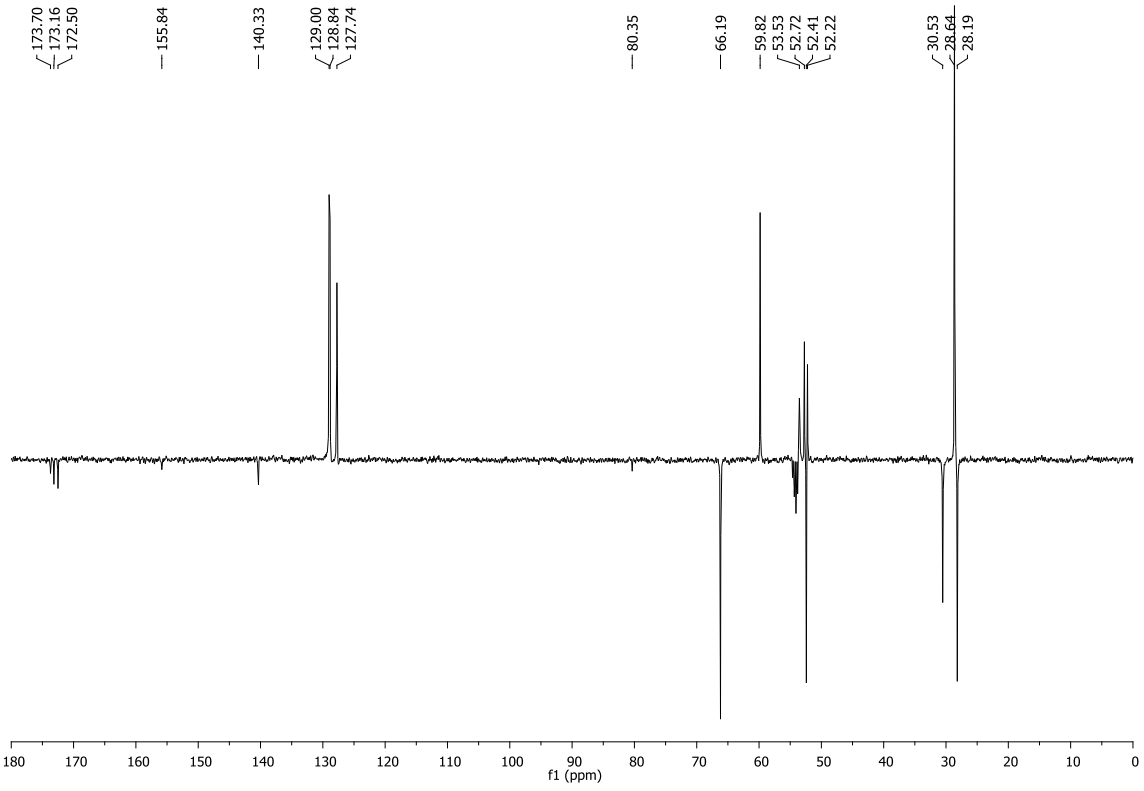

81: HO-DKP8-CO_2Me

^{1}H-NMR (400 MHz, CD_2Cl_2):

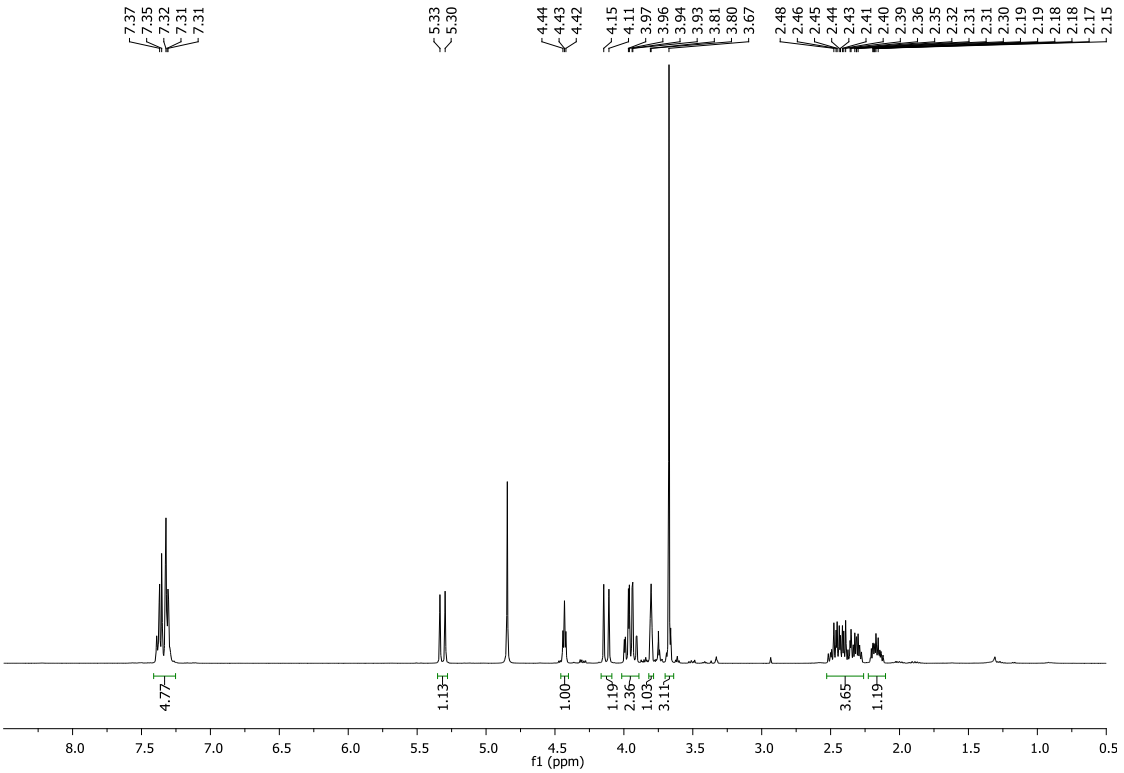

^{13}C-NMR (101 MHz, CD_3OD):

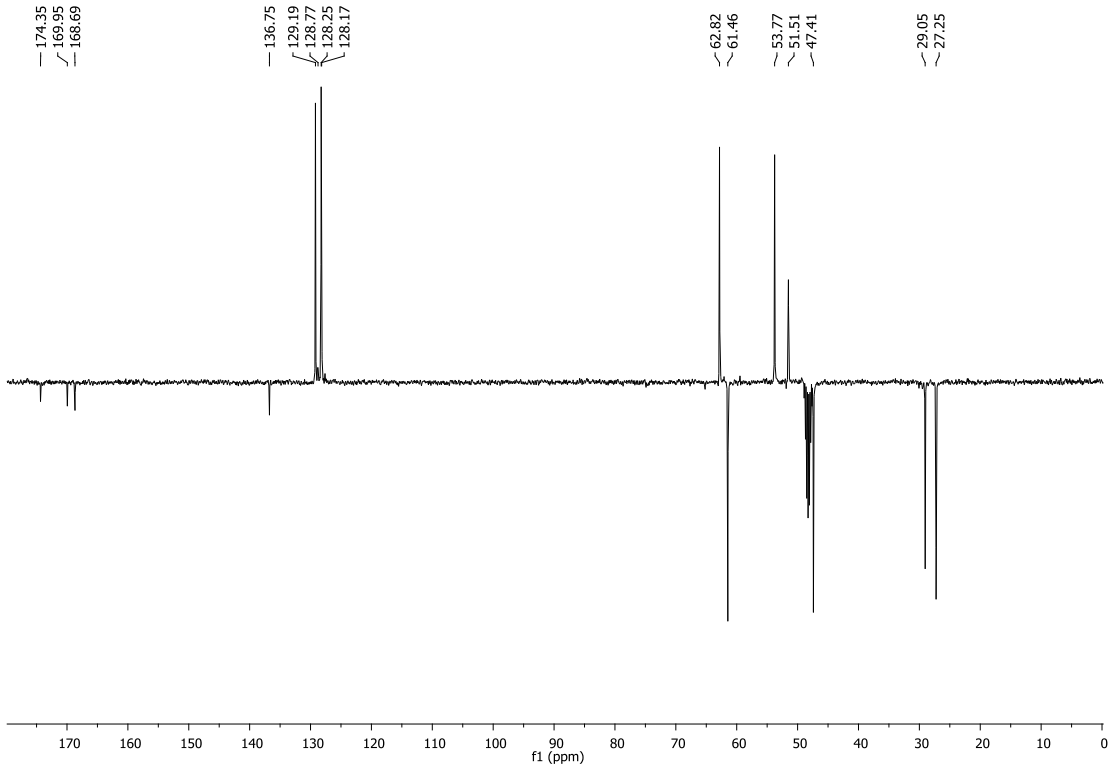

82: N_3-DKP8-CO_2Me

^{1}H-NMR (400 MHz, $CDCl_3$):

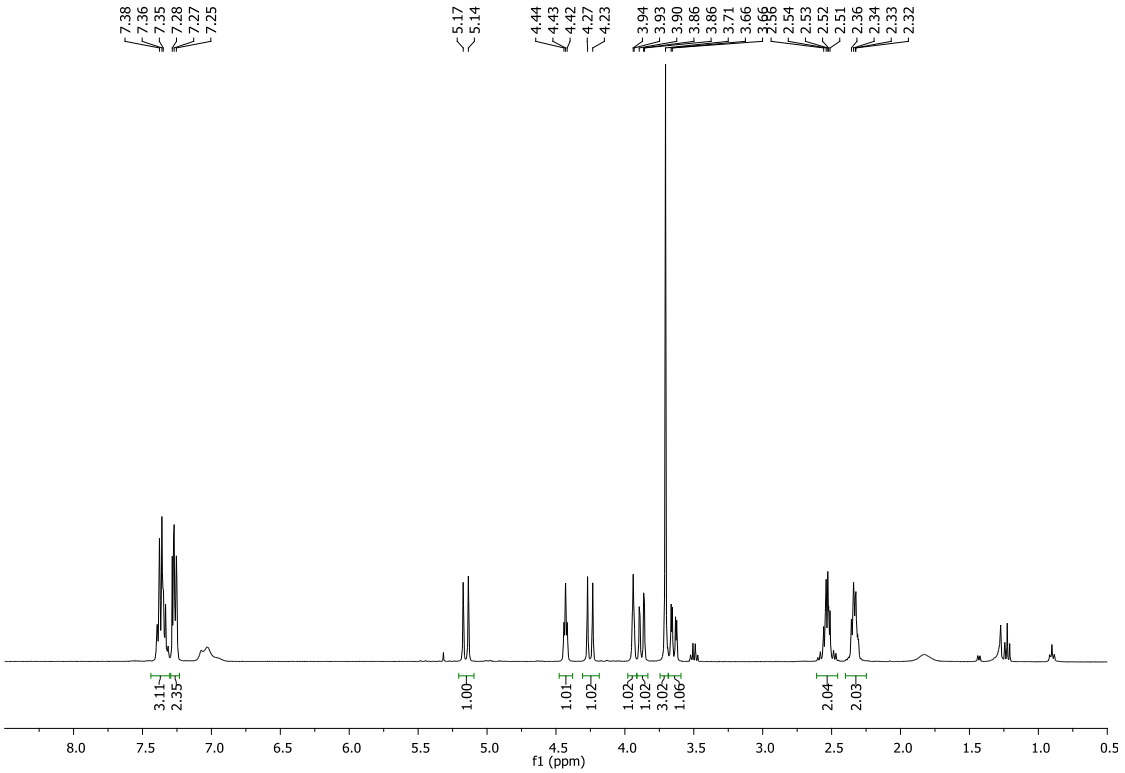

^{13}C-NMR (101 MHz, $CDCl_3$):

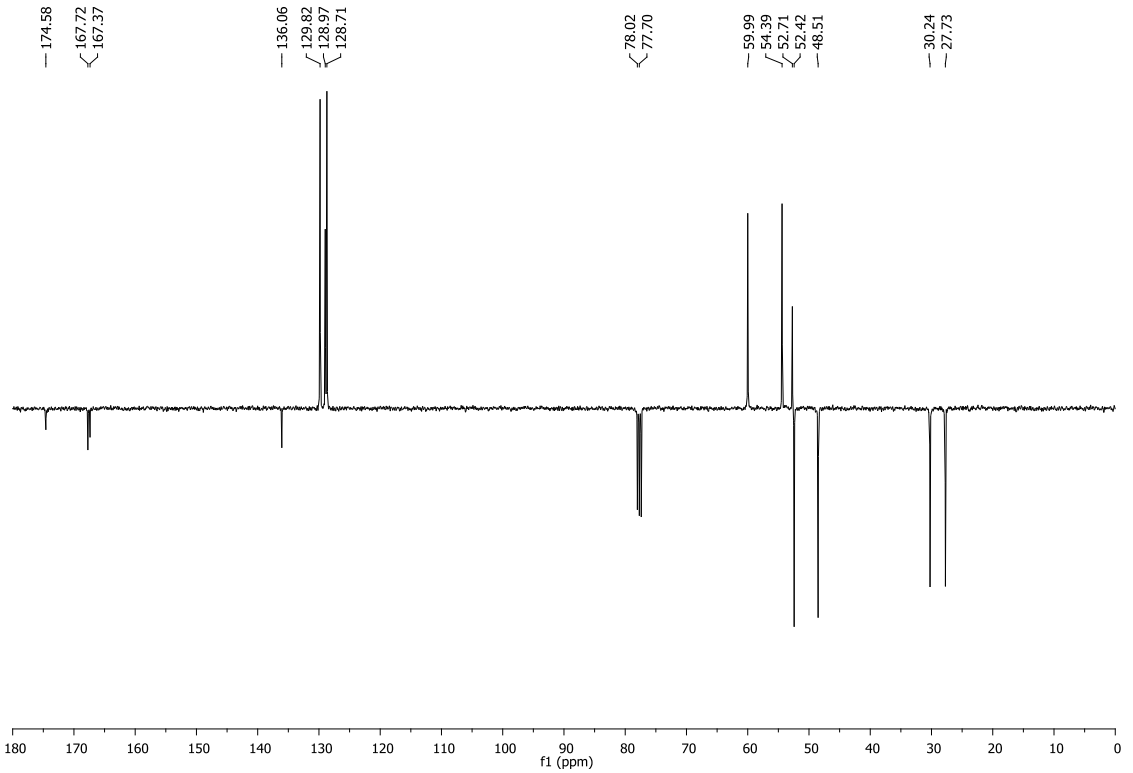

84: NHBoc-DKP8-CO_2Me

^{1}H-NMR (400 MHz, $CDCl_3$):

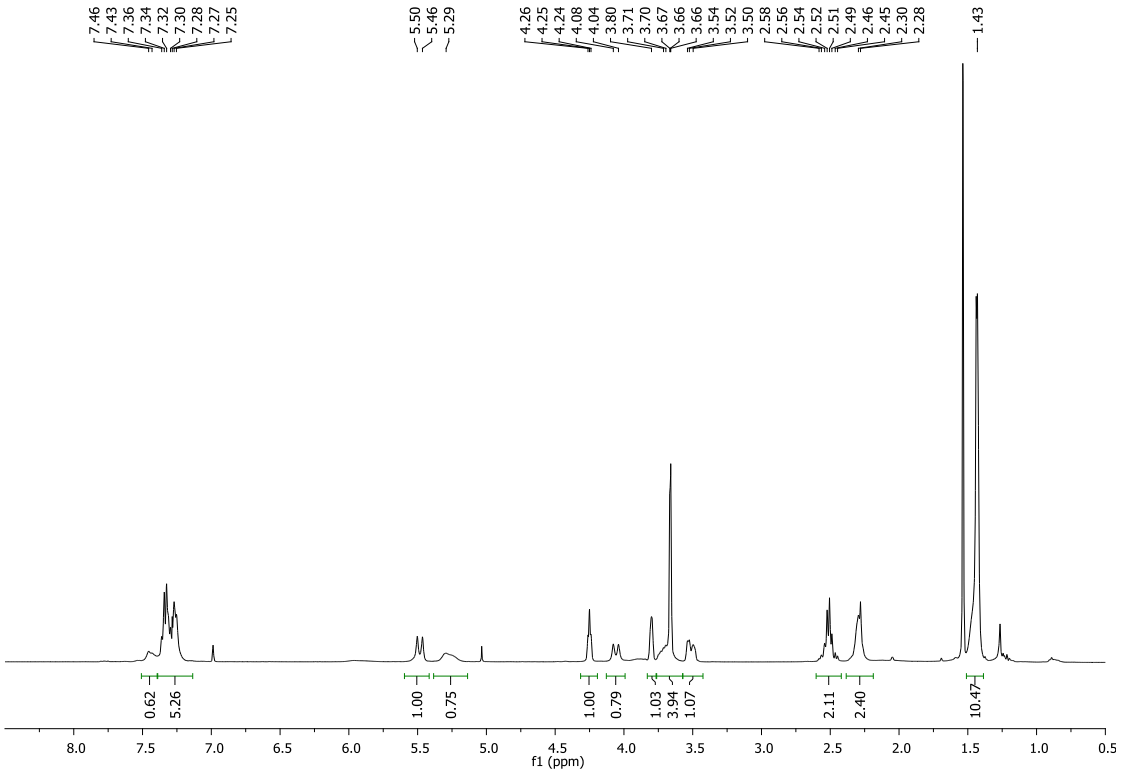

^{13}C-NMR (101 MHz, $CDCl_3$):

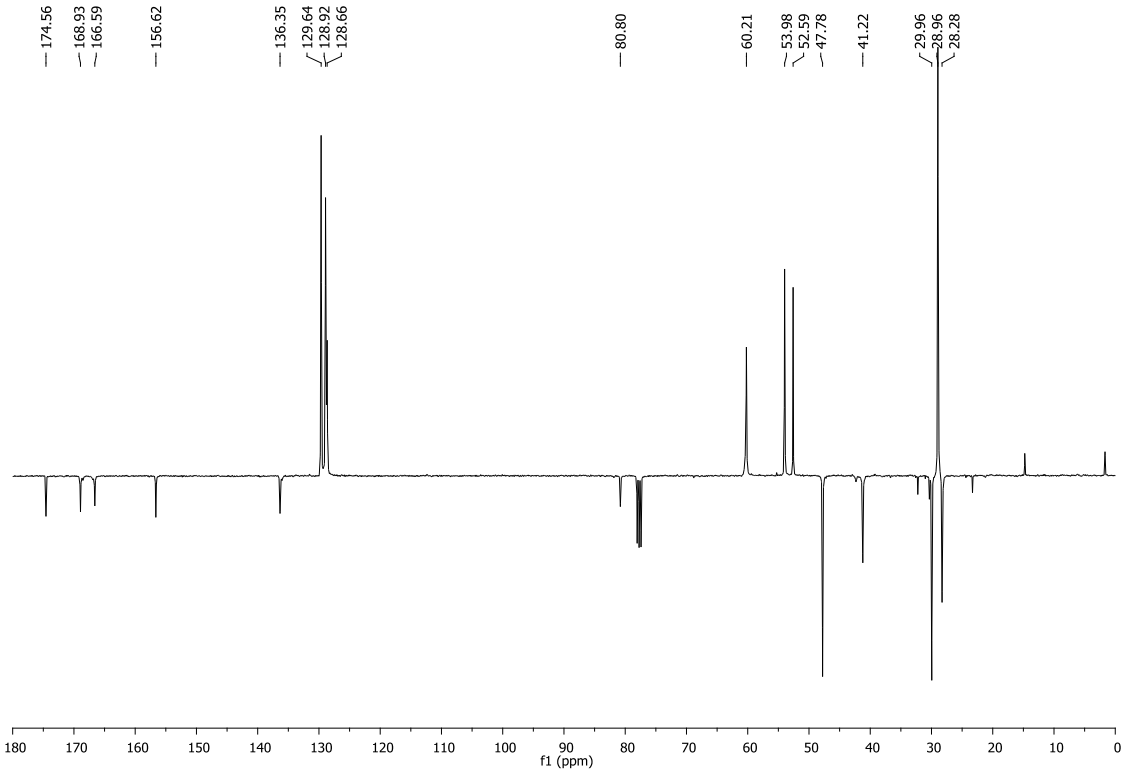

112: (*N*-Boc-Arg(Mtr)-Gly-OBn)

^{1}H NMR (400 MHz, CD_2Cl_2):

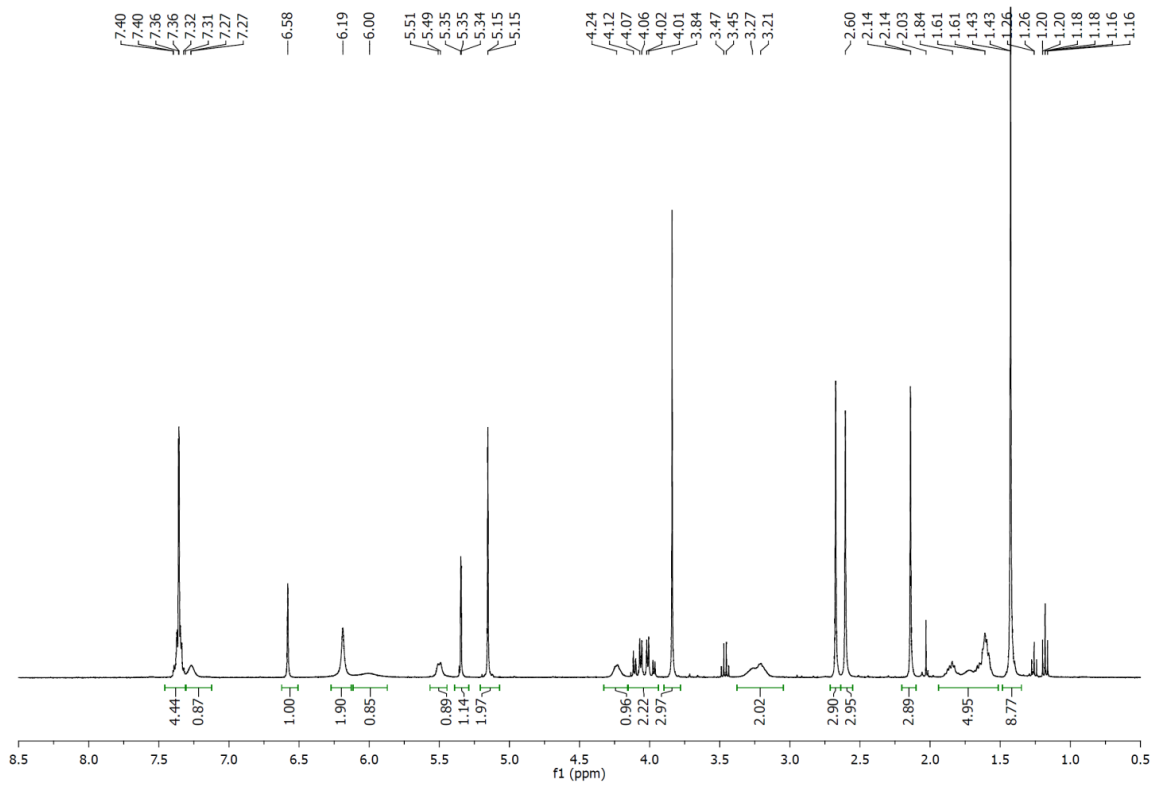

^{13}C NMR (101 MHz, CD_2Cl_2):

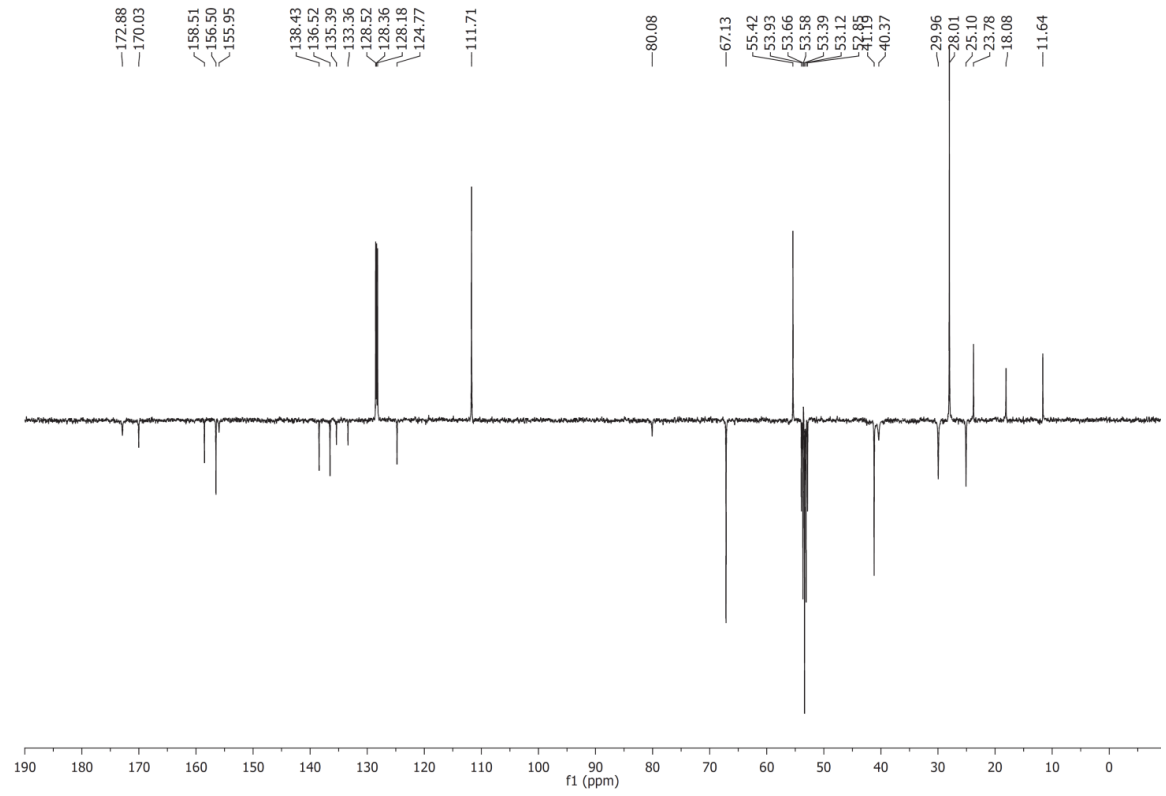

113 a: (Boc-DKP3-Arg(Mtr)-Gly-OBn)

^{1}H NMR (400 MHz, CD_2Cl_2):

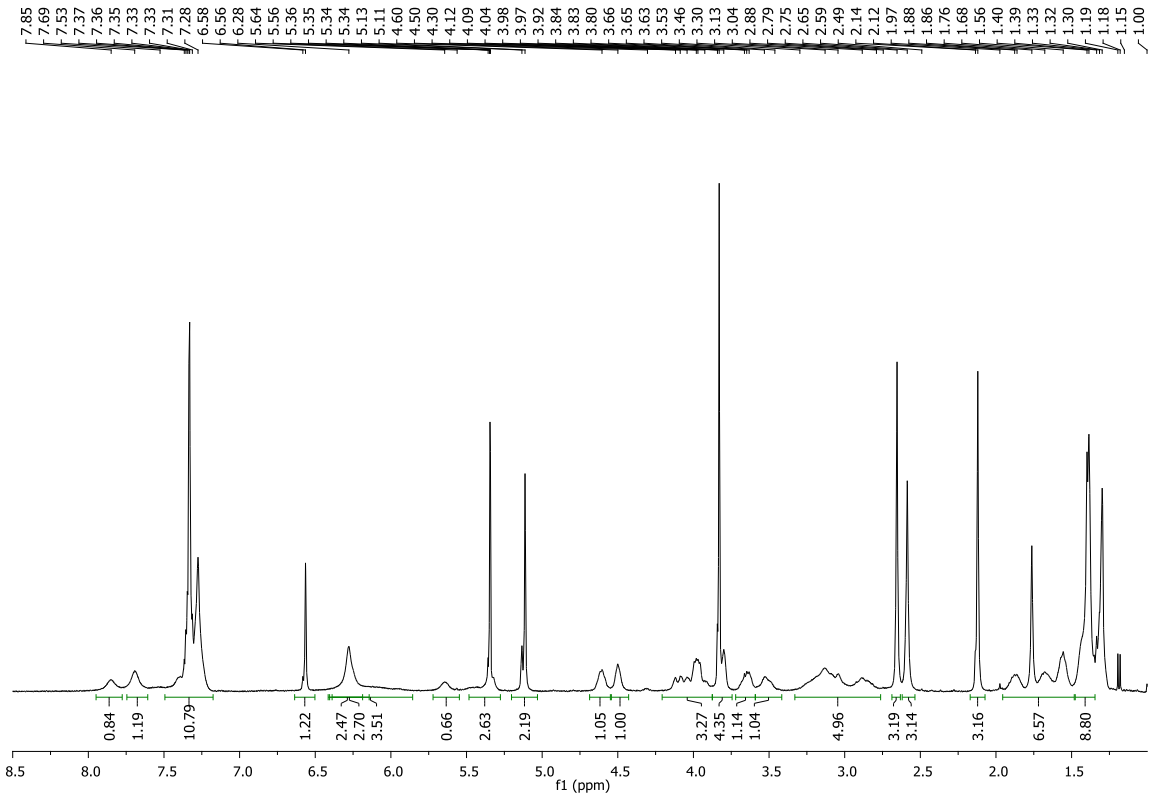

^{13}C NMR (101 MHz, CD_2Cl_2):

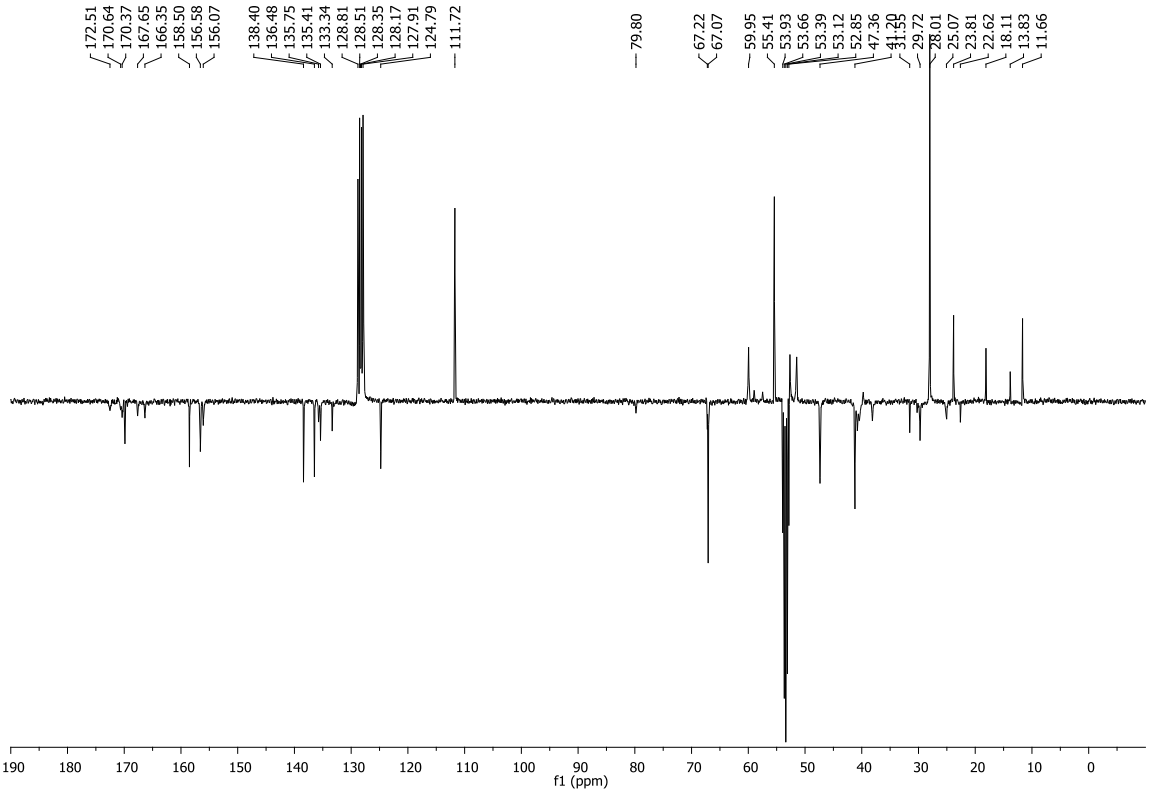

114 a: (Cbz-Asp(O*t*Bu)-DKP3-Arg(Mtr)-Gly-OBn

^{1}H NMR (400 MHz, CD_2Cl_2):

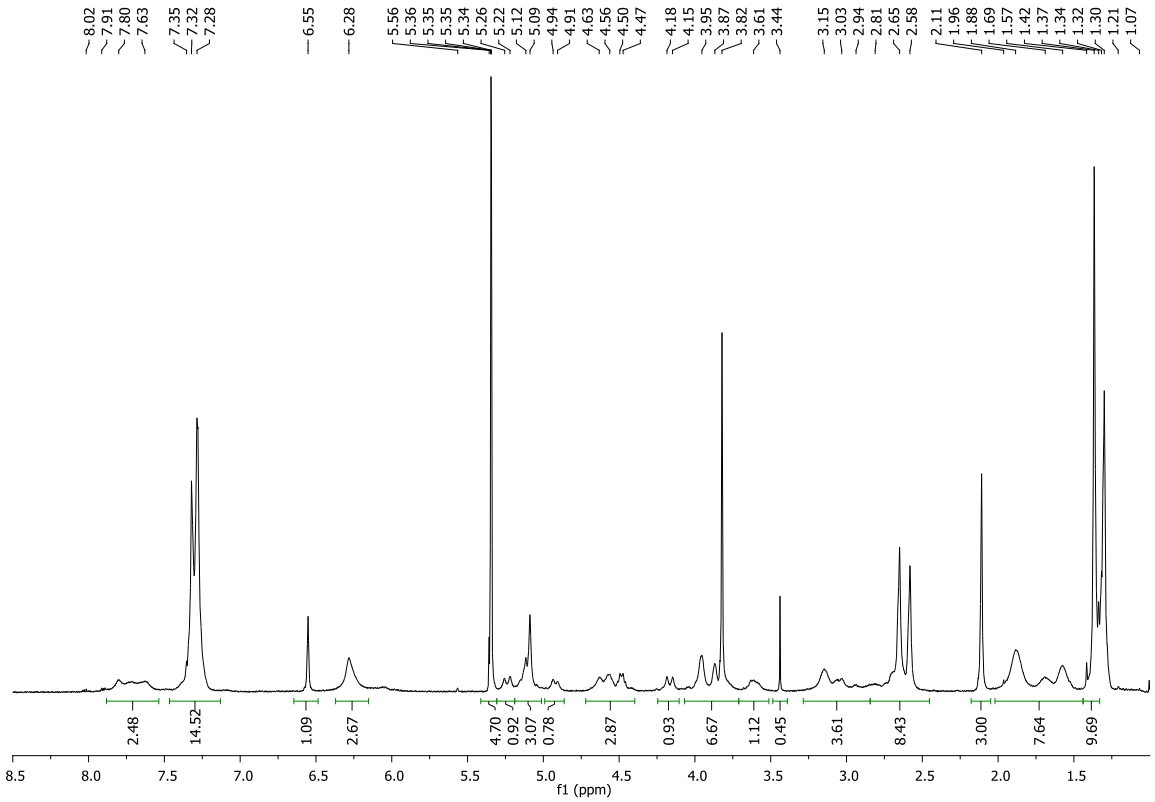

^{13}C NMR (101 MHz, CD_2Cl_2):

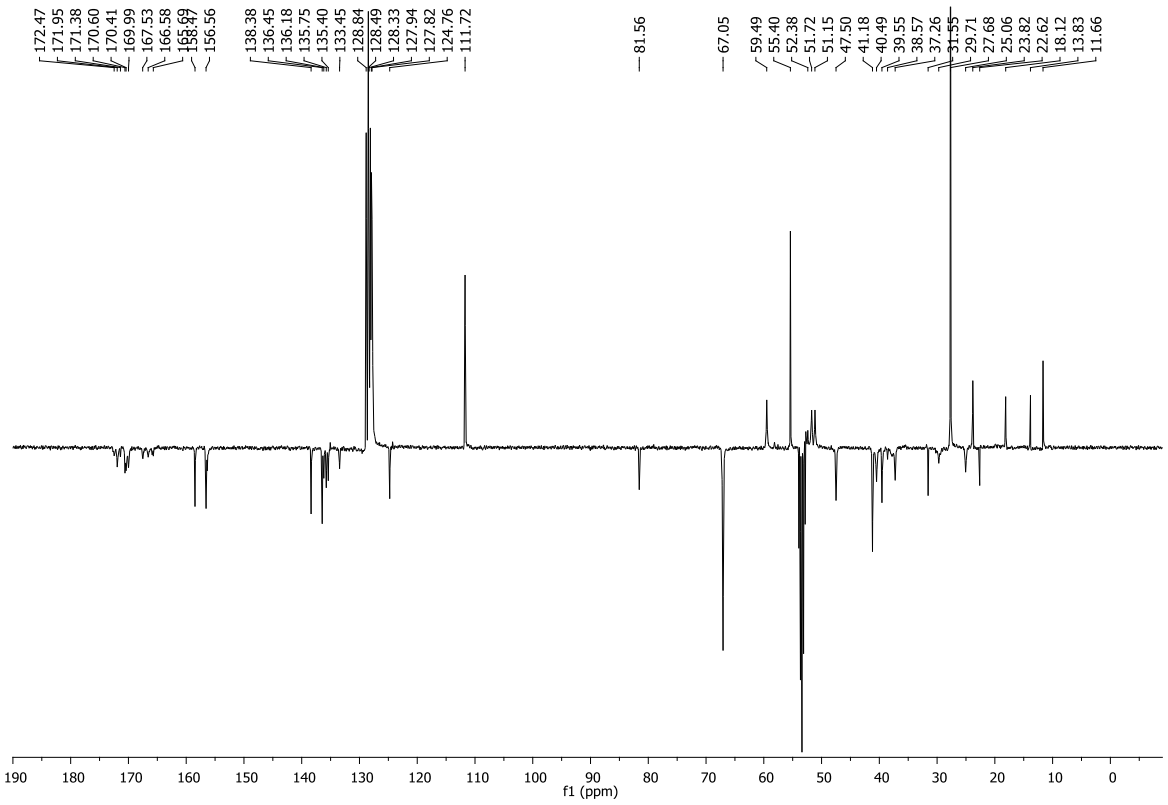

116 a: (*Cyclo*[Arg(Mtr)-Gly-Asp(O*t*Bu)-DKP3])

^{1}H NMR (400 MHz, CD_3OD):

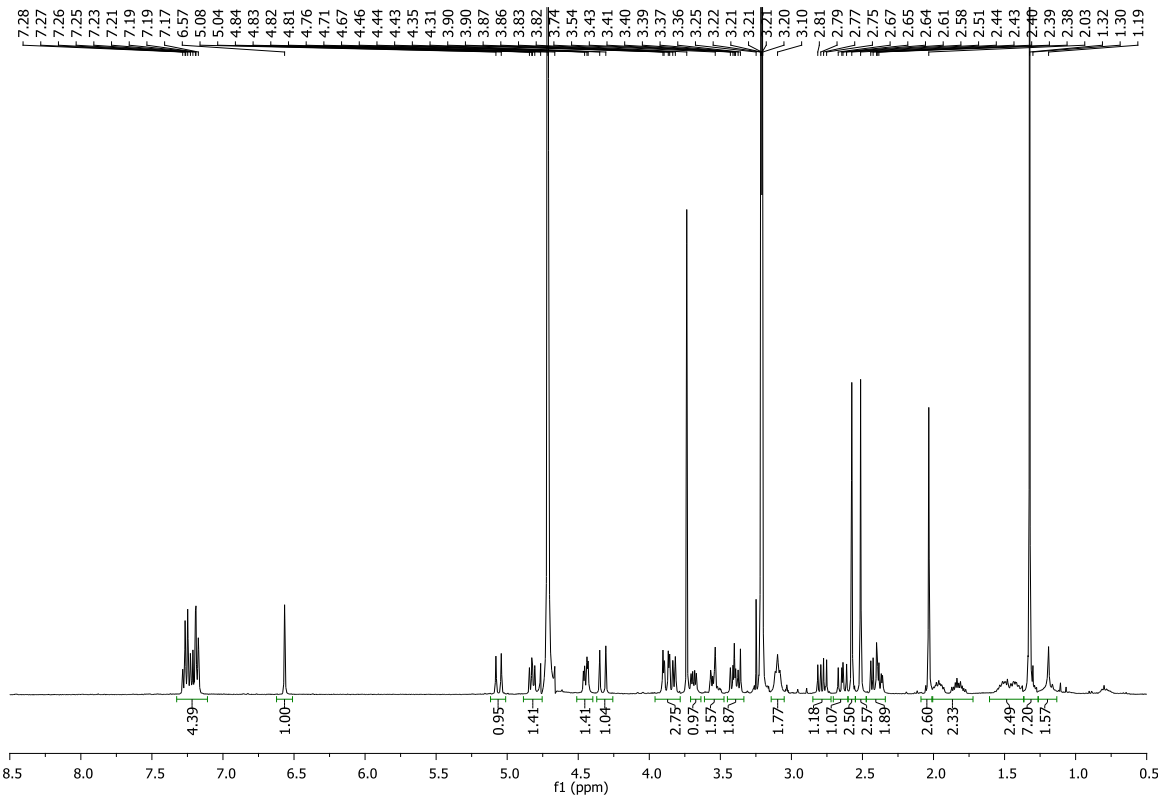

^{13}C NMR (101 MHz, CD_3OD):

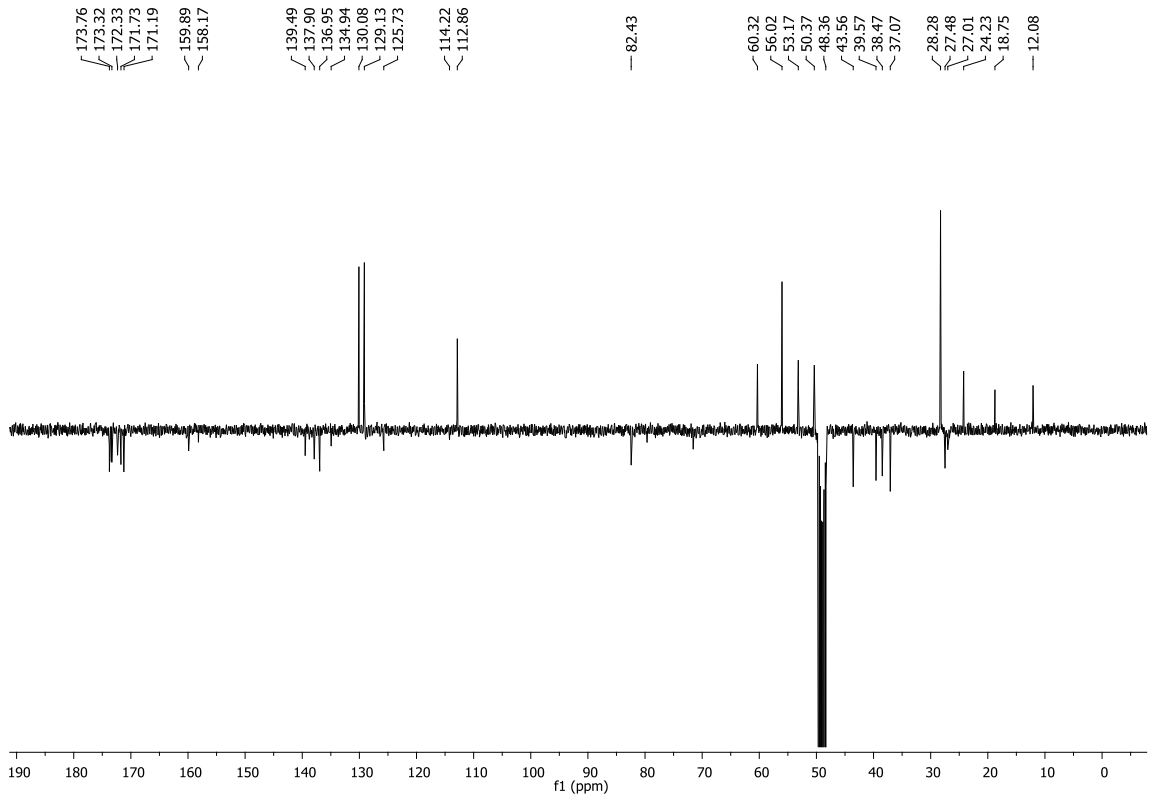

102: (*Cyclo*[Arg-Gly-Asp-DKP-3])

^{1}H NMR (600 MHz, H_2O/D_2O 9:1):

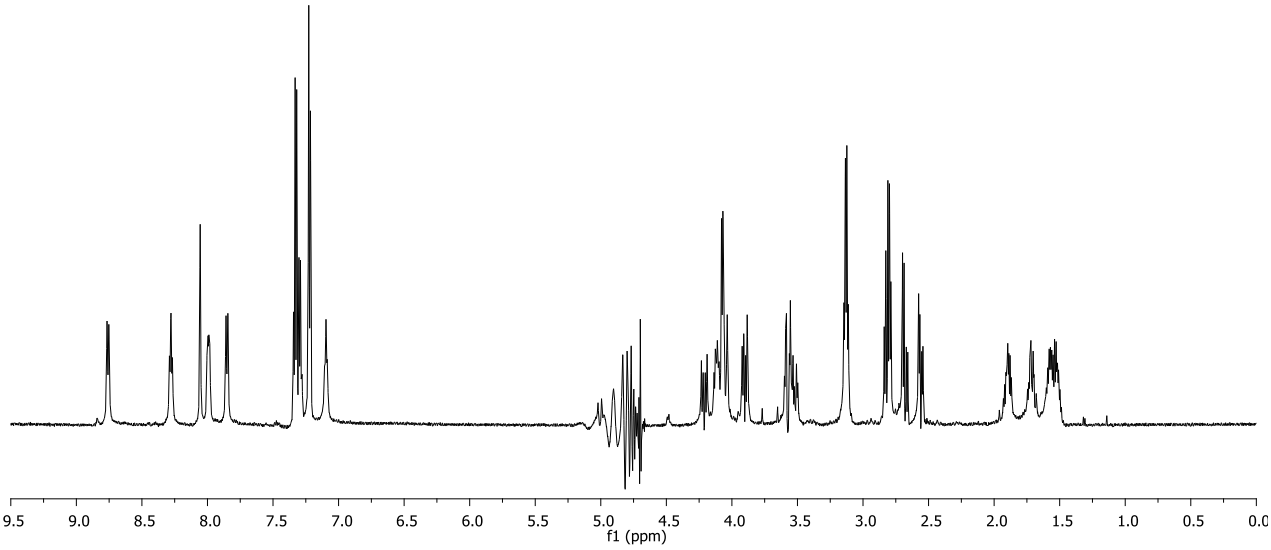

113 b: (*N*-Boc-DKP4-Arg(Mtr)-Gly-OBn)

^{1}H NMR (400 MHz, Acetone-d_6):

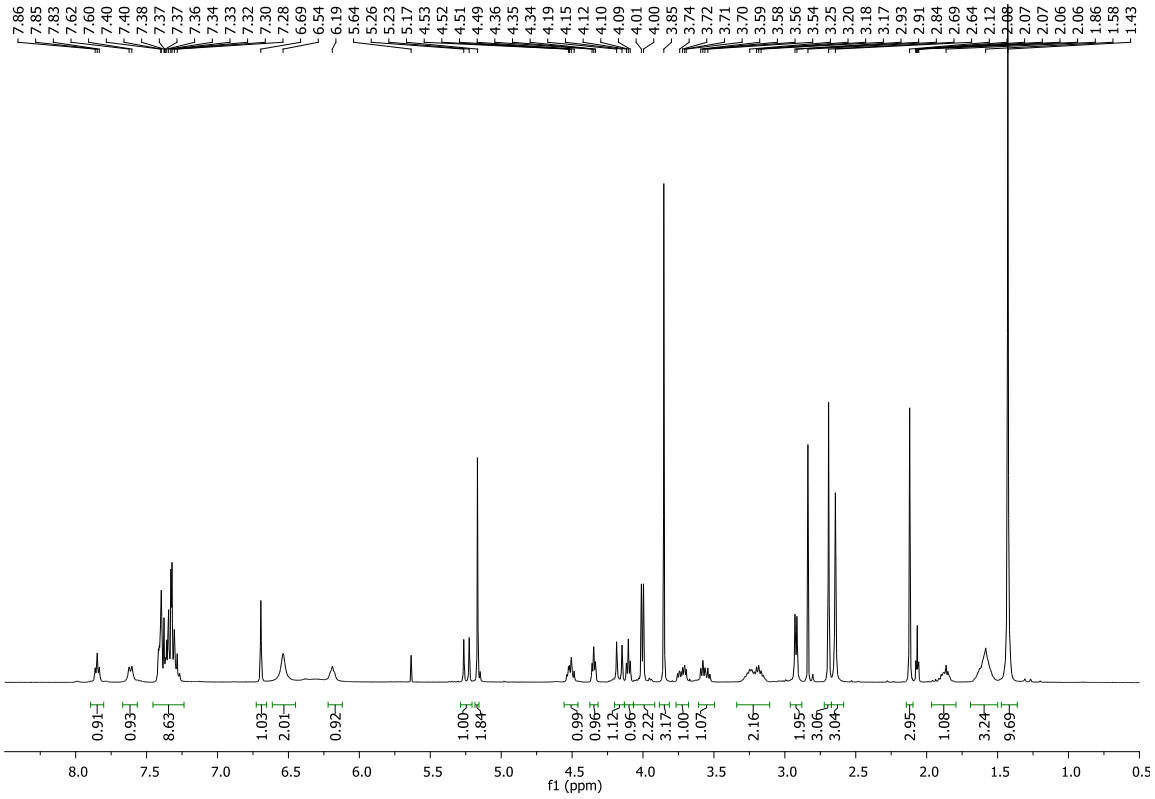

^{13}C NMR (101 MHz, Acetone-d_6):

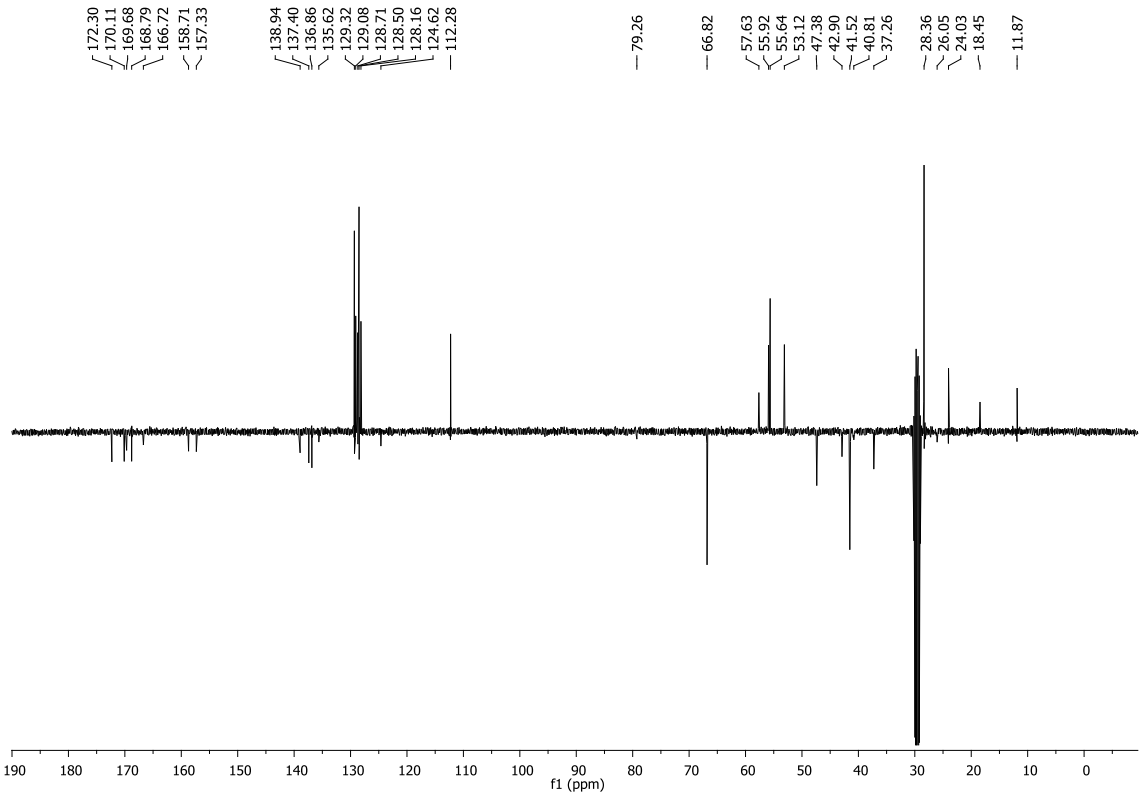

114 b: (Cbz-Asp(O*t*Bu)-DKP4-Arg(Mtr)-Gly-OBn)

^{1}H NMR (400 MHz, Acetone-d_6):

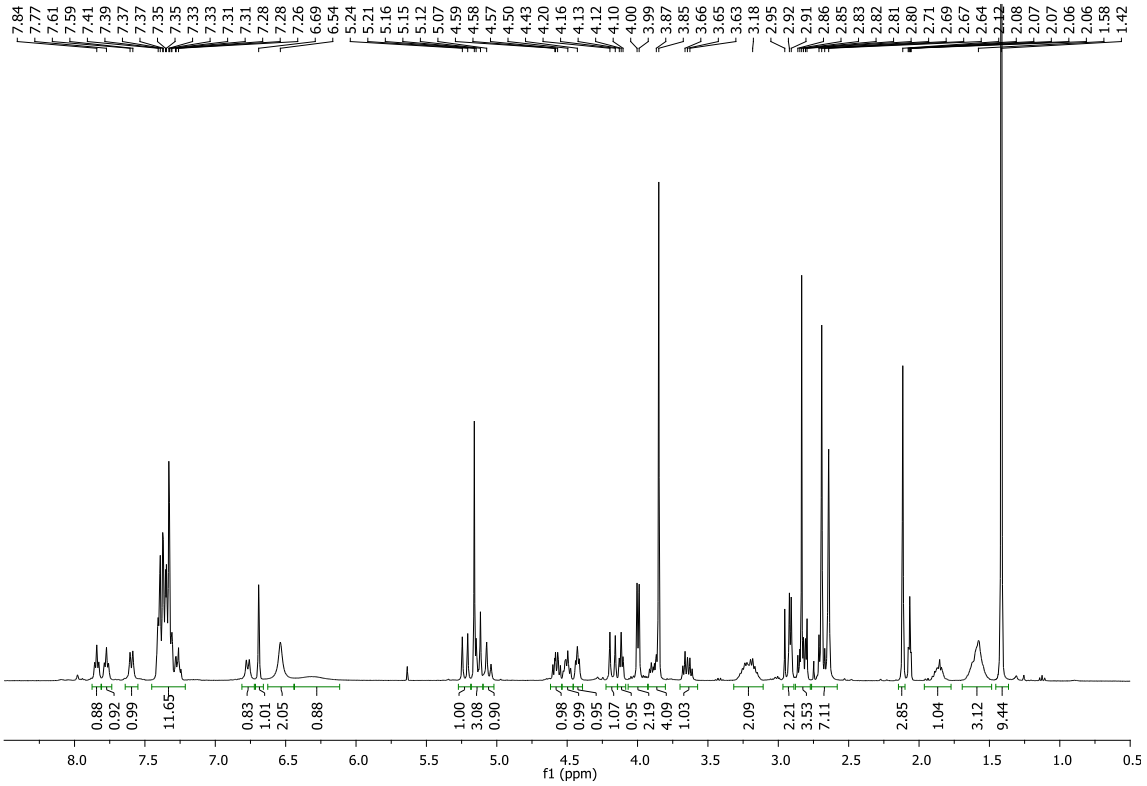

^{13}C NMR (101 MHz, Acetone-d_6):

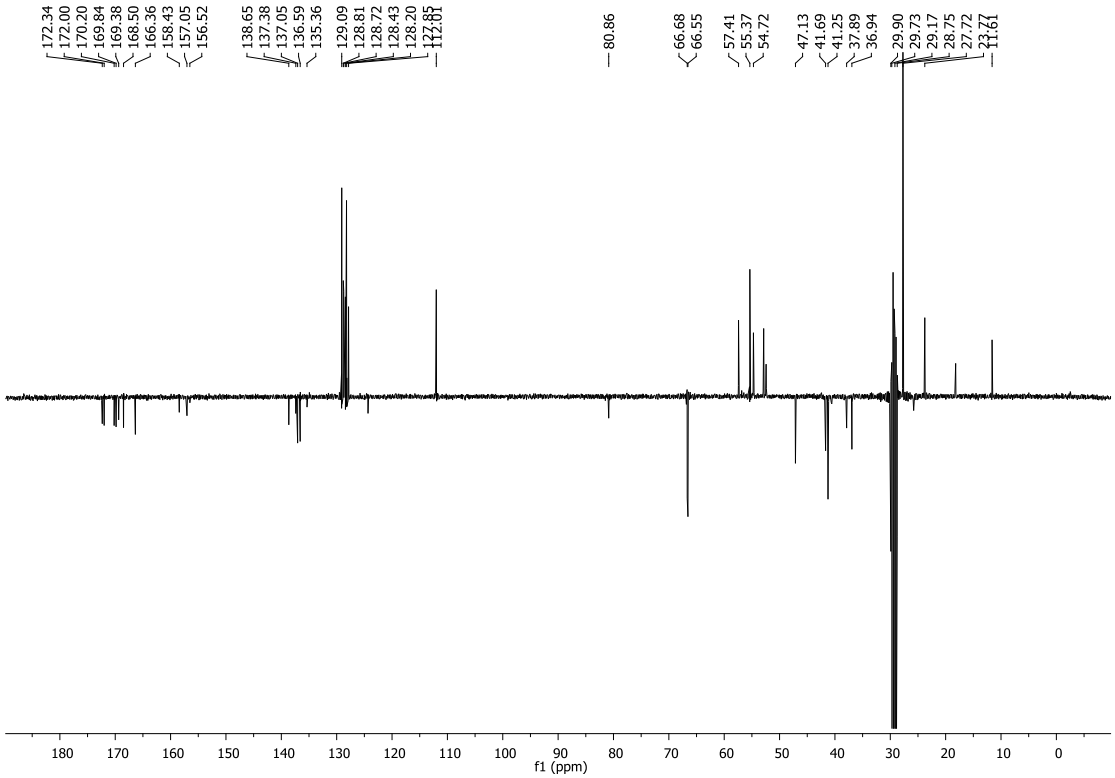

116 b: (*Cyclo*[Arg(Mtr)-Gly-Asp(O*t*Bu)-DKP4])

^{1}H NMR (400 MHz, CD_3OD):

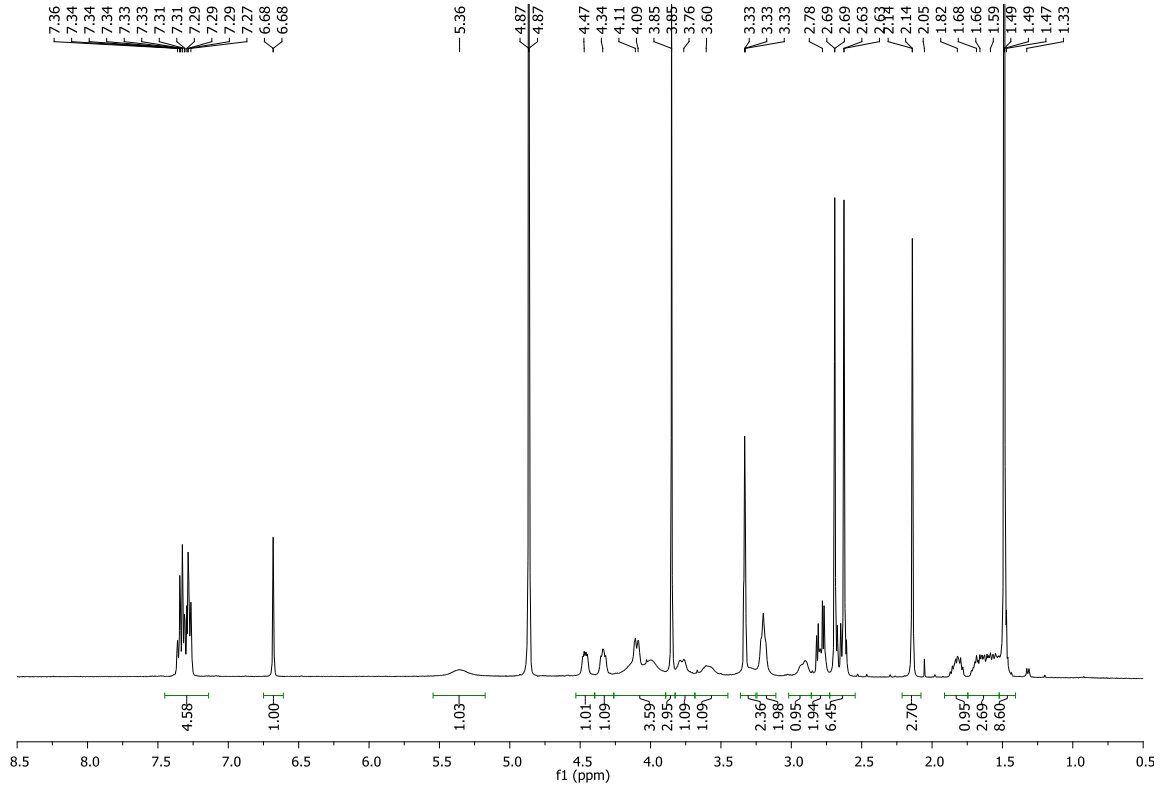

^{13}C NMR (101 MHz, CD_3OD):

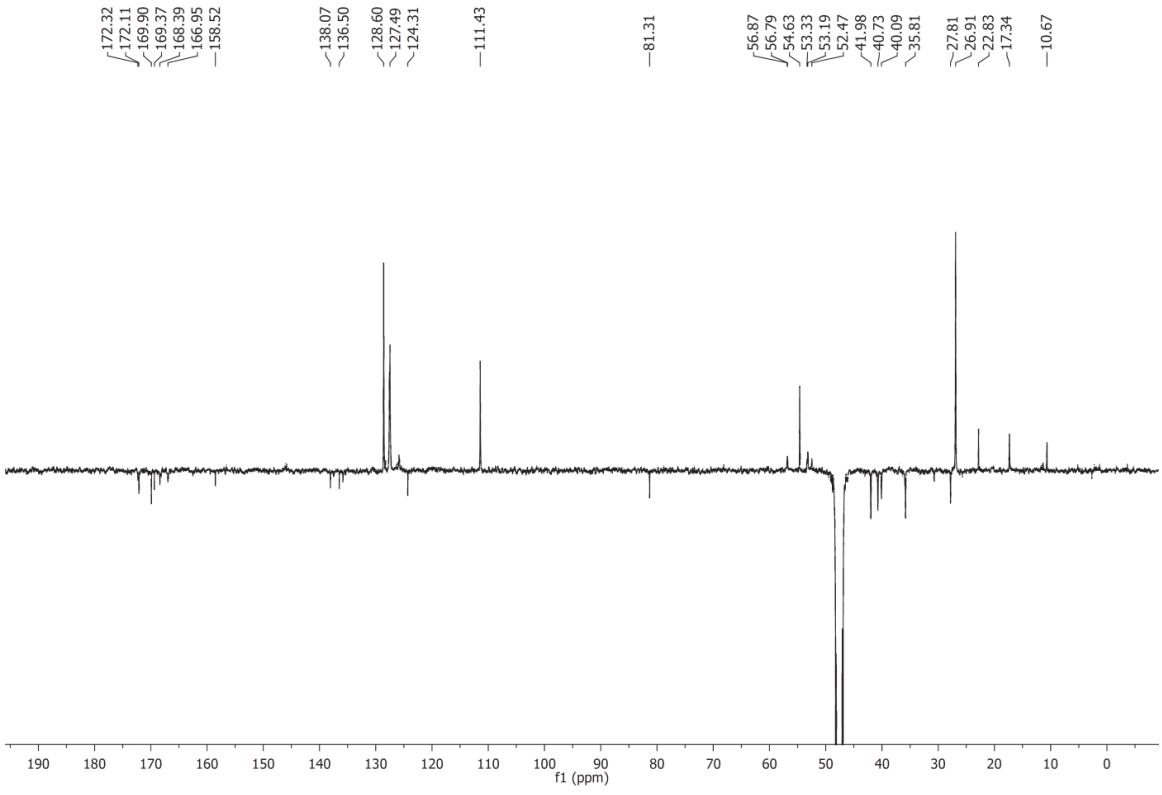

103: (*Cyclo*[Arg-Gly-Asp-DKP4])

^{1}H NMR (400 MHz, H_2O/D_2O 9:1):

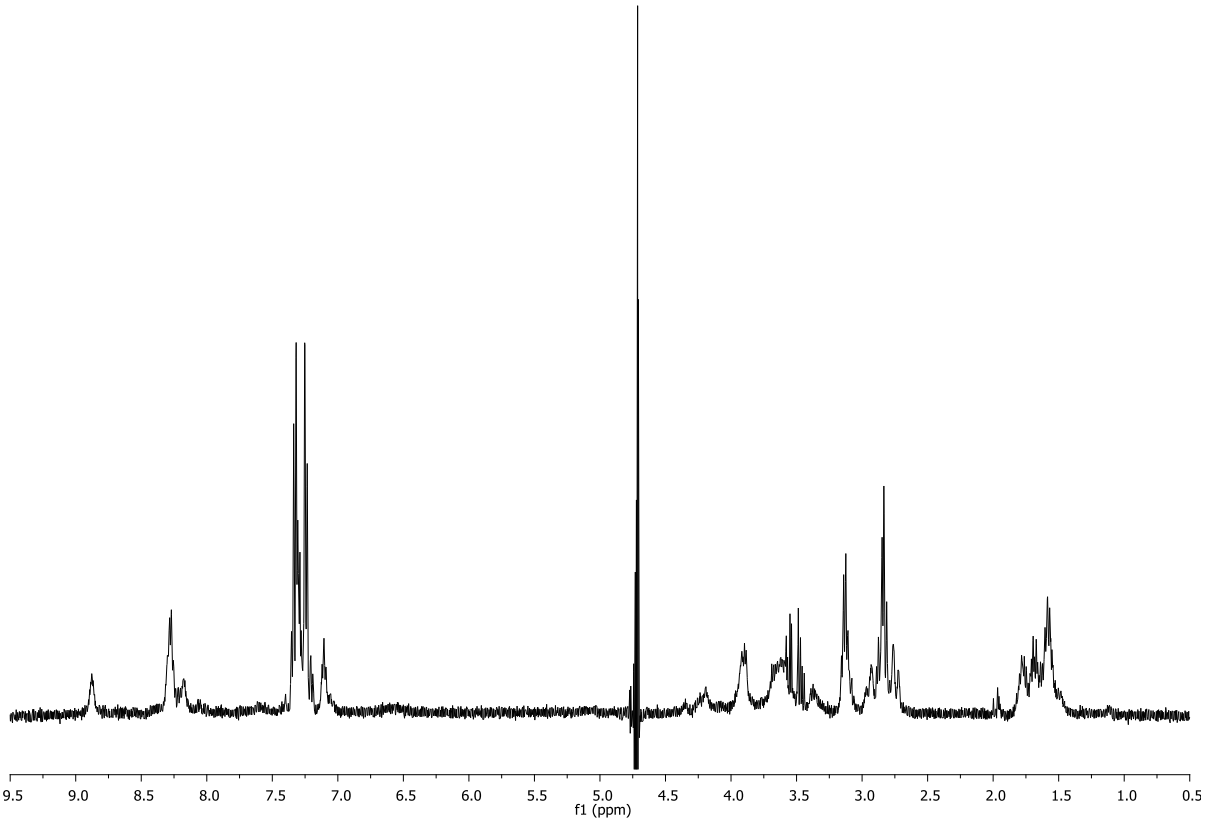

113 c: (*N*-Boc-DKP5-Arg(Mtr)-Gly-OBn)

^{1}H NMR (400 MHz, CD_2Cl_2):

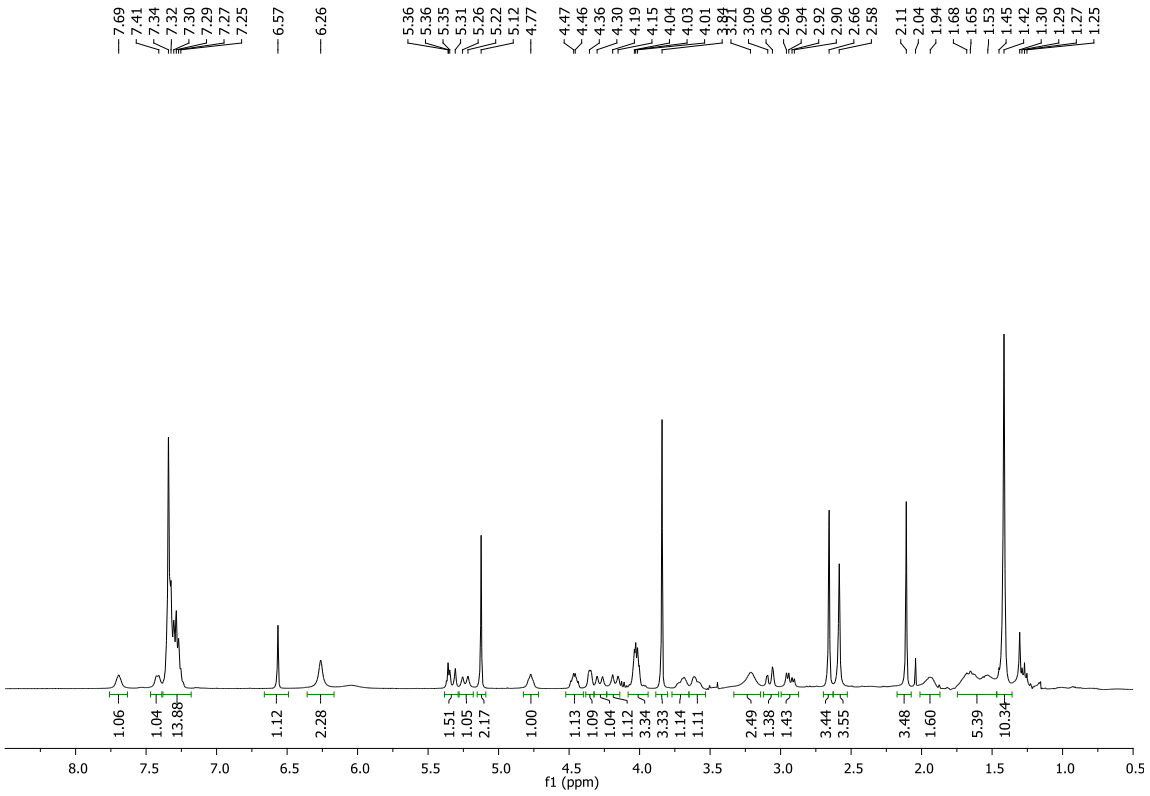

^{13}C NMR (101 MHz, CD_2Cl_2):

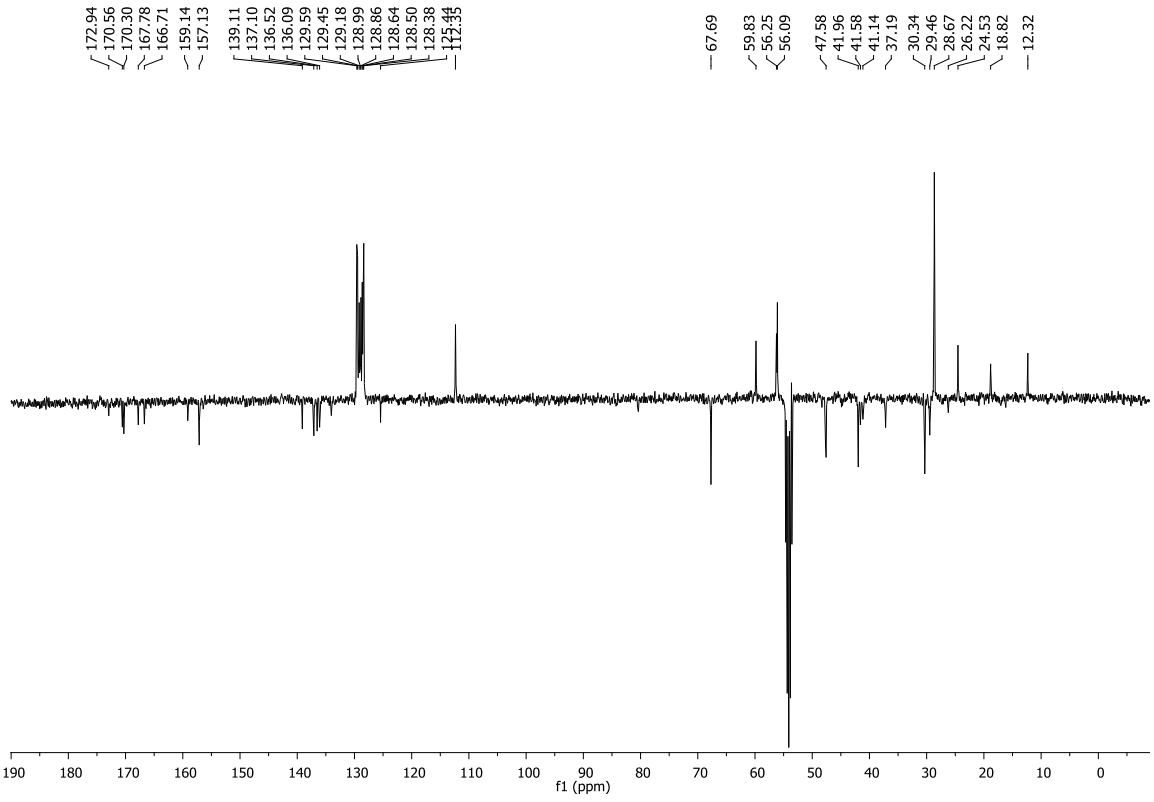

114 c: (Cbz-Asp(O*t*Bu)-DKP5-Arg(Mtr)-Gly-OBn)

^{1}H NMR (400 MHz, Acetone-d_6):

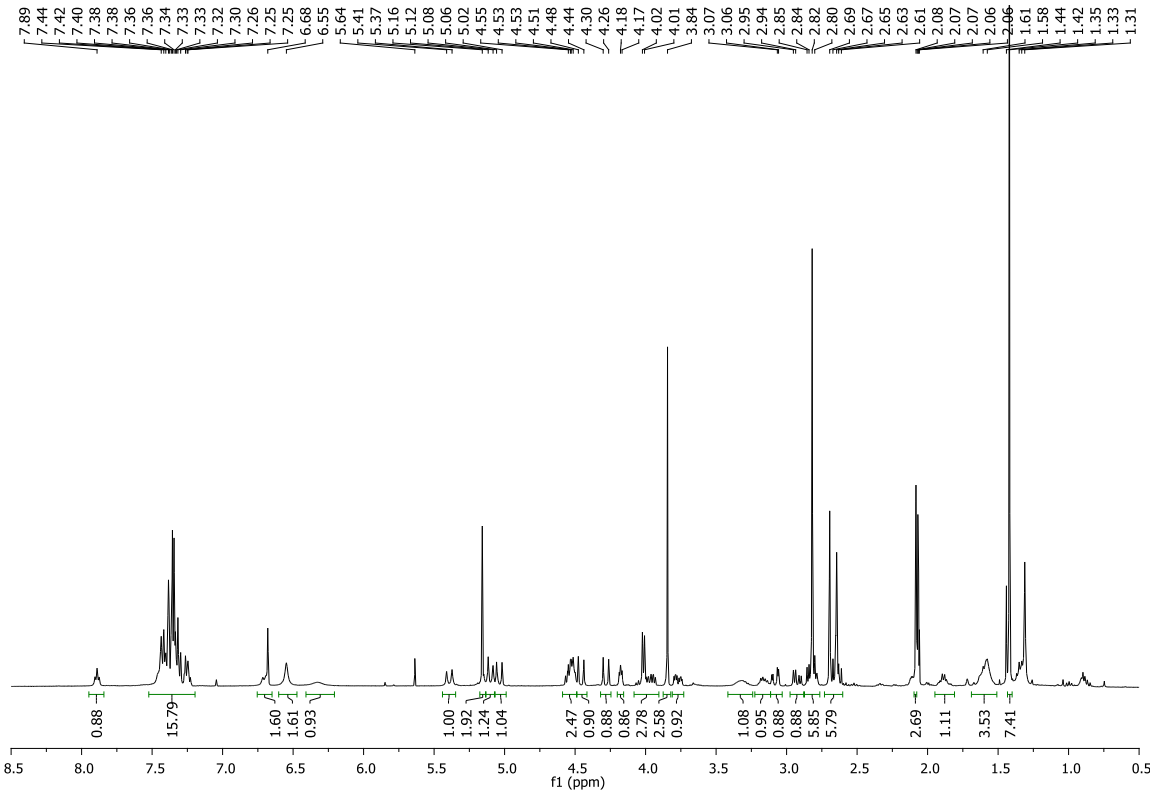

^{13}C NMR (101 MHz, Acetone-d_6):

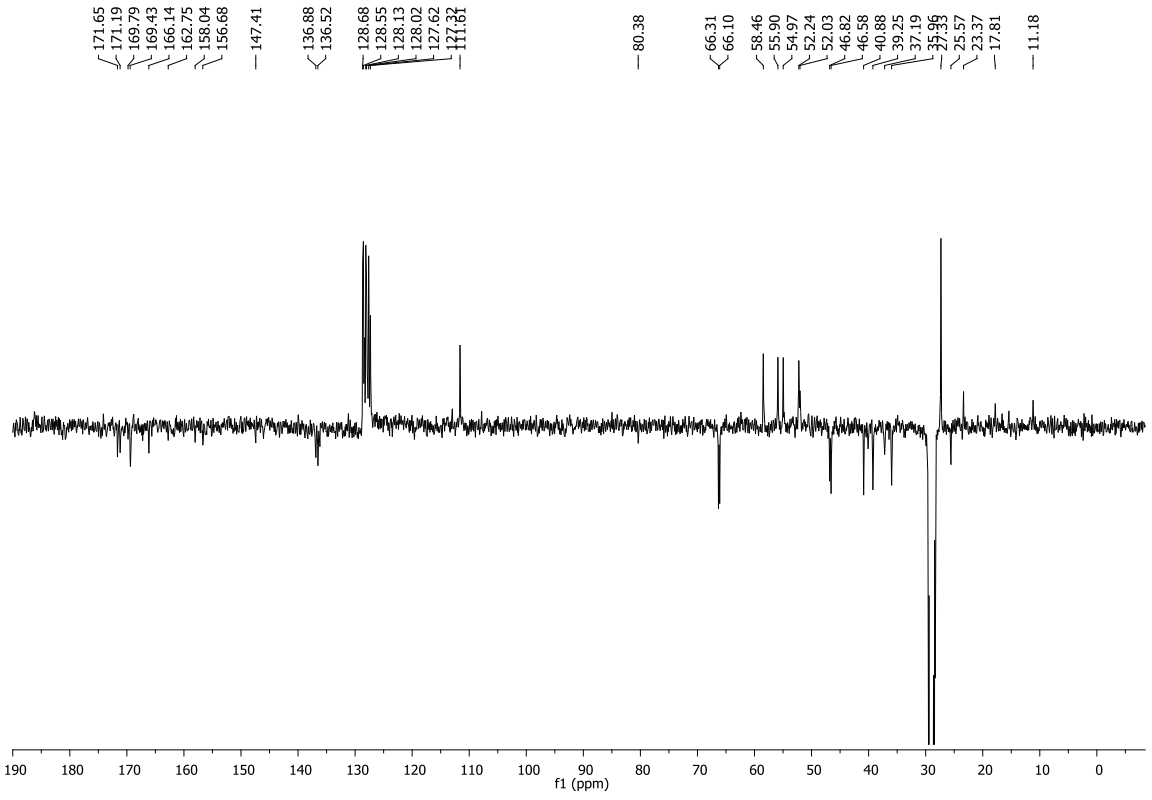

116 c: (*Cyclo*[Arg(Mtr)-Gly-Asp(O*t*Bu)-DKP5]):

^{1}H NMR (400 MHz, Acetone-d_6):

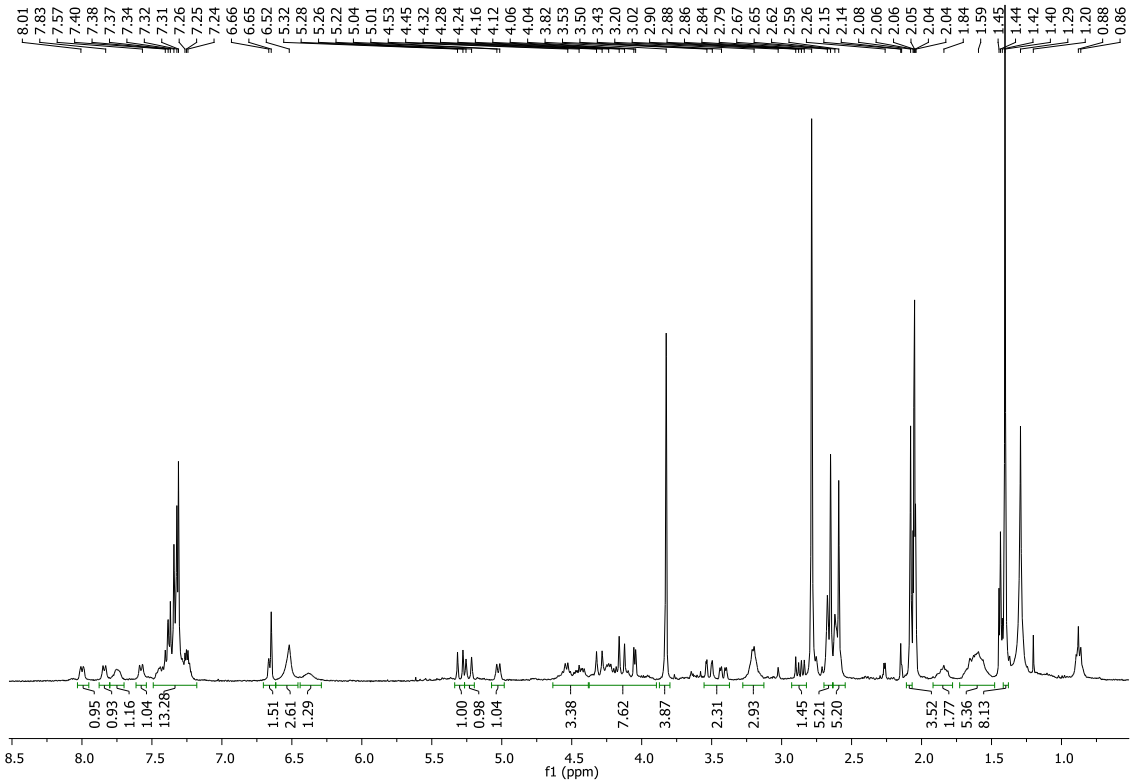

^{13}C NMR (101 MHz, Acetone-d_6):

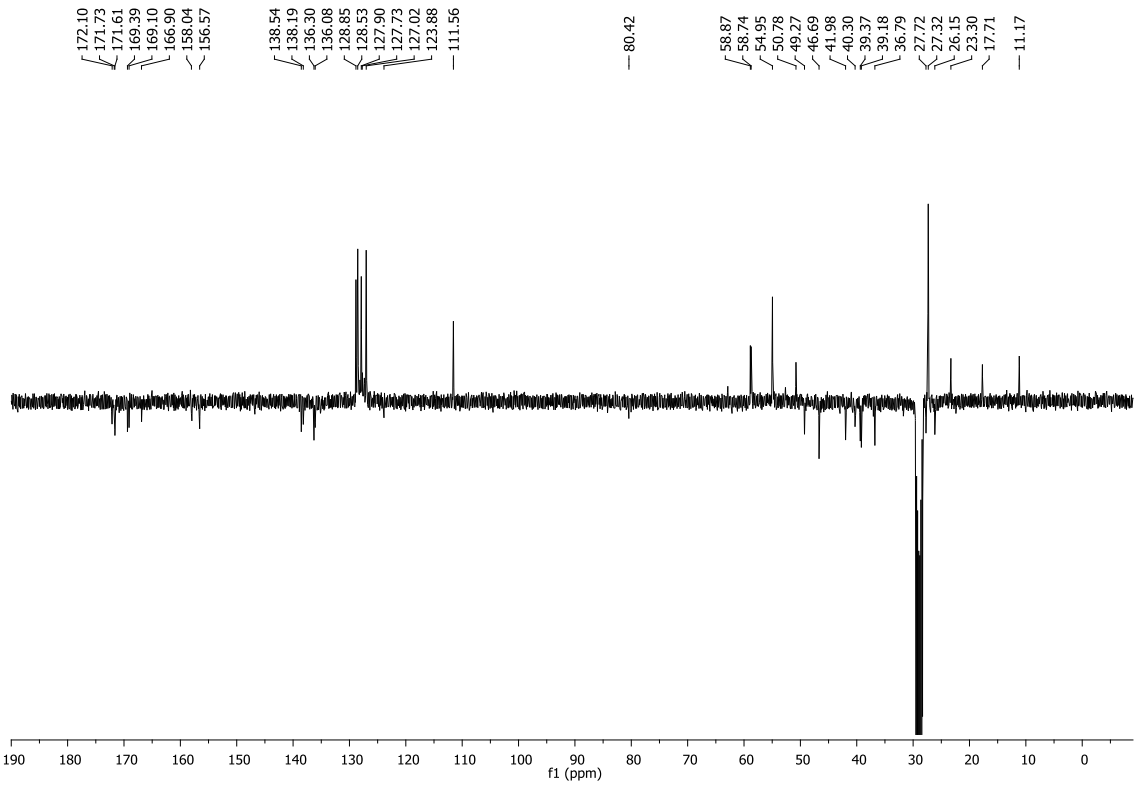

104: (*Cyclo*[Arg-Gly-Asp-DKP5])

^{1}H NMR (400 MHz, H_2O/D_2O 9:1):

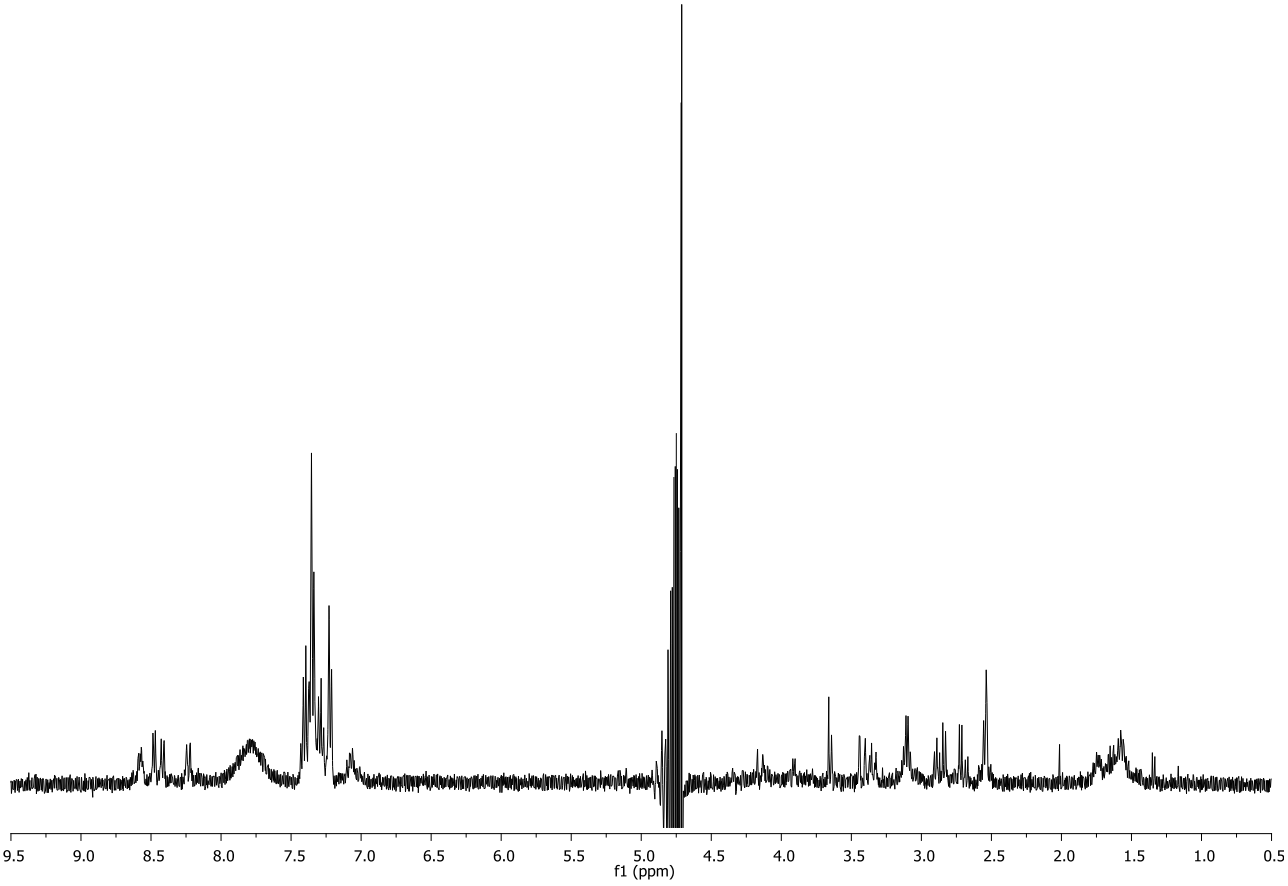

113 d: (Boc-DKP6-Arg(Mtr)-Gly-OBn)

^{1}H NMR (400 MHz, Acetone-d_6):

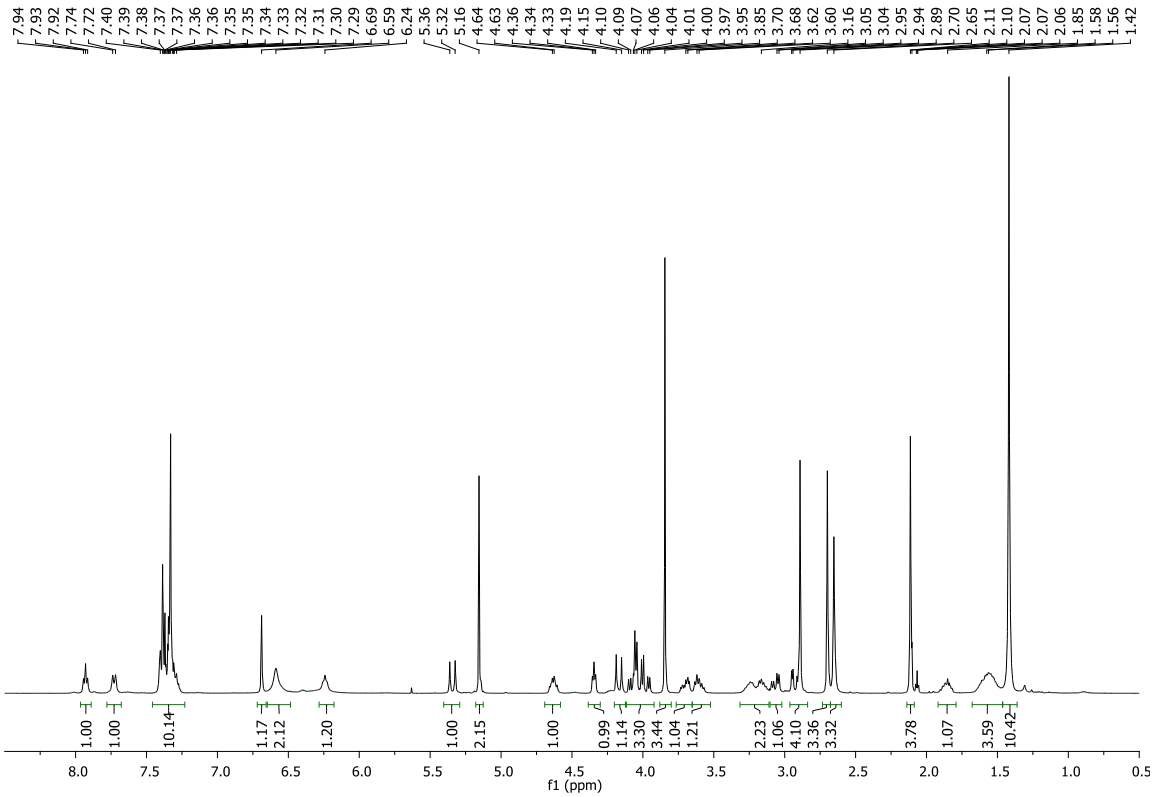

^{13}C NMR (101 MHz, Acetone-d_6):

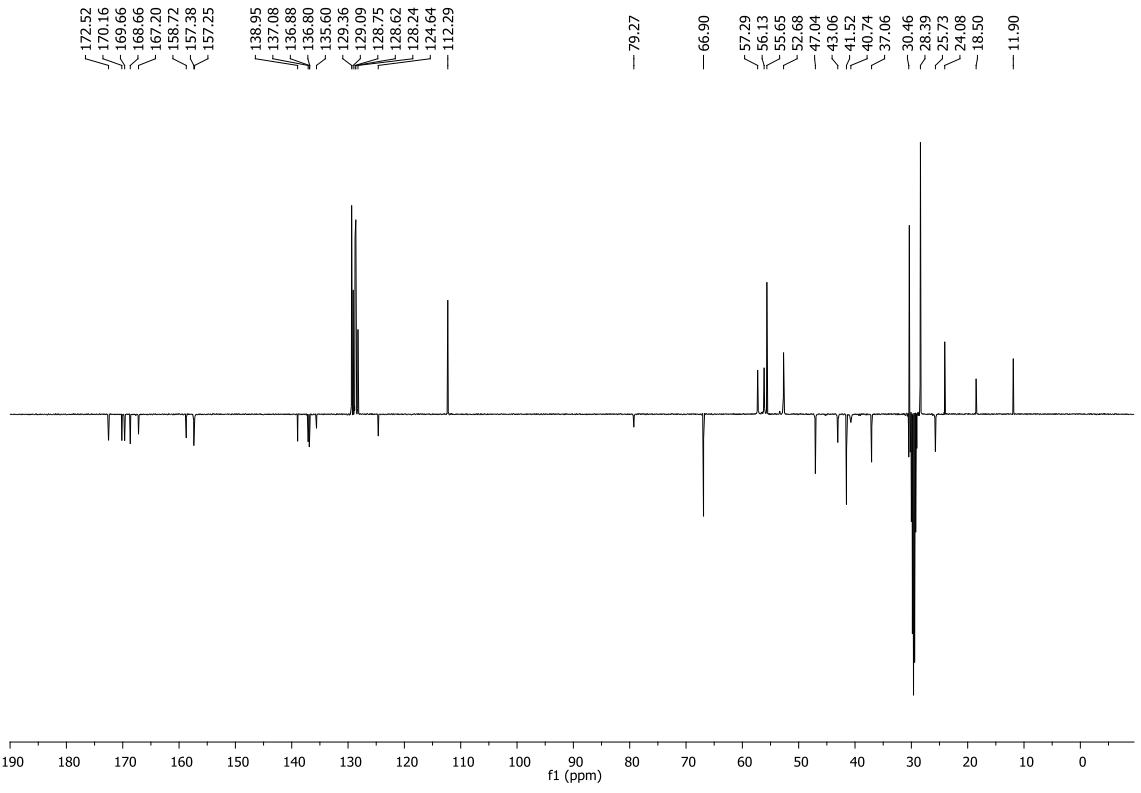

114 d: (Cbz-Asp(O*t*Bu)-DKP6-Arg(Mtr)-Gly-OBn)

^{1}H NMR (400 MHz, Acetone-d_6):

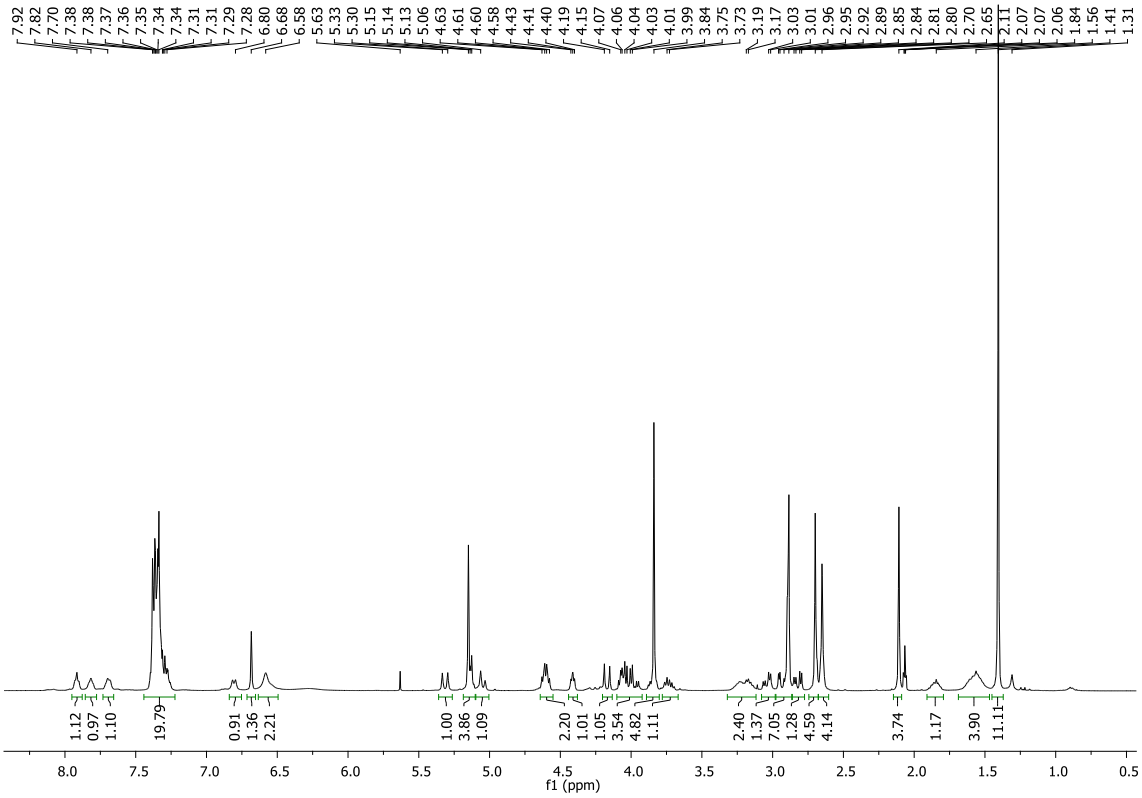

^{13}C NMR (101 MHz, Acetone-d_6):

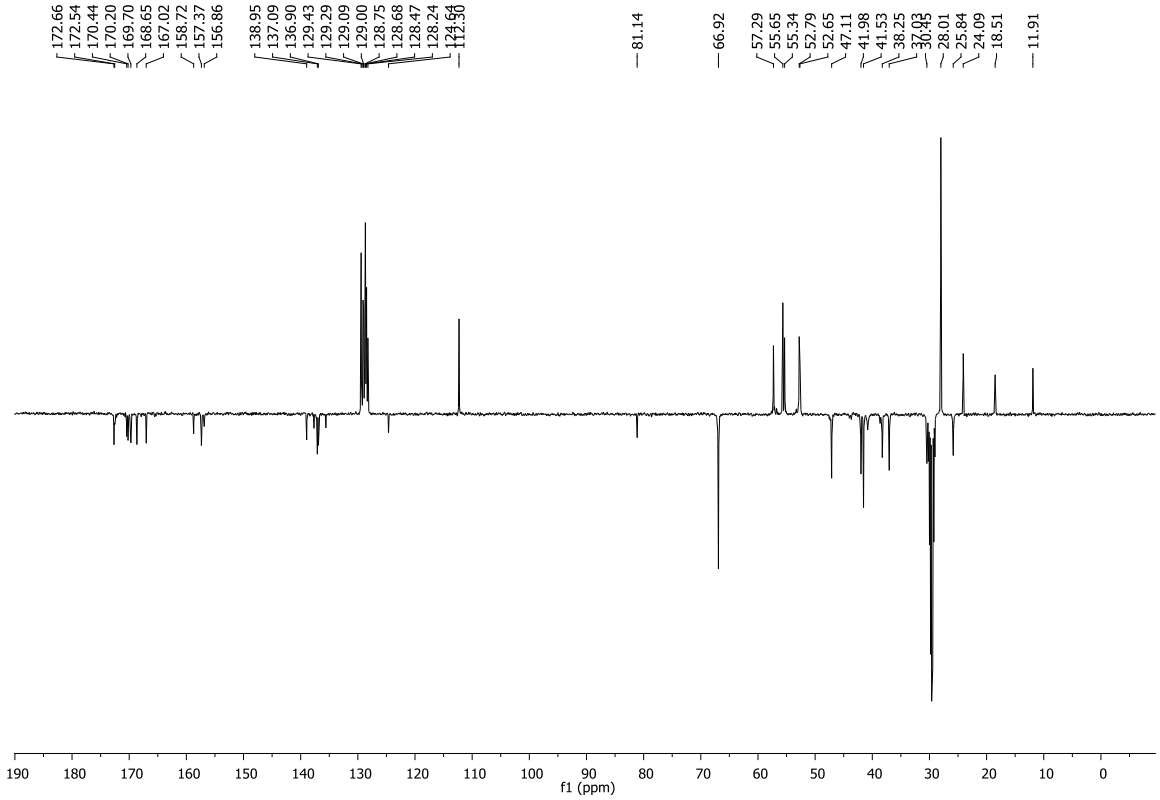

116 d: (*Cyclo*[Arg(Mtr)-Gly-Asp(O*t*Bu)-DKP6])

^{1}H NMR (400 MHz, DMSO-d_6):

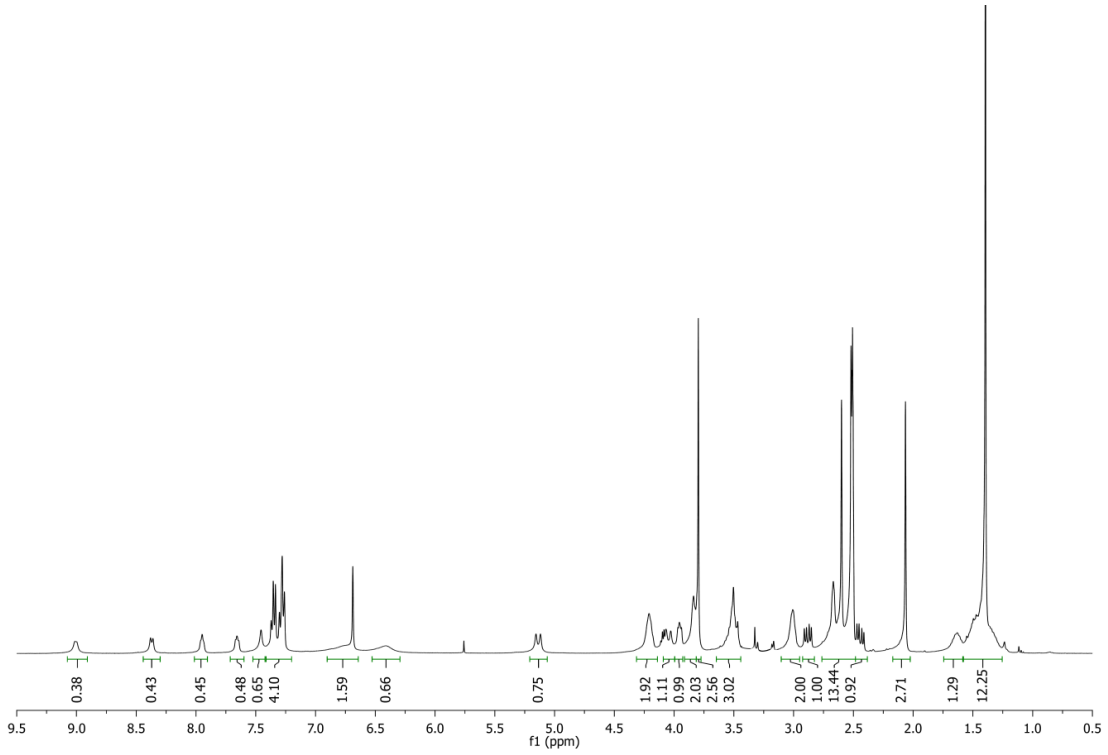

^{13}C NMR (101 MHz, DMSO-d_6):

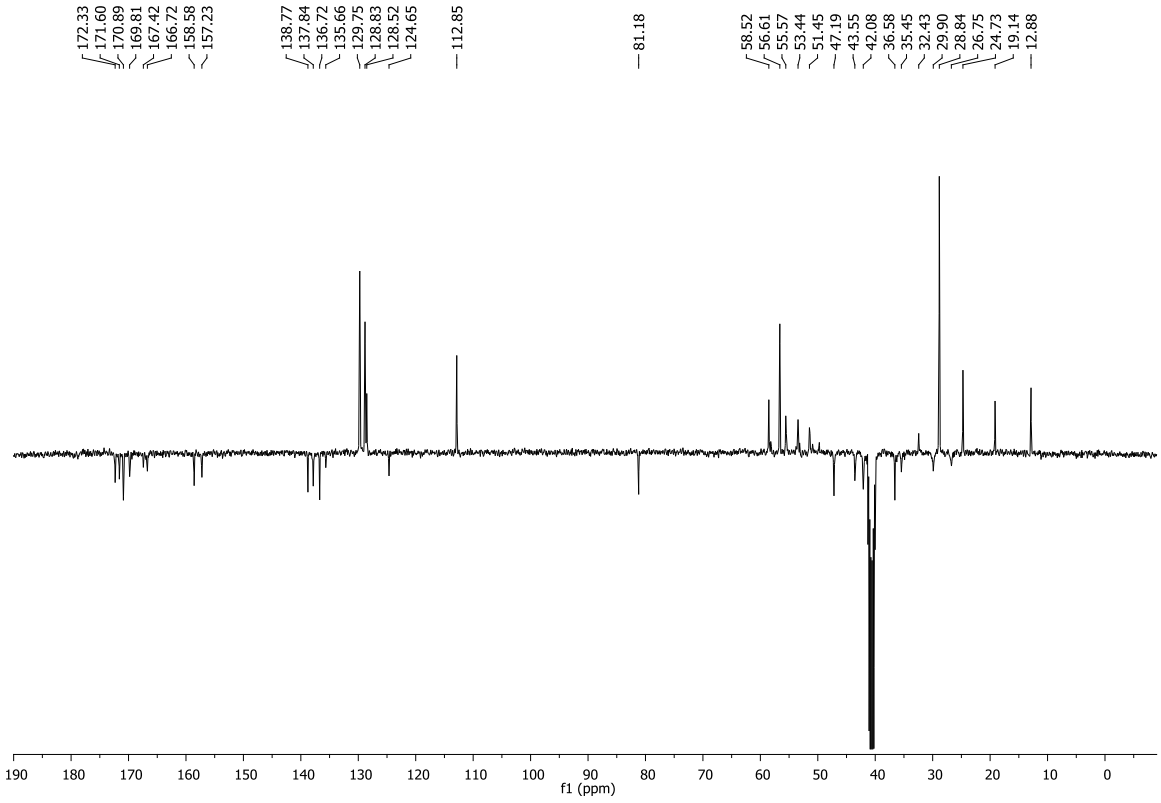

105: (*Cyclo*[Arg-Gly-Asp-DKP6])

^{1}H NMR (400 MHz, H_2O/D_2O 9:1):

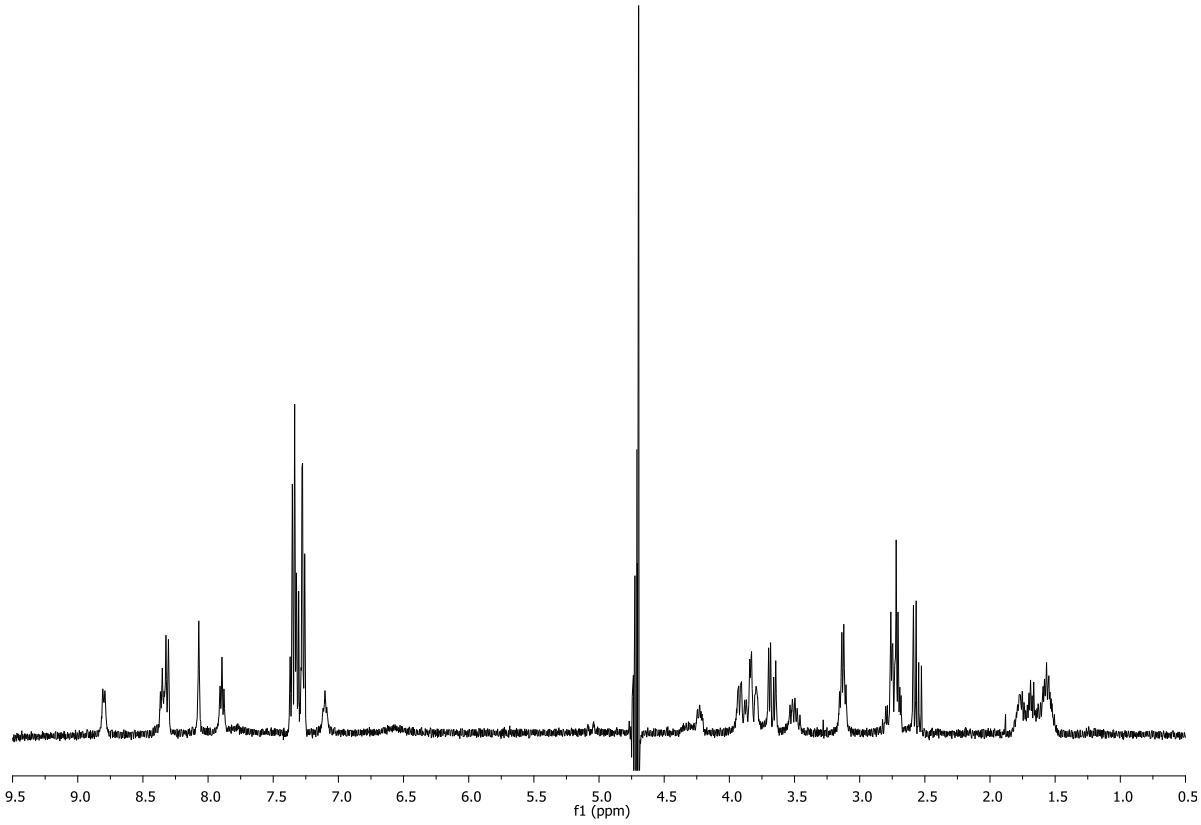

113 e: (*N*-Boc-DKP7-Arg(Mtr)-Gly-OBn)

^{1}H NMR (400 MHz, Acetone-d_6):

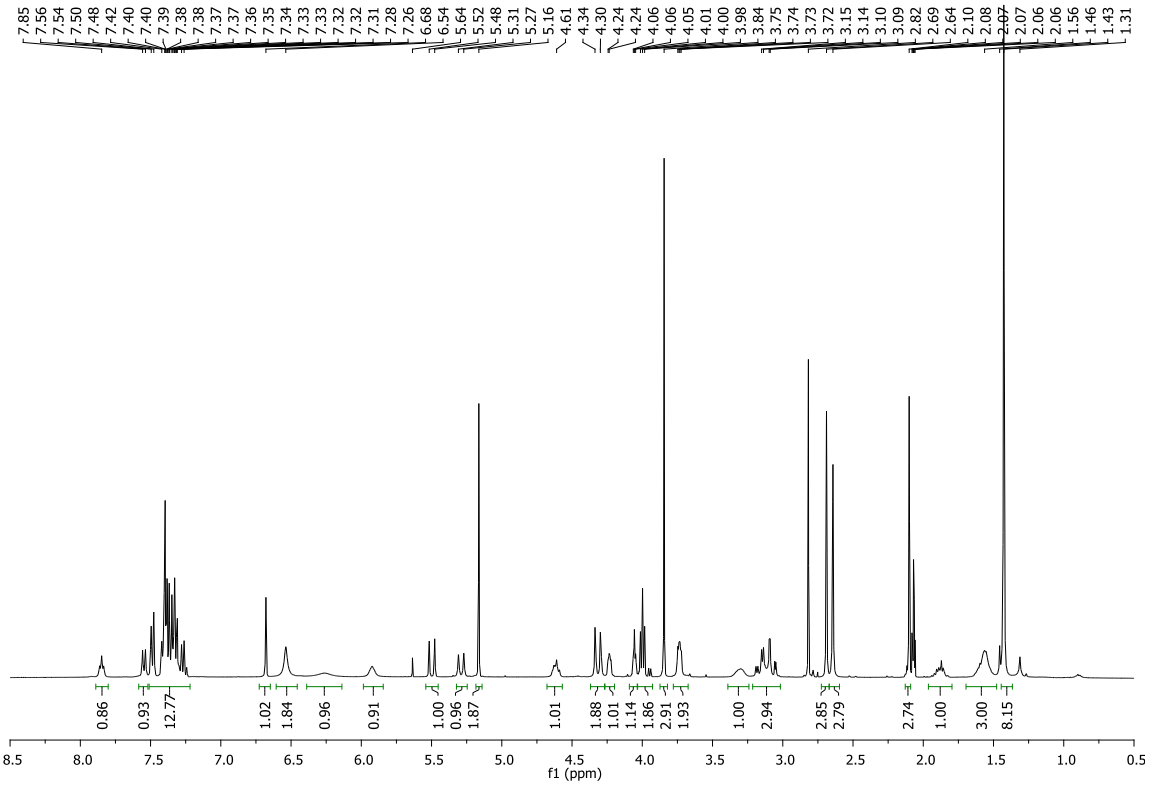

^{13}C NMR (101 MHz, Acetone-d_6):

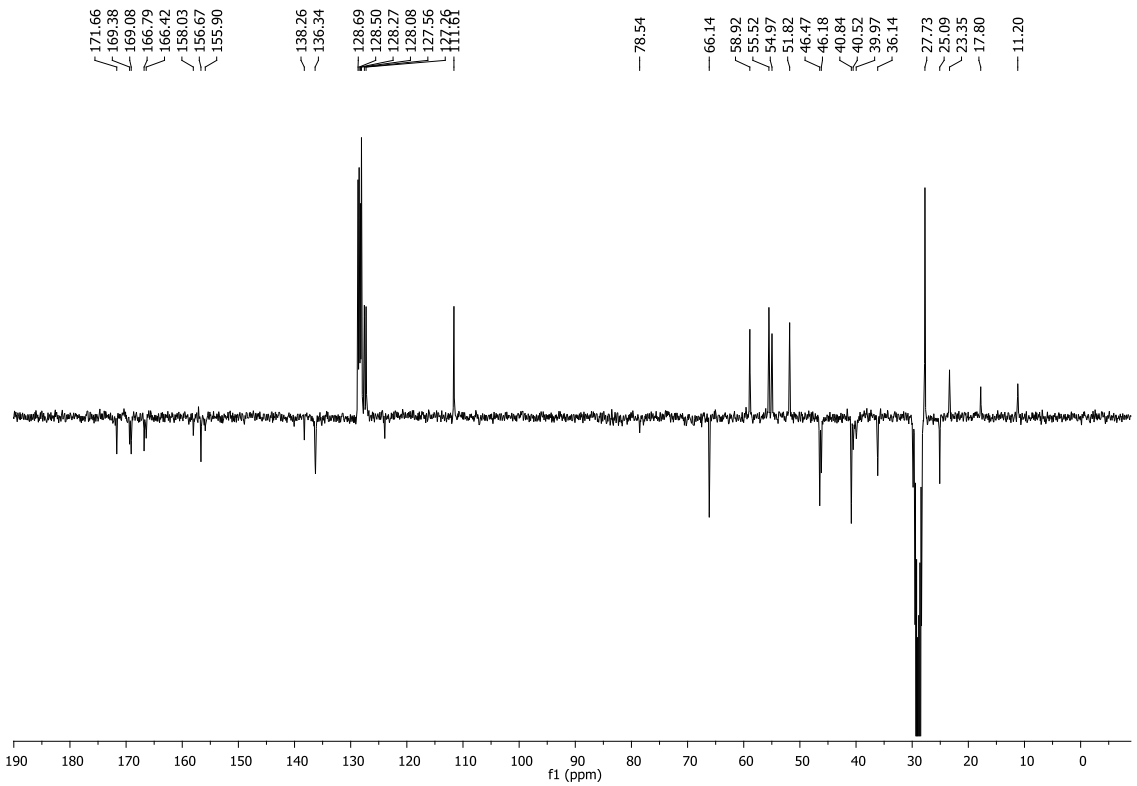

114 e: (Cbz-Asp(O*t*Bu)-DKP7-Arg(Mtr)-Gly-OBn)

^{1}H NMR (400 MHz, Acetone-d_6):

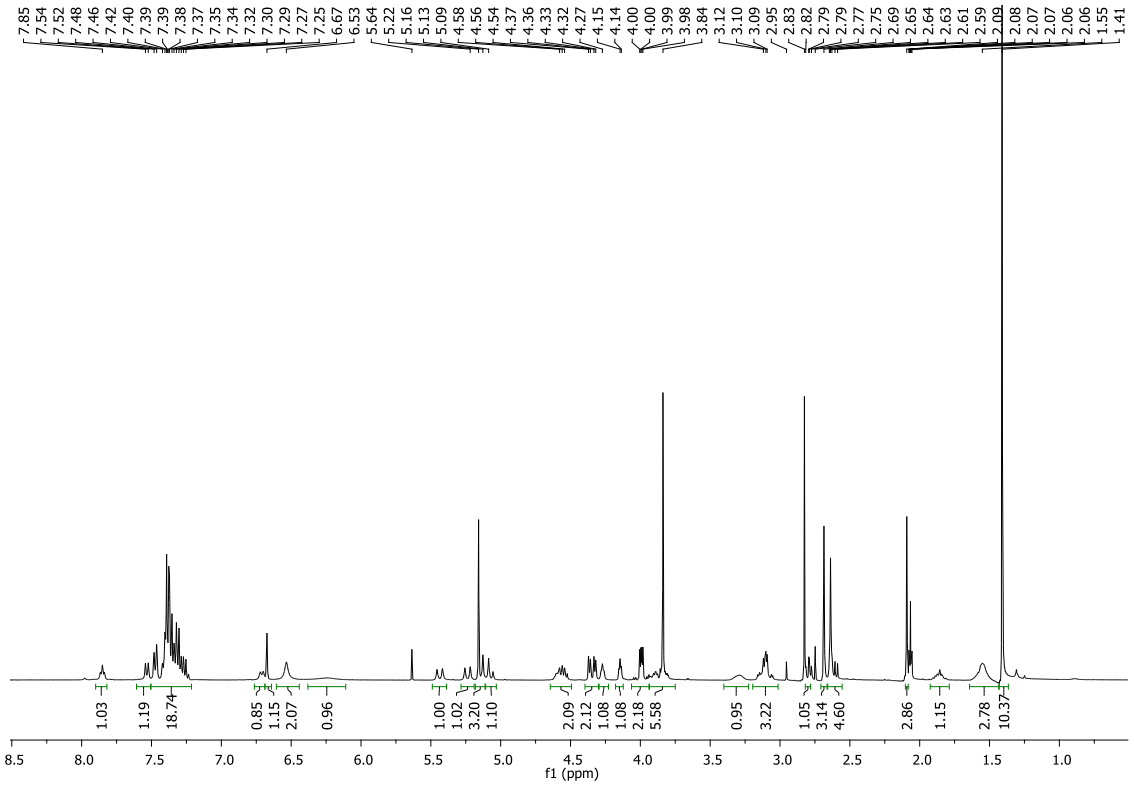

^{13}C NMR (101 MHz, Acetone-d_6):

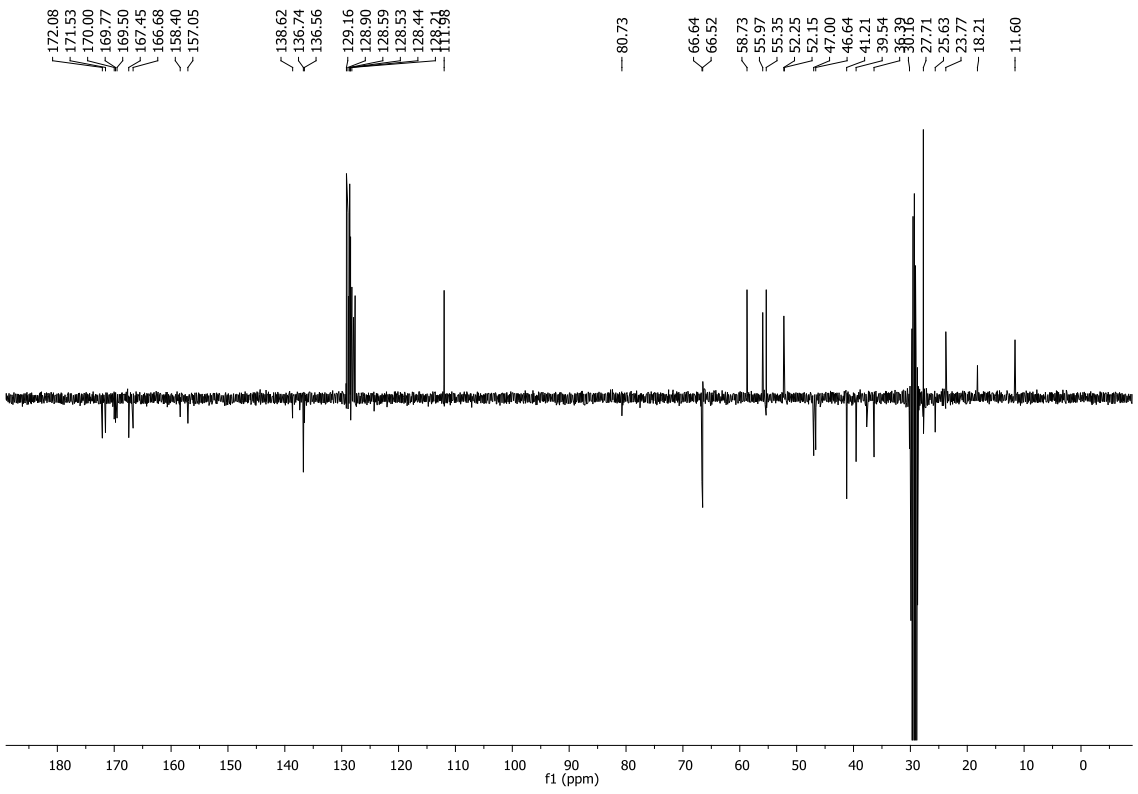

116 e: (*Cyclo*[Arg(Mtr)-Gly-Asp(O*t*Bu)-DKP7])

^{1}H NMR (400 MHz, CD_3OD):

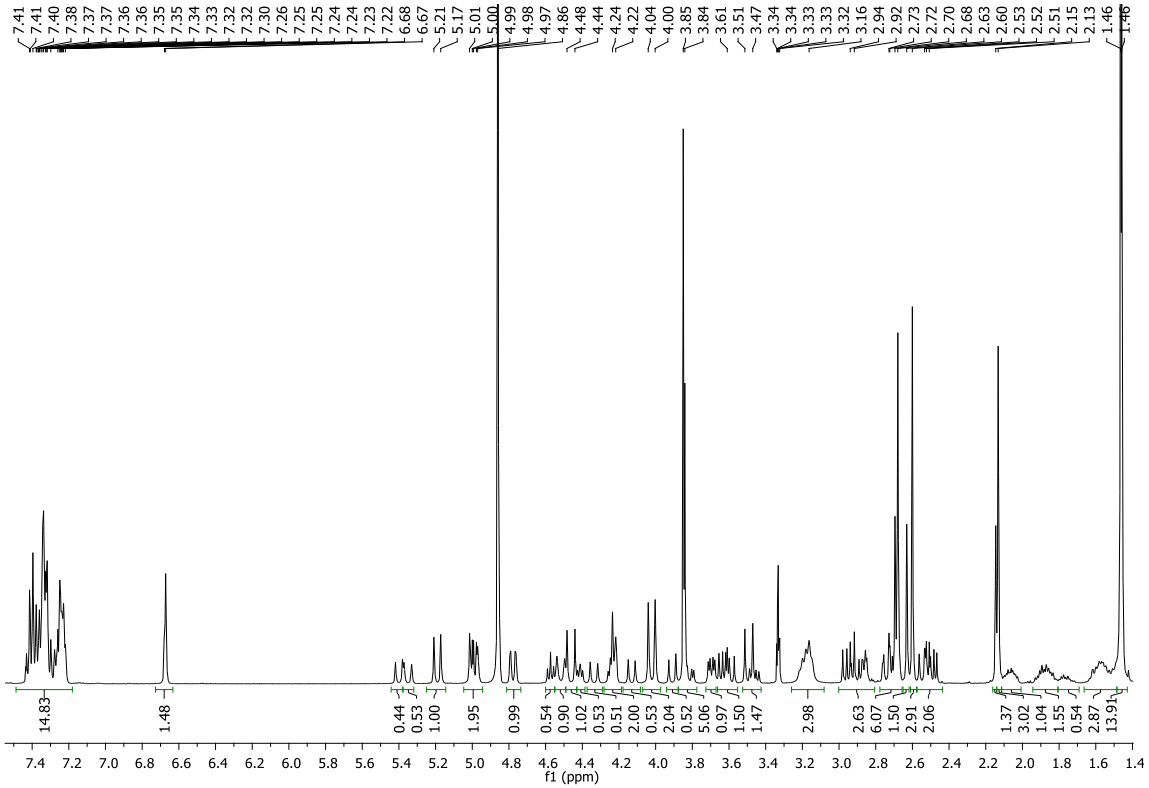

^{13}C NMR (101 MHz, CD_3OD):

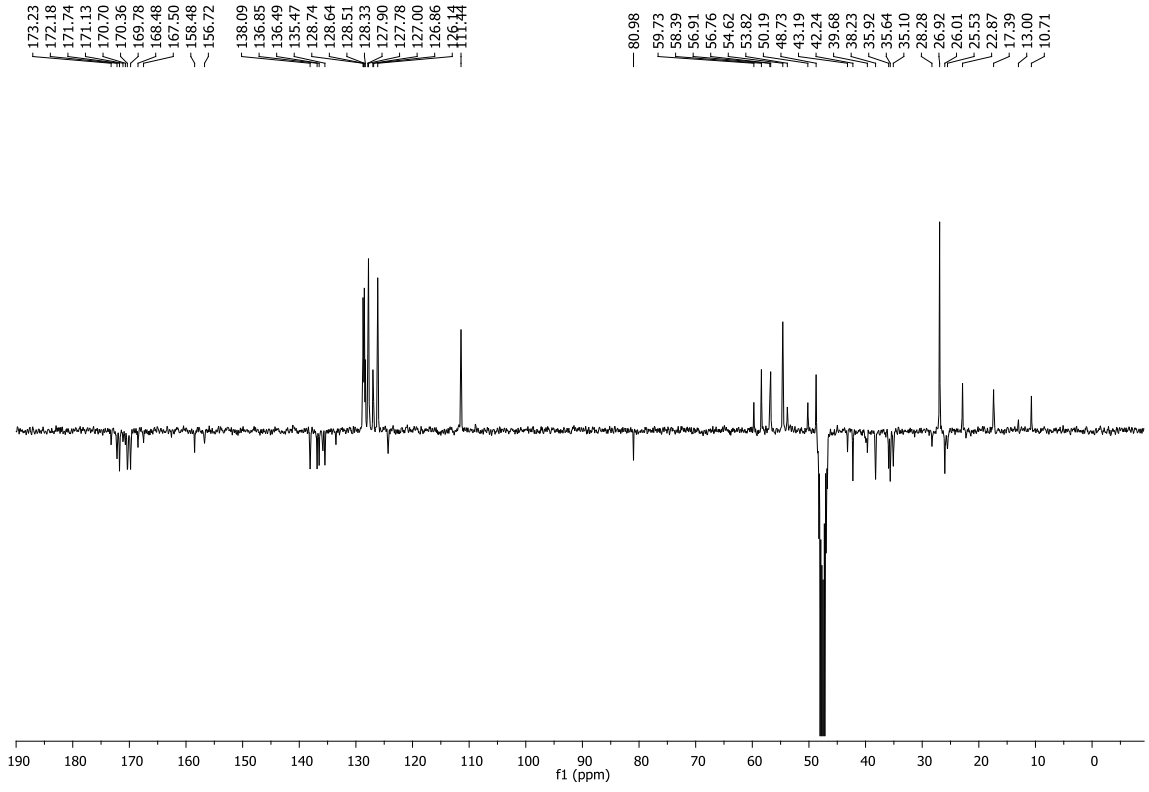

106 A (*Cyclo*[Arg-Gly-Asp-DKP7-A])

^{1}H NMR (400 MHz, H_2O/D_2O 9:1):

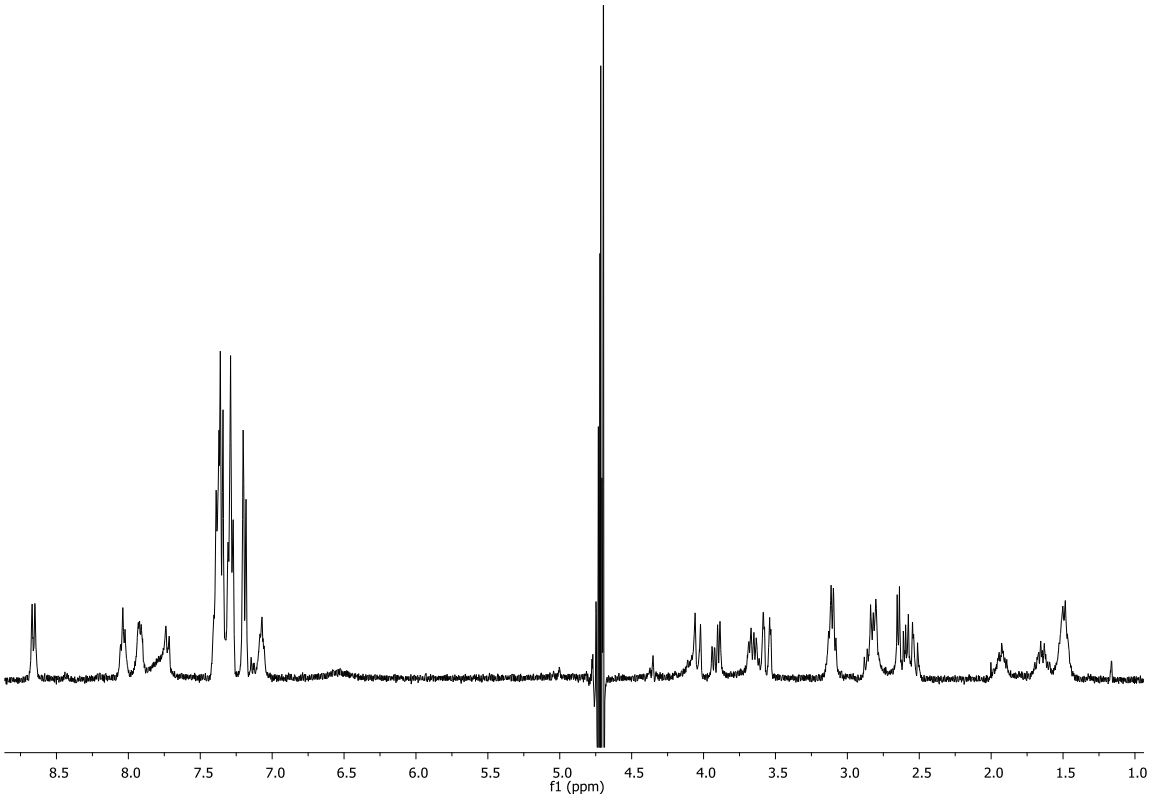

106 B (*Cyclo*[Arg-Gly-Asp-DKP7-B])

^{1}H NMR (400 MHz, H_2O/D_2O 9:1)

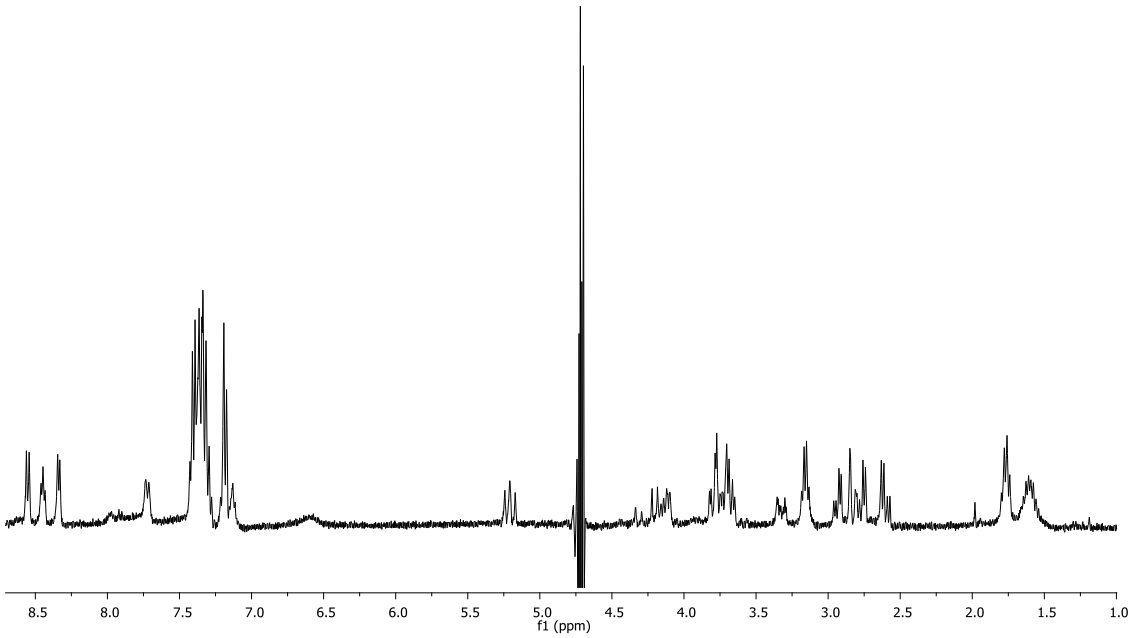

113 f: (*N*-Boc-DKP8-Arg(Mtr)-Gly-OBn)

^{1}H-NMR (400 MHz, CD_3OD):

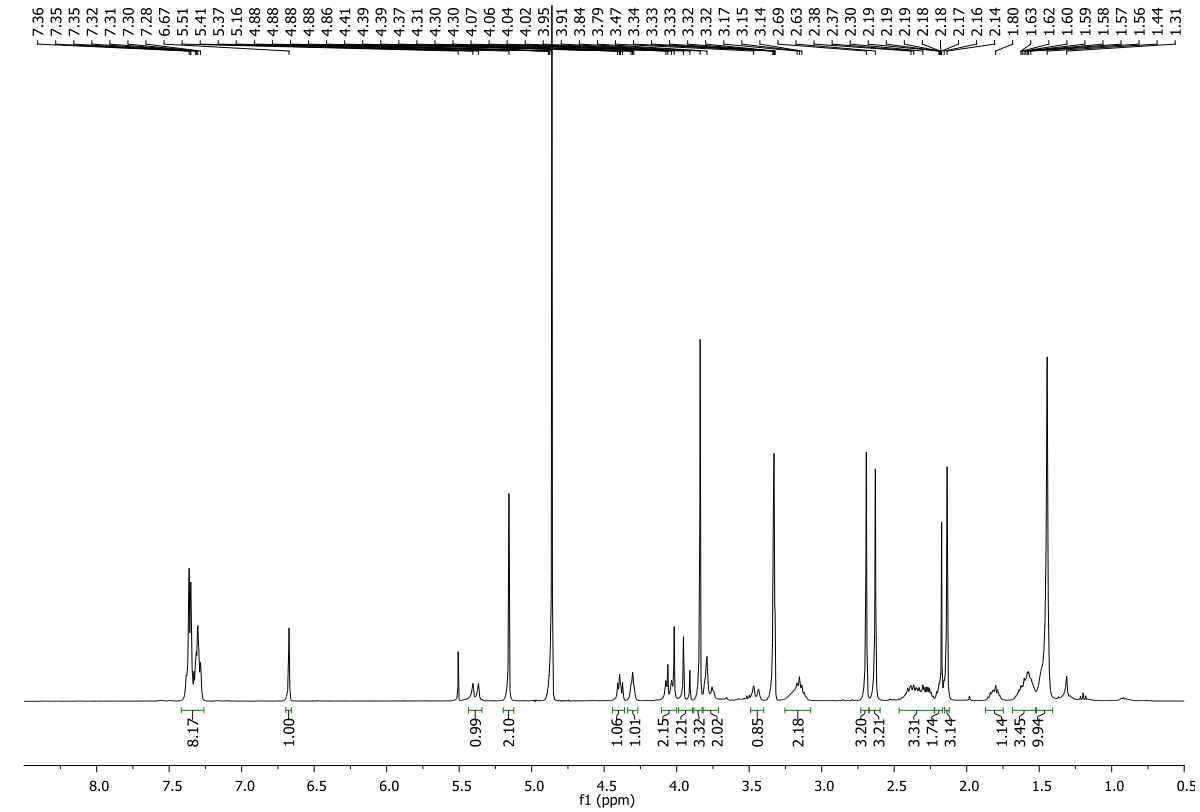

^{13}C-NMR (101 MHz, CD_2Cl_2):

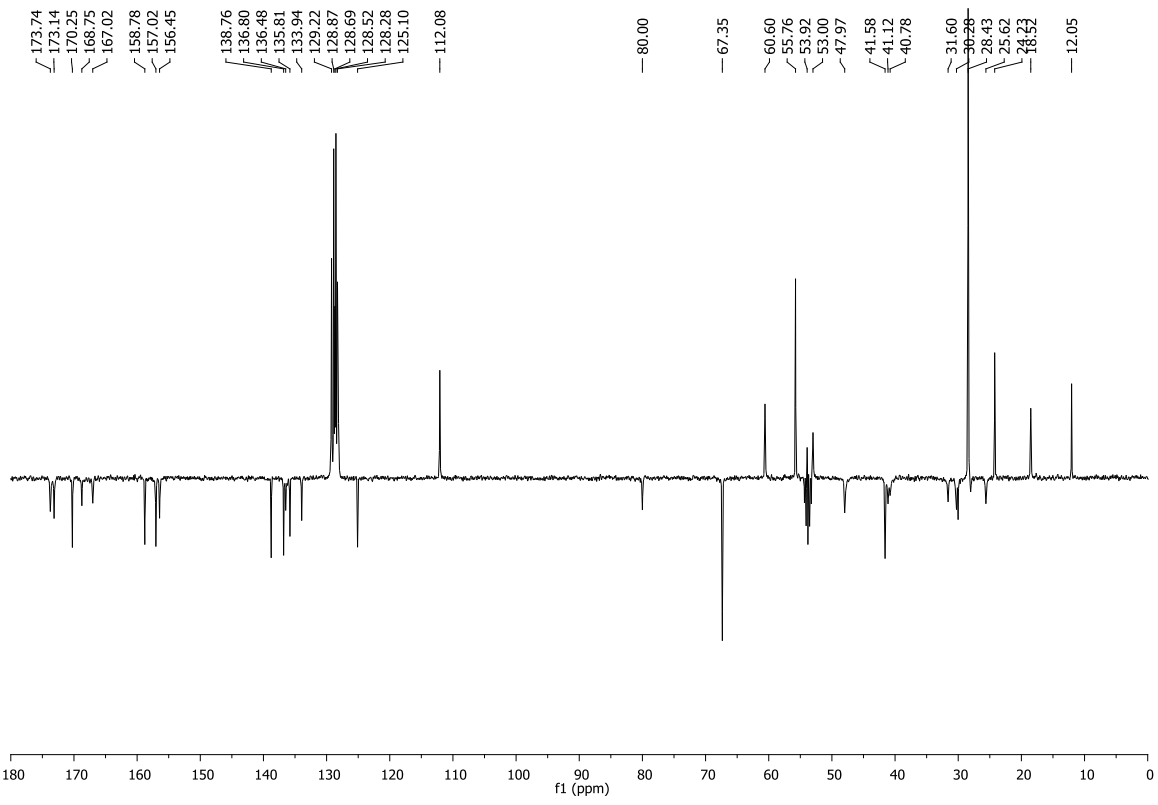

114 f: (*N*-Cbz-Asp(O*t*Bu)-DKP8-Arg(Mtr)-Gly-OBn)

^{1}H-NMR (400 MHz, Acetone-d_6):

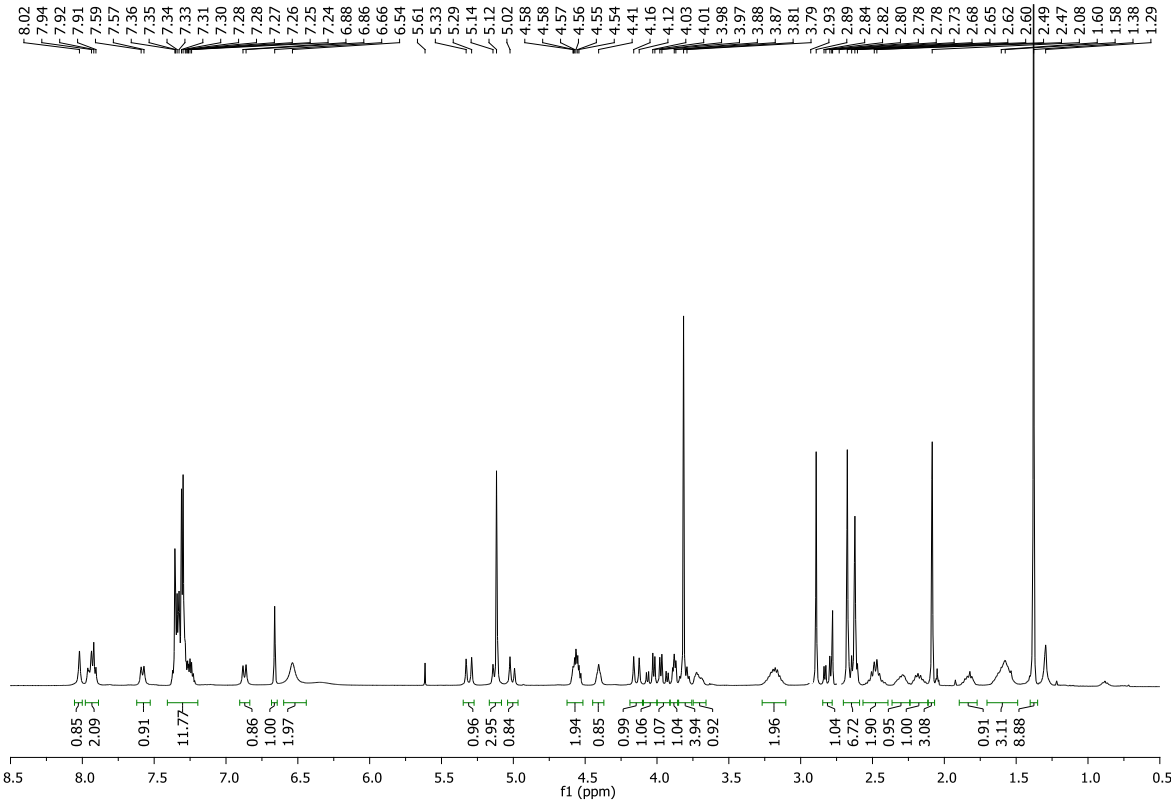

^{13}C-NMR (101 MHz, Acetone-d_6):

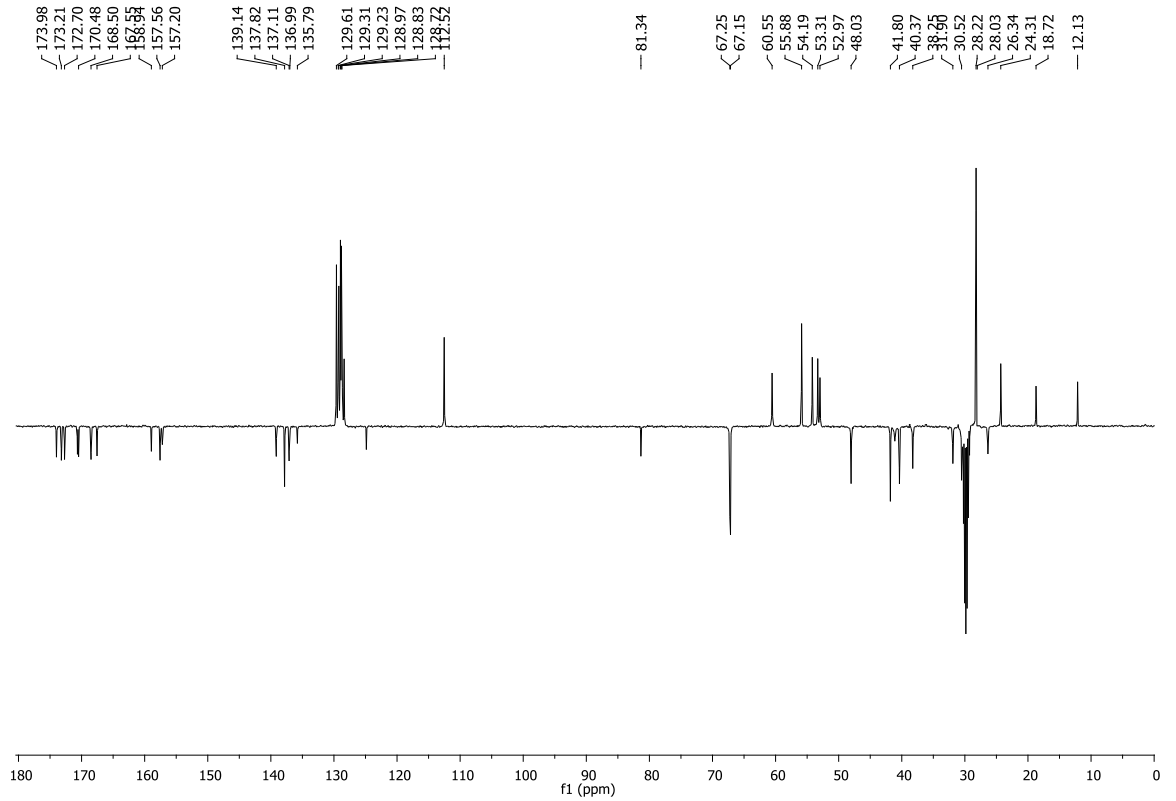

116 f: Cyclo[Arg(Mtr)-Gly-Asp(O*t*Bu)-DKP8]

^{1}H-NMR (400 MHz, CD_3OD):

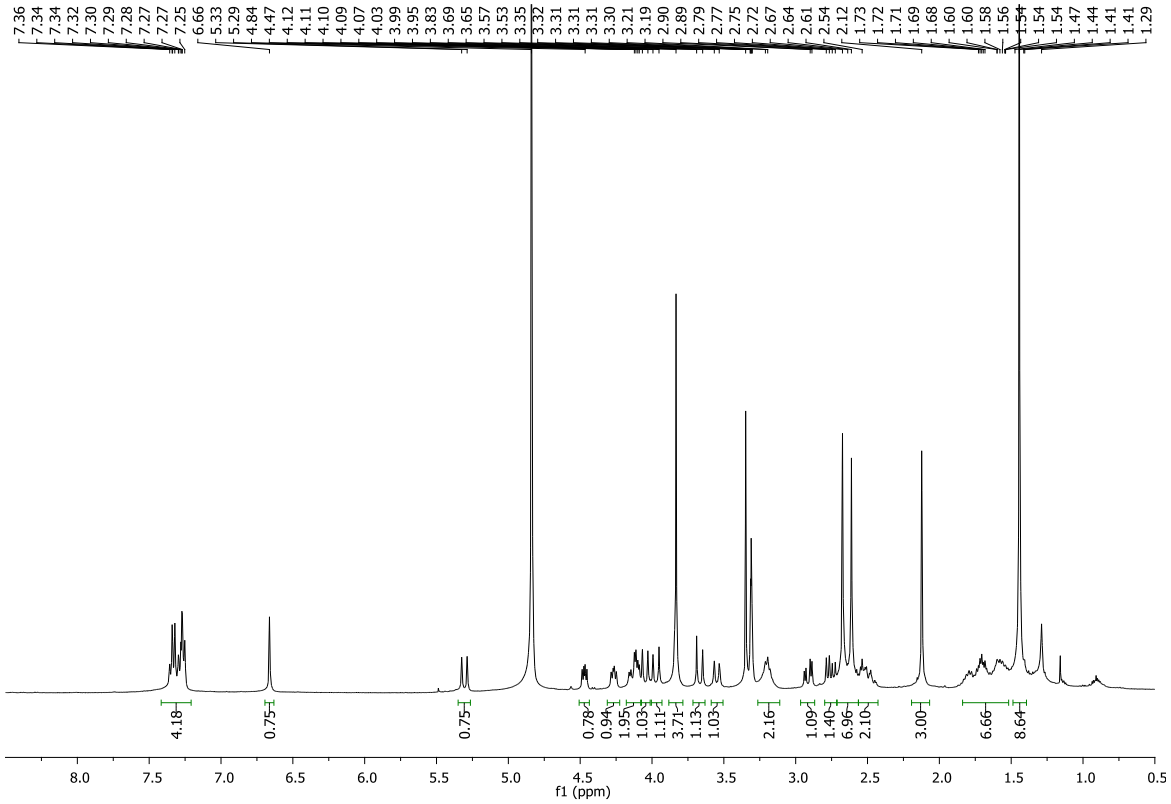

^{13}C-NMR (101 MHz, CD_3OD):

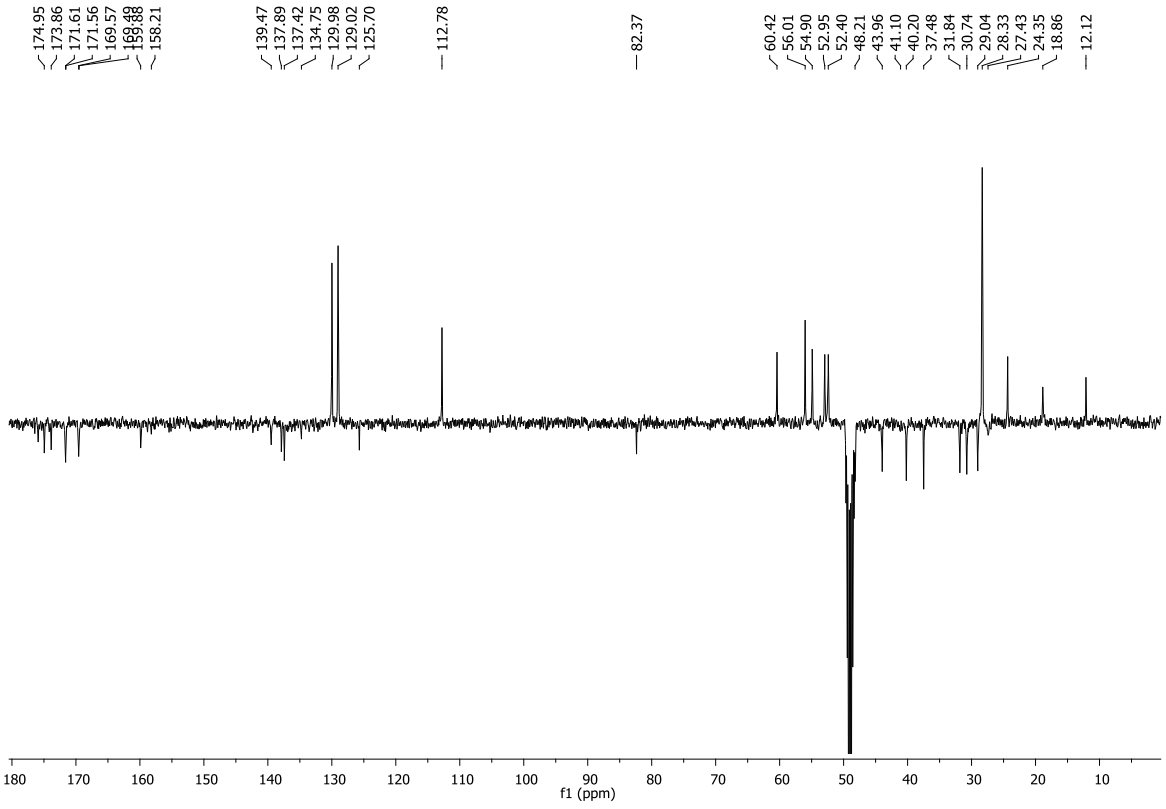

107: Cyclo[Arg-Gly-Asp-DKP8]

^{1}H NMR (400 MHz, D_2O):

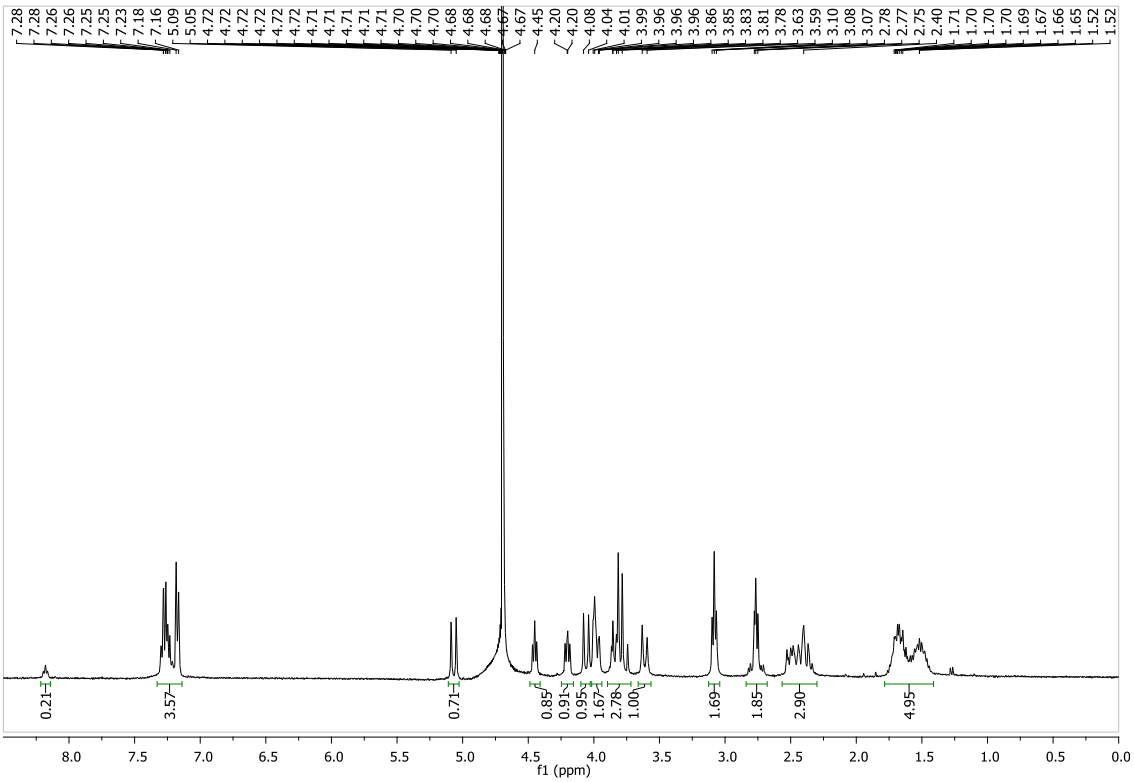

120 a: Cbz-Arg(Mtr)-DKP2-isoAsp(OtBu)-Gly-OH

^{1}H NMR (400 MHz, MeOD):

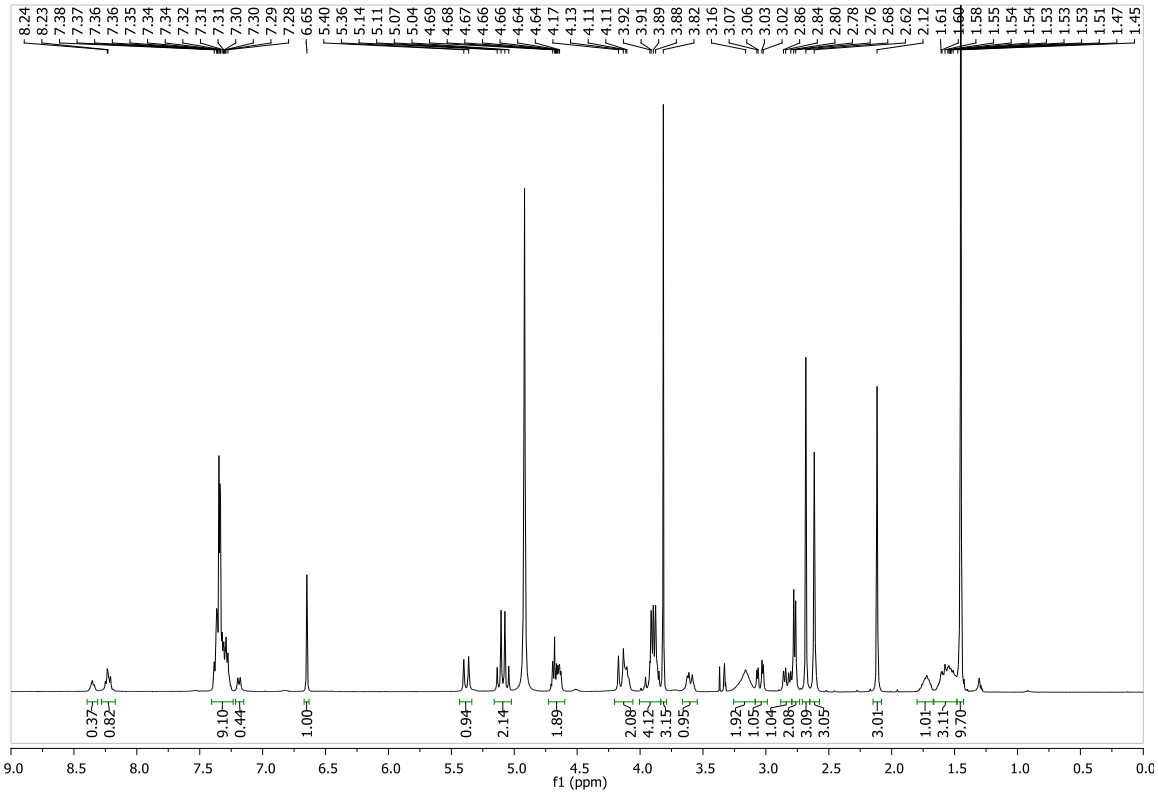

^{13}C NMR (101 MHz, MeOD):

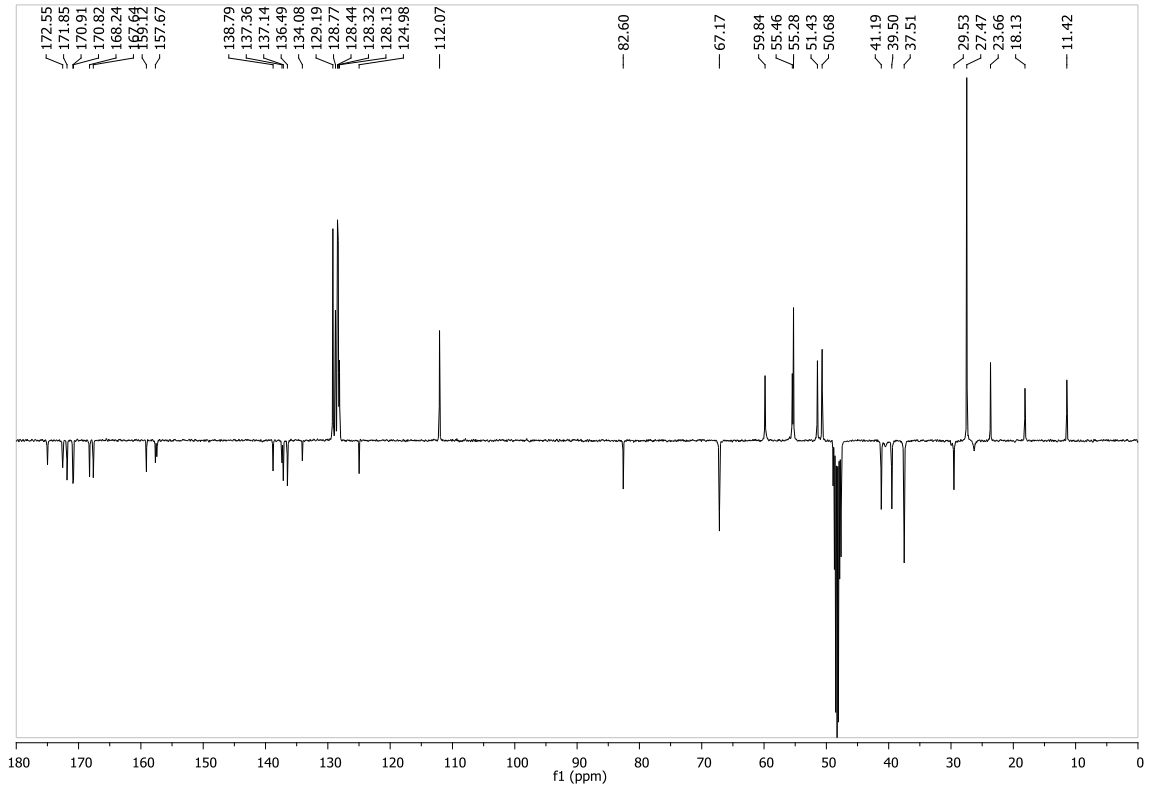

120 b: Cbz-Arg(Mtr)-DKP3-*iso*Asp(O*t*Bu)-Gly-OH

^{1}H NMR (400 MHz, MeOD):

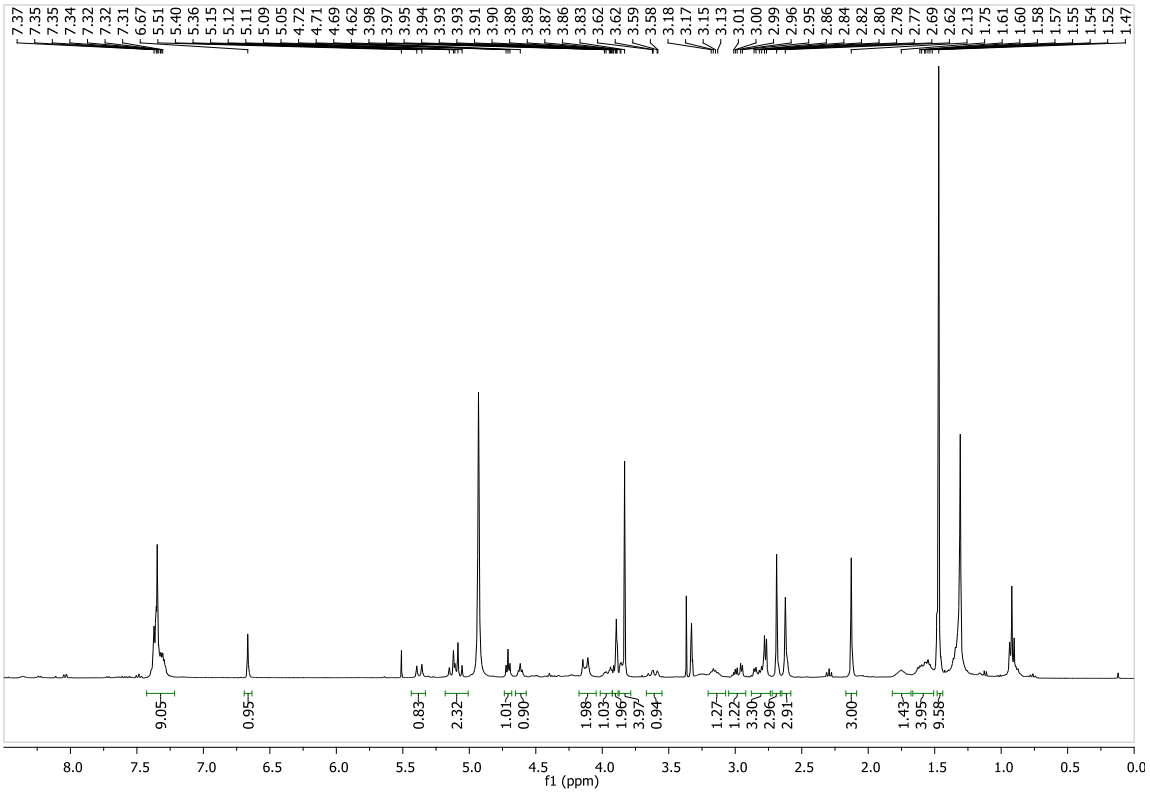

^{13}C NMR (101 MHz, MeOD):

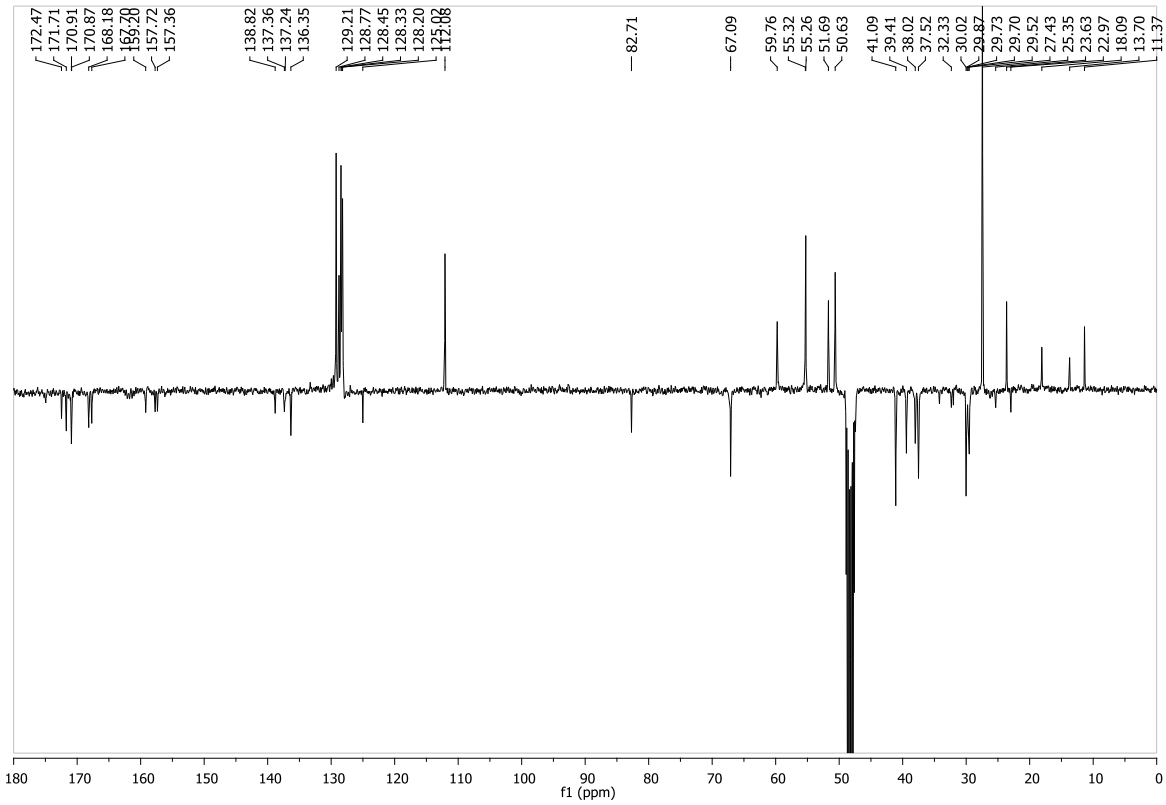

122 a: *Cyclo* [*iso*Asp(O*t*Bu)-Gly-Arg(Mtr)-DKP2]

^{1}H NMR (400 MHz, MeOD):

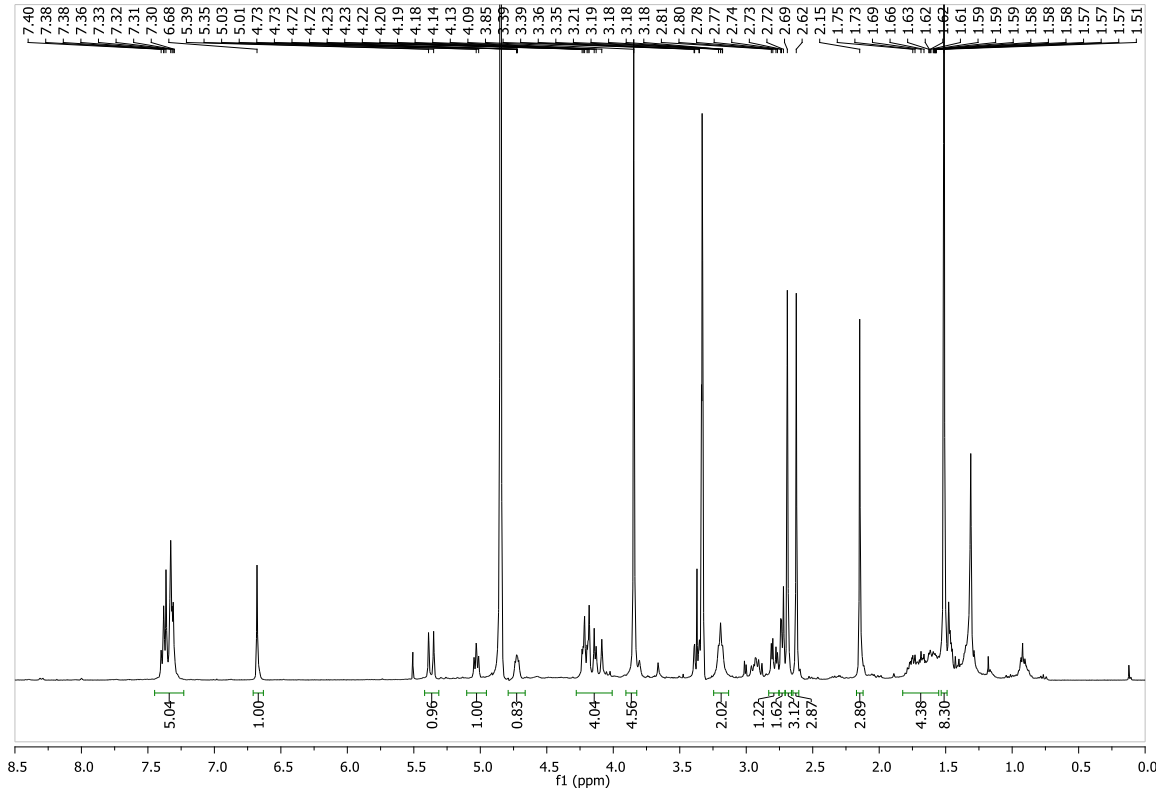

^{13}C NMR (101 MHz, MeOD):

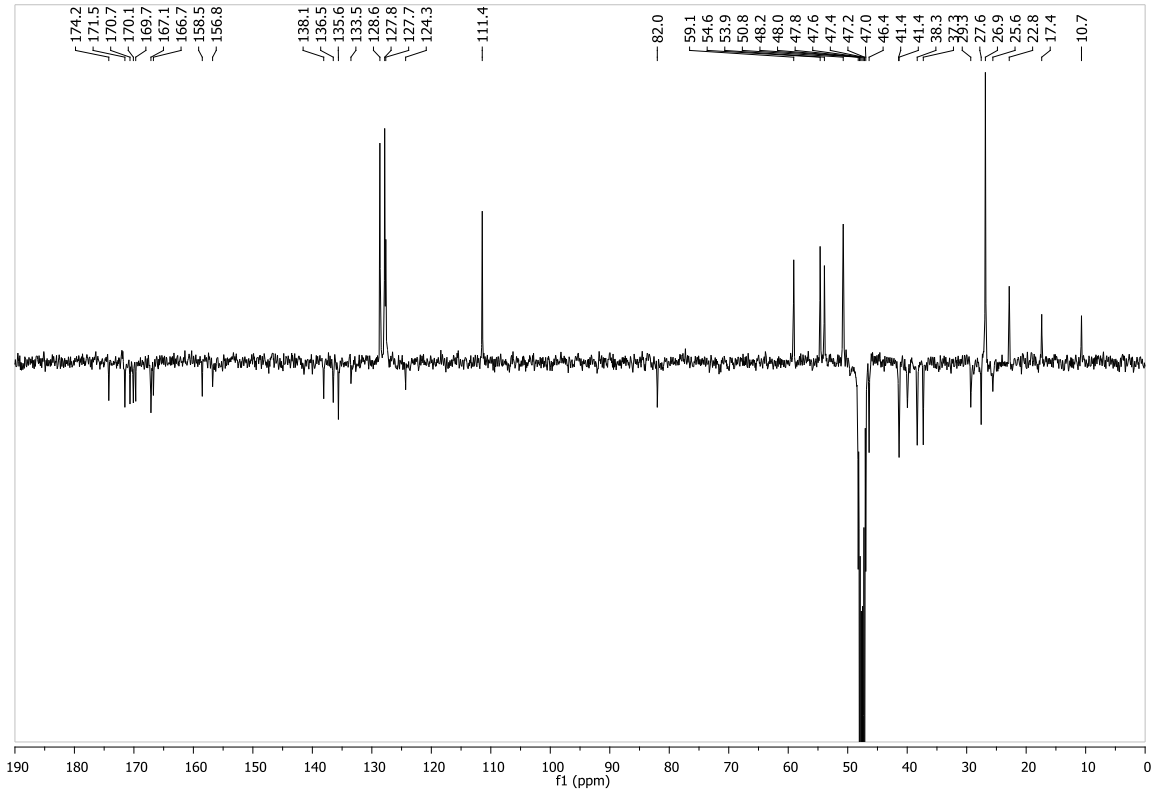

122 b: *Cyclo* [*iso*Asp(O*t*Bu)-Gly-Arg(Mtr)-DKP3]

^{1}H NMR (400 MHz, MeOD):

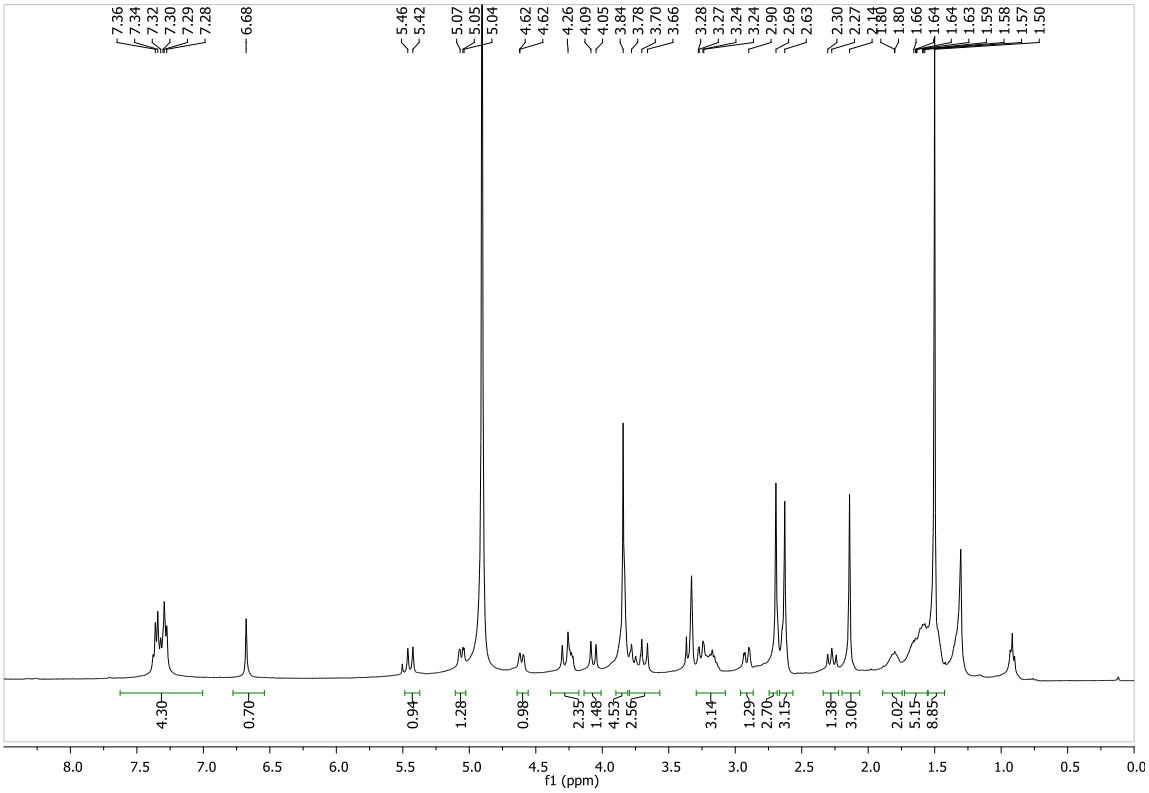

^{13}C NMR (101 MHz, MeOD):

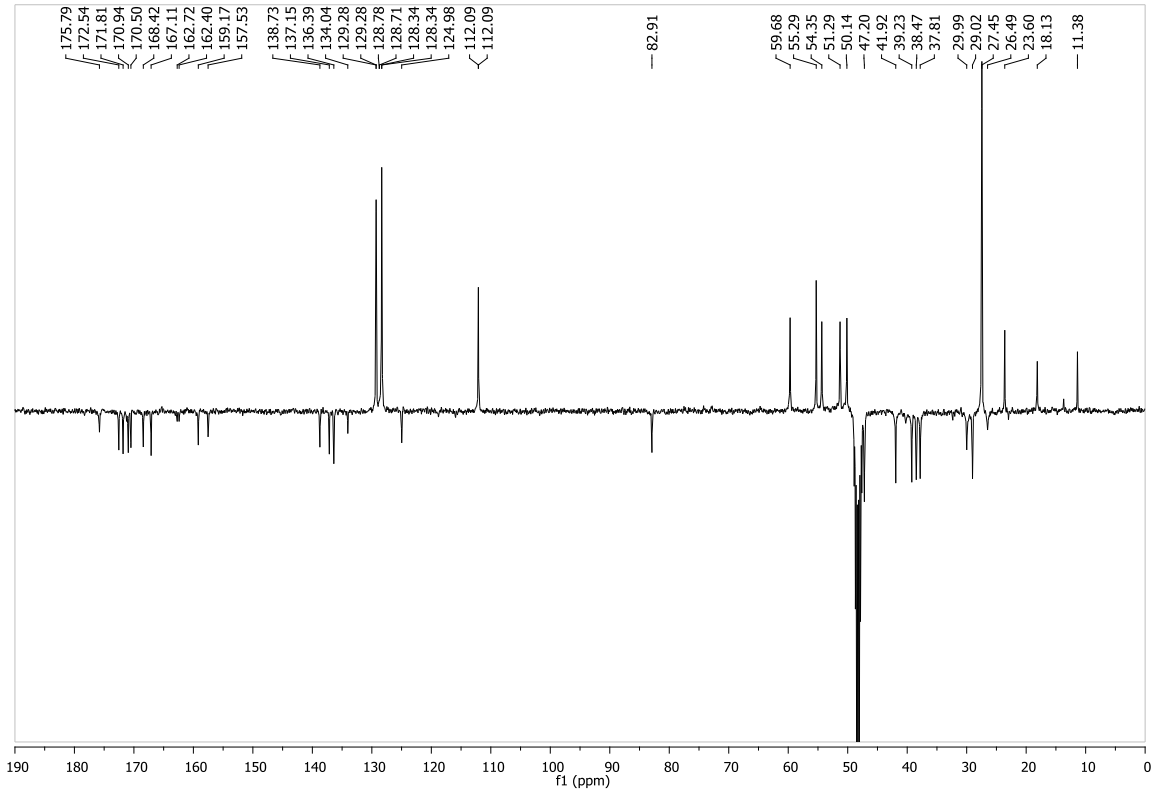

Fmoc-L-Ala-L-Ala-OSu

^{1}H NMR (300 MHz, $CDCl_3$):

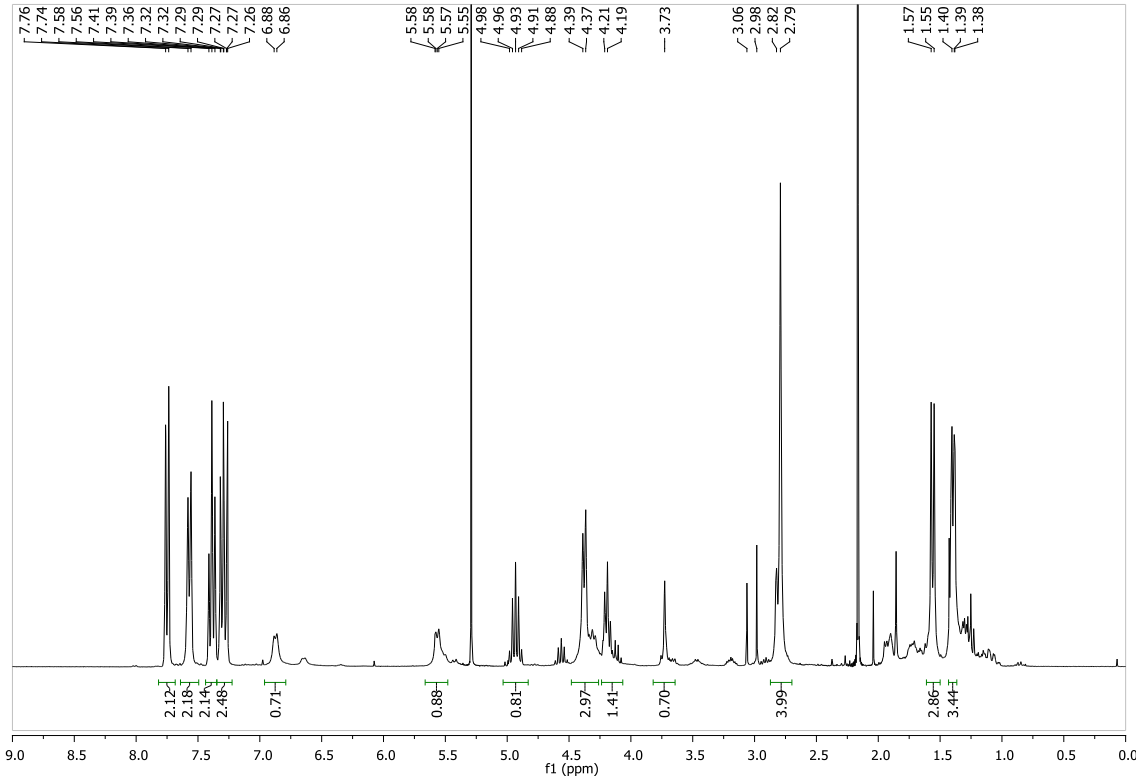

127

^{1}H NMR (600 MHz, DMSO, 310 K)